MATHEMATICAL MODELLING: THEORY AND APPLICATIONS

CHAOS IN ELECTRONICS

M.A. van Wyk and W.-H. Steeb

Springer-Science+Business Media, B.V.

Chaos in Electronics

MATHEMATICAL MODELLING:
Theory and Applications

VOLUME 2

This series is aimed at publishing work dealing with the definition, development and application of fundamental theory and methodology, computational and algorithmic implementations and comprehensive empirical studies in mathematical modelling. Work on new mathematics inspired by the construction of mathematical models, combining theory and experiment and furthering the understanding of the systems being modelled are particularly welcomed.

Manuscripts to be considered for publication lie within the following, non-exhaustive list of areas: mathematical modelling in engineering, industrial mathematics, control theory, operations research, decision theory, economic modelling, mathematical programming, mathematical system theory, geophysical sciences, climate modelling, environmental processes, mathematical modelling in psychology, political science, sociology and behavioural sciences, mathematical biology, mathematical ecology, image processing, computer vision, artificial intelligence, fuzzy systems, and approximate reasoning, genetic algorithms, neural networks, expert systems, pattern recognition, clustering, chaos and fractals.

Original monographs, comprehensive surveys as well as edited collections will be considered for publication.

The titles published in this series are listed at the end of this volume.

Chaos in Electronics

by

M. A. van Wyk
Technikon Southern Africa,
and
Rand Afrikaans University,
Johannesburg, South Africa

and

W.-H. Steeb
Rand Afrikaans University,
Johannesburg, South Africa

Springer-Science+Business Media, B.V.

A C.I.P. Catalogue record for this book is available from the Library of Congress.

ISBN 978-90-481-4857-8 ISBN 978-94-015-8921-5 (eBook)
DOI 10.1007/978-94-015-8921-5

Printed on acid-free paper

Contents

List of Symbols

$\emptyset$	empty set
$\mathbf{Z}$	set of integers
$\mathbf{N}$	set of positive integers: natural numbers
$\mathbf{R}$	set of real numbers
$\mathbf{R}^+$	nonnegative real numbers
$\mathbf{C}$	set of complex numbers
$\mathbf{R}^N$	N-dimensional real linear space
$\mathbf{e}_n$	n-th vector of the standard basis of $\mathbf{R}^N$
S^1	unit circle
I	unit interval
$A \subset B$	subset A of the set B
$A \cap B$	intersection of the sets A and B
$A \cup B$	union of the sets A and B
$A \times B$	Cartesian product of the sets A and B
Int A	interior of the set A
$B(\mathbf{x}; r)$	open ball of radius r centered at $\mathbf{x}$
$\tilde{B}(\mathbf{x}; r)$	closed ball of radius r centered at $\mathbf{x}$
$\dim(\mathcal{M})$	dimension of the manifold $\mathcal{M}$
$T_{\mathbf{x}}\mathcal{M}$	tangent space at the point $\mathbf{x}$ on the manifold $\mathcal{M}$
W^s, W^u	stable and unstable manifolds
W^s_{loc}, W^u_{loc}	local stable and unstable manifolds
$x := y$	x is defined as y
$x \equiv y$	x is identical (or equivalent) to y
f, g, h, F	scalar-valued functions
$\mathbf{f}$, $\mathbf{g}$, $\mathbf{h}$, $\mathbf{F}$, $\mathbf{G}$, $\mathbf{H}$	vector-valued functions
$f \circ g$	composition of mappings $(f \circ g)(x) := f(g(x))$
$f^{(n)}$	n-th iterate of the function f, i.e. f composed n-times
$D\mathbf{f}$, $D_{\mathbf{x}}\mathbf{f}$	Jacobian matrix of the function $\mathbf{f}$ (with respect to $\mathbf{x}$)
$\mathcal{D}(f)$	domain of the function f
$\mathcal{R}(f)$	range of the function f
$f\|A$	restriction of the function f to the set A
supp f	support of the function f
C^n	n-times differentiable
$\mathbf{x} \cdot \mathbf{y}$, $\langle \mathbf{x}, \mathbf{y} \rangle$	scalar product (inner product)
$\mathbf{x} \times \mathbf{y}$	cross product (vector product)

$\mathbf{x} \oplus \mathbf{y}$	direct sum
$\mathbf{x} \otimes \mathbf{y}$	Kronecker product
$\mathrm{tr}(\mathbf{A})$	trace of the square matrix $\mathbf{A}$
$\det(\mathbf{A})$	determinant of the matrix $\mathbf{A}$
λ	eigenvalue, Lyapunov exponent
$\lambda(\mathbf{A})$	spectrum of eigenvalues of the matrix $\mathbf{A}$
$\mathbf{I}$	unit matrix, identity operator
$\mathbf{A}^T$	transpose of matrix $\mathbf{A}$
$\chi_{\mathbf{A}}$	characteristic function of the set $\mathbf{A}$
$(\,,\,)$	Poisson bracket
$\delta_{j,k}$	Kronecker delta, 1 if $j = k$ and 0 otherwise
$\delta(t)$	Dirac delta
$\|\cdot\|$	norm
$O(\cdot)$	remaining higher order terms of a series
Φ	flow of a vector field or map
x^*, $\mathbf{x}^*$	fixed point or periodic point of a map or differential equation
$\bar{x}$	complex conjugate
x^+, x^-	right- and left-limit of the real number x
$\lfloor x \rfloor$	greatest integer less than or equal to x
e	$\mathrm{e} := \exp(1) \equiv 2.71828\ldots$
π	$\pi := 3.14159\ldots$
$\mathrm{sgn}(\cdot)$	Signum function
$\mathrm{sat}(\cdot)$	Saturation function
$\mathrm{card}(A)$	Cardinality of the set A
$x \approx y$	approximate equality of numbers or vectors
$\Re(z)$	real part of the complex number z
$\Im(z)$	imaginary part of the complex number z
j	$:= \sqrt{-1}$

Preface

Many dynamical systems in physics, chemistry and biology exhibit complex behaviour. The apparently random motion of a fluid is the best known example. However also vibrating structures, electronic oscillators, magnetic devices, lasers, chemical oscillators, and population kinetics can behave in a complicated manner. One can find irregular oscillations, which is now known as chaotic behaviour. The research field of nonlinear dynamical systems and especially the study of chaotic systems has been hailed as one of the important breaktroughs in science this century. The simplest realization of a system with chaotic behaviour is an electronic oscillator. The purpose of this book is to provide a comprehensive introduction to the application of chaos theory to electronic systems. The book provides both the theoretical and experimental foundations of this research field. Each electronic circuit is described in detail together with its mathematical model. Controlling chaos of electronic oscillators is also included.

End of proofs and examples are indicated by ■. Inside examples the end of proofs are indicated with □.

We wish to express our gratitude to Catharine Thompson for a critical reading of the manuscript.

Any useful suggestions and comments are welcome.

Email address of the first author: MVANWYK@TSAMAIL.TRSA.AC.ZA
Email address of the first author: WHS@RAU3.RAU.AC.ZA

Home page of the authors: http://zeus.rau.ac.za/steeb/steeb.html

Chapter 1

Introduction

1.1 What is Chaos?

The term *chaos* as used here refers to the seemingly unpredictable behaviour exhibited by deterministic models. A deterministic model is a mathematical model or equation containing no element of chance. Chaos can only be exhibited by nonlinear systems. Roughly speaking, a nonlinear system is said to be *chaotic* if it exhibits sensitive dependence on initial conditions and has an infinite number of different periodic responses. If, for a system, the state space trajectories originating from two closely spaced initial conditions diverge exponentially, locally speaking, then we say the system exhibits sensitive dependence on initial conditions.

Example 1.1 Consider the system described by the equation

$$x_{n+1} = (10x_n) \pmod 1,$$

together with the two initial conditions

$$x_0 = 0.86957634547\ldots, \qquad y_0 = 0.86958908371\ldots.$$

We observe that x_0 and y_0 differ only slightly. Applying the given mathematical model to these initial conditions iteratively, produces the orbits

$$x_1 = 0.6957634547\ldots, \qquad y_1 = 0.6958908371\ldots,$$

$$x_2 = 0.957634547\ldots, \qquad y_2 = 0.958908371\ldots,$$

$$x_3 = 0.57634547\ldots, \qquad y_3 = 0.58908371\ldots,$$

$$x_4 = 0.7634547\ldots, \qquad y_4 = 0.8908371\ldots,$$

$$x_5 = 0.634547\ldots, \qquad y_5 = 0.908371\ldots,$$

etc.. Clearly the two orbits diverge. Divergence is only local, since the separation distance between these orbits will always be less than 1. We therefore see that the model considered here shows sensitive dependence on initial conditions. It is easy to see that

$$x^* = 0.123123123\ldots \equiv 0.(123)^{\infty},$$

is a periodic solution of the above model. With a little effort we can show that our model has a countably infinite number of periodic solutions. Formally, it can be shown that the above mathematical model exhibits chaos. ■

At this stage it is important to realize that chaos is not the result of noise or interference, although these may often be additional complicating factors, especially in numerical simulations and in experimental systems. Experimental observations show that chaos "mixes" orbits in state space in the same way a baker mixes bread dough by kneading it. Local instability (i.e. sensitivity to initial conditions) is the result of the stretching operations of the kneading process while global stability (i.e. boundedness) is the result of the folding operations of the kneading process. To summarize, a chaotic system contains, as ingredients, unpredictability resulting from its sensitive dependence on initial conditions and regularity which is the result of the infinite number of periodic solutions which it possesses.

1.2 Historical Account

In 1831, Faraday studied shallow water waves, in a container, vibrating vertically with a given frequency ω. In his experiments he observed the sudden appearance of subharmonic motion at the frequency $\omega/2$ under certain conditions. This experiment was later repeated by Lord Rayleigh who discussed this experiment in the classic treatise *Theory of Sound* published in 1877. This experiment has been repeatedly studied after the mid 20-th century. The reason why researchers have returned to this experiment is because it had become clear that the sudden appearance of subharmonic motion often occurs as the prelude to chaos.

Poincaré, who is considered to be the originator of dynamical system theory, discovered what is today known as homoclinic trajectories in state space. In 1892, this was published in his work on celestial mechanics, consisting of three volumes. Only in 1962 did Smale prove that Poincaré's homoclinic trajectories are chaotic limit sets.

Van der Pol and Van der Mark were engineers. In 1927 they studied the behaviour of a neon bulb RC oscillator driven by a sinusoidal voltage source [816]. They discovered that by increasing the capacitance in the circuit, sudden jumps from the drive frequency, say ω to $\omega/2$ to $\omega/3$ etc., occurred in the response. These frequency jumps were observed, or more accurately heard, with a telephone receiver. They found that

this process of *frequency demultiplication* (as they called it) eventually led to irregular noise. In fact, what they observed (in today's language) turned out to be caused by *bifurcations* and *chaos*. In 1944, Levinson conjectured that Birkhoff's remarkable curves might occur in the behaviour of some third-order system. This conjecture was answered affirmative in 1949.

Birkhoff, who was a mathematician, proved his famous *Ergodic Theorem* in 1931. He also discovered what he termed *remarkable curves* or *thick curves* which were also studied by Charpentier in 1935. Later these turned out to be a chaotic attractor of a discrete system. These curves have also been found to be *fractal* with dimension between 1 and 2.

In 1936 Chaundy and Phillips [128] studied the convergence of sequences defined by quadratic recurrence formulae. Essentially they investigated the logistic map. They introduced the terminology that a sequence oscillates *irrationally*. Today this is known as chaotic oscillations.

Intrigued by the discovery made by Van der Pol and Van der Mark, two mathematicians, Cartwright and Littlewood [115] embarked on a theoretical study of the system studied earlier by Van der Pol and Van der Mark. In 1945, they published a proof of the fact that the driven Van der Pol system can exhibit nonperiodic solutions. Later, Levinson [479] referred to these solutions as *singular behaviour*.

Melnikov [542] introduced his perturbation method for chaotic systems in 1963. This method is mainly applied to driven dynamical systems.

In 1963, Lorenz, a meteorologist, studied a simplified model for thermal convection numerically. The model (today called the *Lorenz model*) consisted of a completely deterministic system of three nonlinearly coupled ordinary differential equations. He discovered that this simple deterministic system exhibited irregular fluctuations in its response without any element of randomness being introduced into the system from outside.

Cook and Roberts [183] discovered chaotic behaviour exhibited by the Rikitake two-disc dynamo system in 1970. This is a model for the time evolution of the earth magnetic field.

In 1971, Ruelle and Takens introduced the term *strange attractor* for dissipative dynamical systems. This happened at a time when they were still unaware of the Lorenz model as an example. Ruelle and Takens also proposed a new mechanism for the onset of turbulence in the dynamics of fluids. From about this time onward, research done in the field of dynamical systems exploded and therefore only a few highlights of events that followed are mentioned.

It was in 1975 that chaos was formally defined for one-dimensional transformations by Li and Yorke [482]. They went further and presented sufficient conditions for so-

called *Li-Yorke chaos* to be exhibited by a certain class of one-dimensional mappings. The reader is referred to Appendix A for their definition and theorem. In 1976, May called attention to the very complicated behaviour which included period-doubling bifurcations and chaos exhibited by some very simple population models. In 1978, Feigenbaum discovered scaling properties and universal constants (*Feigenbaum's number*) in one-dimensional mappings. Thereafter the idea of a *renormalization group* was introduced for studying chaotic systems. In 1980, Packard *et al.* [609] introduced the technique of state space reconstruction using so-called *delay coordinates.* This technique was later placed on a firm mathematical foundation by Takens [784]. In 1983, Chua [144] discovered a simple electronic circuit for synthesizing a specific third-order piecewise-linear ordinary differential equation. This circuit became known as *Chua's circuit.* What makes this circuit so remarkable is that its dynamical equations have been proven to exhibit chaos in a rigorous sense. Ott, Grebogi and Yorke, in 1990, presented a method for controlling unstable trajectories embedded in a chaotic attractor.

Independently of these events and during the same time, there was another course of events leading to the field of chaos. This was the study of nonintegrable Hamiltonian systems in classical mechanics. Research in this field has led to the formulation and proof of the *Kolmogorov-Arnold-Moser* (KAM) theorem in the early 1960's. Numerical studies have shown that when the conditions stated by the KAM theorem fails, then stochastic behaviour is exhibited by nonintegrable Hamiltonian systems.

1.3 Examples of Chaotic Systems

The most well-known example of a chaotic system, is the *logistic equation*,

$$x_{n+1} = rx_n(1 - x_n), \qquad 1 \leq r \leq 4, \quad x_0 \in [0, 1],$$

which is a simple model for population dynamics. For certain values of the parameter r, of which $r = 4$ is one, the system exhibits chaotic behaviour.

In the field of numerical analysis, chaos is abundant. Even such a simple procedure as finding the roots of a given function may fail, the reason for this being chaos.

Example 1.2 In an attempt to find the root x^* of the function

$$f(x) := \left(\frac{4x - 3}{x}\right)^{\frac{1}{3}},$$

numerically, one would apply the *Newton-Raphson method.* By this method, successive estimates of the root of f are related according to

$$x_{n+1} = x_n - \frac{f(x_n)}{\frac{df}{dx}(x_n)},$$

where x_n denotes the n-th estimate of the root x^* based on an initial guesstimate x_0. For the given function, the Newton-Raphson algorithm takes the form

$$x_{n+1} = 4x_n(1 - x_n),$$

which is precisely the logistic map with $r = 4$. Unless we guessed $x_0 = x^*$, the sequence $\{x_n\}_{n=0}^{\infty}$ may either be periodic, chaotic or unbounded and hence the actual root is not approached by this scheme. ■

Even the process of numerical integration, the very means we use to study chaotic systems numerically, may result in chaos if the integration step size is too large [343].

Chaos has been discovered in bio-systems, meteorology, cosmology, economics, population dynamics, chemistry, physics and mechanical and electrical engineering and many other areas. Numerous examples of chaotic systems encountered in different disciplines can be found in [556] and [822]. A number of chaotic toys are also discussed in [556].

1.4 Organization of the Book

As the title of the book *Chaos in Electronics* suggests, this book is about chaotic circuits and systems in electrical and electronic engineering. Starting with Chapter 2, a review of the theory for the analysis of chaotic systems, is presented. Examples are used to illustrate the use of these techniques for the analysis of chaotic systems. Those readers who are not familiar with the basic definitions and ideas of chaos theory, should first consult Appendix A of this book. In Appendix A the theory of one-dimensional mappings is used as a vehicle for conveying and demonstrating basic ideas in chaos. For extensions to higher-dimensional mappings and differential equations, the reader may consult the bibliography for references to books on these subjects.

Chapters 3 to 6 constitute a comprehensive (although not exhaustive) survey of electronic circuits and systems encountered in research publications on chaos. These chapters are organized as follows. Chapter 3 presents electronic circuits which are described by one-dimensional maps and Chapter 4 electronic systems described by higher-dimensional maps. Chapters 5 and 6 focus on continuous-time systems with Chapter 5 presenting autonomous circuits while Chapter 6 surveys driven electronic systems.

One of the aspects of chaos research which enjoys much attention currently is the aspect of controlling chaos. Chapter 7 presents a survey on methods of controlling chaos. Finally, Chapter 8 concludes the book by taking a look at the future aspects of chaos research as far as electronic engineering is concerned.

Chapter 2

Analysis of Chaotic Systems

2.1 Introduction

In this chapter we describe several methods for the analysis of nonlinear and chaotic systems. We start by introducing the concept of an attractor and its dimension. Several different dimensions associated with an attractor are defined, among which are the capacity and Hausdorff dimension.

The harmonic balance method is a technique used to predict conditions for the existence of limit cycles for a nonlinear system. In the next section the harmonic balance method will be discussed. It will then be used to derive conditions for the presence of chaos and bifurcations for some systems.

In Section 2.4 we see that the presence of a snap-back repeller based at a saddle point is sufficient for a system to be chaotic. A theorem by Marotto and another by Shiraiwa and Kurata, which state sufficient conditions for a system to be chaotic, are presented here.

Melnikov's method, which consists of perturbation analysis of a homoclinic trajectory for a system is presented in Section 2.5. From this method the conditions for the existence of chaos are derived. These are then applied to a number of experimental systems in order to find conditions for these systems to exhibit chaos.

Hopf bifurcation refers to the bifurcation of a fixed point to a limit cycle. In Section 2.6 the Hopf bifurcation theorems for maps as well as for vector fields are presented together with examples. Appart from being important in itself, the Hopf bifurcation also has significance as the initial step in the Ruelle-Takens scenario and period-doubling route to chaos.

In Section 2.7 Lyapunov exponents are introduced. Thereafter, estimation of Lyapunov exponents from the time series of a system is discussed. This is of great importance since it enables one to obtain numerical evidence of chaos in real life systems.

Shil'nikov's method provides conditions for a system with a homoclinic trajectory to be chaotic. The geometric properties of the chaos here reminds one of a horseshoe and is therefore referred to as horseshoe chaos. This is the subject of Section 2.8.

The notion of symbolic dynamics is the topic of Section 2.9. The method of symbolic dynamics refers to the identification of the so-called shift map operating on a sequence space, with the dynamical equation of the system operating on state space. Since the shift map is chaotic, establishing a one-to-one correspondence of it to the system being studied proves that the system is chaotic.

Section 2.10 approaches chaos from the point of view of random processes. The power spectral density of a random process is defined here and illustrated for a chaotic system. We also show by means of an example that it is possible for a system not to have a power spectral density, in the sense that convergence of the limit in the definition of the power spectral density fails to converge.

2.2 Attractors and their Dimensions

In this section we introduce the concepts of an attractor, basin of attraction and dimension of an attractor. Roughly speaking, an attractor is a geometric form that characterizes long-term behaviour in the state space, that is, it is what the behaviour of a dynamical system settles down to or is attracted to. The basin of attraction is that set of initial values for which the system's response is attracted to the attractor in state space. Concerning the dimension of an attractor, we may think of the dimension as giving, in some way, the amount of information necessary to specify the position of a point on the attractor to within a given accuracy. The dimension is also a lower bound on the number of essential variables needed to model the dynamics of the system.

In this section we consider discrete-time autonomous dynamical systems of the form

$$\mathbf{x}_{n+1} = \mathbf{f}(\mathbf{x}_n), \qquad \mathbf{x}_n \in \mathbf{R}^N, \quad n \in \mathbf{N}, \tag{2.1}$$

as well as continuous-time autonomous dynamical systems of the form

$$\frac{d\mathbf{x}}{dt} = \mathbf{f}(\mathbf{x}(t)), \qquad \mathbf{x}(t) \in \mathbf{R}^N, \quad t \in \mathbf{R}^+, \tag{2.2}$$

for appropriate functions $\mathbf{f} : \mathbf{R}^N \to \mathbf{R}^N$, where $N \in \mathbf{N}$. Let $\Phi : \mathbf{T} \times \mathbf{R}^N \to \mathbf{R}^N$ denote the *flow* (discrete or continuous) generated by the dynamical system. For discrete-time systems $\mathbf{T} := \mathbf{N}$, and for continuous-time systems $\mathbf{T} := \mathbf{R}^+$.

Definition 2.1 Consider the system (discrete or continuous) described by the function $\mathbf{f} : \mathbf{R}^N \to \mathbf{R}^N$. The *attractor* of the system is a compact set A, with the property that there is a neighbourhood of A such that for almost every initial condition the limit set of the orbit as $n \to +\infty$ or $t \to +\infty$, is A. ■

Remark The phrase "almost every" here signifies the set of initial conditions in this neighbourhood for which the corresponding limit set can be covered with a set of cubes of arbitrarily small volume (i.e. has Lebesgue measure zero).

Example 2.2 Simple examples of nonchaotic attractors are fixed points, limit cycles and tori. ■

Example 2.3 There is numerical evidence that the Lorenz equations

$$\begin{aligned} \frac{dx_1}{dt} &= \sigma(x_2 - x_1), \\ \frac{dx_2}{dt} &= rx_1 - x_2 - x_1x_3, \\ \frac{dx_3}{dt} &= x_1x_2 - bx_3, \end{aligned}$$

possess a chaotic attractor for $\sigma = 10$, $b = 8/3$, $r = 28$ (see Figure 2.1). ■

Example 2.4 The nonlinear sampled-data control system described by the coupled maps (see Chapter 4)

$$x_{1,n+1} = px_{1,n} - qx_{1,n}^2 + qe(x_{2,n} - x_{1,n}), \tag{2.3}$$

$$x_{2,n+1} = px_{2,n} - qx_{2,n}^2 + qe(x_{1,n} - x_{2,n}), \tag{2.4}$$

is chaotic for $p = 3.004166$, $q = 4.008332$, $e = 0.1$. The chaotic attractor is shown in Figure 2.2. ■

Definition 2.5 The *basin of attraction* of the attractor A is the closure of the set of all initial conditions that approaches A. ■

Example 2.6 For the logistic map $f : I \to I$ defined as

$$f(x) = rx(1 - x), \tag{2.5}$$

with $r = 4$, the attractor and the basin of attraction are both I. For $r > 4$ the attractor and basin of attraction are both the Cantor set Λ defined in Example A.51. ■

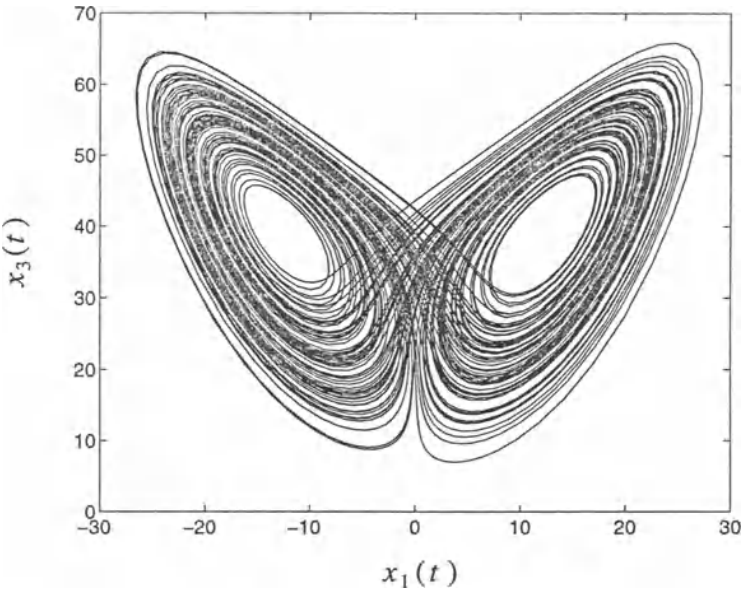

Figure 2.1: Chaotic attractor of the Lorenz equations.

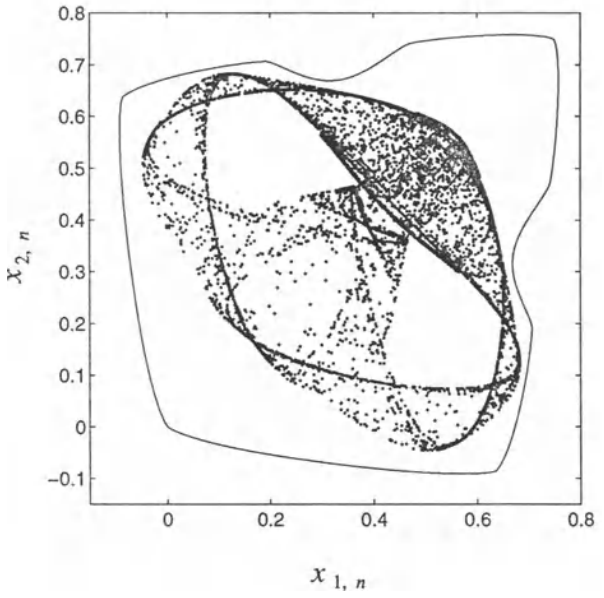

Figure 2.2: Chaotic attractor and basin of attraction boundary of the coupled maps (2.3) and (2.4).

Example 2.7 The basin of attraction for the zigzag map is $\mathbf{R}^+$, but the attractor is a closed interval contained in the interval $[1-c, 1+b-c-1/a]$. ■

Example 2.8 For the sampled-data system (Example 2.4) the basin of attraction is the connected area enclosed by the solid line (the basin of attraction boundary) shown in Figure 2.2. ■

2.2.1 Definitions of Dimension

In this section we define and discuss four different concepts of dimension. The first two of these, the capacity and the Hausdorff dimension, require only a metric (i.e. a distance function) for their definition, and consequently we refer to them as *metric dimensions*. The other dimensions we discuss are the information dimension and the pointwise dimension. These dimensions require both a metric and a probability measure for their definitions, and hence are referred to as *probabilistic dimensions*. Finally the Lyapunov dimension and correlation dimension are introduced.

Definition 2.9 The *capacity* of a set is defined as

$$d_C := \lim_{\epsilon \to 0} \frac{\ln M(\epsilon)}{\ln(1/\epsilon)}, \tag{2.6}$$

where, if the set in question is a bounded subset of an N-dimensional Euclidean space $\mathbf{R}^N$, then $M(\epsilon)$ is the minimum number of N-dimensional cubes of side length ϵ needed to cover the set. ■

Example 2.10 For a point, a line, and an area, we have $M(\epsilon) = 1$, $M(\epsilon) \propto \epsilon^{-1}$, and $M(\epsilon) \propto \epsilon^{-2}$ respectively, and (2.6) yields $d_C = 0, 1$ and 2 respectively as expected. ■

However, for more general sets (dubbed *fractals* by Mandelbrot [508]), d_C can be noninteger as illustrated by the next example.

Example 2.11 Calculate the capacity of the middle thirds Cantor set.

The middle thirds Cantor set is obtained by the limiting process of deleting middle thirds from each remaining subinterval, as illustrated in Figure 2.3. If we choose $\epsilon = (1/3)^m$ with $m \in \mathbf{N}$, then $M = 2^m$, and (2.6) yields

$$d_C = \frac{\ln 2}{\ln 3} = 0.630\ldots .$$

■

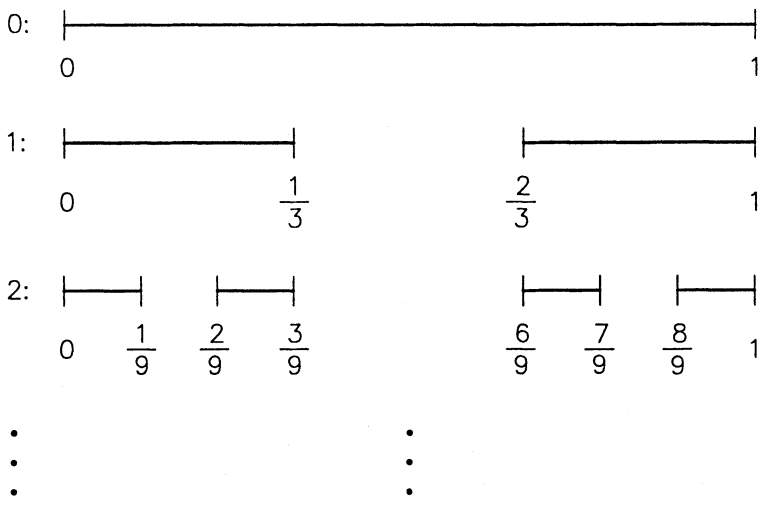

Figure 2.3: The first few steps in the construction of the middle thirds Cantor set.

If we are content to know where the set that is being studied lies to within an accuracy ϵ, then the location of the set is specified by the position of the $M(\epsilon)$ cubes covering the set. Equation (2.6) implies that for small ϵ,

$$\ln N(\epsilon) \approx d_C \ln(1/\epsilon).$$

Therefore, the capacity tells us how much information is required to specify the location of the set to within a given accuracy. If the set has a very fine-scaled structure, as it does for chaotic attractors, then it may be beneficial to introduce some form of coarse-graining into the description of the set. In this case, ϵ may be thought of as specifying the degree of coarse-graining. Then, by taking the limit $\epsilon \to 0$ the capacity is obtained.

Example 2.12 [247] Calculate the capacity of the generalized baker's map

$$x_{1,n+1} = \begin{cases} \lambda_a x_{1,n}, & \text{if } 0 \le x_{2,n} < \alpha \\ \frac{1}{2} + \lambda_b x_{1,n}, & \text{if } \alpha \le x_{2,n} \le 1 \end{cases},$$

$$x_{2,n+1} = \begin{cases} \frac{1}{\alpha} x_{2,n}, & \text{if } 0 \le x_{2,n} < \alpha \\ \frac{1}{1-\alpha}(x_{2,n} - \alpha), & \text{if } \alpha \le x_{2,n} \le 1 \end{cases},$$

where $\alpha \in (0,1)$.

Note that the attractor is a product of a Cantor set along x_1 and the interval $[0,1]$ along x_2. Thus the capacity is in the form

$$d_C = 1 + \bar{d}_C\,,$$

where $\bar{d}_C$ is the dimension of the attractor in the x_1-direction. We now write $M(\epsilon)$ as

$$M(\epsilon) = M_a(\epsilon) + M_b(\epsilon)\,,$$

where $M_a(\epsilon)$ and $M_b(\epsilon)$ are the number of x_1-intervals of length ϵ needed to cover that part of the attractor which lies in the x_1-intervals $[0,\lambda_a]$ and $[1/2, 1/2+\lambda_b]$ respectively. From the scaling property, $M_a(\epsilon) = M(\epsilon/\lambda_a)$, and $M_b(\epsilon) = M(\epsilon/\lambda_b)$, giving

$$M(\epsilon) = M(\epsilon/\lambda_a) + M(\epsilon/\lambda_b).$$

For small ϵ we now assume $N(\epsilon) \approx k\epsilon^{\bar{d}_C}$, and obtain

$$k\left(\frac{1}{\epsilon}\right)^{\bar{d}_C} = k\left(\frac{\lambda_a}{\epsilon}\right)^{\bar{d}_C} + k\left(\frac{\lambda_b}{\epsilon}\right)^{\bar{d}_C},$$

which simplifies to

$$1 = \lambda_a^{\bar{d}_C} + \lambda_b^{\bar{d}_C}.$$

This is a transcendental equation for $\bar{d}_C$. In obtaining this expression, we have made the strong assumption that $M(\epsilon) \approx k\epsilon^{\bar{d}_C}$ for small ϵ, which implies the existence of the limit given in the definition of capacity. For rigorous arguments concerning the existence of this limit, the reader is referred to [247]. Note that the above transcendental expression for $\bar{d}_C$ is monotonically decreasing. Therefore $\bar{d}_C$ obtained from solving this expression and consequently d_C are unique. ■

The capacity, first introduced by Kolmogorov in 1958 [444], may be viewed as a simplified version of the Hausdorff dimension, which was originally introduced by Hausdorff in 1918 [346]. For attractors it seems that these two dimensions are generally equal, while it is possible to construct simple sets for which the Hausdorff dimension and the capacity differ.

To define the Hausdorff dimension of a set lying in $\mathbf{R}^N$ consider a covering of the set with N-dimensional cubes of variable edge lengths. This gives a set $\{\epsilon_i\}$ of edge lengths associated with this covering. Let $\mathcal{C}$ be the set of all such coverings of our set. Define the quantity $l_d(\epsilon)$ by

$$l_d(\epsilon) := \inf_{\mathcal{C}} \sum_i \epsilon_i^d\,,$$

where $d \in \mathbf{R}^+$ which is still to be specified. Now let

$$l_d = \lim_{\epsilon \to 0} l_d(\epsilon).$$

Hausdorff showed that there exists a critical value of d above which $l_d = 0$ and below which $l_d = \infty$.

Definition 2.13 The *Hausdorff dimension* of a set is the critical value, $d = d_H$. ■

We may now ask what the value of l_d is when d is precisely d_H. Precisely at $d = d_H$, l_d may either be 0, positive finite or ∞. Concerning the relationship between the capacity and Hausdorff dimension, it can easily be shown that

$$d_C \geq d_H \,.$$

Example 2.14 [247] Calculate the Hausdorff dimension for the generalized baker's map.

The Hausdorff dimension d_H can be calculated by an argument that is very similar to the one used for computing the capacity. Let $\bar{d}_H \equiv d_H - 1$ be the Hausdorff dimension along x_1. Applying the scaling property of the map to the quantity $l_d(\epsilon)$, we obtain

$$l_d(\epsilon) = \lambda_a^d l_d\left(\frac{\epsilon}{\lambda_a}\right) + \lambda_b^d l_d\left(\frac{\epsilon}{\lambda_b}\right).$$

Substituting $l_d(\epsilon) = E_H(\epsilon)\epsilon^{-(\bar{d}-d)}$ into the above equation, we find that $E_H(\epsilon)$ satisfies

$$E_H(\epsilon) = \lambda_a^{\bar{d}} E_H(\epsilon/\lambda_a) + \lambda_b^{\bar{d}} E_H(\epsilon/\lambda_b)\,.$$

It can be shown (see [247]) that the limit $\epsilon \to 0$ yields $l_d = \infty$ for $d < \bar{d}_C$ and $l_d = 0$ for $d > \bar{d}_C$. Hence, we conclude that the Hausdorff dimension and capacity are equal, that is, $d_H = d_C$ for the generalized baker's map. ■

Before defining the information dimension of an attractor, we introduce the concept of natural measure associated with an attractor. For each cube $C \subset \mathbf{R}^N$ and initial condition $\mathbf{x}_0$ in the basin of attraction, we define

$$T(C;\mathbf{x}_0) := \sum_i \Delta t_i(C;\mathbf{x}_0)\,,$$

where

$$\Delta t_i(C;\mathbf{x}_0) := \sup\left\{\tau \in \mathbf{R}^+ \;\middle|\; \Phi(t_i(C;\mathbf{x}_0)+\gamma;\mathbf{x}_0) \in C \text{ for all } \gamma \in [0,\tau)\right\}.$$

Here $t_i(C;\mathbf{x}_0)$ is the i-th time of entry of the trajectory (starting at $\mathbf{x}_0$) into the cube C. Thus, $\Delta t_i(C;\mathbf{x}_0)$ is the time the trajectory (starting at $\mathbf{x}_0$) spends in C during the i-th visit to C. Now, define

$$\mu(C;\mathbf{x}_0) := \lim_{T_s\to\infty} \frac{T(C;\mathbf{x}_0)}{T_s}\,,$$

where T_s is the total time extent of the trajectory starting at $\mathbf{x}_0$. Thus for each cube C and initial condition $\mathbf{x}_0$ in the basin of attraction, $T(C;\mathbf{x}_0)$ is the total time that the trajectory originating from $\mathbf{x}_0$ spends in C as time approaches infinity. Viewing μ as a real-valued set function suggests that μ is a measure-like function. Under certain conditions μ can be shown to be a measure.

Definition 2.15 If for each cube C in $\mathbf{R}^N$

$$\mu(C) = \mu(C; \mathbf{x}),$$

for a.e. $\mathbf{x}$ in the basin of attraction of the attractor, then μ is a measure on the Borel subsets of $\mathbf{R}^N$ contained in the basin of attraction of the attractor, termed the *natural measure* of the attractor [247]. ■

The natural measure gives the relative probability of different regions of the attractor of being visited, as obtained from time averages, and therefore is the "natural" measure to consider. The natural measure thus provides a measure of the relative frequency with which a trajectory visits different regions of the attractor.

Definition 2.16 The *information dimension* d_I of an attractor is defined by

$$d_I := \lim_{\epsilon \to 0} \frac{I(\epsilon)}{\ln(1/\epsilon)},$$

where

$$I(\epsilon) := \sum_{i=1}^{M(\epsilon)} \mu(C_i) \ln \frac{1}{\mu(C_i)},$$

and C_i is the i-th cube in the covering of the attractor and $M(\epsilon)$ is the number of cubes (each with edge length ϵ) required to cover the attractor. ■

The information dimension originally introduced by Balatoni and Renyi in 1956 (see [247]), is a generalization of the capacity that takes into account the relative probability of the cubes used to cover the set. To see this, assume that all cubes in the covering are equi-probable. Then

$$\mu(C_i) = \frac{1}{M(\epsilon)},$$

for each i and hence we have $d_I = d_C$. However, for unequal probabilities, $I(\epsilon) < \ln M(\epsilon)$ so that in general $d_C \geq d_I$.

In information theory the quantity $I(\epsilon)$ (used in the definition of the information dimension) is the amount of information necessary to specify the state of the system to within an accuracy ϵ (refer to Appendix A, or equivalently, it is the information obtained in making a measurement that is uncertain by an amount ϵ. Since for small ϵ, $I(\epsilon) \approx d_I \ln(1/\epsilon)$ we may interpret d_I as determining how fast the information necessary to specify a point on the attractor increases as ϵ decreases [247].

Example 2.17 [247] Calculate the information dimension for the generalized baker's map.

By a similar argument as before we arrive at the form

$$d_I = 1 + \bar{d}_I\,,$$

for the information dimension of the generalized baker's map. From the geometry of this map, we deduce that

$$I(\epsilon) = I_a(\epsilon) + I_b(\epsilon)\,,$$

where $I_a(\epsilon)$ and $I_b(\epsilon)$ are associated with the x_1 intervals $[a,\, \lambda_a]$ and $[1/2,\, \lambda_b + 1/2]$ respectively. Let the total probability associated with the interval $[0, \lambda_a]$ be α, and that with interval $[1/2,\, \lambda_b + 1/2]$ be $\beta = 1 - \alpha$. Assuming that $M(\epsilon)$ strips of width ϵ are required to cover the whole attractor, then from the scaling property of the baker's map, covering the strip $[0, \lambda_a]$ at resolution $\epsilon\lambda_a$ also requires $M(\epsilon)$ strips. This gives

$$I_a(\epsilon\lambda_a) = \alpha\left(\ln\left(\frac{1}{\alpha}\right) + I(\epsilon)\right).$$

Substituting ϵ for $\epsilon\lambda_a$ into the above expression produces

$$I_a(\epsilon) = \alpha \ln\left(\frac{1}{\alpha}\right) + \alpha I\left(\frac{\epsilon}{\lambda_a}\right).$$

A similar argument, this time for the second interval, yields

$$I_b(\epsilon) = \beta \ln\left(\frac{1}{\beta}\right) + \beta I\left(\frac{\epsilon}{\lambda_b}\right).$$

Combining the expression for $I(\epsilon)$, $I_a(\epsilon)$ and $I_b(\epsilon)$ gives

$$I(\epsilon) = \alpha I\left(\frac{\epsilon}{\lambda_a}\right) + \beta I\left(\frac{\epsilon}{\lambda_b}\right) + H(\alpha)\,, \tag{2.7}$$

where

$$H(\alpha) := \alpha \ln\left(\frac{1}{\alpha}\right) + (1-\alpha)\ln\left(\frac{1}{1-\alpha}\right).$$

Intuitively we assume that

$$I(\epsilon) = \bar{d}_I \ln(1/\epsilon)\,, \tag{2.8}$$

for small ϵ (refer to [247] where this assumption is shown to be rigorous). Using the expressions in (2.7) and (2.8) to eliminate $I(\epsilon), I(\epsilon/\lambda_a)$, and $I(\epsilon/\lambda_b)$, we obtain

$$\bar{d}_I = \frac{H(\alpha)}{\alpha \ln(1/\lambda_a) + \beta \ln(1/\lambda_b)}.$$

■

Alexander and Yorke (see [247]) have computed the information dimension of the generalized baker's map for the special case $\alpha = 1/2$, $\lambda = \lambda_a = \lambda_b$, where $\lambda > 1/2$. For uncountably many values of λ they find that $d_I = 2$, although there are certain special values of λ for which $d_I < 2$.

Definition 2.18 Let

$$d_P(\mathbf{x}) := \lim_{\epsilon \to 0} \frac{\ln \mu(B_\epsilon(x))}{\ln \epsilon},$$

where $B_\epsilon(\mathbf{x})$ denotes the ball of radius ϵ centred about the point $\mathbf{x}$ on the attractor and μ represents the natural measure. If $d_P(\mathbf{x})$ is independent of $\mathbf{x}$ for μ-a.e. $\mathbf{x}$, then we call $d_P(\mathbf{x}) = d_P$ the *pointwise dimension* of the attractor. ■

Intuitively, the pointwise dimension d_P is the exponent with which the total probability of being contained in a ball decreases as the radius of the ball decreases. Roughly speaking, for small ϵ, $\mu(B_\epsilon(x)) \propto \epsilon^{d_P}$.

Example 2.19 [247] The pointwise dimension of the generalized baker's map is given by

$$d_P = 1 + \frac{H(\alpha)}{\alpha \ln(1/\lambda_a) + \beta \ln(1/\lambda_b)},$$

which is precisely the information dimension d_I for the generalized baker's map. ■

It is usually found that the metric dimensions assume a common value. When this is the case, this common value (say d_F) is referred to as the *fractal dimension.* When the probabilistic dimensions assume a common value (say d_μ), we refer to it as the *dimension of the natural measure.* The following conjecture is by Farmer *et al.* [247].

Conjecture 2.20 For a typical chaotic attractor the capacity and Hausdorff dimensions have a common value d_F, and the information dimension and the pointwise dimension have a common value d_μ. ■

However, [244] reports about nonpathological sets for which the capacity and Hausdorff dimension differ. This casts doubt on the validity of the above conjecture.

Example 2.21 [244] Consider the set

$$A := \{x_n\}_{n=1}^{\infty} \cup \{0\},$$

where

$$x_n := n^{-p}, \qquad \text{for each } n \in \mathbf{N},$$

and some (fixed) $p > 0$. Show that the capacity and Hausdorff dimension differ from each other.

We first calculate the capacity of the set A. For some fixed $\epsilon > 0$ the set A is partitioned into two classes: those points which are separated from their neighbours by a distance of less than ϵ and those that are separated from their neighbours by greater than ϵ. Call these two mutually disjoint sets of points $I_1(\epsilon)$ and $I_2(\epsilon)$ respectively. Let $n(\epsilon)$ be chosen such that $x_{n(\epsilon)}$ is the first point of the sequence x_n whose nearest neighbour is within a distance ϵ from it. Then clearly $x_{n(\epsilon)}$ is in $I_1(\epsilon)$ and satisfies

$$x_{n(\epsilon)} - x_{n(\epsilon)+1} \leq \epsilon \leq x_{n(\epsilon)-1} - x_{n(\epsilon)} .$$

Bounds on the number $M(\epsilon)$ of ϵ-intervals required to cover A will now be determined. Since $x_{n(\epsilon)} \in I_1(\epsilon)$ we conclude that $I_2(\epsilon)$ contains the first $n(\epsilon) - 1$ points and $I_1(\epsilon)$ the rest of the points of $\{x_n\}$. Therefore, $I_2(\epsilon)$ can be covered with $n(\epsilon) - 1$ ϵ-intervals while the sum of the lengths of the ϵ-intervals required to cover $I_1(\epsilon)$ minimally, will be less than the length of the interval $[0, x_{n(\epsilon)}]$. Thus if at most $M(\epsilon)$ ϵ-intervals are required to cover A, then $M(\epsilon)$ satisfies the inequalities

$$(n(\epsilon) - 1)\epsilon \leq M(\epsilon)\epsilon \leq (n(\epsilon) - 1)\epsilon + x_{n(\epsilon)} ,$$

that is,

$$n(\epsilon) - 1 \leq M(\epsilon) \leq n(\epsilon) - 1 + \frac{n(\epsilon)^{-p}}{\epsilon} .$$

For sufficiently small ϵ both $n(\epsilon)$ and $n(\epsilon)^{-p}/\epsilon$ approach $\epsilon^{-1/(1+p)}$ and hence

$$M(\epsilon)\epsilon^d \approx \epsilon^{d-1/(1+p)} .$$

Since the preceding expression goes to zero only if $d > 0$ as ϵ tends to zero, we deduce that

$$d_C = \frac{1}{1+p} .$$

Next we calculate the Hausdorff dimension of A. Covering the k-th point of the sequence $\{x_n\}$ with an interval of length ϵ^k for ϵ sufficiently small we then have that

$$\epsilon^d + \epsilon^{2d} + \epsilon^{3d} + \ldots = \frac{\epsilon^d}{1 - \epsilon^d} ,$$

which is finite for each $d > 0$ only and hence

$$d_H = 0 .$$

■

The Lyapunov dimension was first introduce by Kaplan and Yorke in 1978 (refer to [257]) as a lower bound on the fractal dimension [618]. In order to introduce the Lyapunov dimension, we assume that $\{\lambda_i^1\}_{i=1}^N$ is the spectrum of one-dimensional Lyapunov exponents (Section 2.7) in order of decreasing magnitude.

Definition 2.22 The *Lyapunov dimension* d_L is defined by

$$d_L := k - \frac{\sum_{i=1}^{k} \lambda_i}{\lambda_{k+1}},$$

where k is the greatest natural number such that

$$\sum_{i=1}^{k} \lambda_i > 0.$$

For the cases $\lambda_1 < 0$ and $\lambda_1 + \ldots + \lambda_N > 0$ we define $d_L = 0$ and $d_L = N$, respectively. ■

Examples of calculating the Lyapunov dimension are given in later chapters. The last dimension that will be discussed is the correlation dimension which was first introduced by Grassberger and Procaccia [296]. The difficulties encountered in calculating the Hausdorff dimension numerically from the time series served as motivation for introducing the correlation dimension. Suppose that $\{\mathbf{x}_i\}_{i=1}^{M}$ is an M-point time series obtained from the system being investigated.

Definition 2.23 The *correlation dimension* d_G is defined by

$$d_G := \lim_{\epsilon \to 0} \frac{\ln C(\epsilon)}{\ln \epsilon},$$

where

$$C(\epsilon) := \lim_{M \to \infty} \frac{1}{M^2} \sum_{i,j=1 \; i \neq j}^{M} \theta(\epsilon - \|\mathbf{x}_i - \mathbf{x}_j\|)$$

with θ the *Heaviside step function* [417] namely

$$\theta(y) := \begin{cases} 0, & \text{if } y < 0 \\ 1/2, & \text{if } y = 0 \\ 1, & \text{if } y > 0 \end{cases},$$

and $\|\cdot\|$ some norm. The quantity $C(\epsilon)$ is termed the *correlation integral.* ■

Example 2.24 [296] The correlation dimension of the logistic map for $r = 3.5699\ldots$ is

$$d_G \approx 0.538.$$

■

Example 2.25 [296] The correlation dimension of the Hénon map with parameter values $a = 1.4$ and $b = 0.3$ is

$$d_G \approx 1.26 .$$

■

In [296] it is shown that $d_I \leq d_H \leq d_G$ thus estimating d_H from below and above. The correlation dimension was generalized by Pawelzik and Schuster [624] to obtain a whole spectrum of dimensions called generalized dimensions. An algorithm was proposed by the authors for estimating the generalized dimensions from the time series with slightly more effort than needed to calculate the correlation integral.

2.3 Harmonic Balance Method

A method for the analysis of chaotic systems based on the harmonic balance principle [410] was proposed by Genesio and Tesi in [273]. In this section we briefly review the harmonic balance method and thereafter discuss the method as proposed by Genesio and Tesi. However, before proceeding we first discuss different standard forms into which dynamical systems described by differential equations can be casted. A specific standard form, namely the so-called Lur'e form, is used in Genesio and Tesi's method.

2.3.1 Nonlinear State Equations

We consider here systems which can be represented by state equations of the form

$$\begin{pmatrix} d\mathbf{x}/dt \\ d\mathbf{z}/dt \end{pmatrix} = \begin{pmatrix} \mathbf{P} & \mathbf{0} \\ \mathbf{0} & \mathbf{Q} \end{pmatrix} \begin{pmatrix} \mathbf{x} \\ \mathbf{z} \end{pmatrix} + \begin{pmatrix} -\mathbf{b}\phi(\mathbf{x}, \mathbf{z}) \\ \psi(\mathbf{x}) \end{pmatrix} , \tag{2.9}$$

$$y = \mathbf{c}^T \mathbf{x} , \tag{2.10}$$

where $y \in \mathbf{R}$, $\mathbf{P} \in \mathbf{R}^{N \times N}$, $\mathbf{Q} \in \mathbf{R}^{M \times M}$, $\mathbf{b}, \mathbf{c}, \mathbf{x} \in \mathbf{R}^N$, $\mathbf{z} \in \mathbf{R}^M$ with $\phi : \mathbf{R}^N \times \mathbf{R}^M \to \mathbf{R}$ and $\psi : \mathbf{R}^N \to \mathbf{R}^M$ nonlinear functions. Here, $\mathbf{c}^T$ denotes the transpose of the vector $\mathbf{c}$. It is assumed that $(\mathbf{P}, \mathbf{b})$ is controllable [783], [455]. To be able to apply the harmonic balance method [410] we first have to rewrite (2.9) and (2.10) as a scalar differential equation or integro-differential equation, by eliminating the state variables in (2.9). Denoting the transformation from $\mathbf{x}$ to its controllable phase variable form by the $N \times N$ matrix $\mathbf{M}$, we define the output of the system as

$$y = \mathbf{e}_1^T \mathbf{M} \mathbf{x} , \qquad \mathbf{e}_1^T := (1, 0, \ldots, 0) , \tag{2.11}$$

giving

$$\mathbf{x} = \mathbf{M}^{-1} \begin{pmatrix} 1 \\ D \\ \vdots \\ D^{N-1} \end{pmatrix} y = \mathbf{d}(D)y \tag{2.12}$$

where $D := d/dt$ such that $D\mathbf{x} = d\mathbf{x}/dt$, and $\mathbf{d}(D)$ is an N-dimensional differential operator defined by

$$\mathbf{d}(D) := \mathbf{M}^{-1} \begin{pmatrix} 1 \\ D \\ \vdots \\ D^{N-1} \end{pmatrix}.$$

Using this notation, the first equation in (2.9) may be solved for $\mathbf{x}$ to obtain

$$\mathbf{x} = -(\mathbf{I}D - \mathbf{P})^{-1}\mathbf{b}\phi(\mathbf{x}, \mathbf{z}). \tag{2.13}$$

Substituting (2.13) for $\mathbf{x}$ in (2.10) and using (2.12) yields

$$\left(\mathbf{c}^T(\mathbf{I}D - \mathbf{P})^{-1}\mathbf{b}\right)^{-1} y + \phi(\mathbf{d}(D)y, \mathbf{z}) = 0. \tag{2.14}$$

In a similar way, we can show that the second equation in (2.9) may be written as

$$\mathbf{z} = (\mathbf{I}D - \mathbf{Q})^{-1}\psi(\mathbf{d}(D)y). \tag{2.15}$$

Equations (2.14) and (2.15) are of the form

$$q_1(D)y + f(y, Dy, \ldots, D^{N-1}y; z_1, \ldots, z_M) = 0, \tag{2.16}$$

and

$$q_2(D)z_i = \sum_{k=1}^{M} p_{i,k}(D)g_k(y, Dy, \ldots, D^{N-1}y), \quad i = 1, 2, \ldots, M, \tag{2.17}$$

respectively, where q_1 is a polynomial of degree N and q_2 and p_{ik} are two polynomials of degree M and less than M respectively defined by

$$q_1(D) := \frac{1}{\mathbf{c}^T(\mathbf{I}D - \mathbf{P})^{-1}\mathbf{b}}, \tag{2.18}$$

$$q_2(D) := \mathrm{Den}((\mathbf{I}D - \mathbf{Q})^{-1}), \tag{2.19}$$

$$p_{i,k}(D) := \mathrm{Num}((\mathbf{I}D - \mathbf{Q})^{-1})_{i,k}, \quad i, k = 1, 2, \ldots, M, \tag{2.20}$$

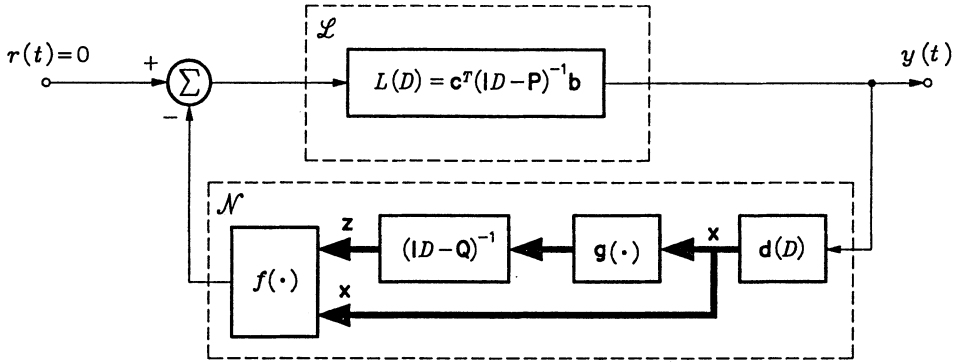

Figure 2.4: Block diagram of the nonlinear feedback system described by (2.16) to (2.22).

and $f : \mathbf{R}^N \times \mathbf{R}^M \to \mathbf{R}$ and $\mathbf{g} = (g_1, \ldots, g_M)^T : \mathbf{R}^N \to \mathbf{R}^M$ are nonlinear mappings defined respectively by

$$f(y, Dy, \ldots, D^{N-1}y; z_1, \ldots, z_M) := \phi(\mathbf{d}(D)y, \mathbf{z}), \tag{2.21}$$

$$g_k(y, Dy, \ldots, D^{N-1}y) := \psi_k(\mathbf{d}(D)y), \qquad k = 1, 2, \ldots, M. \tag{2.22}$$

Here Den$(\cdot)$ and Num$(\cdot)$ respectively denote the denominator and numerator of their arguments. The system (2.16) to (2.22) is depicted graphically in Figure 2.4. In Figure 2.4, $\mathcal{L}$ denotes the linear part described by $L(D) := 1/q_1(D)$ while $\mathcal{N}$ denotes the nonlinear part of the system.

The general system (2.16) and (2.17) can usually assume more simple forms, among which the following is important,

$$f(y, Dy, \ldots, D^{N-1}y) = p(D)h(y), \tag{2.23}$$

with $M = 0$. Systems which are described by (2.23) are called *Lur'e systems* [834].

Example 2.26 [273] Rewrite the Rössler equations

$$\begin{aligned} \frac{dx_1}{dt} &= -x_2 - x_3, \\ \frac{dx_2}{dt} &= x_1 + \sigma x_2, \\ \frac{dx_3}{dt} &= \alpha + x_3(x_1 - \rho), \end{aligned}$$

in the form (2.16) to (2.22).

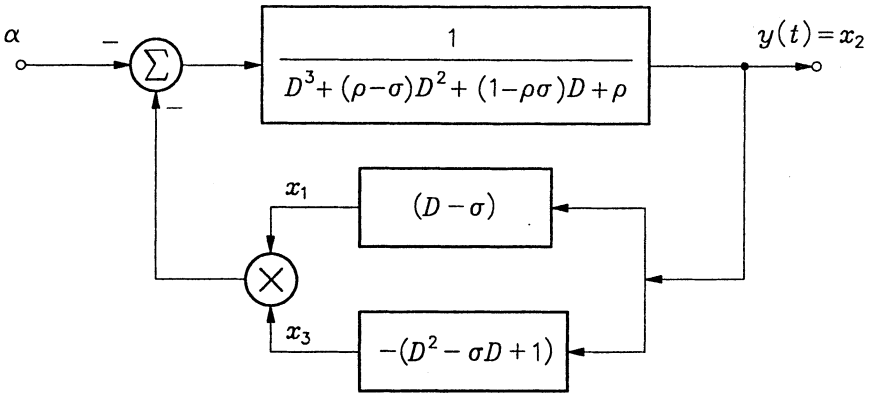

Figure 2.5: Rössler equations in feedback form.

For the Rössler equations we have

$$\mathbf{P} = \begin{pmatrix} 0 & -1 & -1 \\ 1 & \sigma & 0 \\ 0 & 0 & -\rho \end{pmatrix}, \qquad \mathbf{b} = \begin{pmatrix} 0 \\ 0 \\ 1 \end{pmatrix}.$$

Since the output $y(t)$ is not defined suppose that $y := x_2$, i.e.

$$\mathbf{c} = (0,\ 1,\ 0)^T.$$

Substituting the above expressions for $\mathbf{P}$, $\mathbf{b}$ and $\mathbf{c}$ in (2.18), the form (2.16) (with $m = 0$) becomes

$$\frac{d^3y}{dt^3} + (\rho - \sigma)\frac{d^2y}{dt^2} + (1 - \rho\sigma)\frac{dy}{dt} + \rho y + \alpha + \left(\frac{dy}{dt} - \sigma y\right)\left(-\frac{d^2y}{dt^2} + \sigma\frac{dy}{dt} - y\right) = 0.$$

This equation is depicted in Figure 2.5. Notice that the input of the system in Figure 2.5 is nonzero, namely α. ■

Example 2.27 [273] Cast the Lorenz equations

$$\begin{aligned} \frac{dx_1}{dt} &= -\sigma x_1 + \sigma x_2, \\ \frac{dx_2}{dt} &= \rho x_1 - x_2 - x_1 x_3, \\ \frac{dx_3}{dt} &= x_1 x_2 - \mu x_3, \end{aligned}$$

in the form (2.16) to (2.22).

For the Lorenz system we have

$$\mathbf{P} := \begin{pmatrix} -\sigma & \sigma \\ \rho & -1 \end{pmatrix}, \quad \mathbf{b} := \begin{pmatrix} 0 \\ 1 \end{pmatrix}, \quad \phi(\mathbf{x}, z) := x_1 z, \quad \mathbf{Q} := -\mu, \quad \psi(\mathbf{x}) := x_1 x_2,$$

with $z := x_3$. Assuming $y := x_1$, the above system can be rewritten in the form of (2.16) and (2.17), namely

$$\frac{1}{\sigma}\frac{d^2y}{dt^2} + \left(1 + \frac{1}{\sigma}\right)\frac{dy}{dt} + (1-p)y + yz = 0, \qquad \frac{dz}{dt} = -\mu z + y\left(\frac{1}{\sigma}\frac{dy}{dt} + y\right).$$

■

2.3.2 The Harmonic Balance Method

The objective of the harmonic balance method (which is a member of a class of techniques termed *averaging methods* [452]) is to predict the conditions required for a nonlinear ordinary differential equation to have limit cycles, and to find approximate solutions from the given ordinary differential equation for these limit cycles.

The hypothetical foundation underlying this method will now be stated [410]. Consider nonlinear differential equations of the form (see (2.16) and (2.17))

$$q_1(D)y + f(y, Dy, \ldots, D^{N-1}y; z_1, \ldots, z_M) = 0, \tag{2.24}$$

and

$$q_2(D)z_i = \sum_{k=1}^{M} p_{ik}(D)g_k(y, Dy, \ldots, D^{N-1}y), \qquad i = 1, 2, \ldots, M. \tag{2.25}$$

We assume that this system allows a solution of the form

$$y_1(t) = a_0 + a_1(t)\sin\omega t, \qquad a_1, \omega > 0$$

where $a_1(t)$ is slowly varying compared to the period $2\pi/\omega$ of the solution. This implies that $a_1(t)$ is nearly constant over a cycle. Notice that, in order to prevent any resonance from being present in the steady state solutions $z_{i,1}(t)$, $i = 1, 2, \ldots, M$ admitted by (2.25), we demand that the polynomial q_2 has no roots at $\pm j\omega$ with $j := \sqrt{-1}$.

We assume that the nonlinear function f of (2.24) admits a Fourier series

$$f(y_1, Dy_1, \ldots, D^{n-1}y_1; z_{1,1}, \ldots, z_{M,1} = \sum_{k=-\infty}^{\infty} F_k(a_0, a_1, \omega)e^{jk\omega t},$$

where F_k is the complex k-th harmonic coefficient [775], given by

$$F_k(a_0, a_1, \omega) = \frac{\omega}{2\pi} \int_{-\pi/\omega}^{\pi/\omega} f(y_1, Dy_1, \ldots, D^{N-1}y_1; z_{1,1}, \ldots, z_{M,1}) e^{-jk\omega t}\, dt\,.$$

In the case of Lur'e systems, we assume that h in (2.23) admits a Fourier series.

The final hypothesis is called the *filtering hypothesis* [535], [410]. We assume that along the loop (see Figure 2.4) the linear subsystem $\mathcal{L}$ strongly attenuates subharmonics (i.e. frequencies which are rational fractions of the fundamental frequency ω) and superharmonics (i.e. frequencies of which the fundamental frequency is a rational fraction) generated by the nonlinear subsystem $\mathcal{N}$. Then, discarding of all harmonics higher than one, yields

$$\begin{aligned} f(y_1, Dy_1, \ldots, D^{N-1}y_1; z_{1,1}, \ldots, z_{M,1}) \;\approx\; & F_{-1}(a_0, a_1, \omega) e^{-j\omega t} + F_0(a_0, a_1, \omega) + \\ & F_1(a_0, a_1, \omega) e^{j\omega t}\,. \end{aligned}$$

Substituting this expression for f into (2.24), taking the Fourier transform of the result and comparing coefficients of corresponding harmonic components, we obtain the relations

$$q_1(0)a_0 + F_0(a_0, a_1, \omega) = 0\,, \tag{2.26}$$

$$q_1(j\omega)a_1 + 2jF_1(a_0, a_1, \omega) = 0\,. \tag{2.27}$$

The relations (2.26) and (2.27) constitute the harmonic balance method for dynamical systems described by (2.24) and (2.25). In control theory terminology the harmonic balance method is known as the *describing function method.*

2.3.3 Genesio-Tesi Procedure

In this section our attention will be devoted to the class of Lur'e systems. Before proceeding, we define the notion of interaction between a fixed point and a limit cycle.

Definition 2.28 [273] A fixed point (y-component) y^* and limit cycle $y_c(t)$ of a system is said to interact if

$$y^* \in [\min_t(y_c(t)), \max_t(y_c(t))]\,.$$

■

Interaction between a fixed point y^* and a limit cycle $y_c(t)$ implies that there exists a monotonic increasing sequence $\mathcal{T} := \{t_1, t_2, t_3, \ldots\}$ such that

$$y_c(t) = y^*, \qquad \text{for each } t \in \mathcal{T}\,. \tag{2.28}$$

From the previous section we see that the sequence $\mathcal{T}$ exists if and only if

$$a_1 \geq |y^* - a_0|. \tag{2.29}$$

The Genesio-Tesi procedure for determining chaotic behaviour of a dynamical system in Lur'e form requires:

i) The existence of an interacting stable limit cycle and unstable fixed point;

ii) Suitable filtering effect along the system.

Conjecture 2.29 [273] A Lur'e system exhibits chaotic behaviour if an unstable fixed point and a stable limit cycle interact with a suitable filtering effect along the system. ■

The conditions required by this conjecture give an approximate necessary condition for the existence of a homoclinic orbit, whose perturbation under suitable circumstances may give rise to chaos [314] as will be seen in Section 2.5. The fixed points of a Lur'e system are obtained from (2.16) and (2.23) as

$$y^* + L(0)h(y^*) = 0\,, \tag{2.30}$$

where

$$L(D) := \frac{p(D)}{q_1(D)}\,. \tag{2.31}$$

The predicted limit cycle can be found by application of the harmonic balance method. Using (2.23) in (2.26) and (2.27) and assuming $a_0 \neq 0$, we obtain

$$L(0)N_0(a_0, a_1) = -1\,, \quad \text{and} \quad L(j\omega)N_1(a_0, a_1) = -1\,, \tag{2.32}$$

where

$$\begin{aligned} N_0(a_0, a_1) &:= \frac{1}{2\pi a_0} \int_{-\pi}^{\pi} h(a_0 + a_1 \sin\theta)\, d\theta\,, \\ N_1(a_0, a_1) &:= \frac{j}{\pi a_1} \int_{-\pi}^{\pi} h(a_0 + a_1 \sin\theta) e^{-j\theta}\, d\theta\,. \end{aligned}$$

If the nonlinearity does not change the phase of the fundamental frequency component, then the last expression in (2.32) reduces to

$$\frac{L(j\omega)}{\pi a_1} \int_{-\pi}^{\pi} h(a_0 + a_1 \sin\theta) \sin\theta\, d\theta = -1\,. \tag{2.33}$$

Moreover, if a limit cycle does exist, then it follows immediately that

$$\Im(L(j\omega)) = 0\,,$$

since a_1 is real and hence we conclude that the oscillation frequency ω of the limit cycle is independent of the nonlinearity, if the limit cycle exists.

A valuable characteristic of the Genesio-Tesi procedure is that most of the conditions considered can be translated into algebraic relations which involve the system parameters. The only aspect of a qualitative nature is the filtering effect along the system.

Example 2.30 [273] Use the Genesio-Tesi procedure to study the system

$$\begin{aligned}
\frac{dx_1}{dt} &= \alpha(x_2 - x_1 - h(x_1))\,,\\
\frac{dx_2}{dt} &= x_1 - x_2 + x_3\,,\\
\frac{dx_3}{dt} &= -\beta x_2\,,
\end{aligned}$$

where $h : \mathbf{R} \to \mathbf{R}$ is defined by

$$h(x) := -\left(\frac{m_0 - m_1}{2G}\right)(|x + B| - |x - B|) - \frac{m_1}{G}x\,,$$

for the parameter values $m_0 = 0.8$, $m_1 = 0.5$, $B = 1$ and $G = 0.7$.

This system, which describes Chua's circuit (see Chapter 5), can be represented in the form of Figure 2.4 according to the Lur'e model (2.23) with $y := x_1$. The linear part of the system is described by the transfer function [273]

$$L(s) = \frac{\alpha(s^2 + s + \beta)}{s^3 + (1 + \alpha)s^2 + \beta s + \alpha\beta}\,.$$

The steps outlined above are now performed. The y-components of the system's fixed points are

$$y^*_{-1} = -3/2\,, \qquad y^*_0 = 0\,, \qquad y^*_1 = 3/2\,.$$

We restrict our attention to the region of the (α, β)-plane which satisfy the following inequality [273],

$$1 < \alpha < \beta < (1 + \alpha)^2/4\,.$$

Two predicted (stable) limit cycles are found by numerical evaluation of the terms N_0 and N_1. These predicted limit cycles are symmetrical with respect to the origin of the phase space and their projections onto the y-axis enclose the fixed points y^*_{-1}

and y_1^*. Therefore, their interaction with the fixed point (y-component) y_0^* must be considered. The condition at which this interaction begins is

$$a_1 = |a_0| = U\,, \tag{2.34}$$

where U is the unique solution of $N_0(U,U) = -1$. By defining $V := -N_1(U,U)$, the curve corresponding to (2.34) in the (α,β)-plane is

$$\beta = V\alpha + V(1-V)\alpha^2\,,$$

which is the border of the chaotic region in the (α,β)-plane. This is found to be in good agreement with theoretical conclusions (refer to the bifurcation diagram in [154]). ■

For a more detailed analysis of this example, the reader is referred to the discussions given by Genesio and Tesi in [273] and [271]. Genesio and Tesi have also proposed a scheme [273] based on the harmonic balance method, by which period doubling bifurcations can be predicted. In [271] Genesio and Tesi describe a refinement of their procedure for predicting chaos in a nonlinear system.

2.4 Snap-Back Repellers

2.4.1 Marotto's Theorem

The theorem by Li and Yorke (see Proposition A.54) which gives sufficient conditions for a scalar difference equation to exhibit chaotic behaviour inspired Marotto [513] to find conditions that would guarantee a nonlinear multi-dimensional difference equation to behave chaotically. He concluded that the existence of an orbit which begins arbitrarily close to an unstable fixed point of the multi-dimensional difference equation, is repelled from this point as iteration progresses but suddenly snaps back to hit this fixed point precisely, is sufficient to imply chaotic behaviour.

Definition 2.31 Assume that $\mathbf{x}^* \in \mathbf{R}^N$, $N \in \mathbf{N}$ is an unstable fixed point of the nonlinear mapping $\mathbf{f} : \mathbf{R}^N \to \mathbf{R}^N$ and that $\mathbf{f}$ is expanding everywhere in the closed ball $\tilde{B}(\mathbf{x}^*;r)$ for some $r > 0$. Then $\mathbf{x}^*$ is said to be a *snap-back repeller* of $\mathbf{f}$ if there exists a point $\mathbf{x}_0 \in \tilde{B}(\mathbf{x}^*;r)$ with $\mathbf{x}_0 \neq \mathbf{x}^*$, but $\mathbf{f}^{(m)}(\mathbf{x}_0) = \mathbf{x}^*$ and $|D\mathbf{f}^{(m)}(\mathbf{x}_0)| \neq 0$ for some positive integer m. ■

Remark Requiring that $\mathbf{f}$ be expanding everywhere in some closed ball $\tilde{B}(\mathbf{x}^*; r)$ is equivalent to requiring that the eigenvalues of $D\mathbf{f}(\mathbf{x})$ are greater than unity in norm, for all $\mathbf{x} \in \tilde{B}(\mathbf{x}^*; r)$.

Theorem 2.32 (Marotto's Theorem) If the mapping $\mathbf{f} : \mathbf{R}^n \to \mathbf{R}^n$, $n \geq 1$ possesses a snap-back repeller then $\mathbf{f}$ is chaotic.

Proof: See [513]. ■

Example 2.33 For the logistic map $f : I \to I$,

$$f(x) = rx(1 - x),$$

with $r \geq 3.680$, Marotto's theorem guarantees the existence of a snap-back repeller for f. (See [513], [217].) ■

Example 2.34 [343] Consider the N-dimensional autonomous differential equation of the form

$$\frac{d\mathbf{x}}{dt} = \mathbf{f}(\mathbf{x}), \tag{2.35}$$

where $\mathbf{f} : \mathbf{R}^N \to \mathbf{R}^N$ is a continuous differentiable mapping with two distinct roots $\mathbf{x}_1^*$ and $\mathbf{x}_2^*$ satisfying

$$\det\left(D\mathbf{f}(\mathbf{x}_1^*)\right) \neq 0, \qquad \det\left(D\mathbf{f}(\mathbf{x}_2^*)\right) \neq 0.$$

Then there exists a positive constant T such that numerical solution of (2.35) obtained using *Euler's finite difference scheme* with integration step size Δt, namely

$$\mathbf{x}((n+1)\Delta t) = \mathbf{x}(n\Delta t) + \Delta t\, \mathbf{f}(\mathbf{x}(n\Delta t)),$$

exhibits chaos for all $\Delta t > T$. ■

Although Marotto's theorem is remarkable, it is difficult to apply especially to multi-dimensional systems. The reason for this difficulty is that in order to prove the existence of snap-back repellers the global properties of the discrete-time systems must be known.

2.4.2 Shiraiwa and Kurata's Theorem

Before stating Shiraiwa and Kurata's theorem, which is a generalization of Marotto's theorem, we introduce some notation. Let $\mathcal{M}$ be a smooth *manifold* [755], [83] of dimension N and $T_{\mathbf{x}}\mathcal{M}$ be the *tangent space* of $\mathcal{M}$ at a point $\mathbf{x}$ of $\mathcal{M}$. Let $\mathbf{f} : \mathcal{M} \to \mathcal{M}$ be a C^1-map and denote the associated tangent map of $\mathbf{f}$ at $\mathbf{x} \in \mathcal{M}$ by $T_{\mathbf{x}}\mathbf{f} : T_{\mathbf{x}}\mathcal{M} \to T_{\mathbf{f}(\mathbf{x})}\mathcal{M}$. Supposing that $\mathbf{x}^* \in \mathcal{M}$ is a hyperbolic fixed point of $\mathbf{f}$, we define E^s (respectively E^u) as the *direct sum* of the generalized eigenspaces of $T_{\mathbf{x}^*}\mathbf{f}$ which possess only eigenvalues of modulus less than 1 (respectively greater than 1). Then E^s and E^u are $T_{\mathbf{x}^*}\mathbf{f}$-invariant vector subspaces of $T_{\mathbf{x}^*}\mathcal{M}$ under $\mathbf{f}$ and

$$T_{\mathbf{x}^*}\mathcal{M} = E^s \oplus E^u ,$$

since $\mathbf{f}$ is hyperbolic. The stable and unstable manifold theorems (see Appendix B) guarantee the existence of $W^s_{loc}(\mathbf{x}^*)$ and $W^u_{loc}(\mathbf{x}^*)$, the local stable and unstable manifolds respectively of $\mathbf{f}$ at its fixed point $\mathbf{x}^*$.

Theorem 2.35 (The Shiraiwa-Kurata Theorem) Let $\mathbf{f} : \mathcal{M} \to \mathcal{M}$ be a C^1-map and let $\mathbf{x}^* \in \mathcal{M}$ be a hyperbolic fixed point of $\mathbf{f}$. If

i) $N_u := \dim E^u > 0$,

ii) there exists a point $\mathbf{y} \in W^u_{loc}(\mathbf{x}^*)$ different from $\mathbf{x}^*$ and a positive integer m such that $\mathbf{f}^{(m)}(\mathbf{y}) \in W^s_{loc}(\mathbf{x}^*)$, and

iii) there exists an N_u-dimensional disk B^u embedded in $W^u_{loc}(\mathbf{x}^*)$ such that

1) B^u is a neighbourhood of $\mathbf{y}$ in $W_{loc}(\mathbf{x}^*)$,

2) $\mathbf{f}^{(m)}|B^u : B^u \to \mathcal{M}$ is an embedding, and

3) $\mathbf{f}^{(m)}(B^u)$ intersects $W^s_{loc}(\mathbf{x}^*)$ transversally at $\mathbf{f}^{(m)}(\mathbf{y})$,

then $\mathbf{f}$ is chaotic in the Li-Yorke sense (see Appendix B).

Proof: Refer to [729] for details of the proof. ■

In [813], Ushio and Hirai studied the existence of chaos in piecewise-linear sampled-data control systems. First, they showed that a discrete-time system with a piecewise-linear element is chaotic if its associated (lower-dimensional) unstable subsystem has a snap-back repeller. Thereafter, they applied this result to a piecewise-linear sampled-data control system to derive conditions under which this system is exhibits chaos. For examples the reader is referred to Chapter 4.

2.5 Melnikov's Method

We now describe a method by Melnikov [542] for analyzing the motion near separatrices of near-integrable systems. The method yields a criterion for the onset of stochasticity near the separatrix of an integrable system which undergoes a dissipative perturbation. It is known that a generic Hamiltonian perturbation always yields chaotic motion in a layer surrounding the separatrix in the phase portrait [484]. For a dissipative perturbation, the motion near the separatrix is not necessarily chaotic. It is therefore important to predict under what conditions chaos first appears. Melnikov's method is discussed widely by Holmes [362], Greenspan and Holmes [306], Salam *et al.* [683], Lichtenberg and Lieberman [484] and numerous others. However before discussing Melnikov's method we present some definitions.

For the purpose of presenting the required definitions, we consider the autonomous system of ordinary differential equations

$$\frac{d\mathbf{x}}{dt} = \mathbf{f}(\mathbf{x}), \qquad \mathbf{f}(\mathbf{x}) : \mathbf{R}^N \to \mathbf{R}^N . \tag{2.36}$$

Definition 2.36 (E-Homoclinic Trajectory) [539] Suppose the system (2.36) has a fixed point $\mathbf{x}^*$. A solution $\mathbf{x}(t)$ of (2.36) which satisfies

$$\lim_{|t|\to\infty} \mathbf{x}(t) = \mathbf{x}^* ,$$

is said to be *E-homoclinic* or just *homoclinic.* ■

Let $\mathbf{P} : \Sigma^{t_0} \to \Sigma^{t_0}$ be the Poincaré map defined by the intersections of the flow with the surface of section

$$\Sigma^{t_0} := \left\{ (\mathbf{x}, t) \in \mathbf{R}^N \times S^1_T \middle| \, t = t_0 \right\} , \tag{2.37}$$

for some fixed $t_0 \in [0, T)$.

Definition 2.37 (P-Homoclinic Trajectory) [539] Suppose that $\mathbf{x}^*(t)$ is a period-T solution of (2.36). For a solution $\mathbf{x}(t)$ of (2.36), $\mathbf{P}$ is defined by

$$\mathbf{P}(\mathbf{x}(t_0)) := \mathbf{x}(t_0 + T).$$

If $\mathbf{x}(t)$ satisfies

$$\lim_{|n|\to\infty} \mathbf{P}^{(n)}(\mathbf{x}(t_0)) = \mathbf{x}^*(t_0) ,$$

then it is said to be *P-homoclinic.* ■

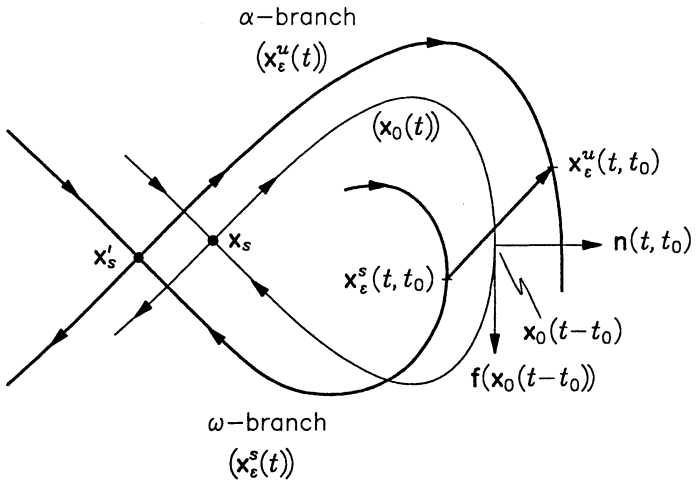

Figure 2.6: Poincaré maps of the unperturbed system (thin line) and the perturbed system (thick line).

Now, consider a two-dimensional autonomous system of the form (2.36) where $\mathbf{f} : \mathbf{R}^2 \to \mathbf{R}^2$ is a smooth function. Suppose the system (2.36) is being perturbed and that the equation of motion describing the perturbed system is of the form

$$\frac{d\mathbf{x}}{dt} = \mathbf{f}(\mathbf{x}) + \epsilon \mathbf{g}(\mathbf{x}, t), \tag{2.38}$$

where $\mathbf{g} : \mathbf{R}^2 \times S^1 \to \mathbf{R}^2$ is smooth, T-periodic in t and ϵ is a small positive number. Now, suppose that the system (2.36) has a saddle point $\mathbf{x}_s$ and an E-homoclinic trajectory $\mathbf{x}_0(t)$ connected to $\mathbf{x}_s$. For both the unperturbed and perturbed systems we consider the induced Poincaré maps (say $\mathbf{P}$ and $\mathbf{P}_\epsilon$ respectively) defined on the time-T surface of section

$$\Sigma^{t_0} := \left\{ (\mathbf{x}, t) \in \mathbf{R}^2 \times S^1 \middle| t = t_0 \in [0, T) \right\}.$$

These Poincaré maps are depicted in Figure 2.6. (Note that Figure 2.6 shows the projections of the Poincaré maps for each $t_0 \in [0, T)$ onto Σ^{t_0} and hence the continuous curves instead of discrete points are obtained.) For the unperturbed system the Poincaré map has an E-homoclinic orbit (the word *orbit* is used to emphasize that the Poincaré section consists of a discrete trajectory). It is fundamental, as illustrated in Figure 2.6, that the saddle fixed point $\mathbf{x}_s$ of the unperturbed system (2.36) is perturbed into a saddle fixed point $\mathbf{x}_s'(\epsilon)$ for the Poincaré map $\mathbf{P}_\epsilon$ and that in general, the E-homoclinic orbit of the Poincaré map $\mathbf{P}$ (thin line in Figure 2.6) is broken to give rise to stable and unstable invariant manifolds ($W^s(\mathbf{x}_s')$ and $W^u(\mathbf{x}_s')$ respectively) for the perturbed system (2.38). These manifolds intersect Σ^{t_0} to form two sets of invariant curves associated with $\mathbf{x}_s'(\epsilon)$ (the thick lines in Figure 2.6):

those which converge to $\mathbf{x}_s'(\epsilon)$ as t tends to infinity are called a pair of ω-branches (or *ω-invariant set*) and those which converge to $\mathbf{x}_s'(\epsilon)$ as t tends to minus infinity are called a pair of α-branches (or *α-invariant set*). The trajectories in phase space of the perturbed system associated with the ω- and α-branches will be denoted by $\mathbf{x}_\epsilon^s(t)$ (stable trajectory) and $\mathbf{x}_\epsilon^u(t)$ (unstable trajectory).

Melnikov's method consists of estimating the separation $d(t_0)$ (see (2.45) below for the definition) between α- and ω-branches at time $t = t_0$. With $d(t_0) < 0$ for all $t_0 \in \mathbf{R}$, we have the situation in Figure 2.7(a); with $d(t_0) > 0$ for all $t_0 \in \mathbf{R}$ we have Figure 2.7(b); and if $d(t_0)$ changes sign for some t_0 then an E-homoclinic orbit of the Poincaré map $\mathbf{P}_\epsilon$ and hence a P-homoclinic trajectory for the perturbed system (2.38) exists. The existence of transversal P-homoclinic orbits (points) implies, via the Smale-Birkhoff theorem (Appendix B), that some iterate of the Poincaré map has an invariant hyperbolic (i.e., structurally stable) set, namely a Smale horseshoe. A horseshoe contains a countable infinity of unstable periodic orbits, an uncountable set of bounded, nonperiodic orbits, and a dense orbit. The sensitive dependence on initial conditions which it engenders in the flow of the differential equation is of great practical interest. However, there is no theorem which assures that a horseshoe is an attractor. In general, a horseshoe may not always be an attractor. For example, if there is no domain of attraction, the horseshoe is asymptotically unstable, and we cannot observe any horseshoe attractor. Therefore, the existence of a transversal P-homoclinic orbit does not always imply the existence of a chaotic attractor. On the other hand, in many cases the chaotic attractor resulting from a horsehoe can be observed.

To calculate $d(t_0)$, we need the stable and unstable trajectories $\mathbf{x}_\epsilon^s(t)$ and $\mathbf{x}_\epsilon^u(t)$ to first order in ϵ. Writing

$$\mathbf{x}_\epsilon^{s,u}(t,t_0) = \mathbf{x}_0(t-t_0) + \epsilon \mathbf{x}_1^{s,u}(t,t_0) + O(\epsilon^2)\,, \tag{2.39}$$

where t_0 is an arbitrary initial time, and inserting (2.39) into (2.38) we obtain to first order

$$\frac{d\mathbf{x}_1^{s,u}}{dt} = D\mathbf{f}(\mathbf{x}_0(t-t_0)) \cdot \mathbf{x}_1^{s,u} + \epsilon \mathbf{g}(\mathbf{x}_0(t-t_0), t)\,. \tag{2.40}$$

We must solve this equation for $\mathbf{x}_\epsilon^s(t)$ for $t > t_0$ and $\mathbf{x}_\epsilon^u(t)$ for $t < t_0$ with the condition that

$$\mathbf{x}_\epsilon^s(t)|_{t\to\infty} = \mathbf{x}_\epsilon^u(t)|_{t\to-\infty} = \mathbf{x}_s'(\epsilon)\,.$$

The vector difference between the two solutions is

$$\mathbf{d}(t,t_o) = \mathbf{x}_\epsilon^u(t,t_0) - \mathbf{x}_\epsilon^s(t,t_0) = \mathbf{x}_1^u(t,t_0) - \mathbf{x}_1^s(t,t_0)\,.$$

The *Melnikov distance* $\Delta(t,t_0)$ is defined by

$$\Delta(t,t_0) := \mathbf{n}(t,t_0) \cdot \mathbf{d}(t,t_0)\,, \tag{2.41}$$

Figure 2.7: Stable and unstable orbits for the hyperbolic fixed point $\mathbf{x}'_s$ of the perturbed system: (a) The unstable trajectory lies outside the stable trajectory; (b) The stable trajectory lies outside the unstable trajectory; (c) Intersection of the stable and unstable trajectories.

which is the projection of $\mathbf{d}(t,t_0)$ onto the normal $\mathbf{n}(t,t_0)$ to the unperturbed P-homoclinic orbit $\mathbf{x}_0$ at time $t-t_0$. From (2.36) we see that $\mathbf{f}(\mathbf{x}_0(t-t_0))$ is tangential to $\mathbf{x}_0(t-t_0)$ and hence a normal vector to $\mathbf{x}_0(t-t_0)$ is

$$\mathbf{n}(t,t_0) = \begin{pmatrix} -f_2(\mathbf{x}_0(t-t_0)) \\ f_1(\mathbf{x}_0(t-t_0)) \end{pmatrix}. \tag{2.42}$$

Introducing the wedge operator $\wedge : \mathbf{R}^2 \times \mathbf{R}^2 \to \mathbf{R}$ defined by

$$\mathbf{x} \wedge \mathbf{y} := x_1 y_2 - x_2 y_1 ,$$

and substituting (2.42) for $\mathbf{n}(t,t_0)$ in (2.41), we obtain

$$\Delta(t,t_0) = \mathbf{f}(\mathbf{x}_0(t-t_0)) \wedge \mathbf{d}(t,t_0) .$$

Now, we write

$$\Delta(t,t_0) = \Delta^s(t,t_0) - \Delta^u(t,t_0) ,$$

where

$$\Delta^{s,u}(t,t_0) = \mathbf{f}(\mathbf{x}_0(t-t_0)) \wedge \mathbf{x}_1^{s,u}(t,t_0) .$$

Differentiating this expression with respect to time, gives

$$\begin{aligned} \frac{d\Delta^s}{dt}(t,t_0) &= \left(\frac{d\mathbf{f}}{dt}(\mathbf{x}_0(t-t_0))\right) \wedge \mathbf{x}_1^s(t,t_0) + \mathbf{f}(\mathbf{x}_0(t-t_0)) \wedge \frac{d\mathbf{x}_1^s}{dt}(t,t_0) \\ &= \left(D\mathbf{f}(\mathbf{x}_0(t-t_0)) \cdot \frac{d\mathbf{x}_0}{dt}(t,t_0)\right) \wedge \mathbf{x}_1^s(t,t_0) + \mathbf{f}(\mathbf{x}_0(t,t_0)) \frac{d\mathbf{x}_1^s}{dt}(t,t_0) , \end{aligned}$$

by application of the chain rule. Using (2.36) and (2.39) in the last expression, produces

$$\begin{aligned} \frac{d\Delta^s}{dt}(t,t_0) &= [D\mathbf{f}(\mathbf{x}_0(t-t_0)) \cdot \mathbf{f}(\mathbf{x}_0(t-t_0))] \wedge \mathbf{x}_1^s(t,t_0) \\ &\quad + \mathbf{f}(\mathbf{x}_0(t-t_0)) \wedge [D\mathbf{f}(\mathbf{x}_0(t-t_0)) \cdot \mathbf{x}_1^s(t,t_0)] \\ &\quad + \mathbf{f}(\mathbf{x}_0(t-t_0)) \wedge \mathbf{g}(\mathbf{x}_0(t-t_0),t) \\ &= \operatorname{tr}[D\mathbf{f}(\mathbf{x}_0(t-t_0))]\, \mathbf{f}(\mathbf{x}_0(t-t_0)) \wedge \mathbf{x}_1^s(t,t_0) \\ &\quad + \mathbf{f}(\mathbf{x}_0(t-t_0)) \wedge \mathbf{g}(\mathbf{x}_0(t-t_0)t) \\ &= \operatorname{tr}[D\mathbf{f}(\mathbf{x}_0(t-t_0))]\, \Delta^s(t,t_0) + \mathbf{f}(\mathbf{x}_0(t-t_0)) \wedge \mathbf{g}(\mathbf{x}_0(t-t_0),t) , \end{aligned}$$

where $\operatorname{tr}(\cdot)$ denotes the *trace* of a matrix. This is a scalar differential equation in $\Delta^s(t,t_0)$. Integrating this equation over the domain of definition $t=t_0$ to $t=\infty$ and presupposing the exponential convergence property (see [306]), results in

$$\Delta^s(t_0,t_0) := \int_{t_0}^{\infty} \mathbf{f}(\mathbf{x}_0(t-t_0)) \wedge \mathbf{g}(\mathbf{x}_0(t-t_0),t) \exp\left(-\int_0^{t-t_0} \operatorname{tr}\left(D\mathbf{f}(\mathbf{x}_0(s))\right) ds\right) dt .$$

Similarly one obtains an analogous result for $\Delta^u(t_0, t_0)$. Combining these results, we obtain the *Melnikov integral*

$$\begin{aligned} M(t_0) &:= \Delta(t_0, t_0) \\ &= \int_{-\infty}^{\infty} \mathbf{f}(\mathbf{x}_0(t-t_0)) \wedge \mathbf{g}(\mathbf{x}_0(t-t_0), t) \exp\left(-\int_0^{t-t_0} \mathrm{tr}\left[D\mathbf{f}(\mathbf{x}_0(s))\right] ds\right) dt . \end{aligned} \tag{2.43}$$

This integral was first derived by Holmes in 1980 [362]. Note that if the unperturbed vector field $\mathbf{f}$ is that of a Hamiltonian function H_0 then $\mathrm{tr}\,(D\mathbf{f}(\mathbf{x}_0(s))) = 0$ and the Melnikov integral becomes

$$\begin{aligned} M(t_0) &= \int_{-\infty}^{\infty} \mathbf{f}(\mathbf{x}_0(t-t_0)) \wedge g(\mathbf{x}_0(t-t_0), t)\, dt \\ &= \int_{-\infty}^{\infty} \mathbf{f}(\mathbf{x}_0(t)) \wedge \mathbf{g}(\mathbf{x}_0(t), t+t_0)\, dt . \end{aligned}$$

By further assuming that the perturbation vector $\mathbf{g}$ is Hamiltonian with Hamiltonian function H_1, then the Melnikov integral reduces to [683].

$$M(t_0) = -\int_{-\infty}^{\infty} (H_0, H_1)_{\mathbf{q},\mathbf{p}}\, dt ,$$

where

$$(H_0, H_1)_{\mathbf{q},\mathbf{p}} := \sum_{i=1}^{2} \left(\frac{\partial H_0}{\partial q_i} \frac{\partial H_1}{\partial p_i} - \frac{\partial H_0}{\partial p_i} \frac{\partial H_1}{\partial q_i} \right), \tag{2.44}$$

is called the *Poisson bracket* and $\{q_1, q_2\}$ and $\{p_1, p_2\}$ are the generalized coordinates and momenta, respectively [287].

The relationship between the separation distance $d(t_0)$ between $\mathbf{x}_\epsilon^u(t_0)$ and $\mathbf{x}_\epsilon^s(t_0)$ and $M(t_0)$ is given by

$$\begin{aligned} d(t_0) &:= \frac{\mathbf{n}(t_0, t_0) \cdot \mathbf{d}(t_0, t_0)}{\|\mathbf{n}(t_0, t_0)\|} \\ &= \frac{\mathbf{f}(\mathbf{x}_0(t_0)) \wedge [\mathbf{x}_\epsilon^u(t_0, t_0) - \mathbf{x}_\epsilon^s(t_0, t_0)]}{\|\mathbf{f}(\mathbf{x}_0(t_0))\|} \\ &= \frac{\epsilon}{\|\mathbf{f}(\mathbf{x}_0(t_0))\|} M(t_0) + O(\epsilon^2) . \end{aligned} \tag{2.45}$$

The following theorem [306] gives conditions under which the Melnikov integral can serve as a measure of the presence of chaos. (See also [238]).

Theorem 2.38 If $M(t_0)$ has at least one zero of multiplicity one (i.e. for some $t_0 = t_0'$ $M(t_0') = 0$ and $(dM/dt)(t_0') \neq 0$) then for $\epsilon > 0$ sufficiently small the stable manifold $W^s(\mathbf{x}_s'(\epsilon))$ and unstable manifold $W^u(\mathbf{x}_s'(\epsilon))$ intersect transversally. Moreover if $M(t_0)$ is bounded away from zero then

$$W^u(\mathbf{x}_s'(\epsilon)) \cap W^s(\mathbf{x}_s'(\epsilon)) = \emptyset\,,$$

(see Figure 2.7). ■

Corollary 2.39 Suppose that the Melnikov function $M(t_0, \epsilon)$ has a quadratic zero at $t_0 = t_0'$, that is

$$M(t_0', \epsilon_b) = 0\,, \qquad \text{and} \qquad \frac{\partial M}{\partial t_0}(t_0', \epsilon_b) = 0\,,$$

but

$$\frac{\partial^2 M}{\partial t^2}(t_0', \epsilon_b) \neq 0\,, \qquad \text{and} \qquad \frac{\partial M}{\partial \epsilon}(t_0', \epsilon_b) \neq 0\,.$$

Then $\epsilon_B = \epsilon_b + O(\epsilon)$ is a bifurcation value for which quadratic homoclinic tangencies occur in the system (2.38). ■

We now turn to examples.

Example 2.40 Under the assumption of small periodic forcing, small DC current bias and small junction conductance, the dynamics of the Josephson junction is described by [686]

$$\begin{pmatrix} dx_1/dt \\ dx_2/dt \end{pmatrix} = \begin{pmatrix} x_2 \\ -\sin x_1 + \epsilon(-d_0 x_2 + \rho' + A' \sin \omega' t') \end{pmatrix},$$

where $d_0 \in \mathbf{R}^+$ is a constant. Study this system by means of Melnikov's method.

The unperturbed system is exactly the system that describes the motion of a one-dimensional undamped pendulum, which is a Hamiltonian system with Hamiltonian function

$$H(x_1, x_2) = \frac{1}{2}x_2^2 - \cos x_1\,. \tag{2.46}$$

Two E-homoclinic trajectories exist for the unperturbed system (see Chapter 6, Section 6.6). These two E-homoclinic trajectories are explicitly described by

$$\mathbf{x}_0(t') = \begin{pmatrix} x_{0,1}(t') \\ x_{0,2}(t') \end{pmatrix} = \begin{pmatrix} \pm 2 \arctan(\sinh t') \\ \pm 2 \operatorname{sech} t' \end{pmatrix}. \tag{2.47}$$

The Melnikov integral is given by

$$\begin{aligned} M(t_0) &= \int_{-\infty}^{\infty} \begin{pmatrix} x_{0,2}(t') \\ -\sin x_{0,1}(t') \end{pmatrix} \wedge \begin{pmatrix} 0 \\ -d_0 x_{0,2}(t') + \rho' + A' \sin \omega'(t'+t_0) \end{pmatrix} dt' \\ &= \int_{-\infty}^{\infty} x_{0,2}(t')(\rho' - d_0 x_{0,2}(t') + A' \sin \omega'(t'+t_0))\, dt' \\ &= \int_{\pm\pi}^{\pm\pi} \rho' dx_{0,1} - d_0 \int_{-\infty}^{\infty} (\pm 2\mathrm{sech}\, t')^2\, dt' + \left(\int_{-\infty}^{\infty} \pm 2\mathrm{sech}\, t' \cos \omega' t'\, dt' \right) A' \sin \omega' t_0 . \end{aligned}$$

where we have used $(dx_{0,1}/dt')(t') = x_{0,2}(t')$ and the fact that

$$\int_{-\infty}^{\infty} \mathrm{sech}\, \tau \sin \omega' \tau\, d\tau = 0 ,$$

since the integrand is an odd function. Evaluating $M(t_0)$ explicitly yields

$$M(t_0) = \pm 2\pi\rho' - 8d_0 \pm A' \left[2\pi \mathrm{sech} \left(\frac{\pi\omega'}{2} \right) \right] \sin \omega' t_0 .$$

Represent the upper E-homoclinic orbit of the unperturbed system (that is the E-homoclinic trajectory in the $x_2 > 0$ half plane of the Poincaré map) by Γ^u and the lower E-homoclinic trajectory by Γ^l. The separation between the upper stable and unstable manifolds is described by

$$M^u(t_0) = 2\pi\rho' - 8d_0 + A' R(\omega') \sin \omega' t_0 ,$$

where

$$R(\omega') := 2\pi \mathrm{sech} \left(\frac{\pi\omega'}{2} \right) > 0 .$$

For $M^u(t_0)$ to have a zero of multiplicity one at some $t_0 = t_0'$, it is necessary and sufficient that

$$|-2\pi\rho' + 8d_0| < A' R(\omega') . \tag{2.48}$$

Subject to this condition the stable and unstable manifolds intersect transversely. For the case

$$|1 - 2\pi\rho' + 8d_0| = A' R(\omega') ,$$

the zero at some $t_0 = t_0'$ is of multiplicity two, implying that stable and unstable manifolds intersect tangentially. Analogously, for Γ^l the lower E-homoclinic orbit, the Melnikov function is

$$M^l(t_0) = -\pi\rho' - 8d_0 - A' R(\omega') \sin \omega' t_0 .$$

Zeros of multiplicity one and two are guaranteed by

$$|2\pi\rho' + 8d_0| < A'R(\omega')\,, \tag{2.49}$$

and

$$|2\pi\rho' + 8d_0| = A'R(\omega')\,,$$

respectively. Conditions (2.48) and (2.49) guarantee the existence of P-homoclinic trajectories for the perturbed system. ■

Example 2.41 The response of a conventional phase-locked loop can be shown to be described by the following nonautonomous system (see Section 6.4)

$$\begin{pmatrix} dx_1/dt \\ dx_2/dt \end{pmatrix} = \begin{pmatrix} x_2 \\ -h(x_1) - \beta\left(1 + (2\zeta/\beta - 1)\,(dh/dx)(x_1)\right) x_2 \end{pmatrix} + \begin{pmatrix} 0 \\ \beta\sigma + m\beta\sin\Omega t + m\Omega\cos\Omega t \end{pmatrix},$$

where $h : S^1 \to \mathbf{R}$ describes the characteristics of the phase detector utilized by the phase-locked loop and $2\zeta - \beta \geq 0$. Use Melnikov's method to study this system.

To be able to apply Melnikov's method here it is required that h and dh/dx have converging Fourier series. If β, ζ and m are of ϵ-order, we can choose the unperturbed system to be Hamiltonian. However, if we regard only m and not β and ζ to be of ϵ-order the unperturbed system becomes non-Hamiltonian. Only the latter case is investigated here. For the case being considered we have $\mathbf{f} : S^1 \times \mathbf{R} \to S^1 \times \mathbf{R}$ defined by

$$\mathbf{f}(\mathbf{x}) := \begin{pmatrix} x_2 \\ -h(x_1) - \beta\left(1 + (2\zeta/\beta - 1)\,(dh/dx)(x_1)\right) x_2 + \beta\sigma_c \end{pmatrix},$$

and $\epsilon\mathbf{g} : S^1 \times \mathbf{R} \times \mathbf{R} \to S^1 \times \mathbf{R}$, given by

$$\epsilon\mathbf{g}(\mathbf{x}, t) := \begin{pmatrix} 0 \\ \beta\Delta\sigma + m\beta\sin\Omega t + m\Omega\cos\Omega t \end{pmatrix},$$

with σ_c the critical detuning at which there exists an E-homoclinic trajectory for the unperturbed system, and $\Delta\sigma$ is a small deviation from σ_c (i.e. $\sigma = \sigma_c + \Delta\sigma$). Using the expression in (2.43), the Melnikov integral for this system is given by (see [238])

$$M(t_0) = \beta\Delta\sigma I_3 + m\sqrt{(\beta^2 + \Omega^2)([I_1(\Omega)]^2 + [I_2(\Omega)]^2)}\,\sin(\Omega t_0 + \theta)\,, \tag{2.50}$$

where

$$
\begin{aligned}
I_1(\Omega) &:= \int_{-\infty}^{\infty} x_{0,2}(t)\mathrm{e}^{p(t)} \sin \Omega t \, dt \,, \\
I_2(\Omega) &:= \int_{-\infty}^{\infty} x_{0,2}(t)\mathrm{e}^{p(t)} \cos \Omega t \, dt \,, \\
I_3 &:= \int_{-\infty}^{\infty} x_{0,2}(t)\mathrm{e}^{p(t)} \, dt \\
p(t) &:= \beta t + (2\zeta - \beta) \int_0^t \frac{dh}{dx}(x_{0,1}(\tau)) \, d\tau \,, \\
\theta &:= \arctan\left(\frac{\beta I_1(\Omega) + \Omega I_2(\Omega)}{\beta I_2(\Omega) - \Omega I_1(\Omega)}\right) .
\end{aligned}
\tag{2.51}
$$

As before $\mathbf{x}_0(t) := (x_{0,1}(t),\ x_{0,2}(t))$ represents the E-homoclinic trajectory of the unperturbed system which in general cannot be obtained explicitly. (In [236] however, an analytical expression for the E-homoclinic trajectory is derived by means of piecewise-linear analysis for the case when the phase detector function is triangular.) For $M(t_0)$ in (2.50) to have zeros, it is required that the integrals $I_1(\Omega)$, $I_2(\Omega)$ and I_3 are convergent and that there exists an interval for Ω on which at least one of $I_1(\Omega)$ and $I_2(\Omega)$ is nonzero.

The convergence of the integrals $I_1(\Omega)$, $I_2(\Omega)$ and I_3 defined above is presented in [238]. For the sake of completeness, we reproduce this convergence proof. Before starting however, we notice that since

$$
-x_{0,2}(t)\mathrm{e}^{p(t)} \leq x_{0,2}(t)\mathrm{e}^{p(t)} \sin \Omega t \leq x_{0,2}(t)\mathrm{e}^{p(t)} \,,
$$

and

$$
-x_{0,2}(t)\mathrm{e}^{p(t)} \leq x_{0,2}(t)\mathrm{e}^{p(t)} \cos \Omega t \leq x_{0,2}(t)\mathrm{e}^{p(t)} \,,
$$

we have

$$
-I_3 \leq I_1(\Omega) \leq I_3 \quad \text{and} \quad -I_3 \leq I_2(\Omega) \leq I_3 \,, \tag{2.52}
$$

and hence we need only show that I_3 converges. Since $x_{0,2}(t)$ is a bounded and smooth function with

$$
\lim_{|t| \to \infty} x_{0,2}(t) = 0 \,,
$$

it will suffice to show that $x_{0,2}(t)\mathrm{e}^{p(t)}$ tends to zero fast enough for I_3 to be convergent. Recalling that $x_{0,2}(t)$ is a component of the E-homoclinic trajectory of the unperturbed system, we realize that the rate with which $x_{0,2}(t)$ approaches the saddle point at t close to $-\infty$ and $+\infty$ is approximately equal to the unstable and stable

eigenvalues respectively of the linearized vector field of the unperturbed system at the saddle point $\mathbf{x}_s = (x_{1,s}, 0)$. The eigenvalues of the linearized system (at $\mathbf{x}_s$)

$$\frac{d\mathbf{u}}{dt} = D\mathbf{f}(\mathbf{x}_s)\mathbf{u}\,,$$

with

$$D\mathbf{f}(\mathbf{x}_s) = \begin{pmatrix} 0 & 1 \\ a' & -\beta + (2\zeta - \beta)a' \end{pmatrix},$$

and

$$\lambda_u = \frac{b + \sqrt{b^2 - 4a'}}{2} > 0\,, \qquad \lambda_s = \frac{b - \sqrt{b^2 - 4a'}}{2} < 0\,,$$

where

$$a' := -\frac{dh}{dx}(x_{1,s})\,, \qquad b := -\left(\beta - (2\zeta - \beta)a'\right).$$

Thus for t close to $-\infty$ we have approximately

$$x_{0,2}(t) = K_1 \mathrm{e}^{\lambda_u t}\,,$$

whereas for t close to $+\infty$, $x_{0,2}(t)$ can be approximated by

$$x_{0,2}(t) = K_2 \mathrm{e}^{\lambda_s t}\,,$$

for some $K_1, K_2 \in \mathbf{R}$. For $\tau \approx \pm\infty$ we have $x_{0,1}(\tau) \approx x_{1,s}$ and $(dh/dx)(x_{0,1}(\tau)) \approx a'$. Since $(dh/dx)(x_{0,1}(\tau))$ is bounded for all τ, there exists a $t_c \in \mathbf{R}^+$ such that

$$\int_0^{t_c} \frac{dh}{dx}(x_{0,1}(\tau))\, d\tau\,,$$

has some finite value K_3 where t_c is chosen such that $x_{0,1}(\tau) \approx x_{1,s}$ for $|\tau| > t_c$. Therefore $p(t)$ is well approximated by

$$p(t) = \beta t + (2\zeta - \beta)(K_3 - a'(t - t_c)) = (\beta - (2\zeta - \beta)a')t + K_4\,,$$

where

$$K_4 := (2\zeta - \beta)K_3 + a'(2\zeta - \beta)t_c\,.$$

Using this expression for $p(t)$ together with the above asymptotic approximations for $x_{0,2}(t)$, we notice that $x_{0,2}(t)\mathrm{e}^{p(t)}$ is of the order of

$$\mathrm{e}^{(\lambda_u + \beta - (2\zeta - \beta)a')t}\,,$$

for t close to $-\infty$ and of the order of

$$\mathrm{e}^{(\lambda_s + \beta - (2\zeta - \beta)a')t}\,,$$

if t is close to $+\infty$. From this we conclude that $x_{0,2}(t)e^{p(t)}$ tends to zero exponentially if

$$\lambda_u + \beta - (2\zeta - \beta)a' > 0\,, \tag{2.53}$$

and

$$\lambda_s + \beta - (2\zeta - \beta)a' < 0\,, \tag{2.54}$$

for t close to $\pm\infty$. Thus I_3 and consequently $I_1(\Omega)$ and $I_2(\Omega)$ converge under the above two conditions.

Next we must prove that $I_2(\Omega)$ and $I_3(\Omega)$ are not identically zero. We note that the Fourier transform of $x_{0,2}(t)e^{p(t)}$ is given by

$$\mathcal{F}\left(x_{0,2}(t)e^{p(t)}\right) = I_2(\Omega) - jI_1(\Omega). \tag{2.55}$$

Since $x_{0,2}(t)e^{p(t)}$ is not identically zero, Parseval's theorem [775] implies that $[I_1(\Omega)]^2 + [I_2(\Omega)]^2$ is not identically zero for some interval of Ω.

Now we return to find the zeros of $M(t_0)$. Assuming that the conditions in (2.53) and (2.54) hold, it follows from (2.50) that $M(t_0) = 0$ when

$$\left|\frac{\beta\,\Delta\sigma\,I_3}{m\sqrt{(\beta^2+\Omega^2)([I_1(\Omega)]^2+[I_2(\Omega)]^2)}}\right| \leq 1\,. \tag{2.56}$$

Strict inequality in (2.56) implies that $M(t_0)$ has zeros of multiplicity one thereby guaranteeing that the perturbed system has transversal P-homoclinic trajectories. Strict equality in (2.56) implies that $M(t_0)$ has quadratic zeros which in turn corresponds to a perturbed system having P-homoclinic trajectories on which homoclinic tangencies occur. ■

In the last example, as mentioned above, an explicit expression for the E-homoclinic trajectory of the unperturbed system does not exist. The E-homoclinic trajectory must therefore be calculated numerically, followed by numerical calculation of the integrals I_1, I_2 and I_3, in order to evaluate (2.53), (2.54) and (2.56). However, it is sometimes possible to write an approximate expression for the E-homoclinic trajectory from physical considerations or by the use of perturbation methods. These can then be used to obtain an analytic approximation to the Melnikov integral and from it approximate conditions for the existence of P-homoclinic trajectories for the perturbed system (see [246]).

Extension of Melnikov's method to higher dimensions as mentioned by Salam *et al.* in [683] was employed by Gruendler [310]. However this extension will not be discussed here. Melnikov's method has also been applied to maps of dimension $N \geq 2$. In this respect the reader is referred to [484] and [471].

2.6 Hopf Bifurcation

In 1970, David Ruelle and Floris Takens and in 1978 Ruelle, Takens and Newhouse pointed out the strong similarity in the behaviour of turbulent flows and strange attractors, suggesting that turbulence results from a strange attractor regime in the Navier-Stokes equation (see [672]). Moreover, this regime is reached through the *Ruelle-Takens scenario* involving a sequence of Hopf bifurcations, namely from a fixed point to a periodic orbit, then to a quasiperiodic orbit (lying on a two-dimensional torus), and then, after the third bifurcation, it is likely that the system possesses a strange attractor with sensitivity to initial conditions. This scenario is confirmed by some experiments with real fluids, where the power spectra exhibit a broad band when the third independent frequency is about to appear. The *Hopf bifurcation theorem* describes the emergence of periodic solutions from a fixed point of a map of the form

$$\mathbf{x}_{n+1} = \mathbf{f}(\mathbf{x}_n; r), \quad \mathbf{f} : \mathbf{R}^N \times \mathbf{R} \to \mathbf{R}^N,$$

or of a vector field of the form

$$\frac{d\mathbf{x}}{dt} = \mathbf{f}(\mathbf{x}; r), \quad \mathbf{f} : \mathbf{R}^N \times \mathbf{R} \to \mathbf{R}^N,$$

if the bifurcation parameter r varies through a critical value r_0. In the next two sections we discuss the Hopf bifurcation of maps and flows respectively.

2.6.1 Hopf Bifurcation of Maps

We state the Hopf bifurcation theorem for maps without proof, followed by an example of its use.

Theorem 2.42 (Hopf Bifurcation Theorem)

i) (Hypotheses) The system

$$\mathbf{x}_{n+1} = \mathbf{f}(\mathbf{x}_n; r), \quad \mathbf{f} : \mathbf{R}^N \times \mathbf{R} \to \mathbf{R}^N, \tag{2.57}$$

satisfies the following conditions:

1) An isolated fixed point $\mathbf{x}^*(r)$ exists.
2) The function $\mathbf{f}$ is C^k $(k \geq 3)$ in the neighbourhood of $(\mathbf{x}^*(r_0); r_0)$.
3) The Jacobian $D_{\mathbf{x}}\mathbf{f}(\mathbf{x}^*(r); r)$ possesses a pair of complex conjugate, simple eigenvalues

$$\lambda(r) := \mathrm{e}^{\alpha(r)+jw(r)},$$

and $\bar{\lambda}(r)$, such that at the critical value $r = r_0$,

$$|\lambda(r_0)| = 1, \quad [\lambda(r_0)]^3 \neq 1, \quad [\lambda(r_0)]^4 \neq 1, \quad \text{and} \quad \frac{d|\lambda|}{dr}(r_0) > 0.$$

4) The remaining $N-2$ eigenvalues of the critical Jacobian $D_{\mathbf{x}}\mathbf{f}(\mathbf{x}^*(r_0);r_0)$ are contained inside the unit circle

$$\{z \in \mathbf{C} |\ |z| < 1\}\ .$$

ii) (Existence) There exists a real number $\epsilon_0 > 0$ and a C^{k-1} function

$$r(\epsilon) = r_0 + r_1\epsilon + r_3\epsilon^3 + O(\epsilon^4)\,,$$

such that for each $\epsilon \in (0, \epsilon_0]$ the map $\mathbf{f}$ has an invariant manifold $H(r)$, i.e. $\mathbf{f}(H(r);r) = H(r)$. The manifold $H(r)$ is C^r diffeomorphic to a circle and consists of points at a distance $O(|r|^{1/2})$ of $\mathbf{x}^*(r)$, for $r = r(\epsilon)$.

iii) (Uniqueness) Each compact invariant manifold close to $\mathbf{x}^*(r)$ for $r = r(\epsilon)$ is contained in $H(r) \cup \{0\}$.

iv) (Stability) If $r_3 < 0$ (respectively $r_3 > 0$) then for $r < 0$ (respectively $r > 0$), the fixed point $\mathbf{x}^*(r(\epsilon))$ is stable (respectively unstable) and for $r > 0$ (respectively $r < 0$) the fixed point $\mathbf{x}^*(r(\epsilon))$ is unstable (respectively stable) and the surrounding manifold $H(r(\epsilon))$ is attracting (respectively repelling). When $r_3 < 0$ (respectively $r_3 > 0$) the bifurcation at $r = r(\epsilon)$ is said to be *supercritical* (respectively *subcritical*). ■

Example 2.43 Use the Hopf bifurcation theorem to study the *bimap* defined by the system (see [499])

$$\begin{pmatrix} x_{1,n+1} \\ x_{2,n+1} \end{pmatrix} = \begin{pmatrix} f(x_{1,n}, x_{2,n}) \\ f(x_{2,n}, x_{1,n}) \end{pmatrix},$$

where $f : I \times I \to I \times I$ is defined by

$$f(x_1, x_2) := b(3x_2 + 1)x_1(1 - x_1), \qquad b \in \mathbf{R}\,.$$

For convenience we distinguish between two groups of fixed points of the bimap:

i) on the x_1-axis

$$\mathbf{x}_0^* = (0,0)^T, \qquad \mathbf{x}_1^* = \left(\frac{b-1}{b}, 0\right)^T, \qquad \mathbf{x}_2^* = \left(0, \frac{b-1}{b}\right)^T,$$

ii) on the diagonal

$$\mathbf{x}_3^* = \left(\frac{1}{3} - \frac{1}{3}\sqrt{4 - \frac{3}{b}},\ \frac{1}{3} - \frac{1}{3}\sqrt{4 - \frac{3}{b}}\right)^T,$$

$$\mathbf{x}_4^* = \left(\frac{1}{3} + \frac{1}{3}\sqrt{4 - \frac{3}{b}},\ \frac{1}{3} + \frac{1}{3}\sqrt{4 - \frac{3}{b}}\right)^T.$$

We only consider the fixed points on the diagonal here. Notice that these fixed points exist only for $b \geq 3/4$. For $b > 3/4$ a stable period-2 orbit exists, given by the points $\mathbf{x}_1$ and $\mathbf{x}_2$,

$$\mathbf{x}_1^T = \left(\frac{2b(b+1) - \sqrt{b(b+1)(4b^2-3)}}{b(4b+3)}, \frac{2b(b+1) + \sqrt{b(b+1)(4b^2-3)}}{b(4b+3)} \right),$$

$$\mathbf{x}_2^T = \left(\frac{2b(b+1) + \sqrt{b(b+1)(4b^2-3)}}{b(4b+3)}, \frac{2b(b+1) - \sqrt{b(b+1)(4b^2-3)}}{b(4b+3)} \right).$$

This period-2 orbit looses stability via a Hopf bifurcation which occurs at $b = b_0$, where $b_0 := 0.957$, and gives rise to a stable limit cycle for $b \in (b_0, b_0 + \delta]$ for some $\delta > 0$. ■

The orbits of the map $\mathbf{f}$ on the invariant manifold $H(r)$ can be fixed points, periodic or even quasiperiodic. Perhaps the easiest way to see this is to take a continuous-time system that exhibits Hopf bifurcation such as the Van der Pol system

$$\frac{dx_1}{dt} = rx_1 - x_2 - x_1^3, \qquad \frac{dx_2}{dt} = x_1,$$

which describes an electrical circuit with a triode vacuum tube [389]. The fixed point $(x_1, x_2) = (0, 0)$ exhibits a Hopf bifurcation at $r = 0$, producing a periodic trajectory with period say T_0. Next, consider the time-T_0 Poincaré map of this periodic solution. Since the points on the Poincaré section lie on an invariant manifold (Theorem 2.42) that is diffeomorphic to a circle, it follows that the orbit of the Poincaré map must be a fixed point for $T = T_0$, periodic if T_0/T is rational and quasi-periodic if T_0/T is irrational, since these Poincaré sections are diffeomorphic to translations of the circle [217].

2.6.2 Hopf Bifurcation of Flows

The version of the Hopf bifurcation theorem for flows stated here is given in [552]. Thereafter two examples which demonstrate the application of this theorem are discussed.

Theorem 2.44 (Hopf Bifurcation Theorem)

i) (Hypotheses) The system

$$\frac{d\mathbf{x}}{dt} = \mathbf{f}(\mathbf{x}; r), \quad \mathbf{f} : \mathbf{R}^N \times \mathbf{R} \to \mathbf{R}^N, \tag{2.58}$$

satisfies the following conditions:

1) An isolated fixed point $\mathbf{x}^*(r)$ exists.

2) The function $\mathbf{f}$ is C^k, $(k \geq 4)$ in a neighbourhood of $(\mathbf{x}^*(r_0); r_0)$.

3) The Jacobian $D_{\mathbf{x}}\mathbf{f}(\mathbf{x}^*(r); r)$ possesses a pair of complex conjugate, simple eigenvalues

$$\lambda(r) := \alpha(r) + j\omega(r)\,,$$

and $\bar{\lambda}(r)$, such that at the critical value $r = r_0$,

$$\alpha(r_0) = 0\,, \quad \frac{d\alpha}{dr}(r_0) > 0\,, \quad \text{and} \quad \omega_0 := \omega(r_0) > 0\,.$$

4) The remaining $N - 2$ eigenvalues of the critical Jacobian $D_{\mathbf{x}}\mathbf{f}(\mathbf{x}^*(r_0); r_0)$ lie in the open left-half complex plane.

ii) (Existence) There exists a real number $\epsilon_0 > 0$ and a C^{k-1} function

$$r(\epsilon) = r_0 + r_2\epsilon^2 + O(\epsilon^3)\,,$$

such that for each $\epsilon \in (0, \epsilon_0]$ there is a nonconstant periodic solution $\mathbf{x}(t; \epsilon)$ of (2.58) near $\mathbf{x}^*(r)$ for $r = r(\epsilon)$. The period of $\mathbf{x}(t; \epsilon)$ is a C^{k-1} function

$$T(\epsilon) = (2\pi/\omega_0)\left(1 + T_2\epsilon^2\right) + O(\epsilon^3)\,,$$

and its amplitude grows as $O(\epsilon)$.

iii) (Uniqueness) If $r_2 \neq 0$ then there is an $\epsilon_1 \in (0, \epsilon_0]$ such that for each $\epsilon \in (0, \epsilon_1]$, the periodic trajectory $\mathbf{x}(t; \epsilon)$ is the only periodic solution of (2.58) for $r = r(\epsilon)$ that lies in a neighbourhood of $\mathbf{x}^*(r(\epsilon))$.

iv) (Stability) Exactly one of the characteristic exponents of $\mathbf{x}(t, \epsilon)$ approaches 0 as $\epsilon \downarrow 0$, and it is given by a C^{k-1} function,

$$\beta(\epsilon) = \beta_2\epsilon^2 + O(\epsilon^3)\,, \qquad \beta_2 := -2r_2\frac{d\alpha}{dr}(r_0)\,.$$

Moreover, the periodic solution $\mathbf{x}(t; \epsilon)$ is orbitally asymptotically stable if $\beta(\epsilon) < 0$ but is unstable if $\beta(\epsilon) > 0$. If $r_2 \neq 0$ then the periodic solutions $\mathbf{x}(t; \epsilon)$, $0 < \epsilon \leq \epsilon_1$ occur for $r > r_0$ or for $r < r_0$. The bifurcation is said to be *supercritical* in the former and *subcritical* in the latter case. ■

If r_2 and β_2 are both nonzero, the direction of bifurcation (i.e. $r > r_0$ or $r < r_0$) and the stability of the oscillations are determined (for small ϵ) by the coefficients r_2 and β_2, respectively. From the relationship between β_2 and r_2 we can see that the oscillations are stable (respectively unstable) if they are supercritical (respectively subcritical).

Example 2.45 The *model-reference adaptive-control* (MRAC) strategy is used to construct an adaptive direct current (DC) servo system. The complete adaptive control system is described by the following set of ordinary differential equations (see [549]).

Plant:

$$\frac{d\theta}{dt} = y\,, \quad \frac{dy}{dt} = \frac{-\mu y - Fe + k_y y + k_u u + d}{J}\,, \quad e := y - y_m\,, \quad u := r - \theta - F_v y\,.$$

Model:

$$\frac{dy_m}{dt} = \frac{1}{J_m} u\,.$$

Adaptation law:

$$\frac{dk_u}{dt} = -eu - \sigma k_u\,, \qquad \frac{dk_y}{dt} = -ey - \sigma k_y\,.$$

The definitions of the symbols used are:

θ : angular rotation of motor shaft,

y : angular velocity of motor shaft,

y_m : reference model state variable corresponding to y,

r : reference input for positioning,

J : inertia of load,

J_m : reference model parameter corresponding to J,

μ : coefficient of viscous friction torque acting on motor shaft,

k_u, k_y : adjustable gains,

F : fixed positive gain for stabilization of the adaptive system,

F_v : fixed gain for velocity feedback loop,

d : bounded disturbance input,

σ : positive real parameter.

The aim of the adaptation is to adjust k_u and k_y so that the dynamics of the whole system approaches that of the reference model which is described by

$$\frac{d\tilde{\theta}_m}{dt} = \tilde{y}_m\,, \quad \frac{d\tilde{y}_m}{dt} = \frac{(r - F_v\tilde{y}_m - \tilde{\theta}_m)}{J_m}\,.$$

Now, study the system by means of the Hopf bifurcation theorem.

For the case $\mu = 0$, $k_y = 0$ the fixed point of the system as a whole (assuming constant inputs r and d) is given by

$$\boldsymbol{\xi}^* := (\theta^*, y^*, y_m^*, k_u^*)^T = (r, 0, -d/F, 0)^T.$$

The characteristic equation of the linearized system about the fixed point $\boldsymbol{\xi}^*$ is

$$(s + \sigma)p(s) = 0\,, \tag{2.59}$$

where

$$p(\lambda) := \lambda^3 + \frac{F}{J}\lambda^2 + \frac{FF_v}{JJ_m}\lambda + \frac{F}{JJ_m}.$$

Applying the Routh-Hurwitz test (Appendix B), we find that the fixed point $\boldsymbol{\xi}^*$ is asymptotically stable if and only if

$$FF_v - J > 0\,.$$

Thus, if $FF_v - J < 0$, then $\boldsymbol{\xi}^*$ is unstable, with exactly two roots of $p(\lambda)$ having positive real parts, while the remaining root of $p(\lambda)$ is in the open left-half complex plane (here the Routh-Hurwitz test produces two sign changes). By solving the auxiliary equation obtained from the Routh-Hurwitz test for $FF_v - J = 0$, we obtain the purely imaginary roots of $p(\lambda)$ namely

$$\lambda_{1,2}(J) = \pm j\frac{1}{\sqrt{J_m}}, \qquad j := \sqrt{-1}\,.$$

Differentiating $p(\lambda) = 0$ with respect to J and solving for $d\lambda/dJ$, we obtain

$$\frac{d\lambda}{dJ} = \frac{(F/J^2)\lambda^2 + (FF_v/J^2J_m)\lambda + (F/J^2J_m)}{3\lambda^2 + (2F/J)\lambda + (FF_v/JJ_m)}.$$

Substituting $\lambda_{1,2} = \pm j/\sqrt{J_m}$ and $FF_v = J$ into this expression for $d\lambda/dJ$, yields

$$\Re\left(\frac{d\lambda}{dJ}\right) = \frac{1}{2F\,(F^2 + J_m)} > 0\,.$$

From Theorem 2.44, a Hopf bifurcation occurs at the point where $J = FF_v$ as J increases. This has been verified experimentally by Mitobe and Adachi in [549]. ■

Remark In [307] it is proven that the stability of the fixed point and the surrounding periodic trajectory (resulting from the Hopf bifurcation) are opposites of one another.

Example 2.46 [537] Consider the tunnel-diode oscillator shown in Figure 2.8(a). A typical voltage-current characteristic for the tunnel-diode is shown in Figure 2.8(b). The state equations describing the dynamics of the system are

$$\frac{di_L}{dt} = \frac{1}{L}v_C\,, \qquad \frac{dv_c}{dt} = \frac{1}{C}g(V_B - v_C) - \frac{1}{C}i_L\,.$$

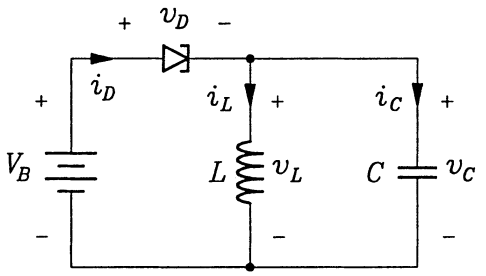

(a)

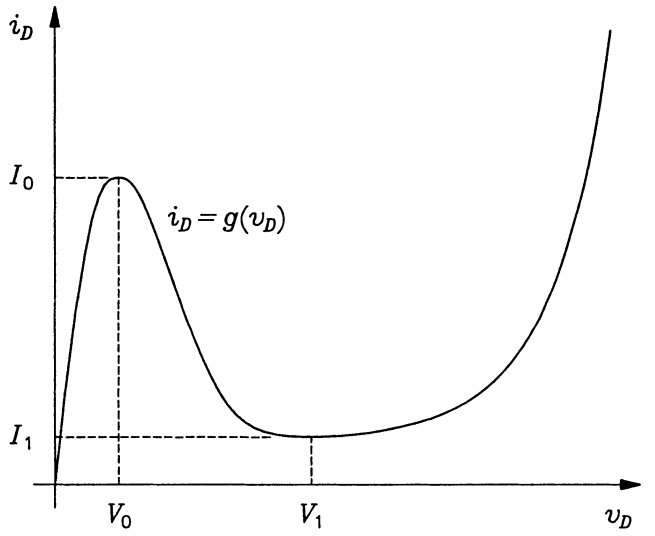

(b)

Figure 2.8: (a) Tunnel-diode oscillator circuit; (b) Typical voltage-current curve for a tunnel-diode.

Here the function $g : \mathbf{R} \to \mathbf{R}$ describes the tunnel-diode's voltage-current relationship. Derive the conditions for Hopf bifurcations to occur.

By defining

$$x_1 := \frac{i_L}{I_0}, \qquad x_2 := \frac{v_C}{V_0}, \qquad \tau := \omega t, \qquad \omega := \frac{1}{LC},$$
$$\beta := \frac{I_0}{V_0}\sqrt{\frac{L}{C}}, \qquad r := \frac{V_B}{V_0}, \qquad h(x) := \frac{1}{I_0} g(V_0 x),$$

we can write the dynamical equations in the following dimensionless form,

$$\frac{dx_1}{d\tau} = \frac{1}{\beta} x_2, \qquad \frac{dx_2}{d\tau} = \beta \left(h(r - x_2) - x_1 \right),$$

where r is taken to be an adjustable parameter of the system. As a result of the normalization, h is a linearly scaled version of g and $g(V_0) = I_0$ corresponds with $h(1) = 1$. The fixed point $\mathbf{x}^*(r)$ of the system is

$$\mathbf{x}^*(r) := (h(r), 0)^T.$$

We assume that g is a C^4 function and hence so is h. The Jacobian matrix evaluated at $\mathbf{x}^*(r)$ is given by

$$J(\mathbf{x}^*(r)) = \begin{pmatrix} 0 & \frac{1}{\beta} \\ -\beta & -\beta \frac{dh}{dr}(r) \end{pmatrix}. \tag{2.60}$$

The eigenvalues of $J(\mathbf{x}^*(r))$ are

$$\lambda_1(r), \lambda_2(r) = -\frac{\beta}{2}\frac{dh}{dr}(r) \pm \sqrt{\left(\frac{\beta}{2}\frac{dh}{dr}(r)\right)^2 - 1} = \alpha(r) \pm \sqrt{\alpha^2(r) - 1},$$

where

$$\alpha(r) := -\frac{\beta}{2}\frac{dh}{dr}(r).$$

From Figure 2.8(b), we note that two values of v_D exist where the real parts of the eigenvalues vanish, namely at $v_D = V_0$ and $v_D = V_1$. This corresponds with $r = r_0$ and $r = r_1$ respectively, where $r_0 := 1$ and $r_1 := V_1/V_0$. Since h is a C^4 function, its continuity guarantees the existence of a neighbourhood B_i of the point $r = r_i$ such that

$$0 \leq \left| \frac{dh}{dr}(r_i) \right| < \frac{2}{\beta},$$

for $i = 0, 1$. Clearly for each $r \in B_i$, $(i = 0, 1)$ the eigenvalues λ_1 and λ_2 are complex and are given by

$$\lambda_1(r), \lambda_2(r) = \alpha(r) \pm j\sqrt{1 - \alpha^2(r)}.$$

In order to comment on the stability of the fixed point $\mathbf{x}^*(r)$, we apply the Routh-Hurwitz test to the linearized system. From this we deduce that $\mathbf{x}^*(r)$ is stable if and only if

$$-\mathrm{tr}\,[J(\mathbf{x}^*(r))] = \beta\frac{dh}{dr}(r) > 0\,.$$

Consequently $\mathbf{x}^*(r)$ is stable if $r \in [0, r_0) \cup (r_1, \infty)$ and unstable if $r \in (r_0, r_1)$. Now, consider first the point $r = r_0$. We have

$$\frac{d\alpha}{dr}(r_0) = -\frac{1}{2}\frac{d^2g}{dr^2}(r_0) > 0\,,$$

since the function h has a local maximum at $r = r_0$. According to Theorem 2.44 it follows that a Hopf bifurcation occurs at $r = r_0$ and there exists a stable limit cycle for each $r \in [r_0, r_0 + \delta)$ for some $\delta > 0$ since the fixed point $\mathbf{x}^*(r)$ is unstable for $r \in [r_{01}, r_{01} + \delta)$. Since $(dh/dr)(r_0) = 0$, it follows directly from the expression for the eigenvalues that the bifurcation frequency at $r = r_0$ is $\omega_0 = 1$.

Next consider the point $r = r_1$. By defining another parameter $s := -r$, we obtain

$$\frac{d\alpha}{ds}(r_1) = -\frac{d\alpha}{dr}(r_1) = \frac{\beta}{2}\frac{d^2h}{dr^2}(r_1) > 0$$

since h has a local minimum at $r = r_1$, and consequently, using the same argument as before, we conclude that a Hopf bifurcation occurs at $s = -r_1$ and that there exists a $\delta > 0$ such that a stable limit cycle exists for $s \in [-r_1, -r_1 + \delta)$. Alternatively we have that a stable limit cycle exists for $r \in (r_1 - \delta, r_1]$, since the fixed point $\mathbf{x}^*(r)$ is unstable for $r \in (r_{02} - \delta, r_{02}]$. ■

Interesting research has been done over the past two decades concerning the Hopf bifurcation. In 1976, Hsü established the existence of periodic solutions to the equations describing the Belousov-Zaikin-Zhabotinskii reaction by application of the Hopf bifurcation theorem (see [369]). In the same year, the book written by Marsden and McCracken with the title, *The Hopf Bifurcation and its Applications* was first published. (reference [515]).

In 1979 Mees and Chua [537] derived a frequency domain version of the Hopf bifurcation theorem for vector fields. In the same article the authors also proposed a graphical version of the Hopf bifurcation theorem. Application of their results was demonstrated with examples.

In 1993 Heidemann, Bode and Purwins [350] studied a two-component reaction-diffusion system. They studied an electronic model consisting of a one-dimensional array of resistively coupled nonlinear LC-oscillators with an S-shaped nonlinearity, similar to the Bonhoeffer-Van der Pol oscillators. Propagating and standing fronts between Hopf- and Turing-type domains were observed experimentally. Their numerical results demonstrated the interaction of front propagation and phase diffusion

within the domains. They concluded with the remark that it is desirable to study front propagation and phase diffusion phenomena by means of the Ginzburg-Landau equations.

Singh and his coworkers [737] studied the effect of internal noise and Hopf bifurcations in hollow cathode gas discharges. They showed that the self-induced oscillations in the hollow cathode discharge undergo backward Hopf bifurcations driven by the discharge current. The effect of internal noise is modelled using a phenomenological complex Ginzburg-Landau type model. Based on their observations and the proposed model, they have shown that the effect of internal noise is reflected by the appearance of a metastable window.

2.7 Lyapunov Exponents

Lyapunov exponents [722] measure the average expansion of a small volume element in orthogonal directions along trajectories in state space. The spectrum of one-dimensional Lyapunov exponents characterizes the attractor in state space. Table 2.1 summarizes the properties of Lyapunov exponents for different attractors for the case of an N-dimensional dynamical system. Therefore, if the spectrum of one-dimensional Lyapunov exponents can be calculated, the attractor in state space can be identified. The aim of this section is to discuss means of estimating numerically the Lyapunov exponents from the equation of motion and the time evolution of a dynamical system.

2.7.1 Lyapunov Exponents from Dynamical Equations

Consider an N-dimensional system whose time evolution is described by

$$\mathbf{x}(t) = \Phi(t; \mathbf{x}(t_0)), \qquad \Phi : \mathbf{T} \times \mathbf{R}^N \to \mathbf{R}^N,$$

with $\mathbf{x}(t_0) = \mathbf{x}_0 \in \mathbf{R}^N$ and $t_0 \geq 0$ the initial conditions. Here the set $\mathbf{T}$ denotes $\mathbf{R}^+$ for a continuous-time system, and $\mathbf{T}$ denotes $\mathbf{N}$ for a discrete-time system. Thus, $t \geq t_0$ is either a real number or integer depending on whether the system is continuous or discrete. The solution of the associated *variational equation* or *linearized equation* of the system is

$$\mathbf{y}(t) = D_{\mathbf{x}}\Phi(t; \mathbf{x}(t_0))\mathbf{y}(t_0),$$

for each $t \geq t_0$. Here $\mathbf{y}(t) \in T_{\mathbf{x}(t)}\mathbf{R}^N$. The symbol $T_{\mathbf{x}(t)}\mathbf{R}^N$ denotes the tangent space at the solution point $\mathbf{x}(t)$ in $\mathbf{R}^N$. It can be shown that there exists an N-dimensional orthonormal basis $\{\mathbf{v}_i\}_{i=1}^N$ such that the i-th one-dimensional Lyapunov exponent $\lambda_i^1(\mathbf{x}_0) := \lambda^1(\mathbf{x}_0, \mathbf{v}_i)$ and $\lambda_1^1 \geq \lambda_2^1 \geq \cdots \geq \lambda_N^1$, where

$$\lambda^1(\mathbf{x}_0, \mathbf{y}_0) := \lim_{t\to\infty} \frac{1}{t} \ln \frac{\|D_{\mathbf{x}}\Phi(t; \mathbf{x}_0)\mathbf{y}_0\|}{\|\mathbf{y}_0\|},$$

Attractor	Lyapunov Exponents
Stable Fixed point	$0 > \lambda_1^1 \geq \cdots \geq \lambda_N^1$
Limit cycle	$\lambda_1^1 = 0\,,\ 0 > \lambda_2^1 \geq \cdots \geq \lambda_N^1$
2-Periodic (Torus)	$\lambda_1^1 = \lambda_2^1 = 0\,,\ 0 > \lambda_3^1 \geq \cdots \geq \lambda_N^1$
k-Periodic (k-Torus)	$\lambda_1^1 = \cdots = \lambda_k^1 = 0\,,\ 0 > \lambda_{k+1}^1 \geq \cdots \geq \lambda_N^1$
Chaotic	$\lambda_1^1 > 0\,,\ 0 \geq \lambda_2^1 \geq \cdots \geq \lambda_N^1\,,\ \sum_{i=1}^N \lambda_i^1 < 0$
Hyperchaotic	$\lambda_1^1 \geq \lambda_2^1 > 0\,,\ 0 \geq \lambda_3^1 \geq \cdots \geq \lambda_N^1\,,\ \sum_{i=1}^N \lambda_i^1 < 0$

Table 2.1: Identification of attractors by means of their Lyapunov exponents.

where $\|\cdot\|$ denotes some norm. It can be shown that the Lyapunov exponent is independent of the norm used.

Next we describe a method by which the one-dimensional Lyapunov exponents can be calculated numerically. Choose an arbitrary post-transient initial condition (i.e. an initial condition on the state space attractor) say $\mathbf{x}(t_0) = \mathbf{x}_0$ and an arbitrary orthonormal basis $\{\mathbf{w}_i\}_{i=1}^N$ in the tangent space $T_{\mathbf{x}_0}\mathbf{R}^N$. Ideally, we would now solve the nonlinear equations of motion with the initial condition $\mathbf{x}(t_0) = \mathbf{x}_0$ and the associated variational equations for the N different initial conditions $\{\mathbf{w}_i\}_{i=1}^N$, as time approaches infinity. However, as time progresses along the fiducial trajectory (i.e. the trajectory passing through $\mathbf{x}_0$) the transformed tangent space vectors $\{D_{\mathbf{x}}\Phi(t;\mathbf{x}_0)\}_{i=1}^N$ asymptotically align with the local direction of most rapid expansion and diverge in magnitude. Due to the finite precision of computer arithmetic, the collapse towards a common direction causes the tangent space orientation of all transformed tangent space vectors to become indistinguishable. These problems can be surmounted by periodic application of the *Gram-Schmidt orthogonalization* (GSO) procedure to the transformed basis.

Suppose that the evolved basis after the j-th renormalization is $\{\mathbf{v}_i(j)\}_{i=1}^N$. Then the Gram-Schmidt orthogonalization procedure produces the following orthonormal set $\{\mathbf{w}_i(j+1)\}_{i=1}^N$ of vectors:

$$\mathbf{w}_1(j+1) = \frac{\mathbf{v}_1(j)}{\|\mathbf{v}_1(j)\|} \tag{2.61}$$

$$\mathbf{w}_2(j+1) = \frac{\mathbf{v}_2(j) - \langle \mathbf{v}_2(j), \mathbf{w}_1(j+1)\rangle \mathbf{w}_1(j+1)}{\|\mathbf{v}_2(j) - \langle \mathbf{v}_2(j), \mathbf{w}_1(j+1)\rangle \mathbf{w}_1(j+1)\|} \tag{2.62}$$

$$\vdots$$

$$\mathbf{w}_N(j+1) = \frac{\mathbf{v}_N(j) - \sum_{i=1}^{N-1} \langle \mathbf{v}_N(j), \mathbf{w}_i(j+1)\rangle \mathbf{w}_i(j+1)}{\|\mathbf{v}_N(j) - \sum_{i=1}^{N-1} \langle \mathbf{v}_N(j), \mathbf{w}_i(j+1)\rangle \mathbf{w}_i(j+1)\|} \tag{2.63}$$

where $\langle \cdot, \cdot \rangle$ represents the inner product. Since Gram-Schmidt orthogonalization preserves the orientation of the first vector in the system (namely $\mathbf{v}_1(j)$), the direction of the vector $\mathbf{w}_1(j+1)$ will converge to the local direction associated with the maximal one-dimensional Lyapunov exponent λ_1^1 as time increases (and hence as j increases).

However, the vector $\mathbf{w}_2(j+1)$ will not eventually converge in direction to the local direction associated the Lyapunov exponent λ_2. Instead, $\mathbf{w}_1(j+1)$ and $\mathbf{w}_2(j+1)$ eventually span the two-dimensional subspace that is most rapidly expanding, despite repeated execution of the Gram-Schmidt re-orthogonalization. The area spanned by $\mathbf{w}_1(j+1)$ and $\mathbf{w}_2(j+1)$ expands as $e^{(\lambda_1^1+\lambda_2^1)t}$. In general the vectors $\{\mathbf{w}_i(j+1)\}_{i=1}^k$, $k = 1, 2, 3, \ldots, N$ eventually span the k-volume of most rapid expansion which then expands as (see [70] and [71])

$$\exp\left(\sum_{i=1}^{k} \lambda_i^1 t\right).$$

Projecting the evolved vectors $\{\mathbf{v}_1(j)\}_{i=1}^k$ onto the new orthogonal basis, produces the k-tuples $\{\gamma_i(j)\}_{i=1}^N$ and $\{\alpha_i(j)\}_{i=1}^N$ defined by

$$\gamma_i(j) := \langle \mathbf{v}_i(j), \mathbf{w}_i(j+1)\rangle, \qquad \alpha_i(j) := \ln|\gamma_i(j)|, \qquad i = 1, 2, \ldots, k.$$

It can be shown that

$$\frac{\|\mathbf{v}_1(j) \wedge \mathbf{v}_2(j) \wedge \cdots \wedge \mathbf{v}_k(j)\|}{\|\mathbf{w}_1(j) \wedge \mathbf{w}_2(j) \wedge \cdots \wedge \mathbf{w}_k(j)\|} = |\gamma_1(j)\gamma_2(j)\cdots\gamma_k(j)|,$$

for each j. Here $\mathbf{u} \wedge \mathbf{v}$ denotes the *Grassman product* of the two vectors $\mathbf{u}$ and $\mathbf{v}$ (see [755]). Using the definition for the (maximal) k-dimensional Lyapunov exponent

$$\begin{aligned} \lambda_1^k &= \lim_{M\to\infty} \frac{1}{M\tau} \sum_{j=1}^{L} \ln|\gamma_1(j)\gamma_2(j)\cdots\gamma_k(j)| \\ &= \lim_{M\to\infty} \frac{1}{M\tau} \sum_{j=1}^{L} (\alpha_1(j) + \alpha_2(j) + \ldots + \alpha_k(j)), \end{aligned}$$

together with the relationship [722]

$$\lambda_1^k = \lambda_1 + \lambda_2 + \ldots + \lambda_k,$$

produces

$$\lambda_i^1 = \lim_{M\to\infty} \frac{1}{M\tau} \sum_{j=1}^{M} \alpha_i(j), \qquad i = 1, 2, \ldots, k.$$

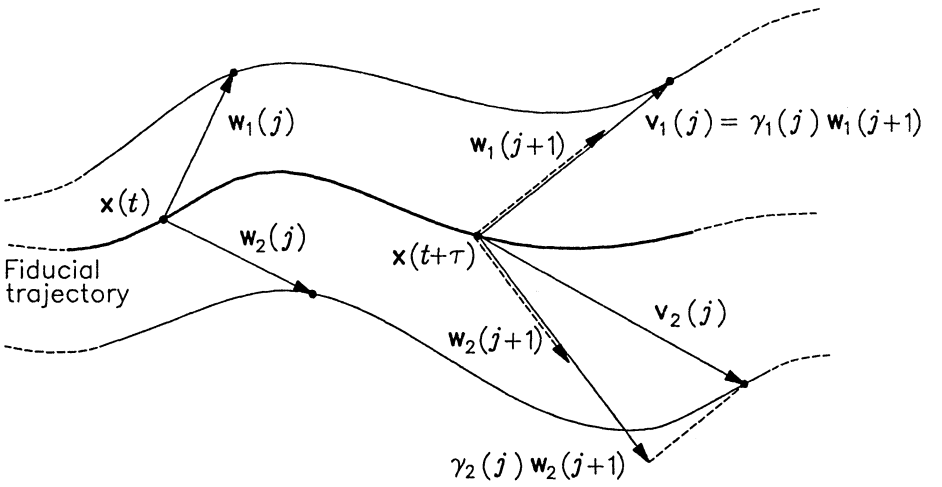

Figure 2.9: Illustration of the Gram-Schmidt orthogonalization procedure applied to a flow.

Thus averaging $\alpha_i(j)$ over j along the fiducial trajectory produces an estimate for the one-dimensional Lyapunov exponent λ_i^1. Here τ is the time interval between two successive Gram-Schmidt orthogonalizations and $\alpha_i(j)$ is referred to as the incremental expansion exponent of the i-th basis vector after the j-th renormalization. Figure 2.9 serves as an illustration of the renormalization procedure.

To wrap up, we notice that the first k vectors from the set $\{\mathbf{w}_i(j)\}_{i=1}^N$ facilitate a means of estimating the k largest one-dimensional Lyapunov exponents. The rate at which renormalization is performed (determined by τ) is not critical, so long as neither the magnitude divergences nor the orientation convergences have exceeded computer limits.

Example 2.47 For the Hénon map

$$\begin{pmatrix} x_{1,n+1} \\ x_{2,n+1} \end{pmatrix} = \begin{pmatrix} 1 - ax_{1,n}^2 + x_{2,n} \\ bx_{1,n} \end{pmatrix}$$

the associated variational equation is

$$\begin{pmatrix} y_{1,n+1} \\ y_{2,n+1} \end{pmatrix} = \begin{pmatrix} -2ax_{1,n} & 1 \\ b & 0 \end{pmatrix} \begin{pmatrix} y_{1,n} \\ y_{2,n} \end{pmatrix}.$$

Now, consider the case $a = 1.4$ and $b = 0.3$. Numerical calculation of the one-dimensional Lyapunov exponents produces

$$\lambda_1^1 \approx 0.4183, \qquad \lambda_2^1 \approx -1.6222.$$

■

Example 2.48 Consider the Lorenz system $d\mathbf{x}/dt = \mathbf{f}(\mathbf{x})$ given by

$$\begin{pmatrix} dx_1/dt \\ dx_2/dt \\ dx_3/dt \end{pmatrix} = \begin{pmatrix} -\sigma x_1 + \sigma x_2 \\ r x_1 - x_2 - x_1 x_3 \\ x_1 x_2 - b x_3 \end{pmatrix}.$$

The variational equation of the Lorenz system is

$$\begin{pmatrix} dy_1/dt \\ dy_2/dt \\ dy_3/dt \end{pmatrix} = \begin{pmatrix} -\sigma & \sigma & 0 \\ r - x_3 & -1 & -x_1 \\ x_2 & x_1 & -b \end{pmatrix} \begin{pmatrix} y_1 \\ y_2 \\ y_3 \end{pmatrix}.$$

For the case $(\sigma, r, b) = (16, 4, 40)$ numerical estimation of the one-dimensional Lyapunov exponent gives

$$\lambda_1^1 \approx 1.37, \quad \lambda_2^1 \approx 0.00, \quad \lambda_3^1 \approx -22.37.$$

The divergence of the vector field $\mathbf{f}(\mathbf{x})$ of the Lorenz model is

$$\mathrm{tr}\,(D\mathbf{f}(\mathbf{x})) \equiv \lambda_1^1 + \lambda_2^1 + \lambda_3^1 = -\sigma - b - 1 = -21.$$

■

Another technique for calculating the Lyapunov exponents is discussed by Shimada and Nagashima in [722]. The method proposed by Shimada and Nagashima calculates the maximal one-, two- up to N-dimensional Lyapunov exponents for an N-th order system.

2.7.2 Lyapunov Exponents from Time Series

Algorithm Description

In the previous section it was assumed that the dynamical equations of motion of the system under investigation are available. However, it often happens that the

system being studied is a physical system of which the equations of motion are not readily available. In such cases one usually has access to physical quantities of the system (e.g. its state variables). In order to study such a system numerically on a digital computer, the time evolution of these quantities must be sampled and stored in the computer memory. This sampled signal will be referred to as a *time series.* In this section a method will be described by which the spectrum of one-dimensional Lyapunov exponents of a system can be calculated from the time series of a single state variable. The method presented here is essentially the method as described in [691].

Consider an N-th order dynamical system (continuous or discrete). First suppose that we have access to the complete state vector $\mathbf{x} \in \mathbf{R}^N$ of the system. Let $\{\mathbf{x}_j\}_{j=1}^L$ denote the time series of the state vector along a post-transient trajectory of the system. Here L is some very large integer. Consider a small ball of radius ϵ, centred at the point $\mathbf{x}_j$, find any set of M points $\{\mathbf{x}_{k_i}\}_{i=1}^M$ included in the ball and let $\{\mathbf{y}_i\}_{i=1}^M$ be the set of vectors with

$$\mathbf{y}_i := \mathbf{x}_{k_i} - \mathbf{x}_j\,, \quad i = 1, 2, \ldots, M\,.$$

After evolution of a time interval $\tau = m\Delta t$ (with Δt the sampling period), the orbital point $\mathbf{x}_j$ will proceed to $\mathbf{x}_{j+m}$ and the neighbouring points $\{\mathbf{x}_{k_i}\}$ to $\{\mathbf{x}_{k_i+m}\}$. The displacement vector $\mathbf{y}_i$ thus evolves to

$$\mathbf{z}_i := \mathbf{x}_{k_i+m} - \mathbf{x}_{j+m},$$

for each $i = 1, 2, \ldots, M$. Choosing the radius ϵ of the ball (centred at $\mathbf{x}_j$) sufficiently small, the set $\{\mathbf{y}_i\}$ may be regarded as vectors in the tangent space $T_{\mathbf{x}_j}\mathbf{R}^N$ and $\{\mathbf{z}_i\}$ as the τ-evolved tangent vectors in $T_{\mathbf{x}_{j+m}}\mathbf{R}^N$ associated with $\{\mathbf{y}_i\}$ for a suitable m not too large. Thus we may write

$$\mathbf{z}_i = \mathbf{A}_j\mathbf{y}_i\,, \quad i = 1, 2, \ldots, M\,,$$

where $\mathbf{A}_j \in \mathbf{R}^{N\times N}$ and

$$\mathbf{A}_j \approx D\Phi(\tau; \mathbf{x}_j)\,.$$

The least squares estimate $\mathbf{A}_j$ of the linearized flow $D\Phi(\tau; \mathbf{x}_j)$ is obtained by solving

$$\min_{\mathbf{A}_j} J(\mathbf{A}_j), \qquad J(\mathbf{A}_j) := \frac{1}{M}\sum_{i=1}^{M} \|\mathbf{z}_i - \mathbf{A}_j\mathbf{y}_i\|_2^2\,,$$

J being the *cost function.* The least squares solution of this is given by (see Appendix C)

$$\mathbf{A}_j = \left(\sum_{i=1}^{M} \mathbf{z}_i\mathbf{y}_i^T\right)\left(\sum_{i=1}^{M} \mathbf{y}_i\mathbf{y}_i^T\right)^{-1}, \tag{2.64}$$

provided that $M \geq N$ and that there is no degeneracy. Thus (2.64) provides a method to estimate the linearized flow at each point $\mathbf{x}_j$ along the experimentally observed trajectory.

To estimate the spectrum of one-dimensional Lyapunov exponents we proceed as follows. Choose an arbitrary orthonormal basis say $\{\mathbf{w}_i(1)\}_{i=1}^N$. After the k-th iterate of the process ($k \geq 0$) we are at the point $\mathbf{x}_{km+1}$ on the trajectory. Using (2.64) we can estimate the linearized flow matrix $\mathbf{A}_{km+1}$ at $\mathbf{x}_{km+1}$. Using the orthonormal basis $\{\mathbf{w}_i(k+1)\}_{i=1}^N$ of the tangent space $T_{\mathbf{x}_{km+1}}\mathbf{R}^N$, we can calculated its τ-evolution $\{\mathbf{v}_i(k+1)\}_{i=1}^N$ from

$$\mathbf{v}_i(k+1) = \mathbf{A}_{km+1}\mathbf{w}_i(k+1).$$

Now, applying the Gram-Schmidt orthogonalization procedure to renormalize $\{\mathbf{v}_i(k+1)\}_{i=1}^N$ we obtain the orthonormal basis $\{\mathbf{w}_i(k+2)\}_{i=1}^N$ in the tangent space $T_{\mathbf{x}_{(k+1)m+1}}\mathbf{R}^N$. The incremental expansion exponents for the time evolution from $\mathbf{x}_{km+1}$ to $\mathbf{x}_{(k+1)m+1}$ along the trajectory measured along the axes of the basis $\{\mathbf{w}_i(k+2)\}_{i=1}^N$ are given by

$$\alpha_i(k+1) = \ln|\langle \mathbf{v}_i(k+1), \mathbf{w}_i(k+2)\rangle|, \quad i = 1, 2, \ldots, N.$$

The process must be repeated for $k = 0, 1, 2, \ldots, K$, (K large, but $Km \leq L$) where we assume some arbitrary orthonormal basis $\{\mathbf{w}_i(1)\}_{i=1}^N$ at step $k = 0$. After completion of the above process, the spectrum of one-dimensional Lyapunov exponents $\{\lambda_i^1\}_{i=1}^N$ can be estimated from the set of exponents of incremental expansion $\{\alpha_i(j)\}_{i,j}$ as follows:

$$\lambda_i^1 = \frac{1}{Km\Delta t}\sum_{j=1}^{K}\alpha_i(j), \quad i = 1, 2, \ldots, N.$$

If the time series $\{\mathbf{x}_j\}$ is generated by a map which was not derived from a continuous-time system then one should set $\Delta t = 1$.

So far we have assumed that the complete state vector is accessible. Next, we assume that only a single *observable* (in the control theoretical sense) state variable x is accessible and produces the time series $\{x_j\}$. The state space may be reconstructed by the method of *delay coordinate embedding* (see [609]), as follows

$$\mathbf{x}_i := \left(x_i,\, x_{i-r},\, \ldots,\, x_{i-(d-1)r}\right)^T, \qquad i = 1, 2, 3, \ldots,$$

where $\mathbf{x}_i \in \mathbf{R}^d$ and d is a positive integer. Here the delay time t_d was taken to be $t_d = r\Delta t$ with r a positive integer.

Usually the actual dimension N is unknown and d has to be guessed. Takens [784] showed that for $d \geq 2N$, the reconstructed state space attractor is diffeomorphic to the actual state space attractor of the system. One problem that arises when d is chosen too large, is that the spectrum of one-dimensional Lyapunov exponents contains spurious Lyapunov exponents in addition to the true Lyapunov exponents. In this regard refer to [620] and [772] for a detailed discussion. In the paper [1] two methods of determining the dimension of the underlying dynamics are presented.

Once the time series $\{\mathbf{x}_j\}$ is generated by means of the time delay coordinate embedding, the algorithm as described for the previous case may be used to estimate the spectrum of one-dimensional Lyapunov exponents.

Various other methods for estimating the one-dimensional Lyapunov exponents from time series may be found in the literature. Some estimate only the maximal one-dimensional Lyapunov exponent, for example [196]. In [860] a method is devised for estimating only the non-negative Lyapunov exponents (of dimension 1 and higher) from a time series. Also included in this article is a FORTRAN program listing. Another Jacobian method which uses the QR decomposition for calculating the spectrum of one-dimensional Lyapunov exponents was proposed by Eckmann and coworkers in [230]. A comparison of different QR decomposition based methods for computing Lyapunov exponents was conducted in [269].

Implementation of the Algorithm

We have implemented the algorithm for calculating the spectrum of one-dimensional Lyapunov exponents (as described in the previous section) in MATLAB. This program is listed in Appendix D. The program takes as input, a vector time series, that is, state space reconstruction must be performed prior to invoking this routine. This gives the flexibility to provide the program with a vector time series of reconstructed states or actual states of the system being studied. In the program an upper limit is imposed on M, the number of members found in the ϵ-neighbourhood of the point under consideration. The upper limit on M is 20. This means that the search for a neighbouring point stops when either the data record is exhausted or when $M = 20$. In the case when the data record is exhausted and $M \geq N$, then the algorithm is executed as described in the previous section. However if $M \leq N$, to prevent ill-conditioning, the program then doesn't calculate the linearized flow matrix under these circumstances. Instead it uses the linearized flow matrix calculated in the previous iteration. Only when a point is found for which $M \geq N$, is the linearized flow matrix calculated again. Although this is a crude approximation, it still provides a better estimate than would be obtained with the ill-conditioned data. On the other hand, this happens infrequently and hence these rough approximations are removed by the filtering effect of averaging.

As far as the performance is concerned, the estimated values of the Lyapunov exponents seem to be very sensitive to the choice of the evolution time $\tau = m\Delta t$ between the linearized flow matrix estimation, the neighbourhood radius ϵ and even the choice of neighbours in the ϵ-neighbourhoods used for the estimation of the linearized flow matrices.

A MATLAB routine to generate a reconstructed state vector time series from a given scalar time series by means of delay coordinate embedding is listed in Appendix D. The reconstructed state vector time series is then used in conjunction with the MATLAB program described earlier to estimate the Lyapunov exponents.

To choose the parameters K, Δt, ϵ and m, great care must be taken to ensure that the estimates of the Lyapunov exponents are representative. K should be chosen large,

say $K \geq 1000$ to ensure sufficient averaging of the varying incremental expansion exponents. As far as Δt is concerned, it should be small enough to ensure that:

i) The evolved basis vectors produce a well-conditioned evolved basis matrix (i.e. the matrix containing the evolved basis vectors as its columns). This is essential for the proper operation of the Gram-Schmidt orthogonalization procedure which doesn't produce an orthogonal basis if the previous evolved basis is ill-conditioned. We have found that even the *modified Gram-Schmidt orthogonalization* (MGSO) procedure breaks down for a severely ill-conditioned evolved basis.

ii) Also, by the nature of our estimation technique $\tau = m\Delta t$ must be small enough so that the evolved difference vectors may still be considered to be tangent vectors.

The above arguments also apply to the choice of m. The choice of ϵ must also be such that the difference vectors and their respective evolved counter parts qualify as tangent vectors.

2.8 Shil'nikov's Method

We restrict our attention to three-dimensional dissipative continuous systems and only to homoclinic trajectories. There are also results concerning Shil'nikov's method for higher dimensional systems, for nondissipative systems and for heteroclinic trajectories, but these will not be discussed here. For results on nondissipative systems, the reader is referred to [852], while for results concerning heteroclinic trajectories the reader should consult [203].

For the case of a homoclinic trajectory, the basic idea behind Shil'nikov's method is to construct a Poincaré map from two constituent maps: one which corresponds to the linearized flow near the associated fixed point and another which describes the behaviour in a neighbourhood of the homoclinic trajectory away from the fixed point. This Poincaré map is termed the *Shil'nikov map*. If the Shil'nikov map behaves qualitatively the same as the Smale horseshoe map, then the Shil'nikov map exhibits horseshoe chaos and hence the original third-order system is chaotic.

Consider the third-order autonomous dynamical system

$$\frac{d\mathbf{x}}{dt} = \mathbf{f}(\mathbf{x}), \qquad t \in \mathbf{R}, \quad \mathbf{x} \in \mathbf{R}^3, \tag{2.65}$$

where the vector field $\mathbf{f} : \mathbf{R}^3 \to \mathbf{R}^3$ is of class C^p, $(p \geq 1)$.

Theorem 2.49 (Shil'nikov Theorem) Consider a third-order autonomous system described by (2.65), where $\mathbf{f}$ is a C^2 vector field on $\mathbf{R}^3$. Let $\mathbf{x}^*$ be a fixed point for (2.65). Suppose that:

i) The fixed point $\mathbf{x}^*$ is a saddle focus, whose characteristic exponents are of the form

$$\gamma, \quad \sigma \pm j\omega, \quad \gamma, \sigma, \omega \in \mathbf{R},$$

with $\omega \neq 0$, and satisfy the *Shil'nikov inequality*, that is,

$$|\gamma| > |\sigma| > 0.$$

ii) There exists a homoclinic trajectory $\mathcal{H}$ based at $\mathbf{x}^*$.

Then

i) The Shil'nikov map defined in a neighbourhood of $\mathcal{H}$ possesses a countable number of Smale horseshoes in its discrete dynamics.

ii) For any sufficiently small C^1-perturbation $\mathbf{g}$ of $\mathbf{f}$, the perturbed system

$$\frac{d\mathbf{x}}{dt} = \mathbf{g}(\mathbf{x}), \quad \mathbf{x} \in \mathbf{R}^3, \tag{2.66}$$

has at least a finite number of Smale horseshoes in the discrete dynamics of the Shil'nikov map defined near $\mathcal{H}$.

iii) Both the unperturbed system (2.65) and the perturbed system (2.66) exhibit horseshoe chaos.

■

Remarks

i) Conclusions (ii) and (iii) of Theorem 2.49 indicate what is called the *structural stability property* of horseshoe chaos, that is, it remains in existence despite minor perturbations in the vector field. This has important implications for both the numerical and experimental investigation of chaos, since the environmental parameters in these contexts do vary with time and are known to only a finite precision. However, unlike horseshoe chaos, the existence of the homoclinic trajectory itself is *not* guaranteed to be structurally stable.

ii) The inequality $|\gamma| > |\sigma|$ in the Shil'nikov inequality is crucial, in the sense that if it is reversed, the Smale horseshoes disappear and chaos is extinguished. The boundary $|\sigma| = \gamma$ is the *bifurcation point* between regular and chaotic behaviour.

iii) Perhaps the most difficult aspect of applying Shil'nikov's method is the rigorous establishment of the existence of a homoclinic trajectory for the system (2.65).

Shil'nikov's method has also been extended to piecewise-C^2 vector fields for which the fixed point $\mathbf{x}^*$ is in the interior of one of the domains and the homoclinic trajectory $\mathcal{H}$ is bounded away from all other fixed points and is not tangent to any of the boundary surfaces [805].

Example 2.50 [203] Study the dimensionless form of the state equations for Chua's circuit, namely

$$\begin{aligned} \frac{dx_1}{dt} &= \alpha(x_2 - x_1 - f(x_1)), \\ \frac{dx_2}{dt} &= x_1 - x_2 + x_3\,, \\ \frac{dx_3}{dt} &= -\beta x_2\,, \end{aligned}$$

where

$$f(x) := \begin{cases} bx - a + b, & \text{if} \quad x \leq -1 \\ ax, & \text{if} \quad |x| \leq 1 \\ bx + a - b, & \text{if} \quad x \geq 1 \end{cases},$$

with α, β, a and b parameters of the system.

The system possesses three distinct saddle foci, one in the interior of each domain, namely

$$\mathbf{x}^*_{-1} := (-k, 0, k)^T\,, \quad \mathbf{x}^*_0 := (0,0,0)^T\,, \quad \mathbf{x}^*_1 := (k, 0, -k)^T\,,$$

with $k := (b-a)/(b+1)$ and $b \neq -1$. Because of the piecewise-linear nature of the vector fields, a precise analysis of the qualitative dynamics in each domain is tenable. This, together with the parameterization of the vector fields, makes it possible to establish formally the existence of an odd-symmetrically related pair of homoclinic trajectories $\mathcal{H}^{\mp}$ based at the origin. This nontrivial task was first performed in [154]. For the following parameter values

$$\alpha = 11.5996022\,, \quad \beta = 15\,, \quad a = -1.142857143\,, \quad b = -0.7142857143\,,$$

a homoclinic trajectory based at the origin was calculated numerically [203]. For the above parameter values the eigenvalues of the origin are

$$\gamma \approx 2.9399\,, \qquad \sigma \pm j\omega \approx -1.1414 \pm j2.6743\,,$$

thus satisfying the Shil'nikov inequality. An application of the homoclinic Shil'nikov method to this system then proves the existence of horseshoe chaos in Chua's circuit. ■

2.9 Symbolic Dynamics

The method of *symbolic dynamics* consists of finding a one-to-one correspondence between the dynamics of the dynamical system under investigation and the dynamics of the so-called shift map (to be defined later) on a subset of the sequence space associated with some set of symbols. This technique appears to have originally been applied by Hadamard [320] to study geodesics on surfaces of negative curvature and Birkhoff [82], [80] in his studies of dynamical systems. However, the first exposition of symbolic dynamics as an independent subject was given by Morse and Hedlund [560]. Levinson used these ideas in his work on the forced Van der Pol equation (see [479]), which inspired Smale to construct the horseshoe map (see [747], [744]). In [15] to [17], Alekseev gives a systematic account of the technique and applies it to problems arising from celestial mechanics. Many other references regarding symbolic dynamics and its applications can be found in the bibliographies of the above mentioned references and of [561]. In recent times there has been a flood of applications of this technique. In the sequel, we first introduce the necessary definitions, followed by results on the dynamics of the shift map. Finally an example illustrating the application of symbolic dynamics will be presented. Several applications of symbolic dynamics appear in later chapters.

Let $S := \{1, 2, \ldots, N\}$ ($N \in \{2, 3, 4, \ldots\}$) be our collection of symbols. As will become clear later, S may actually be any set of N distinct symbols. The sequence space Σ^N associated with S is defined by

$$\Sigma^N := \cdots \times S \times S \times \cdots = \prod_{i=-\infty}^{\infty} S .$$

Thus Σ^N contains all bi-infinite sequences of symbols of S. For convenience, an element s of Σ^N will be written as

$$s = \cdots s_{-2} s_{-1} . s_0 s_1 s_2 \cdots , \qquad s_i \in S ,$$

for each $i \in \mathbf{Z}$. It often suffices to consider only one-sided sequences. In this case Σ^N represents the set of all one-sided sequences, that is,

$$s \in \Sigma^N \iff s = s_0 s_1 s_2 \cdots , \quad s_i \in S ,$$

for each $i \in \mathbf{N}_0$. Defining the function $d : \Sigma^N \times \Sigma^N \to [0, \infty)$, by

$$d(s, u) := \sum_{i=-\infty}^{\infty} \frac{1}{2^{|i|}} \frac{|s_i - u_i|}{1 + |s_i - u_i|} , \tag{2.67}$$

we then have the following result.

Proposition 2.51 The pair $\left(\Sigma^N, \alpha\right)$ with d defined by (2.67) is a metric space which is compact, totally disconnected and perfect in a topological sense.

Proof: Refer to [853]. ■

Lemma 2.52 For $s, u \in \Sigma^N$:

i) If $d(s,u) < 1/2^{M+1}$, $M \in \mathbf{N}$ then $s_i = u_i$ for all $|i| \leq M$;

ii) If $s_i = u_i$ for $|i| \leq M$ then $d(s,u) \leq 1/2^{M-1}$.

Proof: See [853]. ■

Now that we have established the structure of Σ^N, we wish to define the shift map.

Definition 2.53 The map $\sigma : \Sigma^N \to \Sigma^N$ defined

$$s = \cdots s_{-2}s_{-1}.s_0s_1s_2\cdots \mapsto \sigma(s) := \cdots s_{-2}s_{-1}s_0.s_1s_2s_3\cdots ;$$

or $[\sigma(s)]_i = s_{i+1}$, is termed the *shift map.* ■

When the domain of σ is taken to be Σ^N it is often referred to as the *full shift on N symbols.*

Proposition 2.54 The shift map σ has the following properties:

i) σ is surjective;

ii) σ is continuous.

Proof: See [853]. ■

The dynamical properties of the shift map is described by the following proposition.

Proposition 2.55 The shift map σ has

i) a countable infinity of periodic orbits consisting of orbits of all periods,

ii) an uncountable infinity of nonperiodic orbits, and

iii) a dense orbit.

Proof: See [853]. ■

The shift map $\sigma : \Sigma^N \to \Sigma^N$ has N fixed points, namely

$$s_i^* = \cdots ii.iii \cdots, \quad i = 1, 2, 3, \ldots, N.$$

Proposition 2.56 The shift map σ is chaotic.

Proof: We first prove that σ has sensitive dependence on initial conditions. Suppose that $s, u \in \Sigma^N$ such that

$$\frac{1}{2^{M+1}} < d(s,u) < \frac{1}{2^M},$$

for some $M \in \mathbf{N}$. Then by Lemma 2.52 ((i) and the contrapositive of (ii)) we see that $s_i \neq u_i$ for some $M \leq |i| \leq M+2$, that is, either $M \leq i \leq M+2$ or $-(M+2) \leq i \leq -M$. Obviously the latter is not of interest, since by choosing $s, u \in \Sigma^N$ such that they agree everywhere except at the $-M$-th position, we see that under iteration of σ, $d(s,u)$ decreases monotonically, and therefore we consider only the case $M \leq i \leq M+2$. Then $[\sigma(s)]_i \neq [\sigma(u)]_i$ for some $M-1 < i \leq M+1$ and hence

$$\frac{1}{2^M} < d(\sigma(s), \sigma(u)) < \frac{1}{2^{M-1}}.$$

Applying the above argument iteratively, we have that

$$\frac{1}{2^{M-k+1}} < d\left(\sigma^{(k)}(s), \sigma^{(k)}(u)\right) < \frac{1}{2^{M-k}}, \qquad k = 1, 2, 3, \ldots, M,$$

and hence $d\left(\sigma^{(k)}(s), \sigma^{(k)}(u)\right)$ grows monotonically for $k = 1, 2, \ldots, M$. Thus the shift map σ has sensitive dependence on initial conditions.

The topological transitivity follows from the fact that σ has a dense orbit as stated by Proposition 2.54(iii) (see [217]).

If $s \in \Sigma^N$ is an arbitrary periodic point of σ, then we can construct periodic points of differing periods arbitrarily close (with respect to the metric d defined earlier) to s. For example, let $u = \cdots u_{-2}u_{-1}.u_0u_1u_2 \cdots$ be defined by

$$\begin{aligned}
u_i &:= s_i && \text{for each} \quad |i| \leq M, \\
u_{-(M+1)} &= u_{M+1} := k, && \text{for some} \quad k \in S, \quad k \neq s_{M+1}, \\
u_i &:= u_{i-2(M+1)}, && \text{for each} \quad i > M+1, \\
u_i &:= u_{i+2(M+1)}, && \text{for each} \quad i < -M-1,
\end{aligned}$$

where $M \in \mathbf{N}$ was chosen arbitrarily. Then $u \in \Sigma^N$ is a period-$2(M+1)$ point of σ and by Lemma 2.52(ii) we have $d(s,u) \leq 1/2^{M-1}$. Since M was chosen arbitrarily we conclude that the periodic points of σ are dense in Σ^N. Thus by Definition A.49 σ is chaotic. ■

Example 2.57 [217] Consider the logistic map f (refer to (2.5)) for $r > 2+\sqrt{5}$. For this case the iterates of the logistic map tend to $-\infty$ for all points except those points in the Cantor set Λ (see [217]). Now let

$$I_1 := \{x \in [0,1/2] | \, f(x) \leq 1\}, \quad I_2 := \{x \in [1/2,1) | \, f(x) \leq 1\},$$

and define the mapping $h : \Lambda \to \Sigma^2$ as follows. For $x \in \Lambda$,

$$h(x) := s_0 s_1 s_2 \cdots,$$

where

$$s_j := \begin{cases} 1 & \text{if } f^{(j)}(x) \in I_1 \\ 2 & \text{if } f^{(j)}(x) \in I_2 \end{cases}.$$

In [217] the mapping h is shown to be a homeomorphism. Consequently f is topologically conjugate to the shift map σ via h, and therefore the logistic map is chaotic for $r > 2+\sqrt{5}$. ■

Up to now we have assumed that all symbol sequences in Σ^N are admissible. In what follows, we discuss the restriction of the shift map σ to subsets of Σ^N.

Definition 2.58 Let $\mathbf{A} \in \mathbf{R}^{N \times N}$ be a matrix constructed according to the following rule: $(\mathbf{A})_{i,j} = 1$ if the ordered pair of symbols ij may appear in an admissible symbol sequence, and $(\mathbf{A})_{i,j} = 0$ if the ordered pair of symbols ij may not appear in an admissible symbol sequence. The matrix $\mathbf{A}$ is called the *transition matrix* and the set of all admissible symbol sequences is denoted by $\Sigma^N_{\mathbf{A}}$, that is,

$$\Sigma^N_{\mathbf{A}} := \left\{ \{\cdots s_{-2} s_{-1} . s_0 s_1 s_2 \cdots\} \in \Sigma^N \middle| \, (\mathbf{A})_{s_i, s_{i+1}} = 1, \text{ for each } i \in \mathbf{Z} \right\}.$$

■

The restriction of σ to $\Sigma^N_{\mathbf{A}}$, namely $\sigma|\Sigma^N_{\mathbf{A}}$ is called the *subshift map* of finite type. Usually the symbol σ is used for both versions of the shift map.

Definition 2.59 The transition matrix $\mathbf{A}$ is said to be *irreducible* if there is a $k \in \mathbf{N}$ such that $(\mathbf{A}^k)_{i,j} \neq 0$ for each $1 \leq i, j \leq N$. ■

In essence, Definition 2.59 states that a transition matrix $\mathbf{A}$ is irreducible if for some $k \in \mathbf{N}$ a transition from any symbol $s_1 \in S$ to any symbol $s_2 \in S$ can be made in k iterates of the subshift map σ. It is easy to show that this transition can be made in $(\mathbf{A})_{s_1, s_2}$ distinct ways.

Definition 2.60 Let $\mathbf{A}$ be a transition matrix and let $s_1 s_2 s_3 \cdots s_k$, $s_i \in S$, $i = 1, \ldots, k$, be a finite string of symbols of length k for some $k \in \mathbf{N}$. Then we call $s_1 s_2 s_3 \cdots s_k$ an *admissible string of length* k if $(\mathbf{A})_{s_i, s_{i+1}} = 1$, for $i = 1, \ldots, k-1$. ■

Lemma 2.61 Suppose $\mathbf{A}$ is an irreducible transition matrix and let $K > 0$ be the smallest integer such that $(\mathbf{A}^K)_{i,j} \neq 0$ for all $1 \leq i, j \leq N$. Then, given any $i, j \in S$, there exists an admissible string of length $k \leq K - 1$, such that $i s_1 s_2 \cdots s_k j$ is an admissible string of length $k + 2$.

Proof: See [852]. ■

The next proposition presents some results concerning the topological structure of the sequence space $\Sigma_{\mathbf{A}}^N$.

Proposition 2.62 Suppose $\mathbf{A}$ is an irreducible transition matrix. Then the metric space $(\Sigma_{\mathbf{A}}^N, d)$ (where d is defined by (2.67)) is compact, totally disconnected and perfect.

Proof: See [852]. ■

Next we present propositions describing the dynamical structure of the subshift map.

Proposition 2.63 Suppose $\mathbf{A}$ is an irreducible transition matrix. Then the subshift map σ has:

i) a countable infinity of periodic orbits in $\Sigma_{\mathbf{A}}^N$,

ii) an uncountable infinity of nonperiodic orbits in $\Sigma_{\mathbf{A}}^N$, and

iii) a dense orbit in $\Sigma_{\mathbf{A}}^N$.

Proof: The reader is referred to [852] for the proof. ■

Proposition 2.64 Suppose that $\mathbf{A}$ is an irreducible transition matrix. Then the subshift map σ is chaotic on $\Sigma_{\mathbf{A}}^N$.

Proof The proof is similar to the proof of Proposition 2.56 and is therefore omitted. ■

Example 2.65 [440] The dynamics of a (zero input) second-order digital filter (realized in direct form) with an overflow nonlinearity is described by the nonlinear map $\mathbf{f} : J^2 \to J^2$ (where $J := [-1, 1]$), defined by

$$\mathbf{f}(\mathbf{x}) := \begin{pmatrix} x_2 \\ g(bx_1 + ax_2) \end{pmatrix}, \quad \mathbf{x} := (x_1, x_2)^T, \quad a \in \mathbf{R}, \quad b = -1, \tag{2.68}$$

(see Section 4.3) where the overflow property of the accumulator is described by the map

$$g : \mathbf{R} \to J, \quad g(y) := (y + 1) \,(\mathrm{mod}\, 2) - 1 .$$

As shown in Section 4.3, $\mathbf{f}$ may be written in the form

$$\mathbf{f}(\mathbf{x}) = \begin{pmatrix} 0 & 1 \\ -1 & a \end{pmatrix} \begin{pmatrix} x_1 \\ x_2 \end{pmatrix} + \begin{pmatrix} 0 \\ 2 \end{pmatrix} v \; = \; \mathbf{A}\mathbf{x} + \mathbf{B}v , \tag{2.69}$$

where

$$\mathbf{A} := \begin{pmatrix} 0 & 1 \\ -1 & a \end{pmatrix}, \quad \mathbf{B} := \begin{pmatrix} 0 \\ 2 \end{pmatrix}, \quad v := -\left\lfloor \frac{-x_1 + ax_2}{2} + \frac{1}{2} \right\rfloor .$$

The eigenvalues of $\mathbf{A}$ are $q_{1,2} = (a \pm \sqrt{a^2 - 4})/2$. The integer v is the vertical translation required to return a point to the phase space J^2. We have thus transformed the nonlinear autonomous system (2.68) into a linear nonautonomous system where v is the input drive which depends on the state of the system. The integer v may assume any value in the set

$$\{-l_1, \ldots, -1, 0, 1, \ldots, l_1\},$$

where $l_1 > 0$ is the least integer such that

$$2l_1 - 1 \leq \sup_{\mathbf{x} \in J^2} \|\mathbf{A}\mathbf{x}\|_\infty < 2l_1 + 1 .$$

Observe that $\mathbf{f}$ is a bijection (see [158]) with inverse

$$\mathbf{f}^{-1}(\mathbf{x}) = \begin{pmatrix} a & -1 \\ 1 & 0 \end{pmatrix} \begin{pmatrix} x_1 \\ x_2 \end{pmatrix} + \begin{pmatrix} 2 \\ 0 \end{pmatrix} w , \qquad w := -\left\lfloor \frac{ax_1 - x_2 + 1}{2} \right\rfloor , \tag{2.70}$$

and

$$w \in \{-l_2, \ldots, -1, 0, 1, \ldots, l_2\} ,$$

where $l_2 > 0$ is the least integer satisfying

$$2l_2 - 1 \leq \sup_{\mathbf{x} \in J^2} \|\mathbf{A}^{-1}\mathbf{x}\|_\infty < 2l_2 + 1 .$$

It follows that $l := l_1 = l_2$.

Next we define partitions of the phase space J^2 by

$$\begin{aligned} I_m &:= \left\{ \mathbf{x} \in J^2 \,\middle|\, \left\lfloor \frac{-x_1 + ax_2 + 1}{2} \right\rfloor = m \right\} \\ &= \left\{ \mathbf{x} \in J^2 \,\middle|\, 2m - 1 \leq -x_1 + ax_2 < 2m + 1 \right\}, \end{aligned}$$

and

$$\begin{aligned} J_m &:= \left\{ \mathbf{x} \in J^2 \,\middle|\, \left\lfloor \frac{ax_1 - x_2 + 1}{2} \right\rfloor = m \right\} \\ &= \left\{ \mathbf{x} \in J^2 \,\middle|\, 2m - 1 \leq ax_1 - x_2 < 2m + 1 \right\}, \end{aligned}$$

for $m = 0, \pm 1, \pm 2, \ldots, \pm l$.

Define Σ as the set of all bi-infinite sequences of symbols from the set

$$S := \{-l, \ldots, -1, 0, 1, \ldots, l\}.$$

Given an initial condition $\mathbf{x} \in J^2$ we define the map $h : J^2 \to \Sigma$ by

$$\mathbf{x} \mapsto h(\mathbf{x}) = \cdots s_{-2} s_{-1} . s_0 s_1 s_2 \cdots =: s,$$

where

$$s_i := \begin{cases} -m & \text{for } \mathbf{f}^{(i)}(\mathbf{x}) \in I_m \text{ if } i \geq 0 \\ -n & \text{for } \mathbf{f}^{(i)}(\mathbf{x}) \in J_n \text{ if } i < 0 \end{cases},$$

The map h is clearly well-defined. Let $\Sigma_{\mathbf{f}} := h(J^2)$ and hence the sequence s is admissible if $s \in \Sigma_{\mathbf{f}}$.

Now we rewrite (2.69) and (2.70) as second order difference equations, respectively

$$x_{2,n+1} - ax_{2,n} + x_{2,n-1} = 2s_n, \quad \text{if } n \geq 0, \tag{2.71}$$

$$x_{2,n-2} + x_{2,n} - ax_{2,n-1} = 2s_{n-1}, \quad \text{if } n < 0. \tag{2.72}$$

It is clear that the orbit $\{x_{2,n}\}$ and the symbol sequence $\{s_n\}$ are uniquely determined for the given initial conditions $x_{2,0}$ and $x_{2,-1}$. Thus, for $n \geq 0$

$$s_n = -\left\lfloor \frac{ax_{2,n} - x_{2,n-1} + 1}{2} \right\rfloor, \qquad x_{2,n+1} = ax_{2,n} - x_{2,n-1} + 2s_n,$$

while for $n \leq 0$

$$s_n = -\left\lfloor \frac{-x_{2,n} + ax_{2,n-1} + 1}{2} \right\rfloor, \qquad x_{2,n-2} = -x_{2,n} + ax_{2,n-1} + 2s_{n-1}.$$

We can now state conditions for an admissible sequence to determine a unique orbit for (2.68).

Proposition 2.66 [440] If $|a| > 2$ then $|q_1| \neq 1$, $|q_2| \neq 1$ and any admissible sequence determines a unique orbit of (2.68). Explicitly, the orbit identified with the sequence $s = \ldots s_{-2}s_{-1}.s_0 s_1 s_2 \ldots \in \Sigma_{\mathbf{f}}$ is given by the convolution sum

$$x_{2,n} = \sum_{k=-\infty}^{\infty} x_{n-k} s_k \,,$$

where $\{x_n\}$ is the impulse response of the system (2.71) and (2.72) given by

$$x_n = \frac{2}{\sqrt{a^2-4}} \rho^{|n|} \,, \qquad \rho := \min(q_1, q_2) \,.$$

Proof: Refer to [440]. □

In [158] it is shown that if $|a| \leq 2$ then the map h is neither injective nor surjective. Consequently by Propositions 2.64 and 2.66 it follows that (2.68) is chaotic for $|a| > 2$. The case $|a| \leq 2$ is discussed in Section 4.3. ■

In [313] Guckenheimer applied the method of symbolic dynamics to the Van der Pol equation to give a topological characterization of the set of aperiodic solutions for parameter values for which the equation appears structurally stable.

2.10 Power Spectral Density

Consider a real N-dimensional continuous-time stochastic process $\mathbf{x}(t)$ (see [612], [349]). (More precisely, $\mathbf{x}$ is one sample function of the stochastic process.) In the sequel it will be assumed that $\mathbf{x}(t)$ is stationary in the wide sense i.e. the probability density function $\rho_{\mathbf{x}(t)}$ and the joint probability density function $\rho_{\mathbf{x}(t+\tau),\mathbf{x}(t)}$ are independent of time t. The *probabilistic autocorrelation function* of $\mathbf{x}(t)$ is defined by

$$\mathbf{R}_{\mathbf{xx}}(\tau) := E\left[\mathbf{x}(t+\tau)\mathbf{x}^T(t)\right] \,,$$

with

$$E\left[\mathbf{x}(t+\tau)\mathbf{x}^T(t)\right] := \int_{-\infty}^{\infty} \cdots \int_{-\infty}^{\infty} \rho_{\mathbf{x}(t+\tau),\mathbf{x}(t)}(\boldsymbol{\xi}, \boldsymbol{\eta}) \boldsymbol{\xi}\boldsymbol{\eta}^T \, d\xi_1 \cdots d\xi_N \, d\eta_1 \cdots d\eta_N \,,$$

or alternatively, using $E[\mathbf{x}] := (E[x_1], \ldots, E[x_N])^T$, we have

$$E[x_i(t+\tau)x_j(t)] := \int_{-\infty}^{\infty} \int_{-\infty}^{\infty} \widetilde{\rho}_{x_i(t+\tau),x_j(t)}(\xi_i, \eta_j) \, d\xi_i \, d\eta_j \,,$$

for each $i, j = 1, 2, \ldots, N$, where $\widetilde{\rho}_{x_i(t+\tau),x_j(t)}$ is the induced joint probability density function of $x_i(t+\tau)$ and $x_j(t)$, given by

$$\widetilde{\rho}_{x_i(t+\tau),x_j(t)}(\xi_i, \eta_j) := \int_{-\infty}^{\infty} \cdots \int_{-\infty}^{\infty} \rho_{\mathbf{x}(t+\tau),\mathbf{x}(t)}(\boldsymbol{\xi}, \boldsymbol{\eta})\, d\xi_1 \cdots \widehat{d\xi_i} \cdots \widehat{d\eta_j} \cdots d\eta_N\,,$$

for each $i, j, = 1, 2, \ldots, N$. Here $\widehat{d\xi_i}$ and $\widehat{d\eta_j}$ indicate that the integrals corresponding to $d\xi_i$ and $d\eta_j$ respectively are omitted. If in addition we assume the stochastic process $\mathbf{x}(t)$ is ergodic (i.e. time-average and ensemble averages coincide, [612]), then the probabilistic and time autocorrelation functions are equal, namely,

$$\mathbf{R}_{\mathbf{xx}}(\tau) = \lim_{\widetilde{T}\to\infty} \frac{1}{2\widetilde{T}} \int_{-\widetilde{T}}^{\widetilde{T}} \mathbf{x}(t+\tau)\mathbf{x}^T(\tau)\, dt\,,$$

and the *Power Spectral Density* (PSD) of $\mathbf{x}(t)$ is time-invariant and is defined by

$$\mathbf{S}_{\mathbf{xx}}(\omega) := \int_{-\infty}^{\infty} \mathbf{R}_{\mathbf{xx}}(\tau) \mathrm{e}^{-j\omega\tau}\, d\tau\,, \qquad j := \sqrt{-1}\,.$$

In the case of a real N-dimensional discrete-time stochastic process $\mathbf{x}_n$ which is both wide-sense stationary and ergodic, the autocorrelation function of $\mathbf{x}_n$ is given by

$$\mathbf{R}_{\mathbf{xx}}(m) = \lim_{M\to\infty} \frac{1}{2M-1} \sum_{i=-M}^{M} \mathbf{x}_{i+m}\mathbf{x}_i^T\,, \tag{2.73}$$

and the power spectral density is given by

$$\mathbf{S}_{\mathbf{xx}}(\omega) = \sum_{k=-\infty}^{\infty} \mathbf{R}_{\mathbf{xx}}(k)\mathrm{e}^{-j\omega k}, \qquad -\pi \le \omega \le \pi\,. \tag{2.74}$$

The power spectral density of a signal may contain line components (which are the result of periodic components of the signal) and a continuous component (which is the result of the aperiodic component of the signal) as described in [92]. The properties of the autocorrelation function and the power spectral density are listed in [349], [348].

Example 2.67 Calculate the autocorrelation function and the power spectral density function for the scalar signal

$$x(t) = A\cos(\omega_0 t + \theta)\,,$$

where $A, \omega \in \mathbf{R}^+$ and $\theta \in [0, 2\pi)$.

The time-average autocorrelation function of $x(t)$ is

$$\begin{aligned} R_{xx}(\tau) &= \lim_{\widetilde{T}\to\infty} \frac{1}{2\widetilde{T}} \int_{-\widetilde{T}}^{\widetilde{T}} A^2 \cos(\omega_0 t + \omega_0 \tau + \theta) \cos(\omega_0 t + \theta)\, dt \\ &= \lim_{\widetilde{T}\to\infty} \frac{A^2}{4\widetilde{T}} \int_{-\widetilde{T}}^{\widetilde{T}} (\cos \omega_0 \tau + \cos(2\omega_0 t + \omega_0 \tau + \theta))\, dt \\ &= \frac{A^2}{2} \cos \omega_0 \tau \,. \end{aligned} \tag{2.75}$$

Taking the Fourier transform of (2.75) yields

$$S_{xx}(\omega) = \frac{A^2}{4}\delta(\omega - \omega_0) + \frac{A^2}{4}\delta(\omega + \omega_0)\,,$$

where δ denotes the Dirac delta function. Since $x(t)$ here is periodic, the power spectral density of $x(t)$ consists of two line components, one at $\omega = -\omega_0$ and one at $\omega = \omega_0$. ■

Numerous examples of the power spectral densities calculated from the time signals of chaotic systems are presented in the later chapters. Since chaotic signals are not periodic, their power spectral densities contain a continuous spectral component as opposed to signals of periodic and quasi-periodic attractors whose power spectral densities are discrete, that is, contain only line components.

Example 2.68 The nonlinear sampled-data control system described in Example 2.4 is chaotic for $p = 3.004166$, $q = 4.008332$, $e = 0.1$. These parameter values correspond with a sampling period of $T = 2.2$ for the system. For the system output y_n defined by

$$y_n := \frac{x_{1,n} + x_{2,n}}{2}\,,$$

the power spectral density is shown in Figure 2.10. ■

Studying chaotic signals using spectral analysis, also reveals other properties of the chaotic attractor. For example, a saddle-type periodic trajectory with slow expansion generates spectral peaks at multiples of the fundamental frequency of the periodic trajectory. The greater the characteristic exponent associated with the expansion, the wider and lower these peaks become.

We end this section with the interesting observation that there are time responses for which the autocorrelation and hence the power spectral density function do not exist.

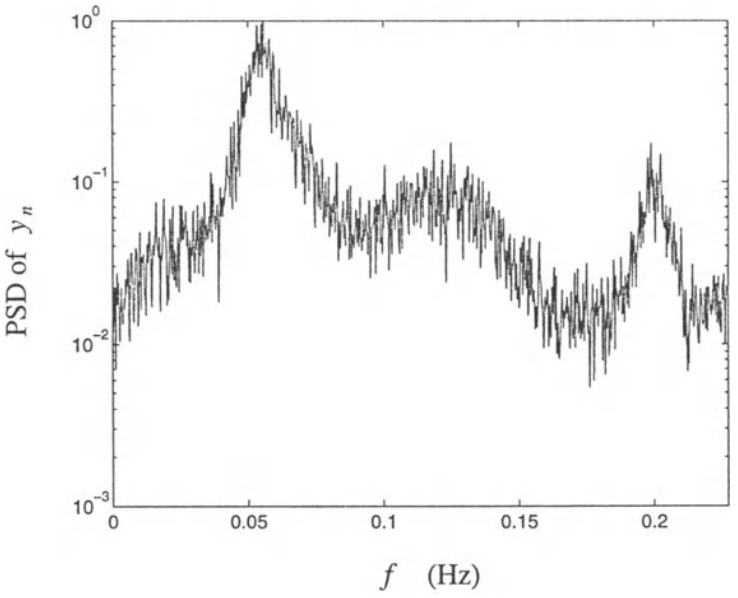

Figure 2.10: Power spectral density of the output y_n of the sampled-data system.

Example 2.69 [92] Consider the dynamical system described by the smooth quadratic vector field

$$\begin{pmatrix} dx_1/dt \\ dx_2/dt \\ dx_3/dt \end{pmatrix} = \begin{pmatrix} -x_2x_3 \\ x_1x_3 \\ -x_3^2 \end{pmatrix}. \tag{2.76}$$

Show that this system has neither an autocorrelation function, nor a power spectral density function.

This system may be viewed as an oscillator [92] with state variables x_1 and x_2, each of which is frequency modulated by x_3 which in turn evolves according to

$$\frac{dx_3}{dt} = -x_3^2.$$

For initial condition $\mathbf{x} = (1, 0, 1)^T$, the solution can be shown to be given by [92]

$$\begin{pmatrix} x_1(t) \\ x_2(t) \\ x_3(t) \end{pmatrix} = \begin{pmatrix} \cos(\log(t+1)) \\ \sin(\log(t+1)) \\ (t+1)^{-1} \end{pmatrix}. \tag{2.77}$$

To show that the autocorrelation does not exist we only consider $R_{x_1x_1}(0)$. Let

$$\begin{aligned} U_{\tilde{T}} &:= \frac{1}{\tilde{T}} \int_0^{\tilde{T}} x_1^2 \, dt \\ &= \frac{1}{2} + \frac{1}{10}\left(\cos\left(2\log(1+\tilde{T})\right) + 2\sin\left(2\log(1+\tilde{T})\right)\right) + \\ &\quad \frac{1}{10\tilde{T}}\left(\cos\left(2\log(1+\tilde{T})\right) + 2\sin\left(2\log(1+\tilde{T})\right) - 1\right). \end{aligned}$$

Thus

$$\begin{aligned} \limsup_{\tilde{T}\to\infty} U_{\tilde{T}} &= \frac{1}{2}\left(1 + \frac{1}{\sqrt{5}}\right), \\ \liminf_{\tilde{T}\to\infty} U_{\tilde{T}} &= \frac{1}{2}\left(1 - \frac{1}{\sqrt{5}}\right), \end{aligned}$$

from which we conclude that x_1 and hence $\mathbf{x}$ has no autocorrelation and consequently no power spectral density function. ■

Chapter 3

One-dimensional Maps in Electronics

3.1 Introduction

In this chapter we consider electronic circuits which are described by one-dimensional maps. In Section 3.2 a switched-capacitor circuit described by a nonlinear one-dimensional map is discussed. For a specific choice of the parameters, this map is equivalent to the logistic map. The bifurcations exhibited by this circuit as one of its parameters is varied, are studied.

A controlled switched-mode power converter is studied in Section 3.3. It is shown here that under certain assumptions, the converter is described by the zigzag map introduced in Appendix A. The dynamics of the zigzag map (and hence the idealized power converter) is studied in detail here. Conditions for the zigzag map and hence the switched-mode power converter to exhibit chaos are discussed.

The next section is devoted to the study of chaotic noise generation. The output transformation approach to generating noise with a prescribed invariant density is discussed. A switched-capacitor circuit for generating noise is discussed followed by a literature survey on the subject of noise generation using chaotic systems.

In Section 3.5 Sigma-Delta modulators are studied for chaotic behaviour. It is shown that for an integration loop gain constant greater than one, a single-loop Sigma-Delta modulator is chaotic. Some theoretical and numerical results are presented.

3.2 Switched Capacitor Circuit: Logistic Map

Since switched-capacitor circuits are important in *Very Large Scale Integration* (VLSI) technology, any potential anomaly or failure mechanisms, as a result of the onset of chaos, should be fully analyzed. The circuit to be discussed here is also of circuit-theoretical interest because its dynamic equation is equivalent to the well-known logistic map. Since the logistic map is the simplest chaotic polynomial discrete map, the chaotic circuit to be described below is the simplest chaotic circuit described by a first-order discrete map.

3.2.1 Circuit Description

The switched-capacitor circuit shown in Figure 3.1(a) was first studied by Rodriguez-Vazquez *et al.* in 1985 (see [659]). It consists of a battery with voltage V_s, a linear capacitor C_s, a nonlinear switched-capacitor component and three analogue switches. The states of the switches are controlled by a two-phase clock defined by the ϕ^e and ϕ^o. Here, ϕ^e is a square wave with a duty cycle of 50 percent and ϕ^o is in anti-phase with ϕ^e. The switches controlled by the clock signals ϕ^e and ϕ^o turn on in synchronization with the rising edges of ϕ^e and ϕ^o, respectively.

The characteristics of the nonlinear switched-capacitor component (here called a Forward Euler Switched Capacitor (FESC) resistor) is defined by

$$q_n - q_{n-1} = k v_{n-1}^2 =: \Delta q_n \,,$$

where q_n is the charge in the FESC resistor after the n-th clock period, Δq_n is the net charge flowing into the FESC resistor during the n-th clock period, v_{n-1} is the voltage sampled across the FESC resistor during the $(n-1)$-th period and k is an arbitrary positive constant. In order for readers to repeat the experiment, Rodriguez-Vazquez

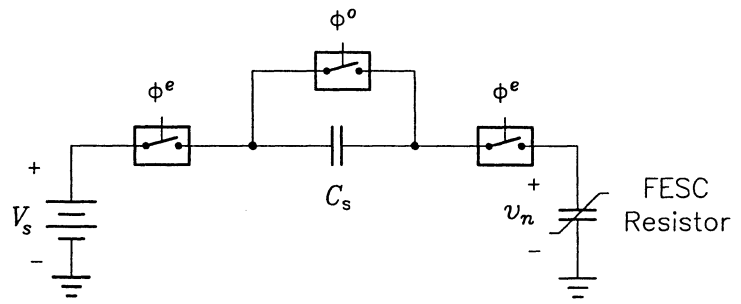

Figure 3.1: Nonlinear switched-capacitor circuit.

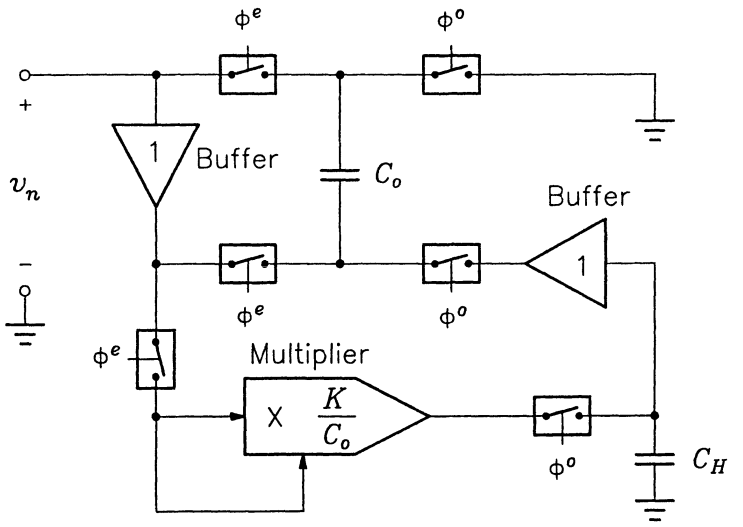

Figure 3.2: Off-the-shelf realization of the FESC resistor.

et al. suggested the circuit shown in Figure 3.2 as an off-the-shelf realization of the FESC resistor.

3.2.2 Analysis

Due to the charge conservation principle the net charge flowing into the FESC resistor during the $(n+1)$-th clock cycle equals the net charge flowing out of the (linear) capacitor C_s and because the voltage across C_s is zero at the start of each cycle, we have

$$C_s(V_s - v_{n+1}) = \Delta q_{n+1}\,,$$

and hence

$$v_{n+1} = V_s - \frac{k}{C_s} v_n^2\,. \tag{3.1}$$

By introducing the transformation defined by

$$x_n := a v_n + b, \qquad a, b \in \mathbf{R}\,,$$

we obtain

$$x_{n+1} = \frac{(C_s V_s a^2 + C_s a b - b^2 k) + k x_n (1 - 2b x_n)}{a C_s}\,.$$

By requiring that

$$C_s V_s a^2 + b C_s a - b^2 k = 0, \quad \text{and} \quad 2b = 1\,,$$

we finally have

$$x_{n+1} = r x_n (1 - x_n),$$

with

$$r = \frac{k}{aC_s}, \qquad b = \frac{1}{2}, \tag{3.2}$$

$$a = -\frac{b}{2V_s}\left(1 \pm \sqrt{1 + 4k\frac{V_s}{C_s}}\right) = -\frac{1}{4V_s}\left(1 \pm \sqrt{1 + 4k\frac{V_s}{C_s}}\right). \tag{3.3}$$

Thus with the choice of a and b made here, we have found (3.1) to be linearly conjugate to the logistic map. The dynamics of the logistic map have been studied in great depth by Devaney [217]and others. Since r depends on V_s through (3.2) and (3.3), the bifurcation analysis of the switched-capacitor circuit may be related to that of the logistic map by using V_s as the bifurcation parameter. The bifurcation tree shown in Figure 3.3 (with r as bifurcation parameter) was generated by means of computer simulation.

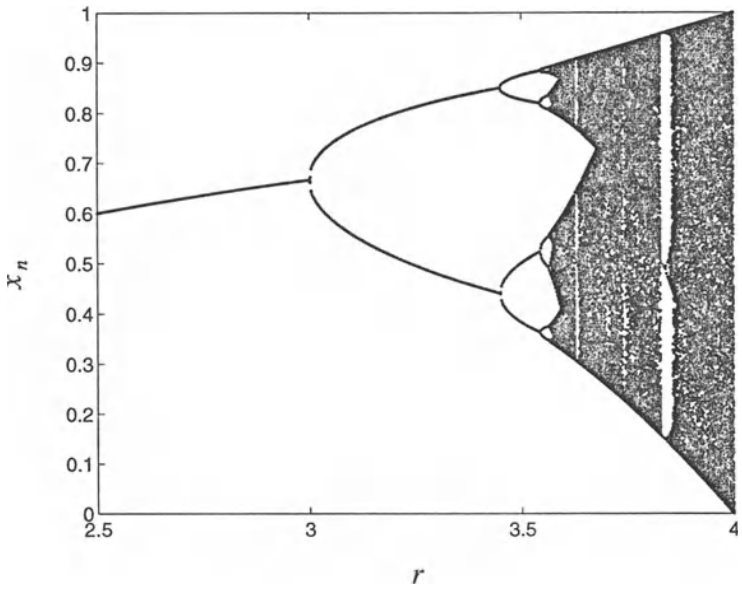

Figure 3.3: Bifurcation tree for the logistic map with r as the bifurcation parameter.

Analogue circuits for synthesizing the logistic map have been proposed and studied by Briggs [98], Mishina *et al.* [548] (refer to Chapter 4) and Jefferies *et al.* [400]. The implementations proposed by Briggs and Mishina *et al.* are much more complex than the one proposed by Rodriguez-Vazquez and coworkers discussed here.

3.3 Controlled Switched-Mode Converter: Zigzag Map

Hamill and Jeffries [328] first analyzed a switched-mode DC-to-DC converter for chaotic response. Because of the periodic switching nature of switched-mode power converters they were able to derive a three segment piecewise-linear difference equation of first order, called the zigzag map, that relates the output currents of two consecutive switching cycles. In this section we present their results and derive further results concerning the dynamics of the zigzag map.

3.3.1 Functional Description

Before considering the switched-mode power converter analyzed by Hamill and Jeffries [328] we are going to explain briefly the operation of a pulse-width modulator (PWM). A pulse-width modulator generates a square pulse train of fixed frequency, the duty cycle of which is determined by a control input (a voltage in our case). Different types of pulse-width modulation schemes are leading edge, trailing edge and dual edge pulse-width modulation. Figure 3.4(a) shows a simple dual edge pulse-width modulator. It consists of a triangular-wave generator (IC_1 and IC_2) and a comparator (IC_3). The comparator compares the triangular-wave with the control input voltage. While the triangular-wave $v_w(t)$ exceeds the (possibly time-varying) control input voltage $v_c(t)$, the output of the comparator $v_o(t)$ remains positive and constant and while $v_c(t)$ exceeds $v_w(t)$, $v_o(t)$ remains negative and constant. This is illustrated in Figure 3.4(b) for some arbitrary $v_c(t)$. By replacing the triangular-wave generator with a positive slope (respectively negative slope) ramp-wave generator a leading edge (respectively trailing edge) pulse-width modulator is obtained.

The functional block diagram of the switched-mode DC-to-DC converter (*buck converter*) studied by Hamill and Jeffries is shown in Figure 3.5. The pulse-width modulator employed in this DC-to-DC converter is a trailing edge pulse-width modulator. It is obvious that the buck converter in Figure 3.5 will only operate as intended if $V_I > V_O$. The circuit works as follows. The actual load current $i(t)$ is compared with the desired load current I_{ref}. The difference between I_{ref} and $i(t)$ drives the control input of the pulse-width modulator, thereby controlling the duty cycle of the pulse-width modulator's output, which in turn controls (by means of a power switching element) the duty cycle of the current pulses applied to the choke L. For example if $i(t)$ is less than I_{ref} then the duty cycle of the pulse-width modulator is increased and hence the average current through the choke increases proportional to the increased duty cycle. On the other hand if $i(t)$ is greater than I_{ref} the duty cycle is decreased resulting in a drop of the average current through the choke.

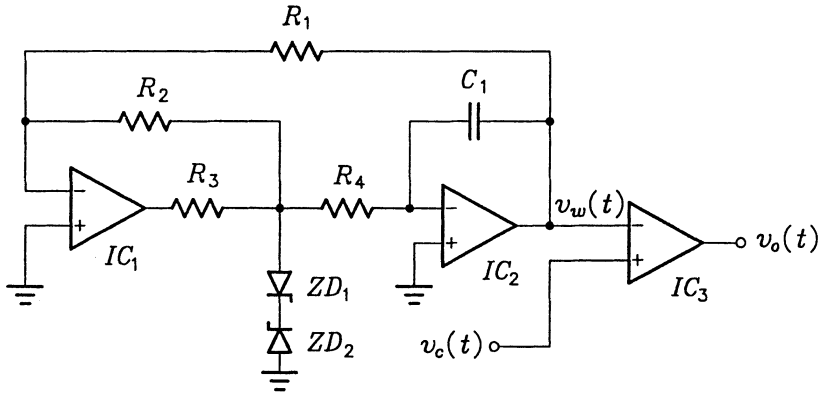

(a)

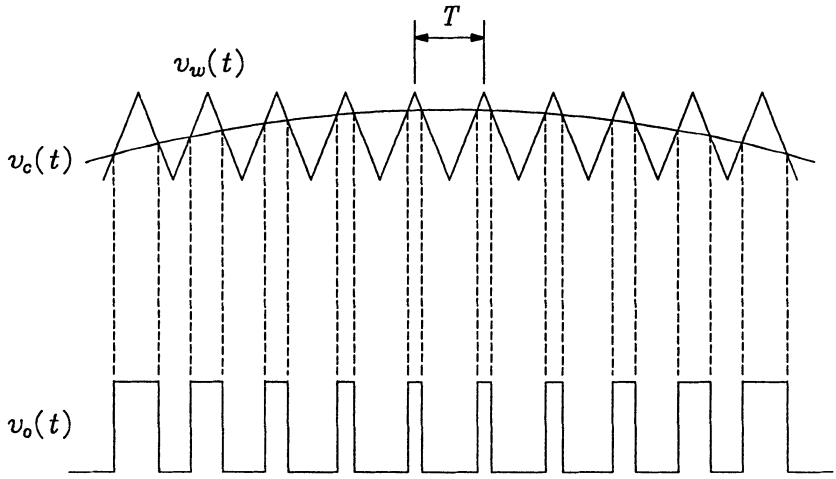

(b)

Figure 3.4: (a)A simple dual edge pulse-width modulator circuit; (b) A typical dual edge pulse-width modulated signal.

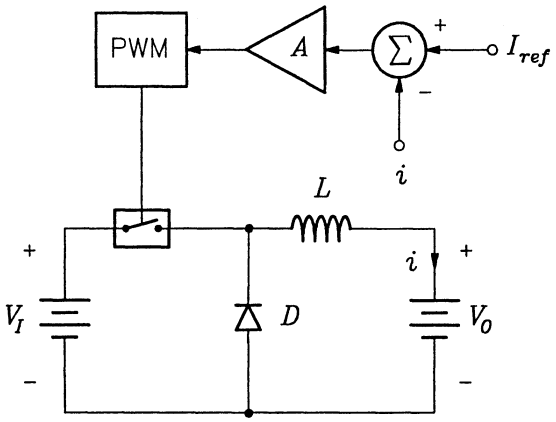

Figure 3.5: Block diagram of the switched-mode DC-to-DC converter studied by Hamill and Jeffries.

3.3.2 Analysis

First we state all assumptions under which the analysis will be performed. All components are assumed to be ideal. For simplicity it is assumed that the current $i(t)$ in the choke is always nonzero, that is, operation is confined to the usual continuous-current mode. However, this assumption is not restrictive and may easily be removed (see [328]). The load is taken to be a constant voltage sink. It is assumed that the switching frequency is constant with period T and that the switch operates with a duty cycle of D, where $D \in [0, 1]$.

By abusing the notation, the choke current at the end of the n-th switching cycle of operation is $i_n := i(nT)$. Let D_n be the duty cycle during the n-th cycle. At the start of the $(n+1)$-th cycle the switch is then closed for a time $D_{n+1}T$ during which the current rises linearly (since the voltage $(V_I - V_O)$ across the choke is being held constant) to the value

$$i_n + \frac{(V_I - V_O)D_{n+1}T}{L}.$$

Next the switch is opened for the remainder of the switching cycle during which the free-wheeling diode conducts. During this time interval the voltage across the choke is once again constant namely $-V_O$, thereby causing the current to fall linearly by an amount $V_O(1 - D_{n+1})T/L$. The relationship between the currents i_{n+1} and i_n is given by

$$i_{n+1} - i_n = \frac{1}{L} \int_{nT}^{(n+1)T} v_L(t)\, dt$$

$$= \frac{1}{L}\left[(V_I - V_O)\int_{nT}^{(n+D_{n+1})T} dt - V_O \int_{(n+D_{n+1})T}^{(n+1)T} dt\right]$$

from which we derive

$$i_{n+1} = i_n + \frac{(V_I D_{n+1} - V_O)T}{L}. \tag{3.4}$$

Equation (3.4) is a difference equation relating the currents at the end of two consecutive cycles. The current-error signal $e(t)$ is given by

$$e(t) = A(I_{ref} - i(t)),$$

where I_{ref} is the reference current, and A is a gain constant. The duty cycle for the $(n+1)$-th cycle is obtained by filtering (i.e. averaging) the current-error signal and thereafter limiting the filtered signal so as to ensure that $D_{n+1} \in [0,1]$. Since any low pass filter introduces phase lag, the simplest possible (or perhaps most idealized) model for describing the relationship between the duty cycle for the $(n+1)$-th cycle is

$$D_{n+1} = \text{sat}(e_n),$$

where $e_n := e(nT)$ and

$$\text{sat}(x) := \begin{cases} 0, & \text{if } x \leq 0 \\ x, & \text{if } 0 < x < 1 \\ 1, & \text{if } x \geq 1 \end{cases}.$$

Substituting the above expressions for D_{n+1} and $e(t)$ into (3.4) we obtain

$$i_{n+1} = i_n + \frac{V_I T}{L}\,\text{sat}(A[I_{ref} - i_n]) - \frac{V_O T}{L}.$$

By making the substitutions

$$x_n := \frac{i_n}{I_{ref}}, \quad a := AI_{ref}, \quad b := \frac{V_I T}{I_{ref} L}, \quad c := \frac{V_O T}{I_{ref} L},$$

the above difference equation can be written in dimensionless form, namely

$$x_{n+1} = x_n + b\,\text{sat}(a[1 - x_n]) - c, \tag{3.5}$$

with $b > c$ since $V_I > V_O$. Explicitly (3.5) yields

$$x_{n+1} = \begin{cases} x_n + b - c, & \text{if } x_n \leq (a-1)/a \\ (1-ab)x_n + ab - c, & \text{if } (a-1)/a < x_n < 1 \\ x_n - c, & \text{if } 1 \leq x_n \end{cases}.$$

An instance of the above difference equation is depicted in Figure 3.6.

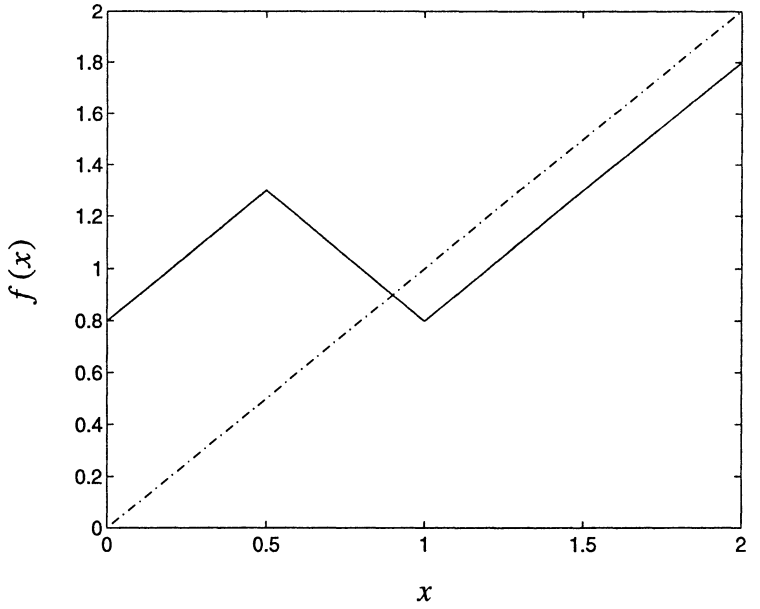

Figure 3.6: The zigzag map for $a = 2$, $b = 1$, and $c = 0.201$.

3.3.3 Stability Analysis

For convenience we write

$$f(x;a,b,c) = \begin{cases} f_L(x;a,b,c), & \text{if } x \leq (a-1)/a \\ f_C(x;a,b,c), & \text{if } (a-1)/a < x < 1 \\ f_R(x;a,b,c), & \text{if } 1 \leq x \end{cases} .$$

where

$$\begin{aligned} f_L(x;a,b,c) &:= x + b - c, \\ f_C(x;a,b,c) &:= (1-ab)x + ab - c, \\ f_R(x;a,b,c) &:= x - c. \end{aligned}$$

When no confusion is possible, we write $f_L(x)$, $f_C(x)$ and $f_R(x)$ instead of using the above more involved notation.

The zigzag map has a single fixed point x^* namely

$$x^* = 1 - \frac{c}{ab}.$$

Since $c < b$ we have $x^* \in ((a-1)/a,\ 1)$. The slope of the zigzag map at the fixed point is

$$\frac{df}{dx}(x^*) = 1 - ab.$$

It is clear that the fixed point x^* is stable if and only if $|1-ab| < 1$. Thus, for stability of x^* it is required that $0 < ab < 2$. When $ab = 2$ the fixed point is nonhyperbolic. Inspection of the k-th return map for $k = 2, 4, 6, \ldots$ reveals that each of these maps contains an identical segment that lies on the line $x_{n+k} = x_n$. Hence the zigzag map has infinitely many nonhyperbolic period-2 orbits for $ab = 2$.

For the case $ab > 2$ (i.e. $|1 - ab| > 1$) the fixed point x^* is unstable and there exists a single unstable period-2 orbit passing through the point

$$x = 1 + (ab - 2)\frac{c}{ab}.$$

We observe that because $f(x) > x$ for $x < (a-1)/a$ and $f(x) < x$ for $x > 1$ it follows that all orbits approach the interval

$$A := [f(1),\ f((a-1)/a)] = [1 - c,\ 1 + b - c - 1/a].$$

Once an orbit is in A it can never escape from A even though orbits are repelled by the fixed point x^*. The domain of attraction is $\mathbf{R}^+$ and therefore after any initial transient response has decayed every orbit lies entirely in the interval A.

In order to find the domain in the parameter space for which f is chaotic, we construct conditions for which a repelling period-3 orbit is guaranteed to exist. These conditions together with the fact that f is continuous will then guarantee that f is chaotic in the Li-Yorke sense (see Appendix A). First we consider the case $b > 2c$ (i.e. $b - c > c$). For f to have a repelling period-3 solution in this case, it is clear that at least one of the points on this period-3 orbit must lie in the interval $[(a-1)/a, 1-c/ab)$. The two possible hyperbolic period-3 orbits for f with $b > 2c$ are shown in Figure 3.7. From Figure 3.7 we observe that a necessary condition of f to afford such a hyperbolic period-3 orbit is

$$f^{(2)}\left(\frac{a-1}{a}\right) \geq 1 \qquad \Longleftrightarrow \qquad b \geq 2c + \frac{1}{a} > 2c. \tag{3.6}$$

Proposition 3.1 Sufficient conditions for the zigzag map f to have a repelling period-3 orbit are $a \leq 1/c$ and $ab \geq 3$.

Proof: We note that

$$a \leq \frac{1}{c} \qquad \Longleftrightarrow \qquad f(1) \geq \frac{a-1}{a},$$

and

$$\frac{3}{b} \leq a \leq \frac{1}{c} \qquad \Longleftrightarrow \qquad f^{(3)}(1) \geq 1.$$

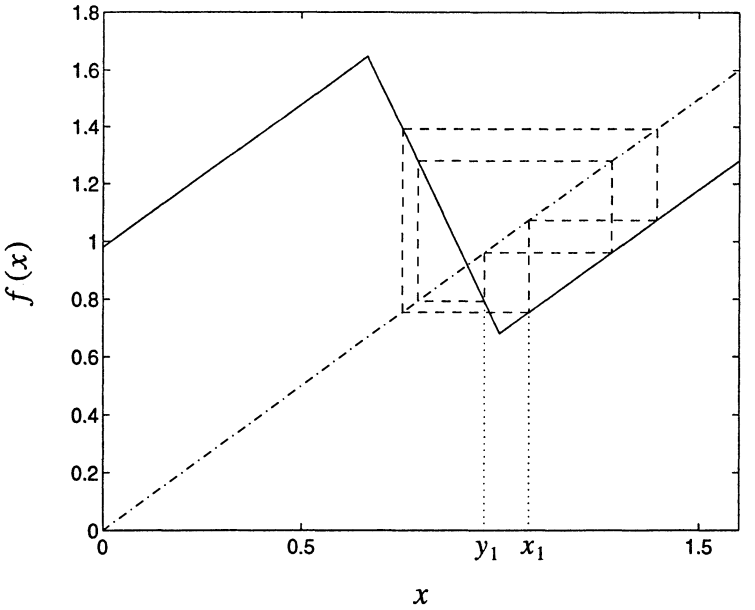

Figure 3.7: Possible hyperbolic period-3 orbits affordable by f if $b > 2c$.

Since for arbitrary constants $a > 0$, $b > c > 0$ we have

$$f^{(2)}(1) \le f\left(\frac{a-1}{a}\right) \implies f^{(2)}(1) - c \le f\left(\frac{a-1}{a}\right) - c$$
$$\implies 1 \le f^{(3)}(1) \le f^{(2)}\left(\frac{a-1}{a}\right),$$

and hence the condition $3/b \le a \le 1/c$ implies the condition in (3.6).

Now, define the set B as

$$B := [1-c, f_C^{-1}(1+c)] = [1-c, 1-2c/(ab-1)]\,.$$

Note that $x^* \notin B$ and that

$$B \cap f^{(k)}(B) = \emptyset, \quad \text{for } k = 1,2 \qquad \text{and} \qquad B \subseteq f^{(3)}(B),$$

and hence by the intermediate value theorem there exists a period-3 point of f in B. Thus we have established the existence of the period-3 orbit in the interval A that contains x_1. By a similar argument the existence of the period-3 orbit that contains y_1 is proved.

To comment on the hyperbolicity of the period-3 orbits, we notice that each of these periodic orbits contains at least one point in the interval $[(a-1)/a, 1]$ and hence

$$\left|\frac{df^{(3)}}{dx}(x)\right| \ge ab - 1 \ge 2\,, \qquad \text{for } x \in \{x_1, y_1\},$$

since $ab \geq 3$. Hence both of these period-3 orbits are repelling. ■

Remark The condition $a \leq 1/c$ in the above ensures that the segment of the zigzag map described by f_L is excluded from the attractor and hence has no effect on the dynamics. Any point in the set A (defined earlier) that can be reached from the left can also be reached from the right and hence for $a \leq 1/c$ the zigzag map may be considered as a two-segment piecewise-linear (unimodal) map described by f_C and f_R.

Referring to Figure 3.7 we observe that the difference between the two period-3 orbits $\{x_1, x_2, x_3\}$ and $\{y_1, y_2, y_3\}$ is that x_1 and y_1 lie on opposite sides of the point $x = 1$. Solving

$$x_1 = f^{(3)}(x_1) = f_R(f_C(f_R(x_1))) ,$$

gives

$$x_1 = 1 + (ab - 3)\frac{c}{ab} .$$

The condition $1 \leq x_1 < 1+c$ reduces to the requirement $ab \geq 3$ which is in accordance with Proposition 3.1. For the other period-3 orbit we have to solve

$$y_1 = f^{(3)}(y_1) = f_R(f_C(f_C(y_1))) ,$$

which gives

$$y_1 = 1 + \left(\frac{ab-3}{ab-2}\right)\frac{c}{ab} .$$

Imposing the conditions $x^* < y_1 \leq 1$ leads to the requirement $ab \geq 3$ which satisfies the conditions of the Proposition 3.1. From the above we conclude that for $ab < 3$ no period-3 orbit exists, for $ab = 3$ a single period-3 orbit exists (since $x_1 = y_1 = 1$) and for $ab > 3$ two distinct period-3 orbits coexist. Therefore $ab = 3$ is a bifurcation point and the period-3 orbit at this point is structurally unstable.

Proposition 3.2 If $ab \geq 3$ and $a \leq 1/c$ then the zigzag map f is chaotic in the set A.

Proof: Since f is continuous and for $ab \geq 3$, $a \leq 1/c$ possesses a repelling period-3 orbit contained in A (Proposition 3.1), f is chaotic on A in the Li-Yorke sense by Proposition A.54. ■

The period-2 orbit of f in A (which by Sarkovskii's theorem (see Appendix B) is the second-last number in Sarkovskii's ordering of the natural numbers) could also have been shown to exist by realizing that $C \cap f(C) = \emptyset$ and $C \subset f^{(2)}(C)$, with

$$C := [1 - c, 1 - c/ab).$$

This is consistent with the definition of Li-Yorke chaos for one-dimensional maps. In order to analyze the zigzag map for the case $c < b < 2c$ (i.e. $0 < b - c < c$), we note the linear topological conjugacy

$$h(f(x;a,b,c)) = f(h(x);a,b,b-c)\,,$$

where the diffeomorphism $h : \mathbf{R} \to \mathbf{R}$ is defined by

$$h(x) := 2x_s - x\,, \tag{3.7}$$

with

$$x_s := \frac{1}{2}\left(\frac{a-1}{a} + 1\right) = \frac{2a-1}{2a}\,.$$

Hence the analysis of the zigzag map for the case $b > 2c$ also holds for the case $c < b < 2c$ via the linear topological conjugacy (3.7) established above.

3.3.4 Invariant Density and Lyapunov Exponent

In this section we study the invariant density and the associated Lyapunov exponent for the case

$$b > 2c\,, \qquad a \leq \frac{1}{c}\,, \qquad ab = k\,, \quad \text{for} \quad k = 3,4,\ldots\,,$$

The last two conditions guarantee the point $x = 1$ to be hyperbolic and of period-k as we shall see shortly. Also, under the above conditions the attractor lies in the interval

$$A = \left[f(1), f^{(2)}(1)\right] = [1-c, 1+(k-2)c]\,.$$

Proposition 3.3 For $ab = k$, $k = 3,4,\ldots$ with $a \leq 1/c$ a structurally unstable hyperbolic period-k orbit appears. This period-k orbit is unstable. As ab increases beyond k this orbit bifurcates to two unstable period-k orbits containing the points

$$x_1 := 1 + (ab-k)\frac{c}{ab}\,, \qquad \text{and} \qquad y_1 := 1 - \left(\frac{ab-k}{ab-2}\right)\frac{c}{ab}\,,$$

respectively.

Proof: To prove the proposition one has to solve

$$x_1 = \left(f_R^{(k-2)} \circ f_C \circ f_R\right)(x_1), \qquad \text{and} \qquad y_1 = \left(f_R^{(k-2)} \circ f_C^{(2)}\right)(y_1),$$

subject to the inequalities

$$1 \leq x_1 < 1 + c\,, \qquad \text{and} \qquad x^* < y_1 \leq 1\,,$$

respectively. The details of the proof are left to the reader. ■

For the case when ab equals some positive integer, the structurally unstable period-k orbit, which exists by the above proposition, contains both boundary points of the attractor as points on it. This enables us to calculate analytically the invariant density for this case. To obtain the invariant density $\rho : \mathbf{R} \to \mathbf{R}^+$ for the case under consideration, we must iterate the expression

$$\begin{aligned}\rho_{n+1}(x) &= \rho_n\left(f_C^{-1}(x)\right)\left|\frac{df_C^{-1}}{dx}(x)\right|\chi_{[f(1),f^{(2)}(1)]}(x) + \\ &\quad \rho_n\left(f_R^{-1}(x)\right)\left|\frac{df_R^{-1}}{dx}(x)\right|\chi_{[f(1),f^{(3)}(1)]}(x) \\ &= \frac{1}{k-1}\rho_n\left(\frac{k-(x+c)}{k-1}\right)\chi_{[1-c,1+(k-2)c]}(x) + \rho_n(x+c)\chi_{[1-c,1+(k-3)c]}(x)\,,\end{aligned} \tag{3.8}$$

which is obtained from the Frobenius-Perron integral equation. By letting

$$\rho_0(x) = \frac{1}{(k-1)c}\chi_{[1-c,1+(k-2)c]}(x),$$

and performing the iterations using (3.8) we find that ρ_n is of the form

$$\rho_n(x) = \frac{1}{c}\sum_{i=1}^{k-1} a_i(n)\,\chi_{[1-c,1+(k-i-1)c]}(x), \qquad n = k, k+1, \ldots \tag{3.9}$$

where $\{a_i(n)\}_{i=1}^{k-1}$ is a set of nonnegative real constants. From (3.9) we obtain

$$\begin{aligned}\rho_n\left(\frac{k-(x+c)}{k-1}\right) &= \frac{1}{c}\sum_{i=1}^{k-1} a_i(n)\,\chi_{[1-c,1+(k-i-1)c]}\left(\frac{k-(x+c)}{k-1}\right) \\ &= \frac{1}{c}\sum_{i=1}^{k-1} a_i(n)\,\chi_{[1-(k^2-(i+2)k+(i+2))c,1+(k-2)c]}(x)\,,\end{aligned} \tag{3.10}$$

and

$$\begin{aligned}\rho_n(x+c) &= \frac{1}{c}\sum_{i=1}^{k-1} a_i(n)\,\chi_{[1-c,1+(k-i-1)c]}(x+c) \\ &= \frac{1}{c}\sum_{i=1}^{k-1} a_i(n)\,\chi_{[1-2c,1+(k-i-2)c]}(x)\,.\end{aligned} \tag{3.11}$$

Thus, substituting (3.10) and (3.11) into (3.8), yields

$$\begin{aligned}\rho_{n+1}(x) &= \frac{1}{c}\left\{\frac{1}{k-1}\sum_{i=1}^{k-1} a_i(n)\right\}\chi_{[1-c,1+(k-2)c]}(x) + \\ &\quad \frac{1}{c}\sum_{j=2}^{k-1} a_{j-1}(n)\,\chi_{[1-c,1+(k-j-1)c]}(x)\,.\end{aligned} \tag{3.12}$$

By replacing n by $n+1$ in (3.9) and equating this to (3.12), we obtain

$$\begin{aligned} a_1(n+1) &= \frac{1}{k-1}\sum_{i=1}^{k-1} a_i(n), \\ a_i(n+1) &= a_{i-1}(n), \qquad i = 2,3,4,\ldots,k-1. \end{aligned} \tag{3.13}$$

Taking the limit $n \to \infty$ for (3.13) and defining

$$a_i := \lim_{n\to\infty} a_i(n), \qquad i = 1,2,\ldots,k-1,$$

we finally have

$$a_1 = a_2 = \ldots = a_{k-1}. \tag{3.14}$$

Since the area under the invariant density ρ must be unity, we have the additional condition

$$\sum_{n=1}^{k-1}\sum_{m=1}^{n} a_m = 1,$$

which together with (3.14) gives

$$\sum_{n=1}^{k-1} n a_r = 1, \qquad \text{for each } r = 1,2,\ldots,k-1,$$

and consequently

$$a_r = \frac{2}{(k-1)k}, \qquad \text{for each } r = 1,2,\ldots,k-1,$$

where we have used the identity

$$1+2+3+\ldots+n \equiv \frac{n(n+1)}{2}.$$

We therefore have

$$\rho(x) = \begin{cases} \dfrac{2}{ck}, & \text{if } 1-c \le x \le 1 \\ \dfrac{2(k-n)}{c(k-1)k}, & \text{if } 1+(n-2)c < x \le 1+(n-1)c, \quad n = 2,3,\ldots,k-1. \\ 0, & \text{otherwise} \end{cases} \tag{3.15}$$

The ergodic theorem is finally used to obtain the Lyapunov exponent, namely

$$\lambda = \int_A \ln\left|\frac{df}{dx}(x)\right| \rho(x)\,dx = \int_{1-c}^{1} \ln\left|\frac{df_c}{dx}(x)\right| \rho(x)\,dx = \frac{2}{k}\ln(k-1). \tag{3.16}$$

Using (3.16) we find for the case $b = 1$ and $c = 0.201$ that $\lambda|_{k=3} \approx 0.462$ and $\lambda|_{k=1} \approx 0.549$.

3.3.5 Simulation Results

The zigzag map was studied numerically in detail [328] for the parameter values $b = 1$ and $c = 0.201$ with a the bifurcation parameter. For $0 < a < 2/b$ there exists a unique stable fixed point. When $a = 2/b$ a bifurcation in the state space orbit occurs. The fixed point has now become unstable and an attracting period-2 solution has appeared. For $a > 2/b$ intermittency occurs. The effect is that of an apparently noisy period-2 subharmonic, the "noise" worsening as a is increased. In reality what is happening is that successive period-doubling bifurcations are occurring as a increases. The period-doubling persists until $a = 3/b$ at which point the zigzag map becomes chaotic and remains so for $a \geq 3/b$. For the special case when $k = b/c$ is an integer and $k > 1$ any chaotic region terminates at $a = 1/c$, where a period-k attractor emerges and persists as a is increased without limit. However when b/c is close to an integer $k > 1$, a period-k appears intermittently [328]. For the case at hand $b/c \approx 4.975$ and hence for $a > 4.975$ an intermitting period-5 subharmonic emerges. The above results are summarized in the bifurcation diagram shown in Figure 3.8.

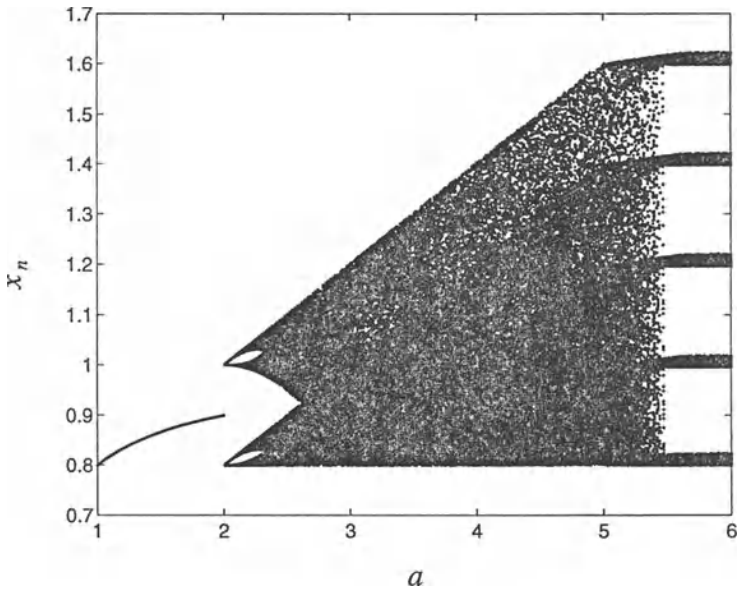

Figure 3.8: Bifurcation diagram for the zigzag map with $b = 1$, $c = 0.201$ and a as the bifurcation parameter.

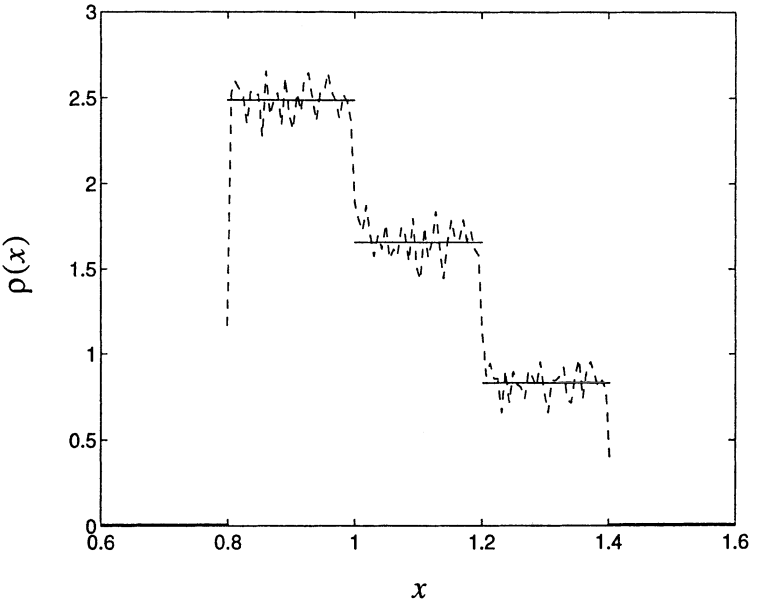

Figure 3.9: Invariant density for the zigzag map with $a = 4$, $b = 1$, $c = 0.201$: histogram estimate (dashed line) and the graph of the analytical expression (3.15) (solid line).

The invariant density calculated numerically from the time evolution, for the case $a = 4$, $b = 1$, $c = 0.201$ is shown in Figure 3.9. For the sake of comparison, the graph of the analytical expression for the invariant density (3.15) is also plotted in this figure. The numerical calculation of the Lyapunov exponent for the cases

$$a = 3\,, \quad b = 1\,, \quad c = 0.201\,,$$

and

$$a = 4\,, \quad b = 1\,, \quad c = 0.201\,,$$

yields $\lambda \approx 0.4618$ and $\lambda \approx 0.5507$ respectively. This compares favourably with the theoretical results obtained in the previous section. In the paper by Hamill *et al.* [327] the Lyapunov exponent as a function of the parameter a was plotted for the case $b = 1$, $c = 0.2$. The reader is referred to [327] for further details.

3.4 Chaotic Noise Generators

3.4.1 Transformation of Random Variables

Suppose we are given a one-dimensional map $f : X \to X$, $X \subset \mathbf{R}$ which exhibits chaos. Let ρ_f be its invariant density. We wish to find the monotonic increasing function $g : X \to Y$, $Y \subset \mathbf{R}$ such that the topological conjugate one-dimensional map $h := g \circ f \circ g^{-1}$ has some prescribed invariant density ρ_h. Since the sequences $\{x_n\}_{n=1}^{\infty}$ and $\{y_n\}_{n=1}^{\infty}$ generated by

$$x_{n+1} = f(x_n), \qquad \text{and} \qquad y_{n+1} = h(y_n),$$

respectively, may be viewed as sample functions (determined by the selected initial conditions) of two ergodic stochastic processes [612], we conclude that ρ_f and ρ_h are related by

$$\rho_h(y) = \rho_f(x) \left| \frac{dy}{dx} \right| ,$$

where, by assumption $y = g(x)$. Thus

$$\left| \frac{dg}{dx}(x) \right| = \frac{\rho_f(x)}{\rho_h(g(x))} . \tag{3.17}$$

Assuming g to be monotonic increasing, (3.17) may be written as

$$\frac{dg^{-1}}{dx}(x) = \frac{\rho_h(x)}{\rho_f(g^{-1}(x))} .$$

Integrating this expression yields

$$g^{-1}(x) = \int_{-\infty}^{x} \frac{\rho_h(\zeta)}{\rho_f(g^{-1}(\zeta))} \, d\zeta , \tag{3.18}$$

where without loss of generality we have assumed that the integration constant is zero. In order to solve the integral equation (3.18) we present the following result.

Proposition 3.4 Consider the integral equation

$$\phi(y) = \int \psi(\phi(y), y) \, dy , \tag{3.19}$$

where $\phi : \mathbf{R} \to \mathbf{R}^+$ and $\psi : \mathbf{R}^2 \to \mathbf{R}^+$ are both Borel-integrable functions. If there exist Borel-integrable functions $f_1, f_2 : \mathbf{R} \to \mathbf{R}^+$ such that

$$\psi(x, y) = \frac{f_1(y)}{f_2(x)} , \tag{3.20}$$

for each $(x, y) \in \mathbf{R}^2$ then the composite function

$$\phi = g_2^{-1} \circ g_1$$

is a solution of (3.19) where the functions $g_1, g_2 : \mathbf{R} \to \mathbf{R}$ are Borel-integrable functions which are given by

$$g_1(y) = \int f_1(y)\, dy\,, \tag{3.21}$$

and

$$g_2(x) = \int f_2(x)\, dx\,, \tag{3.22}$$

respectively.

Proof: Suppose there exist Borel-integrable functions $f_1, f_2 : \mathbf{R} \to \mathbf{R}^+$ such that supp $f_1 \subseteq$ supp f_2, satisfying the hypothesis (3.20). Manipulating (3.22) yields

$$g_2^{-1}(z) = \int \frac{1}{f_2(g_2^{-1}(z))}\, dz\,, \qquad z := g_2(x).$$

Calculating $g_2^{-1} \circ g_1$ we finally get

$$g_2^{-1}(g_1(y)) = \int \frac{1}{f_2(g_2^{-1}(g_1(y)))} \frac{dg_1}{dy}(y)\, dy = \int \frac{f_1(y)}{f_2(g_1^{-1}(g_2(y)))}\, dy\,,$$

which completes the proof. ■

Applying Proposition 3.4 to (3.18), we immediately obtain

$$y = F_h^{-1}(F_f(x)), \tag{3.23}$$

that is, $g = F_h^{-1} \circ F_f$ where F_f and F_h are *probability distribution functions* associated with ρ_f and ρ_h respectively, defined by

$$F_f(x) := \int_{-\infty}^{x} \rho_f(\xi)\, d\xi\,, \tag{3.24}$$

and

$$F_h(y) := \int_{-\infty}^{y} \rho_h(\xi)\, d\xi\,, \tag{3.25}$$

respectively. Note that in the derivation of (3.23) we have used the fact that the monotonicity of F_f and F_h on their respective domains guarantee the existence of F_f^{-1} and F_h^{-1} respectively. In the next section we use (3.23) to generate chaotic signals with prescribed invariant densities.

3.4.2 Generating Chaos with Prescribed Distribution

Consider the one-dimensional discrete-time dynamical system $x_{n+1} = f(x_n)$ where $f : I \to I$ is given by

$$f(x) := \begin{cases} \gamma x, & \text{if } 0 \leq x \leq 1/\gamma \\ \dfrac{\gamma}{\gamma - 1}\left(x - \dfrac{1}{\gamma}\right), & \text{if } 1/\gamma < x \leq 1 \end{cases} \tag{3.26}$$

where the parameter $\gamma \in (1, \infty)$. Chua and coworkers studied this map in [166]. The dynamical properties of this map are summarized in the following proposition.

Proposition 3.5 [166] Consider the map $f : I \to I$ defined by (3.26). For almost every $\gamma \in (1, \infty)$, f has the following properties:

i) For each $n \in \mathbf{N}$ there exists a period-n solution of f. Moreover, the total number of periodic solutions of f is countably infinite and all are unstable.

ii) Every quasi-periodic solution of the map $g : I \to I$ defined by $g(x) := f(x) - x$ is periodic.

iii) If x is not a periodic point of f, then x is also not an asymptotically periodic point.

iv) For almost all solutions the iterates of f are uniformly distributed on $[0, 1]$, that is, the invariant density of f is

$$\rho_f(x) = \chi_I(x).$$

In particular, for almost all $x \in I$ the ω-limit set is given by $L(x) = [0, 1]$ and the map f is ergodic.

v) The Lyapunov exponent of f is given by

$$\lambda = \ln \gamma + \left(\frac{1 - \gamma}{\gamma}\right) \ln(\gamma - 1).$$

It follows that $\lambda > 0$ for each $\gamma > 1$.

Proof: The reader is referred to [166] for the proof of the above properties. See also Examples A.21, A.62, A.74 and A.76 in Appendix A for the proofs of properties (iv) and (v). ■

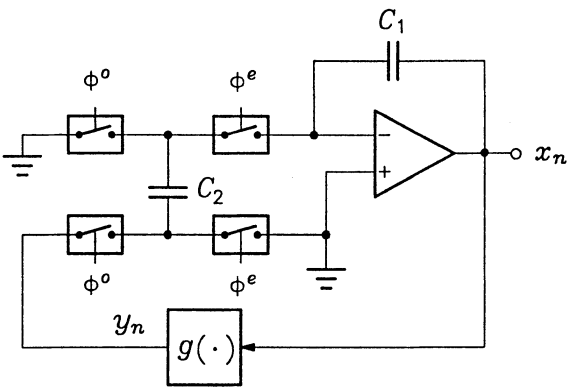

Figure 3.10: (a) Functional circuit diagram of the nonlinear switched-capacitor loop.

The nonlinear switched-capacitor circuit shown in Figure 3.10 for synthesizing the one-dimensional discrete-time system (3.26) was described in [166]. During the clock phase "odd", switches connected to gate signals ϕ^o and ϕ^e close and open respectively and therefore C_2 is charged to $-y_n$ (where $y_n = g(x_n)$). During the clock phase "even", switches connected to gate signals ϕ^o and ϕ^e open and close respectively and hence the integrator integrates the input signal to produce an output voltage of x_{n+1}, where (recalling the charge conservation principle)

$$C_1(x_{n+1} - x_n) = C_2 y_n \qquad \Longrightarrow \qquad x_{n+1} = x_n + \frac{C_2}{C_1} g(x_n).$$

Choosing $C_1 = C_2$ we have $x_{n+1} = x_n + g(x_n)$. Since $x_{n+1} = f(x_n)$, we obtain

$$g(x_n) = f(x_n) - x_n = \begin{cases} (\gamma - 1)x_n\,, & \text{if} \quad 0 \le x_n \le 1/\gamma \\ \dfrac{1}{\gamma - 1}(x_n - 1)\,, & \text{if} \quad 1/\gamma < x_n \le 1 \end{cases} . \tag{3.27}$$

Notice that g is also piecewise-linear. Each segment of the function g can be implemented by the circuit shown in Figure 3.11.

The switch S is open during every "even" phase and closes during the "odd" phase only if $V_3 > V_4$; otherwise it remains open. During the even phase the capacitor C_3 is charged to voltage $V_2 - V_1$. If $V_3 > V_4$ then all the charge in C_3 is transferred to the capacitor C_4 during the next odd phase.

To synthesize the function g of (3.27) two subcircuits of the type in Figure 3.11 are required. For the first we require that

$$V_1 = 1\text{V}\,, \quad V_2 = x_n\,, \quad V_3 = x_n\,, \quad V_4 = 1/\gamma\,, \quad C_3 = C/(\gamma - 1) \quad \text{and} \quad C_4 = C\,.$$

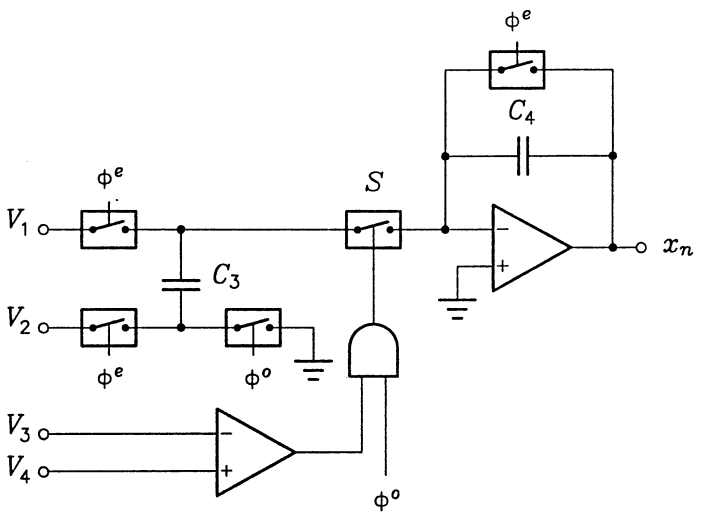

Figure 3.11: Switched-capacitor building block for piecewise-linear functions.

For the second we put

$$V_1 = 0\text{V}\,,\quad V_2 = x_n\,,\quad V_3 = 1/\gamma\,,\quad V_4 = x_n\,,\quad C_3 = (\gamma - 1)C \quad \text{and} \quad C_4 = C\,.$$

The complete circuit implementing the map g is shown in Figure 3.12 which completes the circuit for synthesizing the map f. In [166] TL074C operational amplifiers and HEP4066BP analogue switches were used to implement the circuit that synthesizes f.

We now analyze the map f numerically for the case $\gamma = \sqrt{3}$. For all numerical experiments we use the initial condition $x_0 = 0.21$ and the first 3000 samples are disregarded in order to get rid of the effects of transient response. The time response for this case is shown in Figure 3.13(a). Figure 3.13(b) shows the power spectral density for the case under investigation. As can be seen from Figure 3.13(b), the power spectral density is reminiscent of narrow band noise. Histogram estimates of the probability density confirm that the samples of the time evolution of f are distributed uniformly on the unit interval I. Numerical calculation of the Lyapunov exponent from the time series yields $\lambda \approx 0.6813$ which provides numerical evidence that f is chaotic for $\gamma = \sqrt{3}$. The correlation dimension which is calculated from the time series was found to be $d_G \approx 0.8509$ (see also [166]).

Next we consider maps which are topologically conjugate to the map f of (3.26). Although such a map would also be chaotic when f is chaotic, its invariant density function would differ depending on the transformation relating this map to f, as was shown in the previous section. Recalling that iterates of the map f are uniformly distributed on the interval $[0, 1]$, the transformation of $\{x_n\}$ (the iterates of f) to

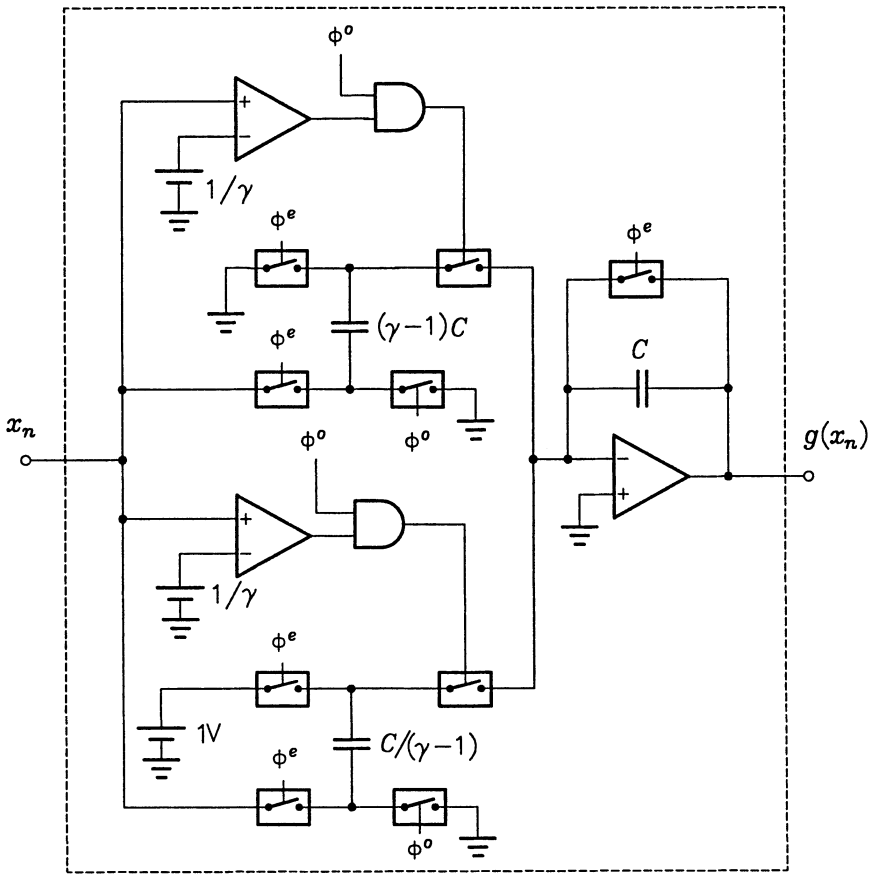

Figure 3.12: Complete functional circuit for synthesizing function g.

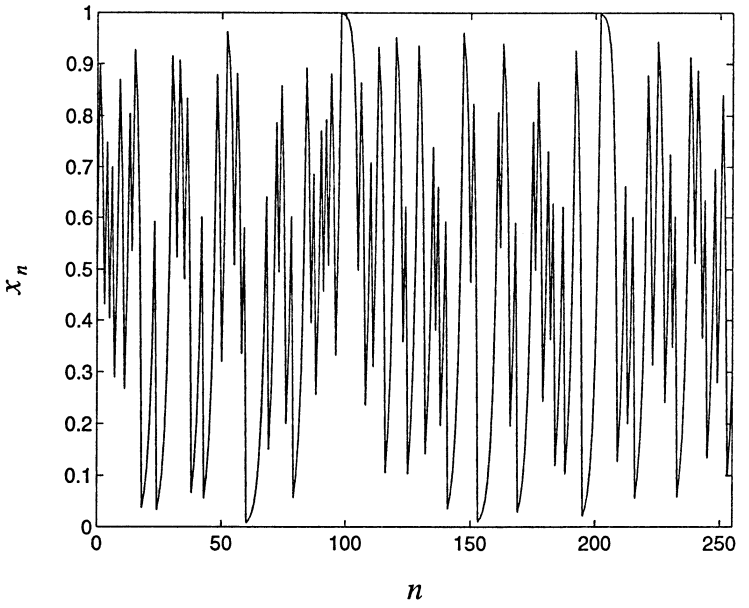

(a)

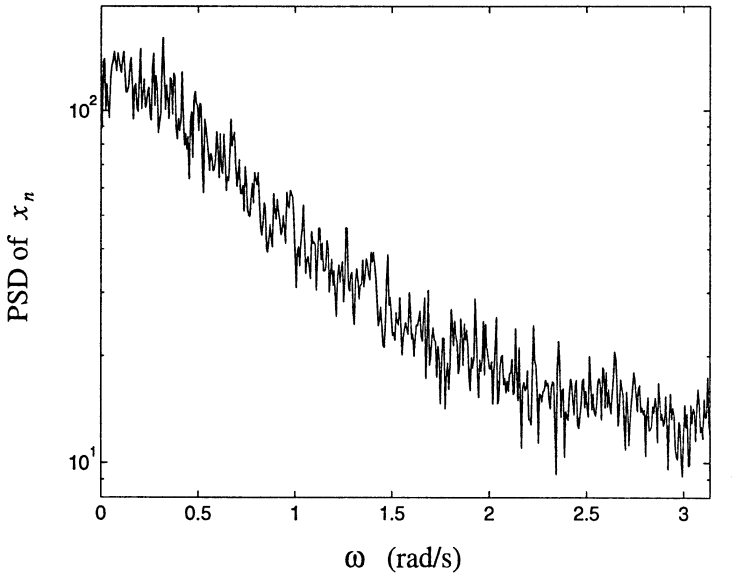

(b)

Figure 3.13: (a) Time evolution of the map f; (b) Power spectral density of the time evolution.

$\{y_n\}$ (the transformed response having the prescribed invariant density ρ_h) simplifies to

$$y_n = F_h^{-1}(x_n)\,, \tag{3.28}$$

where F_h is the probability distribution function of the map h which is given by

$$h = F_h^{-1} \circ f \circ F_h\,.$$

Here F_h is related to ρ_h according to (3.25).

Example 3.6 Suppose that we require a map h whose iterates are distributed exponentially, that is, h has invariant density ρ_h given by

$$\rho_h(y) = \begin{cases} \beta e^{-\beta(y-\mu)}, & \text{if } x \geq \mu \\ 0, & \text{if } x < \mu \end{cases}\,, \tag{3.29}$$

where $\beta > 0$ and $\mu \in \mathbf{R}$.

Using (3.28) with

$$F_h(y) = 1 - e^{-\beta(y-\mu)}\,,$$

which is obtained by integrating ρ_h (see (3.25)), we see that $\{y_n\}$ and $\{x_n\}$ are related by

$$y_n = \mu - \beta^{-1}\ln(1 - x_n)\,. \tag{3.30}$$

For the case $\gamma = \sqrt{3}$, $\beta = 1$, $\mu = 0$, the iterates $\{y_n\}$ of h were calculated. In addition a histogram estimate of the invariant density ρ_h of $\{y_n\}$ was calculated. This is shown in Figure 3.14. In order to compare this with an actual exponential distribution, we have fitted the function in (3.29) to the measured probability density function, using the method of steepest descent to minimize the mean square error. As can be seen from Figure 3.14 the agreement is good. ■

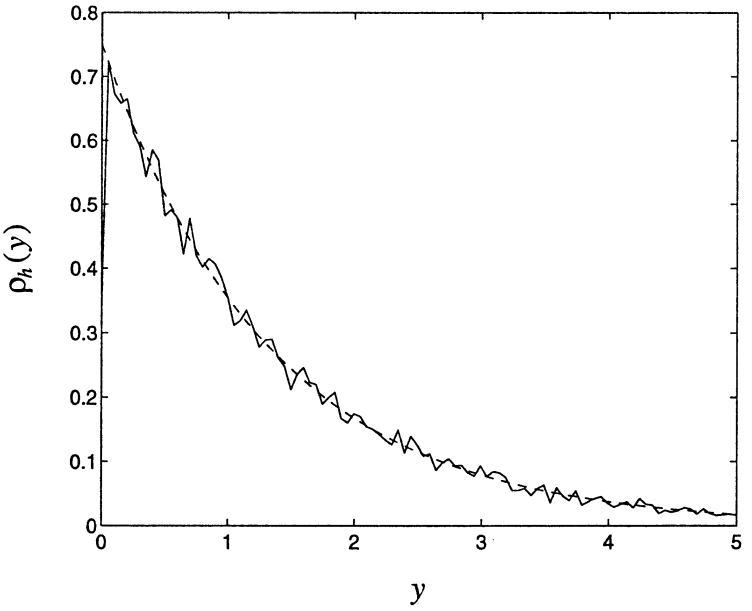

Figure 3.14: Probability density function of the map h: histogram estimate (solid line) and the exact exponential probability density function (dashed line).

3.4.3 Survey on Literature

In addition to the work done by Chua and coworkers in [166] which was discussed in the previous section, several others have also realized the potential of chaotic systems to be used as noise generators. Bernstein and Lieberman [75] have studied a chaotic first-order *digital phase-locked loop* (DPLL) for use as a random number generator. They have shown that the first-order DPLL is described by the circle map

$$x_{n+1} = f(x_n) := \left(x_n + \frac{k}{1 - A \sin x_n} \right) (\mathrm{mod}\ 2\pi), \tag{3.31}$$

where $k, A \in \mathbf{R}$. The graph of this map is plotted in Figure 3.15 for parameter values $A = 0.25$ and $k = 8.5$. To obtain random binary digits from the system they defined the output y_n as

$$y_n := \begin{cases} 1, & \text{if } x_n \in [0, \pi) \\ 0, & \text{if } x_n \in [\pi, 2\pi) \end{cases},$$

for each $n \in \mathbf{N}$. Assuming information was obtained by observing the system output at, say, time $n = 0$, they studied the average rate of information loss of the map in (3.31) when no further observations were made. This was done by calculating the time evolution of the information observed initially. The time evolution of the

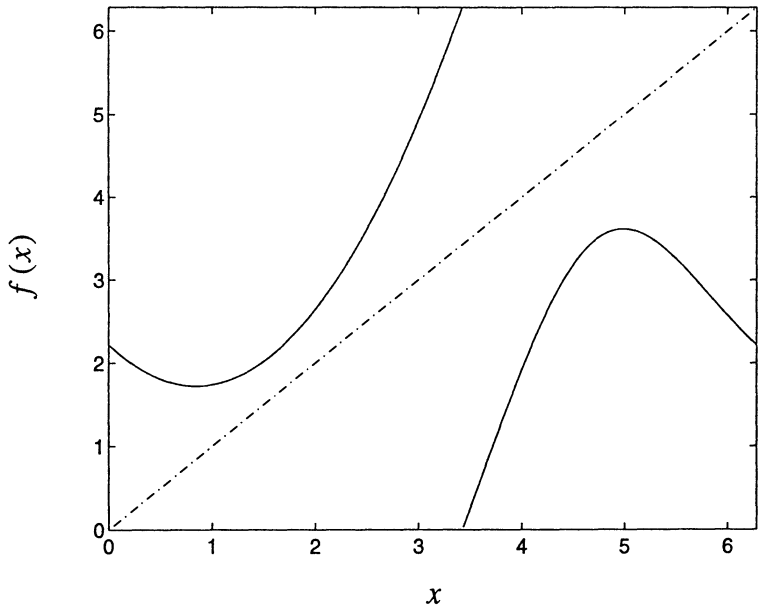

Figure 3.15: Graph of the circle map (3.31) for $A = -0.25$ and $k = 8.5$.

information is given by

$$H_n = \int_0^{2\pi} \rho_n(x) \ln\left(\frac{\rho_n(x)}{\rho(x)}\right) dx\,,$$

where the information available at time $n = 0$ is determined by the probability density function ρ_0 which in turn is determined by the outcome of the initial observation made. Here ρ is the invariant density of the system. The successive probability densities ρ_n, $n = 1, 2, \ldots$ were obtained by means of iterating the Frobenius-Perron equation, starting with ρ_0. As n increases, ρ_n converges towards ρ, the invariant density resulting in H_n approaching 0. The invariant density for the case $A = -0.25$ and $k = 8.5$ as we calculated by numerical iteration of the Frobenius-Perron equation, is shown in Figure 3.16. The iteration was performed at 4096 uniformly spaced points in the interval $[0, 2\pi]$. Applying Birkhoff's ergodic theorem, numerical integration produces the value $\lambda \approx 0.5332$ for the Lyapunov exponent.

Now suppose that a "1" is observed at the system output. The probability density ρ_0 corresponding with this information is shown in Figure 3.17. The first four subsequent iterates of the probability density function ρ_0 are shown in Figure 3.18. The loss of information based on the single observation made (i.e. no subsequent observations are made) is shown in Figure 3.19. The functional circuit for the first-order DPLL studied by Bernstein and Lieberman is shown in Figure 3.20.

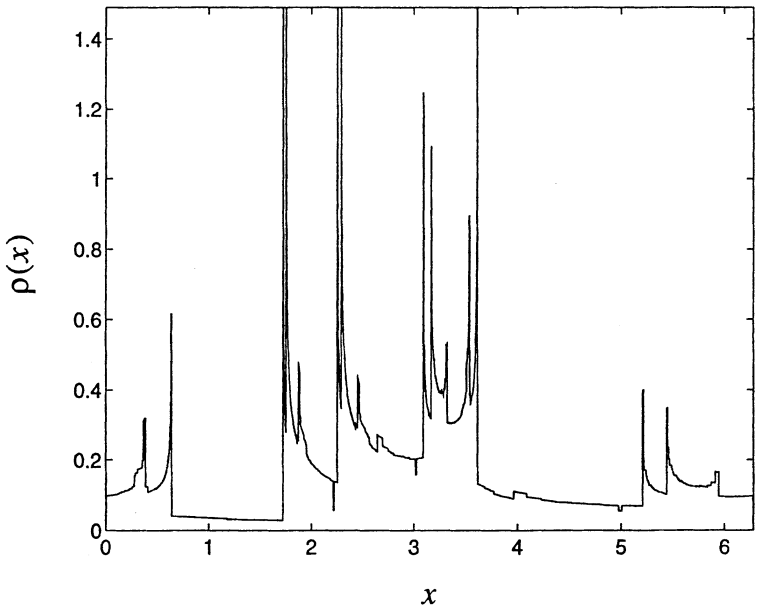

Figure 3.16: Invariant density for the circle map (3.31) with $A = -0.25$ and $k = 8.5$.

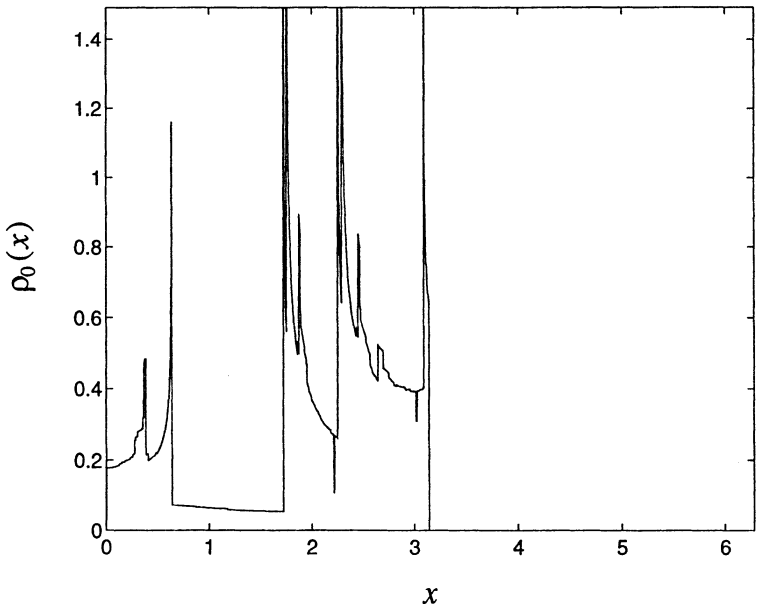

Figure 3.17: Probability density based on the observation of a "1".

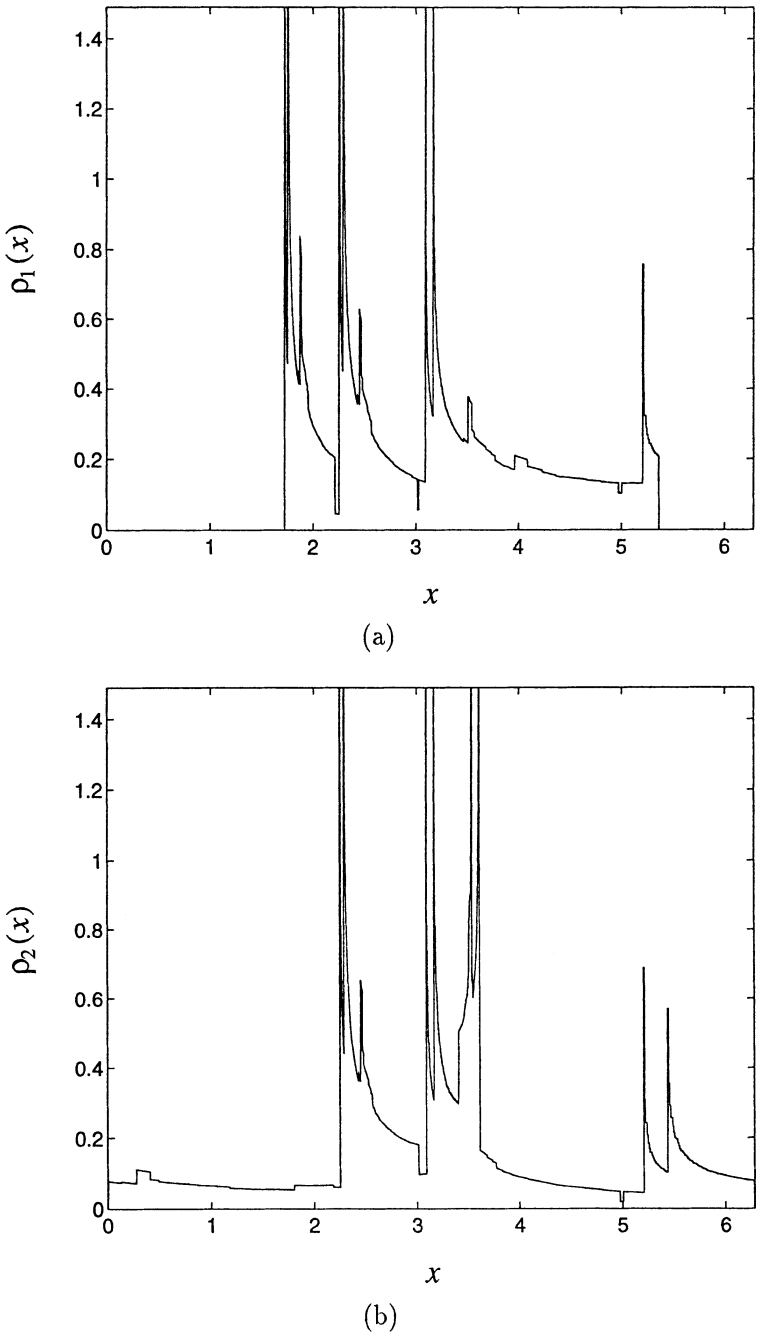

Figure 3.18: First four subsequent probability density functions after iterating the system in the absence of additional observations.

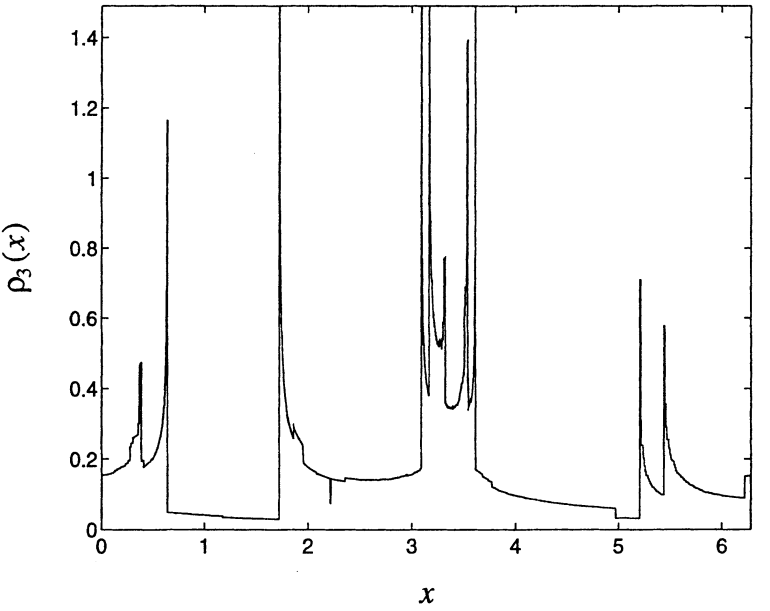

(c)

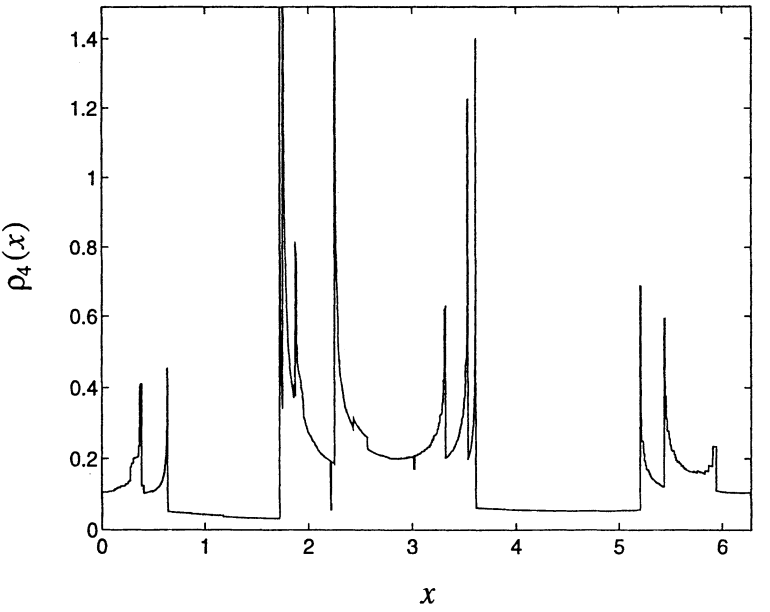

(d)

Figure 3.18: (Continued)

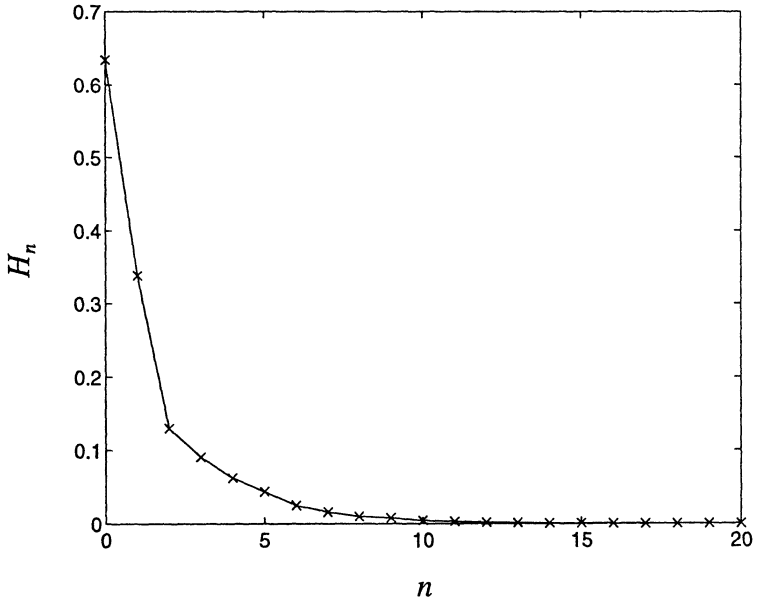

Figure 3.19: Loss of information about the system's state as time progresses.

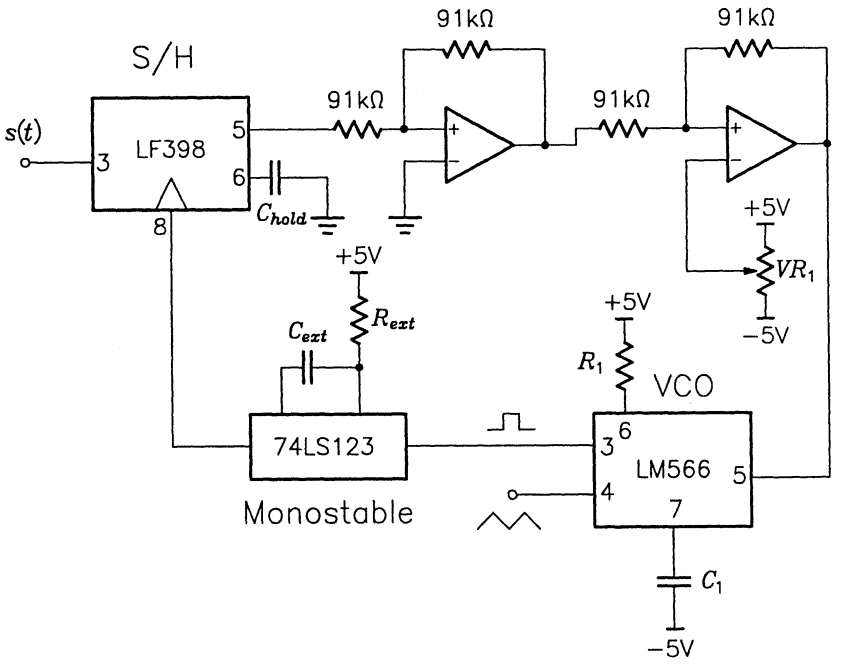

Figure 3.20: Functional circuit diagram for the DPLL studied by Bernstein and Lieberman.

McGonigal and Elmasry devised an electronic circuit for synthesizing the logistic map. Their measurements showed the output power spectral density to be approximately white (see [530]). Using the period-doubling property of the logistic map they were able to operate this circuit as a 2- and 4-valued oscillator.

A method for the generation of noise with seemingly arbitrary power spectral density and probability density was studied by Murch and Bates in [568]. Their method was based on the use of hierarchies of recursive loops generating variable-gain sequences.

In [211] a switched-capacitor circuit which realizes a one-dimensional map was proposed for generating $1/f^{\delta}$ noise. This switched-capacitor circuit exhibits the *hopping transition*, which was previously found to be a mechanism for the appearance of $1/f^{\delta}$ divergencies.

Another switched-capacitor circuit which generates $1/f^{\delta}$ noise was presented by Murao and his collaborators (see [567]). The proposed circuit used logarithmic and antilogarithmic amplifiers for realizing the nonlinear term x^z. The map describing the dynamical behaviour of the circuit is

$$x_{n+1} = f(x_n) := \begin{cases} x + ux^z, & \text{if } 0 \le x \le a \\ (x-a)/(1-a), & \text{if } a < x \le 1 \end{cases},$$

where $u > 0$ and $1 < z < 2$. The authors calculated the power spectral density of the circuit output by an indirect method which is based on the Galerkin approximation to the Frobenius-Perron integral operator. Results obtained this way were in good agreement with measured results.

3.5 Sigma-Delta Modulators

The increasing use of digital techniques has led to significant research interest in the analogue-to-digital and digital-to-analogue converters which serve as interfaces between digital processing systems and real-world analogue signals. Ideally, these interfaces should be implemented in VLSI technology so as to maximize reliability and minimize cost of the complete system. While modern VLSI techniques produce very high-speed and high-density digital circuits, they restrict the dynamic range and precision of the analogue stages. Conventional analogue-to-digital conversion techniques require high precision components and often don't take advantage of the very high speeds permitted by the VLSI technology.

These disadvantages are overcome with oversampled analogue-to-digital converters. The structure is simple and is tolerant of circuit imperfections and component matching inaccuracies. The quantization can be coarse—in the basic implementation, the

quantizer has just two levels. To permit accurate signal reconstruction with such a quantizer the signal is sampled at a rate much higher than the usual Nyquist rate, and a large number of the resultant coarse representations of the signal are used to generate a single high resolution representation.

Sigma-Delta ($\Sigma\Delta$) modulation is the most popular method used for realizing oversampled analogue-to-digital converters. In its simplest form the $\Sigma\Delta$ modulator is a single-loop system in which a one-bit quantizer is used together with a discrete time integrator inside the feedback loop. This basic structure can be extended by adding more feedback loops, increasing the number of quantization levels or altering the forward path transfer function. Since in such complex systems stability often becomes a problem, the most commonly used $\Sigma\Delta$ structures are the single- and double-loop modulators.

An important feature of $\Sigma\Delta$ modulation is the appearance of periodic orbits in the output bit stream. As a result, the quantization noise of the single-loop system is not white, but rather contains discrete spikes at frequencies depending on the input. This "periodic noise" can be particularly objectionable in audio applications. Higher order systems suffer from this problem to a lesser extent than does the single-loop system.

Oversampled $\Sigma\Delta$ modulation as a method of analogue-to-digital conversion in electronic circuits was first studied by Inose and Yasuda [387] and Candy [111]. The technique is now finding widespread use in such applications as digital signal processing systems, voiceband telecommunication systems and commercial compact disc players [282], [547].

3.5.1 Analysis

The structure of a single-loop $\Sigma\Delta$ modulator is depicted in Figure 3.21. The modulator consists of a discrete time accumulator (also referred to as an integrator) and a one-bit quantizer located in the outer loop. The input to the modulator is denoted by x_n and the input signal to the delay element is denoted by u_n. Throughout this section we assume that the input is fixed to some $x \in (-1, 1]$. Under this assumption the first order difference equation that describes the behaviour of the $\Sigma\Delta$ modulator in Figure 3.21 is

$$u_{n+1} = f(u_n) := pu_n + x - q(u_n), \tag{3.32}$$

with the quantizer function q defined by

$$q(u) := \operatorname{sgn}(u).$$

For the ideal case (i.e. $p = 1$) with the initial state $u_0 \in [x - 1, x + 1)$ the dynamics are equivalent to that of the circle map (see [217]). For this case the output bit stream is periodic if x is rational and quasiperiodic if x is irrational. The case of

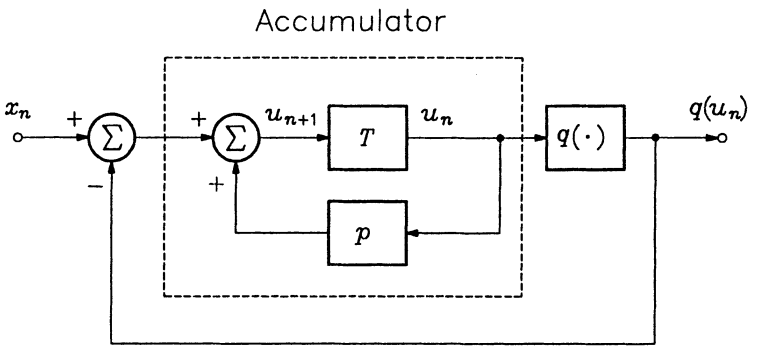

Figure 3.21: Block diagram of a single-loop $\Sigma\Delta$ modulator.

leaky integration (i.e. $p < 1$) was studied by [473], [250] and [613]. For this case it has been shown that almost all constant inputs yield a periodic output sequence and an asymptotically periodic quantizer error sequence. The remainder of our discussion of the $\Sigma\Delta$ modulator will focus on the case $p > 1$.

The fixed points of f are

$$u^*_{-1} := \frac{x+1}{1-p}, \qquad u^*_1 := \frac{x-1}{1-p},$$

and for $x = 0$ we also have the fixed point $u^*_0 = 0$. Since $p > 1$, both fixed points are unstable. Notice that if $x + 1 < u^*_1$ and $x - 1 > u^*_{-1}$, i.e. if $|x| < -1 + 2/p$, then each orbit starting inside the interval (u^*_{-1}, u^*_1) will eventually remain inside $[x-1, x+1]$. This means, if $|x| < -1 + 2/p$ then $[x-1, x+1]$ contains the attractor of f with $[u^*_{-1}, u_1]$ the basin of attraction of this attractor (see also [250]).

We now focus our attention on the case $x = 0$. For this case the bifurcation diagram with p as the bifurcation parameter is shown in Figure 3.22. The band boundaries of the bifurcation diagram are given by [250]

$$\begin{aligned} \pm 1, F^{\pm}_1(p), \ldots, F^{\pm}_6(p) \quad & \text{for} \quad 1 < p < p_1\,, \\ \pm 1, F^{\pm}_1(p), F^{\pm}_2(p) \quad & \text{for} \quad p_1 < p < \sqrt{2}\,, \\ \pm 1 \quad & \text{for} \quad \sqrt{2} < p \leq 2\,, \end{aligned}$$

where $p_1 \approx 1.1892$ and

$$F^{\pm}_j(p) := \pm f^{(j)}(1; p, 0).$$

Here $f(u; p, x)$ is $f(u)$ in (3.32) with explicit indication of the parameters p and x.

Assuming that for a given choice of parameters the invariant density ρ of f has a support with nonzero Lebesgue measure (i.e. f is ergodic), then application of the

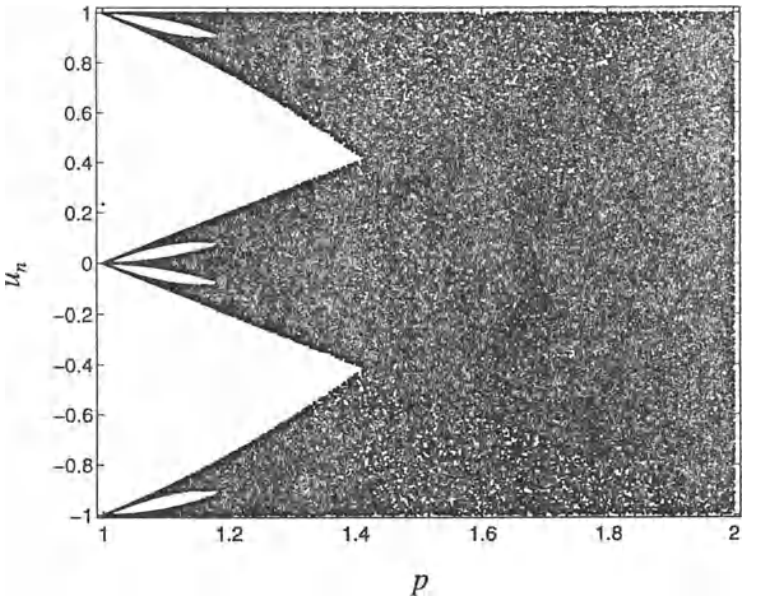

Figure 3.22: Bifurcation diagram for $x = 0$: p vs. u_n.

Birkhoff ergodic theorem yields

$$\lambda = \int_{-1}^{1} \ln \left| \frac{df}{du}(u) \right| \rho(u)\, du = \ln p \int_{-1}^{1} \rho(u)\, du = \ln p. \tag{3.33}$$

For $p = 2$ it is easy to show that the map f is linearly conjugate to the Bernoulli shift map $g : I \to I$ where

$$g(u) := 2u \,(\text{mod } 1).$$

The invariant density associated with $p = 2$ is therefore

$$\rho(u) = \frac{1}{2}\chi_{(-1,1)}(u),$$

where $\chi_{(-1,1)}$ is the characteristic function of the interval $(-1, 1) \in \mathbf{R}$. The Lyapunov exponent for $p = 2$ is $\lambda = \ln 2$.

We saw in Section 3.3 that it is possible to calculate invariant densities analytically for special cases of parameter values of mappings. Now, consider the parameter value $p = \sqrt{2}$ which is deduced from the requirement

$$f^{(2)}(-1) = f(1) \qquad \Longleftrightarrow \qquad f_-^{(2)}(-1) = f_+(1),$$

where

$$f_-(u) := pu + 1\,, \qquad f_+(u) := pu - 1\,.$$

The Frobenius-Perron equation for the map f is given by

$$\rho_{n+1} = P\rho_n, \tag{3.34}$$

where the Frobenius-Perron operator P is defined by

$$(P\rho_n)(u) := \frac{1}{p}\rho_n\left(\frac{u-1}{p}\right) + \frac{1}{p}\rho_n\left(\frac{u+1}{p}\right), \qquad (p = \sqrt{2}, \text{ fixed}). \tag{3.35}$$

The fixed point of the Frobenius-Perron operator must now be determined. Since the Frobenius-Perron operator is linear and contracting [467], we consider its iterates. As initial density ρ_0 we consider

$$\rho_0(u) = \frac{1}{2}\chi_{(-1,1)}(u). \tag{3.36}$$

Then

$$\begin{aligned}
\rho_1(u) &= (P\rho_0)(u) \\
&= \frac{1}{2p}\left(\chi_{(-1,1-p]}(u) + 2\chi_{(1-p,p-1)}(u) + \chi_{[p-1,1)}(u)\right) \qquad (3.37) \\
&= \frac{1}{\sqrt{2}}\rho_0(u) + \frac{1}{2\sqrt{2}}\chi_{(1-p,p-1)}(u). \qquad (3.38)
\end{aligned}$$

Next, using (3.37) we have

$$\rho_2(u) = (P\rho_1)(y) = \rho_0(u) - \frac{1}{4}\left(\delta_{1-p}(u) + \delta_{p-1}(u)\right),$$

where, for fixed $y \in \mathbf{R}$

$$\delta_y(u) := \begin{cases} 1, & \text{if } u = y \\ 0, & \text{if } u \neq y \end{cases}.$$

Using the results

$$(P\delta_{1-p})(u) = \frac{1}{\sqrt{2}}\delta_{p-1}(u), \qquad (P\delta_{p-1})(u) = \frac{1}{\sqrt{2}}\delta_{1-p}(u),$$

we obtain

$$\rho_3(u) = \rho_1(u) - \frac{1}{4\sqrt{2}}\left(\delta_{1-p}(u) + \delta_{p-1}(u)\right).$$

Continuing in this way, we obtain

$$\rho_{2k}(u) = \rho_0(u) - \frac{1}{4}\left(\sum_{i=1}^{k}\frac{1}{2^{i-1}}\right)\left(\delta_{1-p}(u) + \delta_{p-1}(u)\right),$$

and

$$\rho_{2k+1}(u) = \rho_1(u) - \frac{1}{4\sqrt{2}}\left(\sum_{i=1}^{k}\frac{1}{2^{i-1}}\right)\left(\delta_{1-p}(u)\delta_{p-1}(u)\right),$$

for each $k = 0, 1, 2, \ldots$. Taking the limit $k \to \infty$, the above expressions yield

$$\rho_0^*(u) := \lim_{k\to\infty} \rho_{2k}(u) = \rho_0(u) - \frac{1}{2}\left(\delta_{1-p}(u) + \delta_{p-1}(u)\right), \tag{3.39}$$

and

$$\rho_1^*(u) := \lim_{k\to\infty} \rho_{2k+1}(u) = \rho_1(u) - \frac{1}{2\sqrt{2}}\left(\delta_{1-p}(u) + \delta_{p-1}(u)\right), \tag{3.40}$$

where ρ_0 and ρ_1 are given by (3.36) and (3.38). It is easily verified that

$$\rho_1^* = P\rho_0^*, \qquad \rho_0^* = P\rho_1^*,$$

and hence $\{\rho_0^*, \rho_1^*\}$ is a period-2 orbit of the Frobenius-Perron operator (3.35). Thus repeated iteration of the Frobenius-Perron equation has produced a period-2 orbit instead of a fixed point as one would expect. The question now is how does one obtain the fixed point of the Frobenius-Perron operator. The answer to this question is given by the following lemma.

Lemma 3.7 If $\{\rho_i^*\}_{i=0}^{m-1}$, $m \in \mathbf{N}$ is a period-m orbit of the Frobenius-Perron operator P of the map $f : X \subset \mathbf{R} \to X$, then ρ^* defined by

$$\rho^*(u) := \frac{1}{m}\sum_{i=0}^{m-1} \rho_i^*(u), \quad \text{for each} \quad u \in X,$$

is a fixed point of P.

Proof: Using the linearity of P, we have

$$\begin{aligned} P\left(\frac{1}{m}\sum_{i=0}^{m-1}\rho_i^*\right)(u) &= \frac{1}{m}\sum_{i=0}^{m-1}(P\rho_i^*)(u) \\ &= \frac{1}{m}\sum_{i=0}^{m-1}\rho_{i+1}^*(u) \\ &= \frac{1}{m}\sum_{i=0}^{m-1}\rho_i^*(u), \end{aligned}$$

since $\rho_m^* = \rho_0^*$ by definition of $\{\rho_i^*\}_{i=1}^{m-1}$ and consequently

$$\rho^*(u) := \frac{1}{m}\sum_{i=0}^{m-1} \rho_i^*(u), \quad u \in X,$$

is a fixed point of P. ■

Thus a fixed point of P in (3.35) is

$$\begin{aligned}\rho^*(u) &= \frac{\rho_0^*(u)+\rho_1^*(u)}{2} \\ &= \frac{1+\sqrt{2}}{4}\chi_{(-1,1)}(u)+\frac{1}{4\sqrt{2}}\chi_{(1-p,p-1)}(u)-\frac{1+\sqrt{2}}{4}\left(\delta_{1-p}(u)+\delta_{p-1}(u)\right).\end{aligned}$$

Explicitly, ρ^* is given by

$$\rho^*(u)=\begin{cases}\dfrac{1+\sqrt{2}}{4\sqrt{2}}, & \text{if } \sqrt{2}-1<|u|<1 \\ 0, & \text{if } |u|=\sqrt{2}-1 \\ \dfrac{1+\sqrt{2}}{4}, & \text{if } 1-\sqrt{2}<u<\sqrt{2}-1\end{cases}. \tag{3.41}$$

In order to verify this result, we attempted to calculate the invariant density by numerical iteration of the Frobenius-Perron equation (3.34) and (3.35). As initial condition we assumed the uniform density given by (3.36). Figure 3.23 shows the converged even and odd densities, ρ_0^* and ρ_1^*. To be able to compare these with the corresponding analytical expressions, we write explicit expressions for both ρ_0^* and ρ_1^*, namely

$$\rho_0^*(u)=\begin{cases}\dfrac{1}{2}, & \text{if } \sqrt{2}-1<|u|<1 \\ 0, & \text{if } |u|=\sqrt{2}-1 \\ \dfrac{1}{2}, & \text{if } 1-\sqrt{2}<u<\sqrt{2}-1\end{cases}, \tag{3.42}$$

and

$$\rho_1^*(u)=\begin{cases}\dfrac{1}{2\sqrt{2}}, & \text{if } \sqrt{2}-1<|u|<1 \\ 0, & \text{if } |u|=\sqrt{2}-1 \\ \dfrac{1}{\sqrt{2}}, & \text{if } 1-\sqrt{2}<u<\sqrt{2}-1\end{cases}. \tag{3.43}$$

The agreement was found to be excellent. The average of the numerical estimates of ρ_0^* and ρ_1^* were then calculated and used as initial conditions for the numerical iteration of the Frobenius-Perron equation. This indeed turned out to be the fixed point of the Frobenius-Perron equation (see Figure 3.23(c)) and was found to be in good agreement with ρ in (3.41). The zero points of ρ can explained by referring to the bifurcation diagram with the observation that at $p=(\sqrt{2})^+$ there is band merging. For example, for the case $p=1.415$ (studied in [250]) numerical iteration of the Frobenius-Perron equation (starting with the uniform density) produced a

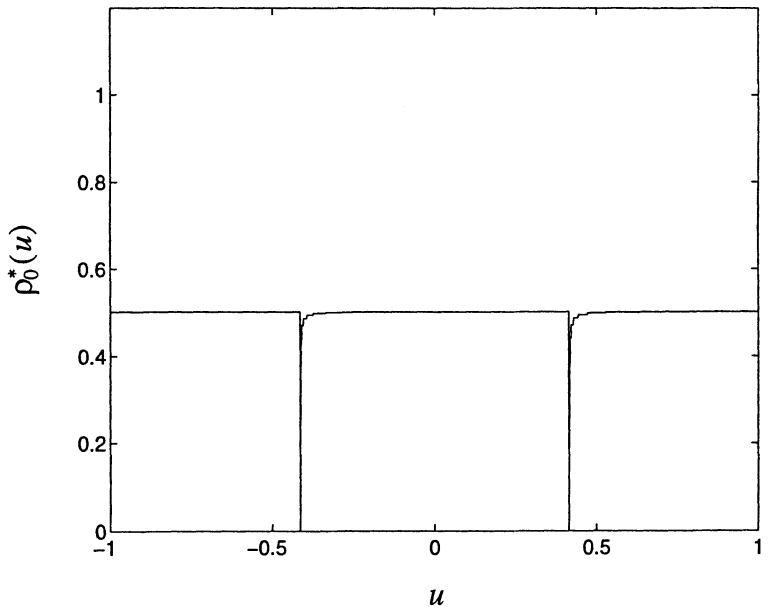

(a)

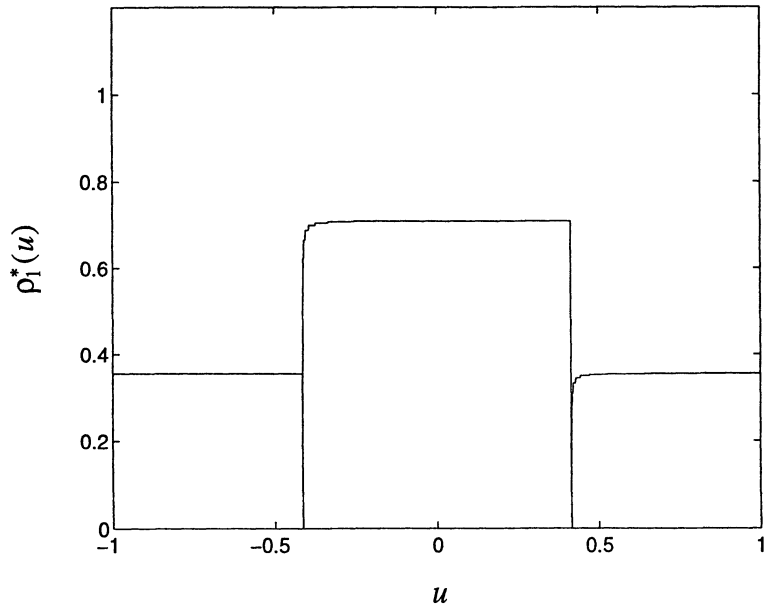

(b)

Figure 3.23: Numerical solution of the Frobenius-Perron equation starting with the uniform density (3.36): period-2 solution (a) Even iterate; (b) Odd iterate; (c) Fixed point.

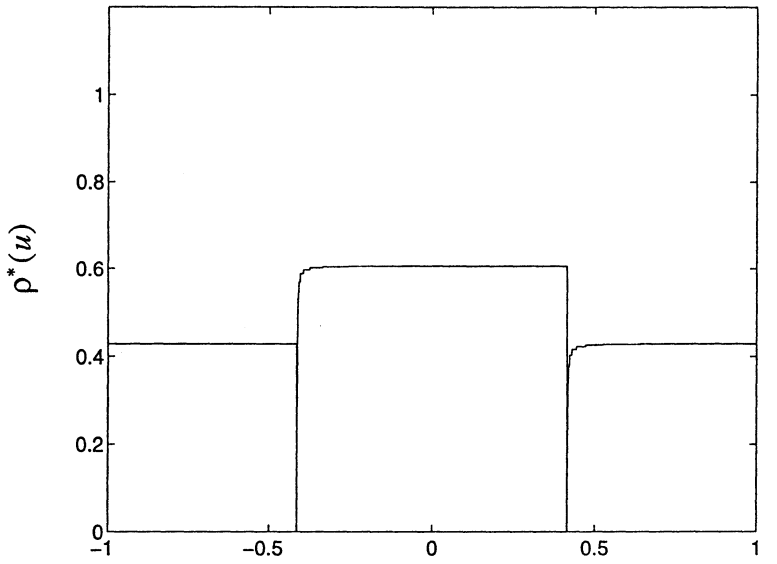

(c)

Figure 3.23: (Continued)

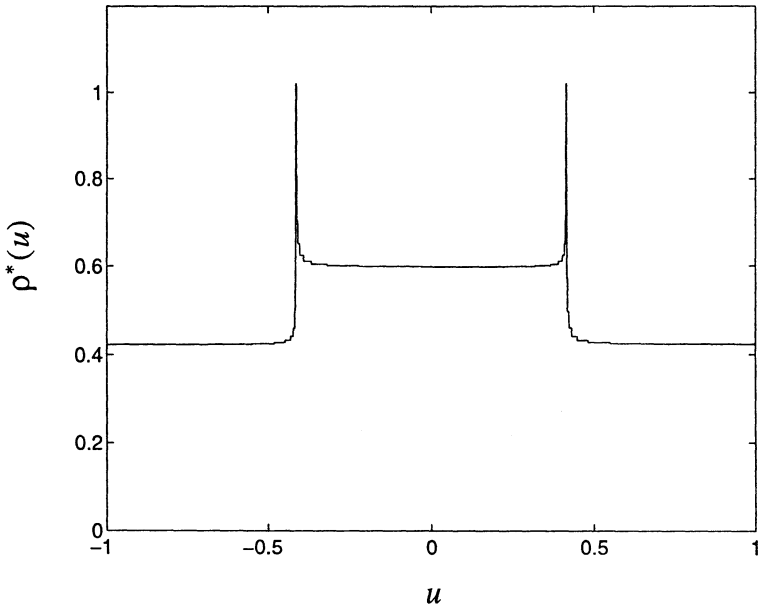

Figure 3.24: Numerically calculated invariant density for the case $p = 1.415$.

period-2 orbit from which the fixed point was then calculated as explained above. This fixed point of the Frobenius-Perron equation obtained is shown in Figure 3.24. Clearly the band merging is indicated by the impulses at $u = \pm 0.415$.

Further investigation of the case $p = \sqrt{2}$ showed that by using different densities as initial conditions for the Frobenius-Perron equation, different period-2 solutions could be produced. Moreover, any such period-2 solution can be expressed as a convex linear combination of ρ_0^* and ρ_1^* given by (3.39) and (3.40), that is,

$$\tilde{\rho}_0 = \alpha\rho_0^* + (\alpha - 1)\rho_1^*, \qquad \tilde{\rho}_1 = (\alpha - 1)\rho_0^* + \alpha\rho_1^*,$$

for some $\alpha \in [0, 1]$. It follows easily that the periodicity of $\{\rho_0^*, \rho_1^*\}$ under P implies the periodicity of $\{\tilde{\rho}_0, \tilde{\rho}_1\}$ under P for each (fixed) $\alpha \in [0, 1]$. As an example, consider as initial density the Gaussian density restricted to the interval $(-1, 1)$, namely

$$\rho_0(u) = \frac{1}{A} e^{-u^2/\sigma^2} \chi_{(-1,1)}(u), \tag{3.44}$$

for $\sigma := 1/\sqrt{10}$ and

$$A := \int_{-1}^{1} e^{-u^2/\sigma^2}\, du\,.$$

The numerical estimates of the period-2 orbit $\{\tilde{\rho}_0, \tilde{\rho}_1\}$ of P and the associated fixed point $\tilde{\rho} := (\tilde{\rho}_0 + \tilde{\rho}_1)/2$ of P are shown in Figure 3.25. Although the periodic orbit obtained here differs from that obtained earlier for the uniform density (3.36), the fixed points are identical. Since by (3.33) the Lyapunov exponent is $\lambda = \ln\sqrt{2}$ we conclude that f is chaotic for $p = \sqrt{2}$ from a numerical point of view.

The chaotic nature of the map f was analyzed in [250] by using symbolic dynamics. For further details, the reader is referred to this article.

Although the presence of chaos is usually considered to be undesirable, it can be put to good use in $\Sigma\Delta$ modulators. Schreier [703] showed that chaos can be used to destabilize undesirable limit cycles which in audio applications manifest as objectionable tones. Schreier found that the amount of chaos introduced in the modulator must be sufficient to adequately destabilize troublesome limit cycles, yet be small enough to ensure proper operation of the modulator.

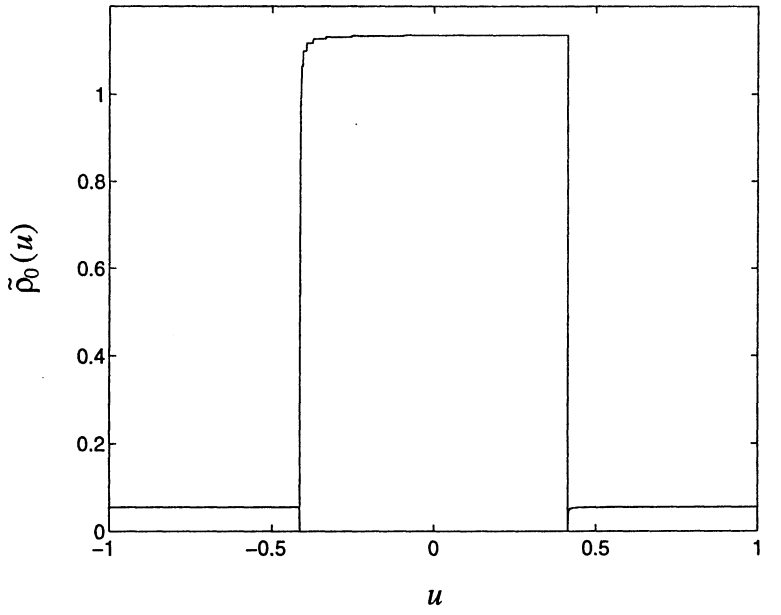

(a)

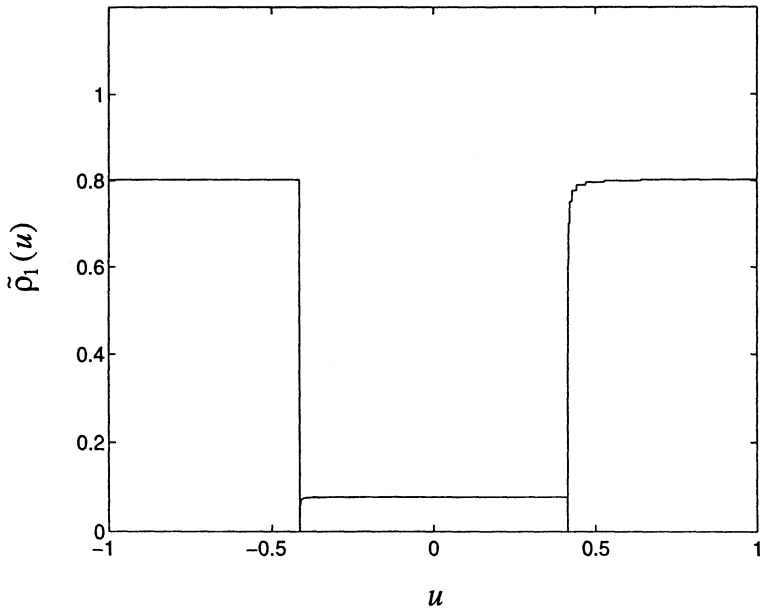

(b)

Figure 3.25: Numerical solution of the Frobenius-Perron equation starting with the Gaussian density (3.44): period-2 solution (a) Even iterate; (b) Odd iterate; (c) Fixed point.

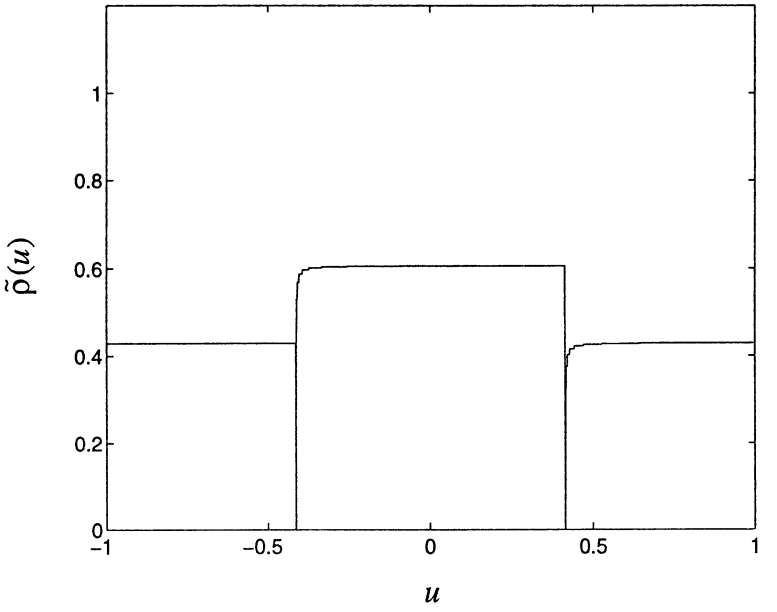

(c)

Figure 3.25: (Continued)

Chapter 4

Higher Dimensional Maps in Electronics

4.1 Introduction

In this chapter we take a look at electronic circuits of which the dynamical behaviour is described by higher dimensional maps. Many electronic systems and circuits operate discretely in time and are therefore described by mappings rather than differential equations.

In Section 4.2 we discuss a circuit proposed and investigated by Mishina *et al.* [548]. This circuit synthesizes two logistic maps which may or may not be coupled depending on the position of a switch. At first it may seem a little odd to design a circuit that mimics a theoretical model, as one would prefer rather to analyze real-life circuits and systems and derive analytical results for it. However, this is not really that artificial, since in Chapter 3 we discussed a switched-capacitor circuit of which the dynamics was described by the logistic map. On the other hand, synthesizing theoretical models provides one with the opportunity to study these models in a real-life environment which is not so idealistic and friendly as studying them on computer or on paper. Hence one is faced with new challenges, e.g. minimizing noise interference in the circuit and establishing accurate measurement procedures using non-ideal apparatus and instruments. In this section the results of Mishina are compared with numerical results we have obtained for the same system of equations.

In Section 4.3 the behaviour of an infinite impulse response (IIR) digital filter with fixed tap weights and which utilizes a two's complement adder with overflow is discussed. Interesting behaviour is exhibited by this filter ranging from simple limit cycles, quasi-periodic behaviour to chaos and fractals [158], [156], [440].

Allowing the weights of a digital filter to vary during operation provides additional degrees of freedom which may be utilized to achieve the objectives of the filtering process especially when operating in a nonstationary environment [348]. In this case the filter is said to be adaptive. In the case of a finite impulse response (FIR) filter the weights may assume arbitrary values without jeopardizing the operation of the filter. However, in the case of an IIR digital filter, arbitrary values of the weights may cause the filter to become unstable and hence the weights must be kept in the stability region in weight space. Adaptive IIR filters are considered in Section 4.4. For the adaptive IIR filter, the algorithm for adapting the filter weights is usually nonlinear and is therefore one of the elements in such a filter which may cause the filter to behave chaotically. That this is indeed so is demonstrated for a simple IIR filter with a single adjustable weight [504]. Such complex behaviour as bifurcations and chaos is exhibited by this simple filter.

Another potential source of chaos synonymous with discrete-time systems is the rounding error. In Section 4.5 the concept of a mixed state is first introduced. A mixed state version of the Shiraiwa-Kurata theorem [814] is then used to find analytical conditions under which a typical digital control system's response is chaotic. A specific example of such a system is presented.

Yet another aspect important for the proper operation of discrete-time systems is the selection of its sampling period. For linear systems the well-known Nyquist sampling criterion gives minimal requirements under which continuous-time signals may be reconstructed from their sampled counterparts. In Section 4.6 it is shown for a class of sampled-data systems that there exists a sampling period $T^* \in \mathbf{R}^+$ such that there systems are chaotic for all sampling periods $T > T^*$. In closing two examples of such systems are discussed.

4.2 Coupled Logistic Map

Mishina *et al.* [548] devised a circuit which demonstrates experimentally the dynamics of the logistic map as well as the dynamics of two coupled logistic maps. Instead of implementing the logistic map in its standard form, they implemented the map on the interval $[-1, 1]$ defined by

$$x_{n+1} = 1 - ax_n^2, \qquad a \in \mathbf{R}$$

which is topologically conjugated to the logistic map $f : [0, 1] \to [0, 1]$

$$f(x) = rx(1 - x),$$

via a function of the form [217]

$$h(x) = mx + c \qquad m, c \in \mathbf{R}.$$

Mishina *et al.* proposed a circuit to model the equation

$$\begin{pmatrix} x_{1,n+1} \\ x_{2,n+1} \end{pmatrix} = \begin{pmatrix} 1 - a_1 x_{1,n}^2 + b_1(x_{2,n} - x_{1,n}) \\ 1 - a_2 x_{2,n}^2 + b_2(x_{1,n} - x_{2,n}) \end{pmatrix} . \tag{4.1}$$

In the following we restrict our attention to the case $a := a_1 = a_2$. The fixed points of (4.1) for this case are

$$\begin{aligned} \mathbf{x}_1^* &= \left(\frac{-1 - 2b_1 - \Delta_1}{2a}, \frac{-1 - 2b_2 + \Delta_1}{2a} \right), \\ \mathbf{x}_2^* &= \left(\frac{-1 - 2b_1 + \Delta_1}{2a}, \frac{-1 - 2b_2 - \Delta_1}{2a} \right), \\ \mathbf{x}_3^* &= \left(\frac{-1 + \Delta_2}{2a}, \frac{-1 + \Delta_2}{2a} \right), \\ \mathbf{x}_4^* &= \left(\frac{-1 - \Delta_2}{2a}, \frac{-1 - \Delta_2}{2a} \right), \end{aligned} \tag{4.2}$$

where

$$\Delta_1 := \sqrt{1 + 4(a - b_1 b_2)}, \qquad \Delta_2 := \sqrt{1 + 4a}.$$

The Jacobian matrix of the map (4.1) is given by

$$D\mathbf{f}(x_1, x_2) := \frac{\partial \mathbf{f}}{\partial(x_1, x_2)}(x_1, x_2) = \begin{pmatrix} -b_1 - 2ax_1 & b_1 \\ b_2 & -b_2 - 2ax_2 \end{pmatrix} .$$

The eigenvalues of the Jacobian matrix are

$$\lambda_1, \lambda_2 = -d \pm \sqrt{d^2 - 2a(b_2 x_1 + b_1 x_2 + 2a x_1 x_2)} ,$$

with

$$d := \frac{b_1 + b_2 + 2a(x_1 + x_2)}{2} .$$

Evaluation of the eigenvalues of $D\mathbf{f}(x_1, x_2)$ at the fixed points yields

$$\begin{aligned} \lambda_1, \lambda_2|_{\mathbf{x}_1^*} &= 1 + \frac{(b_1 + b_2)}{2} \pm \sqrt{1 + 4a + (b_1 - b_2)\Delta_1 + \frac{(b_1^2 - 14 b_1 b_2 + b_2^2)}{4}} , \\ \lambda_1, \lambda_2|_{\mathbf{x}_2^*} &= 1 + \frac{(b_1 + b_2)}{2} \pm \sqrt{1 + 4a + (b_2 - b_1)\Delta_1 + \frac{(b_1^2 - 14 b_1 b_2 + b_2^2)}{4}} , \\ \lambda_1|_{\mathbf{x}_3^*} &= 1 - \Delta_2 , \\ \lambda_2|_{\mathbf{x}_3^*} &= 1 - b_1 - b_2 - \Delta_2 , \\ \lambda_1|_{\mathbf{x}_4^*} &= 1 + \Delta_2 , \\ \lambda_2|_{\mathbf{x}_4^*} &= 1 - b_1 - b_2 + \Delta_2 . \end{aligned}$$

Instead of studying the stability properties of the fixed points we rather analyze (4.1) numerically. The reader is referred to [836], [267] for the stability analysis of coupled logistic maps. However, the circuit studied by Mishina *et al.* is first discussed before we present numerical results obtained for the coupled logistic maps.

4.2.1 Circuit Description

The circuit of the one-dimensional map implemented by Mishina *et al.* is shown in Figure 4.1. An analogue multiplier IC_1 is used as a squarer; a variable resistor VR_1 sets the gain. The potentiometers VR_2 and VR_3 make provision for input balance and output-offset adjustment, respectively. They are adjusted so that the output voltage at pin 4 becomes $0V$, $10V$ and $10V$ for input voltages of $0V$, $10V$ and $-10V$ at pin 6, respectively. Denote the input to the analogue multiplier by the state variable $X_{1,n} \in [-10, 10]$. Then the output of the multiplier is $X_{1,n}^2/10$. This is fed to the operational amplifier IC_2 via the potentiometer VR_4. The attenuation provided by VR_4 is represented by the factor $A_1 \in [0, 1]$. IC_2 is a subtractor with output $10 - A_1 X_n/5$ which is fed to another operational amplifier IC_3 acting as an adder. The operational amplifier IC_4 is configured as a differential amplifier with unity gain. IC_4 subtracts $X_{1,n}$ from $X_{2,n}$, the state variable of the second one-dimensional map circuit, and then feeds this difference via the attenuator VR_5 (represented by $B_1 \in [0, 1]$) to the non-inverting input of IC_3. The output of IC_3, namely $X_{1,n+1}$ is thus given by

$$X_{1,n+1} = 10\left(1 - 2A_1\left(\frac{X_{1,n}}{10}\right)^2\right) + B_1(X_{2,n} - X_{1,n}).$$

$X_{1,n+1}$ is then delayed and applied to the pin 2 of IC_4. This is achieved by feeding $X_{1,n+1}$ to the series connected sample-and-hold devices, IC_5 and IC_6.

Similarly the state variable $X_{2,n}$ of the second one-dimensional map circuit evolves according to

$$X_{2,n+1} = 10\left(1 - 2A_2\left(\frac{X_{2,n}}{10}\right)^2\right) + B_2(X_{1,n} - X_{2,n}).$$

Note that the term in brackets in Figure 4.1 applies to the second map's circuit which is identical to the circuit for the first map. The integrated circuit devices used are AD533H (for IC_1), LF356 (for IC_2 to IC_4) and LF398 (for IC_5 and IC_6).

Finally, note that normalizing the above two equations by defining $x_{i,n} := X_{i,n}/10$, $a_i := 2A_i$, $b_i := B_i$ for $i = 1, 2$, produces the system (4.1). Hence we have shown that the proposed circuit implements the coupled logistic maps with the restriction $a_i \in [0, 2]$, $b_i \in [0, 1]$ for $i = 1, 2$. The block diagram depicting the experimental setup of the coupled maps is shown in Figure 4.2.

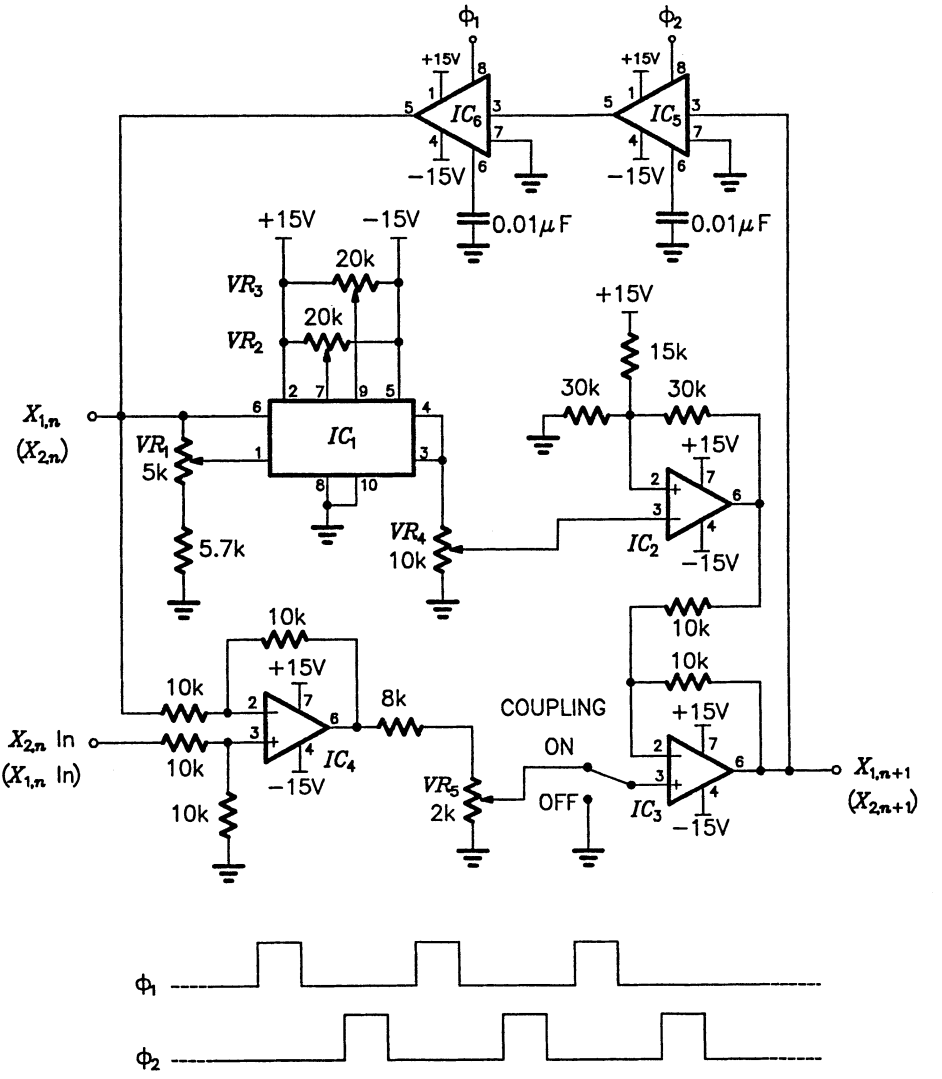

Figure 4.1: Circuit model for the one-dimensional logistic map studied by Mishina and coworkers.

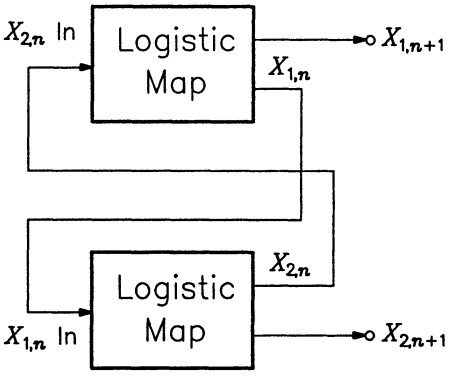

Figure 4.2: Block diagram of the coupled the coupled maps.

4.2.2 Simulation Results

For the case when the circuit is configured as two independent one-dimensional maps, the reader is referred to Mishina *et al.* [548] for a discussion of the dynamics observed. When the coupling switch is closed, the two one-dimensional maps are mutually coupled. In this section the behaviour of the coupled system (4.1) will be studied numerically.

In order to study (4.1) numerically, we first put the coupling parameters $b_1 = 0.4$ and $b_2 = 0.35$. Then by increasing a gradually from zero we obtain the phase plane plots shown in Figure 4.3 for various values of a. For $a = 0.48$ a stable torus exists (see Figure 4.3(a)). As a increases the elliptic patterns in Figure 4.3(a) become more irregular This can be seen from the phase portraits in Figures 4.3(b) and 4.3(c) for $a = 0.55$ and $a = 0.62$, respectively. For $a = 0.663$, $a = 0.67$ and $a = 0.8$ strange attractors appear as can be seen from Figure 4.3. The results obtained are qualitatively in good agreement with experimental results obtained by Mishina *et al.* [548]. For experimental results obtained from the coupled maps refer to [548].

Several endomorphisms of a plane have been constructed by coupling two logistic maps. Gardini *et al.* [267] studied one such endomorphism using critical curves. This enabled them to find absorbing and invariant areas, inside which global bifurcations of the attracting sets (i.e. fixed points, closed invariant curves, periodic or chaotic attractors) take place. The basins of attraction of the absorbing areas were determined together with their bifurcations [267]. Another such endomorphism was studied numerically by Villet and Steeb in [836]. They found the coupled maps to exhibit regular (i.e. periodic or quasi-periodic) motion, chaotic and hyperchaotic motion. In some regions the coupled maps were found to be globally unstable.

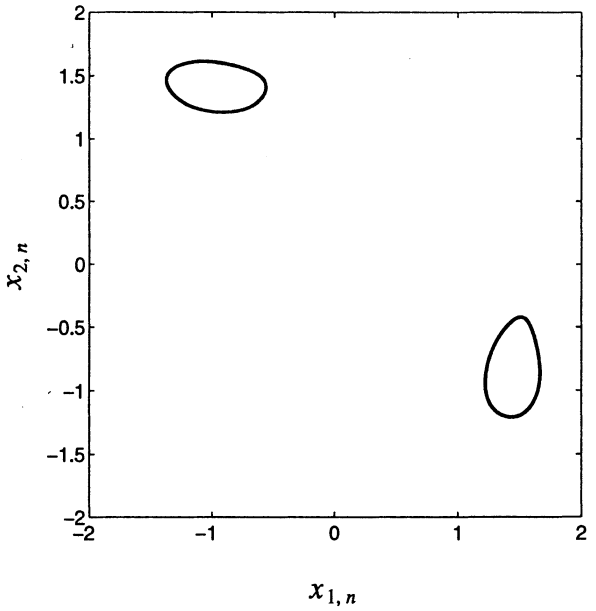

(a)

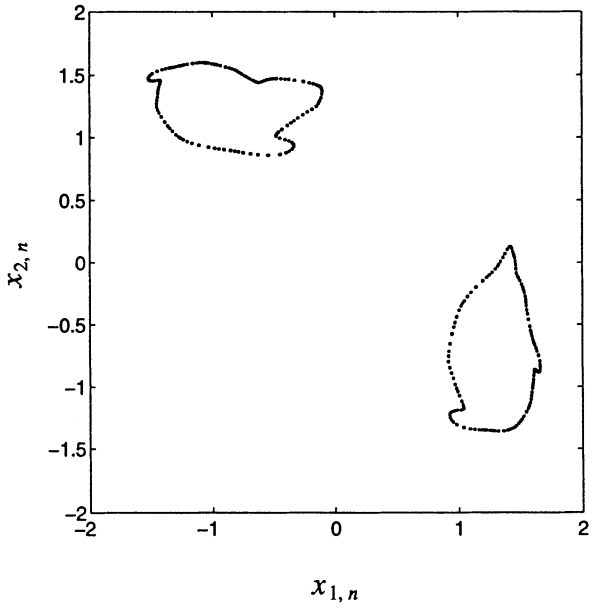

(b)

Figure 4.3: Phase portraits of (4.1) for $b_1 = 0.4$ and $b_2 = 0.35$: (a) stable torus ($a = 0.48$); (b) deformed torus ($a = 0.55$); (c) deformed torus ($a = 0.62$); (d) chaotic attractor ($a = 0.663$); (e) quasi-periodic attractor ($a = 0.6653$); (f) chaotic attractor ($a = 0.67$); (g) chaotic attractor ($a = 0.82$).

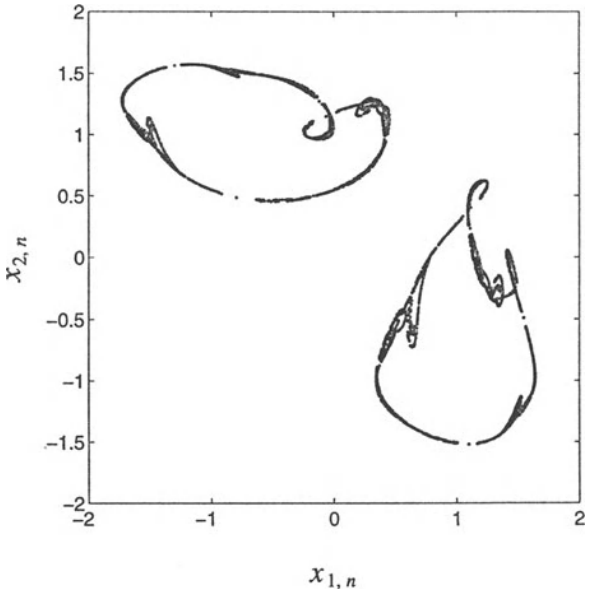

(c)

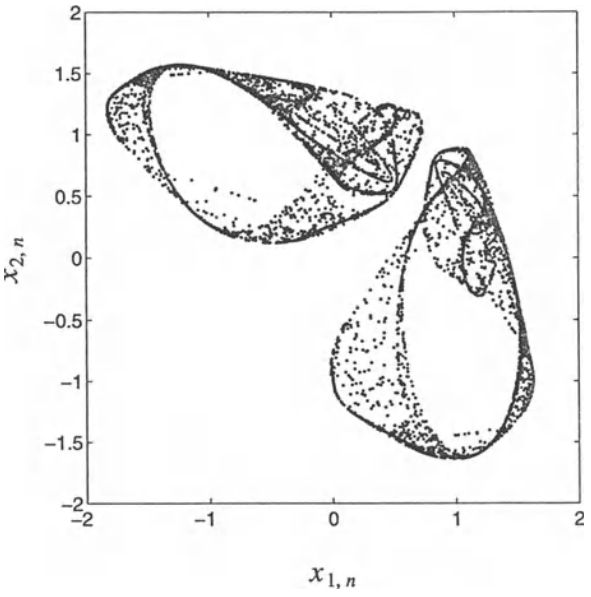

(d)

Figure 4.3: (Continued)

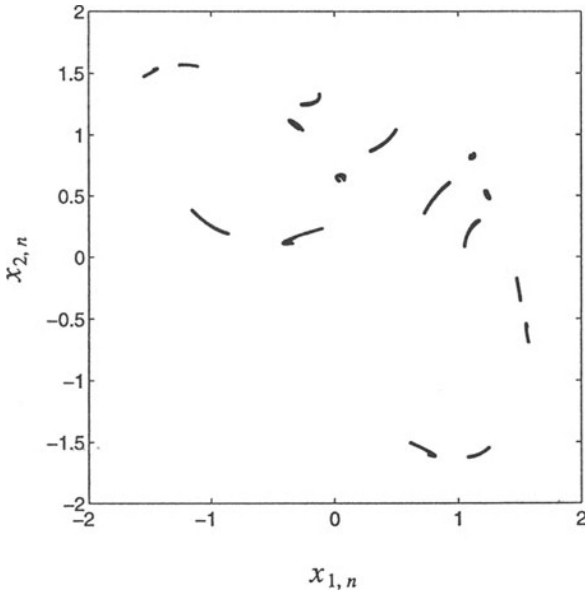

(e)

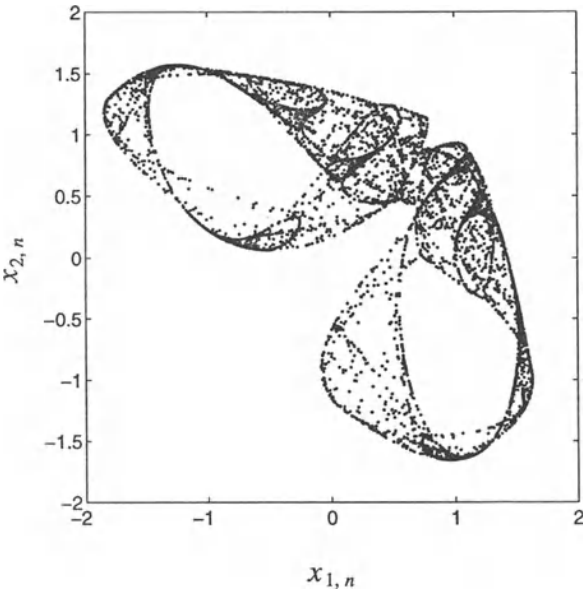

(f)

Figure 4.3: (Continued)

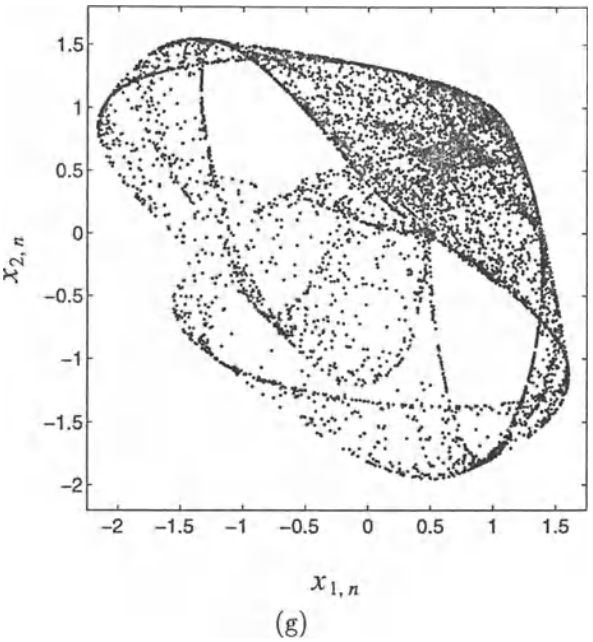

Figure 4.3: (Continued)

4.3 Chaos in Digital Filters

Chua, Lin [158], [156] and Kocarev [440] studied a second-order infinite impulse response (IIR) filter for chaotic phenomena. The nonlinear component in the filter implementation under investigation is a two's complement adder with overflow. The filter was found to exhibit chaos on the boundary of the stable region of the idealized linear filter (i.e. the filter with no overflow). Moreover, the phase portrait of the filter under investigation exhibits a fractal geometry. The second-order IIR filter is realized in direct-form as shown in Figure 4.4.

In order to rule out the effect of finite wordlength, we assume all quantities to be represented arbitrarily accurately, thereby retaining only the effect of the adder overflow nonlinearity, which in normalized form, is then modelled by the map $g : \mathbf{R} \to J$,

$$g(x) := (x+1) \,(\mathrm{mod}\ 2) - 1\,,$$

where $J := [-1, 1]$. With zero-input present, the filter is described by the nonlinear difference equation $\mathbf{x}_{n+1} = \mathbf{f}(\mathbf{x}_n)$ with $\mathbf{f} : J^2 \to J^2$ is defined by

$$\mathbf{f}(\mathbf{x}) := \begin{pmatrix} x_2 \\ g(bx_1 + ax_2) \end{pmatrix}, \qquad \mathbf{x} := (x_1, x_2)^T, \tag{4.3}$$

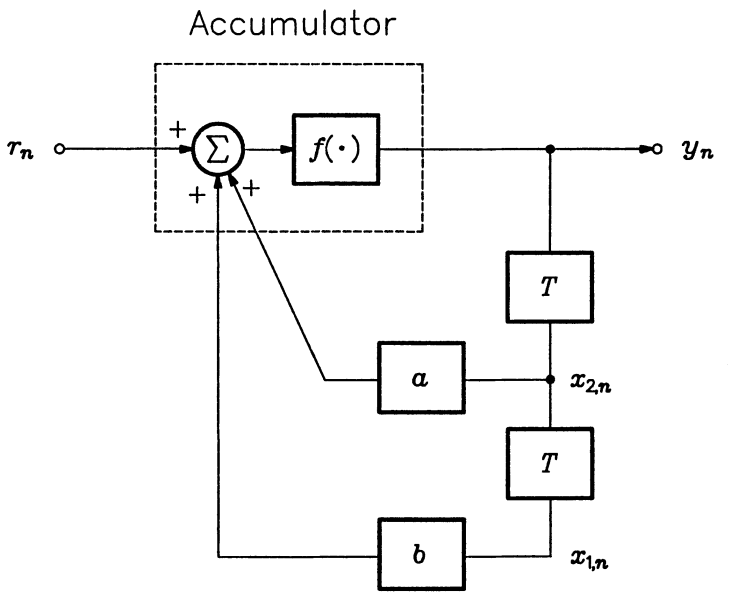

Figure 4.4: Direct-form realization of the second-order IIR filter.

and initial condition $\mathbf{x}_0 := (x_{1,0}, x_{2,0})^T \in J^2$. Using the identity

$$\frac{u}{v} \equiv \left\lfloor \frac{u}{v} \right\rfloor + \frac{u \,(\mathrm{mod}\, v)}{v}, \qquad u, v \in \mathbf{R}, \quad v \neq 0,$$

we may rewrite the function g in the form

$$g(x) = x - 2\left\lfloor \frac{x+1}{2} \right\rfloor. \tag{4.4}$$

Here $\lfloor x \rfloor$ denotes the greatest integer less than or equal to $x \in \mathbf{R}$. Using (4.4), we then cast (4.3) into the following form

$$\mathbf{f}(\mathbf{x}) = \mathbf{A}\mathbf{x} + \mathbf{B}v, \tag{4.5}$$

where

$$\mathbf{A} := \begin{pmatrix} 0 & 1 \\ b & a \end{pmatrix}, \qquad \mathbf{B} := \begin{pmatrix} 0 \\ 2 \end{pmatrix}, \qquad v := -\left\lfloor \frac{bx_1 + ax_2}{2} + \frac{1}{2} \right\rfloor.$$

The eigenvalues of $\mathbf{A}$ are

$$q_1, q_2 = \frac{a \pm \sqrt{a^2 + 4b}}{2}. \tag{4.6}$$

Viewing (4.5) in the phase space, we note that v is the vertical translation required to return a point to the domain J^2. We have thus transformed the original nonlinear autonomous system into a linear nonautonomous system (4.5), where v is the input to this system. Notice that v may only assume integer values in the range $-l_1$ to l_1, where $l_1 \in \mathbf{N}$, such that

$$2l_1 - 1 \leq \sup_{\mathbf{x} \in J^2} \|\mathbf{Ax}\|_\infty < 2l_1 + 1 .$$

The equivalent idealized linear filter with zero input is described by

$$\mathbf{x}_{n+1} = \mathbf{A}\mathbf{x}_n . \tag{4.7}$$

Since $\det(A) = -b$, we see that the transformation properties of (4.7) as well as (4.5) can be vastly different for different ranges of values of b. For $|b| > 1$ this transformation is area-expansive while for $|b| = 1$ it is area-preserving. For $0 < |b| < 1$ this transformation is area-contractive. This transformation is orientation-preserving for negative values of b and orientation-changing for positive values of b. In order to determine for which a and b values the system is asymptotically stable, we have to find the regions in the (a, b)-plane for which $|q_1| \leq 1$ and $|q_2| \leq 1$ (using (4.6)). For the case of real eigenvalues, (that is, $b \geq -a^2/4$), $|q_1| \leq 1$ and $|q_2| \leq 1$ yield the domain

$$S_R := \left\{ (a, b) \in \mathbf{R}^2 \,\middle|\, -\frac{a^2}{4} \leq b \leq 1 + a - 2a\,u(a) \right\}, \tag{4.8}$$

with

$$u(a) := \begin{cases} 0, & a < 0 \\ 1, & a \geq 0 \end{cases} .$$

For the case of complex eigenvalues (i.e. $b < -a^2/4$), $|q_1| \leq 1$ and $|q_2| \leq 1$ translate to the domain

$$S_C := \left\{ (a, b) \in \mathbf{R}^2 \,\middle|\, -1 \leq b < -\frac{a^2}{4} \right\}. \tag{4.9}$$

Combining (4.8) and (4.9), we conclude that the fixed point $\mathbf{x}^* = \mathbf{0}$ of the system (4.7) is asymptotically stable inside the triangular region

$$S := S_R \cup S_C = \left\{ (a, b) \in \mathbf{R}^2 \,\middle|\, b \leq 1 + a, \quad b \leq 1 - a, \quad b \geq -1 \right\}.$$

As in [158] and [440], we restrict the discussion to the case $b = -1$. This is on (i.e. $|a| \leq 2$) and off (i.e. $|a| > 2$) the lower boundary of the stable region of the linear system. As was mentioned earlier, the nonlinear and linear systems are both area- and orientation-preserving along the line $b = -1$. Along the path $b = -1$, (4.5) and (4.7) become

$$\mathbf{x}_{n+1} = \mathbf{f}(\mathbf{x}_n) = \begin{pmatrix} 0 & 1 \\ -1 & a \end{pmatrix} \begin{pmatrix} x_{1,n} \\ x_{2,n} \end{pmatrix} + \begin{pmatrix} 0 \\ 2 \end{pmatrix} v , \tag{4.10}$$

with

$$v = -\left\lfloor \frac{-x_{1,n} + ax_{2,n} + 1}{2} \right\rfloor ,$$

and

$$\mathbf{x}_{1,n+1} = \begin{pmatrix} x_{1,n+1} \\ x_{2,n+1} \end{pmatrix} = \begin{pmatrix} 0 & 1 \\ -1 & a \end{pmatrix} \begin{pmatrix} x_{1,n} \\ x_{2,n} \end{pmatrix} .$$

The function $\mathbf{f}$ is bijective with inverse $\mathbf{f}^{-1}$,

$$\mathbf{f}^{-1}(\mathbf{x}_n) = \begin{pmatrix} a & -1 \\ 1 & 0 \end{pmatrix} \begin{pmatrix} x_{1,n} \\ x_{2,n} \end{pmatrix} + \begin{pmatrix} 2 \\ 0 \end{pmatrix} w ,$$

where

$$w := -\left\lfloor \frac{ax_{1,n} - x_{2,n} + 1}{2} \right\rfloor .$$

We now give some examples of the dynamical behaviour of (4.10) for different values of a. The one-dimensional Lyapunov exponents of the system are given by [440]

$$\lambda_i = \ln |q_i|, \qquad i = 1, 2 . \tag{4.11}$$

For $|a| < 2$ the eigenvalues of $\mathbf{A}$ are complex with $q_2 = \bar{q}_1$ and

$$|q_1|^2 = |q_2|^2 = q_1 q_2 = 1 .$$

Then all periodic points of (4.10) are elliptic [440]. By (4.11) the Lyapunov exponents are $\lambda_1 = \lambda_2 = 0$, and therefore the system (4.10) is not chaotic.

As an example, consider the case $a = 0.5$. Chua and coworkers (see [158] and [440]) showed that vastly different types of dynamical behaviour are exhibited for the case $a = 0.5$ for initial conditions in different domains in J^2. For an arbitrary initial condition $\mathbf{x}_0$ in the elliptic shaped region Π_0, defined by

$$\Pi_0 := \left\{ \mathbf{x} \in J^2 \middle| r(\mathbf{x}) < 1 \right\}, \quad \text{with} \quad r(\mathbf{x}) := \left(\frac{(x_1 + x_2)^2}{2 + a} + \frac{(x_1 - x_2)^2}{2 - a} \right)^{\frac{1}{2}} ,$$

the orbit lies on an ellipse passing through the point $\mathbf{x}_0$ and which is described by

$$\left\{ \mathbf{x} \in J^2 \middle| r(\mathbf{x}) = r(\mathbf{x}_0) \right\} .$$

Figure 4.5(a) shows the orbit of the nonlinear system $\mathbf{x}_{n+1} = \mathbf{f}(\mathbf{x}_n)$ (in (4.10)) for $\mathbf{x}_0 = (-0.6, 0.6)^T$. For the initial condition $\mathbf{x}_0 = (-0.616, 0.616)^T$ the orbit travels periodically among 10 ellipses as shown in Figure 4.5(b). However, extremely complex geometrical structure is exhibited in the phase space for the case

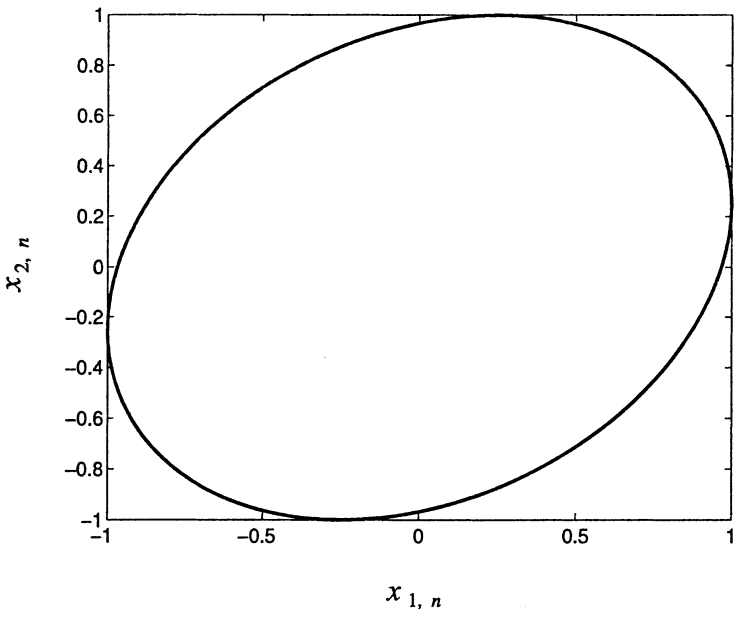

(a)

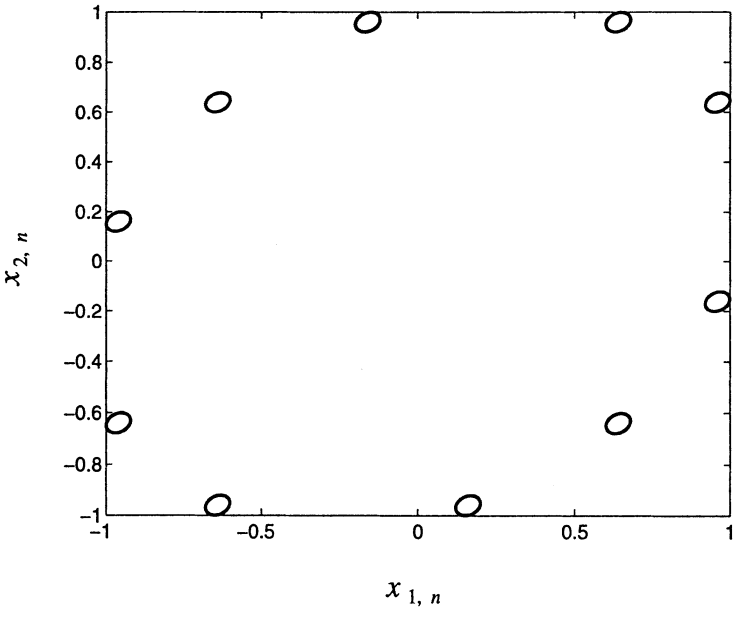

(b)

Figure 4.5: Orbits for $a = 0.5$ for different initial conditions: (a) $\mathbf{x}_0 = (-0.6, 0.6)^T$; (b) $\mathbf{x}_0 = (-0.616, 0.616)^T$; (c) $\mathbf{x}_0 = (-0.6135, 0.6135)^T$.

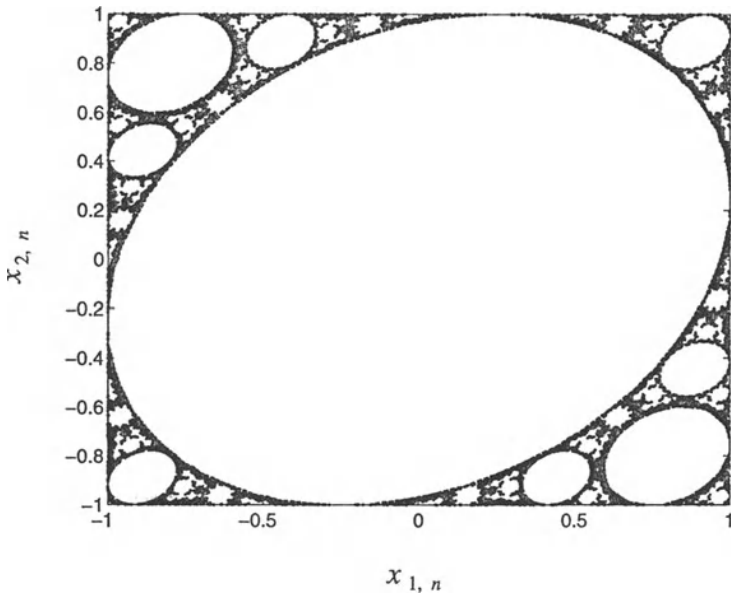

(c)

Figure 4.5: (Continued)

$\mathbf{x}_0 = (-0.6135, 0.6135)^T$. The orbit visits infinitely many ellipses and exhibits self-similar geometric structure as is evident from Figure 4.5(c).

Next, we consider the case when $|a| = 2$ which corresponds to

$$q_1 = q_2 = \pm 1 .$$

For this case all periodic points are parabolic [440] and the system $\mathbf{x}_{n+1} = \mathbf{f}(\mathbf{x}_n)$ is integrable, i.e. the line

$$x_2 = x_1 + x_{2,0} - x_{1,0} ,$$

is invariant, and the system may be written in the form

$$\begin{pmatrix} x_{1,n+1} \\ z_{n+1} \end{pmatrix} = \begin{pmatrix} 1 & 1 \\ 0 & 1 \end{pmatrix} \begin{pmatrix} x_{1,n} \\ z_n \end{pmatrix} + \begin{pmatrix} 2 \\ 0 \end{pmatrix} s_n ,$$

where $z_n := x_{2,n} - x_{1,n}$. For this case an orbit can have different qualitative behaviours depending on rationality or irrationality of z_0 (see [440]). If z_0 is rational, then each orbit consists of only finitely many parabolic periodic points. If z_0 is an irrational number, then each orbit consists of an infinite number of points which are dense on a circle. For $|a| = 2$, the system $\mathbf{x}_{n+1} = \mathbf{f}(\mathbf{x}_n)$ has $\lambda_1 = \lambda_2 = 0$ and thus is not chaotic.

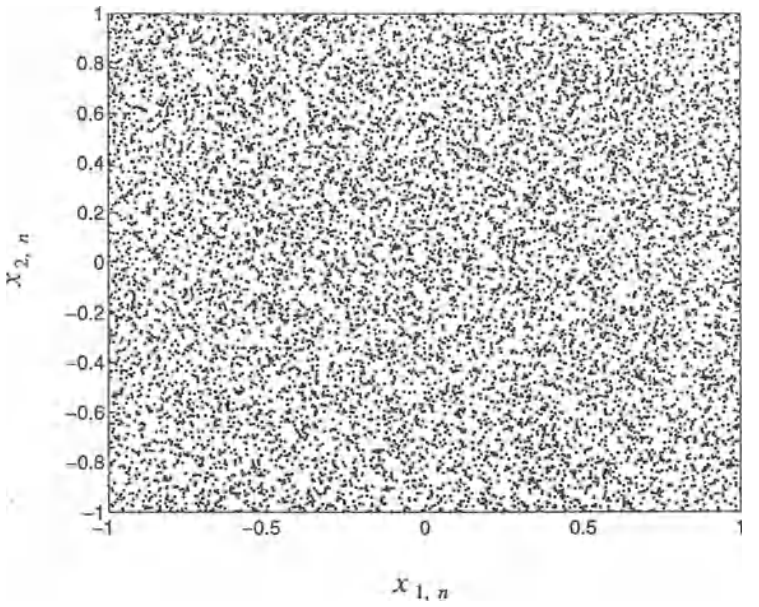

Figure 4.6: Chaotic orbit for the case $a = 3$.

Finally, consider the case $|a| > 2$ or equivalently

$$|q_1| > 1 > |q_2| .$$

For this case we have $\lambda_1 > 0 > \lambda_2$, and thus the system $\mathbf{x}_{n+1} = \mathbf{f}(\mathbf{x}_n)$ is chaotic. In Chapter 2, Example 2.65 we have shown, using symbolic dynamics, that this system is indeed chaotic for the case $|a| > 2$. An orbit for $a = 3$ is shown in Figure 4.6. For a detailed analysis of the topological structure of orbits, the reader is referred to [158].

Chua and Lin also studied a third-order IIR filter (see [157]). Computer simulations performed by them showed that the third-order filter with an overflow nonlinearity exhibits much richer dynamics than the second-order filter discussed here. The three-dimensional orbit of the system always lies on several parallel planes. These planes are reached at different points to create the chaotic behaviour and complex geometrical structure. The number and location of these planes are determined by the parameters of the filter and the initial conditions. Chua and Lin developed a seven-value symbolic dynamics for describing the complex behaviour of this filter.

In practice a digitally implemented digital filter has finite wordlength. The question now arises: is it possible for a filter with finite wordlength to exhibit chaos? In theory a continuum of states are required for a system to exhibit chaotic behaviour. However, in [487] Lin and Chua found through simulation that for sufficiently large wordlength, the dynamics of the finite wordlength system becomes almost indistinguishable from the truly chaotic dynamics of its infinite wordlength counterpart.

4.4 Chaotic Behaviour in an Adaptive IIR Filter

Adaptive *auto-regressive moving-average* (ARMA) predictors are classical tools in signal processing, e.g. for speech modelling, digital speech transmission, information storage, etc. They are also used in the field of control for the regulation of time-varying processes. Although the optimality requirements depend on the applications, the stability conditions are always present due to the recursive structure of predictors which includes a moving average (MA) path with possibly unstable poles. Figure 4.7 shows the block diagram of an adaptive ARMA predictor in the $\mathcal{Z}$-plane.

Introducing vector notation for the past input samples

$$\mathbf{s}_n := (s_{n-1}, \ldots, s_{n-p})^T ,$$

and past error samples

$$\mathbf{e}_n := (e_{n-1}, \ldots, e_{n-q})^T ,$$

the system is described by

$$e_n = s_n - \mathbf{a}_n^T \mathbf{s}_n - \mathbf{b}_n^T \mathbf{e}_n , \tag{4.12}$$

with the time-varying transfer function of the predictor which is of the form

$$H_n(z) = \frac{1 - A_n(z)}{1 + B_n(z)} ,$$

with

$$A_n(z) := \mathcal{Z}(a_{m,n}) = \mathbf{a}_n^T \mathbf{z}_p , \quad \text{and} \quad B_n(z) := \mathcal{Z}(b_{m,n}) = \mathbf{b}_n^T \mathbf{z}_q ,$$

where $z := \mathrm{e}^{j\omega/f_s}$, $j := \sqrt{-1}$, f_s is the sampling frequency and

$$\mathbf{z}_m := (z^{-1}, z^{-2}, \ldots, z^{-m})^T , \qquad m \in \mathbf{N} .$$

The positive integers p and q denote the AR and MA orders respectively, while $\mathbf{a}_n \in \mathbf{R}^p$ and $\mathbf{b}_n \in \mathbf{R}^q$ denote the time-varying filter coefficients of the AR and MA parts, respectively. This predictor is said to be an ARMA(p, q)-predictor. In the classical formalism the problem is to adapt $H_n(z)$ in order to minimize some cost function while controlling the zeros of the MA part $1 + \mathbf{b}_n^T \mathbf{z}_q$ to remain strictly inside the unit circle, using stability constraints if necessary. The cost function usually is the time or ensemble mean of the squared prediction error e_n^2.

When the predictor in Figure 4.7(a) is merely autoregressive (AR), the stochastic gradient algorithm with constant adaption speed β, also known as the *least mean square* (LMS) algorithm,

$$\mathbf{a}_{n+1} = \mathbf{a}_n + \beta e_n \mathbf{s}_n , \qquad \beta > 0 , \tag{4.13}$$

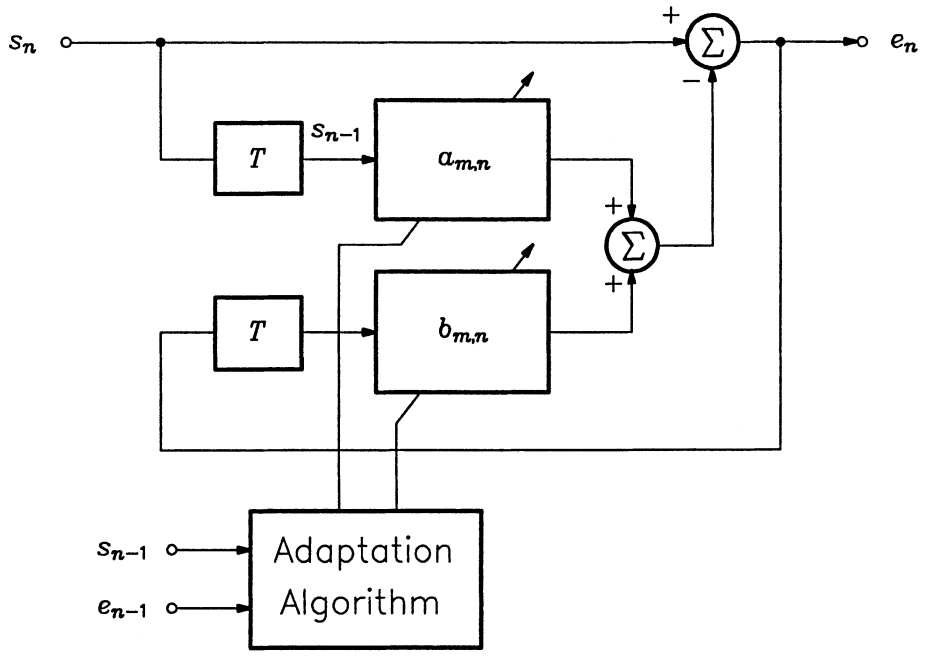

Figure 4.7: Block diagram of an ARMA(p, q) predictor.

is the simplest stochastic algorithm that converges to the optimal weight vector $\hat{\mathbf{a}}$, thereby minimizing the cost function. For sufficiently small β, convergence is known to be in the quasi-mean-square sense [504], [348], that is,

$$E\left(|\mathbf{a}_n - \hat{\mathbf{a}}|^2\right) \propto \beta,$$

with E here denoting the expectation functional. The amount by which the final value of the mean-squared error, averaged over an ensemble of adaptive filters, deviates from the minimum-squared error that is produced by the optimal Wiener filter is termed the *misadjustment.*

AR predictors are always stable and their spectral responses have broad peaks but arbitrarily deep notches [348]. The addition of a MA part to the predictor makes it possible to model frequency responses with sharp peaks and/or notches. (A purely AR predictor is characterized by a spectral response having arbitrarily narrow peaks and broad valleys.) However, the optimal choice of parameter vectors $\mathbf{a}_n$ and $\mathbf{b}_n$ becomes much more complex. When β is small a close approximation of the stochastic gradient algorithm is obtained [407] by using a recursively filtered version of e_n (respectively s_n) in the increment of $\mathbf{b}_n$ (respectively $\mathbf{a}_n$). Very often in signal processing applications the recursion may be omitted. This results in the so-called *recursive* LMS algorithm

comprising of (4.13) together with

$$\mathbf{b}_{n+1} = \mathbf{b}_n + \beta e_n \mathbf{e}_n \,. \tag{4.14}$$

Equations (4.4) to (4.14) can be rewritten in the form

$$\mathbf{a}_{n+1} = (\mathbf{I} - \beta \mathbf{s}_n \mathbf{s}_n^T)\mathbf{a}_n + \beta(s_n - \mathbf{b}_n^T \mathbf{e}_n)\mathbf{s}_n \,, \tag{4.15}$$

$$\mathbf{b}_{n+1} = (\mathbf{I} - \beta \mathbf{e}_n \mathbf{e}_n^T)\mathbf{b}_n + \beta(s_n - \mathbf{a}_n^T \mathbf{s}_n)\mathbf{e}_n \,, \tag{4.16}$$

$$e_n = -\mathbf{a}_n^T \mathbf{s}_n - \mathbf{b}_n^T \mathbf{e}_n + s_n \,. \tag{4.17}$$

Using the state vector $\mathbf{x}_n := (\mathbf{a}_n^T, \mathbf{b}_n^T, \mathbf{e}_n^T)^T$, the system (4.15) to (4.17) may be viewed as a nonautonomous, nonlinear discrete-time system of order $p + 2q$, namely

$$\mathbf{x}_{n+1} = \mathbf{F}(\mathbf{x}_n; s_n, \ldots, s_{n-p}) \,. \tag{4.18}$$

Given the input samples $s_n, \ldots, s_{n-p}$ the nonlinearity arises in, for example, the term $-\beta \mathbf{e}_n \mathbf{e}_n^T \mathbf{b}_n$ in (4.16). For $\beta = 0$ the system (4.15) to (4.17) is a simple recursive linear filter. This implies that the degree of nonlinearity of $\mathbf{F}$ is determined by the parameter β. Based on the observation that the severity of the nonlinearity is directly proportional to β, it is expected that the qualitative behaviour of the predictor would depend on β. Therefore we choose β as the bifurcation parameter. For a small speed β, the behavior is understood thanks to the *self-stabilization* property of the recursive LMS. Adjusting $\mathbf{b}_n$ adaptively using the recursive LMS, causes it to reach the boundary of the stability region (because the domain of stability is bounded), thereby causing the predictor to become unstable. This type of drift is referred to as bursting. When this happens the output error consists of a linear term at the input frequency f and a nonlinear term at the frequency of the unstable pole. In contrast to the LMS algorithm the recursive LMS algorithm inverts the drift, using the bursting output error to reinforce stability. For small β the behaviour is therefore expected to be quasi-periodic.

For large β (say, $1/2 < \beta < 1$) the self-stabilization phenomenon is still present as before. However, the analysis is more complex. For fast adaptation (i.e. large β), there are values of β which induce abrupt changes (bifurcations) in the global behaviour of the system output, and values for which the dynamics are chaotic.

Example 4.1 The complex dynamical behaviour of the adaptive ARMA predictor utilizing the recursive LMS is evidenced in the simplest case, namely the ARMA(0, 1)-predictor (i.e. a predictor with no AR part) described by

$$b_{n+1} = b_n(1 - \beta e_{n-1}^2) + \beta e_{n-1} s_n \,, \tag{4.19}$$

$$e_n = -b_n e_{n-1} + s_n \,. \tag{4.20}$$

This nonautonomous, nonlinear discrete system is of order 2 with state vector $\mathbf{x}_n := (b_n, e_{n-1})^T$ in (4.18).

For the purpose of the analysis, we choose the input to be a unit amplitude sinusoid,

$$s_n = \sin k\phi\,, \qquad \phi := 2\pi\frac{f}{f_s}\,,$$

where f_s is the rate at which the sinusoid of frequency f is sampled. This discrete sinusoid is described by the difference equation,

$$s_{n+1} = 2\cos\phi\; s_n - s_{n-1}\,. \tag{4.21}$$

Defining the state vector as $\mathbf{x}_n := (x_{1,n}, x_{2,n}, x_{3,n}, x_{4,n})^T$ where

$$x_{1,n} := s_n\,, \qquad x_{2,n} := s_{n-1}\,, \qquad x_{3,n} := b_n\,, \qquad x_{4,n} := e_{n-1}\,,$$

the system (4.19), (4.20) and (4.21) may be written as an autonomous system of order 4, namely

$$x_{1,n+1} = 2\cos\phi\; x_{1,n} - x_{2,n}\,, \tag{4.22}$$

$$x_{2,n+1} = x_{1,n}\,, \tag{4.23}$$

$$x_{3,n+1} = x_{3,n}\left(1 - \beta x_{4,n}^2\right) + \beta x_{4,n} x_{1,n}\,, \tag{4.24}$$

$$x_{4,n+1} = -x_{3,n}x_{4,n} + x_{1,n}\,. \tag{4.25}$$

This system is of the form

$$\mathbf{x}_{n+1} = \mathbf{G}(\mathbf{x}_n)\,.$$

A given state $\mathbf{x}_n$ may have no, one or two inverse images and consequently the $\mathbf{F}$-transformation is not invertible. As a matter of fact $\mathbf{F}$ is an endomorphism [467]. The Jacobian of $\mathbf{F}$ described by (4.19) and (4.20),

$$J(x_{3,n}, x_{4,n}) = \det(D\mathbf{F}(x_{3,n}, x_{4,n}; x_{1,n})) = -x_{3,n} + \beta x_{4,n+1} x_{4,n}\,,$$

vanishes when $x_{4,n+1} = x_{3,n}/\beta x_{4,n}$. The equation

$$J(x_{3,n}, x_{4,n}) = 0\,,$$

characterizes a critical curve C of which the successive images $\mathbf{F}^{(k)}(C)$, $k = 1, \ldots$ in the (x_3, x_4)-plane might constitute the boundary of a stable, no-escape region where the system may be chaotic [316].

To demonstrate the bifurcation phenomena we assume $f_s = 8$ kHz, $f = 1257$ Hz. We consider $\beta \in [0.5, 0.8]$. For $\beta = 0.5$ the response of the system is quasi-periodic (see Figure 4.8).

As can be seen from Figure 4.8, bifurcations occur as β increases with the attractor becoming more irregular as β increases. The attractor shown in Figure 4.8(d) remains almost unchanged for a small interval of values of β with $\beta \approx 0.7347$ as its lower bound. Only local bifurcations occur as β sweeps from 0.7347

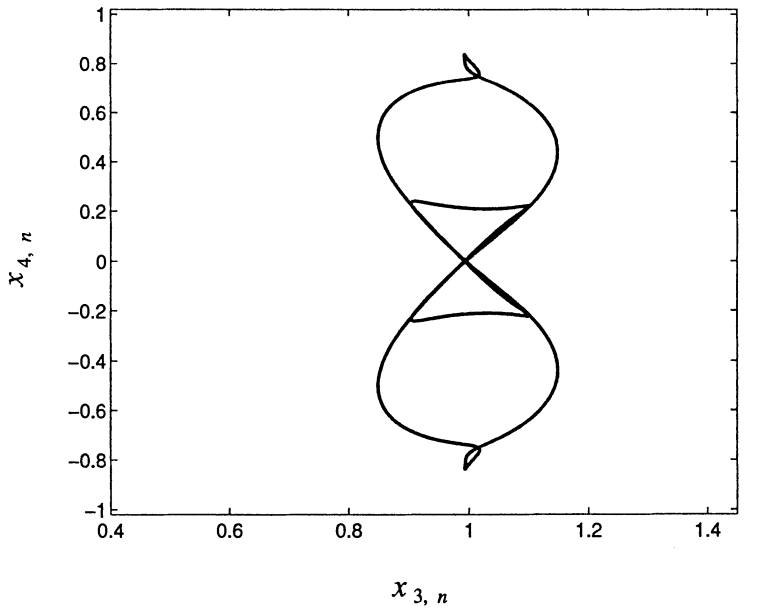

(a)

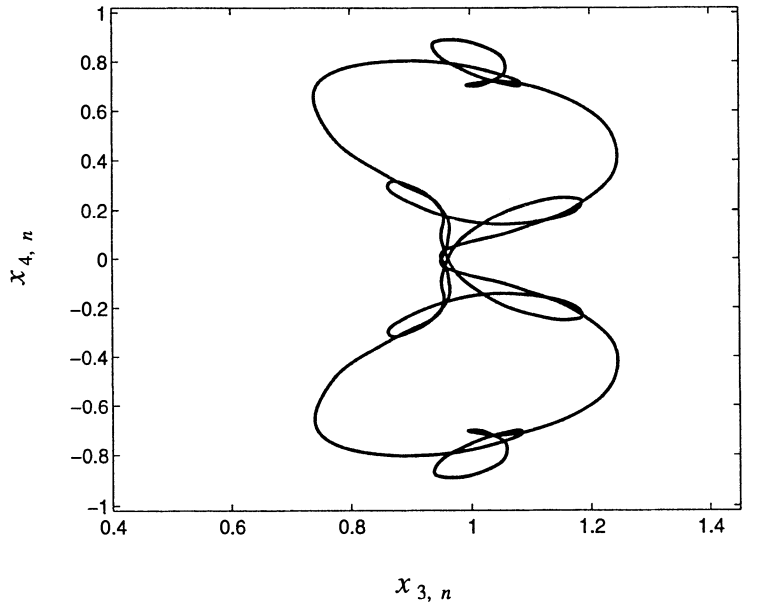

(b)

Figure 4.8: Phase portraits of (4.22) to (4.25) for $f_s = 8$ kHz, $f = 1257$ Hz and:(a) $\beta = 0.5$; (b) $\beta = 0.65$; (c) $\beta = 0.68$; (d) $\beta = 0.7347$; (e) $\beta = 0.74377$.

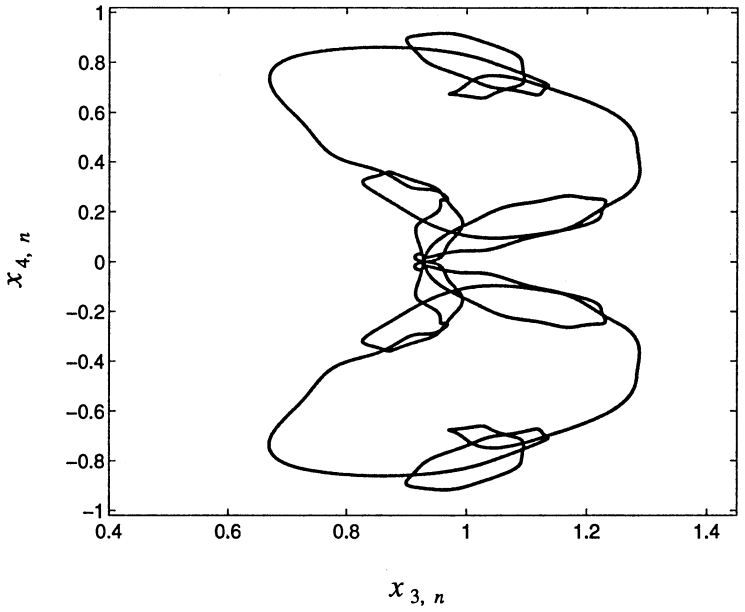

(c)

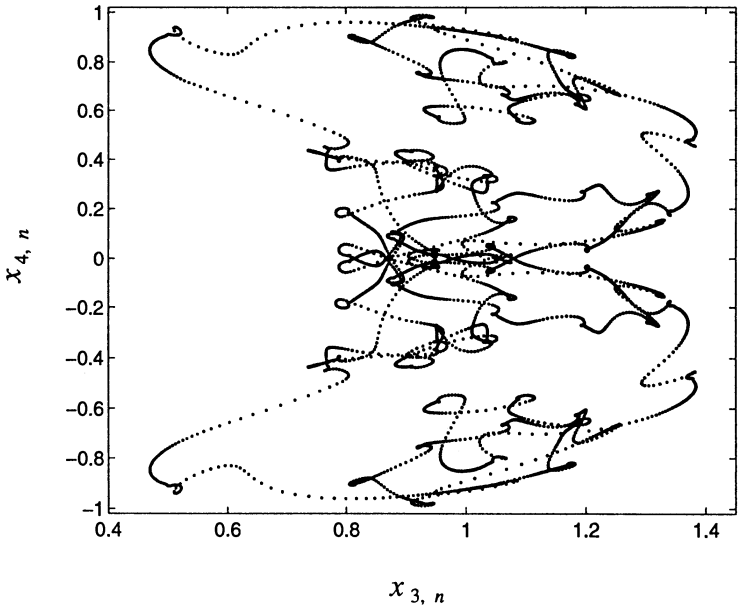

(d)

Figure 4.8: (Continued)

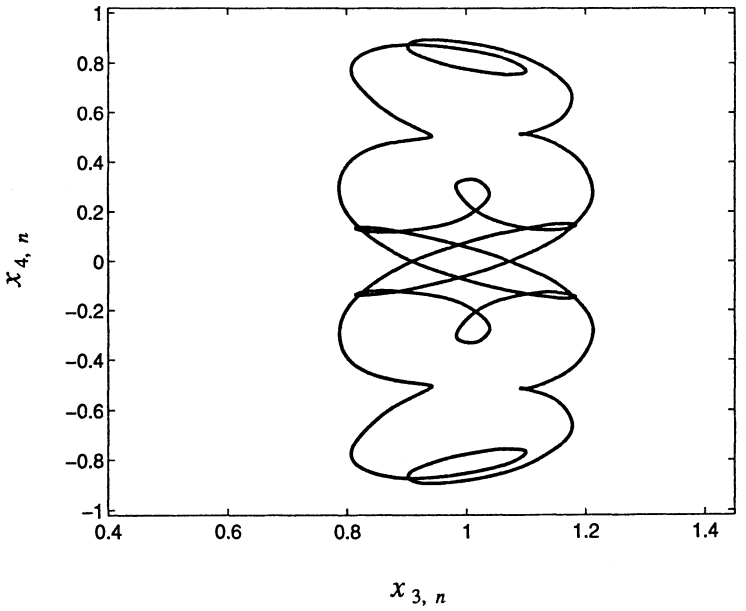

(e)

Figure 4.8: (Continued)

to 0.74374. For $\beta \approx 0.74374623$ the attractor bifurcates back to a smooth quasi-periodic attractor which remains essentially unchanged for further small increases in β. This quasi-periodic attractor is shown in Figure 4.8(e) for $\beta = 0.73477$. Increasing β further, leads to more bifurcations and eventually the system becomes unstable for some critical value of β.

For $f = 500$ Hz, $f_s = 8$ kHz and $\beta \in [0.5, 0.8]$, bifurcations (as β increases) eventually leads to chaos [504]. For this case, Macchi and Jaidane-Saidane reported successive period doublings and triplings as the bifurcation parameter increases. For $\beta = 0.8$ a strange attractor appears as shown in Figure 4.9. From Figure 4.9(b) it is clear that the power spectral density of the output error e_n contains a broadband component which is indicative of chaos. Macchi and Jaidane-Saidane found that the system exhibited sensitive dependence on initial conditions for the current choice of parameters. For more simulation results of the system (4.22) to (4.25), the reader is referred to [504].

Finally we note that, by combining state variables, one can obtain interesting plots. For example, define

$$y_{1,n} := |x_{1,n}|x_{4,n}\,, \qquad y_{2,n} := |x_{1,n}|x_{3,n}\,.$$

For $f = 500$ Hz, $f_s = 8$ kHz and $\beta = 0.8$, as before, the plot of $y_{1,n}$ vs. $y_{2,n}$ strongly resembles the face of a cartoon bulldog (see Figure 4.10(a)). The eyes, flabby cheeks,

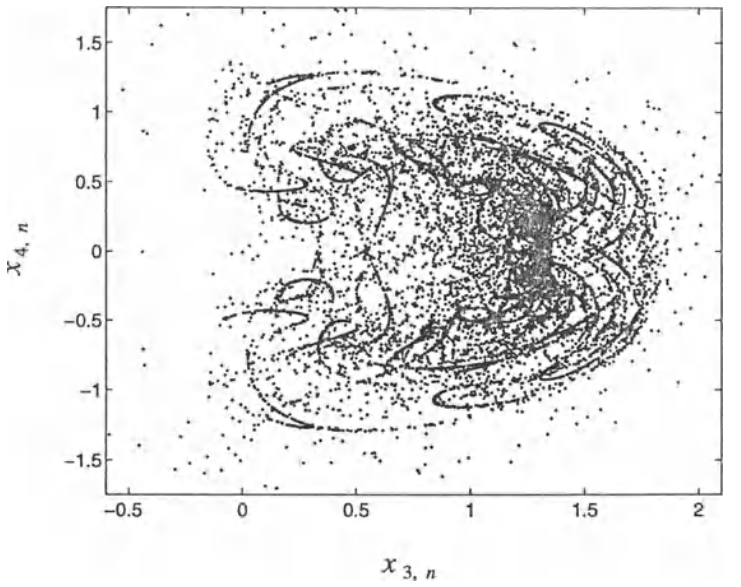

(a)

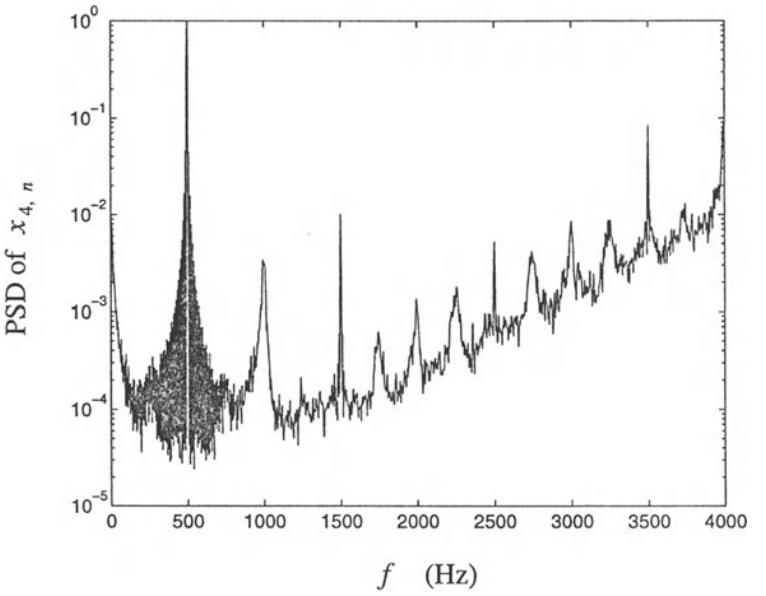

(b)

Figure 4.9: Chaotic attractor for $f_s = 8$ kHz, $f = 500$ Hz and $\beta = 0.8$: (a) Phase portrait; (b) Power spectral density of e_n.

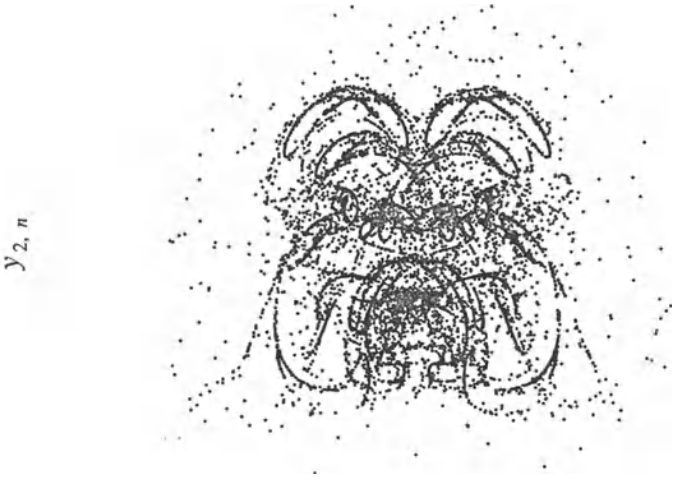

(a)

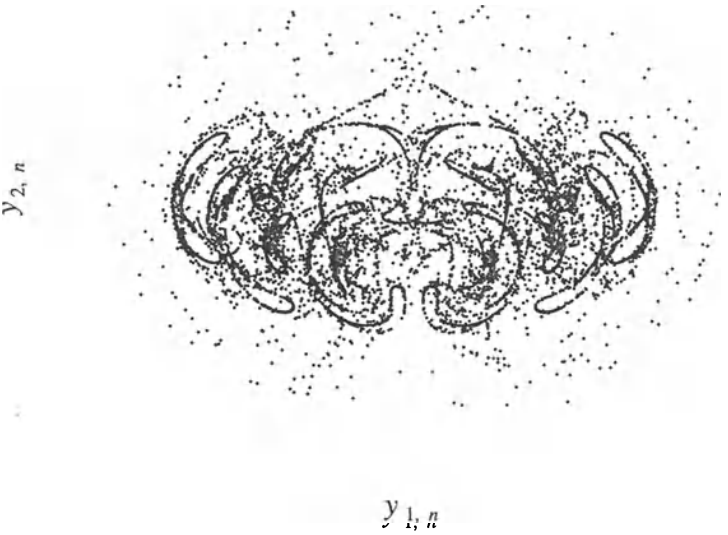

(b)

Figure 4.10: (a) Cartoon bulldog; (b) Abstract buffalo.

nostrils, lips, lower jaw and muscular neck can be clearly distinguished. (Spot the hidden silky-coated dog! A maltese poodle or collie.) For the same choice of parameters and

$$y_{1,n} := x_{1,n}x_{3,n}\,, \qquad y_{2,n} := x_{1,n}x_{4,n}\,.$$

the plot of $y_{1,n}$ vs. $y_{2,n}$ in Figure 4.10(b) (using a bit of imagination) vaguely resembles the head of a buffalo. Clearly, playing with chaotic systems can be both educational and entertaining at the same time! ■

4.5 Chaotic Rounding Error in Digital Control Systems

A standard problem in the field of control systems is that of a *plant* (the system to be controlled) which exhibits undesirable response in some sense and has to be controlled by another system called a *compensator* or *controller* to correct the response. The response of the plant is usually qualitatively expressible in terms of dynamic response criteria such as the rise time, settling time, percentage overshoot etc. The motivation for this approach is that it is usually either not possible or very expensive to make appropriate adjustments to the plant itself. Then the only alternative that remains is to insert a controller into the control loop which adjusts the overall system transfer function to achieve the desired response.

The development of the large scale integration (LSI) technology in recent years has facilitated the implementation of digital compensators in control systems. One of the most important problems encountered is that of the finite-wordlength limitation of digital compensators. The effects of finite-wordlength in digital filters and control systems have been studied by many authors [636], [614], [174], [55], [741], [559]. However, all of them present estimates of the upperbound of the rounding error instead of its influence on the dynamical response of the system being considered.

Ushio and Hsu [814] showed that when appropriate conditions are met, the rounding error in a digital control system due to finite-wordlength could cause the system to exhibit chaotic behaviour. In this sequel we highlight the main results and present an example of a digital control system exhibiting chaos due to finite-wordlength.

4.5.1 Mixed Mapping Model of a Digital Control System

In this section we present a model for a digital control system with finite-wordlength. Our discussion is restricted to a *single-input single-output* (SISO) linear digital control system as shown in Figure 4.11. In order to avoid the use of triples as subscripts later on in this section, we indicate time dependency as $x(n)$ rather than x_n, as we do in

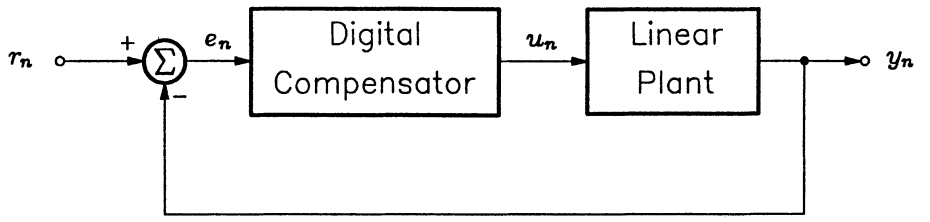

Figure 4.11: Digital control system: plant-controller configuration.

this text. The dynamics of the plant is described by the linear point mapping [455]

$$\mathbf{x}_p(n+1) = \mathbf{A}_p\mathbf{x}_p(n) + \mathbf{b}_p u(n), \tag{4.26}$$

$$y_p(n) = \mathbf{c}_p^T\mathbf{x}_p(n), \tag{4.27}$$

where $\mathbf{x}_p(n)$, $\mathbf{b}_p$, $\mathbf{c}_p \in \mathbf{R}^N$, $u(n)$, $y_p(n) \in \mathbf{R}$, and $\mathbf{A}_p \in \mathbf{R}^{N\times N}$. The dynamics of an ideal digital compensator (i.e. a digital compensator with an infinite-wordlength) is described by a linear point mapping

$$\mathbf{x}_d(n+1) = \mathbf{A}_d\mathbf{x}_d(n) + \mathbf{b}_d e(n), \tag{4.28}$$

$$u(n) = \mathbf{c}_d^T\mathbf{x}_d(n) + d\,e(n), \tag{4.29}$$

where $\mathbf{x}_d(n)$, $\mathbf{b}_d$, $\mathbf{c}_d \in \mathbf{R}^M$, d, $e(n) \in \mathbf{R}$ and $\mathbf{A}_d \in \mathbf{R}^{M\times M}$.

In order to account for the round-off characteristics of a real digital compensator (i.e. a digital compensator with finite-wordlength) we introduce the quantization operator $Q_h : \mathbf{R} \to \mathbf{R}$ defined by

$$Q_h(x) := 10^{-h}\left\lfloor 10^h x + \frac{1}{2}\right\rfloor,$$

where $\lfloor x\rfloor$ denotes the greatest integer less than or equal to $x \in \mathbf{R}$. Here $h \in \mathbf{N}_0$ is called the *wordlength*. It is obvious that Q_h satisfies the identity

$$10^h Q_h(x) \equiv Q(10^h x),$$

where $Q(x) := Q_0(x)$ is termed the *rounding operator*. From the definition of Q_h it is obvious that the rounding operator Q rounds to the closest integer.

In the following we discuss the case where the digital compensator (4.28), (4.29) is realized by a first direct structure [636].The transfer function of the ideal digital compensator is given by

$$\begin{aligned} D(z) &= \mathbf{c}_d^T\left(z\mathbf{I} - \mathbf{A}_d\right)^{-1}\mathbf{b}_d + d \\ &= \frac{\beta_{2M}z^M + \beta_{2M-1}z^{M-1} + \ldots + \beta_M}{z^M + \beta_{M-1}z^{M-1} + \ldots + \beta_0}, \end{aligned} \tag{4.30}$$

where $z := e^{j\omega T}$ with T the sampling period of the system.

In order to apply direct decomposition [455] to (4.30) we introduce the dummy variable $X_{d,M}(z)$ to obtain

$$\frac{U(z)}{E(z)} = \frac{(\beta_{2M}z + \beta_{2M-1} + \beta_{2M-2}z^{-1} + \ldots + \beta_M z^{-M+1})X_{d,M}(z)}{(z + \beta_{M-1} + \beta_{M-2}z^{-1} + \ldots + \beta_0 z^{-M+1})X_{d,M}(z)}.$$

Equating numerators and denominators across the equality of the last expression, gives

$$E(z) = (z + \beta_{M-1} + \beta_{M-2}z^{-1} + \ldots + \beta_0 z^{-M+1})X_{d,M}(z), \tag{4.31}$$

and

$$U(z) = (\beta_{2M}z + \beta_{2M-1} + \beta_{2M-2}z^{-1} + \ldots + \beta_M z^{-M+1})X_{d,M}(z), \tag{4.32}$$

respectively. From (4.31), we obtain

$$zX_{d,M}(z) = -\sum_{j=1}^{M} \beta_{j-1} z^{-(M-j)} X_{d,M}(z) + E(z). \tag{4.33}$$

Since

$$z^p X_{d,i}(z) = X_{d,i+p}(z) \xrightarrow{\mathcal{Z}^{-1}} x_{d,i}(n+p) = x_{d,i+p}(n), \tag{4.34}$$

where $p \in \mathbf{Z}$, (4.33) becomes

$$zX_{d,M}(z) = -\sum_{j=1}^{M} \beta_{j-1} X_{d,j}(z) + E(z).$$

Taking the inverse $\mathcal{Z}$-transform then yields

$$x_{d,M}(n+1) = -\sum_{j=1}^{M} \beta_{j-1} x_{d,j}(n) + e(n). \tag{4.35}$$

Similarly using (4.32) and (4.34) we obtain

$$\begin{aligned} U(z) &= \sum_{j=1}^{M} \beta_{M+j-1} z^{-(M-j)} X_{d,M}(z) + \beta_{2M} z X_{d,M}(z) \\ &= \sum_{j=1}^{M} \beta_{M+j-1} X_{d,j}(z) + \beta_{2M} z X_{d,M}(z). \end{aligned}$$

The inverse $\mathcal{Z}$-transform of this is given by

$$u(n) = \sum_{j=1}^{M} \beta_{M+j-1} x_{d,j}(n) + \beta_{2M} x_{d,M}(n+1). \tag{4.36}$$

Using (4.34), (4.35) and ((4.36)) we may write the system (4.28) and (4.29) in phase-variable canonical form, that is,

$$\mathbf{x}_d(n+1) = \mathbf{\Lambda}_d \mathbf{x}_d(n) + \mathbf{e}_M e(n)\,, \tag{4.37}$$

where

$$\mathbf{x}_d(n) := (x_{d,1}(n),\, x_{d,2}(n),\, \ldots\,, x_{d,M-1}(n)\,, x_{d,M}(n))^T\,,$$

$$\mathbf{\Lambda}_d := \begin{pmatrix} 0 & 1 & 0 & \ldots & 0 & 0 \\ 0 & 0 & 1 & \ldots & 0 & 0 \\ \vdots & \vdots & \vdots & & \vdots & \vdots \\ 0 & 0 & 0 & \ldots & 0 & 1 \\ -\beta_0 & -\beta_1 & -\beta_2 & \ldots & -\beta_{M-2} & -\beta_{M-1} \end{pmatrix},$$

with $\mathbf{e}_M \in \mathbf{R}^M$ the standard basis vector

$$\mathbf{e}_M := (0,\, 0,\, \ldots\,, 0,\, 1)^T\,,$$

and

$$u(n) = \sum_{j=1}^{M} \beta_{M+j-1} x_{d,j}(n) + \beta_{2M} x_{d,M}(n+1)\,.$$

Equation (4.37) is the vector dynamical equation of the ideal digital compensator. The scalar dynamical equations of a real digital compensator are derived from (4.37) and are given by

$$x_{d,i}(n+1) = x_{d,i+1}(n)\,, \qquad i = 1, 2, \ldots, M-1\,, \tag{4.38}$$

$$x_{d,M}(n+1) = \sum_{j=1}^{M} Q_h(-\beta_{j-1} x_{d,j}(n)) + Q_h(e(n))\,, \tag{4.39}$$

$$u(n) = \sum_{j=1}^{M} Q_h(\beta_{M+j-1} x_{d,j}(n)) + Q_h(\beta_{2M} x_{d,M}(n+1))\,. \tag{4.40}$$

Letting

$$z_j(n) := 10^h x_{d,j}(n)\,,$$

then (4.38) to (4.40) may be rewritten as

$$z_i(n+1) = z_{i+1}(n)\,, \qquad i = 1, 2, \ldots, M-1\,,$$

$$z_M(n+1) = \sum_{j=1}^{M} Q(-\beta_{j-1} z_j(n)) + Q(10^h e(n))\,,$$

$$u(n) = 10^h \left(\sum_{j=1}^{M} Q(\beta_{M+j-1} z_j(n)) + Q(\beta_{2M} z_M(n+1)) \right).$$

Defining

$$\mathbf{x}(n) := 10^h \mathbf{x}_p(n)\,,$$

and using

$$e(n) = r(n) - y(n)\,,$$

the real digital compensator is governed by

$$\mathbf{x}(n+1) = \mathbf{A}_p\mathbf{x}(n) + \mathbf{b}_p\left(\sum_{j=1}^{M} Q(\beta_{M+j-1}z_j(n)) + Q(\beta_{2M}z_M(n+1))\right), \quad (4.41)$$

$$z_i(n+1) = z_{i+1}(n)\,, \qquad i = 1,2,\ldots,M-1\,, \quad (4.42)$$

$$z_M(n+1) = \sum_{j=1}^{M} Q(-\beta_{j-1}z_j(n)) + Q(10^h r(n) - \mathbf{c}_p^T\mathbf{x}(n)), \quad (4.43)$$

$$y(n) = 10^{-h}\mathbf{c}_p^T\mathbf{x}(n)\,. \quad (4.44)$$

Equations (4.41) to (4.44) give vector recurrence relations of the form

$$\mathbf{x}(n+1) = \mathbf{G}(\mathbf{x}(n), \mathbf{z}(n))\,, \quad (4.45)$$

$$\mathbf{z}(n+1) = \mathbf{C}(\mathbf{x}(n), \mathbf{z}(n))\,, \quad (4.46)$$

where $\mathbf{x}(n) \in \mathbf{R}^N$, $\mathbf{z}(n) \in \mathbf{Z}^M$, $\mathbf{G} : \mathbf{R}^N \times \mathbf{Z}^M \to \mathbf{R}^N$, $\mathbf{C} : \mathbf{R}^N \times \mathbf{Z}^M \to \mathbf{Z}^M$. Equations (4.45) and (4.46) are nonlinear due to the incorporation of the rounding operator Q.

By defining $S^{(N,M)} := \mathbf{R}^N \times \mathbf{Z}^M$ and

$$\boldsymbol{\zeta}(n) := \begin{pmatrix} \mathbf{x}(n) \\ \mathbf{z}(n) \end{pmatrix},$$

(4.45) and (4.46) can jointly be written as

$$\boldsymbol{\zeta}(n+1) = \mathbf{H}(\boldsymbol{\zeta}(n))\,,$$

where the function $\mathbf{H} : S^{(N,M)} \to S^{(N,M)}$ is defined by

$$\mathbf{H}(\boldsymbol{\zeta}(n)) := \begin{pmatrix} \mathbf{G}(\mathbf{x}(n), \mathbf{z}(n)) \\ \mathbf{C}(\mathbf{x}(n), \mathbf{z}(n)) \end{pmatrix}. \quad (4.47)$$

Definition 4.2 The set $S^{(N,M)}$, $\boldsymbol{\zeta} \in S^{(N,M)}$ and $\mathbf{H}$ are termed a *mixed state space*, a *mixed state* and a *mixed mapping*, respectively. We call $\mathbf{x}(n)$ and $\mathbf{z}(n)$ the *continuous* and *discrete parts* of $\boldsymbol{\zeta}(n)$, respectively. ■

4.5.2 Conditions for the Existence of Chaos

In this section the conditions are derived under which the rounding error of the real digital compensator renders the system chaotic. Consider a system of the form (4.41) to (4.44) whose matrix $\mathbf{A}_p$ is in block-Jordan form, $\beta_2 = 1$ and has constant input $r(n) = 0$. This system is thus given by

$$\begin{pmatrix} \mathbf{x}_1(n+1) \\ \mathbf{x}_2(n+1) \end{pmatrix} = \begin{pmatrix} \mathbf{A}_1 & \mathbf{0} \\ \mathbf{0} & \mathbf{A}_2 \end{pmatrix} \begin{pmatrix} \mathbf{x}_1(n) \\ \mathbf{x}_2(n) \end{pmatrix} + \begin{pmatrix} \mathbf{b}_1 \\ \mathbf{b}_2 \end{pmatrix} (Q(\beta_1 z(n)) + Q(z(n+1))), \tag{4.48}$$

$$z(n+1) = Q(-\beta_0 z(n)) + Q(-\mathbf{c}^T \mathbf{x}(n)), \tag{4.49}$$

$$y(n) = 10^{-h} \mathbf{c}^T \mathbf{x}(n), \tag{4.50}$$

where

$$\mathbf{c}^T := \left(\mathbf{c}_1^T, \mathbf{c}_2^T\right), \qquad \mathbf{c}_1 \in \mathbf{R}^{N_1 \times 1}, \quad \mathbf{c}_2 \in \mathbf{R}^{N_2 \times 1}.$$

By defining $\boldsymbol{\zeta} \in S^{(N_1+N_2,1)}$ to be

$$\boldsymbol{\zeta}^T(n) := \left(\mathbf{x}_1^T(n), \mathbf{x}_2^T(n), z(n)\right),$$

we may write (4.48) and (4.49) more compactly as

$$\boldsymbol{\zeta}(n+1) = \mathbf{H}(\boldsymbol{\zeta}(n)). \tag{4.51}$$

Assume that the absolute values of all the eigenvalues of $\mathbf{A}_1$ and $\mathbf{A}_2$ are respectively greater than and less than one and nonzero. The transfer function of the hypothesized ideal digital compensator is

$$D(z) = \frac{z + \beta_1}{z + \beta_0},$$

which is a phase-lead compensator if $\beta_1 > \beta_0$ and a phase-lag compensator if $\beta_1 < \beta_0$.

It is obvious that the origin i.e. $\boldsymbol{\zeta}_0^* := (\mathbf{0}^T, \mathbf{0}^T, 0)^T$ is a hyperbolic mixed state of (4.51). By the stable and unstable manifold theorems there exists a neighbourhood of $\boldsymbol{\zeta}_0^*$ where $z = 0$ [814] containing local stable and unstable manifolds $W_{loc}^s(\boldsymbol{\zeta}_0^*)$ and $W_{loc}^u(\boldsymbol{\zeta}_0^*)$ respectively of $\mathbf{H}$. Since the existence of an unstable manifold in a neighbourhood of the fixed point of the map $\mathbf{H}$ is a necessary condition for the system to exhibit chaotic behaviour, we have ensured its existence by assuming that $\mathbf{A}_p$ has eigenvalues which are greater than one in absolute value.

Lemma 4.3 By the hypotheses on $\mathbf{A}_i$, $i = 1, 2$, there exist positive definite matrices $\mathbf{P}_i \in \mathbf{R}^{N_i \times N_i}$, $i = 1, 2$, such that, for some positive definite matrices $\mathbf{Q}_i \in \mathbf{R}^{N_i \times N_i}$, $i = 1, 2$, we have

$$(\mathbf{A}_1^{-1})^T \mathbf{P}_1 \mathbf{A}_1^{-1} - \mathbf{P}_1 = -\mathbf{Q}_1, \qquad \mathbf{A}_2^T \mathbf{P}_2 \mathbf{A}_2 - \mathbf{P}_2 = -\mathbf{Q}_2.$$

Proof: Refer to [814] for the proof. ∎

Before stating the main result of this section, we define

$$\rho_i := \inf\left\{\mathbf{x}_i^T\mathbf{P}_i\mathbf{x}_i \,\middle|\, \mathbf{x}_i \in \mathbf{R}^{N_i} \text{ subject to } \mathbf{c}_i^T\mathbf{x}_i = 1/2\right\},$$

for $i = 1, 2$. We now state sufficient conditions for the system (4.51) as described by (4.48) to (4.50), to be chaotic.

Theorem 4.4 If $N_1 > 0$ and the following conditions

$$|\beta_0| < \frac{1}{2}, \quad |\beta_1| < \frac{1}{2}, \tag{4.52}$$

$$\frac{1}{2} < \mathbf{c}_1^T\mathbf{A}_1^{-1}\mathbf{b}_1 < \frac{3}{2}, \tag{4.53}$$

$$\mathbf{b}_1^T(\mathbf{P}_1 - \mathbf{Q}_1 - (\mathbf{A}_1^{-1})^T\mathbf{Q}_1\mathbf{A}_1^{-1})\mathbf{b}_1 < \rho_1, \tag{4.54}$$

$$\mathbf{b}_2^T\mathbf{P}_2\mathbf{b}_2 < \rho_2, \tag{4.55}$$

hold, then (4.51) is chaotic due to rounding error.

Proof: The proof uses a mixed mapping version of the Shiraiwa-Kurata theorem as stated and proved in [814]. For details of the proofs the reader is referred to [814]. ■

Remark If $N_2 = 0$, then condition (4.55) becomes void and

$$\mathbf{A}_1 = \mathbf{A}_p, \qquad \mathbf{b}_1 = \mathbf{b}_p, \qquad \mathbf{c}_1 = \mathbf{c}_p.$$

Corollary 4.5 The conditions (4.54) and (4.55) can be generalized to

$$|\mathbf{c}_1^T(\mathbf{A}_1^{-1})^k\mathbf{b}_1| < \frac{1}{2}, \qquad k = 2, 3, \ldots,$$

and

$$|\mathbf{c}_2^T\mathbf{A}_2^k\mathbf{b}_2| < \frac{1}{2}, \qquad k = 0, 1, \ldots.$$

respectively. ■

Example 4.6 [814] Below is stated the equations of a second-order plant controlled by a first-order digital compensator,

$$\mathbf{x}(n+1) = \begin{pmatrix} 3 & 0 \\ 0 & 0.25 \end{pmatrix}\mathbf{x}(n) + \begin{pmatrix} 2 \\ -1 \end{pmatrix}(Q(\beta_1 z(n)) + Q(\beta_2 z(n)) + Q(-y(n))), \tag{4.56}$$

$$z(n+1) = Q(\beta_1 z(n)) + Q(-y(n)), \tag{4.57}$$

$$y(n) = (1, 0.25)\,\mathbf{x}(n), \tag{4.58}$$

where $\mathbf{x}(n) \in \mathbf{R}^2$ and $z(n) \in \mathbf{Z}$. By Theorem 4.4, the system (4.56) to (4.58) is chaotic as a result of rounding error if

$$|\beta_1| < \frac{1}{2}, \qquad |\beta_2| < \frac{1}{2}. \tag{4.59}$$

Next, we deduce the stability conditions for the corresponding ideal digital control system,

$$\begin{pmatrix} \mathbf{x}(n+1) \\ z(n+1) \end{pmatrix} = \begin{pmatrix} 1 & -0.5 & 2(\beta_1+\beta_2) \\ -1 & 0.5 & -(\beta_1+\beta_2) \\ -1 & -0.25 & \beta_1 \end{pmatrix} \begin{pmatrix} \mathbf{x}(n) \\ z(n) \end{pmatrix}. \tag{4.60}$$

Using the stability criteria for linear point mappings, the stability conditions for the ideal digital compensator (4.60) are given by

$$\begin{aligned} 3\beta_1 + 4\beta_2 + 1 &> 0, \\ 10\beta_1 + 3\beta_2 + 7 &> 0, \\ (3\beta_1 - \beta_2 - 34)(\beta_1 + \beta_2) &> 0, \end{aligned} \tag{4.61}$$

which describes a triangular region that overlaps the square region in the (β_1, β_2)-plane defined by the condition for chaos, namely (4.59). Consider the point $(\beta_1, \beta_2) = (-0.2, 0)$ which lies in the intersection of these two regions in the parameter space. For this choice of parameters the system has a chaotic attractor which is located in 15 (x_1, x_2) real hyperplanes corresponding to

$$z = -7, -6, \ldots, 6, 7.$$

Simulation results of this attractor is shown in Figure 4.12. Because of the system's symmetry about the origin, only the hyperplanes at $z = 0, -1, \ldots, -7$ are displayed. Successive enlargements of regions on the attractor reveals that the chaotic attractor exhibits self-similarity close to the origin [814]. Typical time evolutions of the state variables $x_1(n)$, $x_2(n)$ and $z(n)$ and the output $y(n)$ are shown in Figure 4.13. Computer simulations showed that the motion of (4.56) to (4.58) goes to infinity if the parameters β_1 and β_2 are in the chaotic region but outside the stability region of the ideal digital control system. To date there exists no confirmation that for such choices of parameters, a system actually exhibits chaos. Therefore, it is conjectured that no chaotic attractor exists if the ideal digital control system is unstable. ■

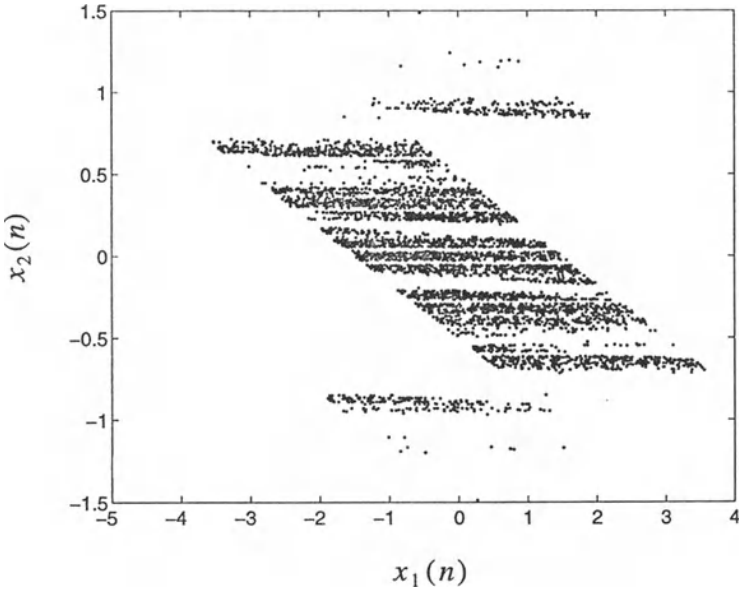

(a)

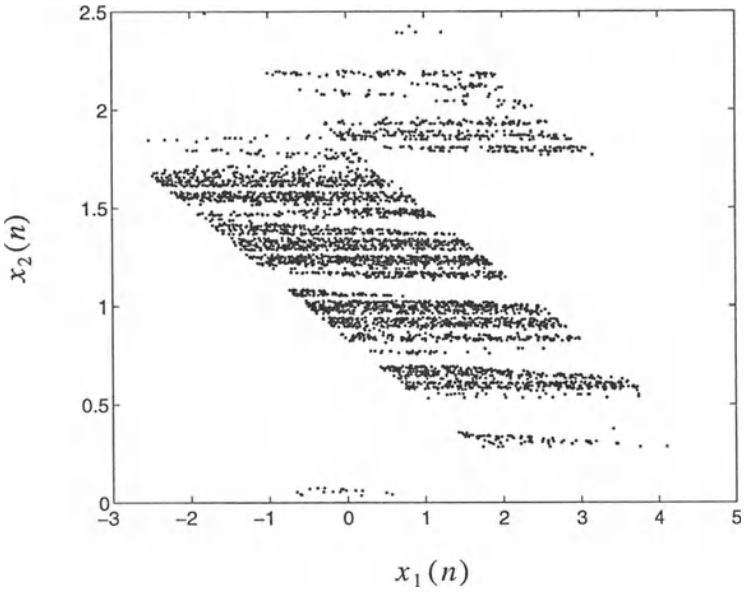

(b)

Figure 4.12: Chaotic attractor in different hyperplanes: (a) $z = 0$; (b) $z = -1$; (c) $z = -2$; (d) $z = -3$; (e) $z = -4$; (f) $z = -5$; (g) $z = -6$; (h) $z = -7$.

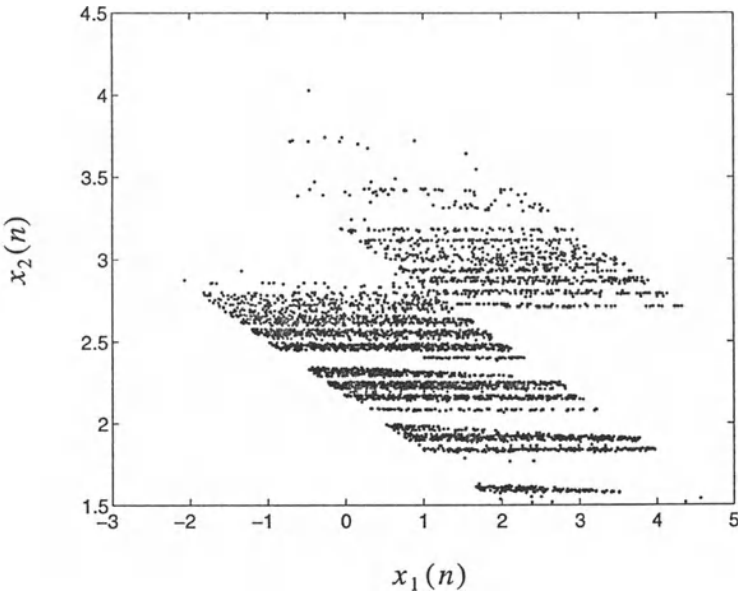

(c)

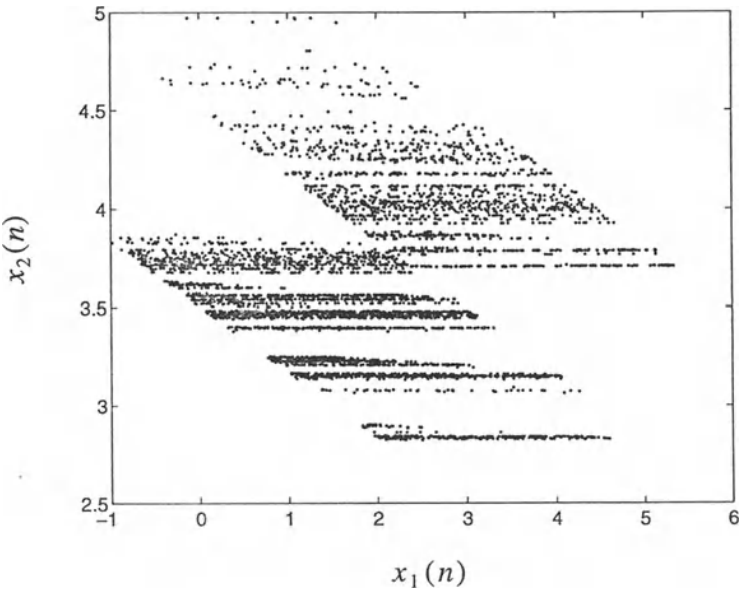

(d)

Figure 4.12: (Continued)

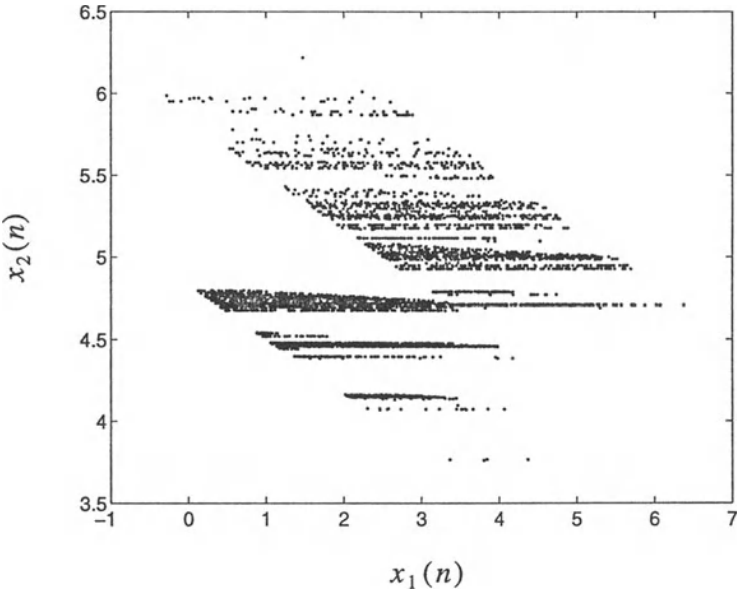

(e)

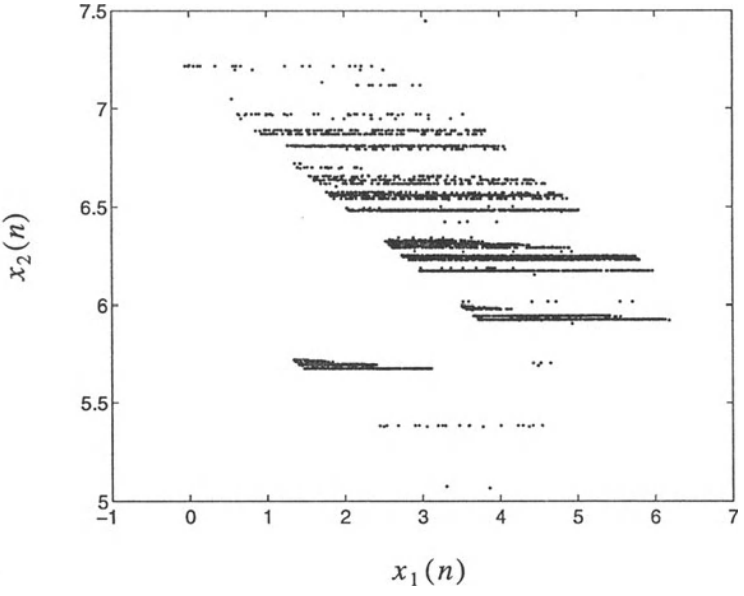

(f)

Figure 4.12: (Continued)

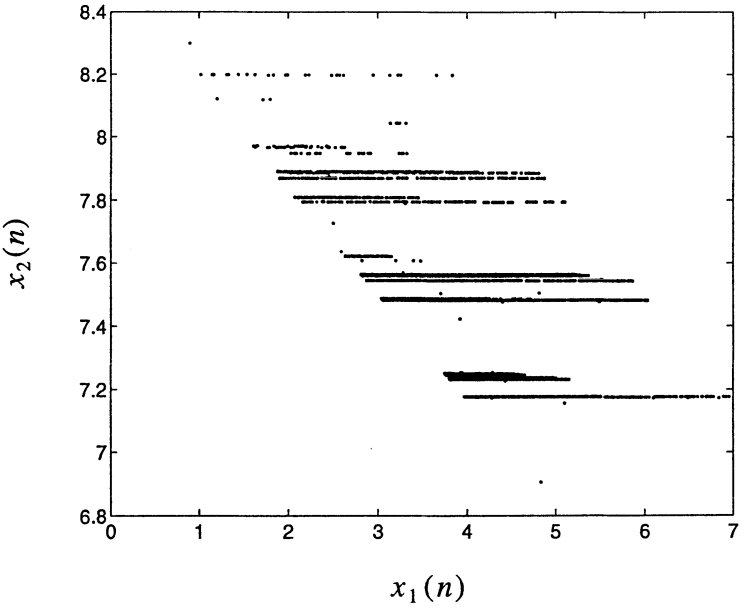

(g)

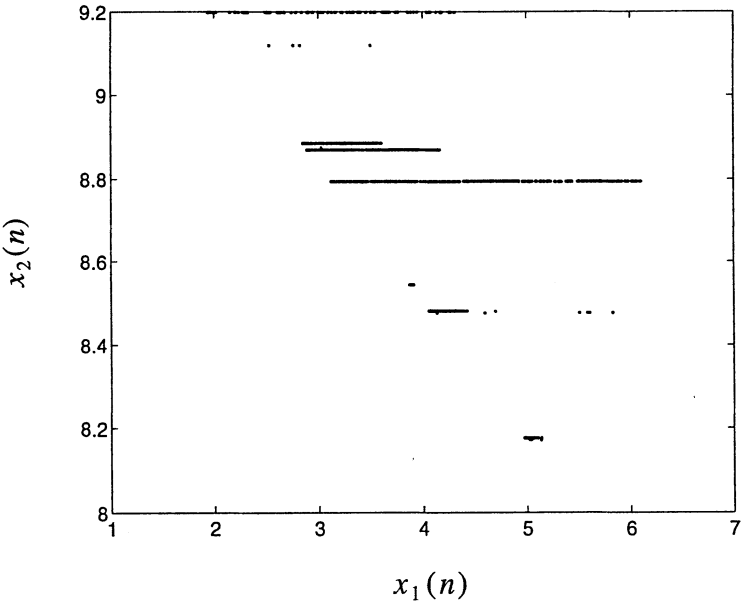

(h)

Figure 4.12: (Continued)

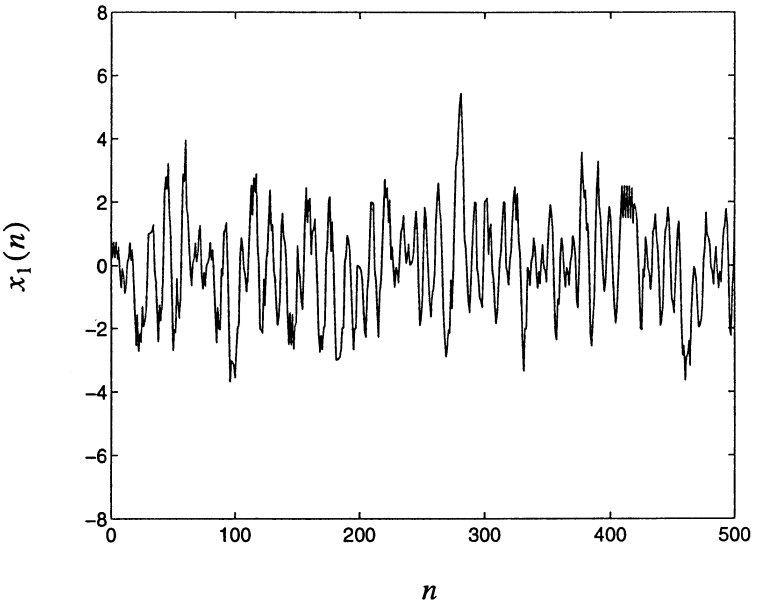

(a)

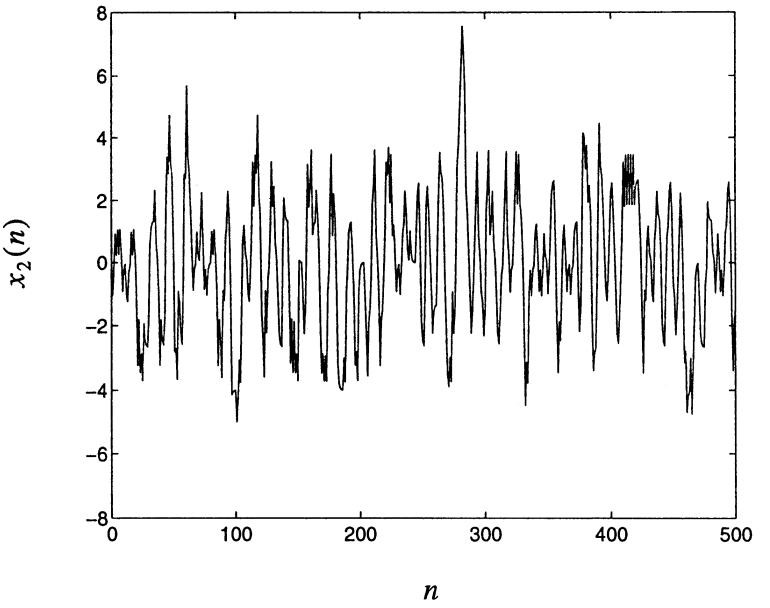

(b)

Figure 4.13: Chaotic time series of the state variables and the output.

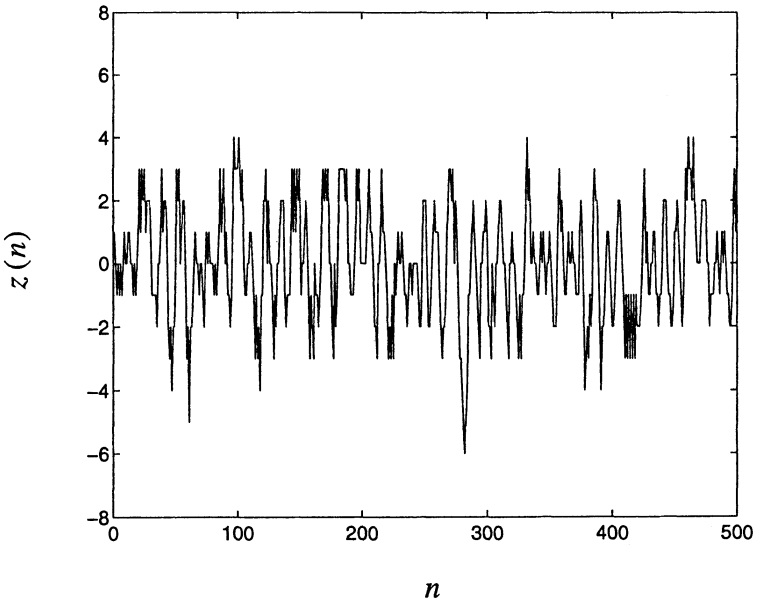

(c)

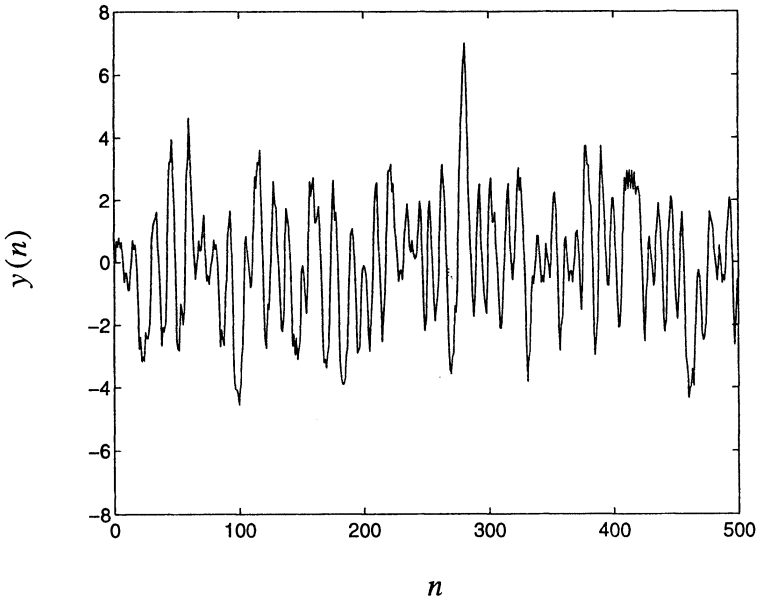

(d)

Figure 4.13: (Continued)

4.6 Chaos in Nonlinear Sampled-Data Control Systems

In applications where a discrete-time control system is used, the input signals to it must first be sampled before they are applied to the discrete-time control system. The choice of sampling frequency is governed by the *Nyquist criterion.* The Nyquist criterion states that the sampling frequency must be at least twice the highest frequency component present in the input signal to prevent *aliasing* from occurring. In effect what happens when the sampling frequency is less than this critical frequency is that all frequencies greater than half the sampling frequency manifest as frequencies less than or equal to half the sampling frequency. The expression that relates the frequency after sampling to the frequency before sampling and the sampling frequency is

$$f_o = \left(f_i + \frac{f_s}{2}\right) (\mathrm{mod}\ f_s) - \frac{f_s}{2},$$

where f_s, f_i and f_o are the sampling frequency, frequency before and after sampling, respectively. The sampling period T and sampling frequency f_s are related by $T = 1/f_s$. Ushio and Hirai [812] proved that there exists a sampling period, say T^*, such that certain sampled-data control systems with sampling period T are chaotic in the Li-Yorke sense for all $T > T^*$. In the sequel we reproduce the main results from [812].

4.6.1 Chaos in State-Feedback Sampled-Data Control Systems

In this section we analyze the nonlinear state-feedback sampled-data control system shown in Figure 4.14. The system studied here is described by

$$\frac{d\mathbf{x}}{dt} = \mathbf{A}\mathbf{x}(t) + \mathbf{B}\mathbf{u}(t), \tag{4.62}$$

$$\mathbf{y}(t) = \mathbf{C}\mathbf{x}(t), \tag{4.63}$$

$$\mathbf{u}(t) = \mathbf{r}(nT) - \mathbf{f}(\mathbf{x}(nT)) \quad \text{for} \quad kT \leq t < (n+1)T, \tag{4.64}$$

where $k = 0, 1, 2, \ldots$, $\mathbf{x}(t) \in \mathbf{R}^N$, $\mathbf{y}(t) \in \mathbf{R}^M$, $\mathbf{r}(t), \mathbf{u}(t) \in \mathbf{R}^L$, $\mathbf{A} \in \mathbf{R}^{N \times N}$, $\mathbf{B} \in \mathbf{R}^{N \times L}$, $\mathbf{C} \in \mathbf{R}^{M \times N}$ and $\mathbf{f} : \mathbf{R}^N \to \mathbf{R}^L$ is a continuously differentiable map. Here T denotes the sampling period. We assume that $\mathbf{A}$ is nonsingular. The solution of (4.62) is given by [783], [455]

$$\mathbf{x}(t) = e^{\mathbf{A}(t-t_0)}\mathbf{x}(t_0) + \int_{t_0}^{t} e^{\mathbf{A}(t-\tau)}\mathbf{B}\mathbf{u}(\tau)d\tau\,. \tag{4.65}$$

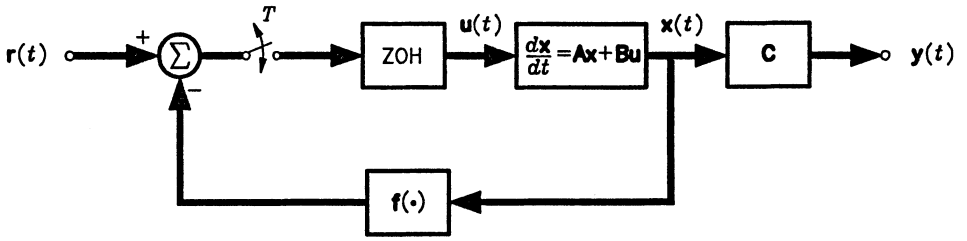

Figure 4.14: Sampled-data control system with nonlinear state-feedback.

From Figure 4.14 it is clear that

$$\mathbf{u}(t) = \mathbf{u}(nT), \qquad nT \leq t < (n+1)T, \quad n \in \mathbf{N}.$$

By defining $\mathbf{x}_n := \mathbf{x}(nT)$, $\mathbf{y}_n := \mathbf{y}(nT)$, $\mathbf{u}_n := \mathbf{u}(nT)$ and $\mathbf{r}_n := \mathbf{r}(nT)$, evaluation of (4.65) at discrete-time instances $t = (n+1)T$ with $t_0 = nT$, $n \in \mathbf{N}_0$, yields [783], [651]

$$\mathbf{x}_{n+1} = \mathrm{e}^{\mathbf{A}T}\mathbf{x}_n + \mathbf{A}^{-1}\left(\mathrm{e}^{\mathbf{A}T} - \mathbf{I}\right)\mathbf{B}\mathbf{u}_n, \tag{4.66}$$

and in addition

$$\mathbf{y}_n = \mathbf{C}\mathbf{x}_n, \tag{4.67}$$

$$\mathbf{u}_n = \mathbf{r}_n - \mathbf{f}(\mathbf{x}_n), \tag{4.68}$$

where $\mathbf{I}$ denotes the $N \times N$ identity matrix. We combine (4.66) to (4.68) to get

$$\mathbf{x}_{n+1} = \mathbf{G}_T(\mathbf{x}_n), \tag{4.69}$$

where

$$\mathbf{G}_T(\mathbf{x}) := \mathbf{x} + \left(\mathrm{e}^{\mathbf{A}T} - \mathbf{I}\right)\mathbf{F}(\mathbf{x}), \tag{4.70}$$

$$\mathbf{F}(\mathbf{x}) := \mathbf{x} + \mathbf{A}^{-1}\mathbf{B}\left(\mathbf{r} - \mathbf{f}(\mathbf{x})\right), \tag{4.71}$$

and we have used the identity [585]

$$\mathbf{A}^{-1}\mathrm{e}^{\mathbf{A}T} = \mathrm{e}^{\mathbf{A}T}\mathbf{A}^{-1}.$$

Since $\mathbf{f} : \mathbf{R}^N \to \mathbf{R}^L$ is a C^1 function by assumption, $\mathbf{G}_T : \mathbf{R}^N \to \mathbf{R}^N$, with $T \in \mathbf{R}^+$ and $\mathbf{F} : \mathbf{R}^N \to \mathbf{R}^N$, as defined above, are both also of class C^1. Concerning the t-dependency of the fixed points of $\mathbf{G}_T$, we have the following lemma.

Lemma 4.7 [812] Any fixed point $\mathbf{x}^*$ of (4.69), satisfies

$$\mathbf{F}(\mathbf{x}^*) = \mathbf{0}\,.$$

Thus any fixed point $\mathbf{x}^*$ of (4.69) is independent of the sampling period.

Proof: Any fixed point $\mathbf{x}^*$ of (4.69) satisfies

$$\begin{aligned} & \mathbf{x}^* = \mathbf{G}_T(\mathbf{x}^*) \\ \Longrightarrow \quad & \mathbf{x}^* = \mathbf{x}^* + \left(\mathrm{e}^{\mathbf{A}T} - \mathbf{I}\right)\mathbf{F}(\mathbf{x}^*) \\ \Longrightarrow \quad & \left(\mathrm{e}^{\mathbf{A}T} - \mathbf{I}\right)\mathbf{F}(\mathbf{x}^*) = \mathbf{0}\,. \end{aligned} \tag{4.72}$$

Because $\mathbf{A}$ is nonsingular, it does not have 0 as an eigenvalue; hence $\mathrm{e}^{\mathbf{A}T}$ does not have $\mathrm{e}^{0T} \equiv 1$ as an eigenvalue. Therefore, $\det\left(\mathrm{e}^{\mathbf{A}T} - \mathbf{I}\right) \neq 0$ which implies $\mathbf{F}(\mathbf{x}^*) = \mathbf{0}$. Since $\mathbf{F}$ is independent of T we conclude that $\mathbf{x}^*$ is independent of T. ■

Theorem 4.8 [812] Let $\mathbf{f} : \mathbf{R}^N \to \mathbf{R}^L$ be a continuously differentiable map. Assume the following conditions:

i) The C^1 map $\mathbf{f} : \mathbf{R}^N \to \mathbf{R}^L$ is such that $\mathbf{G}_T$ in (4.67) has two fixed points, $\mathbf{x}_1^*$ and $\mathbf{x}_2^*$ which satisfy

$$\det(D\mathbf{F}(\mathbf{x}_1^*)) \neq 0\,, \qquad \det(D\mathbf{F}(\mathbf{x}_2^*)) \neq 0\,,$$

that is, both fixed points are hyperbolic.

ii) The real parts of all eigenvalues of $\mathbf{A}$ are positive.

Then there exists a sampling period $T^* > 0$ such that the system (4.62) to (4.64) is chaotic for all $T > T^*$.

Remark Theorem 4.8 still holds if $\mathbf{f} : \mathbf{R}^N \to \mathbf{R}^L$ is of class C^1 on some neighbourhoods of the fixed points $\mathbf{x}_1^*$ and $\mathbf{x}_2^*$.

Before proving this theorem, we state some auxiliary results in the form of lemmas. Conditions (i) and (ii) of Theorem 4.8 are also conditions for these lemmas, although they are not explicitly restated there.

Lemma 4.9 There exist positive numbers r_1 and T_1 such that for all $T > T_1$ and any

$$\mathbf{x} \in \tilde{B}(\mathbf{x}_1^*; r_1) \cup \tilde{B}(\mathbf{x}_2^*; r_1) \neq \emptyset\,,$$

we have

$$\det(D\mathbf{G}_T(\mathbf{x})) \neq 0\,.$$

Proof: See [812] for the details of the proof. ■

Lemma 4.10 There exist positive numbers r_2 and T_2 such that all eigenvalues of $D\mathbf{G}_T(\mathbf{x})$ exceed unity in norm for all $T > T_2$ and all $\mathbf{x} \in \tilde{B}(\mathbf{x}_i; r_2)$, $i = 1, 2$.

Proof: See [812]. ■

Lemma 4.11 Let $U := \text{Int } \tilde{B}(\mathbf{x}_1^*; \epsilon)$ and $V := \text{Int } \tilde{B}(\mathbf{x}_1^*; \epsilon)$ where ϵ is a sufficiently small positive number. There exists a positive number $T_3(\epsilon)$ such that the following two conditions hold for all $T > T_3(\epsilon)$:

i) For each $\mathbf{v} \in V$, the equation $\mathbf{G}_T(\mathbf{x}) = \mathbf{v}$ has at least one solution $\mathbf{x} \in U$;

ii) For each $\mathbf{u} \in U$, the equation $\mathbf{G}_T(\mathbf{y}) = \mathbf{u}$ has at least one solution $\mathbf{y} \in V$.

Proof: This proof makes use Urabe's proposition [810] as stated therein. The reader is referred to [812] for the proof. ■

Here Int A denotes the interior of the set A. We are now in a position to present the proof of Theorem 4.8.

Proof of Theorem 4.8: Let $r^* := \min(r_1, r_2)$ and $T^* := \max(T_1, T_2, T_3(\epsilon))$, where ϵ is a positive number satisfying the conditions

$$U := B(\mathbf{x}_1^*; \epsilon) \subset \text{Int } \tilde{B}(\mathbf{x}_1^*; r^*),$$

and

$$V := B(\mathbf{x}_2^*; \epsilon) \subset \text{Int } \tilde{B}(\mathbf{x}_2^*; r^*).$$

By Lemma 4.10, $\mathbf{x}_1^*$ is a repelling fixed point for all $T > T^*$ with $W_{loc}^u = \tilde{B}(\mathbf{x}_1^*; r^*)$. Moreover, by Lemma 4.11 there exists at least one $\mathbf{v}(T) \in V$ such that

$$\mathbf{G}_T(\mathbf{v}(T)) = \mathbf{x}_1^*(T),$$

and at least one $\mathbf{u}(T) \in U$ such that

$$\mathbf{G}_T(\mathbf{u}(T)) = \mathbf{v}(T),$$

for all $T > T^*$. By Lemma 4.9, for all $T > T^*$,

$$\det\left(D\mathbf{G}_T^{(2)}(\mathbf{u}(T))\right) \neq 0,$$

and thus $\mathbf{G}_T$ is locally bijective so that $\mathbf{u}$ and $\mathbf{v}$ are locally unique. Therefore, we conclude that $\mathbf{x}_1^*$ is a snap-back repeller and consequently, using Marotto's theorem we deduce that the system (4.62) to (4.64) is chaotic for all $T > T^*$. ■

Example 4.12 Consider the sample-data system described by

$$\mathbf{G}_T(\mathbf{x}) = \mathrm{e}^{\mathbf{A}T}\mathbf{x} + \mathbf{A}^{-1}\left(\mathrm{e}^{\mathbf{A}T} - \mathbf{I}\right)\mathbf{B}(\mathbf{r} - \mathbf{f}(\mathbf{x}))\,, \tag{4.73}$$

where

$$\mathbf{A} := \begin{pmatrix} \lambda_1 & 0 \\ 0 & \lambda_2 \end{pmatrix}, \quad \mathbf{B} := \begin{pmatrix} 1 & 0 \\ 0 & 1 \end{pmatrix}, \quad \mathbf{C} := \frac{1}{2}\begin{pmatrix} 1 \\ 1 \end{pmatrix}, \quad \mathbf{r} := \begin{pmatrix} 0 \\ 0 \end{pmatrix}, \tag{4.74}$$

with $\lambda_1, \lambda_2 \in \mathbf{R}^+$ and

$$\mathbf{f}(\mathbf{x}) := \begin{pmatrix} x_1^2 - e_1(x_2 - x_1) \\ x_2^2 - e_2(x_1 - x_2) \end{pmatrix}, \quad e_1, e_2 \in \mathbf{R}\,. \tag{4.75}$$

The function $\mathbf{F}$ in (4.71) is given by

$$\mathbf{F}(\mathbf{x}) = \begin{pmatrix} x_1 + \dfrac{e_1(x_2 - x_1) - x_1^2}{\lambda_1} \\ x_2 + \dfrac{e_2(x_1 - x_2) - x_2^2}{\lambda_2} \end{pmatrix}.$$

Combining (4.73) to (4.75), $\mathbf{x}_{n+1} = \mathbf{G}_T(\mathbf{x}_n)$ is explicitly given by

$$x_{1,n+1} = r_1 x_{1,n} - q_1 x_{1,n}^2 + q_1 e_1(x_{2,n} - x_{1,n})\,, \tag{4.76}$$

$$x_{2,n+1} = r_2 x_{2,n} - q_2 x_{2,n}^2 + q_2 e_2(x_{1,n} - x_{2,n})\,, \tag{4.77}$$

where

$$r_i := \mathrm{e}^{\lambda_i T}, \qquad q_i = \frac{\mathrm{e}^{\lambda_i T} - 1}{\lambda_i} \quad i = 1, 2\,. \tag{4.78}$$

To simplify the analysis, assume that $\lambda := \lambda_1 \equiv \lambda_2$ and $e := e_1 \equiv e_2$. Under these assumptions (4.76) and (4.77) become

$$x_{1,n+1} = r x_{1,n} - q x_{1,n}^2 + q e(x_{2,n} - x_{1,n})\,, \tag{4.79}$$

$$x_{2,n+1} = r x_{2,n} - q x_{2,n}^2 + q e(x_{1,n} - x_{2,n})\,, \tag{4.80}$$

where r is the common value of r_1 and r_2 and q is the common value of q_1 and q_2.

The fixed points of the system (4.79) and (4.80) are obtained by solving the equation $\mathbf{F}(\mathbf{x}^*) = \mathbf{0}$. These are

$$\mathbf{x}_1^* := (0,0)^T\,, \quad \mathbf{x}_2^* := (\lambda, \lambda)^T\,, \quad \mathbf{x}_3^* := (\alpha, \beta)^T\,, \quad \mathbf{x}_4^* := (\beta, \alpha)^T\,,$$

where

$$\alpha, \beta := \frac{\lambda - 2e \pm \sqrt{\lambda^2 - 4e^2}}{2}\,.$$

The Jacobian matrix and the Jacobian of $\mathbf{F}$ are respectively given by

$$D\mathbf{F}(\mathbf{x}) = \begin{pmatrix} 1 - \left(\frac{2x_1 + e}{\lambda}\right) & \frac{e}{\lambda} \\ \frac{e}{\lambda} & 1 - \left(\frac{2x_2 + e}{\lambda}\right) \end{pmatrix},$$

and

$$\det(D\mathbf{F}(\mathbf{x})) = \frac{\lambda^2 - 2(e + x_1 + x_2)\lambda + 2(ex_1 + ex_2 + 2x_1x_2)}{\lambda^2}.$$

Evaluation of the Jacobian at the fixed points yields

$$\begin{aligned} \det(D\mathbf{F}(\mathbf{x}_1^*)) &= 1 - \frac{2e}{\lambda}, & \det(D\mathbf{F}(\mathbf{x}_2^*)) &= 1 + \frac{2e}{\lambda}, \\ \det(D\mathbf{F}(\mathbf{x}_3^*)) &= \frac{4e^2}{\lambda^2} - 1, & \det(D\mathbf{F}(\mathbf{x}_4^*)) &= \frac{4e^2}{\lambda^2} - 1. \end{aligned}$$

From the above results we conclude that

$$\det(D\mathbf{F}(\mathbf{x}_i^*)) \neq 0, \quad \text{for each} \quad e \in \mathbf{R} - \left\{-\frac{\lambda}{2}, \frac{\lambda}{2}\right\}. \tag{4.81}$$

Thus, this systems satisfies the conditions of Theorem 4.8 as long as e does not equal $\pm\lambda/2$. By Theorem 4.8 there exists a $T^* \in \mathbf{R}^+$ such that this system is chaotic for each $T > T^*$.

To demonstrate the behaviour of the system described by (4.79) and (4.80), assume $\lambda = 1/2$, $e = 0.1$. For $T = 2.2$ the system shows numerical evidence of chaos. Various projections of the attractor for this case are shown in Figure 4.15. A typical time evolution of the output y_n after the transient response of the system has decayed, is shown in Figure 4.16(a). The power spectral density of y_n in Figure 4.16(b) suggests that the system is chaotic. For $T = 2.2$ the basin of attraction is connected as shown in Figure 4.17. The solid line in this figure represents the boundary of the basin of attraction. However, as T increases the basin of attraction becomes increasingly disconnected. For example, for $T = 2.23$ the basin of attraction is shown in Figure 4.18. It is evident from this that the attractor has a Cantor set-like structure. As T increases the Lebesgue measure of the basin of attraction approaches zero, that is, in the limit as $T \to \infty$ the basin of attraction becomes a totally disconnected

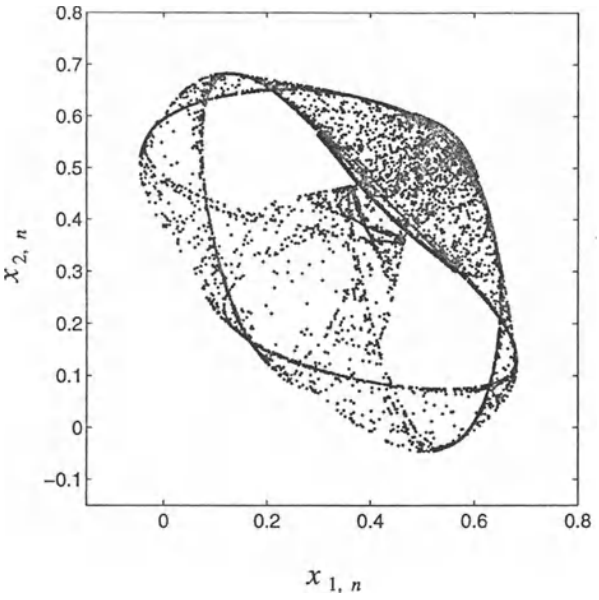

(a)

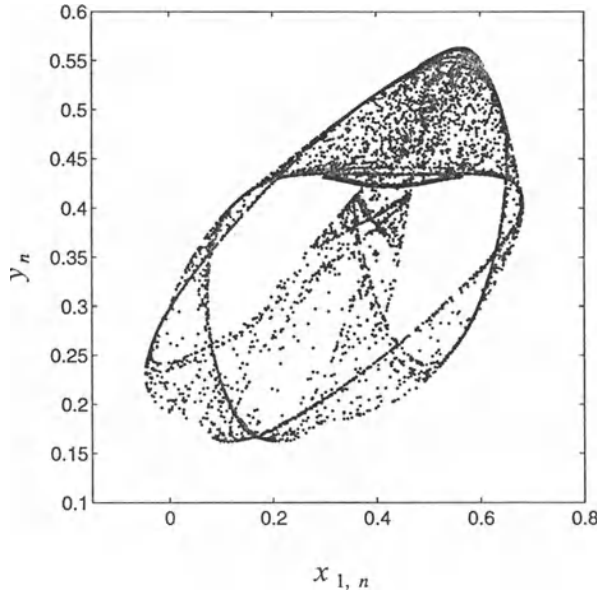

(b)

Figure 4.15: The chaotic attractor of the nonlinear sampled-data system for $T = 2.2$: (a) (x_1, x_2)-plane; (b) (x_1, y)-plane; (c) $(x_{1,n}, x_{1,n+1})$-plane; (d) (y_n, y_{n+1})-plane.

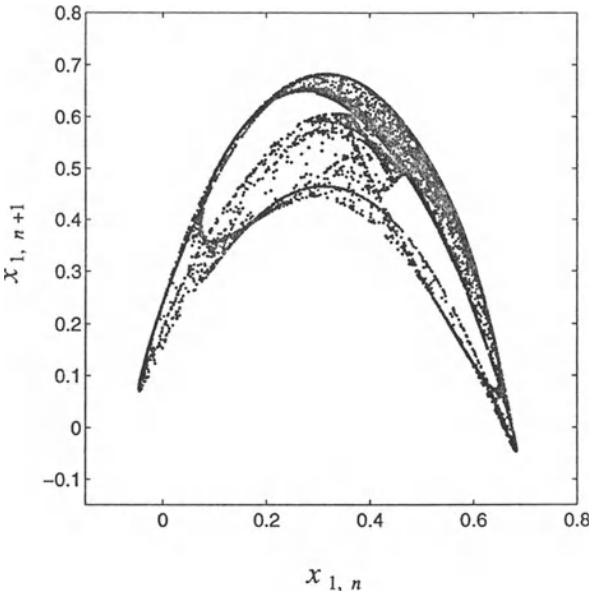

(c)

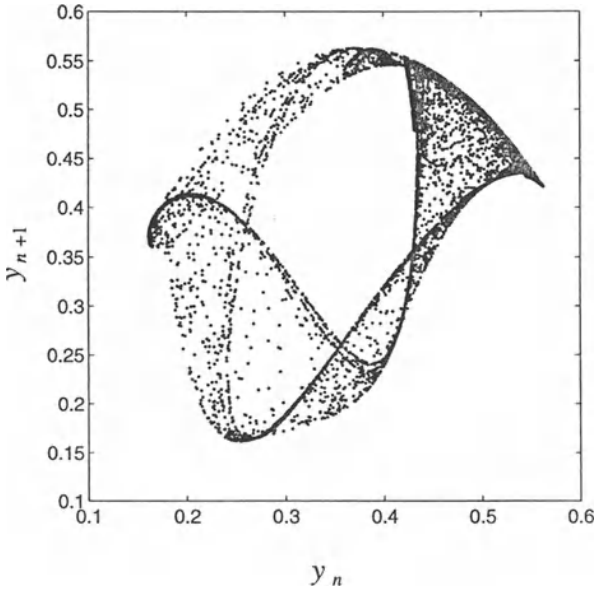

(d)

Figure 4.15: (Continued)

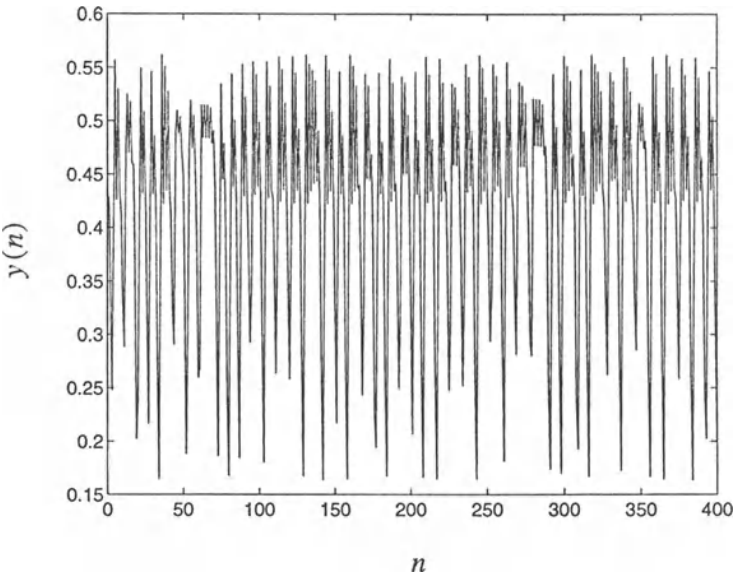

(a)

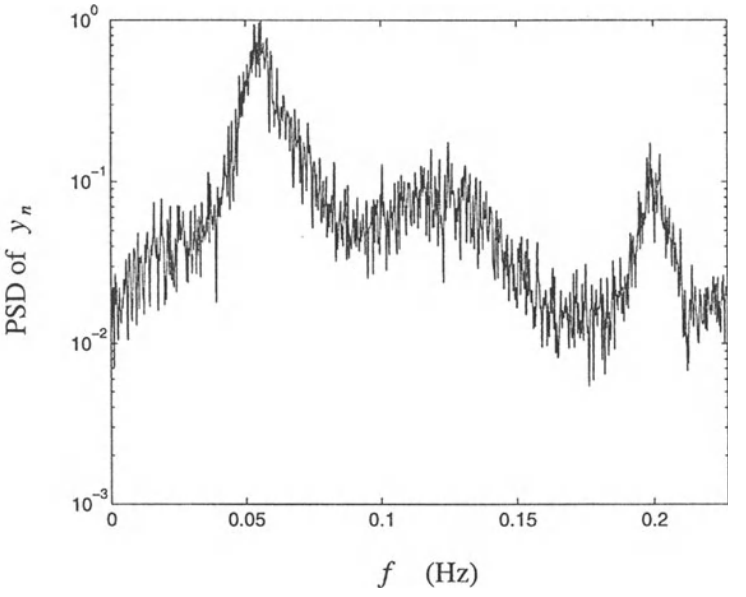

(b)

Figure 4.16: (a) Chaotic time series of the system output y_n for $T = 2.2$; (b) Power spectral density of y_n.

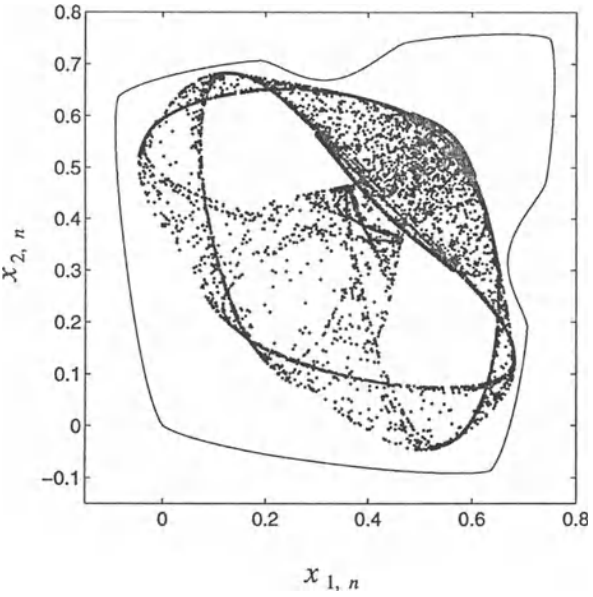

Figure 4.17: Orientation of the basin of attraction relative to the chaotic attractor in the (x_1, x_2)-plane for $T = 2.2$.

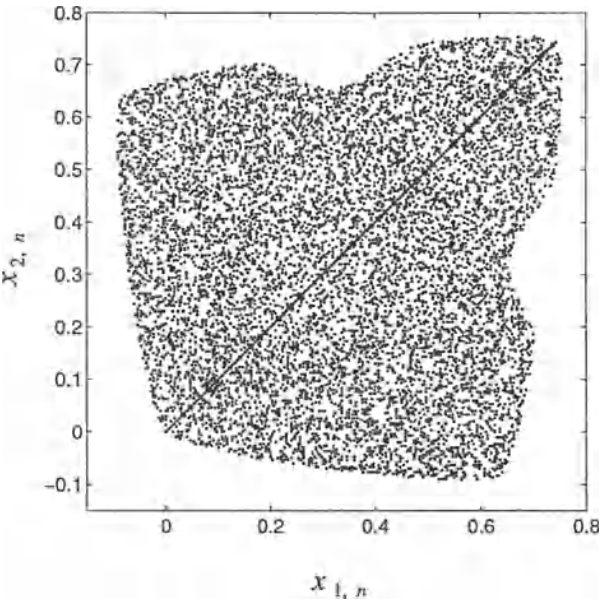

Figure 4.18: The basin of attraction in the (x_1, x_2)-plane for $T = 2.23$.

set. Therefore as T increases, it becomes increasingly difficult to find bounded orbits numerically. Despite this fact, Theorem 4.8 guarantees that the system is chaotic for all $T > T^*$ for some $T^* \in \mathbf{R}^+$.

Before leaving this example, consider the following scaling $z_i := (q/r)x_i$ of the state variables x_i, $i = 1, 2$. Applying this scaling to (4.79) and (4.80), we obtain the scaled system

$$z_{1,n+1} = rz_{1,n}(1 - z_{1,n}) - \epsilon(z_{2,n} - z_{1,n}), \tag{4.82}$$

$$z_{2,n+1} = rz_{2,n}(1 - z_{2,n}) - \epsilon(z_{1,n} - z_{2,n}), \tag{4.83}$$

where $\epsilon := qe$. Thus, we see that the system being studied here is equivalent to the pair of linearly coupled logistic maps in (4.82) and (4.83).

The bifurcation parameters of the scaled system are r and ϵ. As T increases for the original system, the parameters r and ϵ also increase (see (4.78)). On the other hand, for fixed T one is able to adjust the coupling coefficient while r remains unchanged and hence r and ϵ may be adjusted independently from one-another. The system (4.82) and (4.83) was studied numerically in detail by Villet and Steeb in [836].They found this system to exhibit regular, chaotic and hyperchaotic behaviour for appropriate choices of r and ϵ. ■

Example 4.13 Consider the system described by

$$\mathbf{G}_T(\mathbf{x}) = \mathrm{e}^{\mathbf{A}T}\mathbf{x} + \mathbf{A}^{-1}\left(\mathrm{e}^{\mathbf{A}T} - \mathbf{I}\right)\mathbf{B}(\mathbf{r} - \mathbf{f}(\mathbf{x})),$$

where

$$\mathbf{A} := \begin{pmatrix} \lambda_1 & 0 \\ 0 & \lambda_2 \end{pmatrix}, \quad \mathbf{B} := \begin{pmatrix} b_{1,0}^{-1} & 0 \\ 0 & b_{2,0}^{-1} \end{pmatrix}, \quad \mathbf{C} := \frac{1}{2}\begin{pmatrix} 1 \\ 1 \end{pmatrix}, \quad \mathbf{r} := \begin{pmatrix} a \\ 0 \end{pmatrix},$$

where $\lambda_1, \lambda_2 \in \mathbf{R}^+$, $a \in \mathbf{R}$ and $b_{1,0}, b_{2,0} \in \mathbf{R}^+$ are defined later. The mapping $\mathbf{f}$ is taken to be

$$\mathbf{f}(\mathbf{x}) := \mathbf{e}_1 * \mathbf{x} * \mathbf{x} + \mathbf{D}\mathbf{x}, \tag{4.84}$$

where $\mathbf{e}_1$ has its usual meaning and $\mathbf{D}$ is any 2×2 matrix (with real elements) of the form

$$\mathbf{D} := \begin{pmatrix} a_{1,0} & b \\ -1 & a_{2,0} \end{pmatrix},$$

with $b \in \mathbf{R}$ and

$$a_i(T) := \mathrm{e}^{\lambda_i T}, \qquad b_i(T) := \frac{\mathrm{e}^{\lambda_i T} - 1}{\lambda_i}, \qquad i = 1, 2,$$

with $a_{i,0} := a_i(T_0)$ and $b_{i,0} := b_i(T_0)$, $i = 1, 2$ for some value T_0 of the sampling period T. The product $*$ used here is defined by

$$\begin{pmatrix} x_1 \\ x_2 \end{pmatrix} * \begin{pmatrix} y_1 \\ y_2 \end{pmatrix} := \begin{pmatrix} x_1 y_1 \\ x_2 y_2 \end{pmatrix}.$$

The functions $\mathbf{G}_T$ and $\mathbf{F}$ are given by

$$\mathbf{G}_T(\mathbf{x}) = \begin{pmatrix} a_1(T)x_1 + \dfrac{b_1(T)}{b_{1,0}}\,(a - x_1^2 - a_{10}x_1 - bx_2) \\ a_2(T)x_2 + \dfrac{b_2(T)}{b_{2,0}}\,(x_1 - a_{20}x_2) \end{pmatrix},$$

and

$$\mathbf{F}(\mathbf{x}) = \begin{pmatrix} x_1 + \dfrac{a - x_1^2 - a_{1,0}x_1 - bx_2}{\lambda_1 b_{1,0}} \\ x_2 + \dfrac{x_1 - a_{2,0}x_2}{\lambda_2 b_{2,0}} \end{pmatrix}.$$

Notice that

$$\mathbf{G}_{T_0}(\mathbf{x}) = \begin{pmatrix} a - bx_2 - x_1^2 \\ x_1 \end{pmatrix},$$

which is the Hénon map. Thus, $\mathbf{G}_T$ is in a sense a generalization of the Hénon map, since it has embedded in it the Hénon map for the parameter value $T = T_0$. Taking a closer look at $\mathbf{G}_T$ we notice that it is just the Hénon map with a linear term added to it. The fixed points of the map $\mathbf{G}_T$ are the solutions of $\mathbf{F}(\mathbf{x}^*) = \mathbf{0}$, namely

$$\mathbf{x}_1^* := (\alpha, \alpha)^T, \qquad \mathbf{x}_2^* := (\beta, \beta)^T,$$

where

$$\alpha, \beta := \frac{-(b+1) \pm \sqrt{(b+1)^2 + 4a}}{2}.$$

Note, since the fixed points are independent of the sampling period T by Lemma 4.7, these fixed points are necessarily the fixed points of the Hénon map. That the fixed points are independent of T can be seen by noticing that the expressions α and β are independent of $a_i(T)$, $b_i(T)$, $a_{i,0}$, $b_{i,0}$. The Jacobian matrix of $\mathbf{F}$ is

$$D\mathbf{F}(\mathbf{x}) = \begin{pmatrix} -\dfrac{2x_1 + 1}{\lambda_1 b_{1,0}} & \dfrac{-b}{\lambda_1 b_{1,0}} \\ \dfrac{1}{\lambda_2 b_{2,0}} & \dfrac{-1}{\lambda_2 b_{2,0}} \end{pmatrix}.$$

Taking the determinant of $D\mathbf{F}(\mathbf{x})$ we obtain the Jacobian of $\mathbf{F}$ at $\mathbf{x}$, that is,

$$\det\left(D\mathbf{F}(\mathbf{x})\right) = \frac{1 + b + 2x_1}{\lambda_1 b_{1,0} \lambda_2 b_{2,0}}.$$

Evaluating the Jacobian at each fixed point yields

$$\det\left(D\mathbf{F}(\mathbf{x}_1^*)\right) = \frac{\sqrt{1+4a+2b+b^2}}{\lambda_1 b_{1,0}\lambda_2 b_{2,0}},$$

and

$$\det\left(D\mathbf{F}(\mathbf{x}_2^*)\right) = -\frac{\sqrt{1+4a+2b+b^2}}{\lambda_1 b_{1,0}\lambda_2 b_{2,0}}.$$

It is easy to see that

$$\det\left(D\mathbf{F}(\mathbf{x}_i^*)\right) \neq 0, \qquad i = 1,2$$

under the conditions $T_0 < \infty$ and

$$1 + 4a + 2b + b^2 \neq 0.$$

Then by Theorem 4.8 there exists a $T^* \in \mathbf{R}^+$ such that this system is chaotic for each $T > T^*$. ■

In further work Ushio and Hirai [811] observed chaos and crises in two-dimensional nonlinear sampled-data systems. They studied piecewise-linear sampled-data systems by means of the Shiraiwa-Kurata theorem [813]. The reader is referred to [811] and [813] for an in-depth exposition.

Chapter 5

Autonomous Systems in Electronics

5.1 Introduction

The objective of this chapter is to study autonomous nonlinear continuous-time systems in electronics. Such systems have no external inputs and therefore oscillation of these systems must occur at least for some values of system parameters. If this is not so, such a system will not exhibit chaos. Therefore a chaotic autonomous system is usually some kind of oscillator. We start off by discussing Shinriki's circuit in Section 5.2. In essence Shinriki's circuit is a modified Van der Pol oscillator. It was originally presented by Shinriki, Yamamoto and Mori as a circuit which exhibits a type of random waveform (see [728]). It is studied here mainly for Hopf bifurcations. Thereafter we give numerical results obtained by Freire *et al.* in [259] which show that Shinriki's circuit exhibits chaos.

In Section 5.3 we study the circuit proposed by Saito for modeling a quasi-harmonic oscillator. This is done through studying a suitable Poincaré map for this system. Using symbolic dynamics, it is possible to find analytical conditions for which this system shows chaos.

By cascading linear circuits, each of which may be considered to be a filter (at least in the frequency domain) and then closing the loop by adding a nonlinear system which may even be a simple nonlinear amplifier, it is possible to construct an oscillator. As a matter of fact, this is the approach one would use to design an electronic oscillator. From the theory of linear systems it follows that for some values of the system parameters (e.g. a gain factor) the system, being of suitable order, will oscillate. Now if the system contains a nonlinear element such as a nonlinear amplifier one would expect bifurcations and even chaos to occur for certain parameter values. In Section 5.4 we

study such systems. From the numerical results we see that such systems have the potential of shaping the spectral response of a chaotic signal (generated by the system itself) to achieve required specfications.

In the Section 5.5 we study the well-known, perhaps the most famous, Chua's circuit family. Each member of this family is a third-order autonomous piecewise-linear oscillator. We give a short historical overview in which we present the different realizations of the piecewise-linear resistor contained in Chua's oscillator. This resistor is also sometimes called Chua's diode. We also summarize current directions in research on Chua's circuit. Finally, results obtained from a numerical experiment are discussed.

In the last section of this chapter, Section 5.6, we present a discussion of a fourth-order circuit containing two active elements (a nonlinear resistor and a linear negative resistor). This circuit was presented by Matsumoto, Chua and Kobayashi as the first experimental circuit to have generated hyperchaos. Roughly speaking, hyperchaos occurs when a system has two (local) directions of expansion in state space. We present the results of their numerical experiment in this section. These include projections of the attractor onto planes in state space, a Poincaré section, the spectrum of four one-dimensional Lyapunov exponents and the associated Lyapunov dimension of the theoretical circuit model.

5.2 Shinriki's Circuit

5.2.1 Circuit and Model Description

A circuit for modeling a modified Van der Pol oscillator was proposed by Shinriki *et al.* in [728]. The circuit as shown in Figure 5.1 together with an approximating theoretical model was studied by Freire *et al.* [259]. The circuit consists of a resonant circuit and two nonlinear conductances one negative and another positive. The negative nonlinear conductance is realized using the operational amplifier IC_1 (type LM741), resistors R_1 to R_3 and the variable conductance G_1. The positive nonlinear conductance is realized with two sets of series connected diodes connected anti-parallel. The two nonlinear conductances are connected in series. The circuit is closed with a parallel RLC circuit consisting of conductance G_2, inductance L and capacitance C.

For the purpose of deriving an approximate model for the circuit in Figure 5.1, the current-voltage characteristics of two nonlinear elements are approximated by

$$i_a(v) := -a_1 v + a_3 v^3, \qquad a_1, a_3 > 0,$$

for the negative nonlinear conductance and by

$$i_d(v) := b_1 v + b_3 v^3, \qquad b_1, b_3 > 0,$$

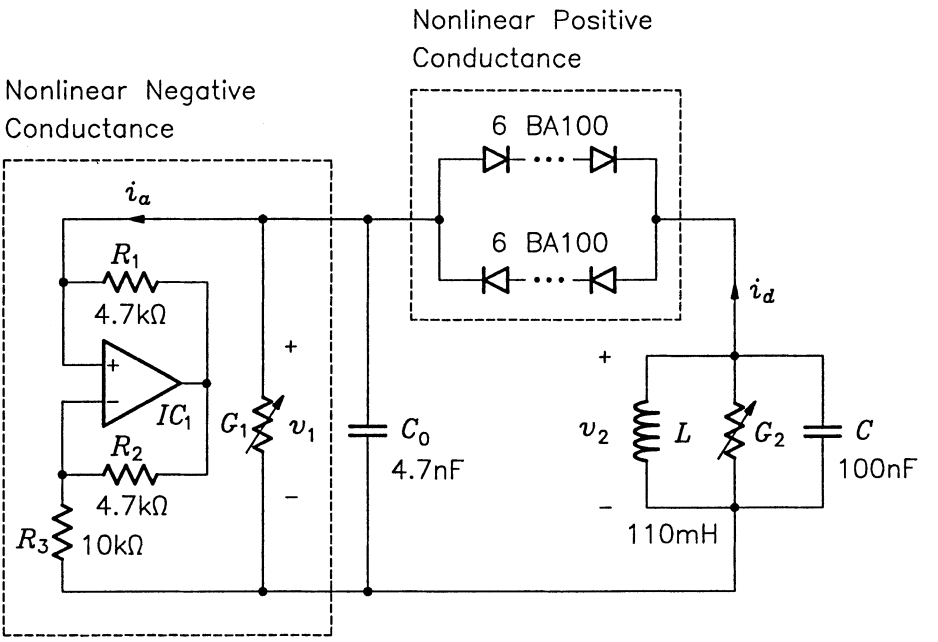

Figure 5.1: Shinriki's circuit.

for the positive nonlinear conductance. The approximation is adequate from a qualitative viewpoint. The state equations which serve as an approximate description of this circuit are derived from the circuit itself by applying Kirchoff's laws and then using the current-voltage approximations stated earlier. Therefore, the state equations for the model are

$$C_0\frac{dv_1}{dt} = -G_1v_1 + a_1v_1 - a_3v^3 + b_1(v_2 - v_1) + b_3(v_2 - v_1)^3, \tag{5.1}$$

$$C\frac{dv_2}{dt} = -i_L - G_2v_2 - b_1(v_2 - v_1) - b_3(v_2 - v_1)^3, \tag{5.2}$$

$$L\frac{di_L}{dt} = v_2, \tag{5.3}$$

with $(v_1, v_2, i_L) \in \mathbf{R}^3$. Here v_1 denotes the voltage across G_1, v_2 is the voltage across G_2, with the rail common to G_1 and G_2 the reference, and i_L the current flowing downward into the inductor L. By making the following substitutions,

$$\omega := \frac{1}{\sqrt{LC}}, \quad \tau := \omega t, \quad x_1 := v_1, \quad x_2 := v_2, \quad x_3 := \frac{1}{\omega C}i_L,$$

and

$$\mu := \frac{G_1 + b_1 - a_1}{\omega C} \qquad \delta := \frac{G_2 + b_1}{\omega C},$$

the system (5.1) to (5.3) may be written in the form

$$\frac{dx_1}{d\tau} = -\mu\frac{C}{C_0}x_1 - \frac{a_3}{\omega C}\frac{C}{C_0}x_1^3 + \frac{b_1}{\omega C}\frac{C}{C_0}x_2 + \frac{b_3}{\omega C}\frac{C}{C_0}(x_2 - x_1)^3, \tag{5.4}$$

$$\frac{dx_2}{d\tau} = \frac{b_1}{\omega C}x_1 - \delta x_2 - x_3 - \frac{b_3}{\omega C}(x_2 - x_1)^3, \tag{5.5}$$

$$\frac{dx_3}{d\tau} = x_2\,. \tag{5.6}$$

To study the behaviour of the system only the parameters G_1 and G_2 will be varied while all other parameters will be kept constant. Because of to the typically small values of b_1 the condition $b_1^2 < C_0/L$ is assumed. The bifurcation parameters are taken to be μ and δ as defined above. The fixed points of the system are

$$\mathbf{x}^*_{-1} := -(\alpha, 0, \beta)^T, \qquad \mathbf{x}^*_0 := (0,0,0)^T, \qquad \mathbf{x}^*_1 := (\alpha, 0, \beta)^T,$$

where

$$\alpha := \sqrt{\frac{-\mu\omega C}{a_3 + b_3}}\,, \qquad \beta := \frac{b_1}{\omega C}\alpha + \frac{b_3}{\omega C}\alpha^3\,.$$

We must now investigate the stability of the fixed points as the bifurcation parameters δ and μ vary.

5.2.2 Fixed Point Stability and Bifurcation Analysis

In this section we study the stability properties of the fixed points of the system (5.4) to (5.6) in the (μ, δ)-plane. First, we fix δ to some positive value and investigate the qualitative behaviour of the system as μ goes from positive values through zero to negative values for points lying above the curve depicted by the solid line in Figure 5.2(a). For $\mu > 0$ the fixed points $\mathbf{x}^*_{-1}$ and $\mathbf{x}^*_1$ are purely imaginary. Because the state variables are constrained to the real plane, these two fixed points are not reachable by trajectories of the system in state space. Hence, for positive values of μ we need only study the fixed point $\mathbf{x}^*_0$. To study the local stability of the fixed point $\mathbf{x}^*_0$, we calculate the eigenvalues of the Jacobian matrix evaluated at $\mathbf{x}^*_0$. The Jacobian matrix evaluated at the origin of the phase space is given by

$$D\mathbf{f}\,(\mathbf{x}^*_0) = \begin{pmatrix} -\dfrac{C}{C_0}\mu & \dfrac{b_1}{\omega C_0} & 0 \\ \dfrac{b_1}{\omega C} & -\delta & -1 \\ 0 & 1 & 0 \end{pmatrix}.$$

For $\mu > 0$ the three characteristic exponents of $\mathbf{x}^*_0$ (i.e. the eigenvalues of $D\mathbf{f}(\mathbf{x}^*_0)$) have negative real parts which implies that the fixed point is hyperbolic and asymptotically

stable. (A fixed point of a flow is *hyperbolic* if all eigenvalues of its Jacobian evaluated at the fixed point have nonzero real part.) For $\mu = 0$, the first and last column of $D\mathbf{f}(\mathbf{x}_0^*)$ are collinear, resulting in one eigenvalue of $D\mathbf{f}(\mathbf{x}_0^*)$ to be zero and hence the fixed point $\mathbf{x}_0^*$ is not hyperbolic. For $\mu < 0$ one characteristic exponent of $\mathbf{x}_0^*$ has a positive real part and the other two have negative real parts, which implies that $\mathbf{x}_0^*$ is hyperbolic and unstable. One is faced with a change in stability which corresponds to a characteristic exponent crossing the imaginary axis. This situation leads us to consider the bifurcation of $\mathbf{x}_0^*$ as the δ-axis in the (μ, δ)-plane is crossed from the region $\mu > 0$ to the region $\mu < 0$.

Thus, maintaining δ constant, the characteristic exponent $\lambda_1(\mu)$ changes from being negative (for $\mu > 0$) to positive (for $\mu > 0$) with $\lambda_1(0) = 0$. The other two characteristic exponents $\lambda_2(\mu)$ and $\lambda_3(\mu)$ remain in the left half of the complex plane. It can be shown (see [259]) that

$$\frac{d\lambda_1}{d\mu}(0) \neq 0\,.$$

The point $\mu = 0$ is a bifurcation point at which $\mathbf{x}_1^*$ and $\mathbf{x}_{-1}^*$ coincide with $\mathbf{x}_0^*$ (i.e. two new (real) fixed points $\mathbf{x}_1^*$ and $\mathbf{x}_{-1}^*$ appear). It can be shown that these two fixed points are asymptotically stable for small negative values of μ. Therefore we conclude that a pitchfork bifurcation occurs at $\mu = 0$ with resulting symmetry of the bifurcating fixed points with respect to change of sign. This symmetry arises from the invariance of the state equations with respect to the transformation $x_1 \mapsto -x_1$, $x_2 \mapsto -x_2$, $x_3 \mapsto -x_3$. The pitchfork bifurcation also occurs for the experimental system and may be ascribed to the presence of the negative nonlinear conductance in the circuit (see [259]).

We now wish to find those values in the (μ, δ)-plane for which Hopf bifurcations associated with the characteristic exponents of $\mathbf{x}_0^*$ are possible. Concerning the hypotheses for Hopf bifurcation, we must find those parameter values in the (μ, δ)-plane for which the Jacobian matrix $D\mathbf{f}(\mathbf{x}_0^*)$ has a conjugate pair of purely imaginary eigenvalues. The characteristic polynomial of $D\mathbf{f}(\mathbf{x}_0^*)$ is given by

$$p(\lambda) := \det(D\mathbf{f}(\mathbf{x}_0^*) - \lambda\mathbf{I}) = -\lambda^3 + T(\mu,\delta)\lambda^2 + S(\mu,\delta)\lambda + D(\mu)\,, \tag{5.7}$$

where

$$T(\mu,\delta) := \operatorname{tr}(D\mathbf{f}(\mathbf{x}_0^*)) = D(\mu) - \delta\,, \tag{5.8}$$

$$S(\mu,\delta) := E + D(\mu)\delta - 1\,, \tag{5.9}$$

$$D(\mu) := \det(D\mathbf{f}(\mathbf{x}_0^*)) = -\zeta\mu\,, \qquad \zeta := \frac{C}{C_0} > 0\,, \tag{5.10}$$

$$E := \frac{b_1^2}{\omega^2 C C_0}\,. \tag{5.11}$$

From the assumptions concerning b_1 made earlier we find that $0 < E < 1$. To find those locations in the (μ, δ)-plane where purely imaginary eigenvalues will occur, we

apply the Routh-Hurwitz test to the characteristic equation

$$p(\lambda) = 0\,. \tag{5.12}$$

Necessary (although not sufficient) conditions for the roots of (5.12) all to lie in the left half of the complex plane are that all coefficients of the characteristic polynomial must be nonzero and must have the same sign, that is,

$$D(\mu),\ S(\mu,\delta),\ T(\mu,\delta) < 0\,. \tag{5.13}$$

From the Routh-Hurwitz test we obtain the additional requirement

$$\frac{T(\mu,\delta)S(\mu,\delta) + D(\mu)}{T(\mu,\delta)} < 0\,,$$

or equivalently (taking the third inequality in (5.13) into account)

$$T(\mu,\delta)S(\mu,\delta) + D(\mu) > 0\,. \tag{5.14}$$

Equations (5.13) and (5.14) constitute a set of necessary and sufficient conditions for all the roots of the characteristic equation (5.12) to have negative real parts. From the first condition in (5.13) we derive that

$$\mu > 0\,. \tag{5.15}$$

Assuming (5.15) to hold, the other two conditions in (5.13) yield respectively

$$\delta > \frac{1-E}{D(\mu)}\,, \tag{5.16}$$

and

$$\delta > D(\mu)\,. \tag{5.17}$$

From the Routh-Hurwitz test we see that the characteristic equation (5.12) has imaginary roots if

$$S(\mu,\delta)T(\mu,\delta) + D(\mu) = 0\,. \tag{5.18}$$

For (5.18) satisfied, the auxiliary equation associated with (5.12) is

$$T(\mu,\delta)\lambda^2 + D(\mu) = 0\,.$$

Its roots which are also roots of (5.12) are given by

$$\lambda_1, \lambda_2 = \pm j\sqrt{\frac{D(\mu)}{T(\mu,\delta)}} = \pm j\sqrt{-S(\mu,\delta)}\,. \tag{5.19}$$

By the conditions imposed on $D(\mu)$, $S(\mu,\delta)$ and $T(\mu,\delta)$ in (5.13), we observe that the square roots in (5.19) are both real and hence the values of λ in (5.19) are imaginary.

Expanding (5.18) by using (5.8) to (5.10) we obtain

$$D(\mu)\delta^2 + \left(E - D^2(\mu) - 1\right)\delta - ED(\mu) = 0\,,$$

which is a quadratic equation in δ with μ-dependent coefficients. Solving this quadratic equation for δ gives

$$\delta_+(\mu),\ \delta_-(\mu) = \frac{(1 + D^2(\mu) - E) \pm \sqrt{(1 + D^2(\mu) - E)^2 + 4ED^2(\mu)}}{2D(\mu)}\,. \tag{5.20}$$

The graphs of $\delta_+(\mu)$ and $\delta_-(\mu)$ are shown in Figure 5.2(a) for the circuit parameters set to those specified in Figure 5.1 and (5.21). In order to make the graphs comparable, we had to magnified the graph of $\delta_-(\mu)$ vertically by a factor of 400. Using the fact that

$$\delta_+(\mu) < D(\mu) < 0\,, \qquad \text{for all} \quad \mu > 0\,,$$

which contradicts (5.17), we have that $\delta_+(\mu)$ is not a valid solution. On the other hand

$$D(\mu) < 0 < \delta_-(\mu)\,, \qquad \text{for all} \quad \mu > 0\,,$$

which is in agreement with (5.17). We must now check if $\delta_-(\mu)$ satisfies (5.16). It can easily be shown that

$$-E < D(\mu)\delta_-(\mu) < 0 < 1 - E\,, \qquad \text{for all} \quad \mu > 0\,,$$

and hence $\delta_-(\mu)$ also satisfies (5.16).

Next we must check that, subject to the condition (5.18), the real characteristic exponent is in the left half of the complex plane as is required by the Hopf bifurcation theorem. However, this is guaranteed by the Routh-Hurwitz test. Alternatively, with (5.18) in effect, we have

$$\lambda_3 = \sum_{k=1}^{3} \lambda_k = T(\mu, \delta_-(\mu)) < 0\,, \qquad \text{for all} \quad \mu > 0\,,$$

by (5.13), where λ_1 is the imaginary characteristic exponent, λ_2 its complex conjugate and λ_3 the real characteristic exponent associated with the fixed point $\mathbf{x}_0^*$.

The last requirement of the Hopf bifurcation theorem, namely that the pair of complex roots of the characteristic equation crosses the imaginary axis with zero velocity, remains to be verified for $\delta_-(\mu)$. We restrict our attention to horizontal crossing of the curve defined by

$$\mathcal{M} := \{(\mu, \delta_-(\mu)) \mid \mu > 0\}\,.$$

We therefore choose δ equal to some constant, say $\delta_0 \in \mathcal{R}(\delta_-)$ and define μ_0 as a value of μ for which

$$\delta_0 = \delta_-(\mu_0)\,.$$

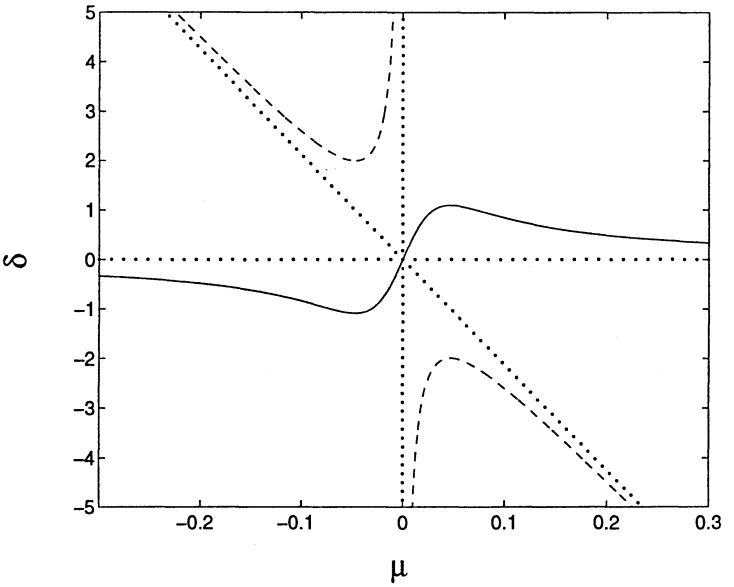

(a)

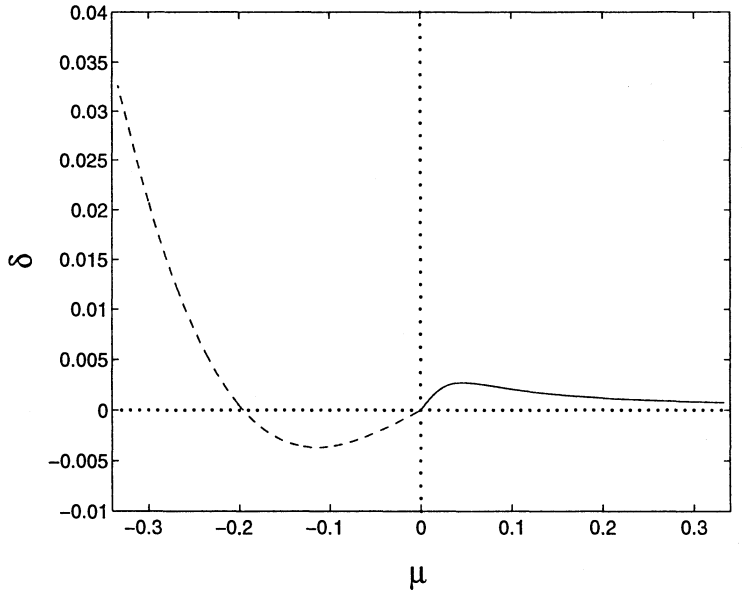

(b)

Figure 5.2: (a) Graphs of $\delta_+(\mu)$ (dashed line) and $\delta_-(\mu)$ (solid line); (b) The complete Hopf bifurcation diagram.

Now differentiating (5.7) with respect to μ and manipulating this to obtain $d\lambda/d\mu$ on one side, gives

$$\frac{d\lambda}{d\mu}(\mu,\delta_0) = \frac{(dT/d\mu)\lambda^2 + (dS/d\mu)\lambda + dD/d\mu}{3\lambda^2 - 2T\lambda - S}\,.$$

Here the (μ,δ_0)-dependency on the right hand side of the last expression was dropped to achieve compactness. Putting $\mu = \mu_0$ in this expression and taking the real part, we obtain

$$\frac{d\Re(\lambda)}{d\mu}(\mu_0,\delta_0) = \frac{\zeta}{2}\left(\frac{S_0 + \delta_0 + 1}{T_0^2 - S_0}\right) \neq 0\,,$$

for all $\mu_0 > 0$ except $\mu_0 = (E+\delta_0)/(\zeta\delta_0)$. Here $S_0 := S(\mu_0,\delta_0)$, $T_0 := T(\mu_0)$ and $\Re(\lambda)$ is the real part of λ. The section of $\delta_-(\mu)$ satisfying the hypotheses of the Hopf bifurcation theorem is depicted by the solid line in Figure 5.2(b).

Since $\delta_-(\mu)$ has a global maximum at $\hat{\mu} := \sqrt{1-E}/\zeta$, namely

$$\hat{\delta} := \delta_-(\hat{\mu}) = 1 - \sqrt{1-E}\,,$$

we conclude that for $\hat{\delta} < b_1/(\omega C)$ or equivalently

$$E < \frac{4\zeta}{(1+\zeta)^2}\,,$$

Hopf bifurcation of the fixed point $\mathbf{x}_0^*$ cannot occur in the experimental system and is therefore only of theoretical interest, since $G_2 \geq 0$ for the experimental system.

The stability and bifurcations of the fixed points $\mathbf{x}_1^*$ and $\mathbf{x}_{-1}^*$ will now be studied briefly. The Jacobian matrix evaluated at the the fixed points $\mathbf{x}_1^*$ and $\mathbf{x}_{-1}^*$ is given by

$$D\mathbf{f}\left(\mathbf{x}_{\pm 1}^*\right) = \begin{pmatrix} 2\dfrac{C}{C_0}\mu & \dfrac{b_1}{\omega C_0} - \left(\dfrac{3b_3}{a_3+b_3}\right)\dfrac{C}{C_0}\mu & 0 \\ \dfrac{b_1}{\omega C} - \left(\dfrac{3b_3}{a_3+b_3}\right)\mu & \left(\dfrac{3b_3}{a_3+b_3}\right)\mu - \delta & -1 \\ 0 & 1 & 0 \end{pmatrix}.$$

Since the expressions for the Jacobian matrices of $\mathbf{x}_1^*$ and $\mathbf{x}_{-1}^*$ are identical, we need only consider one of these two fixed points, say $\mathbf{x}_1^*$. Results obtained for $\mathbf{x}_1^*$ then also apply to $\mathbf{x}_{-1}^*$. First, we determine those points at which $\mathbf{x}_1^*$ has a purely imaginary pair of characteristic exponents. This is achieved by the same process as presented earlier for the fixed point $\mathbf{x}_0^*$ and hence the details of this analysis are not reproduced here. The contour obtained from this analysis is depicted by the dashed line in the (μ,δ)-plane in Figure 5.2(b). In the region above this curve, to the left of the δ-axis in the (μ,δ)-plane the three characteristic exponents have negative real parts, which implies that the fixed point $\mathbf{x}_1^*$ is hyperbolic and asymptotically stable. However, $\mathbf{x}_1^*$ is not hyperbolic at points along this curve, because two of the characteristic exponents

are a purely imaginary conjugate pair while the remaining one is negative real. In the region below the curve (i.e. the dashed line in Figure 5.2(b)) and the μ-axis, one characteristic exponent is real and negative and the other two form a complex conjugate pair with positive real parts. Hence the fixed point $\mathbf{x}_1^*$ is hyperbolic and unstable. A change of stability occurs on crossing this curve, which corresponds to a pair of characteristic exponents crossing the imaginary axis. This leads us to consider the Hopf bifurcation of the fixed point $\mathbf{x}_1^*$ as this curve is crossed. Considering horizontal crossing of the curve depicted by the dashed line in Figure 5.2(b), it can be shown that a Hopf bifurcation occurs as this curve is crossed from right to left, resulting in a small stable limit cycle parametrized by μ to appear.

5.2.3 Numerical Simulation Results

In [259] further bifurcations of the periodic trajectories resulting from the Hopf bifurcation of the fixed points $\mathbf{x}_{\pm 1}^*$ in state space were studied numerically. Freire *et al.* reported to have observed period-doubling bifurcations and chaos. For a complete account of the observations (both numerically and experimentally) made by Freire and coworkers, the reader is referred to [259].

To demonstrate the behaviour of the system (5.4) to (5.6), we select the parameter values

$$\frac{a_1}{\omega C} = 0.1\,, \quad \frac{a_3}{\omega C} = 6 \times 10^{-4}\,, \quad \frac{b_1}{\omega C} = 0.0016\,, \quad \frac{a_1}{\omega C} = 0.05\,. \tag{5.21}$$

In addition we fix δ to the value $\delta_0 := 0.02$. For the parameter value $\mu = -0.051$ we observed a stable periodic solution with a period of $T \approx 6.65$ (refer to Figure 5.3(a)). This period-1 solution (with T as reference) is the result of a Hopf bifurcation. As μ is decreased steadily, period-doubling occurs and a stable period-2 solution appears. Figure 5.3(b) shows a projection of this period-2 solution for the parameter value $\mu = -0.053$. As μ was decreased further, we observed two consecutive period-doublings from period-2 to period-4 to period-8. Figure 5.3(c) and (d) shows these periodic attractors. For $\mu = -0.061$ a chaotic attractor (Figure 5.4) appears which disappears for further decrease in μ.

For $\mu = -0.075$ another chaotic attractor is found which is structurally completely different than the chaotic attractor observed earlier (compare Figures 5.4(a) and 5.5(a)). What happens here is that as μ is decreased, progressive interactions between the two attractors (one associated with each of the fixed points $\mathbf{x}_{\pm 1}^*$) are produced until finally one unique chaotic attractor appears. Interaction between the two attractors already starts to occur from about $\mu = -0.0642$.

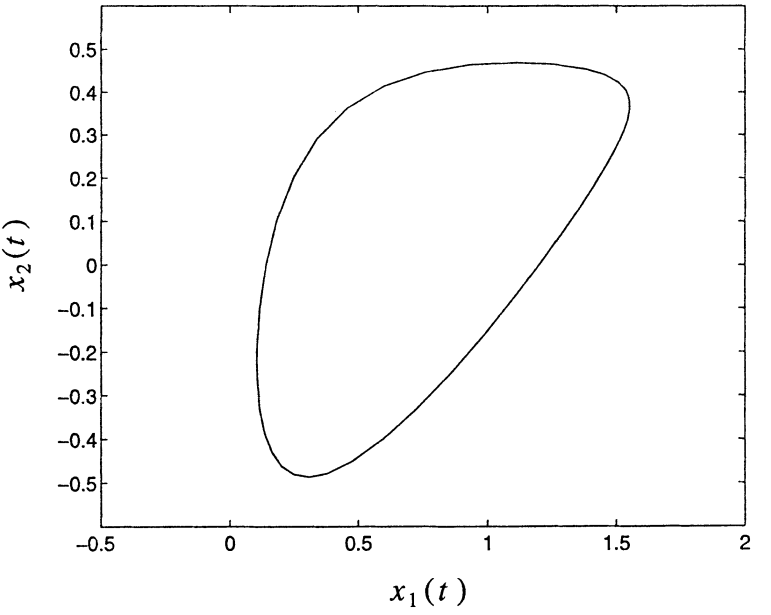

(a)

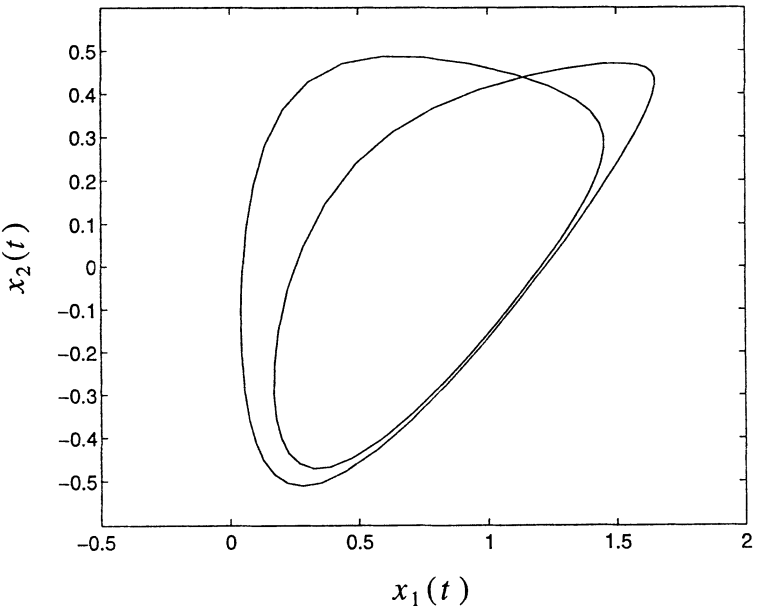

(b)

Figure 5.3: Phase portrait projections: (a) Period-1 limit cycle ($\mu = -0.051$); (b) Period-2 limit cycle ($\mu = -0.053$); (c) Period-4 limit cycle ($\mu = -0.055$); (d) Period-8 limit cycle ($\mu = -0.057$).

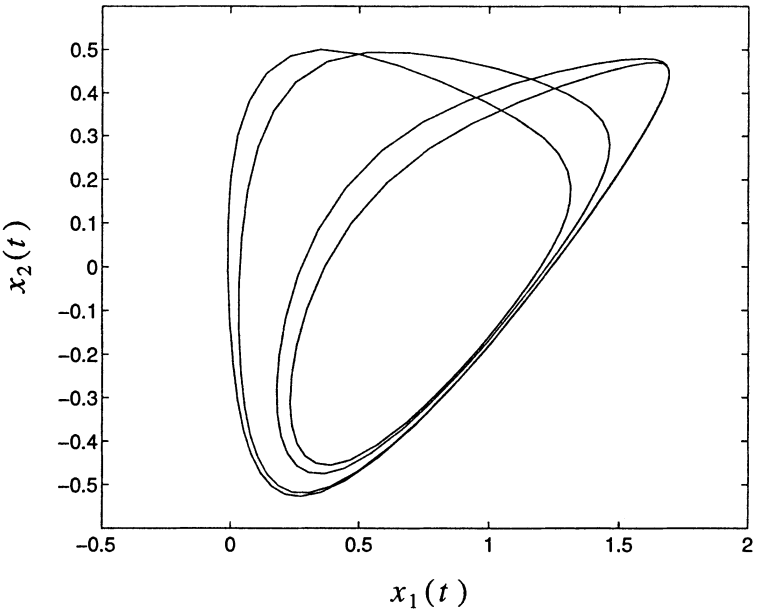

(c)

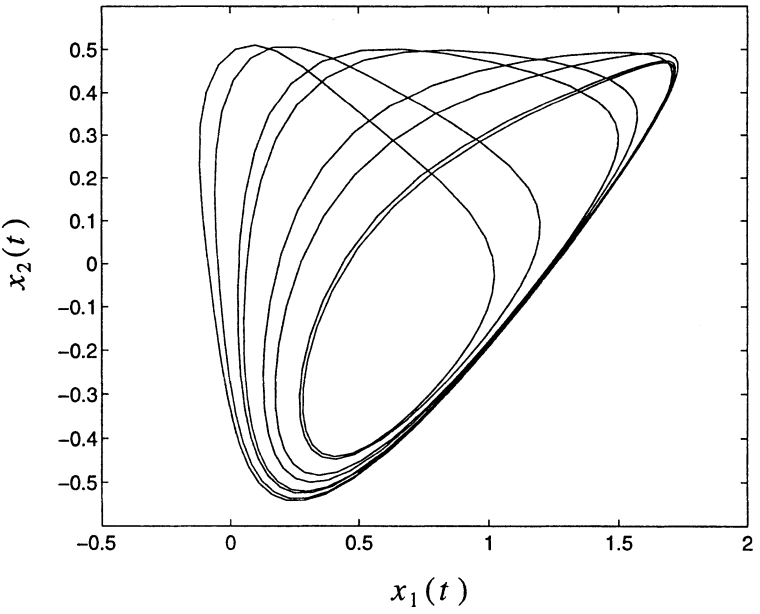

(d)

Figure 5.3: (Continued)

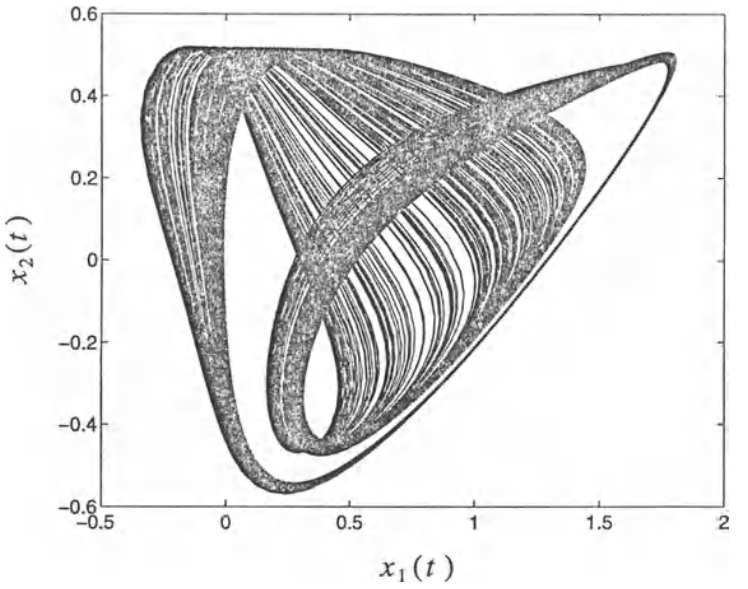

(a)

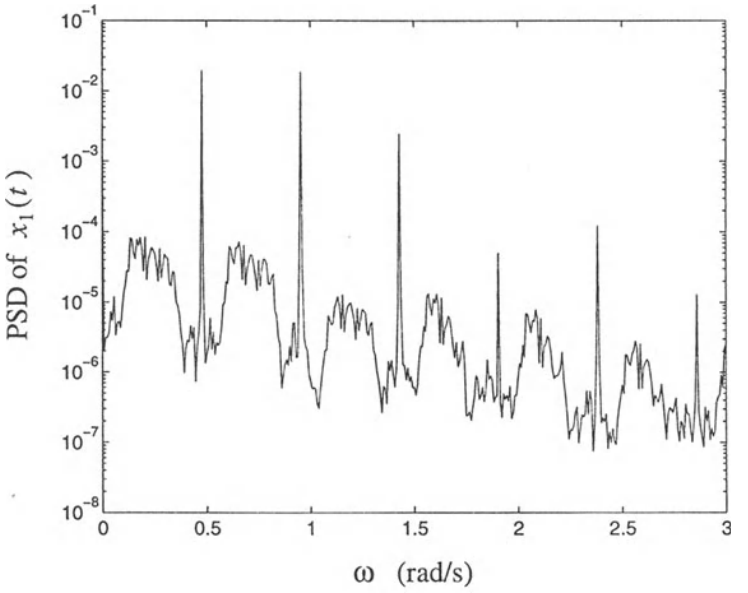

(b)

Figure 5.4: Chaotic attractor for $\mu = -0.061$: (a) Phase portrait; (b) Power spectral density of x_1.

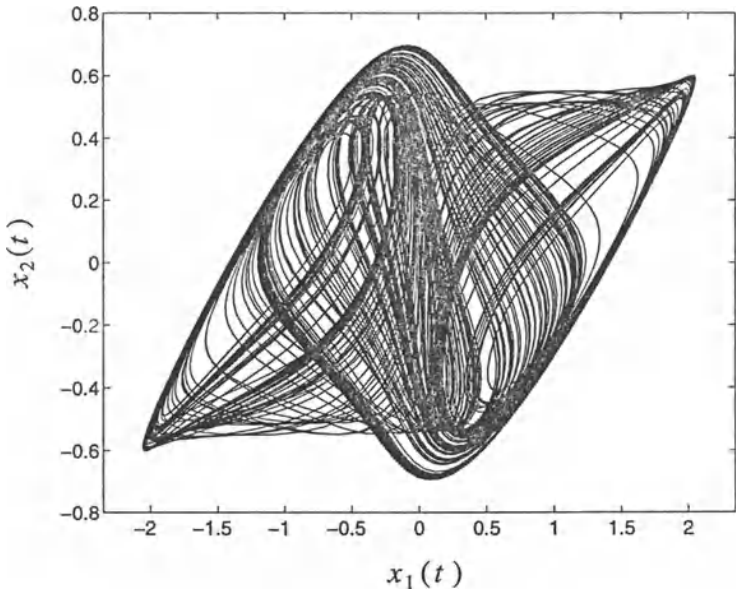

(a)

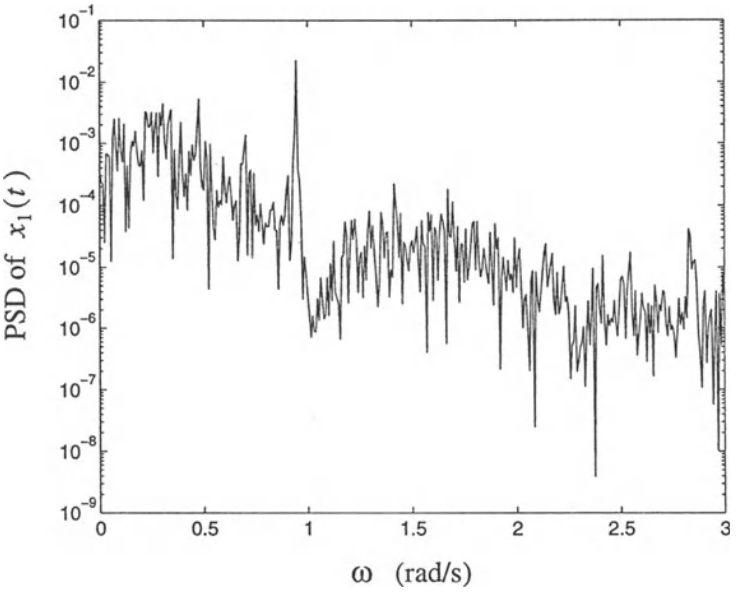

(b)

Figure 5.5: Chaotic attractor for $\mu = -0.075$: (a) Phase portrait; (b) Power spectral density of x_1.

5.3 Quasi-Harmonic Oscillator

5.3.1 The Continuous Chaos Generator

Figure 5.6 shows the circuit proposed and studied by Saito [677]. In this figure, N_1 is a linear, negative conductance with value $-G_1$, $G_1 > 0$. The circuit parameters are selected such that the voltage v oscillates whether the control switch S is opened or closed, that is,

$$0 < \sqrt{\frac{L}{C}} G_1 < 2, \quad \sqrt{\frac{L}{C}} (G_2 - G_1) < 2. \tag{5.22}$$

The voltage across the negative conductance N_1 is

$$v(t) = \frac{d\phi}{dt},$$

where $\phi(t)$ denotes the time-varying magnetic flux in the inductor. For convenience, the initial conditions of the circuit are assumed to satisfy

$$v(0) = 0, \quad \phi(0) > 0. \tag{5.23}$$

For $t \geq 0$, switch S is closed or opened when the trajectory of states intersects the ϕ-axis in the (ϕ, v)-plane as follows:

i) S is closed the moment when $\phi > \phi_t$ and $v = 0$, where ϕ_t is a threshold value for ϕ satisfying

$$\phi_t > 0, \qquad \phi_t > LG_2V_B, \tag{5.24}$$

ii) S is opened the moment when $\phi \leq \phi_t$ and $v = 0$.

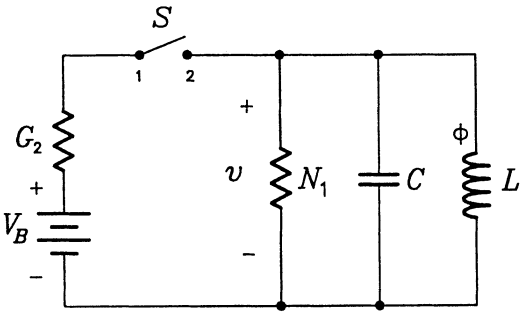

Figure 5.6: Quasi-harmonic oscillator circuit.

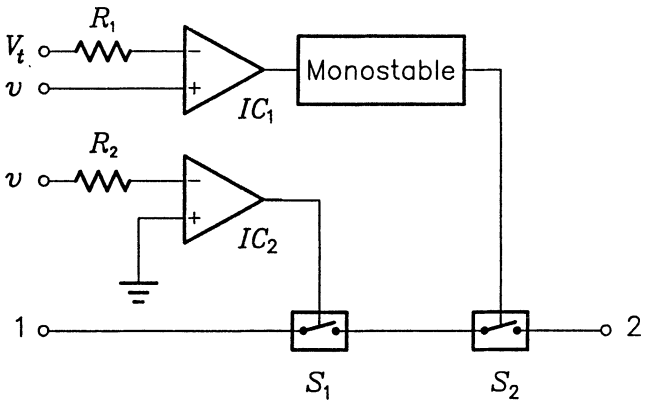

Figure 5.7: Realization of switch S.

The circuit realization of switch S is depicted by Figure 5.7. Here IC_1 is a comparator with threshold voltage V_t which is the maximum value of v along the trajectory passing through the point $(\phi_t, 0)$. The output of IC_1 supplies the input to the monostable multivibrator. The monostable is preset such that its pulsewidth T_p is approximately $(f_1 + f_2)/2$ where f_1 is the resonant frequency when S is open and f_2 is the resonant frequency when S is closed. When v exceeds V_t at some time instant t', the output of IC_1 goes high thereby causing the monostable to generate a pulse which in turn closes switch S_2 approximately from time t' to $t' + T_p$. Thereafter S_2 opens again. IC_2 which is also a comparator closes switch S_1 for the duration during which $v < 0$.

The dynamics of the circuit as a whole is governed by the differential equation

$$\frac{d^2x}{d\tau^2} + x = \begin{cases} 2\delta_1 \dfrac{dx}{d\tau}, & \text{if } S \text{ is open} \\ -2\delta_2 \dfrac{dx}{d\tau} + V_0, & \text{if } S \text{ is closed} \end{cases}, \tag{5.25}$$

where

$$x := \frac{\phi}{\phi_t}, \qquad \tau := \frac{t}{\sqrt{LC}}, \qquad V_0 := \frac{LG_2V_B}{\phi_t},$$

and

$$\delta_1 := \frac{1}{2}\sqrt{\frac{L}{C}}\,G_1, \qquad \delta_2 := \frac{1}{2}\sqrt{\frac{L}{C}}\,(G_2 - G_1).$$

The conditions (5.22) translate to

$$0 < \delta_1 < 1, \qquad -1 < \delta_2 < 1, \qquad V_0 < 1,$$

and the initial conditions (5.23) translate to

$$\frac{dx}{d\tau}(0) = 0, \qquad x(0) > 0. \tag{5.26}$$

From (5.25) and the definitions of δ_1 and δ_2 we see that the system is linear with negative damping when S is open but linear with positive damping (respectively negative damping) for $G_1 < G_2$ (respectively $G_1 > G_2$) when S is closed. Since the differential equation (5.25) is piecewise-linear its general solution is of the form

$$x(\tau) = A_1 e^{\delta_1 \tau} \cos(\omega_1 \tau + \theta_1), \qquad \text{if } S \text{ is open,} \tag{5.27}$$

$$x(\tau) = A_2 e^{-\delta_2 \tau} \cos(\omega_2 \tau + \theta_2) + V_0, \qquad \text{if } S \text{ is closed,} \tag{5.28}$$

where

$$\omega_1 := \sqrt{1 - \delta_1^2}, \qquad \omega_2 := \sqrt{1 - \delta_2^2},$$

with A_1, A_2, θ_1, and θ_2 arbitrary constants. For an initial state which satisfy (5.26), a particular solution is obtained by joining the solutions for the different regions by the continuity of x and $dx/d\tau$. Thus, as the trajectory crosses the boundary from one region to the next, the final state of the current region is taken as the initial state in the next region. For convenience we set

$$L_+ := \left\{ \left(x, \frac{dx}{d\tau} \right) \middle| \frac{dx}{d\tau} = 0, x > 0 \right\}.$$

The assumption that the parameters of the above general solutions satisfy

$$(1 + e^{-\pi\delta_2/\omega_2}) V_0 < e^{-\pi\delta_2/\omega_2},$$

implies that all trajectories starting from L_+ must intersect L_+, and therefore, a Poincaré map $F : L_+ \to L_+$ can be constructed. The Poincaré map is piecewise-linear and given by (see [677])

$$F(x) = \begin{cases} ax, & \text{if } 0 < x \leq 1 \\ bx - c, & \text{if } 1 < x \end{cases}, \tag{5.29}$$

where

$$a := e^{2\pi\delta_1/\omega_1}, \quad b := e^{\pi(\delta_1/\omega_1 - \delta_2/\omega_2)}, \quad c := (\sqrt{a} + b) V_0.$$

Using the conditions on δ_1, δ_2, and V_0 given above and assuming $F(1^+) > 0$, the parameters a, b, and c satisfy

$$a > 1, \quad a > b, \quad b > c.$$

We now restrict our attention to the case [677]

$$1 < b < 2, \qquad b < a < \frac{b}{b-1}, \qquad a(b-1) < c < b,$$

or

$$b < 1, \qquad 1 < a, \qquad b - 1 < c < b.$$

When these conditions are satisfied then $F(a) < a$ and $F(1^+) < 1$ so that the interval $J' := (b-c, a]$ is invariant, i.e. $F(J') \subset J'$ and there is some positive integer n such that $F^{(n)}(x) \in J'$ for all $x \in L_+$, for the case $b < 1$ in the above conditions. For the case $1 < b < 2$, in the above conditions $F(J') \subset J'$ and $F^{(n)}(x) \in J'$ for all $x \in (0, c/(b-1))$. On the other hand, if $F(1^+) > 1$ and $b > 1$, then all orbits diverge; if $F(1^+) > 1$ but $b < 1$, then all orbits converge to the fixed point. If $F(1^+) > 1$ and $F(a) > a$ then no invariant interval exists.

5.3.2 Analysis of the Poincaré Map

As the object of the analysis of this section, consider the transformation $T : I \to I$ given by

$$T(x) := \begin{cases} a(x-D)+1, & \text{if } 0 \le x \le D \\ b(x-D), & \text{if } D < x \le 1 \end{cases}, \tag{5.30}$$

where $(a, b, D) \in U$, with the set U defined as

$$U := \left\{ (a,b,D) \,\middle|\, 0 < D < 1, \quad 0 < a < \frac{1}{D}, \quad 0 < b < \frac{1}{1-D} \right\}.$$

Based on the conditions on the parameters a, b and c, T is topologically conjugate to F, that is, $T = h \circ F \circ h^{-1}$ for

$$h(x) = \frac{x-(b-c)}{a-(b-c))}, \quad \text{and} \quad D = \frac{1-(b-c)}{a-(b-c)}.$$

Concerning the stability properties of the periodic points of T, we have the the following theorem.

Theorem 5.1 If $T(0) < T(1)$ (i.e. T is surjective but not injective and $V_B > 0$ in Figure 5.6), then T has no stable periodic point. If $T(0) > T(1)$ (i.e. T is injective but not surjective and $V_B < 0$), then there exists no unstable periodic point.

Proof: See [677]. ■

Remark If $T(0) = T(1)$, that is, T is into and $V_B = 0$, then T is isomorphic to the rotation of the unit circle.

The (a, b, D)-parameter space may be partitioned into regions as follows:

R_u the parameter region in which $T(0) < T(1)$ is satisfied,

Σ the parameter region in which $T(0) = T(1)$ is satisfied,

R_s the parameter region in which $T(0) > T(1)$ is satisfied.

Roughly speaking, R_u is the chaotic region, R_s is the stable region and Σ is the boundary separating R_u and R_s. Conditions under which the map T is ergodic may be given, using symbolic dynamics. We therefore introduce the following definitions.

Definition 5.2 Define the mapping $\omega : I \to S$ where S is the set of symbols $\{0,1\}$, as

$$\omega(x) := \begin{cases} 0, & \text{if } 0 < T^{(n)}(x) \leq D \\ 1, & \text{if } D < T^{(n)}(x) \leq 1 \end{cases},$$

and

$$\Sigma^2 := S \times S \times \cdots = \prod_{i=0}^{\infty} S.$$

■

Definition 5.3 [569] Define the set $S_1 \subset \Sigma^2$ as the set of all periodic sequences of the form $(0^m 1)^\infty$ and $(01^m)^\infty$, for m any positive integer. ■

Definition 5.4 [677] A period-$(m+1)$ point x^* of T is said to be a $0^m 1$ *periodic point* (respectively a 01^m periodic point) if the sequence

$$\left\{\omega(T^{(0)}(x^*)), \omega(T^{(1)}(x^*)), \omega(T^{(2)}(x^*)), \ldots\right\}, \tag{5.31}$$

is equal to $(0^m 1)^\infty$ (respectively $(01^m)^\infty$). Moreover, x^* is called an S_1 *periodic point* if the sequence in (5.31) is contained in S_1. ■

Theorem 5.5 The region in the (a,b,D)-parameter space for which S_1 periodic points exist is given by

$$(P_1 \cup P_2) \cap U,$$

where

$$P_1 := \left\{(a,b,D) \,\middle|\, \frac{a^{m-1}}{a^{m-1}b + \sum_{i=0}^{m-1} a^i} \leq 1 - D < \frac{a^m}{\sum_{i=0}^{m} a^i}, \; a^m b > 1\right\},$$

$$P_2 := \left\{(a,b,D) \,\middle|\, \frac{b^{m-1}}{ab^{m-1} + \sum_{i=0}^{m-1} b^i} \leq D < \frac{b^m}{\sum_{i=0}^{m} b^i}, \; ab^m > 1\right\}.$$

Proof: See [677]. ■

Theorem 5.6 If there exist unstable S_1 periodic points, then there exists the unique absolutely continuous invariant measure [179], say μ, with respect to T and hence T is ergodic [467].

Proof: See [677]. ■

Theorem 5.7 The density ρ of the measure μ is given by

$$\rho(x) = K \sum_{n=0}^{\infty} \left\{ \frac{W_1}{a^{N_0(1,n)} b^{N_1(1,n)}} I_{(0,T^n(1))}(x) - \frac{W_2}{a^{N_0(0,n)} b^{N_1(0,n)}} I_{(0,T^n(0))}(x) \right\},$$

where K is the normalizing factor and I_A is the characteristic function for μ, with

$$N_j(x,n) = \begin{cases} 0, & \text{if} \quad n = 0 \\ \text{card}\left\{ i \,\middle|\, 0 < i \leq n-1, \omega\left(F^{(i)}(x)\right) = j \right\}, & \text{if} \quad n \geq 1 \end{cases},$$

and

$$W_1 := \sum_{n=0}^{\infty} \frac{1}{a^{N_0(0,n)} b^{N_1(0,n)}}, \quad W_2 := \sum_{n=0}^{\infty} \frac{1}{a^{N_0(1,n)} b^{N_1(1,n)}}.$$

Proof: Refer to [677]. ■

Remark It is important to note that ρ is the Radon-Nikodym derivative [179] of μ with respect to Lebesgue measure. For the special case when μ is differentiable, this coincides with the usual derivative of μ.

For further analytical results and experimental results on the quasi-harmonic oscillator refer to [677].

5.3.3 Numerical Results

We now wish to study numerically the dimensionless differential equation (5.25) and the related Poincaré map T given by (5.30). First, consider the parameter values [677]

$$a = 1.3, \qquad b = 0.226, \qquad D = 0.591.$$

For this selection of parameter values, there exist stable 0^31 periodic points. The corresponding parameters of the dimensionless dynamical equations of the quasi-harmonic oscillator circuit are

$$\delta_1 \approx 0.05119, \qquad \delta_2 \approx 0.4646, \qquad V_0 \approx -0.16056.$$

A typical trajectory for these parameter values, obtained from simulation is shown in Figure 5.8. The period of this periodic trajectory in state space is $T \approx 25.57061$.

Now, for the Poincaré map we select the parameter values [677]

$$a = 1.38, \qquad b = 0.809, \qquad D = 0.653.$$

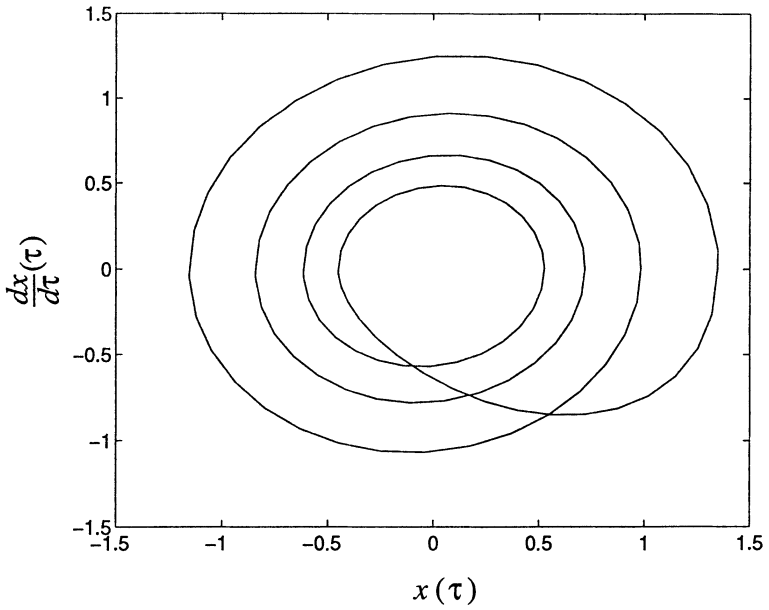

Figure 5.8: 0^31 periodic attractor for $a = 1.38$, $b = 0.8$, $D = 0.591$.

The corresponding parameters for the differential equation in dimensionless form are

$$\delta_1 \approx 0.05119, \qquad \delta_2 \approx 0.11790, \qquad V_0 \approx 0.2642.$$

From the phase portrait shown Figure 5.9(a) it seems that the circuit is chaotic for this choice of parameters. Figure 5.8(b) shows the invariant density for the map T obtained by numerical iteration of the Frobenius-Perron operator, which gives numerical evidence that the Poincaré map is ergodic. Using the Birkhoff ergodic theorem to calculate the Lyapunov exponent numerically, we obtained $\lambda \approx 0.2834$. We therefore conclude that the Poincaré map (and hence the differential equation) shows numerical evidence of chaos for this choice of parameters.

Finally, consider the parameter selection [677],

$$a = 2, \qquad b = 0.8, \qquad D = 0.4.$$

For the equivalent dimensionless continuous-time system the parameters are

$$\delta_1 \approx 0.10965, \qquad \delta_2 \approx 0.17844, \qquad V_0 \approx 0.21076.$$

From the phase portrait shown in Figure 5.10(a) it seems that the circuit is chaotic. Figure 5.10(b) shows the invariant density obtained by the same procedure as for the previous case. From Figure 5.10 we conclude that the Poincaré map is ergodic. Numerical application of the Birkhoff ergodic theorem produces the Lyapunov exponent $\lambda \approx 0.3736$, which is positive and hence the Poincaré map and by implication

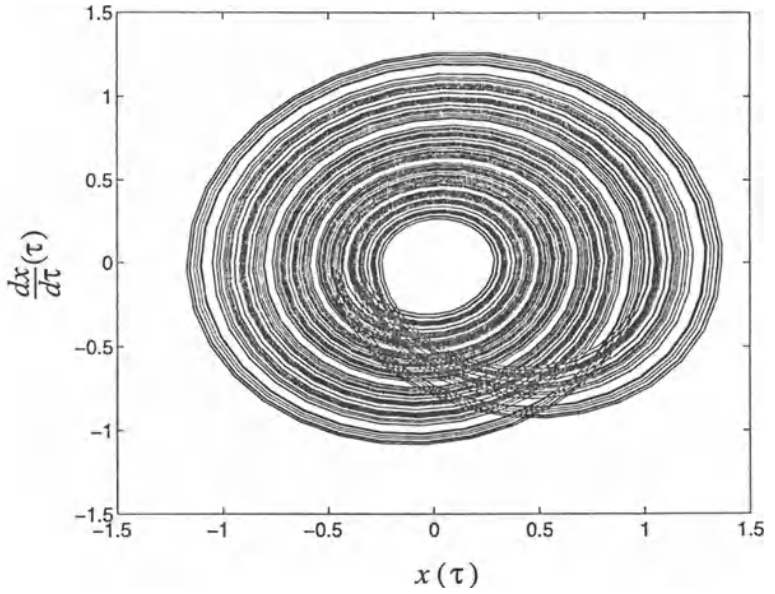

(a)

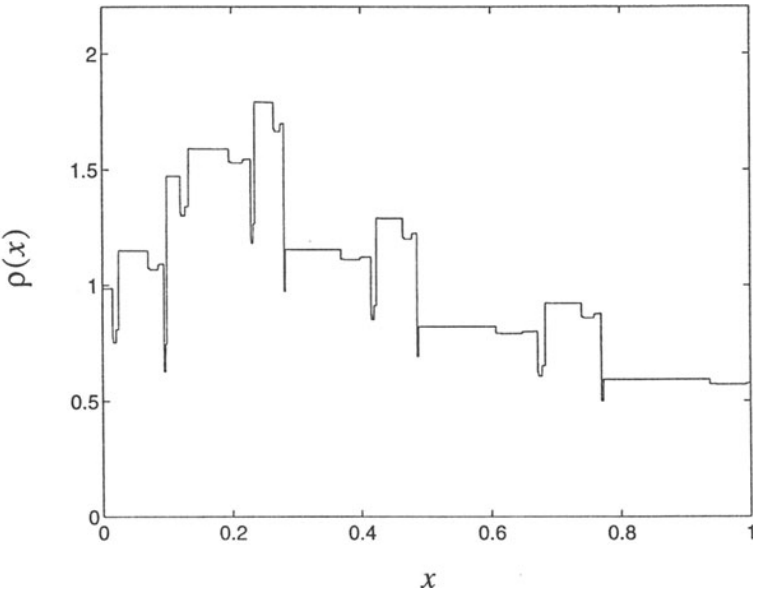

(b)

Figure 5.9: Dynamical response for $a = 1.38$, $b = 0.809$, $D = 0.653$: (a) Phase portrait of the attractor; (b) Invariant density of T.

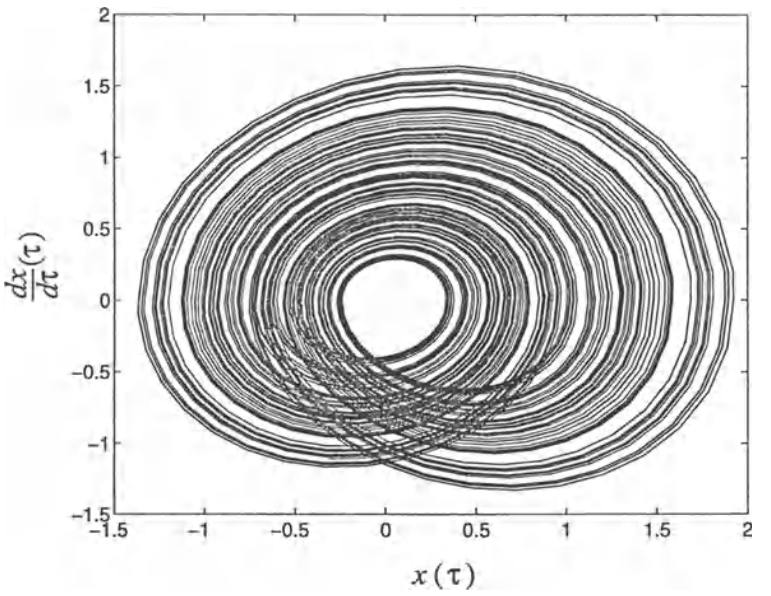

(a)

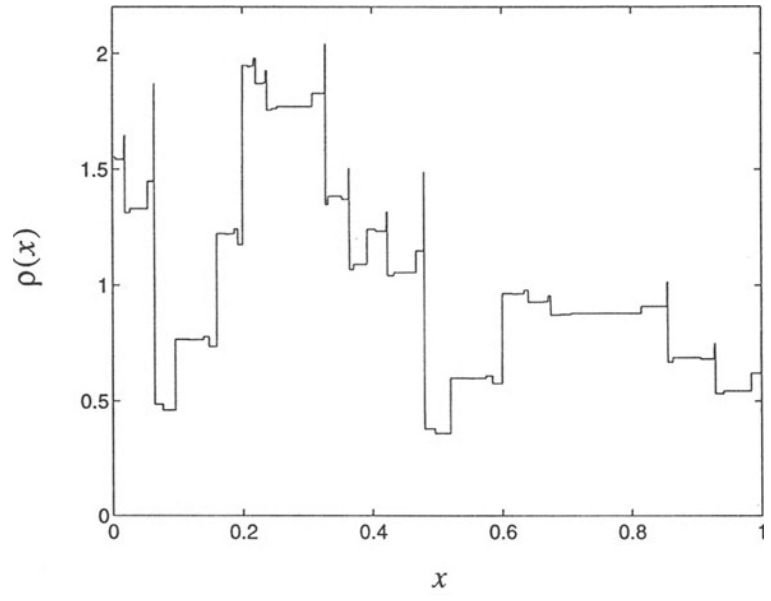

(b)

Figure 5.10: Dynamical response for $a = 2$, $b = 0.8$, $D = 0.4$: (a) Phase portrait of the attractor; (b) Invariant density of T.

the circuit equations show numerical evidence of chaos. Although the state space attractors in Figures 5.9(a) and 5.10(a) look very similar up to a scaling factor, the corresponding invariant densities show that they are in fact very different with regard to the distribution of their trajectories. Another indication of their dissimilarity concerning averaged local expansion between trajectories are the Lyapunov exponents. More numerical results and also experimental results obtained for the quasi-harmonic oscillator may be found in [677].

5.4 Chaotic Ring Self-Excited Oscillatory Systems

5.4.1 Model of a Ring Self-Excited Oscillatory System

Radio-physical models of *ring self-excited oscillatory* systems have been investigated by Aref'yev *et al.* [29] and Dmitriyev *et al.* [222]. The generalized form of this model consists of a first-order lowpass filter, k second-order filters, m bandpass filters, n band rejection filters and a nonlinear amplifier, all cascaded in a closed loop. This is depicted in Figure 5.11.

The equations describing a (k, m, n)-self-excited oscillatory system are given by [62]

$$\tau \frac{dw}{dt} + w = f(z_n), \tag{5.32}$$

$$\frac{d^2x_i}{dt^2} + \alpha_{i,1}\frac{dx_i}{dt} + \omega_{i,1}^2 x_i = \omega_{i,1}^2 x_{i-1}, \qquad i = 1, \ldots, k, \tag{5.33}$$

$$\frac{d^2y_i}{dt^2} + \alpha_{i,2}\frac{dy_i}{dt} + \omega_{i,2}^2 y_i = \omega_{i,2}^2 \frac{dy_{i-1}}{dt}, \qquad i = 1, \ldots, m, \tag{5.34}$$

$$\frac{d^2z_i}{dt^2} + \alpha_{i,3}\frac{dz_i}{dt} + \omega_{i,3}^2 z_i = \frac{d^2z_{i-1}}{dt^2} + \omega_{i,3}^2 z_{i-1}, \qquad i = 1, \ldots, n, \tag{5.35}$$

where

$$x_0(t) := w(t), \quad y_0(t) := x_k(t), \quad z_0(t) := y_m(t),$$

Equation (5.32) describes the first-order lowpass filter, (5.33) describes the k second-order lowpass filters, (5.34) represents the m bandpass filter and (5.35) describes the n band rejection filters. The coefficients $\alpha_{i,j}$ and $\omega_{i,j}$ are the dissipative (i.e. damping) coefficients and resonance frequencies of the second-order filters, while τ is the time constant of the first-order lowpass filter. The nonlinear amplifier is characterized by the nonlinear function $f : \mathbf{R} \to \mathbf{R}$. Here f is chosen to be close in form to the characteristic of a symmetrical *lambda-diode* [29] [62], namely

$$f(z) = Kze^{-z^2},$$

where $K \in [0, \infty)$ is a gain parameter of the nonlinear amplifier. The gain parameter will serve as the bifurcation parameter in the analysis of such systems. The purpose

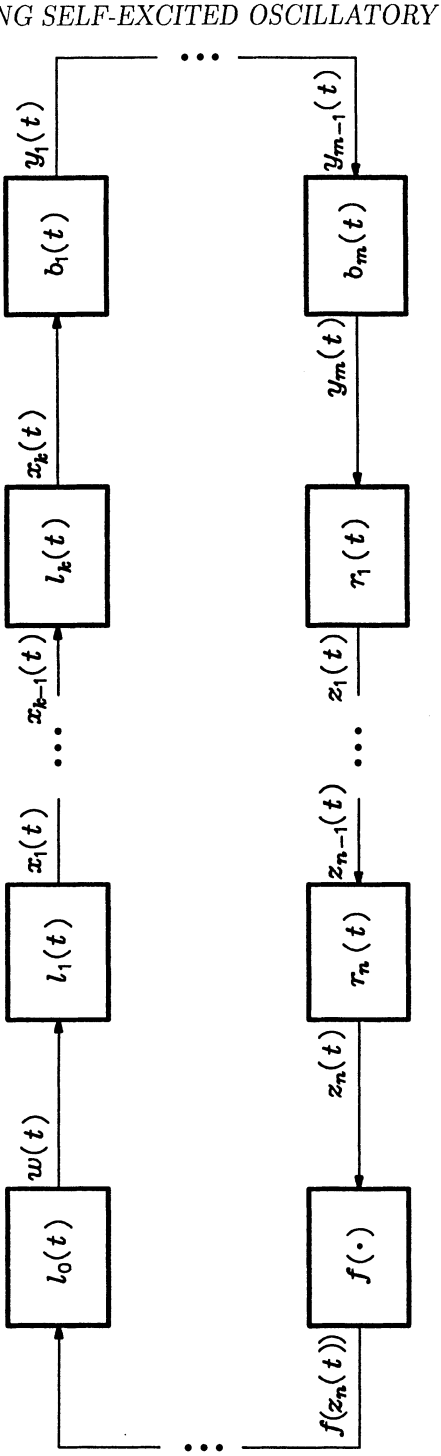

Figure 5.11: Block diagram of the ring self-excited oscillatory system.

of the set of filters in a ring self-oscillatory system is to shape the power spectral density to satisfy specified requirements. The location of passbands and stopbands as well as roll-off rates can be set to meet design specifications.

Example 5.8 The equations for a $(1,1,0)$-self-excited oscillatory system take the form

$$\begin{aligned} \tau\frac{dw}{dt} + w &= Ky_1 e^{-y_1^2}, \\ \frac{d^2x_1}{dt^2} + \alpha_{1,1}\frac{dx_1}{dt} + \omega_{1,1}^2 x_1 &= \omega_{1,1}^2 w, \\ \frac{d^2y_1}{dt^2} + \alpha_{1,2}\frac{dy_1}{dt} + \omega_{1,2}^2 y_1 &= \omega_{1,2}^2 \frac{dx_1}{dt}. \end{aligned}$$

This system can be rewritten as the system of first-order ordinary differential equations,

$$\frac{d\mathbf{u}}{dt}(t) = \mathbf{A}\mathbf{u}(t) + \frac{K}{\tau}\mathbf{e}_1 u_4 e^{-u_4^2}, \tag{5.36}$$

with $\mathbf{e}_1$ the first basis vector of the standard basis for $\mathbf{R}^5$, and

$$\mathbf{u} := (u_1, u_2, u_3, u_4, u_5)^T,$$

$$\mathbf{A} := \begin{pmatrix} -1/\tau & 0 & 0 & 0 & 0 \\ 0 & 0 & 1 & 0 & 0 \\ \omega_{1,1}^2 & -\omega_{1,1}^2 & -\alpha_{1,1} & 0 & 0 \\ 0 & 0 & 0 & 0 & 1 \\ 0 & 0 & \omega_{1,2}^2 & -\omega_{1,2}^2 & -\alpha_{1,2} \end{pmatrix}.$$

Here we have set

$$u_1 := w, \quad u_2 := x_1, \quad u_3 := \frac{dx_1}{dt}, \quad u_4 := y_1, \quad u_5 := \frac{dy_1}{dt}.$$

The system (5.36) has a single unique fixed point given by

$$\mathbf{u}^* := (0,0,0,0,0)^T.$$

For the analysis of the fixed point a more useful form of the above system is

$$\frac{d\mathbf{u}}{dt}(t) = \mathbf{B}\mathbf{u}(t) + \frac{K}{\tau}\mathbf{e}_1 \mathbf{h}(\mathbf{u}(t)), \tag{5.37}$$

where

$$\mathbf{B} := \begin{pmatrix} -1/\tau & 0 & 0 & K/\tau & 0 \\ 0 & 0 & 1 & 0 & 0 \\ \omega_{1,1}^2 & -\omega_{1,1}^2 & -\alpha_{1,1} & 0 & 0 \\ 0 & 0 & 0 & 0 & 1 \\ 0 & 0 & \omega_{1,2}^2 & -\omega_{1,2}^2 & -\alpha_{1,2} \end{pmatrix},$$

$$\mathbf{h}(\mathbf{u}) := (e^{-u_4^2} - 1)u_4 .$$

Notice that $\mathbf{h}$ satisfies $\mathbf{h}(\mathbf{0}) = \mathbf{0}$ and that

$$\lim_{\|\mathbf{u}\|_1 \to 0} \frac{\|\mathbf{h}(\mathbf{u})\|_1}{\|\mathbf{u}\|_1} = 0, \qquad \|\mathbf{u}\|_1 := \sum_{i=1}^{5} |u_i| .$$

The stability of the system (5.37) (and hence of (5.36)) is therefore governed by the sign of the dominant eigenvalue of $\mathbf{B}$ (see [410]).

Since the eigenvalues of $\mathbf{B}$ are functions of K we now choose K as the bifurcation parameter of the ring self-oscillatory system. Using the Routh-Hurwitz test, the critical value K_{cr} of the gain K with regard to stability of $\mathbf{u}^*$ is obtained. When the parameter $K < K_{cr}$ the fixed point $\mathbf{u}^*$ is stable. For the case $K = K_{cr}$ there is a loss of stability and a limit cycle is formed in the phase space of the system. The frequency of the limit cycle is given by one of the two natural frequencies of the self-excited oscillatory system. When $K > K_{cr}$ excitation also occurs at the second natural frequency. A further increase in K causes a restructuring of the modes on the basis of two-frequency oscillations and a change in the structure of the corresponding two-dimensional invariant tori in the phase space.

An increase in K after the excitation of two-frequency oscillations leads to the formation of a strange attractor in the phase space. The specific scenario of the transition to chaotic behaviour depends on the rotation number $\rho := \omega_{1,2}/\omega_{1,1}$. In particular the closeness of strong resonances (i.e. $\rho = 1/1\,,\ 2/1\,,\ 3/1$, etc.) plays an important role. The structure of the strange attractor formed depends very much on the least stable mode which exists for the transition to chaos (see [222]) as dictated by the form of the power spectral density. For the case when the system is chaotic, its spectral response is strongly influenced by the combined frequency response of the cascaded linear filters in the system.

For example, for the system defined by the parameters values

$$\tau = 0.2\,, \quad \omega_{1,1} = 1\,, \quad \omega_{1,2} = 2.5\,, \quad \alpha_{1,1} = 0.5\,, \quad \alpha_{1,2} = 0.2\,, \quad K = 32\,,$$

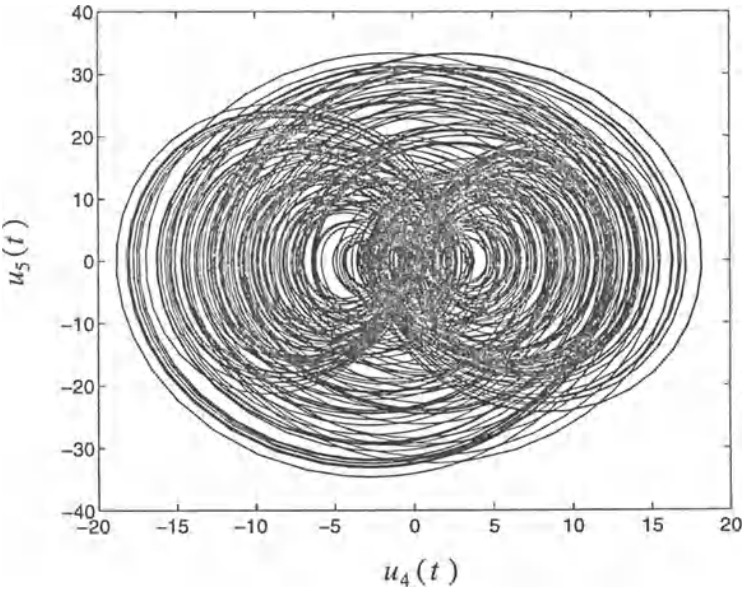

(a)

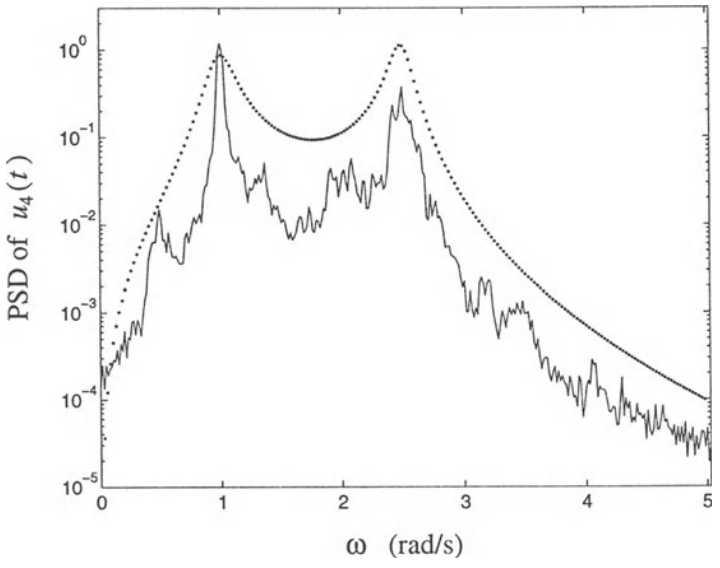

(b)

Figure 5.12: (a) Chaotic attractor; (b) Power spectral density of $u_4(t)$ (solid line) as compared to the squared magnitude of its linear part's frequency response (dotted line).

chaotic behaviour is observed. This is evident from the phase portrait, Figure 5.12(a). Figure 5.12(b) displays the power spectral density (solid line) and the squared magnitude of the spectral response of the system's linear part (i.e. the cascaded filters), depicted by the dotted line. For our choice of parameters the correspondence is remarkable. However the degree of similarity depends also on the rotation number (refer to [62]). ■

In [62], Bel'skii and coworkers present a detailed discussion of (1,1,0)-self-excited oscillatory systems. For various parameter values of these systems, they have calculated Lyapunov and correlation dimensions as well as two-dimensional probability distributions of instantaneous signal values.

5.5 Chua's Circuit Family

5.5.1 Introduction

Chua's circuit and its variations (collectively called Chua's circuit family) in their physical nature constitute a rather simple class of electronic circuits which generates chaos, and consists of four linear elements and one nonlinear circuit element. (However, the *canonical* realization of Chua's circuit family [156] requires an additional linear resistor, and the component configuration is different.) Some members of this circuit family are Chua's circuit itself, the torus circuit and the double hook circuit [157]. This family of circuits is an ideal paradigm for research on chaos by means of both laboratory experiments and computer simulations because it admits an adequate modeling via the language of differential equations. In the simplest case, these equations are written in dimensionless form as we see later. The main reasons why Chua's circuit is a subject of interest not only in engineering, but in other disciplines as well, are the following [718]:

i) Chua's circuit exhibits a number of distinct routes to chaos, e.g. through a period-doubling cascade, the breakdown of an invariant torus, etc. In itself, this makes the study of Chua's circuit a rather universal problem.

ii) Chua's circuit exhibits a chaotic attractor called the *double-scroll attractor*. Three equilibrium states of a saddle-focus type exist in this attractor, which indicates that the double-scroll attractor is multistructural. This is in sharp distinction with other known attractors of three-dimensional systems.

iii) The governing equations are close (in the sense that the bifurcation portraits are close) to the equations defining a three-dimensional normal form for bifurcations of a fixed point with three zero characteristic exponents (for the case with

additional symmetry) and that of a periodic orbit with all three multipliers equal to -1.

iv) In their mathematical nature, the attractors that occur in Chua's circuit family are new and essentially more complicated objects than it seemed before. This conclusion is based on new subtle results on systems with homoclinic tangencies and homoclinic loops of a saddle focus [608], [291].

5.5.2 Brief Historical Review

The first article on Chua's circuit that appeared was written by Matsumoto (see [518]). In this paper Matsumoto reported on numerical evidence of chaos in Chua's circuit. He also reported on a saddle-type hyperbolic periodic orbit which was discovered to be present outside the chaotic attractor. Moreover, for the case when the nonlinear resistor is eventually dissipative (as for example in Figure 5.13(b)), a large stable limit cycle was found to exist outside the chaotic attractor. Following this, Zhong and Ayrom published three articles [875], [874] and [44] in which they reported on the first experimental results confirming chaos in Chua's circuit. Their realization of the two terminal piecewise-linear resistor (also known as *Chua's diode*) in Chua's circuit is depicted in Figure 5.14.

In [874], Zhong and Ayrom studied Chua's circuit for the different circuit parameter values of the piecewise-linear resistor:

Case 1:

$$V_{cc} = 18\text{V}, \quad R_1 = 376\Omega, \quad R_2 = 78\Omega, \quad R_3 = 5.98\text{k}\Omega,$$

$$R_4 = 312\Omega, \quad R_5 = 1.91\text{k}\Omega, \quad R_6 = 52\Omega.$$

Case 2:

$$V_{cc} = 15\text{V}, \quad R_1 = 3.67\text{k}\Omega, \quad R_2 = 1.09\text{k}\Omega, \quad R_3 = 5.43\text{k}\Omega,$$

$$R_4 = 104\Omega, \quad R_5 = 5.36\text{k}\Omega, \quad R_6 = 128\Omega.$$

The operational amplifiers used were both type National/8035 741LN. For component values

$$R = 1.03\text{k}\Omega, \quad C_1 = 0.005\mu\text{F}, \quad C_2 = 0.1\mu\text{F} \quad L = 7.6\text{mH},$$

of Chua's circuit and case 1 of the nonlinear resistor Zhong and Ayrom observed a chaotic attractor in Chua's circuit. In a second experiment (see [874]), this time with

$$C_1 = 0.005\mu\text{F}, \quad C_2 = 0.05\mu\text{F}, \quad L = 7.2\text{mH},$$

and with case 2 of the nonlinear resistor, they observed period-doubling bifurcations (initiated by a Hopf bifurcation) as R was decreased, which eventually led to chaos.

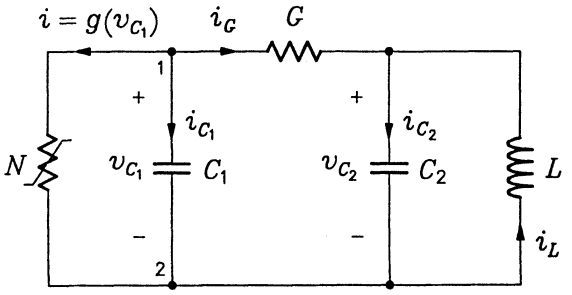

(a)

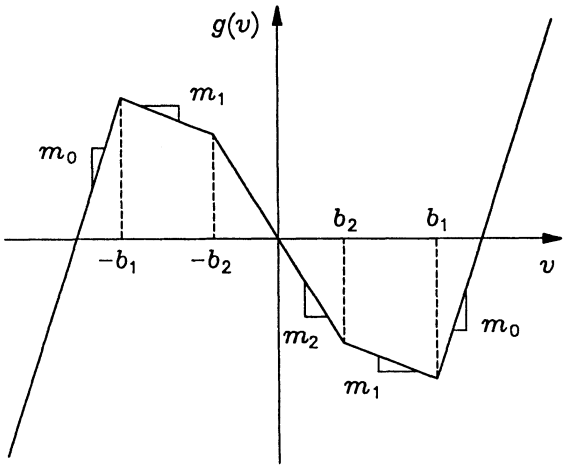

(b)

Figure 5.13: Chua's circuit: (a) Circuit configuration; (b) Constitutive voltage-current relation of the nonlinear resistor.

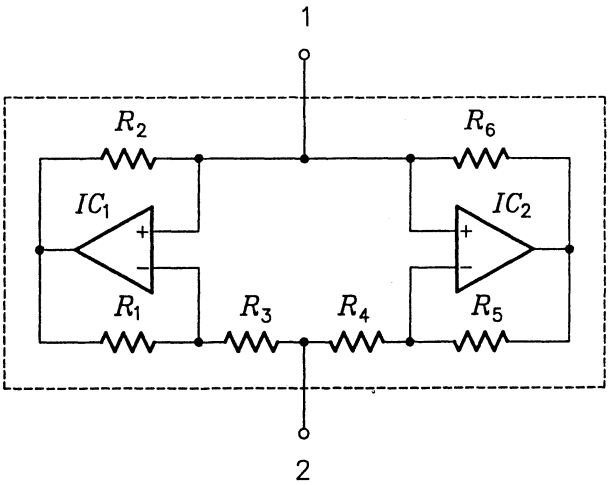

Figure 5.14: The Zhong-Ayrom realization of the piecewise-linear resistor in Chua's circuit.

Later, in [44] the authors also studied Chua's circuit for bifurcations with C_1, L and R as bifurcation parameters. The stable limit cycle associated with the eventual dissipativity of the nonlinear resistor reported by Matsumoto was also observed in their experimental measurements.

Matsumoto, Chua and Komuro studied Chua's circuit in great detail in [522]. Reports of numerical and experimental results were presented by them. They also studied the geometric structure of the double scroll attractor in great detail. This was made possible by the piecewise-linear nature of the dynamical equations. In addition the chaos exhibited by these equations was further studied by the calculation of Lyapunov exponents and the Lyapunov dimension. The spectrum of one-dimensional Lyapunov exponents was found to be of the form $(+, 0, -)$, thereby confirming numerically this circuit's ability to generate chaos. The Lyapunov dimension was found to be between 2 and 3. Calculation and measurement of power spectra were found to be continuous and broad-band, which is reminiscent of chaos. Concerning their experimental circuit, Matsumoto *et al.* proposed an alternative realization of the piecewise-linear resistor in Chua's circuit. As shown in Figure 5.15, it utilizes a single op amp, two diodes and a few resistors. For component values

$$G = 0.0055\mu\text{F}\,, \quad C_2 = 0.0495\mu\text{F}\,, \quad L = 7.07\text{mH}\,, \quad R = 1.428\text{k}\Omega\,, \quad V_{cc} = 15\text{V}\,,$$

the authors observed the double scroll attractor. The bifurcation phenomena of this circuit was reported on in [523].

Yet another realization of the piecewise-linear resistor, using only two transistors, two diodes and a few resistors, was proposed by Matsumoto *et al.* in [525]. This

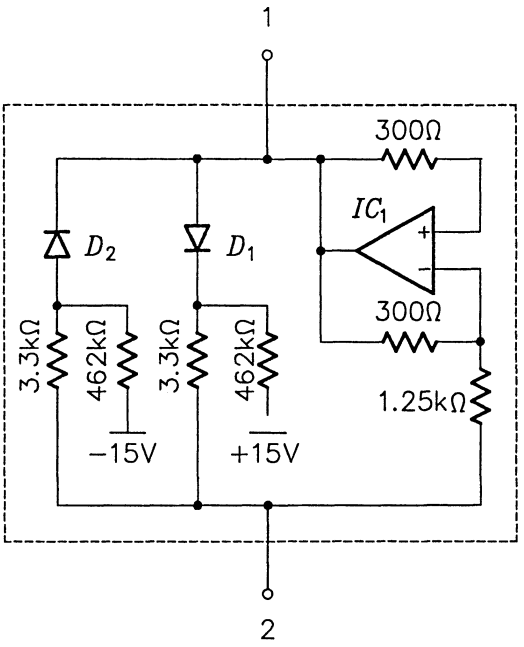

Figure 5.15: The Matsumoto-Chua-Komuro realization of the piecewise-linear resistor in Chua's circuit.

realization of the piecewise-linear resistor is shown in Figure 5.16. As in the case of the Zhong-Ayrom realization, its voltage-current characteristic consists of 5 linear segments (see Figure 5.13(b)). Typical component values used for this realization are

$$R_B = 56\text{k}\Omega\,,\quad R_1 = 1\text{k}\Omega\,,\quad R_2 = 3.3\text{k}\Omega\,,\quad R_3 = 88\text{k}\Omega\,,\quad R_4 = 39\text{k}\Omega\,,\quad V_{cc} = 29\text{V}\,.$$

The authors observed the double scroll attractor in their realization of Chua's circuit for

$$C_1 = 0.0053\mu\text{F}\,,\quad C_2 = 0.047\mu\text{F}\,,\quad L = 6.8\text{mH}\,,\quad R = 1.21\text{k}\Omega\,.$$

They also used SPICE2 electronic circuit simulation package to study their circuit numerically. A good agreement was found to exist between the experimental and numerical results obtained.

About the same time, Chua and coworkers developed a rigorous mathematical proof of chaos generated by the *double scroll equations* (including the equations of Chua's circuit as a special case) which was published in [154]. Their approach was to derive a linearly equivalent class of piecewise-linear differential equations which includes the double scroll equations as a special case. A necessary and sufficient condition for two such piecewise-linear vector fields to be linearly equivalent is that their respective eigenvalues be a scaled version of one-another. In the special case where they are identical, exact equivalence in the sense of linear conjugacy, is the result.

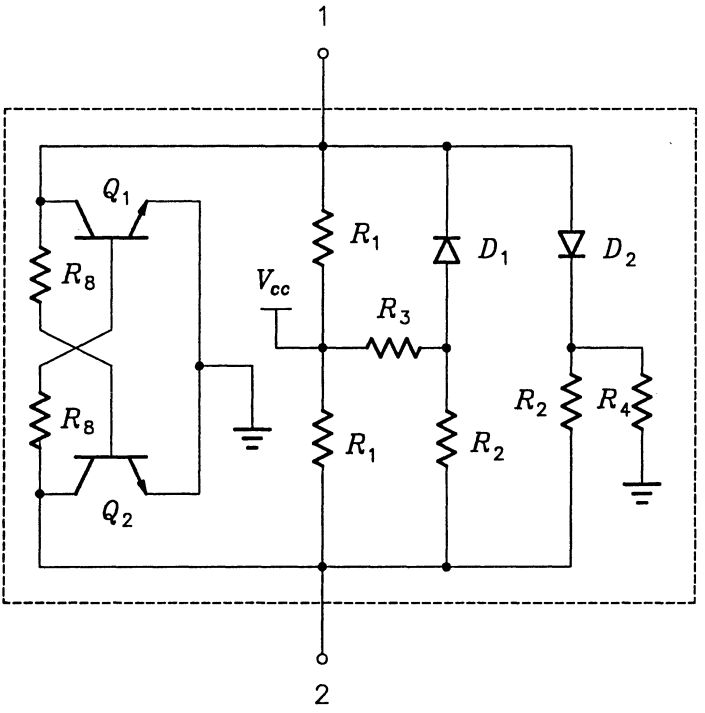

Figure 5.16: The Matsumoto-Chua-Tokumasu realization of the piecewise-linear resistor in Chua's circuit.

An explicit normal form equation in the context of global bifurcation was derived and parametrized by their eigenvalues. Analytical expressions for various Poincaré maps were then derived and used to characterize the birth (i.e. onset) and death (i.e. extinction) of the double scroll attractor, as well as to derive an approximate one-dimensional map in analytic form which was found to be useful for further bifurcation analysis. In particular, the analytical expressions characterizing various half-return maps associated with the Poincaré map were used in a crucial way to prove the existence of a Shil'nikov-type homoclinic orbit, thereby establishing rigorously the chaotic nature of the double scroll equations. These analytical expressions were also fundamental in their in-depth analysis of the birth and death of the double scroll.

In essence Chua, Komuro and Matsumoto analyzed the double scroll equations as an unfolding of a large family of piecewise-linear vector fields in $\mathbf{R}^3$. This enabled them to prove that the chaotic dynamics of the double scroll is quite common, and is robust because the associated horseshoes predicted from Shil'nikov's theorem are structurally stable. In fact, it is exhibited by an infinite family of vector fields (each associated with a piecewise-linear circuit) whose associated piecewise-linear differential equations bear no resemblance to each other. For this reason it is remarkable that the normalized

eigenvalues (a local concept), completely determine the system's global qualitative behaviour.

After the publication of [154], many researchers have contributed with new results concerning Chua's circuit. In the article titled "The Genesis of Chua's Circuit" (reference [144]) a chronological bibliography of papers and articles on Chua's circuit is given. In it Chua also gives a historical anecdote of the development of Chua's circuit. Rigorous results have been obtained through application of Shil'nikov's theorem by Silva [203] and Blázquez and Tuma [84], [85]. Current research on Chua's circuit entails work on sinusoidally driven Chua's circuit [564], [565], stochastic resonance in Chua's circuit [24], spatial disorder and wave fronts in coupled Chua's circuits [573], [634] and time-delayed Chua's circuits [713]. In [718], Shil'nikov also states current and future research issues of interest regarding Chua's circuit.

Concerning numerical analysis of Chua's circuit, Kennedy and Wu have written a PC-based software package called *Adventures in Bifurcation and Chaos* (ABC) for studying Chua's circuit numerically. This package, which is written in Microsoft QuickBASIC for MSDOS machines, simulates three example circuits of which Chua's circuit is one. It generates plots of vector fields, time wavefronts and trajectories. In the case of Chua's circuit, the program calculates and draws fixed points, eigenvalues, eigenspaces and trajectories. The viewing angle of the two-dimensional projection of the three-dimensional state space may be specified to view attractors in a variety of orientations. In addition, the software is accompanied by an extensive database of sets of initial conditions and parameters that produce just about every dynamical behaviour that has been reported for Chua's circuit. This database is being maintained and extended as new attractors are discovered [427]. This software is available from M.P. Kennedy (of University College Dublin, Ireland) on request. For experimental results on Chua's circuit the reader is referred to the bibliography of this book and the bibliography contained in [144].

5.5.3 Numerical Study

The equations that describe Chua's circuit (Figure 5.13(a)) are

$$C_1 \frac{dv_{C_1}}{dt} = G(v_{C_2} - v_{C_1}) - g(v_{C_1}), \tag{5.38}$$

$$C_2 \frac{dv_{C_2}}{dt} = G(v_{C_1} - v_{C_2}) + i_L, \tag{5.39}$$

$$L \frac{di_L}{dt} = -v_{C_2}, \tag{5.40}$$

where v_{C_1}, v_{C_2} and i_L denote the voltage across C_1, the voltage across C_2 and the current through L respectively, and g is the piecewise-linear function (Figure 5.13(b))

$$g(x) := m_0 x + \frac{(m_1 - m_0)}{2}(|x + b_1| - |x - b_1|) + \frac{(m_2 - m_1)}{2}(|x + b_2| - |x - b_2|).$$

For the purpose of our numerical experiment we take the parameters to be

$$C_1 = \frac{1}{9}, \qquad C_2 = 1, \qquad L = \frac{1}{7}, \qquad G = 0.7,$$
$$m_1 = -0.5, \quad m_2 = -0.8, \quad b_1 \to \infty, \quad b_2 = 1.$$

Here $b_1 \to \infty$ implies that the g is a three-segment piecewise-linear function. Therefore the nonlinear resistor is globally active. For the initial conditions

$$v_{C_1}(0) = 0.15264, \quad v_{C_2}(0) = -0.02281, \quad i_L(0) = 0.38127,$$

a chaotic attractor is observed. A saddle-type periodic trajectory also exists in state space (see [522]). For the initial conditions

$$v_{C_1}(0) = 2.532735, \quad v_{C_2}(0) = 1.285458 \times 10^{-3}, \quad i_L(0) = -3.367482,$$

it is observed. The period of this limit cycle is $T = 3.5479$. In practice however, this type of periodic trajectory is not observable, since it is repelling. For finite b_1 and positive m_0 the nonlinear resistor is globally passive and a large stable limit cycle exists. For $b_1 = 3$, $m_0 = 5$ and the initial conditions

$$v_{C_1}(0) = -3.08832, \quad v_{C_2}(0) = -1.0423, \quad i_L(0) = 6.93155,$$

a large stable periodic attractor of period $T = 2.87$ is observed. Projections of the chaotic attractor and saddle-type limit cycle are shown in Figure 5.17. The power spectral densities for each of $v_{C_1}(t)$, $v_{C_2}(t)$ and $i_L(t)$ are plotted in Figure 5.18 when chaos manifests. Next we compute the Lyapunov exponents numerically using the program in Appendix D. The Lyapunov exponents were found to be

$$\lambda_1 \approx 0.23, \quad \lambda_2 \approx 0.0, \quad \lambda_3 \approx -1.78.$$

This shows that the double-scroll attractor is indeed chaotic from a numerical point of view.

We end our discussion of Chua's circuit with a somewhat closer look at the geometrical structure of the double-scroll attractor. For this purpose we rewrite (5.38) to (5.40) in the following dimensionless form [522]

$$\frac{dx_1}{d\tau} = \alpha(x_2 - x_1 - f(x_1)), \tag{5.41}$$
$$\frac{dx_2}{d\tau} = x_1 - x_2 + x_3, \tag{5.42}$$
$$\frac{dx_3}{d\tau} = -\beta x_2, \tag{5.43}$$

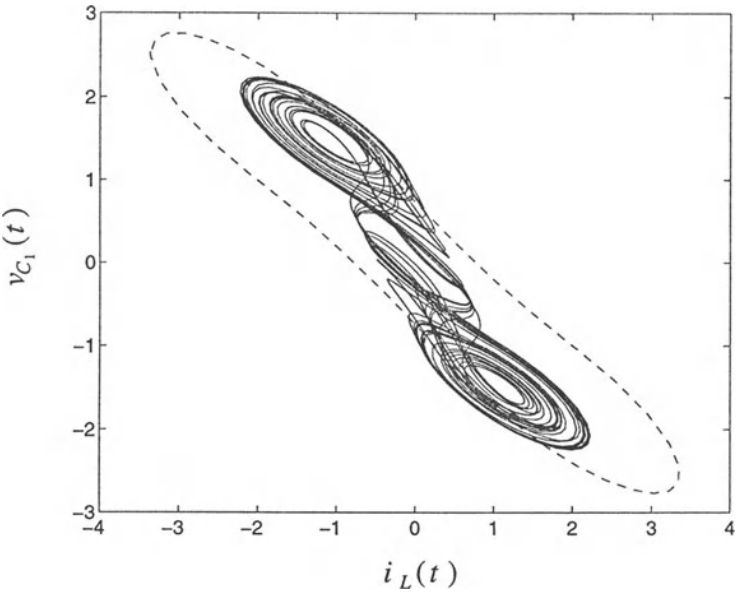

(a)

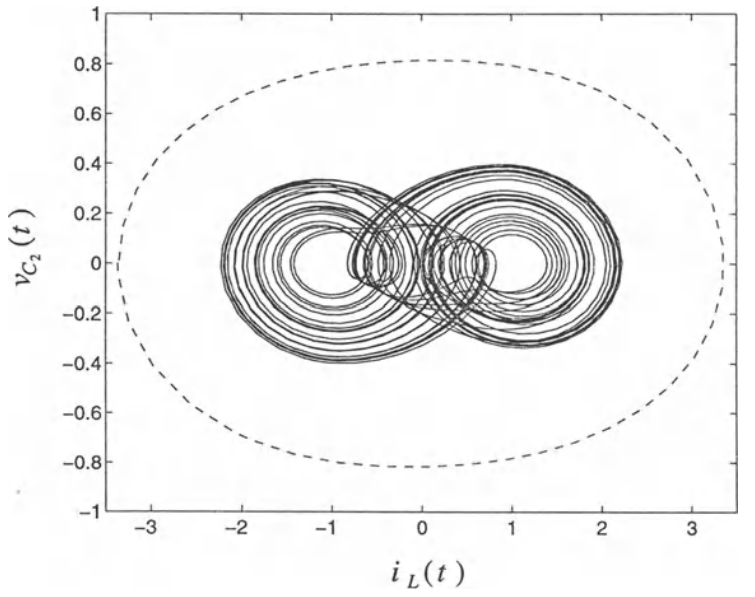

(b)

Figure 5.17: State space projections of the chaotic attractor (solid line) and unstable limit cycle (dashed line): (a) (i_L, v_{C_1})-plane; (b) (i_L, v_{C_2})-plane; (c) (v_{C_1}, v_{C_2})-plane.

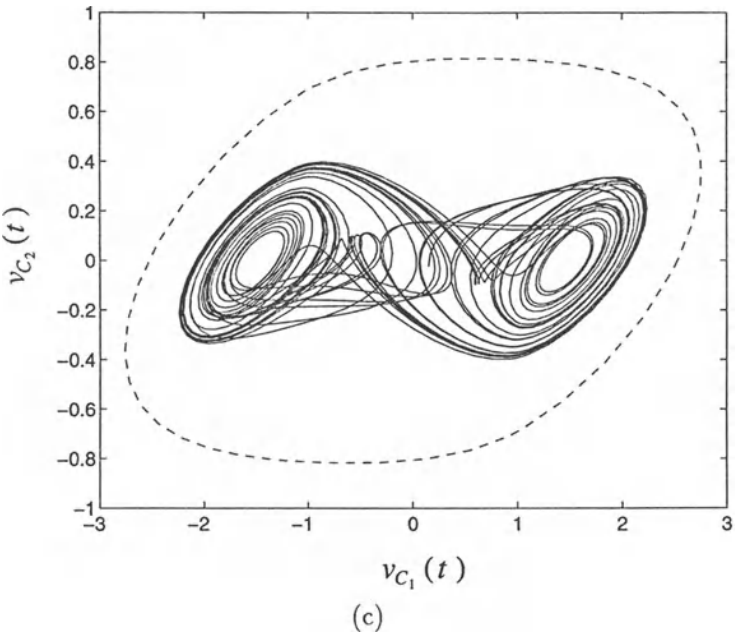

Figure 5.17: (Continued)

where f is the three-segment piecewise-linear function

$$f(x) := \begin{cases} bx - a + b, & \text{if} \quad x \leq -1 \\ ax, & \text{if} \quad |x| \leq 1 \\ bx + a - b, & \text{if} \quad x \geq 1 \end{cases},$$

$$x_1 := \frac{v_{C_1}}{b_2}, \quad x_2 := \frac{v_{C_2}}{b_2}, \quad x_3 := \frac{i_L}{b_2 G}, \quad \tau := \frac{G}{C_2} t,$$

$$a := \frac{m_2}{G}, \quad b := \frac{m_1}{G}, \quad \alpha := \frac{C_2}{C_1}, \quad \beta := \frac{C_2}{(LG)^2}.$$

The system (5.41) to (5.43) has three fixed points, namely

$$\mathbf{x}^*_{-1} := (-k, 0, k)^T, \quad \mathbf{x}^*_0 := (0, 0, 0)^T, \quad \mathbf{x}^*_1 := (k, 0, -k)^T,$$

with $k := (b-a)/(b+1)$, provided that $b \neq -1$. These fixed points are clearly unique if $a \neq b$, and $\mathbf{x}^*_i \in D_i$ for $i = -1, 0, 1$, where

$$\begin{aligned} D_{-1} &:= \{(x_1, x_2, x_3) \mid x_1 \leq -1\}, \\ D_0 &:= \{(x_1, x_2, x_3) \mid |x_1| \leq 1\}, \\ D_1 &:= \{(x_1, x_2, x_3) \mid x_1 \geq 1\}, \end{aligned}$$

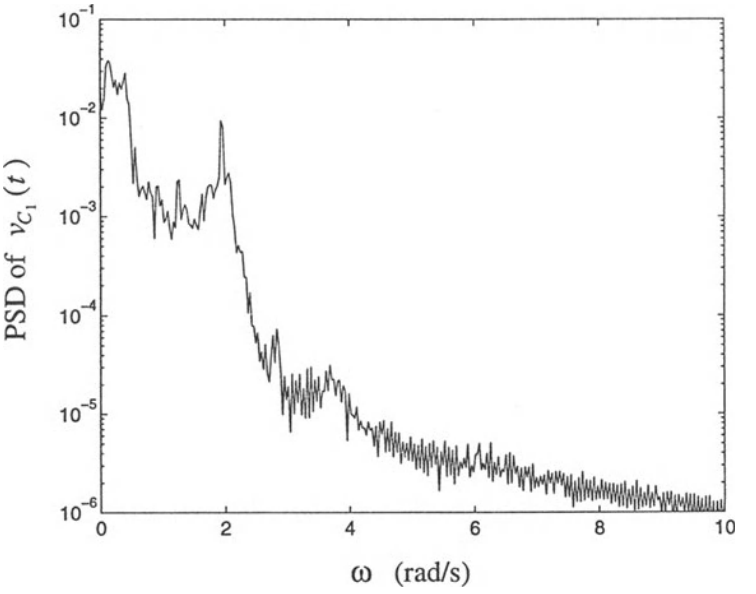

(a)

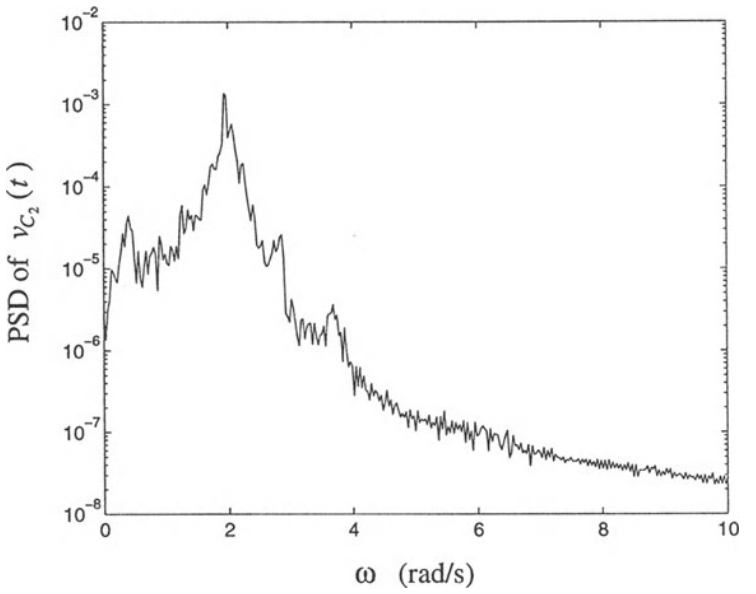

(b)

Figure 5.18: Power spectral densities for the chaotic case: (a) $v_{C_1}(t)$; (b) $v_{C_2}(t)$; (c) $i_L(t)$.

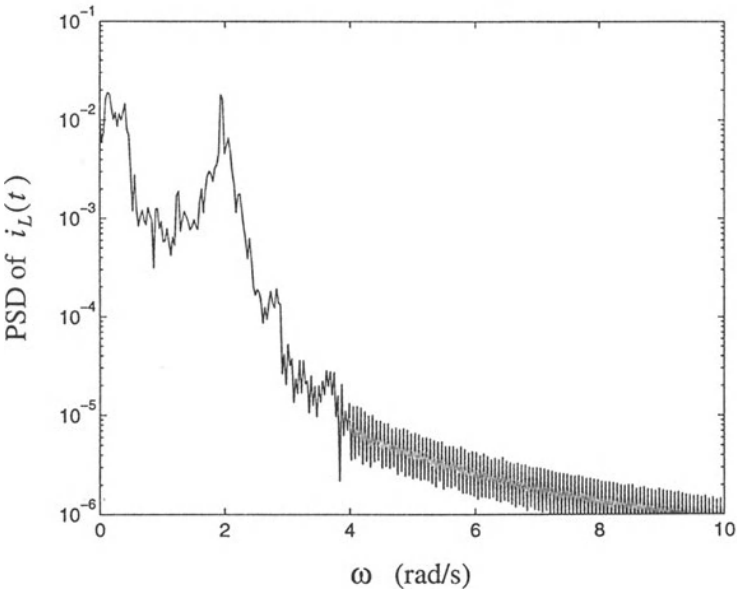

(c)

Figure 5.18: (Continued)

We observe that the system (5.41) to (5.43) is invariant under the transformation $\mathbf{h} : \mathbf{R}^3 \to \mathbf{R}^3$ defined by

$$\mathrm{h}(x_1, x_2, x_3) := (-x_1, -x_2, -x_3)^T .$$

Consequently the system is symmetric about the origin in state space. Since the system is linear in each of the sets D_i for $i = -1, 0, 1$, we can write the system in the form

$$\frac{d\mathbf{x}}{d\tau} := \begin{cases} \mathbf{A}(\alpha, \beta, b)(\mathbf{x} + \mathbf{k}), & \text{if } \mathbf{x} \in D_{-1} \\ \mathbf{A}(\alpha, \beta, a)\mathbf{x}, & \text{if } \mathbf{x} \in D_0 \\ \mathbf{A}(\alpha, \beta, b)(\mathbf{x} - \mathbf{k}), & \text{if } \mathbf{x} \in D_1 , \end{cases}$$

where $\mathbf{x} := (x_1, x_2, x_3)^T$, $\mathrm{k} := (k, 0, -k)^T$ and

$$\mathbf{A}(\alpha, \beta, c) := \begin{pmatrix} -\alpha(c+1) & \alpha & 0 \\ 1 & -1 & 1 \\ 0 & -\beta & 0 \end{pmatrix} .$$

For the parameters of the original systems as assumed above, the corresponding dimensionless parameters are

$$(\alpha, \beta, a, b) = \left(9, \frac{108}{7}, -\frac{8}{7}, -\frac{5}{7}\right) .$$

We also define

$$\mathbf{A}_1 = \mathbf{A}_{-1} := \mathbf{A}\left(9, \frac{108}{7}, -\frac{5}{7}\right) , \qquad \mathbf{A}_0 := \mathbf{A}\left(9, \frac{108}{7}, -\frac{8}{7}\right) .$$

The eigenvalues of these matrices are

$$\lambda(\mathbf{A}_1) = \lambda(\mathbf{A}_{-1}) = \{\gamma_1, \sigma_1 \pm j\omega_1\} , \qquad \lambda(\mathbf{A}_0) = \{\gamma_0, \sigma_0 \pm j\omega_0\} ,$$

where

$$\gamma_1 \approx -3.94 , \quad \sigma_1 \approx 0.19 , \quad \omega_1 \approx 3.05 ,$$

$$\gamma_0 \approx 2.22 , \quad \sigma_0 \approx -0.97 , \quad \omega_0 \approx 2.71 .$$

Let $E^s(\mathbf{x}_i^*)$ and $E^u(\mathbf{x}_i^*)$ denote the stable and unstable eigenspaces respectively of the i-th fixed point. Then

$$\begin{aligned} \dim E^s(\mathbf{x}_{\pm 1}^*) &= \dim E^u(\mathbf{x}_0^*) = 1 , \\ \dim E^u(\mathbf{x}_{\pm 1}^*) &= \dim E^s(\mathbf{x}_0^*) = 2 , \end{aligned}$$

where the eigenspaces are given explicitly by

$$\begin{aligned} E^s(\mathbf{x}_{\pm 1}^*) &:= \left\{ \mathbf{x} \in D_{\pm 1} \,\middle|\, \frac{x_1 \mp k}{\gamma_1^2 + \gamma_1 + \beta} = \frac{x_2}{\gamma_1} = \frac{x_3 \pm k}{-\beta} \right\} , \\ E^u(\mathbf{x}_{\pm 1}^*) &:= \left\{ \mathbf{x} \in D_{\pm 1} \,\middle|\, (\gamma_1^2 + \gamma_1 + \beta)(x_1 \mp k) + \alpha\gamma_1 x_2 + \alpha(x_3 \pm k) = 0 \right\} , \\ E^u(\mathbf{x}_0^*) &:= \left\{ \mathbf{x} \in D_0 \,\middle|\, \frac{x_1}{\gamma_0^2 + \gamma_0 + \beta} = \frac{x_2}{\gamma_0} = \frac{x_3}{-\beta} \right\} , \\ E^s(\mathbf{x}_0^*) &:= \left\{ \mathbf{x} \in D_0 \,\middle|\, (\gamma_0^2 + \gamma_0 + \beta)x_1 + \alpha\gamma_0 x_2 + \alpha x_3 = 0 \right\} . \end{aligned}$$

These eigenspaces are depicted in Figure 5.19, where

$$U_{\pm 1} := D_{\pm 1} \cap D_0 = \{(x_1, x_2, x_3) \,|\, x_1 = \pm 1\} .$$

From the values of the eigenvalues of $\mathbf{A}_{\pm 1}$ we note that projection of trajectories in $D_{\pm 1}$ onto $E^u(\mathbf{x}_{\pm 1}^*)$ produces expanding spirals while projection onto $E^s(\mathbf{x}_{\pm 1}^*)$ produces exponential contracting motion converging to $\mathbf{x}_{\pm 1}^*$. As far as trajectories in D_0 are concerned, projection onto $E^u(\mathbf{x}_0^*)$ yields exponential diverging motion from the fixed point $\mathbf{x}_0^*$, while projection onto $E^s(\mathbf{x}_0^*)$ produces contracting spirals. These different types of motions can be identified in the projections in Figure 5.17. For a detailed analysis and discussion of the attractor's geometrical structure the reader is referred to [522]. Graphical illustrations of trajectories in the different eigenspaces of the fixed points are also presented there.

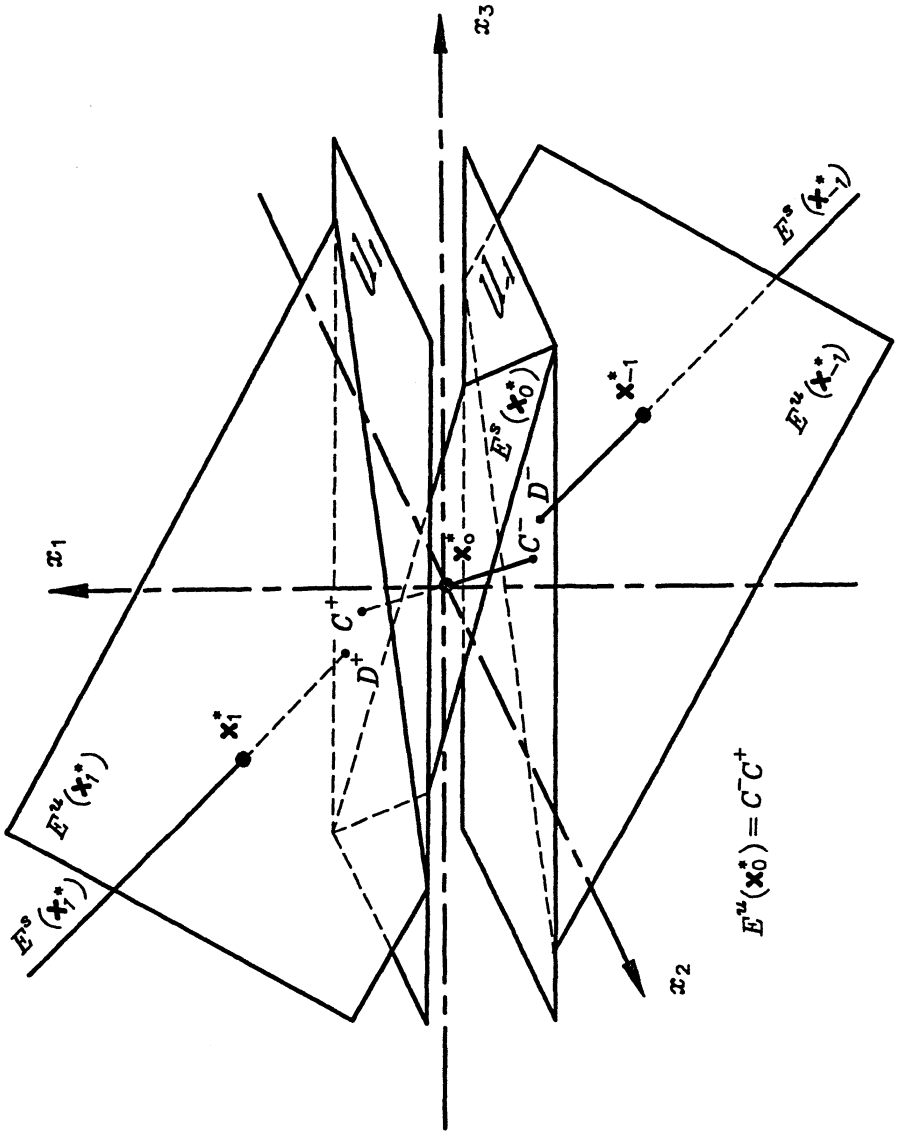

Figure 5.19: Eigenspaces of the fixed points.

5.6 Hyperchaotic Circuit

The phenomenon termed hyperchaos (see definition below) was first observed in a theoretical model by Rössler [666] in 1979. However, the first observation of hyperchaos in a physical system, namely a fourth-order electrical circuit, was reported by Matsumoto *et al.* [521] in 1986. This circuit is the subject of this section. For the purpose of the following definition, let $\{\lambda_i^1\}$ denote the (monotonic decreasing) sequence of one-dimensional Lyapunov exponents, of a given dynamical system.

Definition 5.9 A dynamical system is said to be *hyperchaotic* if $\lambda_1^1 > 0$ and $\lambda_2^1 > 0$. ■

Remark Recall that for chaos to be exhibited by an autonomous continuous-time system, a necessary condition is that it be of order higher than two. However for hyperchaos to be exhibited by a continuous-time system, it is necessary that its order be higher than three, since one Lyapunov exponent is zero [322] and there must always be at least one negative Lyapunov exponent for an attractor to exist in state space.

Consider the circuit of Figure 5.20(a), where the nonlinear resistor N_1 is qualitatively characterized by Figure 5.20(b), i.e. it has a three-segment piecewise-linear voltage-current characteristic. Suppose that N_2 is a negative resistor with resistance $-R$, $R > 0$, and that all other circuit components are linear and passive. The dynamics of the circuit are described by

$$C_1 \frac{dv_{C_1}}{dt} = g(v_{C_2} - v_{C_1}) - i_{L_1}, \tag{5.44}$$

$$C_2 \frac{dv_{C_2}}{dt} = -g(v_{C_2} - v_{C_1}) - i_{L_2}, \tag{5.45}$$

$$L_1 \frac{di_{L_1}}{dt} = v_{C_1} + R i_{L_1}, \tag{5.46}$$

$$L_2 \frac{di_{L_2}}{dt} = v_{C_2}, \tag{5.47}$$

where v_{C_1}, v_{C_2}, i_{L_1} and i_{L_2} denote the voltage across C_1, the voltage across C_2, the current through L_1, and the current through L_2, respectively, and g is the piecewise-linear function of Figure 5.20(b), defined by

$$g(v) := m_0 v + \frac{(m_1 - m_0)}{2}\left(|v+1| - |v-1|\right).$$

The circuit realizations of the nonlinear resistor N_1 and the negative resistor N_2 are shown in Figure 5.21. The operational amplifiers may be replaced by bipolar transistors as in Matsumoto-Chua-Tokumasu realization of the piecewise-linear resistor in the previous section. For the realization of N_1 shown in Figure 5.21(a) Matsumoto

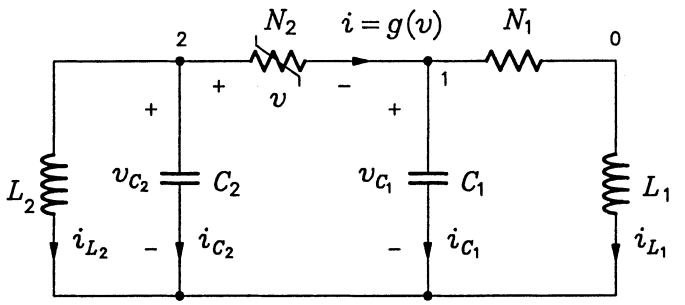

(a)

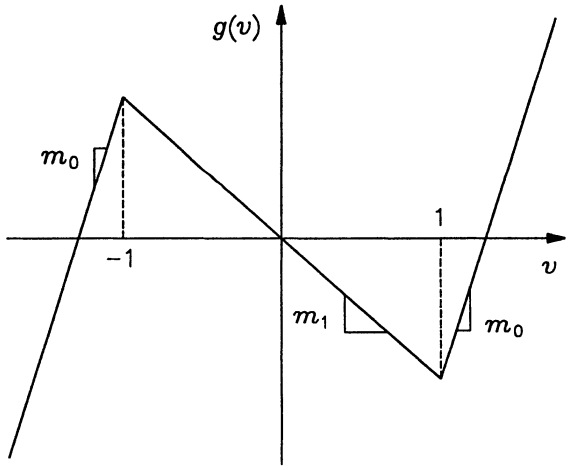

(b)

Figure 5.20: Fourth-order circuit exhibiting hyperchaos: (a) Circuit configuration; (b) Voltage-current characteristic of N_1.

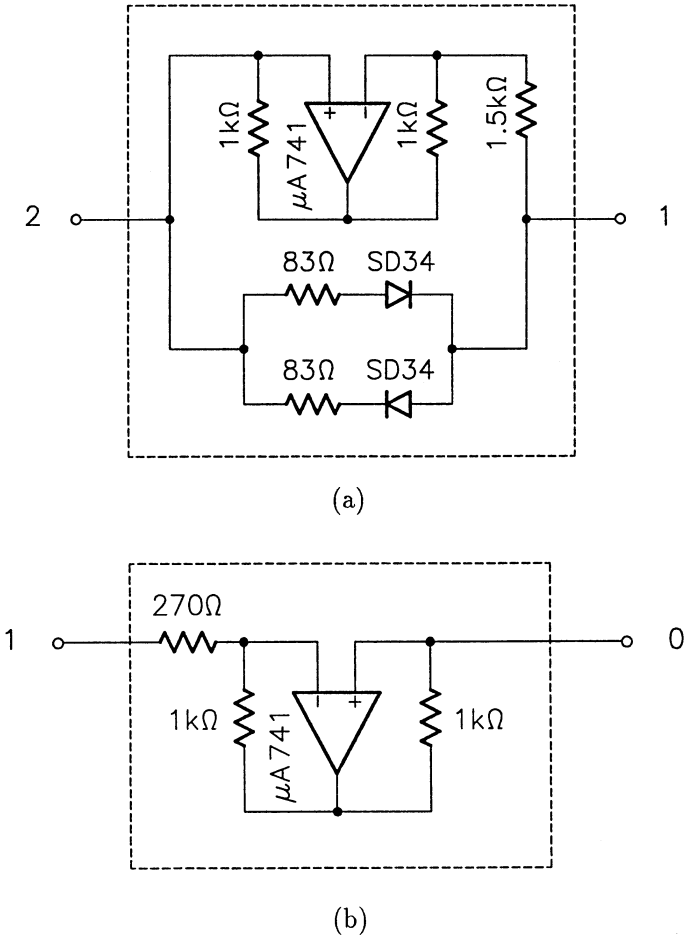

Figure 5.21: Circuit realization of: (a) Nonlinear resistor; (b) Negative resistance.

found that the voltage-current relationship g approximates the measured voltage-current characteristic of N_1 satisfactorily for $m_0 = 3$ and $m_1 = -0.2$.

We now describe numerical results obtained for the system (5.44) to (5.47) for the parameter values [521]

$$m_0 = 3\,, \quad m_1 = -0.2\,, \quad \frac{1}{C_1} = 2\,, \quad \frac{1}{C_2} = 20\,, \quad \frac{1}{L_1} = 1\,, \quad \frac{1}{L_2} = 1.5\,, \quad R = 1\,.$$

As can be seen from the state space projections of the phase portrait, Figure 5.22, the system seems to be (at least) chaotic. The surface of section on the plane

$$v_{C_2} - v_{C_1} = 0\,, \qquad \frac{d}{dt}(v_{C_2} - v_{C_1}) > 0\,, \tag{5.48}$$

and projected onto the (v_{C_1}, v_{L_1})-plane is shown in Figure 5.23. In order to confirm numerically that the equations (5.44) to (5.47) exhibit hyperchaos, Matsumoto and coworkers [521] computed the four one-dimensional Lyapunov exponents for it (using the above set of parameters). These were found to be

$$\lambda_1 \approx 0.24\,, \quad \lambda_2 \approx 0.06\,, \quad \lambda_3 \approx 0.00\,, \quad \lambda_4 \approx -53.8\,.$$

The spectrum of one-dimensional Lyapunov exponents is of the form $(+,+,0,-)$ and hence one may conclude that the theoretical model shows numerical evidence of hyperchaos. Matsumoto *et al.* have also calculated the Lyapunov dimension for the above choice of parameters, to obtain

$$d_L \approx 3 + \frac{0.3}{|-53.8|} \approx 3.006\,,$$

which is a fractal between 3 and 4, and agrees with their experimental observations.

The hyperchaos exhibited by the system (5.44) to (5.47) was also observed by Matsumoto *et al.* for the experimental circuit. In order to analyze the attractor generated by the experimental circuit for hyperchaos, they studied its cross section with the three-dimensional hyperplane

$$\Sigma := \left\{ (v_{C_1}, v_{C_2}, i_{L_1}, i_{L_2}) \in \mathbf{R}^4 \,\middle|\, v_{C_2} - v_{C_1} = 0 \right\}.$$

The measured cross section on the hyperplane had areas where it was thick. They argued that for chaos (which has only one direction of expansion) crossings would have looked much thinner, from which they concluded that the circuit therefore appeared to be hyperchaotic. Matsumoto *et al.* conjectured that for a circuit to exhibit hyperchaos, in addition to being of sufficiently high order, the circuit must include at least two active components.

In [680] and [680], Saito studied a family of circuits containing two active components (an eventually dissipative negative resistor and a linear negative resistor) and two linear inductors and two linear capacitors. In this family every member is of order four. Using singular perturbation theory and defining a suitable Poincaré section he was able to show that members of this family of circuits generate hyperchaos.

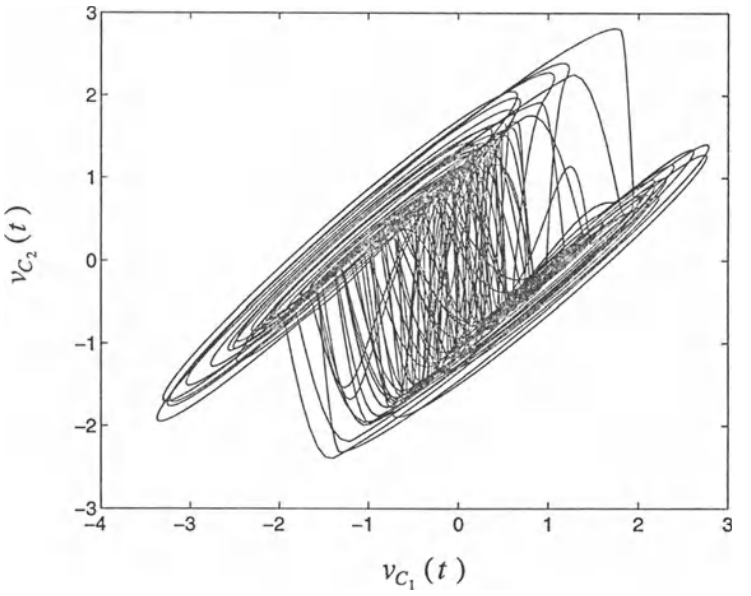

(a)

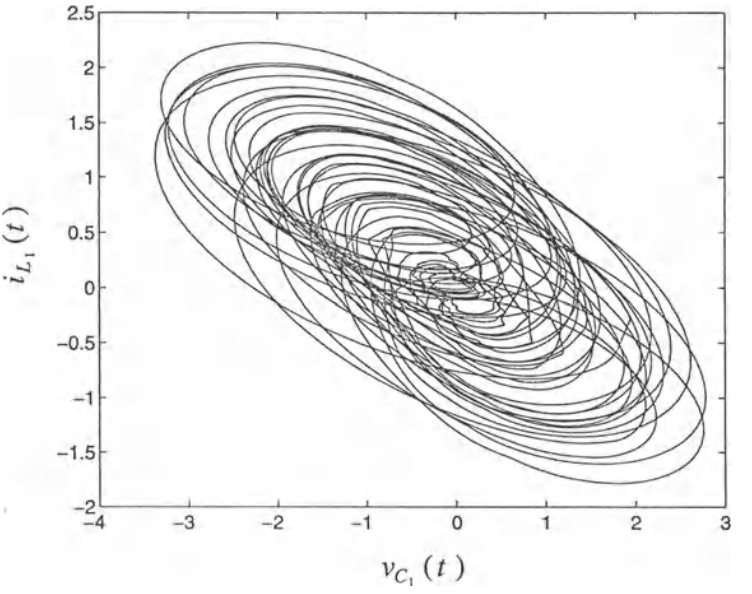

(b)

Figure 5.22: State space projections of the attractor: (a) (v_{C_1}, v_{C_2})-plane; (b) (v_{C_1}, i_{L_1})-plane; (c) (v_{C_1}, i_{L_2})-plane; (d) (v_{C_2}, i_{L_1})-plane; (e) (v_{C_2}, i_{L_2})-plane; (f) (i_{L_1}, i_{L_2})-plane.

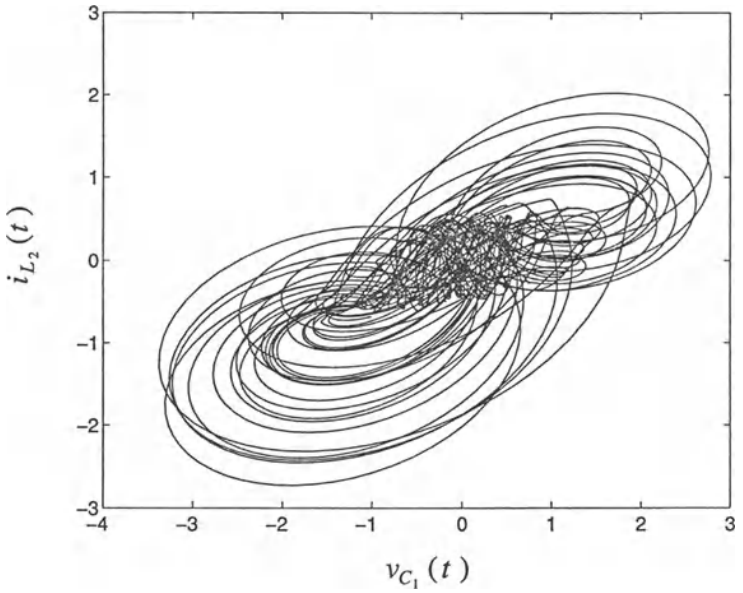

(c)

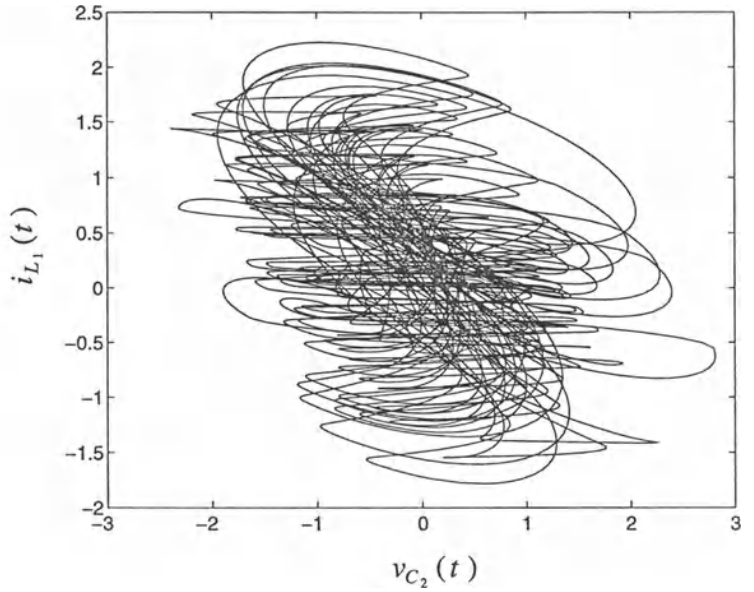

(d)

Figure 5.22: (Continued)

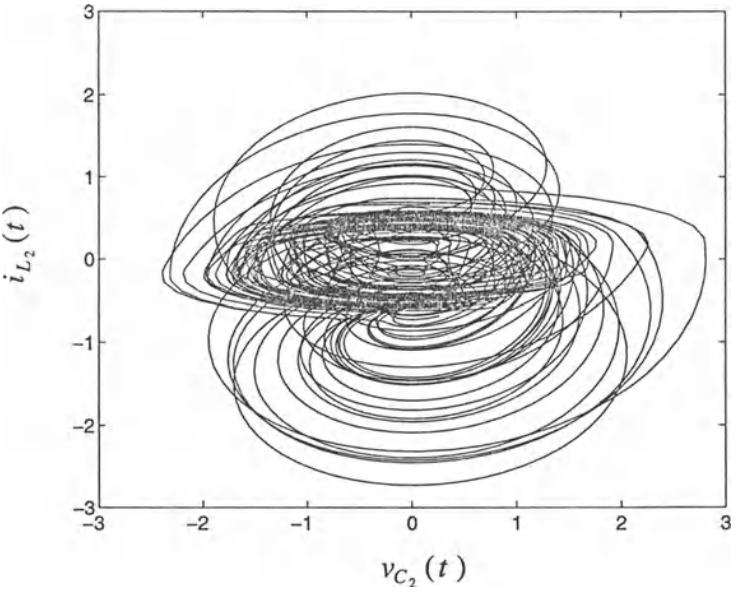

(c)

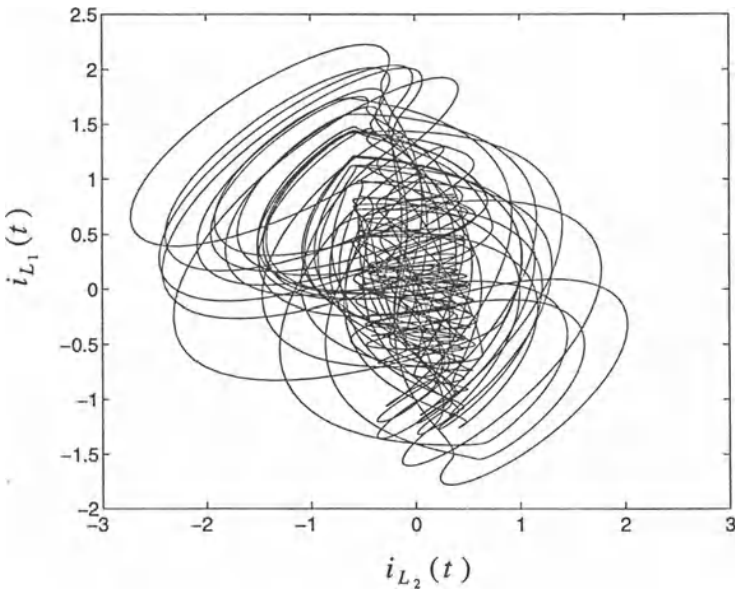

(d)

Figure 5.22: (Continued)

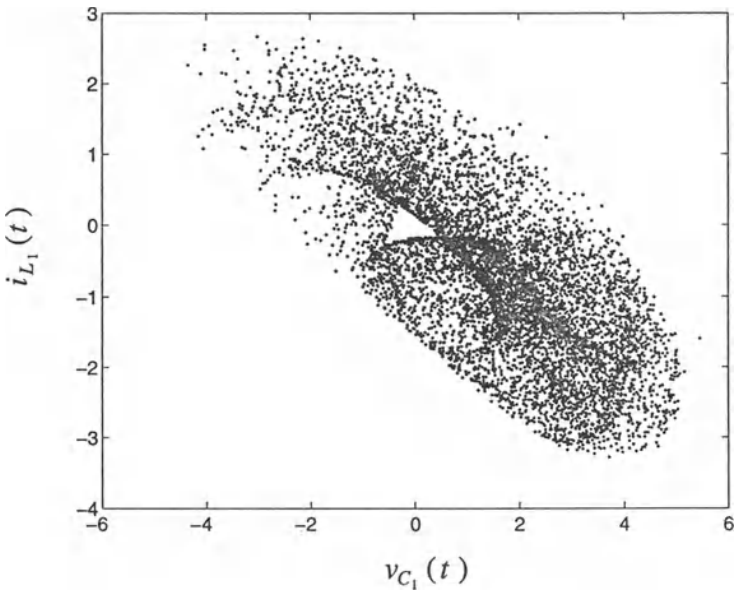

Figure 5.23: Surface of section described by (5.48).

Chapter 6

Driven Systems

6.1 Introduction

The term nonautonomous system or driven system as it is otherwise known, refers to any system that is driven by an external source. Take for instance a phase-locked loop circuit which comes in each radio. It is driven by a frequency modulated signal that is broadcasted and then received by the radio receiver where it is processed before being introduced to the phase-locked loop circuit. The output of the phase-locked loop then is a voice signal which after being amplified can be interpreted by the human. By this description we may say that a phase-locked loop circuit is a driven system. There are many other examples of driven systems which serve us and therefore driven systems constitute an important class of systems. What is more, there are numerous examples of driven systems which under certain circumstances generate chaos. In this chapter we consider such systems. We begin by looking at the simple driven resistance-inductance-capacitance (RLC) circuits with either the inductor or the capacitor nonlinear. It will be seen that even such a simple circuit can exhibit chaotic response under suitable conditions. In Section 6.2.1 we first discuss the case when the inductor is nonlinear . Following this is a discussion of RLC circuits containing a nonlinear capacitor. Usually the nonlinear capacitor comes in the form of a reverse biased diode in which case we refer to such a circuit as a RL-diode circuit.

In Section 6.3 a driven astable multivibrator circuit first studied by Tang, Mees and Chua [788] is discussed. First, the piecewise-constant differential equation that describes the circuit is derived. From the differential equation a discrete piecewise-linear mapping that preserves the dynamics of the differential equation is derived. The analysis of the circuit is then done by studying this mapping. This enables us to prove rigorously that the driven astable multivibrator is chaotic for a certain range of driving frequencies.

Section 6.4 is devoted to the study of chaos generated by phase-locked loops. Although higher order phase-locked loop circuits have been studied in the literature (see for instance [137]), we concentrate on second-order phase locked loop circuits. The phase model of a phase-locked loop is first derived. This model makes it much simpler to study phase-locked loops. Thereafter we embark on a detailed study of chaotic response of second-order phase-locked loops for different operating modes.

In Section 6.5 we study automatic gain control loops for chaos. Automatic gain control loops are utilized in electronic equipment where signals of a constant level are required. One such application is in radio systems where it is used to compensate for the unpleasant fluctuations in voice signal power, by maintaining a constant power output. Conditions leading to the undesirable chaotic response in such system occur are studied.

A Josephson junction is a semiconductor device which finds application in sensitive detectors and superfast computers. Single Josephson junction devices and arrays of mutually coupled Josephson junctions exhibit a wide range of nonlinear phenomena [69] [371] [687] [806]. Section 6.6 is devoted to studying the appearance of chaos in Josephson junctions.

We believe that the understanding of the dynamical behaviour of artificial neural networks will provide fundamental insight into the dynamical behaviour and inner workings of the human brain. Moreover, we believe that this will also have a huge impact on the development of controllers for industrial processes and robots, especially in cases where the process to be controlled is nonlinear and/or time-variant and the control objectives are fuzzy. For such problems linear controllers fall short of achieving the goals set. For these reasons we feel it appropriate to include a section on chaotic response of neural networks. In Section 6.7 we focus our attention on a driven two-cell cellular neural network. This simple system can exhibit chaos. Numerical evidence of this is given. An electronic circuit for implementation of this two-cell cellular neural network which was devised by Zou and Nossek [879] is also presented here with a short discussion of their experimental findings.

In the final section of this chapter, we briefly discuss phase coupled systems. By phase coupled systems we mean two identical systems with coupling to one or both the systems proportional to the difference of the state vectors of the two systems. The amounts of coupling applied to the two systems are equal. From the view point of stability properties of solutions afforded by a single system, this type of coupling is found to be important. Although we restrict our discussion to autonomous systems, the results also apply to driven systems with identical drives.

6.2 Driven *RLC* Circuit

6.2.1 Ferroresonant Circuit

A nonlinear circuit element frequently encountered in power electronics is a nonlinear inductance. When the core of an inductor or transformer is driven into saturation, its inductance reduces. Nonlinear inductance is put to work in magnetic amplifiers, snubber inductors, and inverter transformers (in for example the Royer oscillator). A ferroresonant circuit consists of a nonlinear inductor combined in a circuit with a linear capacitor. Ferroresonant circuits are employed in for instance voltage stabilizers and frequency dividers. Concerning nonlinear phenomena in ferroresonant circuits, multiple steady states in driven ferroresonant circuits were reported as early as 1907 and subharmonics were described in 1926. We refer to [589], [803] for citations to some early work in this field. Multiple periodic steady states, now seen as coexisting stable attractors are still being studied [340].

In this section we consider the periodically driven ferroresonant circuit [153] shown in Figure 6.1. The only nonlinear element is the inductor. This circuit is of importance from a theoretical perspective because it is the simplest circuit that does not satisfy the hypotheses of any of the general theorems [150] which guarantee uniqueness and global asymptotic stability of periodic solutions. In fact, multiple periodic solutions have been obtained both by nonrigorous harmonic balance methods [345] [398], and by computer simulation [398] [276] of similar circuits. This circuit is also important from a practical perspective since its equations model voltage measuring transformers in for example high-voltage equipment. From a practical point of view the presence of extraneous periodic solutions could be catastrophic. For example, a second periodic solution (having the same generator frequency) usually has a much larger amplitude which will damage if not destroy the transformer. Similarly, subharmonic solutions often cause failures in power systems.

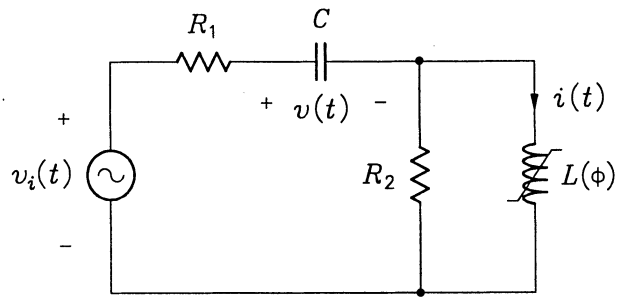

Figure 6.1: Ferroresonant circuit.

Concerning the circuit depicted in Figure 6.1 we assume that the nonlinear inductor's ϕ-i characteristic may be approximated by a piecewise-linear function without hysteresis. In doing so firstly analytical difficulties are overcome so that exact (regional) solutions are attainable, thereby avoiding the errors associated with numerical methods and secondly the complications of magnetic hysteresis are omitted [803] [207]. We assume that the piecewise-linear function $i(\phi)$ is given by

$$i(\phi) := \begin{cases} (\phi + \phi_1)/L_1\,, & \text{if} \quad \phi < -\phi_0 \\ \phi/L_0\,, & \text{if} \quad |\phi| < \phi_0 \\ (\phi - \phi_1)/L_1\,, & \text{if} \quad \phi > \phi_0 \end{cases},$$

where $0 < L_1 < L_0$ and for continuity at $\phi = \pm\phi_0$, ϕ_0 and ϕ_1 are related by

$$\phi_1 = \phi_0 \left(1 - \frac{L_1}{L_0}\right).$$

Choosing ϕ the magnetic flux and v the voltage across the capacitor as state variables, application of Kirchoff's laws yield the state equations as

$$\frac{d\phi}{dt} = -\frac{R_1 R_2}{R_1 + R_2} i(\phi) - \frac{R_2}{R_1 + R_2}(v - E\cos\omega t)\,, \tag{6.1}$$

$$\frac{dv}{dt} = -\frac{R_2}{C(R_1 + R_2)} i(\phi) - \frac{1}{C(R_1 + R_2)}(v - E\cos\omega t)\,. \tag{6.2}$$

Note that these state equations are linear in each of the three strips $\phi < -\phi_0$, $|\phi| < \phi_0$, and $\phi > \phi_0$ of the state space. Introducing the state vector

$$\mathbf{x} := (\phi, v)^T\,,$$

the state equations have the form

$$\frac{d\mathbf{x}}{dt} = \mathbf{A}\mathbf{x} + \mathbf{b}E\cos\omega t + \mathbf{A}\mathbf{d}\,, \tag{6.3}$$

in each of the three strips, where

$$\mathbf{A} := \begin{cases} \mathbf{A}_1\,, & \text{if} \quad x_1 < -\phi_0 \\ \mathbf{A}_0\,, & \text{if} \quad |x_1| < \phi_0 \\ \mathbf{A}_1\,, & \text{if} \quad x_1 > \phi_0 \end{cases},$$

with

$$\mathbf{A}_i := \frac{-1}{R_1 + R_2} \begin{pmatrix} \dfrac{R_1 R_2}{L_i} & R_2 \\ \dfrac{-R_2}{L_i C} & \dfrac{1}{C} \end{pmatrix}, \qquad \text{for} \quad i = 0, 1\,,$$

and

$$\mathbf{b} := \frac{1}{R_1 + R_2} \begin{pmatrix} R_2 \\ 1/C \end{pmatrix},$$

$$\mathbf{d} := \begin{cases} (\phi_1, 0)^T, & \text{if } x_1 < -\phi_0 \\ (0,0)^T, & \text{if } |x_1| < \phi_0 \\ -(\phi_1, 0)^T, & \text{if } x_1 > \phi_0 \end{cases}.$$

In a given region the solution of (6.3) that satisfies the initial condition $\mathbf{x}(t_0)$ at time t_0 is

$$\mathbf{x}(t) = \mathbf{x}_s(t) + e^{\mathbf{A}(t-t_0)}(\mathbf{x}(t_0) - \mathbf{x}_s(t_0)), \tag{6.4}$$

where $\mathbf{x}_s(t)$ is the steady state solution [34] given by

$$\mathbf{x}_s(t) = -E\left(\omega^2\mathbf{I} + \mathbf{A}^2\right)^{-1}(\mathbf{A}\cos\omega t + \omega \sin\omega t)\frac{E}{\omega^2}\mathbf{b} - \mathbf{d}. \tag{6.5}$$

Here steady state means that all terms containing exponentials have decayed and hence the steady state is free of such terms. At the region boundaries $\phi = \pm\phi_0$ the function $i(\phi)$ and thus the piecewise-linear vector field (6.3) is continuous. Therefore the solution can be continued across region boundaries. Anywhere along the boundary between two regions both $\mathbf{x}$ and $d\mathbf{x}/dt$ are continuous functions of time. Consequently for any initial time t_0 and for any initial condition $\mathbf{x}(t_0)$ a unique solution $\mathbf{x}(t)$ of (6.4) for $-\infty < t < +\infty$ can easily be shown to exist [153]. Furthermore, such a solution is eventually uniformly bounded. Finally we make the observation that the vector field (6.3) is symmetric in two respects. It is invariant under the transformation

$$\mathbf{x}(t) \mapsto \mathbf{x}(t+T), \qquad t \in \mathbf{R},$$

and it is symmetric about the origin, that is, the system (6.3) is invariant under the transformation

$$\mathbf{x}(t) \mapsto -\mathbf{x}(t + T/2), \qquad t \in \mathbf{R}.$$

Note that by applying the latter transformation twice we obtain the former which implies that every symmetric solution must be periodic. However the converse of this is only true if the symmetric solution is unique, which as we see is not always the case here. In addition if there exists a nonsymmetrical solution then there exists a second nonsymmetrical solution. This concludes the derivation of the state equations and corresponding solutions.

We now turn to a numerical study of the circuit based on the expressions derived above. In order to study the above system numerically, we assume the following parameter values [153],

$$\omega = 2\pi \times 50\text{rad/s}, \quad R_1 = 50\Omega, \quad R_2 = 10\text{k}\Omega, \quad C = 1.69\mu\text{F},$$

$$L_0 = 33.33\text{H}, \quad L_1 = 1.28\text{H}, \quad \phi_0 = 0.92\text{Vs}.$$

For a drive voltage amplitude $E < 91\text{V}$ there exists a unique globally asymptotically stable period-1 solution. Here the reference period used is the drive voltage's period which is $T = 20\text{ms}$. This trajectory is symmetric about the origin i.e.

$$\mathbf{x}(t + T/2) = -\mathbf{x}(t), \qquad t \in \mathbf{R},$$

and is a scaled replica of the middle trajectory in Figure 6.2. For source voltage amplitudes in the range 91V to 246V Chua *et al.* found three harmonic period-1 solutions. For the case $E = 160\text{V}$ the state space trajectories for the three period-1 solutions are depicted in Figure 6.2. The "×"-symbols on the trajectories indicate the point where

$$t \,(\text{mod } 2\pi) = 0\,.$$

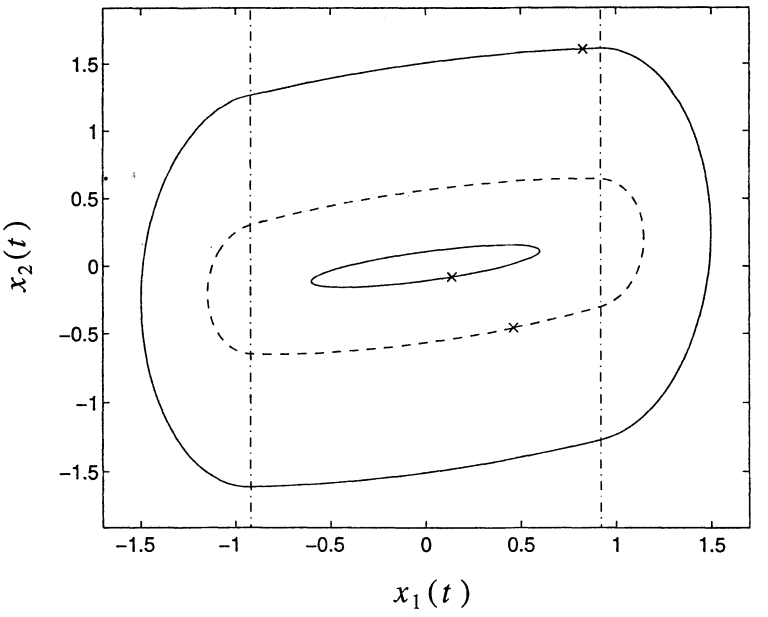

Figure 6.2: Phase portrait of three symmetrical period-1 solutions for the case $E = 160\text{V}$: two stable solutions (solid lines) and an unstable solution (dashed line). The dashed-dotted lines represent $x_1 = \pm\phi_0$.

The smallest period-1 trajectory belongs to the linear circuit relative to the region $|x_1| < \phi_0$. It is, of course, locally stable in the sense that the domain of attraction is a proper subset of the state space. The period-1 solution with the largest state space trajectory was also found to be only locally stable. The period-1 solution "in between" the other two (at least in the projection onto the (x_1, x_2)-plane) is unstable. It is therefore not possible to observe this trajectory starting from an arbitrary initial condition. A point on the trajectory itself is required as initial condition in order for it to be observed. Using the Nelder-Mead minimization routine of MATLAB we have been able to estimate numerically the location where it pierces the plane $t \pmod{2\pi} = 0$. The coordinates of this point were found to be

$$(t \pmod{2\pi}, x_1, x_2) \approx (0,\ 0.452109,\ -143.424724)\,.$$

Using this point we were able to obtain its state space trajectory which is shown in Figure 6.2. As was mentioned above, Figure 6.2 is not the complete state space but merely a projection of it onto the (x_1, x_2)-plane (the third state variable being time). For this reason the unstable period-1 trajectory is *not* a separatrix as one finds for the simple pendulum equation. Notice that all three trajectories in Figure 6.2 are symmetrical about the origin. For the amplitude range 246V to 1694V once again there appears to be a unique, globally asymptotically stable periodic solution of period T which is symmetric about the origin. It is similar in shape to the outer trajectory in Figure 6.2.

All examples of periodic solutions given so far, whether they are unique or not, are symmetrical. However, for E in the range $1694\text{V} < E < 4389\text{V}$, nonsymmetrical solutions exist. There are three periodic solutions in total: two (see earlier discussion) are nonsymmetric period-1 solutions which were found to be locally stable only and the third is a symmetric period-1 solution which is unstable. For the case $E = 2500\text{V}$ these trajectories can be seen in Figure 6.3. In order to obtain a point on the unstable trajectory to enable us to draw it, we utilized the Nelder-Mead minimization routine of MATLAB to obtain a numerical estimate of the point that satisfies $t \pmod{2\pi} = 0$. The coordinates of this point are

$$(t \pmod{2\pi}, x_1, x_2) \approx (0,\ 0.401294,\ 3298.897814)\,.$$

For $E > 4389\text{V}$, there again appears to be only a single, necessarily symmetrical, globally asymptotically stable periodic solution. It approximately follows the periodic solutions of the linear circuits associated with the regions $x_1 > \phi_0$ and $x_1 < -\phi_0$ since the time spent in the region $|x_1| < \phi_0$ is much shorter than the time spent in the other two regions together.

By changing R_2 and C to $R_2 = 50\text{k}\Omega$ and $C = 250\text{nF}$ and keeping the other circuit parameters as specified above Chua *et al.* [153] were able to observe more complex periodic solutions, subharmonics and chaos by once again adjusting the driving amplitude E. For example, for $E = 1800\text{V}$ the globally asymptotically stable period-1

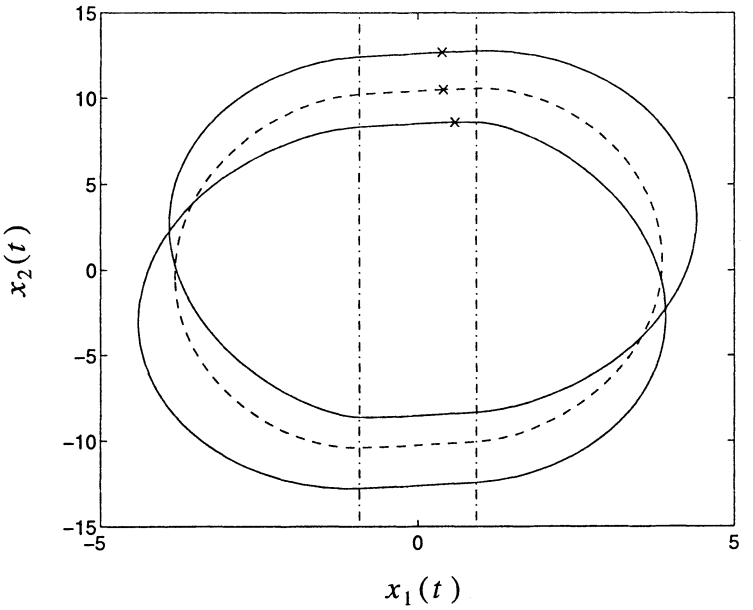

Figure 6.3: Phase portrait of three period-1 solutions for the case $E = 2500$V: two stable nonsymmetric solutions (solid lines) and an unstable symmetric solution (dashed line). The dashed-dotted lines represent $x_1 = \pm\phi_0$.

trajectory in Figure 6.4 was observed. As can be seen this solution is already more complex that those observed earlier. At $E = 1000$V a 1/5-subharmonic was reported to have been observed [153], an indication of qualitative changes taking place. For $E = 800$V the circuit showed numerical evidence of chaos. The phase portrait for this case is shown in Figure 6.5. Figure 6.6 shows typical waveforms for the case $E = 800$V as well as sensitive dependence on initial conditions. Figure 6.7 shows the power spectral density of $x_1(t)$ (i.e. $\phi(t)$) for the case $E = 800$V. Plotted in the same figure is the power spectral density of a pure 50Hz sinusoid with the same power as the 50Hz component in the $x_1(t)$. On comparison of the two power spectral densities in Figure 6.7) we observe that $x_1(t)$ has a broadband component which is not present in the power spectral density of the sinusoid. This indicates chaos.

A ferroresonant circuit of similar constructional topology to the one in Figure 6.1 was studied by Deane and Hamill [207]. Removing the resistor R_2 from the above circuit, the series ferroresonant circuit studied by them is obtained. The state equations of the series ferroresonant circuit can be obtained from (6.1) and (6.2) by taking the limit as R_2 approaches ∞. However, they used a square wave (with adjustable frequency and amplitude) as excitation for the circuit. The response of this circuit was demonstrated numerically in [326] and experimentally in [207]. Observations made showed that the circuit is likely to be chaotic.

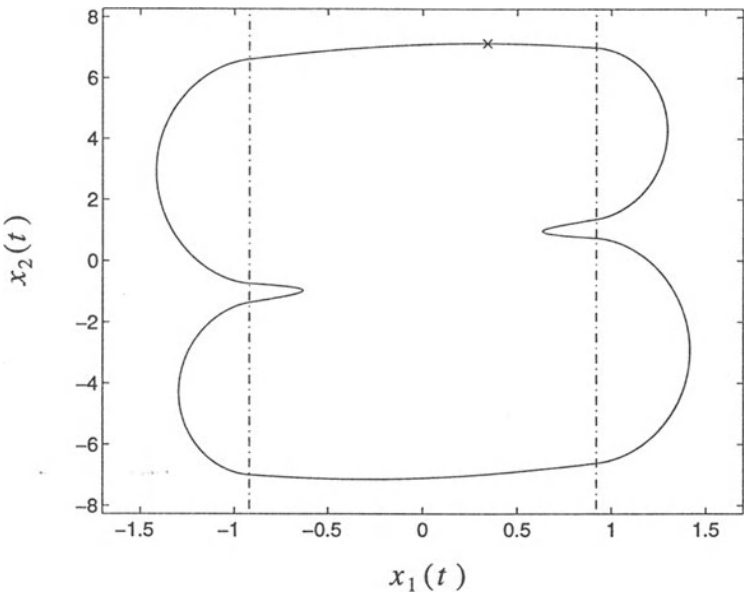

Figure 6.4: Phase portrait of a more complex period-1 solution for $E = 1800$V.

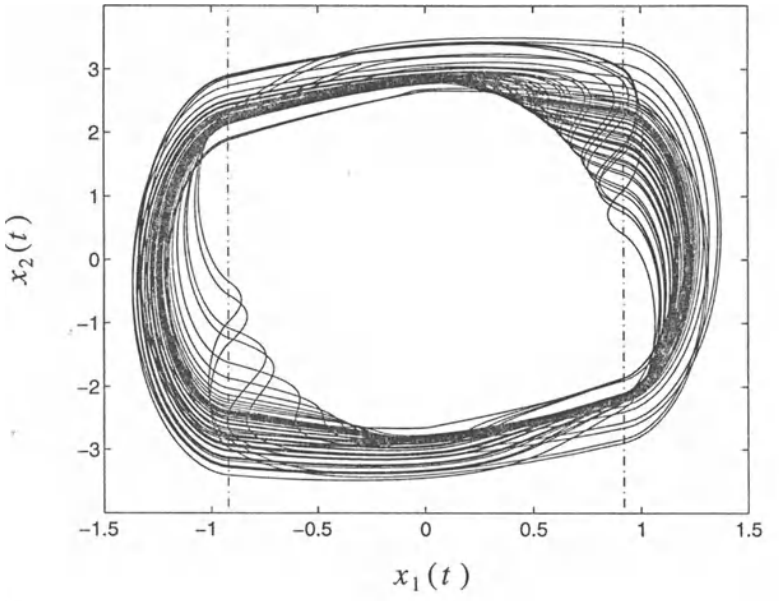

Figure 6.5: Phase portrait of a seemingly chaotic solution for the case $E = 800$V.

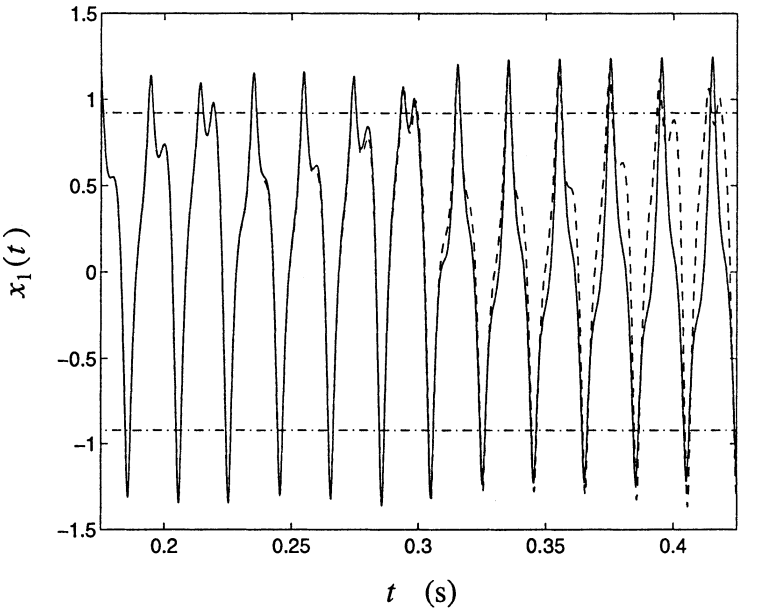

(a)

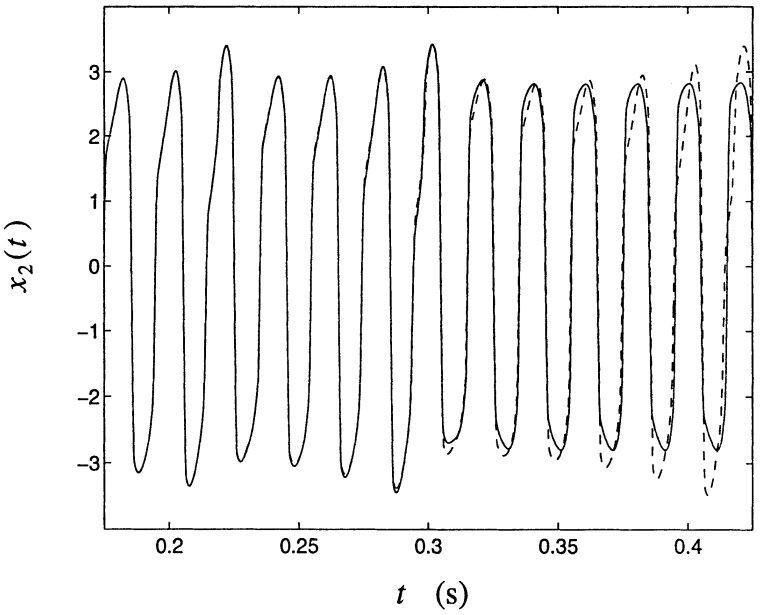

(b)

Figure 6.6: Typical waveforms for $E = 800$V showing sensitive dependence on initial conditions: (a) Waveform for $x_1(t)$ (the dashed-dotted lines represent $x_1 = \pm\phi_0$.); (b) Waveform for $x_2(t)$.

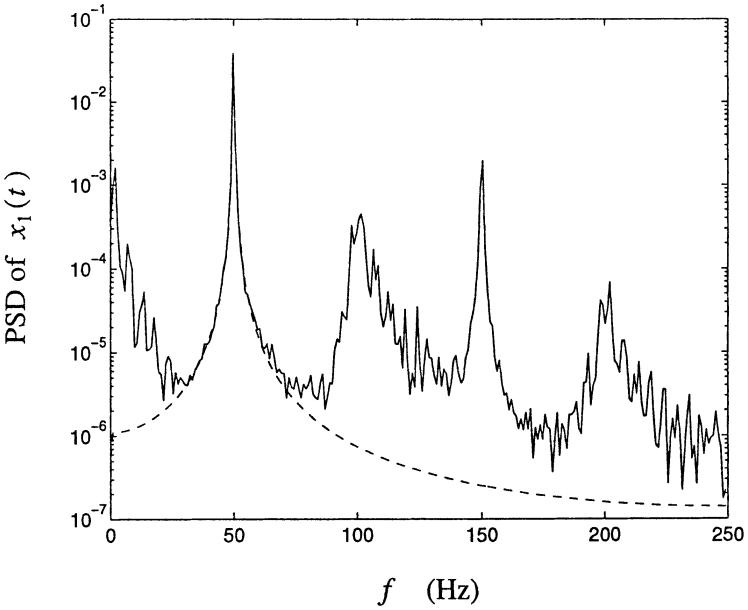

Figure 6.7: Power spectral density of $x_1(t)$ (solid line) for the case $E = 800$V compared to that of a 50Hz sinusoid (dashed line).

6.2.2 Driven *RL*-Varactor Diode Circuits

A diode is characterized by nonlinear conduction (the well-known i-v characteristic curve), by a reverse recovery time τ, and by two types of capacitance, namely the junction capacitance C_j, dominant under reverse bias, and the charge storage capacitance C_s, dominant under forward bias. Ordinary rectifier diodes usually have $C_s > C_j$ and $\tau \approx 1\mu$s. Varactor diodes usually have $C_j > C_s$ and τ between 0.1 and 1μs. For fast signal diodes $\tau \approx 1$ns. The *RL*-varactor diode circuit finds application in RF receivers where it forms part of the frequency selective tuning circuit of the radio receiver. It also finds application as a frequency divider at microwave frequencies. The *RL*-varactor diode circuit shown in Figure 6.8 was studied by a number of researchers (see [493], [793], [794], [376], [46], [661], [116], [103], and [787]).

The dynamics of the system in Figure 6.8 is described by the ordinary differential equation

$$L\frac{d^2q}{dt^2} + R\frac{dq}{dt} + v_d(t) = v_i(t)\,. \tag{6.6}$$

The relationship between the voltage $v_d(t)$ across the varactor diode and the junction capacitance of the varactor diode is of the form

$$C_j(v_d) = \frac{C_0}{(1 + v_d/\phi)^\gamma}\,.$$

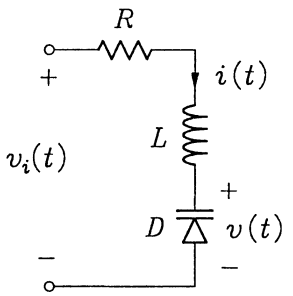

Figure 6.8: Series RL-varactor diode circuit.

It is important to note that this relationship only holds when the diode is reverse biased, that is, when $v_d(t) > 0$.

In the study performed by Linsay in [493], the component values were $R = 180\Omega$ and $L = 100\mu$H, and the diode was an IN 5470 A with $C_0 = 81.8$pF, $\phi = 0.6$V and $\gamma = 0.44$. The circuit was driven sinusoidally from a signal generator with a 50Ω output impedance while the power spectral density was measured at the output, using a spectrum analyzer. Therefore $v_i(t)$ is of the form

$$v_i(t) = V_0 \sin \omega t \,.$$

At very low drive voltages the circuit behaved as a linear RLC circuit with a resonance at $f_1 = 1.78$MHz. The nonlinear behaviour was observed by driving the circuit at this frequency and gradually increasing the drive voltage amplitude. At low amplitude the circuit displayed the frequency multiplication typical of all nonlinear circuits. The first subharmonic appeared at a drive voltage of 1.9V. Linsay found that once a spectral peak has appeared and reached full magnitude it remained essentially unchanged through any further period doubling. Feigenbaum [493] derived the expression

$$X^n_{2k+1} \approx \frac{1}{2\alpha}\left(1 - j(-1)^k\right)\left(1 - j\frac{(-1)^k}{\alpha}\right)\sum_l \frac{1}{j\pi}\left(\frac{X^n_{2l+1}}{(2l+1)-(2k+1)/2}\right),$$

($\alpha := 2.5029\ldots$, $j := \sqrt{-1}$) which estimates the Fourier components of the $(n+1)$-th period-doubling bifurcation from those of the n-th period-doubling bifurcation. Linsay has found his experimental results to be in excellent agreement with this theoretical prediction up to the fourth generation period-doubling bifurcation. Beyond the fifth generation period-doubling bifurcation noise in the system prevented testing of this prediction. Predictions of the Feigenbaum number from the first few period-doubling bifurcations were also found to be in good agreement of the theoretically predicted value of $4.669\ldots$. Increasing the amplitude of the drive voltage further produced chaotic behaviour. This manifested in the the form of a broadband spectral component which appears in the subharmonic region of the spectrum. The broadband component is not white but displays broad peaks about the frequencies $f_1/4$,

$f_1/2$ and $3f_1/4$. Further increases in drive voltage produces period-quintupling, chaos and period-tripling. Period-doubling then produced subharmonics between the $f_1/3$ spectral peaks.

In order to determine the nonlinearity responsible for generating the subharmonics, Linsay replaced the varactor by an 80pF capacitor in parallel with a 1N4154 diode. The experiment was then repeated. In this second experiment no bifurcations occurred, leading Linsay to conclude that the bifurcations in the first experiment were due to the nonlinear junction capacitance.

The purpose of the experiment performed by Testa, Pérez and Jeffries [793] was to compare the dynamical behaviour as fully as possible with that of the simple logistic map. The parameters of the circuit studied by them are: $R = 28\Omega$, $L = 10$mH, 1N953 varactor with $C_0 = 300$pF, $\phi = 0.6$V and $\gamma = 0.5$. They found that at low amplitude driving the system behaved like a high-Q resonant circuit at $f_0 = 93$kHz. As the amplitude V_0 increased the resonant frequency increased and the Q decreased at first. Fixing the driving frequency f near the resonant frequency of the circuit and then increasing the driving amplitude V_0, they found a typical voltage waveform across the varactor diode to be occasionally spiky. During the diode conduction half cycle the voltage across the varactor diode was compressed towards the zero line whereas during the reverse half cycle it had a set of discrete peak values. These peaks during the reverse half cycle were then used to obtain bifurcation diagrams (see [793]). They observed period-doubling bifurcations, band merging and chaos with the drive amplitude as bifurcation parameter. Overall there was a reasonable quantitative agreement between their observations and the logistic model. Their estimations of universal numbers such as Feigenbaum's number where found to be in fair agreement with theoretically predicted values.

Following the publication of the results in [793], Hunt responded with a brief note [376] suggesting that the major cause of the period-doubling bifurcations and chaos was the reverse recovery time effect of the varactor diode rather than it's nonlinear junction capacitance. The reverse recovery time is the time it takes for the minority carriers to recombine.

In the paper [661] the authors Rollins and Hunt have studied the RL-varactor diode circuit in Figure 6.8 with

$$v_i(t) = V_0 \cos \omega t$$

in an attempt to determine what exactly causes this circuit to exhibit period-doubling bifurcations and chaos. The following assumptions concerning the properties of the varactor diode were made [661]:

i) The changing capacitance of the varactor diode is unimportant with regard to the salient features of the response and is therefore neglected.

ii) The diode behaves as an ideal diode with the following added characteristics:

1) There is a finite forward bias voltage V_f. The diode will not conduct until the forward voltage drop reaches V_f and the voltage drop remains at V_f as long as the diode conducts.

2) When the voltage drop is less than V_f the diode does not conduct but acts as a capacitor with fixed capacitance C.

3) When the current through the diode is driven through zero, the diode does not shut off immediately, but continues to conduct for a time equal to the reverse recovery time τ_r. Although it is known that τ_r depends on various factors such as the magnitude of the forward current and the magnitude of the reverse voltage, the very simple functional relationship

$$\tau_r = \tau_m \left(1 - \mathrm{e}^{-|I_m|/I_c}\right) \tag{6.7}$$

is used. Here $|I_m|$ is the magnitude of the most recent maximum forward current, and τ_m and I_c are parameters that describe the characteristics of the particular diode used.

The response of the diode resonator can now be exactly calculated by splitting time into intervals when the diode is either conducting or off. Exact analytic solutions were obtained for each time interval since the dynamical behaviour in the different time intervals is linear. When the diode is conducting, the general solution is of the form

$$i(t) = \frac{V_0}{Z_1}\cos(\omega t - \theta_1) + A\mathrm{e}^{-(R/L)t} + \frac{V_f}{R}\,, \qquad v_d(t) = -V_f\,, \tag{6.8}$$

where

$$Z_1^2 := R^2 + \omega^2 L^2\,, \quad \theta_1 := \arctan\left(\frac{\omega L}{R}\right)\,,$$

and A is a constant determined by the boundary conditions. The general solution when the diode is not conducting is

$$\begin{aligned} i(t) &= \frac{V_0}{Z_2}\cos(\omega t - \theta_1) + B\mathrm{e}^{-(R/L)t}\cos(\omega_2 t + \phi)\,, \\ v_d(t) &= V_0\cos\omega t - Ri(t) - L\frac{di}{dt}(t)\,, \end{aligned} \tag{6.9}$$

where

$$\begin{aligned} Z_2^2 &:= R^2 + \left(\frac{L}{\omega}\right)^2\left(\omega^2 - \omega_0^2\right)^2\,, \quad \omega_0^2 := \frac{1}{LC}\,, \\ \theta_2 &:= \arctan\left(\frac{L\left(\omega^2 - \omega_0^2\right)}{R\omega}\right), \quad \omega_2^2 := \omega_0^2 - \left(\frac{R}{2L}\right)^2\,, \end{aligned}$$

and B and ϕ are constants determined by the boundary conditions.

We now explain how (6.7)–(6.9) are combined to model the RL-diode system studied here. The response of the system may be divided into intervals. During the n-th

interval the response is determined by the constants A_n, B_n and ϕ_n together with the time instances $t_{1,n}$, $t_{2,n}$ and $t_{3,n}$. Here $t_{1,n}$ is the time when the diode first starts to conduct fully. Equation (6.8) is then relevant. The requirement that the current through the diode and the voltage across the diode be continuous at time $t_{1,n}$ determines A_n. The time instant in the n-th cycle during which the current crosses zero is indicated by $t_{2,n}$. At this point we define

$$|I_m|_n := \max_{t\in[t_{1,n},t_{2,n}]} |i(t)| .$$

Using $|I_m|_n$ in (6.7) the time instant $t_{3,n}$ is determined as

$$t_{3,n} = t_{2,n} + \tau_{r,n} .$$

If the current at time $t_{3,n}$ passes through the diode in the reverse direction, the diode stops to conduct as from this moment in time and hence (6.9) is used from hereon to describe the dynamical behaviour. In this case B_n and ϕ_n are determined by the boundary values at time instant $t_{3,n}$. Equation (6.9) remains relevant until $v_d(t)$ reaches the value $-V_f$ once more which happens at time instant $t_{1,n+1}$. However if the current passing through the diode at time instant $t_{3,n}$ is in the forward direction, then $t_{1,n+1} = t_{3,n}$ and the next cycle commences. Thus given the initial value A_1, the current $i(t)$ is determined by the process just described.

The model for the diode in a series diode resonator circuit above proposed by Rollins and Hunt leads directly to an exact one-dimensional mapping for this nonlinear system. Successive values of $|I_m|$ may be expressed as iterations of a one-parameter family of noninvertible one-dimensional unimodal maps of the form [661]

$$|I_m|_{n+1} := f(|I_m|_n, V_0) ,$$

where $|I_m|_n$ is the maximum forward current through the diode during the n-th cycle, the parameter V_0 of the map f is the magnitude of the drive voltage, and the mapping f is given by the procedure described above. Notice in addition that f contains implicitly the circuit parameters R, L, C, τ_m and I_c which in any case are kept constant during the experiment. Using the method outlined above Rollins and Hunt reported to have modelled results and measurements previously obtained by others. Rollins and Hunt concluded that the stability of periodic orbits depends on the shape of the mapping function which, in turn, depends on the circuit parameters and V_0. They reported to have found that if either the forward bias voltage V_f, or the reverse recovery time τ_r, of the diode is set equal to zero, no bifurcations occurred and the period-1 solution was always stable.

Cascais, Dilão and Da Costa [116] studied the *RL*-varactor diode circuit shown in Figure 6.8 with $R = 5\Omega$, $L = 1\text{mH}$ and a varactor diode type BA102 with $C_0 = 50\text{pF}$ and $\phi = 0.6\text{V}$. However, they forced the system with the input signal

$$v_i(t) = U + V_0 \cos \omega t .$$

Throughout the experiment V_0 was kept constant and the bias offset of the sinusoid U was increased monotonically. They observed period-doubling, chaos, band merging and noise-free windows as for the logistic map. In addition, however they observed reverse flip bifurcations (i.e. period-halving).

Azzouz, Duhr and Hasler [46] studied the *RL*-varactor circuit in Figure 6.8 numerically with $R = 15\Omega$ and $L = 10\text{mH}$. Their simulations were performed in SPICE. The model for the diode used by SPICE contained a nonlinear resistor defined by

$$i = I_s \left(e^{v_d/nV_T} - 1 \right) ,$$

a nonlinear capacitor that models the reverse bias junction capacitance,

$$q_2 = \begin{cases} C_{j0}\phi \left(1 - (1 - v_d/\phi)^{1-m}\right)/(1-m), & \text{if } v_d < \phi \\ C_{j0}\phi/(1-m), & \text{if } v_d > \phi \end{cases} ,$$

and a nonlinear capacitor that models the transit time by

$$q_3 = \tau I_s \left(e^{v_d/nV_T} - 1 \right) ,$$

in parallel. Here, I_s is the saturation current of the diode and V_T is known as the thermal voltage and is given by

$$V_T := kT/e ,$$

where k is Boltzmann's constant, T is absolute temperature and e is the magnitude of the electron charge.

In series with this parallel combination is a resistor r_s. To model a varactor diode Azzouz *et al.* chose the following value for parameters: $I_s = 8.3 \times 10^{-15}\text{A}$, $r_s = 9.6\Omega$, $\tau = 4 \times 10^{-6}\text{s}$, $C_{j0} = 300\text{pF}$, $m = 0.4$, $n = 1$, $\phi = 0.75\text{V}$. They observed period-doubling bifurcations and chaos from their numerical experiment.

Finally, we discuss the study of the series *RL*-diode circuit (Figure 6.8) conducted by Matsumoto and coworkers in [524]. The q-v characteristics of the nonlinear capacitance for a *pn*-junction diode assumed by them is shown in Figure 6.9. The motivation for using these characteristics for the nonlinear capacitor is that it is a piecewise-linear approximation to the capacitive behaviour of a *pn*-junction diode. The function in Figure 6.9 is represented mathematically by

$$f(q) := a|q| + bq + E_0 ,$$

where

$$a := \frac{C_2 - C_1}{2C_1C_2} , \qquad b := \frac{C_1 + C_2}{2C_1C_2} .$$

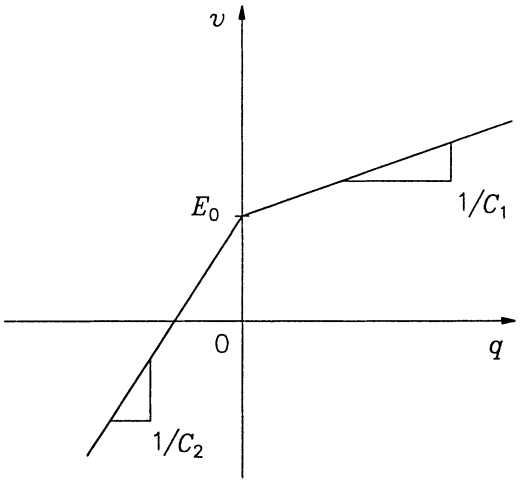

Figure 6.9: The q-v characteristics of the nonlinear capacitor.

Using this approximation, the dynamical behaviour of the circuit is described by

$$L\frac{d^2q}{dt^2} + R\frac{dq}{dt} + a|q| + bq + E_0 = E\sin\omega t\,.$$

By substituting $Q := q/E$ into the differential equation we obtain

$$L\frac{d^2Q}{dt^2} + R\frac{dQ}{dt} + a|Q| + bQ + \frac{E_0}{E} = \sin\omega t\,. \tag{6.10}$$

Notice from (6.10) that if $E_0 = 0$ then (6.10) remains unchanged as E is varied and hence the circuit will not exhibit bifurcations. Therefore, a necessary condition for the circuit to exhibit chaos, is that $E_0 \neq 0$. This is in agreement with observations made by Rollins and Hunt in [661]. Consider the case with circuit parameters,

$$R = 60\Omega\,, \qquad L = 100\mu\text{F}, \qquad \omega = 2\pi \times 700\text{krad/s},$$

$$C_1 = 0.1\mu\text{F}, \quad C_2 = 400\text{pF}, \quad E_0 = 0.1\text{V}.$$

The amplitude E of the sinusoidal driving signal was varied, and the charge q in the nonlinear capacitor observed at time instances $t = nT$ where $T := 2\pi/\omega$. This produced the bifurcation diagram shown in [524]. We repeated this numerical experiment to obtain the bifurcation diagram shown in Figure 6.10 Period-doubling, chaotic and periodic windows, can be seen in Figure 6.10. We found that for values of E in a small neighbourhood about 0.2V there are at least two coexisting periodic attractors. This can be seen by comparing Figure 6.10 with the bifurcation diagram given in [524] around $E = 0.2$V. In a small region between $E = 1.58$V and $E = 1.60$V we also noticed significant deviations from the bifurcation diagram in [524]. Here also it seems that there are coexisting attractors.

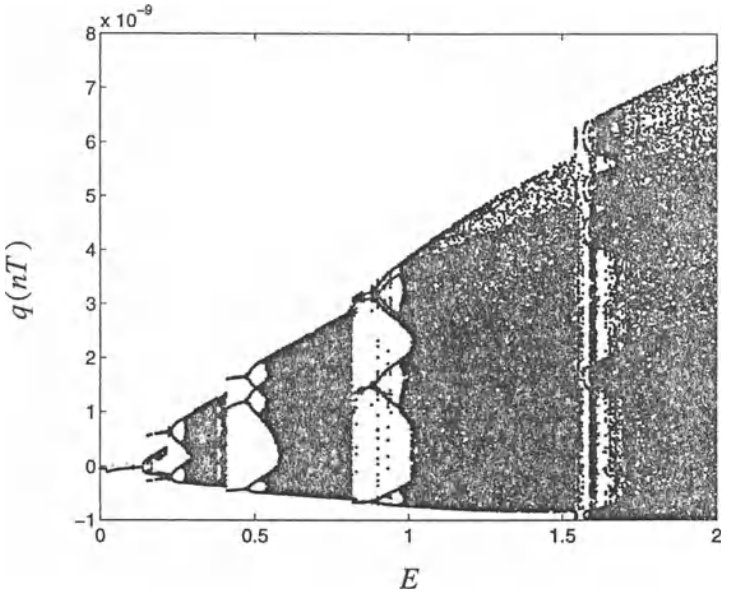

Figure 6.10: Bifurcation diagram.

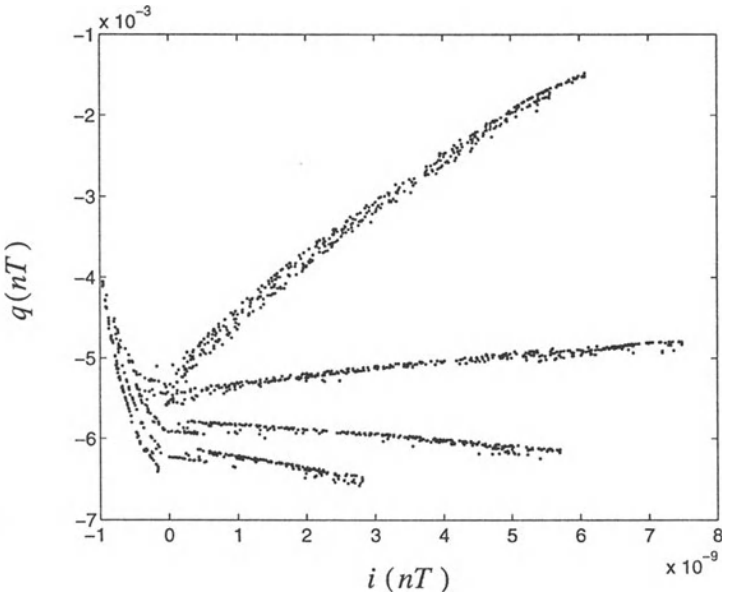

Figure 6.11: Surface of section of the chaotic attractor at $E = 2.0$V.

Strobing the state variables $q(t)$ and $i(t)$ on multiples of the interval $T = 2\pi/\omega$ we obtained the surface of section for $E = 2.0$V (see Figure 6.11). Matsumoto and his coworkers also obtained these results using an experimental RL-diode circuit. They have found that experimentally measured results were in good agreement with theoretical predictions.

Numerous studies concerning the circuit in Figure 6.8 (see [384], [103], [470], [787], [56], [281]) as well as other RLD circuits with completely different component configurations (see [76], [679], [581], [386]) have been conducted.

6.2.3 Coupled RL-Diode Circuits

To our knowledge, Gollub, Brunner and Danly [289] were the first to study coupled diode oscillators experimentally and numerically. Their experimental setup consisted of two (or more) series RL-tunnel diode oscillators (with different natural frequencies). These oscillators were then resistively coupled and/or line coupled. (The terms resistive coupling and line coupling were used in [815] and their meanings will become clear in due course.) Gollub *et al.* observed periodicity, synchronization and chaos from their circuit.

In this section however, we discuss the behaviour exhibited by the coupled RL-diode oscillators shown in Figure 6.12. The diodes used are pn-junction diodes. The discussion presented here is based on the work of Van Buskirk and Jeffries (see [815]). Here we model the pn-junction diode by a nonlinear capacitance $C(v)$ in parallel with an ideal Schockley diode with i-v characteristic,

$$i(v) = I_s \left(e^{v/V_T} - 1 \right) , \qquad V_T := kT/e ,$$

with the parameters k, T, and e as defined previously.

For a single RL-diode resonator (i.e. $N = 1$) the equation of motion is in the form of a driven damped oscillator

$$\frac{d^2 q_1}{dt^2} + a(q_1)\frac{dq_1}{dt} - f(q_1) = A_0 \sin \omega t ,$$

with nonlinear damping coefficient

$$a(q_1) := \frac{R}{L} + \frac{1}{C(q_1)} \frac{\partial i_1}{\partial v_1}(v_1(q_1)) ,$$

and nonlinear restoring force

$$f(q_1) := -\frac{1}{L} \left(v_1(q_1) + R i_1(v_1(q_1)) \right) .$$

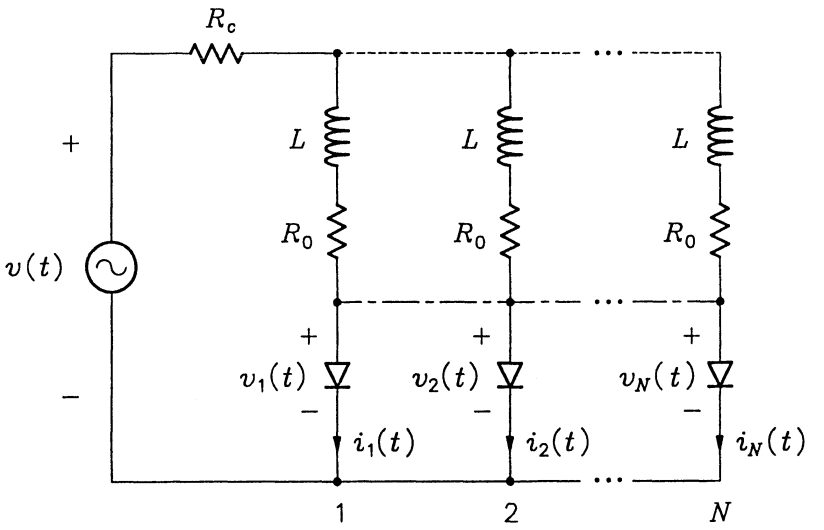

Figure 6.12: N identical RL-diode resonators resistively coupled (dotted line) or line coupled (dash-dotted line).

For positive charge q_1 (i.e. forward injection) $f(q_1) \propto -\ln(q_1 + 1)$ and is almost constant negative, while for negative q_1 there is a strong restoring force $f(q_1) \approx q_1^2$. Thus the restoring force may be viewed as resulting from an ultrasoft spring, which implies that resonant frequency of the system when driven hard can be much lower than for the small forcing case.

Van Buskirk and Jeffries [815] studied the above circuit for $N = 1, 2, 4, 12$ resonators. However, we shall restrict our discussion to the case $N = 2$. For resistive coupling, the coupled equations of motion obtained from Kirchoff's laws are

$$\frac{d^2q_1}{dt^2} + b\frac{dq_1}{dt} + r\left(\frac{dq_1}{dt} + \frac{dq_2}{dt}\right) - f(q_1) = A_0 \sin \omega t, \tag{6.11}$$

$$\frac{d^2q_2}{dt^2} + \beta\left(b\frac{dq_2}{dt} + r\left(\frac{dq_1}{dt} + \frac{dq_2}{dt}\right)\right) - f(q_2) = A_0 \sin \omega t, \tag{6.12}$$

where $r := R_c/L$ is the coupling coefficient,

$$b(q) := \frac{1}{C(q)}\frac{\partial i_1}{\partial v_1} \approx b,$$

$a = b + r$, and a small term $r\,i_2(q_2)$ (respectively $r\,i_1(q_1)$) is neglected in (6.11) (respectively (6.12)). The factor $\beta \approx 1$ is introduced to take into account small differences in the pn-junctions. From (6.11) and (6.12) it is evident that the coupling is through the diode currents via the common resistance R_c.

Concerning the resistively coupled pair of resonators, Van Buskirk and Jeffries studied the circuit in Figure 6.12 for component values: $R_0 = 53\Omega$, $L = 100\text{mH}$, $R_c = 1200\Omega$ and a 1N4723 diode. The drive frequency was $f = f_1 = 27\text{kHz}$. The bifurcation parameter was taken to be V_0, the RMS value of the drive voltage $v(t)$. The bifurcation diagram of the synchronously sampled current through diode (V_0 vs. D_1, $i_{1,n}$) is shown in [815]. After period-doubling to $f_1/2$ there occurs a Hopf bifurcation to a second incommensurate frequency of $f_2 \approx 0.22 f_1$ followed by narrow locked regions and then a wide locked region with winding number $\rho = f_1/f_2 = 9/2$. Then follows period-doubling to chaos, proceeded by an abrupt jump in attractor size, further locking etc. The first (vertically) broad smeared region passing over from left to right (in this figure) denotes the response proceeding the Hopf bifurcation. The smearing is due to the fact that f_2 is incommensurate with respect to f_1.

In an attempt to mimic the bifurcation behaviour of the experimental system, Van Buskirk and Jeffries solved the system (6.11) and (6.12) using $\beta = 19/20$, damping coefficient $b = 0.45$, coupling coefficient $r = 0.6$ and relative drive frequency $\omega = 1.5$. The bifurcation diagram of A_0 vs. $q_{1,n}$ is also shown in [815]. The model agrees with the experimentally observed data in showing first a period-doubling bifurcation, followed by a Hopf bifurcation proceeded by many narrow lockings. However, the results for the model then diverge from that of the experimental system in that the model shows more lockings, becoming wider at larger A_0 as opposed to showing a wide locking and period-doubling to chaos as for the experimental system. Van Buskirk and Jeffries also performed other experiments with the two resistively coupled resonators (see [815]). The authors reported to have observed torus breakup and crises for the resistively coupled resonators. Experimental results are presented in support. They have also studied the case of line coupling in detail. Refer to the above mentioned article for a complete discussion of the results obtained.

6.3 Triggered Astable Multivibrator

Tang *et al.* [788] studied synchronization in the context of the nonlinear phenomenon of chaos. Consider an oscillatory system whose output $x(t)$ behaves as follows. It rises steadily until some upper threshold b is reached, then it falls steadily until it reaches some lower threshold a at which point the process starts to repeat itself. Assuming that this motion is linear (which is not restricting [788]), then the equation of motion of this system is given by the ordinary differential equation

$$\frac{dx}{dt} = \begin{cases} I_0, & \text{if } \dfrac{dx}{dt} > 0, \quad x \leq b \\ -\dfrac{I_0}{\alpha}, & \text{if } \dfrac{dx}{dt} < 0, \quad x \geq a \end{cases},$$

with $0 < a < b$ the two thresholds and α is the ratio of the slopes. When the system is excited additively by a periodic narrow pulse train $d_p(t)$ with period p, the equation

then becomes

$$\frac{dx}{dt}(t^+) = \begin{cases} I_0\,, & \text{if } \dfrac{dx}{dt}(t) > 0 \text{ and } x(t) + d_p(t) < b \\ & \text{or } x(t) + d_p(t) \leq a \\ -\dfrac{I_0}{\alpha}\,, & \text{if } \dfrac{dx}{dt}(t) < 0 \text{ and } x(t) + d_p(t) > a \\ & \text{or } x(t) + d_p(t) \geq b \end{cases}$$

This elementary mathematical model is an extremely accurate description of a host of circuits, one of which is the emitter-coupled astable multivibrator. It is shown in [788] that a free-running (i.e. autonomous) astable multivibrator can be modelled by a nonlinear resistor connected in parallel with a capacitor, while a triggered (i.e. driven) multivibrator can be modelled by a nonlinear resistor, a capacitor and a pulse generator, all connected in series in a closed loop.

6.3.1 Analysis of the Model

In the following we assume without loss of generality that $a = 0$ and that both the signal $x(t)$ and the triggering pulse train $d_p(t)$ are nonnegative. Under this assumption only the upper threshold b matters. We assume that $d_p(t)$ is described by

$$d_p(t) = \begin{cases} c, & \text{if } t = np \\ 0, & \text{otherwise} \end{cases},$$

where $n \in \mathbf{N}$ and $p > 0$. Furthermore we assume

$$q < p < q + \frac{c}{I_0}\,, \tag{6.13}$$

where $q > 0$ is the free-running period of the system. The assumption $p - q < c/I_0$ ensures that a pulse will occur in the first region where it could cause switching. However if $p - q > c/I_0$ the region could be skipped, which would complicate the analysis but would not give rise to any more complicated behaviour.

We define t_n to be the time from the n-th successful triggering back to when the signal was last zero (i.e. when the last cycle started). It is easy to see that the total time between two successive successful triggers, say T, is

$$T = kq + \alpha t_n + t_{n+1}\,,$$

where $k \in \mathbf{N}_0$ and by definition

$$T = lp, \qquad l \in \mathbf{N}\,.$$

Eliminating T amongst the last two expressions, we obtain

$$lp - kq = \alpha t_n + t_{n+1}\,.$$

By the assumption (6.13) we have $k = l$ and hence

$$t_{n+1} = k(p-q) - \alpha t_n\,. \tag{6.14}$$

Under assumption (6.13) it is also obvious that

$$(k-1)(p-q) < \alpha t_n + \frac{(b-c)}{I_0} \leq k(p-q)\,,$$

and hence by the division algorithm, [288], we have

$$\alpha t_n + \frac{(b-c)}{I_0} = (k-1)(p-q) + \left(\alpha t_n + \frac{(b-c)}{I_0}\right) \pmod{(p-q)}. \tag{6.15}$$

Subtracting (6.15) from (6.14) gives

$$t_{n+1} - \frac{(b-c)}{I_0} = (p-q) - \left(\alpha t_n + \frac{(b-c)}{I_0}\right) \pmod{(p-q)}.$$

By dividing this expression throughout by $(p-q)$ and defining the dimensionless quantity

$$x_n := \frac{t_n + (b-c)/I_0}{p-q}\,,$$

we obtain the dimensionless form

$$x_{n+1} = f(x_n) := 1 - (\alpha x_n + \beta) \pmod 1, \tag{6.16}$$

where

$$\beta := \left(\frac{(\alpha+1)(b-c)}{I_0(p-q)}\right) \pmod 1.$$

We have thus derived a one-dimensional mapping which describes the original continuous-time system completely. Next we analyze (6.16) for different values of α (refer to Examples A.6, A.10 and A.32).

The case $\alpha < 1$:

When $\alpha < 1$, f has at least one fixed point and f is a contraction on each of its straight line segments. Consequently all fixed points are stable attractors of the discrete dynamical system (6.16), and every initial state is attracted to a fixed point. It is then trivial to see that these fixed points correspond to periodic solutions of the original continuous-time system, the value of k being fixed for any fixed point.

The case $\alpha = 1$:

In this case $\mathrm{Per}_2(f) = I$, that is, every point in the unit interval is of period-2 (see Example A.10). This means the circuit will be synchronized to an even multiple of p for all initial conditions except those for which $x_n = x_{n+1}$ in which case synchronization to odd multiples is possible.

The case $\alpha > 1$:

The interesting case is when $\alpha > 1$. We can see at once that all the fixed points of f are now unstable. Moreover, iterates $f^{(m)}$ of f consist of straight line segments with slope $(-\alpha)^m$ and so fixed points of all periods are unstable (refer to A.32). Therefore the original continuous-time system can have no stable periodic solutions. This implies that the mapping is always locally expansive in the sense that nearby points get pulled further and further apart, until eventually they are on opposite sides of a discontinuity of f, corresponding to being in different switching cycles of the original system. For $\alpha > 1$ we have the following result.

Proposition 6.1 Every almost-periodic orbit of $x_{n+1} = f(x_n)$, where f is defined by (6.16), is periodic.

Proof: The proof of this proposition is given in [788]. ■

In [788] it is shown that it is possible to associate with each point a kneading sequence [217] and that for the case $\alpha > 1$ the following result.

Proposition 6.2 Any two distinct points $x_1, x_2 \in [0, 1)$ have different kneading sequences.

Proof: Refer to [788]. ■

This proposition implies that the orbits of two distinct points x_1 and x_2 must separate onto different sides of a discontinuous point of f at least once. The iterates of the points may eventually come closer together again but the proposition shows that unless they coincide, they must split again. Thus any two trajectories must either coincide after a finite time or split infinitely often. They cannot approach each other asymptotically since for $\alpha > 1$ the map f is locally expansive. For the case when α is an integer, any point x in the unit interval may be described by its base-α expansion, namely

$$x = \sum_{j=1}^{\infty} \zeta_j \alpha^{-j}, \quad 0 \leq \zeta_j < \alpha \qquad \text{for each} \quad j \in \mathbf{N},$$

and (6.16) may be replaced by (i.e. is topologically equivalent to) the map

$$\zeta_{n+1} = (-\alpha \zeta_n) \pmod 1.$$

Periodic points of f correspond with rational base-α numbers (in the unit interval) in a one-to-one basis. For example, if x is a period-m point of f then $\zeta_{n+m} = \zeta_n$ for each n. The irrational numbers therefore correspond to points on nonperiodic trajectories which are locally repelling.

When α is not an integer, the problem is that while every point has some expansion in base $\lfloor \alpha \rfloor + 1$ that contains its kneading sequence, not every expansion to this base corresponds to a point on the interval. This makes it difficult to attach the expansion to the point. For further details refer to [788].

6.3.2 Numerical Results and Experimental Circuit

The power spectral density for the time response of the output obtained from the original continuous-time system was calculated for the case with parameter values

$$a = 0\,, \quad b = 2\,, \quad c = 3/4\,, \quad I_0 = 2\,, \quad \alpha = 2\,.$$

Using these parameter values we calculated the value of q as

$$q = (1 + \alpha)\frac{b}{I_0} = 3\,,$$

and we took

$$p = q + 0.99\frac{c}{I_0} = 3.3712\,.$$

The calculated power spectral density is shown in Figure 6.13.

To illustrate and confirm the chaotic behaviour predicted, a simple experimental circuit was proposed by Tang *et al.* [788]. This circuit, shown in Figure 6.14, is essentially a triggered astable multivibrator. The circuit is divided into three blocks, namely i) the trigger generator which generates the trigger pulses, ii) the nonlinear resistor (in essence the astable multivibrator and two constant current sources) and adder which adds the trigger pulses to the capacitor voltage and lastly iii) the capacitor which is charged and discharged by the two constant current sources. In the nonlinear resistor subcircuit, a standard timer integrated circuit (IC) the NE555 performs the switching between charging and discharging. The output of the NE555 jumps from 15V down to 0V whenever the threshold input reaches 10V and jumps from 0V to 15V whenever the trigger input (of the NE555 IC) falls below 5V. The two transistors act as two constant current sources. When the output of NE555 is high, Q_1 overcomes Q_2 and charges C_0 linearly. Otherwise Q_1 is off and C_0 is discharged linearly by Q_2. The first NE555 (from the left) generates the triggering signal which is added to the triangular wave signal existing across the capacitor C_0 using an operational amplifier. This signal is then fed into the trigger input of the second NE555 IC.

The circuit was setup by Tang *et al.* [788] such that

$$\alpha \approx 1.5\,, \quad q \approx 1\text{ms}\,, \quad p \approx 1.1\text{ms}\,, \quad a \approx 5\text{V}\,, \quad b \approx 12\text{V}\,, \quad c \approx 2\text{V}\,.$$

The power spectral density of the voltage across capacitor C_0 was measured by them. It agrees with the power spectral density that we have calculated numerically. For a complete discussion of experimental results the reader is referred to [788].

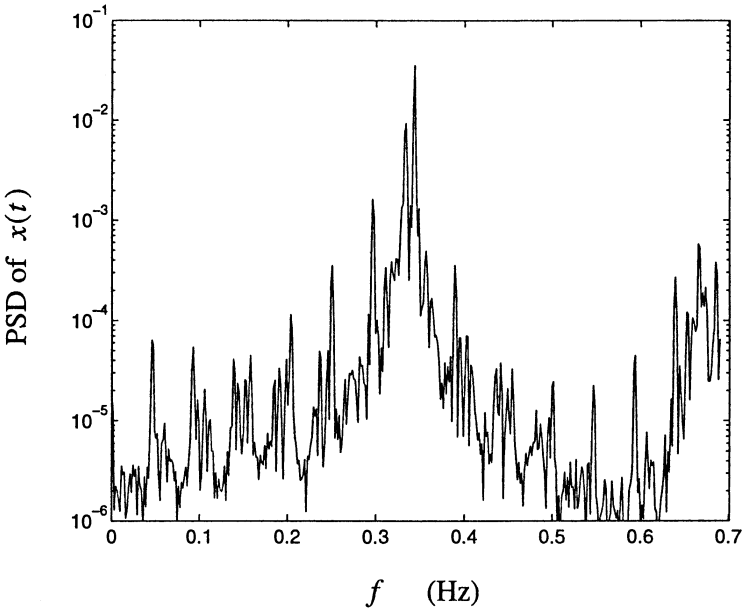

Figure 6.13: Power spectral density of the output $x(t)$.

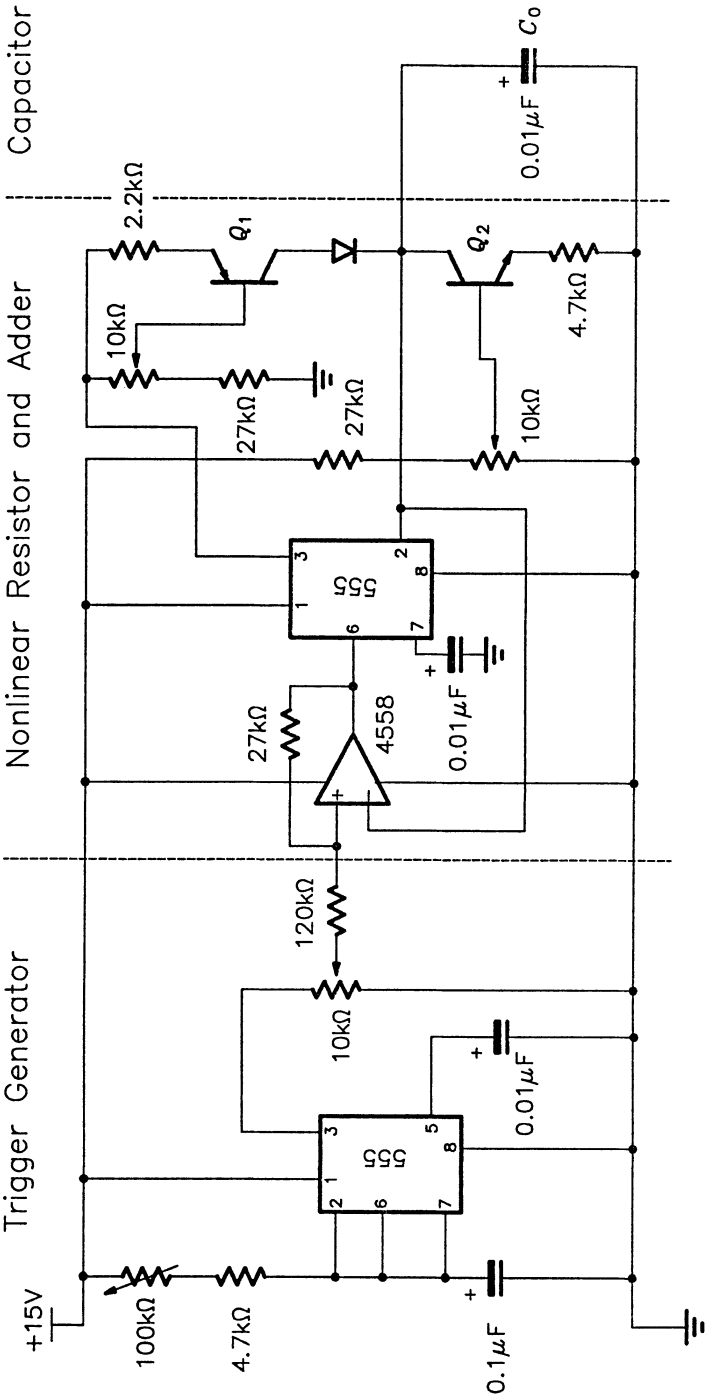

Figure 6.14: Experimental circuit studied by Tang *et al.*

6.4 Phase-Locked Loops

6.4.1 Introduction

The *Phase-Locked Loop* (PLL) was introduced in 1932 by de Bellescize [201]. Considered an exotic device in those days, it gained increased interest in the mid-sixties when it first became available as an integrated circuit. Today phase-locked loops are found in every home (in television receivers, radio equipment and modems) where they perform tasks such as frequency modulation and demodulation, frequency synthesis, data synchronization etc. A phase-locked loop is a circuit which causes a particular system's response to track the response of another one. More precisely a phase-locked loop is a circuit that synchronizes the signal generated by an oscillator with a reference or input signal both in frequency and phase. In the synchronized (or locked) state the phase error between the oscillator's output signal and the reference signal is zero, or very small. If a phase error builds up, a control mechanism acts on the oscillator in such a way that the phase error is once more reduced to a minimum thereby locking the phase of the output signal to the phase of the reference signal.

The functional block diagram of a typical phase-locked loop is shown in Figure 6.15. The phase-locked loop consists of three basic functional blocks: a *Voltage-Controlled Oscillator* (VCO), a *Phase Detector* (PD) or phase comparator and a *Loop Filter* (LF). (In some phase-locked loop circuits a current-controlled oscillator is used instead of a voltage-controlled oscillator.)

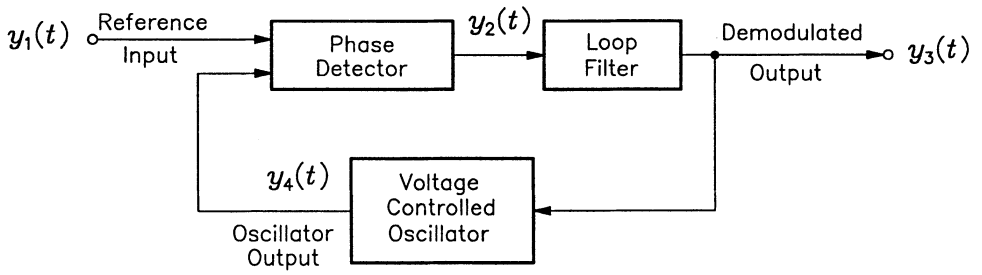

Figure 6.15: Functional block diagram of a phase-locked loop.

To describe the operation of a phase-locked loop we now assume that the phase detector and voltage-controlled oscillator operate in the linear region. Then the transfer characteristics of the phase detector and voltage-controlled oscillator are described by

$$y_2(t) = K_p(\theta_i(t) - \theta_o(t)),$$

and

$$\omega_1(t) = \omega_0 + K_v y_3(t),$$

respectively, where K_p is the gain of the phase detector in V/rad, ω_0 is the centre angular frequency in rad/s of the voltage-controlled oscillator and K_v is the voltage-controlled oscillator gain in $s^{-1}V^{-1}$.

To see how the three building blocks work together, first assume that the angular frequency of the input signal $y_1(t)$ is equal to the centre frequency or free-running frequency ω_0 of the voltage-controlled oscillator. The voltage-controlled oscillator then operates at its centre frequency ω_0. If $\phi(t)$ is zero, the output signal $y_2(t)$ of the phase detector must also be zero. Consequently the output signal of the loop filter $y_3(t)$ will also be zero. This is the condition that permits the voltage-controlled oscillator to operate at its centre frequency. However, if the phase error $\phi(t)$ were nonzero initially, the phase detector would produce a nonzero output signal $y_2(t)$. After some delay the loop filter (being a lowpass filter) would also produce a finite signal $y_3(t)$. This would cause the voltage-controlled oscillator to change its operating frequency in such a way that the phase error approaches zero and finally vanishes.

Assume now that the frequency of the input signal is increased suddenly by an amount $\Delta\omega$. The phase of the input signal then starts leading the phase of the output signal. A phase error is built up and increases with time. The phase detector develops a signal $y_2(t)$, which also increases with time. With a delay given by the loop filter, $y_3(t)$ will also rise. This causes the voltage-controlled oscillator to increase its frequency. This results in the phase error becoming smaller and after some settling time the voltage-controlled oscillator will oscillate at a frequency that is exactly the frequency of the input signal. Depending on the type of loop filter used, the final phase error will have been reduced to zero or perhaps to a small value. The voltage-controlled oscillator now operates at a frequency which is greater than its centre frequency ω_0 by an amount $\Delta\omega$. This will force the signal $y_3(t)$ to settle at a final value of $y_3 = \Delta\omega/K_0$. If the centre frequency of the input signal is frequency-modulated by an arbitrary low-frequency signal, then the output signal of the loop filter is the *demodulated signal* which is an approximation of the low-frequency modulating signal. The phase-locked loop can consequently be used as a *Frequency Modulation* (FM) detector.

6.4.2 Second-Order Phase-Locked Loop

In this section we discuss the work of Endo and Chua [238] [241] on the dynamical behaviour of a second-order phase-locked loop. By utilizing Melnikov's method, they proved that a second-order phase-locked loop used as a FM demodulator exhibits chaotic behaviour when the difference between the carrier frequency f_c of the incoming signal and the free-running frequency f_0 of the voltage-controlled oscillator is greater than the pull-in frequency f_p of the phase-locked loop. Since the operation of a phase-locked loop as a FM demodulator is described widely in the literature [775] [349] [238], we shall not discuss it here.

Derivation of the Dynamical Equation

Next we derive the nonlinear differential equation governing the phase-locked loop's dynamics. Suppose the input signal is a periodic waveform defined by

$$y_1(t) = f_1(\theta_i(t)),$$

where $f_1 : \mathbf{R} \to \mathbf{R}$ is some function describing the basic waveform of the signal y_1 and $\theta_i(t) \in [0, 2\pi)$. The voltage-controlled oscillator output will also be a periodic waveform of the following form

$$y_4(t) = f_4(\theta_o(t)),$$

where $f_4 : \mathbf{R} \to \mathbf{R}$ and $\theta_o(t) \in [0, 2\pi)$. The commonly employed waveforms f_1 and f_4 are sinusoidal, square and pulse waveforms.

The phase detector produces an output $y_2(t)$ proportional to the phase difference between y_1 and y_4 i.e.

$$y_2(t) = K_p h(\phi(t)), \tag{6.17}$$

where $\phi(t) \in [0, 2\pi)$ is defined by

$$\phi(t) := \theta_i(t) - \theta_o(t), \tag{6.18}$$

and is called the *phase error*. Here h is usually a sine wave, triangular wave or a sawtooth wave, depending on the waveforms y_1 and y_4 and the type of phase detector used (see [238]).

Consider as the loop filter a linear time-invariant bandpass filter with transfer characteristic function

$$F(D) := \frac{1 + \tau_2 D}{1 + \tau_1 D}, \tag{6.19}$$

where $D := d/dt$. If $\tau_2 = 0$ then the filter is a first-order lowpass filter. Therefore the input-output characteristic of the loop filter is then given by

$$y_3(t) = F(D)y_2(t). \tag{6.20}$$

The voltage-controlled oscillator is assumed to be described by the first-order linear ordinary differential equation

$$\frac{d\theta_o}{dt} = \omega_0 + K_v y_3(t), \tag{6.21}$$

where ω_0 is the free-running angular frequency of the voltage-controlled oscillator. From the results of (6.17)–(6.21), we can model the phase-locked loop as shown in Figure 6.16. This is called the *phase model* of the phase-locked loop where

$$\alpha_i(t) := \theta_i(t) - \omega_0 t, \qquad \alpha_o(t) := \theta_o(t) - \omega_0 t,$$

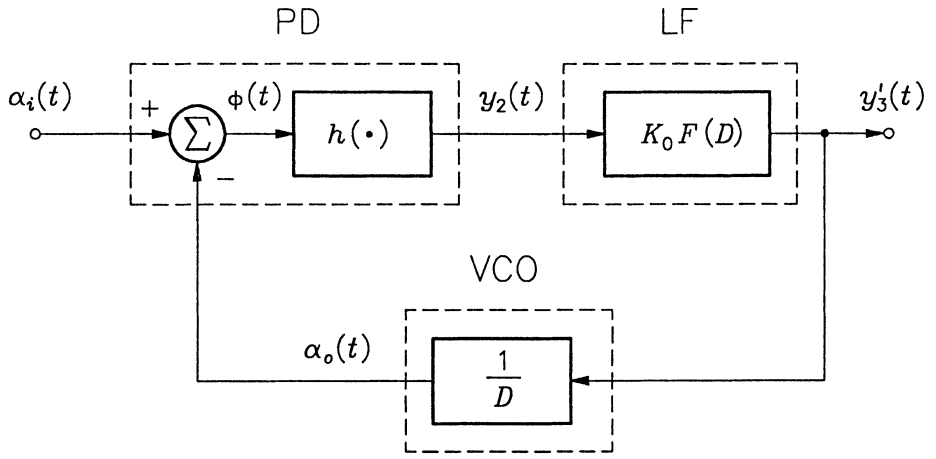

Figure 6.16: Phase model of a phase-locked loop.

which enable us to write (6.21) as

$$\frac{d\alpha_0}{dt} = K_v y_3(t)\,.$$

For simplicity, the gains K_p and K_v are combined to give the total loop gain $K_0 := K_p K_v$ which is associated with $F(D)$ and $y_3'(t) := K_v y_3(t)$ in the block diagram depicted in Figure 6.16. From the block diagram we derive the following nonautonomous second-order nonlinear differential equation

$$\frac{d^2\phi}{dt^2} + \frac{1}{\tau_1}\left(1 + K_0\tau_2\frac{dh}{d\phi}(\phi)\right)\frac{d\phi}{dt} + \frac{K_0}{\tau_1}h(\phi) = \frac{d^2\alpha_i}{dt^2} + \frac{1}{\tau_1}\frac{d\alpha_i}{dt}\,.$$

Assuming that the input signal is modulated by a sinusoidal waveform about some centre carrier frequency ω_c so that

$$\frac{d\theta_i}{dt} = \omega_c + M\sin\omega_m t\,,$$

and hence we have

$$\frac{d\alpha_i}{dt} = \Delta\omega + M\sin\omega_m t\,,$$

where $\Delta\omega := \omega_c - \omega_0$. Here M is the maximum instantaneous carrier frequency deviation and ω_m the frequency of the modulating signal.

We assume (without loss of generality) that $(dh/d\phi)(0) = 1$. Then for the linearized system (obtained by putting $h(\phi) = \phi$) we define the natural angular frequency ω_n and the damping ratio respectively by

$$\omega_n := \sqrt{\frac{K_0}{\tau_1}}\,, \qquad \zeta := \frac{(1 + K_0\tau_2)}{2\sqrt{K_0\tau_1}}\,.$$

By using the above definitions and the following definitions

$$\begin{aligned}
\beta &:= \frac{\omega_n}{K_0} \text{ (normalized natural frequency)},\\
\sigma &:= \frac{\Delta\omega}{\omega_n} \text{ (normalized frequency detuning)},\\
\Omega &:= \frac{\omega_m}{\omega_n} \text{ (normalized modulation frequency)},\\
m &:= \frac{M}{\omega_n} \text{ (normalized maximum frequency)},\\
\tau &:= \omega_n t \text{ (normalized time)},
\end{aligned}$$

we obtain the normalized differential equation

$$\begin{aligned}
\frac{d^2\phi}{d\tau^2} + \beta\left(1 + \left(\frac{2\zeta - \beta}{\beta}\right)\frac{dh}{d\phi}(\phi)\right)\frac{d\phi}{d\tau} \;&+\; h(\phi) = \\
\beta\sigma \;&+\; \beta m \sin\Omega\tau + m\Omega\cos\Omega\tau\,, \qquad (6.22)
\end{aligned}$$

where we have used

$$\beta = \frac{1}{\omega_n\tau_1} = \frac{1}{\sqrt{K_0\tau_1}}.$$

Now we have $2\zeta - \beta = K_0\tau_2\beta$ and hence it is clear that $2\zeta - \beta > 0$ (equivalently $\tau_2 > 0$) for the bandpass filter case and $2\zeta - \beta = 0$ (equivalently $\tau_2 = 0$) for the lowpass filter case.

Analysis of the Phase-Locked Loop

In this section we analyze (6.22) by Melnikov's method for two cases: when the unperturbed system is Hamiltonian, and when it is non-Hamiltonian. For the case when the unperturbed system is Hamiltonian the analysis will only be given for the sinusoidal phase detector function

$$h(\phi) = \sin\phi\,.$$

For the analysis of the case where h is a triangular function of the form

$$h(\phi) = \begin{cases} \dfrac{-a(\pi+\phi)}{(\pi-a)}, & \text{if} \quad \phi < -a \\ \phi, & \text{if} \quad -a < \phi < a \\ \dfrac{a(\pi-\phi)}{(\pi-a)}, & \text{if} \quad \phi > a \end{cases}, \qquad (6.23)$$

with $a > 0$ and $h(\pi + 2\pi n) = h(\pi)$, $n \in \mathbf{Z}$ the condition for homoclinic intersection will only be stated. A detailed derivation for this case is given in [238].

However before we commence we first identify the fixed points (and the stability properties thereof) for the autonomous system. In the case of the phase-locked loop the autonomous system corresponds to the case when the input is grounded so that the voltage-controlled oscillator of the phase-locked loop is running free. This implies that $m = \sigma = 0$ and hence (6.22) reduces to the following homogeneous differential equation,

$$\frac{d^2\phi}{d\tau^2} + \beta\left(1 + \left(\frac{2\zeta - \beta}{\beta}\right)\frac{dh}{d\phi}(\phi)\right)\frac{d\phi}{d\tau} + h(\phi) = 0\,, \tag{6.24}$$

which describes the autonomous phase-locked loop. Putting

$$\frac{d^2\phi}{d\tau^2} = \frac{d\phi}{d\tau} = 0\,,$$

in this differential equation and solving for the fixed points, we obtain (considering $\tau \in S^1$)

$$\mathbf{x}_c := (0,0)^T\,, \qquad \mathbf{x}_s := (\phi_{0,s}, 0)^T\,, \qquad (\mathbf{x} := (\phi, d\phi/dt)^T),$$

where $h(\phi_{0,s}) = 0$, i.e. $\phi_{0,s} = \pi$. To derive the stability properties of the two fixed points we notice that (6.24) may be cast in the form

$$\frac{d^2\phi}{d\tau^2} + u(\phi, d\phi/d\tau) + v(\phi) = 0\,,$$

where

$$u(\phi, d\phi/d\tau) := \beta\left(1 + \left(\frac{2\zeta - \beta}{\beta}\right)\frac{dh}{d\phi}(\phi)\right)\frac{d\phi}{d\tau}\,, \qquad v(\phi) := h(\phi)\,.$$

The system's change in total energy from time τ_0 to time τ can be shown to be given by [410]

$$\mathcal{E}(\tau) - \mathcal{E}(\tau_0) = -\int_{\tau_0}^{\tau} \frac{d\phi}{d\tau} u(\phi, d\phi/d\tau)\, d\tau\,.$$

This expression may be used to comment on the global stability of the system. The potential energy of the system is given by [410]

$$\mathcal{V}(\phi) = \int v(\phi)\, d\phi\,,$$

which can be used to comment on the stability of the fixed points. For the sinusoidal phase detector function it follows that $\mathcal{V}(\phi) = -\cos\phi$ and hence $\mathcal{V}(0)$ is a local minimum of the potential energy function $\mathcal{V}(\phi)$ and hence $\mathbf{x}_c$ is a centre fixed point and consequently stable. On the other hand $\mathcal{V}(\phi_{0,s})$, is a local maximum of the potential energy and therefore $\mathbf{x}_s$ is a saddle fixed point and thus unstable. For the case of a triangular wave phase detector function we also have that $\mathbf{x}_c$ is a centre and $\mathbf{x}_s$ is a saddle point.

The Hamiltonian Case If we regard β, ζ and m in (6.22) to be of ϵ-order, then (6.22) is of the form

$$\frac{d\mathbf{x}}{d\tau} = \mathbf{f}(\mathbf{x}) + \epsilon \mathbf{g}(\mathbf{x}, \tau)\,,$$

where

$$\mathbf{f}(\mathbf{x}) := \begin{pmatrix} y \\ -h(\phi) \end{pmatrix},$$

$$\epsilon \mathbf{g}(\mathbf{x}, \tau) := \begin{pmatrix} 0 \\ -\beta\left(1 + \left(\frac{2\zeta}{\beta} - 1\right)\frac{dh}{d\phi}(\phi)\right) y + \beta\sigma + m\beta \sin \Omega\tau + m\Omega \cos \Omega\tau \end{pmatrix},$$

with $\mathbf{x} := (\phi, y) \in S^1 \times \mathbf{R}$. The unperturbed system is Hamiltonian with Hamiltonian function

$$H(\phi, y) = \frac{1}{2}y^2 - \cos\phi\,.$$

The unperturbed system has a saddle fixed point of

$$\mathbf{x}_s^T := (\phi_s, y_s) = (\pi, 0)\,,$$

and two E-homoclinic trajectories (Γ_0^u for upper one and Γ_0^l for lower one) in the cylindrical coordinate system $(\phi, y) \in S^1 \times \mathbf{R}$, given explicitly by

$$\begin{aligned} \Gamma_0^u &= \{(\phi_0(t), y_0(\tau)) = (2\arcsin(\tanh\tau), 2\operatorname{sech}\tau) \mid \tau \in \mathbf{R}\}\,, \\ \Gamma_0^l &= \{(\phi_0(\tau), y_0(\tau)) = (2\arcsin(\tanh\tau), -2\operatorname{sech}\tau) \mid \tau \in \mathbf{R}\}\,. \end{aligned}$$

In order to find conditions for the existence of P-homoclinic trajectories of the perturbed system, we apply Melnikov's method. The corresponding Melnikov integral is

$$\begin{aligned} M(t_0) = & -4\beta \int_{-\infty}^{\infty} \operatorname{sech}^2 t\, dt \\ & - 4(2\zeta - \beta) \int_{-\infty}^{\infty} \operatorname{sech}^2 t \cos(2\arcsin(\tanh t))\, dt \\ & \pm 2\beta\sigma \int_{-\infty}^{\infty} \operatorname{sech} t\, dt \\ & \pm 2(m\beta \cos \Omega t_0 - m\Omega \sin \Omega t_0) \int_{-\infty}^{\infty} \operatorname{sech} t \sin \Omega t\, dt \\ & \pm 2(m\beta \sin \Omega t_0 + m\Omega \cos \Omega t_0) \int_{-\infty}^{\infty} \operatorname{sech} t \cos \Omega t\, dt \end{aligned}$$

$$= -\frac{16}{3}(\beta+\zeta) \pm 2\beta\sigma\pi + 2m\pi \operatorname{sech}\left(\frac{\pi\Omega}{2}\right)\sqrt{\beta^2+\Omega^2}\,\sin(\Omega t_0+\theta), \tag{6.25}$$

where $\theta := \arctan(\Omega/\beta)$ and where the + sign is for Γ_0^u and the − sign for Γ_0^l. Thus the condition for the existence of P-homoclinic trajectories of the perturbed system is

$$\left|\frac{((16/3)(\beta+\zeta) \mp 2\beta\sigma\pi)\cosh(\pi\Omega/2)}{2m\pi\sqrt{\beta^2+\Omega^2}}\right| \leq 1,$$

where the − sign is for Γ_0^u and the + sign for Γ_0^l. The strict inequality corresponds to transversal homoclinic intersections while the strict equality corresponds to the case when homoclinic tangencies occur.

For the triangular phase detector function (i.e. where h is of the form described by (6.23)), homoclinic intersections are guaranteed by the condition (see [238])

$$\left|\frac{2a\zeta\pi \arcsin\sqrt{a/\pi} + \pi\beta\sqrt{a(\pi-a)} \mp 2\pi\beta\sigma}{2m\sqrt{\beta^2+\Omega^2}\,Q(a,\Omega)}\right| \leq 1, \tag{6.26}$$

(here the − sign is for Γ_0^u and + sign for Γ_0^l) where

$$Q(a,\Omega) := \frac{(1+b)(a\cos\Omega t_1 - \Omega\sqrt{a(\pi-a)}\,\sin\Omega t_1}{(1-\Omega^2)(b+\Omega^2)},$$

$$b := \frac{a}{\pi-a}, \quad t_1 := \arcsin\sqrt{\frac{a}{\pi}}, \quad \Omega \neq 1.$$

The strict inequality ensures transversal intersection while the strict equality leads to homoclinic tangency.

The Non-Hamiltonian Case If we regard only m, but not β and ζ to be of ϵ-order, then the unperturbed system becomes non-Hamiltonian. In this case

$$\mathbf{f}(\mathbf{x}) = \begin{pmatrix} y \\ -h(\phi) - \beta\left(1 + \left(\frac{2\zeta}{\beta} - 1\right)\frac{dh}{d\phi}(\phi)\right)y + \beta\sigma_c \end{pmatrix},$$

$$\epsilon\mathbf{g}(\mathbf{x},\tau) = \begin{pmatrix} 0 \\ \beta\Delta\sigma + m\beta\sin\Omega\tau + m\Omega\cos\Omega\tau \end{pmatrix},$$

where $\sigma = \sigma_c + \Delta\sigma$ with σ_c the critical detuning at which there exists an upper E-homoclinic trajectory for the unperturbed system and $\Delta\sigma$ is a small deviation from σ_c. Endo *et al.* [243] [241] described a numerical scheme for calculating σ_c.

No analytical solution exists for the associated E-homoclinic trajectory in general. However, for the case of a triangular phase detector function, Endo and Chua [236] have derived an expression by means of piecewise-linear analysis.

To find the condition for the existence of a P-homoclinic trajectory for the perturbed system we apply Melnikov's method. The associated Melnikov integral was calculated in Section 2.5 on Melnikov's method (see Example 2.41) and led to the following conditions for the existence of a P-homoclinic trajectory for the perturbed system,

$$\begin{aligned} \lambda_s + \beta - (2\zeta - \beta)a' &< 0\,, \\ \lambda_u + \beta - (2\zeta - \beta)a' &> 0\,, \\ \left| \frac{\beta \Delta \sigma I_3}{m\sqrt{(\beta^2 + \Omega^2)\left([I_1(\Omega)]^2 + [I_2(\Omega)]^2\right)}} \right| &\leq 1\,, \end{aligned}$$

where all symbols appearing in the above expressions are defined in Example 2.41.

Numerical Verification

Endo and Chua [238] verified numerically that the phase-locked loop equation exhibits chaotic behaviour. They calculated numerically the stable and unstable manifolds of the perturbed saddle fixed point for the cases of homoclinic tangencies and homoclinic intersections. They found the parameter values for homoclinic tangencies and intersections obtained from theoretical predictions to be in good agreement with the observations made from their numerical results. They also calculated power spectra for different parameter values. In this section we present some of the numerical results obtained by Endo and Chua. Specifically, we investigate the phase-locked loop with a lowpass filter (i.e. $\beta = 2\zeta$) as loop filter and with a triangular phase detector function as in (6.23) with $a = \pi/2$. We choose $\beta = 0.01$, $\Omega = 4$ and $\sigma = 0.8$ which results in the unperturbed system being Hamiltonian. Using the criterion for the existence of P-homoclinic trajectories, (6.26), we see that for the above parameter values $m = 0.3$ corresponds to the case when there are no intersections while for $m = 0.62$ transversal intersections are predicted. Indeed, computer generated Poincaré maps for the α- and ω-branches of the homoclinic trajectory extending from the saddle fixed point support these predictions (see [238]). The power spectral densities for these two cases are shown in Figure 6.18. It is clear that the phase-locked loop does not behave chaotically for $m = 0.3$. However, for $m = 0.62$ the broadband component hints that the phase-locked loop exhibits chaotic behaviour. For results on the case when the unperturbed system is non-Hamiltonian see [238]. Numerous other numerical experiments have been conducted by Endo and Chua. For more detail concerning this, the reader is referred to [238] and [241].

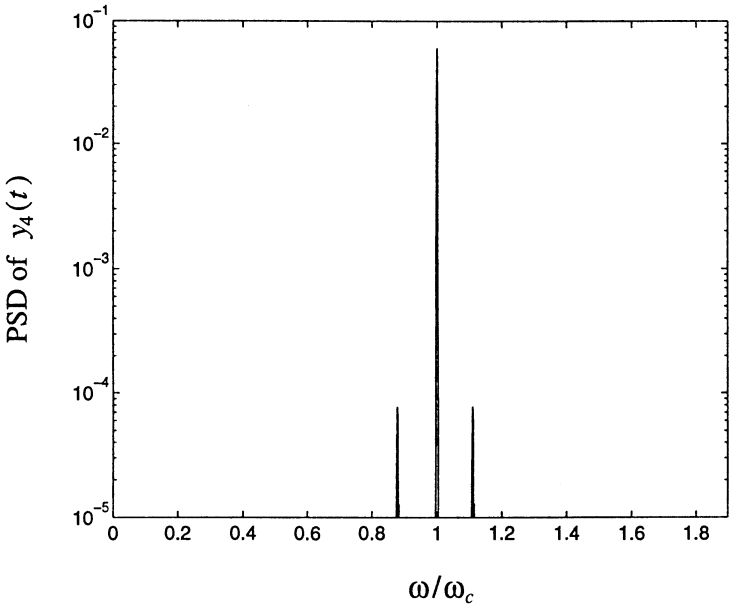

(a)

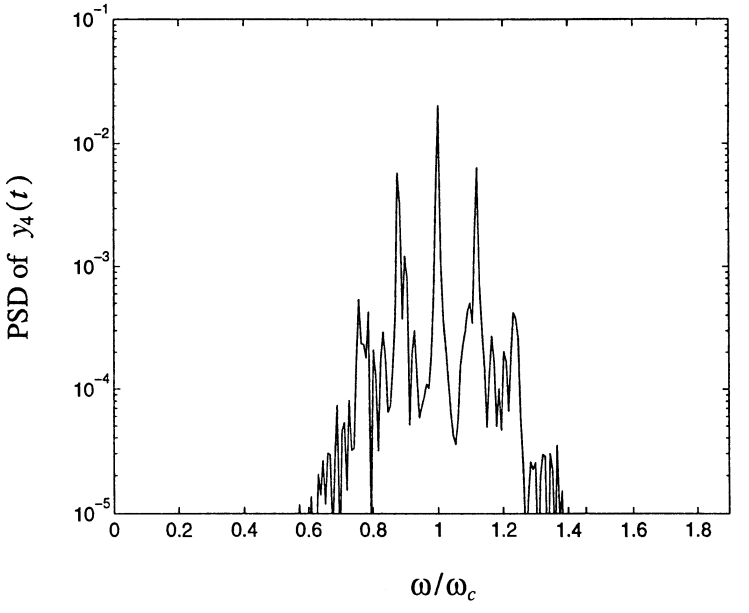

(b)

Figure 6.17: Power spectral density at the voltage-controlled oscillator output for $\beta = 0.01$, $\Omega = 4$, $\sigma = 0.8$: (a) $m = 0.3$ (nonchaotic); (b) $m = 0.62$ (chaotic).

Experimental Verification

Endo and Chua [238] designed and built an experimental phase-locked loop circuit for the purpose of comparing experimental results with the theoretical results. Their circuit is shown in Figure 6.18. The phase-locked loop design equations obtained from the databook are [238]:

$$
\begin{aligned}
f_0 &= \frac{1}{3.7R_0C_0} = 6550\text{Hz (voltage-controlled oscillator's centre frequency)}, \\
K_0 &= \frac{33.6f_0}{V_c} = 18200\text{s}^{-1}\text{V}^{-1} \text{ (total loop gain)}, \\
f_H &= \pm\frac{8f_0}{V_c} = \pm 4366\text{Hz (lock range)}, \\
f_p &= \pm\frac{1}{2\pi}\sqrt{\frac{2\pi f_H}{R_1C_1}} = \pm\frac{0.4393}{\sqrt{C_1}} \text{ (pull-in range)}, \\
f_n &= \frac{1}{2\pi}\sqrt{\frac{K_0}{R_1C_1}} = \frac{0.3578}{\sqrt{C_1}} \text{ (natural frequency)}, \\
\zeta &= \frac{1}{2}\sqrt{\frac{1}{R_1C_1K_0}} = \frac{6.177\times 10^{-5}}{\sqrt{C_1}} \text{ (damping ratio)}.
\end{aligned}
$$

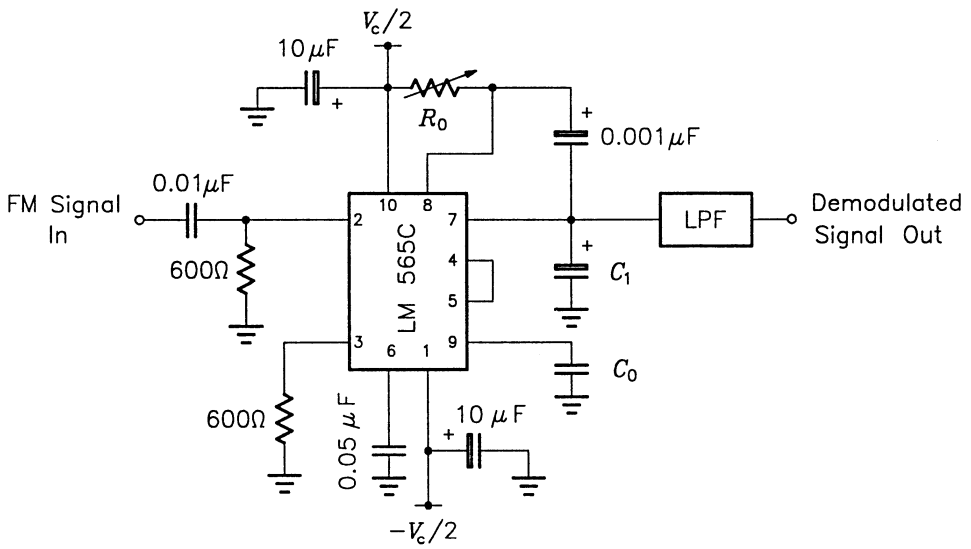

Figure 6.18: Experimental phase-locked loop circuit studied by Endo and Chua. Here $V_c = 12\text{V}$, $R_0 = 12.5\text{k}\Omega$, $C_0 = 0.0033\mu\text{F}$, $R_1 = 3.6\text{k}\Omega$.

For $C_1 = 1.92\mu$F we have $\beta = 0.089$ ($f_n = 258$Hz, $f_p \approx 317$Hz). The other variables f_m and Δf were set to $f_m = 1032$Hz and $\Delta f = 379$Hz giving $\Omega = 4$ and $\sigma = 1.47$. Experimentally it was found for $m < 0.5$ that the phase-locked loop is not chaotic. For m greater than 0.5 the output of the voltage-controlled oscillator may or may not be chaotic, depending on the initial conditions. Both nonchaotic (in-lock) states and chaotic (out-of-lock) states were observed for values of m up to nearly 8. For increasing m from 0.5 to 8 the power spectral density at the voltage-controlled oscillator's output for chaotic response gradually becomes broader. For values of m greater than 8 the phase-locked loop is chaotic only (see [238] for experimental results).

Endo and Chua then selected $C_1 = 0.0489\mu$F which yields $\beta = 0.56$ ($f_n = 1618$Hz, $f_p = 1986$Hz). The input signal's modulation was decreased to $m = 2.2 \times 10^{-4}$. In this case the phase-locked loop was in out-of-lock state, the phase-locked loop's response was fully chaotic. The reader is referred to Endo *et al.* [238] [241] for detailed discussions of all experiments performed by the authors.

Further Work

Endo *et al.* [241] further extended their results for the non-Hamiltonian case. They identified the possible region of chaos for the phase-locked loop equation. In particular they calculated boundary curves numerically in the $(\Omega, m/\Delta\sigma)$-plane which correspond to the onset of homoclinic tangency. This was done for various β and ζ. Poincaré maps were drawn for various parameter values for which homoclinic tangency is predicted by these boundary curves. These results were found to be in good agreement with theoretical predictions.

In 1990 Endo and Chua [237] reported on bifurcation diagrams and fractal basin boundaries for the phase-locked loop equation. They applied a numerical algorithm [420] to derive the bifurcation sets. This algorithm is based on Newton's method for calculating fixed points of the Poincaré map together with the parameter values satisfying the conditions for bifurcations. They obtained detailed one-parameter and two-parameter bifurcation diagrams. Using these bifurcation diagrams they were able to identify and confirm various routes to chaos. They investigated the relationship between the homoclinicity and the fractal basin boundary. The conclusion was reached that the random behaviour of the phase-locked loop in the out-of-lock state was indeed a form of horseshoe chaos spawned by homoclinic trajectories and that the routes to this chaos include an infinite sequence of period-doubling cascade and intermittency.

In 1990 Chu *et al.* [137] studied a third-order phase-locked loop (a phase-locked loop with a second-order loop filter) for tracking frequency-variant signals. By considering this system to be a slowly varying oscillator they were able to prove that the third-order phase-locked loop can exhibit chaotic behaviour. Using Melnikov's method they proved that this phase-locked loop circuit has transversal P-homoclinic trajectories

under certain conditions. In addition they calculated the Lyapunov exponents and Lyapunov dimension to confirm that the phase-locked loop is indeed chaotic for those parameter values for which the theory predicts homoclinic intersections. Boundary curves for the region of transversal homoclinicity were calculated and drawn.

A thorough treatment of a second-order phase-locked loops with a phase detector with triangular phase detector function is given in [236]. In the report [236] a piecewise-linear method was used to derive the Melnikov integral analytically for various cases which included the case of high dissipation. With the analytical expressions available they have been able to evaluate numerical results obtained in previous reports mentioned above.

In 1993 Bradley [95] reported on the constructive utilization of chaos to solve problems experienced with phase-locked loops. Bradley has shown that chaos in phase-locked loops may be exploited to broaden the capture range of a phase-locked loop. An external modulating input is used to throw the unlocked phase-locked loop into a chaotic regime that overlaps with the original capture range. The chaos-inducing modulation is then turned off, allowing the loop's original dynamics to capture the signal.

6.4.3 Coupled Phase-Locked Loops

Mutually interconnected networks of phase-locked loops are frequently used in communication systems. They are designed for achieving synchronization between geographically separated timing clocks [490], [215], [844]. Coupled phase-locked loops have been studied in connection with chaos in [239] and [240] by Endo and Chua. In [240] two phase-locked loops are driven by a master phase-locked loop which is chaotic. It was found that under suitable conditions the two driven phase-locked loops (which are not completely identical) synchronize. Synchronization was achieved only when the Lyapunov exponents of both the driven phase-locked loops are negative [627]. Numerical and experimental results were presented in [240]. In [239] two mutually coupled phase-locked loops were studied numerically and experimentally by Endo and Chua. We review some of their results in this section.

Analytical Model

The configuration of the phase-locked loops which they have studied is shown in Figure 6.19 below. The voltage-controlled oscillator output of PLL 2 is applied to the input of PLL 1 and the inverted voltage-controlled oscillator output of PLL 1 applied to the input of PLL 2. The phase-detector functions or the two phase-locked loops

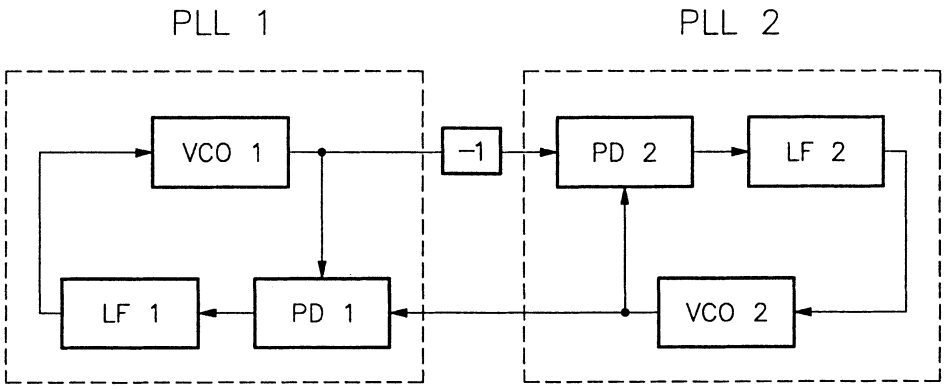

Figure 6.19: Block diagram of two mutually coupled phase-locked loops studied by Endo and Chua.

are identical and are described by

$$h(\phi) = \begin{cases} -\phi - \pi, & \text{if} \quad -\pi \leq \phi < -\pi/2 \\ \phi, & \text{if} \quad |\phi| \leq \pi/2 \\ -\phi + \pi, & \text{if} \quad \pi/2 < \phi < \pi \end{cases}, \tag{6.27}$$

with $h(\pi + n2\pi) = h(\pi)$. The loop filters are simple RC lowpass filters described by the transfer operators,

$$F_i(D) := \frac{1}{1 + R_i C_i D}, \qquad i = 1, 2.$$

From Figure 6.19 the following fourth-order system of nonlinear autonomous ordinary differential equation can be obtained [239]

$$\begin{aligned} \frac{d^2\phi_1}{dt^2} + \frac{1}{\tau_1}\frac{d\phi_1}{dt} + \frac{K_1}{\tau_1} h(\phi_1 - \phi_2) &= \frac{\omega_1}{\tau_1}, \\ \frac{d^2\phi_2}{dt^2} + \frac{1}{\tau_2}\frac{d\phi_2}{dt} + \frac{K_2}{\tau_2} h(\phi_2 - \phi_1) &= \frac{\omega_2}{\tau_2}, \end{aligned}$$

where K_i, ω_i and $\tau_i := R_i C_i$ denotes the total loop gain, free-running angular frequency and time constant respectively of the i-th phase-locked loop. Substituting

$$\alpha_i := \phi_i - \omega t, \qquad i = 1, 2,$$

into the above system of differential equations yields

$$\frac{d^2\alpha_1}{dt^2} + \frac{1}{\tau_1}\frac{d\alpha_1}{dt} + \frac{K_1}{\tau_1} h(\alpha_1 - \alpha_2) = \frac{\Delta\omega}{\tau_1}, \tag{6.28}$$

$$\frac{d^2\alpha_2}{dt^2} + \frac{1}{\tau_2}\frac{d\alpha_2}{dt} + \frac{K_2}{\tau_2} h(\alpha_2 - \alpha_1) = \frac{\Delta\omega}{\tau_2}, \tag{6.29}$$

where ω is called the synchronized angular frequency (which is still to be determined) and $\Delta\omega_i$ denotes the frequency detuning of the i-th phase-locked loop defined by

$$\Delta\omega_i := \omega_i - \omega\,, \qquad i = 1,\, 2\,. \tag{6.30}$$

The fixed points of the system (6.28) and (6.29) are those states for which the two phase-locked loops are phase locked. The fixed points of the system (6.28) and (6.29) are described by

$$h(\alpha_1 - \alpha_2) = \frac{\Delta\omega_1}{K_1}\,, \qquad h(\alpha_2 - \alpha_1) = \frac{\Delta\omega_2}{K_2}\,. \tag{6.31}$$

Referring to (6.27) we note that there may either be none, one, two or three fixed points. Now, since h is an odd function, (6.31) yields

$$\frac{\Delta\omega_1}{K_1} + \frac{\Delta\omega_2}{K_2} = 0\,, \tag{6.32}$$

from which we conclude that $\Delta\omega_1 = 0$ if and only if $\Delta\omega_2 = 0$. Looking back at (6.31) we now realize that

$$\alpha_2 - \alpha_1 = n\pi, \qquad n \in \mathbf{Z}\,, \tag{6.33}$$

if and only if $\Delta\omega_1 = \Delta\omega_2 = 0$. Thus, for the outputs of the voltage-controlled oscillators to be in phase (a special case of (6.33) with $n = 0$) the free-running frequencies of the two voltage-controlled oscillators must be identical. Before continuing this discussion we see that substituting (6.30) in (6.32) gives an expression for the synchronized angular frequency, namely

$$\omega := \frac{K_2\omega_1 + K_1\omega_2}{K_1 + K_2}\,.$$

Now, returning to our discussion, we note that the case where no fixed point exists corresponds to those situations when (from (6.31))

$$\max_{\phi} |h(\phi)| = \frac{\pi}{2} < \left|\frac{\Delta\omega_i}{K_i}\right|\,, \quad i = 1,\, 2\,. \tag{6.34}$$

From (6.34) we derive the condition for synchronization (lock range) in the form

$$\frac{|\omega_1 - \omega_2|}{K_1 + K_2} < \frac{\pi}{2}\,, \tag{6.35}$$

where we have used

$$\begin{aligned} \Delta\omega_1 &:= \left(\frac{K_1}{K_1 + K_2}\right)(\omega_2 - \omega_2)\,, \\ \Delta\omega_2 &:= \left(\frac{K_2}{K_1 + K_2}\right)(\omega_2 - \omega_1)\,. \end{aligned}$$

In order to obtain (6.28) and (6.29) in normalized form we define the normalized time to be

$$\tau := \sqrt{\frac{K_1}{\tau_1}}\,t\,, \tag{6.36}$$

and the state variables

$$x_1 := \alpha_1\,, \quad x_2 := \frac{d\alpha_1}{dt}\,, \quad x_3 := \alpha_2\,, \quad x_4 := \frac{d\alpha_2}{dt}\,. \tag{6.37}$$

Using (6.36) and (6.37) we then rewrite (6.28) and (6.29) in the following normalized form

$$\frac{dx_1}{d\tau} = x_2\,, \tag{6.38}$$

$$\frac{dx_2}{d\tau} = \delta - 2\zeta_1 x_2 - h(x_1 - x_3)\,, \tag{6.39}$$

$$\frac{dx_3}{d\tau} = x_4\,, \tag{6.40}$$

$$\frac{dx_4}{d\tau} = -\frac{r_1}{r_2}\delta - 2\sqrt{\frac{r_1}{r_2}}\,\zeta_2 x_4 - \frac{r_1}{r_2}h(x_3 - x_1)\,, \tag{6.41}$$

where

$$\zeta_i := \frac{1}{2\sqrt{K_i \tau_i}}\,, \qquad i = 1, 2\,,$$

is the damping ratio of the i-th phase-locked loop,

$$\delta := \frac{\omega_1 - \omega_2}{K_1 + K_2}$$

defines the detuning between the phase-locked loops and

$$r_1 := \frac{K_2}{K_1}, \qquad r_2 := \frac{\tau_2}{\tau_1}\,.$$

The condition for synchronization (that is, phase-locking) (6.35) now becomes

$$|\delta| < \frac{\pi}{2}\,.$$

This completes the derivation of the system of equations describing the coupled phase-locked loop system.

Numerical Results and Experiments

In [239] the system (6.38) to (6.41) was studied for a wide range of the damping coefficients. The authors have confirmed by computer simulation and by experiments that two mutually coupled phase-locked loops can generate chaos in the marginally out-of-lock condition for the cases of asymmetric damping, symmetric low damping and symmetric high damping. To demonstrate the behaviour of the system (6.38) to (6.41), consider the damping ratios $\zeta_1 = 0.614$ and $\zeta_2 = 0.331$ and set $r_1 = 3.64$ and $r_2 = 0.9488$ as in [239]. For different values of δ, namely $\delta_a = -0.77348$ (phase-locked

condition), $\delta_b = -0.77456$ (marginal out-of-lock condition), and $\delta_c = -0.79623$ (out-of-lock condition) the power spectral densities for the output of the voltage-controlled oscillator output of PLL 1 is shown in Figure 6.20. We observe that for the phase-locked condition only the fundamental tone is present (Figure 6.20(a)). However, for the marginal out-of-lock condition (Figure 6.20(b)) the power spectral density contains line components as well as a continuous component indicating nonperiodic behaviour. For the out-of-lock condition the power spectral density contains line components only. From the aforegoing one could speculate that perhaps the power spectral densities for the marginal out-of-lock signify that under this condition the system is chaotic. Endo and Chua [239] calculated the Lyapunov spectrum as a function of the free-running frequency of PLL 2 for the case of asymmetrical damping. They found that when the free-running frequencies of the two voltage-controlled oscillators become closer in the out-of-lock condition, the first (i.e. maximal) Lyapunov exponent becomes positive except in the region where phase-locking is achieved. The second Lyapunov exponent was always zero or negative while the third and fourth Lyapunov exponents were always negative. From this we conclude that the system shows numerical evidence of chaos under the marginal out-of-lock condition. Endo and Chua found numerical and experimental results for the case of asymmetrical damping to be in excellent agreement. For results concerning the symmetrical low and high damping case the reader is referred to [239].

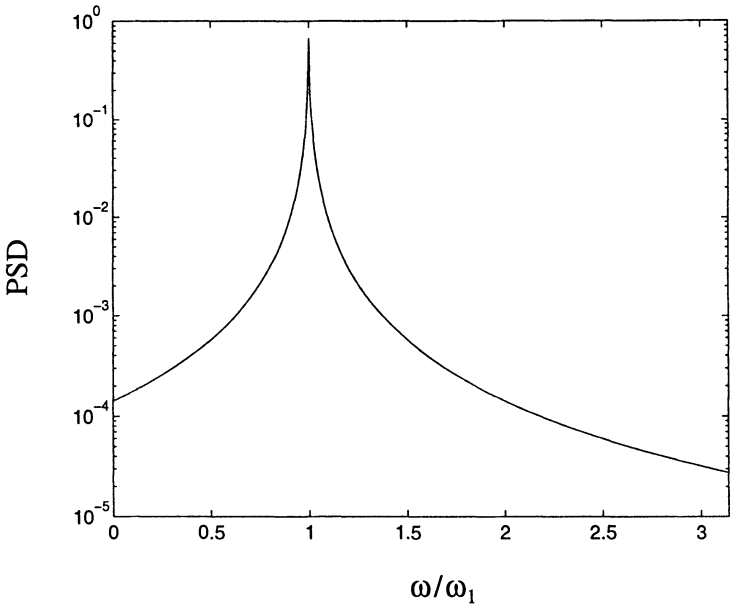

(a)

Figure 6.20: Voltage-controlled oscillator output power spectral density of PLL 1 for asymmetrical damping: (a) Phase-locked condition; (b) Marginal out-of-lock condition; (c) Out-of-lock condition.

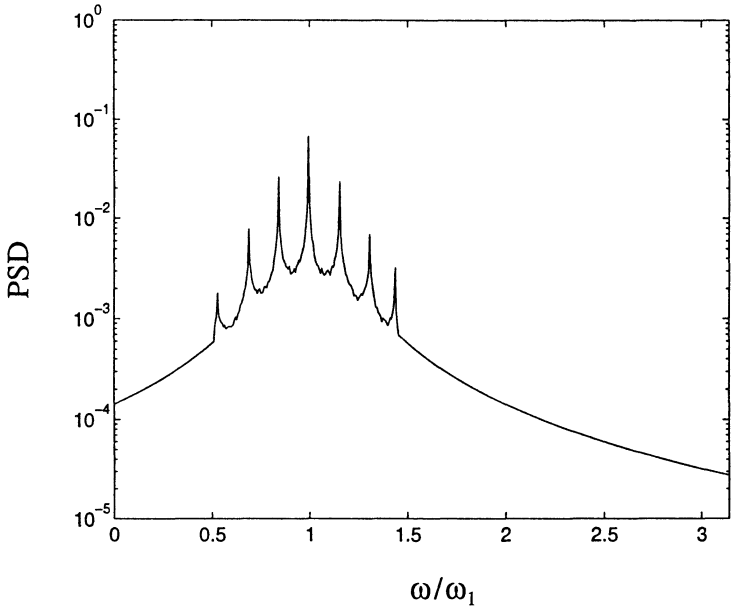

(b)

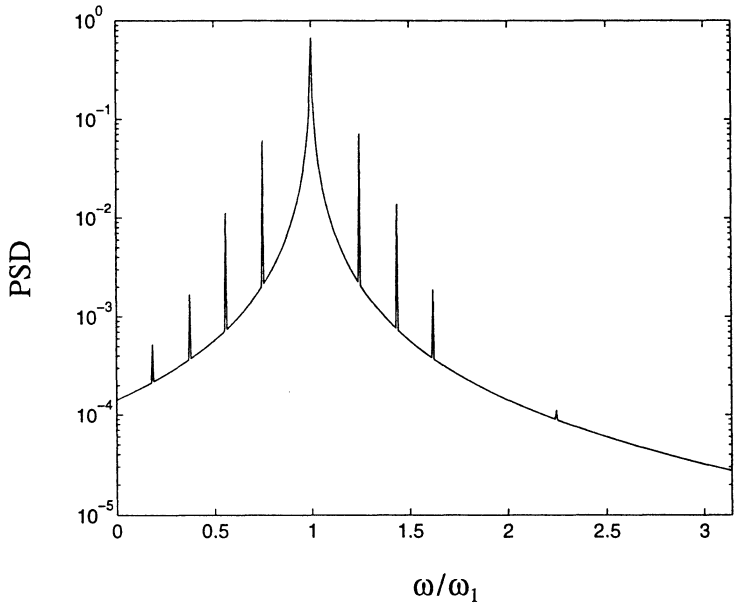

(c)

Figure 6.20: (Continued)

6.5 Automatic Gain Control Loops

The automatic gain control (AGC) loop is one of the most useful nonlinear circuits in modern communication systems. It provides an effective means of automatically adjusting the gain of an amplifier to maintain a relatively constant output level. In most radio frequency receivers, the levels of the received signals are often subject to variation over a wide range. This is due to factors such as presence of barriers, atmospheric layers, reception from different transmission stations, etc. In order to ensure a constant output level, the automatic gain control is introduced in such receivers to combat the wide-range energy variation of received signals and to achieve the automatic volume control. In televisions, automatic gain control performs the tasks of maintaining a fixed picture intensity and establishing more stable synchronizing signals. Automatic gain control loops also find applications in signal encoding and decoding, in modems and in radar detectors to name just a few.

Usually automatic gain control loops are studied using small-signal models which result in the system to be described by a linear system in a small neighbourhood about the operating point. The disadvantage of such an analysis is that the resultant solutions reveal only the local dynamical features of the systems. Global dynamical properties are usually not available from this analysis. In [596] and [303] the hypothesis of small signals is disposed of and the automatic gain control loops are analyzed as first-order nonlinear systems. Chang and coworkers [125] studied automatic gain control loops from a geometric point of view. Specifically an automatic gain control loop which utilizes the square law for gain control was analyzed to find conditions under which it would exhibit chaos.

The functional block diagram of the automatic gain control system studied in [125] is shown in Figure 6.21. As shown, the input or the received signal v_i is amplified by a *Voltage-Controlled Amplifier* (VCA). The voltage dependent gain of the voltage-controlled amplifier is denoted by $p(v_c)$. The control signal v_c for the voltage-

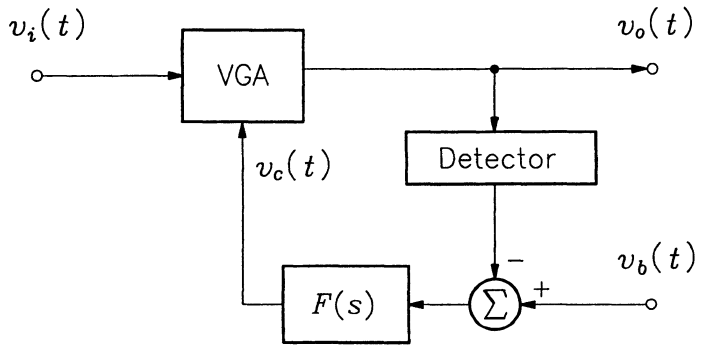

Figure 6.21: Functional block diagram of an automatic gain control loop.

controlled amplifier is obtained by sensing the level of the output signal v_o using a detector and comparing it with the bias signal v_b. The difference signal (error signal)

$$v_e = v_b - v_d\,,$$

is then filtered to suppress rapid fluctuations. This filtered signal is then used to control the gain of the voltage-controlled amplifier. The detector used for sensing the output signal usually implements a square-law, exponential-law or inverse-law etc. (see [790] and [125]). Here we restrict the discussion to the use of a square-law detector. Therefore the output of the detector is

$$v_d = k_d v_o^2\,, \qquad k_d > 0\,.$$

Thus one source of nonlinearity is the output signal detector, while a second source of nonlinearity is the voltage controlled amplifier. For simplicity we assume the voltage-controlled amplifier to be linear so that its output is described by

$$v_o = k_p v_c v_i\,, \qquad k_p > 0\,.$$

We assume the filter to be a second-order lowpass filter with transfer function

$$F(s) = \frac{k_f}{s^2 + a_f s + b_f}\,, \qquad k_f,\, a_f,\, b_f > 0\,.$$

Combining these equations we obtain the following differential equation which describes the dynamics of the automatic gain control loop,

$$\frac{d^2 v_c}{dt^2} + a_f \frac{dv_c}{dt} + b_f v_c = r - \beta v_c^2 v_i^2\,,$$

where

$$r := k_f v_b\,, \qquad \beta = k_d k_f k_p^2\,.$$

We now assume that

$$v_i^2 = m + \epsilon \sin \omega t\,, \qquad m > 0\,,\ \ 0 < \epsilon \ll 1\,.$$

In addition we assume the bias to be small and damping of the lowpass filter to be weak so that

$$r = \epsilon\gamma\,, \quad \text{and} \quad a_f = \epsilon\varphi\,.$$

Using these assumptions the differential equation describing the dynamics of the automatic gain control loop can be written in the form

$$\frac{dx_1}{dt} = x_2\,, \tag{6.42}$$

$$\frac{dx_2}{dt} = -b_f x_1 - \alpha x_1^2 - \epsilon\left(\varphi x_2 - \gamma + \beta x_1^2 \sin \omega t\right)\,, \tag{6.43}$$

where

$$x_1 := v_c\,, \quad x_2 := \frac{dv_c}{dt}\,, \quad \text{and} \quad \alpha := \beta m\,.$$

The system (6.42) and (6.43) may be considered as a perturbation of the unperturbed Hamiltonian system

$$\frac{dx_1}{dt} = x_2\,, \qquad \frac{dx_2}{dt} = -b_f x_1 - \alpha x_1^2\,, \tag{6.44}$$

with Hamiltonian function

$$H(\mathbf{x}) = \frac{1}{2}b_f x_1^2 + \frac{1}{2}x_2^2 + \frac{1}{3}\alpha x_1^3\,, \qquad \mathbf{x} := (x_1, x_2)^T\,.$$

The fixed points of the unperturbed system are

$$\mathbf{x}_c := (0,0)^T\,, \qquad \mathbf{x}_s := (-b_f/\alpha, 0)^T\,.$$

Here $\mathbf{x}_c$ is a centre while $\mathbf{x}_s$ is a saddle point. The point set constituting the homoclinic trajectory containing the fixed point $\mathbf{x}_s$ is given by

$$\Gamma_0 := \left\{\mathbf{x} \in \mathbf{R}^2 \,\middle|\, H(\mathbf{x}) = H(\mathbf{x}_s) \equiv b_f^3/6\alpha^2\right\}\,.$$

To find the time solution of the homoclinic trajectory we must restrict (6.44) to the set Γ_0. Solving $H(\mathbf{x}) = H(\mathbf{x}_s)$ for x_2 and substituting this into the first differential equation in (6.44) gives the differential equation describing the homoclinic trajectory, namely

$$\frac{dx_1}{dt} = \sqrt{\frac{2\alpha}{3}}\left(x_1 + \frac{b_f}{\alpha}\right)\left(\frac{b_f}{2\alpha} - x_1\right)^{1/2}\,.$$

Integrating this differential equation based on the initial condition

$$\mathbf{x}(0) = (b/2\alpha, 0)^T\,,$$

the E-homoclinic trajectory is found to be given by

$$\begin{aligned}\mathbf{x}_0(t) &:= (x_{0,1}(t), x_{0,2}(t))^T \\ &= \left(b_f/2\alpha - (3b_f/2\alpha)\tanh(\sqrt{b_f}\,t/2),\right. \\ &\quad \left.(3b_f^{3/2}/2\alpha)\tanh(\sqrt{b_f}\,t/2)\mathrm{sech}\,2(\sqrt{b_f}\,t/2)\right)^T\,.\end{aligned}$$

We now consider the Poincaré map of the perturbed system

$$\mathbf{P} : \Sigma^{t_0} \to \Sigma^{t_0},$$

where

$$\Sigma^{t_0} := \{(\mathbf{x}, t)\,|\,t = t_0 \in [0, 2\pi/\omega)\} \subset \mathbf{R}^2 \times S^1\,,$$

is the surface of section. The dynamical properties of $\mathbf{P}$ are now considered. For ϵ sufficiently small, the Poincaré map $\mathbf{P}_\epsilon$ for the perturbed system has a saddle fixed point

$$\mathbf{x}_s' = \mathbf{x}_s + O(\epsilon)\,.$$

This follows immediately from the fact that $\mathbf{x}_s$ is hyperbolic and the implicit function theorem. By a similar argument we deduce that the perturbed system also has a sink type fixed point $\mathbf{x}_c'$ close to $\mathbf{x}_c$. To obtain criteria for transversal homoclinic intersections we apply Melnikov's method. The Melnikov integral is given by

$$\begin{aligned} M(t_0,\boldsymbol{\mu}) &= \int_{-\infty}^{\infty} \begin{pmatrix} x_{0,2}(t) \\ -b_f x_{0,1}(t) - \alpha x_{0,1}^2(t) \end{pmatrix} \wedge \\ &\qquad \begin{pmatrix} 0 \\ -\varphi x_{0,2}(t) + \gamma - \beta x_{0,1}^2(t)\sinh\omega(t+t_0) \end{pmatrix} dt \\ &= \int_{-\infty}^{\infty} \left(-\varphi x_{0,2}^2(t) + \gamma x_{0,2}(t) - \beta x_{0,1}^2(t) x_{0,2}(t)\sinh\omega(t+t_0)\right) dt \\ &= \frac{3}{5\alpha^3}\left(2\varphi\alpha b_f^{5/2} - \beta\pi\omega^2(\omega^2 - b_f)(\omega^2 - 4b_f^2)\frac{\cos\omega t_0}{\sinh(\pi\omega/\sqrt{b_1})}\right), \end{aligned}$$

where

$$\boldsymbol{\mu} := (\varphi, b_f, \gamma, \alpha, \beta, \omega)^T.$$

Now $M(t_0,\boldsymbol{\mu})$ has zeros for some t_0 if $\boldsymbol{\mu}$ satisfies

$$R(\boldsymbol{\mu}) := \left|\frac{2\varphi\alpha b_f^{5/2}\sinh\left(\pi\omega/\sqrt{b_f}\right)}{\beta\pi\omega^2(\omega^2 - b_f)(\omega^2 - 4b_f)}\right| \leq 1\,.$$

Here, for strict equality $M(t_0,\boldsymbol{\mu})$ has zeros of even multiplicity greater than zero. For values of $\boldsymbol{\mu}$ corresponding to this case the perturbed system exhibits global homoclinic bifurcations. For strict inequality $M(t_0,\boldsymbol{\mu})$ has simple zeros and hence for this case the system exhibits horseshoe chaos by the Smale-Birkhoff theorem.

By considering the automatic gain control loop as a periodically forced nonlinear system, its local and global dynamical properties are thus described by the above remarks. Since the fixed point $\mathbf{x}_c'$ is stable, it is the proper operating point for the perturbed system in order to maintain a constant output level. However, the automatic gain control loop operates correctly only for values of $\boldsymbol{\mu}$ for which $R(\boldsymbol{\mu}) > 1$. For other values of $\boldsymbol{\mu}$ bifurcations and chaos occur, causing the automatic gain control loop to operate incorrectly.

Chang *et al.* [125] studied the system (6.42) and (6.43) numerically for various parameter values. For the different cases they calculated the invariant manifolds to observe

homoclinic tangencies and homoclinic intersections. They also studied first-order and second-order sampled-data automatic gain control loops by calculating bifurcation diagrams and Lyapunov exponents numerically. The first-order sampled-data automatic gain control loops exhibited a period-doubling route to chaos. The second-order sampled-data automatic gain control loops showed Hopf bifurcation as well as numerical evidence of chaos.

6.6 RF Josephson Junction

Josephson junction devices are used in many applications ranging from supersensitive detectors to superfast computers. This remarkable two-terminal device exhibits extremely rich dynamics and displays a wide variety of exotic nonlinear phenomena. For example, when driven by a DC current source the device is found to oscillate at extremely high frequencies (in the GHz range). The V_{DC}-I_{DC} characteristic is found to be hysteretic. For the case when a sinusoidal current source in parallel with the DC current source drives a Josephson junction the resulting V_{DC}-I_{DC} characteristic changes dramatically. Here discontinuous voltage steps of varying width are observed at rational number multiples of some natural frequency [686].

In this section we wish to discuss the occurrence of the phenomenon of chaos in a simple Josephson junction circuit. The model used for describing the Josephson junction consists of the parallel combination of a linear resistor R, linear capacitor C and a nonlinear inductor described by

$$v(t) = \frac{d\phi}{dt}, \qquad i(t) = I_0 \sin\left(\frac{4\pi e}{h}\phi(t)\right),$$

where ϕ denotes the flux linkage, e denotes the electron charge, h is Planck's constant and R, C and I_0 respectively are the junction resistance, junction capacitance and threshold current associated with the tunneling current. The quantity $(4\pi e/h)\phi$ has an important physical interpretation, namely that it represents the quantum phase difference between the two superconductors which make up the junction. The circuit that we discuss here is shown in Figure 6.22. The equation of motion governing the second-order circuit in Figure 6.22 is

$$C\frac{d^2\phi}{dt^2} + G\frac{d\phi}{dt} + I_0 \sin\left(\frac{4\pi e}{h}\phi\right) = i_s(t),$$

where $G := 1/R$ and $i_s(t)$ is of the form

$$i_s(t) := I_{DC} + I_{AC} \sin \nu t.$$

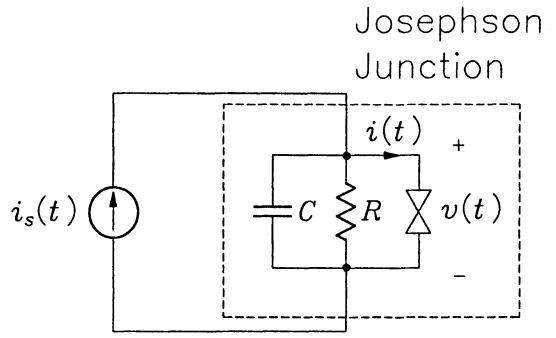

Figure 6.22: Josephson junction circuit model driven by a current source $i_s(t)$.

Using the definitions

$$\rho := \frac{I_{DC}}{I_0}, \qquad \Omega := \left(\frac{4\pi e}{h}\right)\frac{I_0}{G}, \qquad \tau := \Omega t, \qquad \beta := \Omega\frac{C}{G},$$
$$x(\tau) := \frac{4\pi e}{h}\phi(\tau\Omega), \qquad \omega := \frac{\nu}{\Omega}, \qquad \epsilon A' := \frac{I_{AC}}{I_0},$$

where $0 < \epsilon \ll 1$, $A' > 0$, we may write the differential equation in the following dimensionless form,

$$\beta\frac{d^2x}{d\tau^2} + \frac{dx}{d\tau} + \sin x = \rho + \epsilon A' \sin\omega\tau\,. \tag{6.45}$$

Alternatively we may write this second-order differential equation as the following system

$$\frac{dx_1}{d\tau} = x_2\,, \qquad \frac{dx_2}{d\tau} = \frac{\rho - \sin x_1 - x_2 + \epsilon A' \sin\omega\tau}{\beta}, \tag{6.46}$$

where $x_1 := x$ and $x_2 := dx/d\tau$. Referring to this system we see that the dynamics of the Josephson junction are those of the forced pendulum with damping.

Now, consider the instance when only the magnitude of the periodic forcing is small. We now apply Melnikov's method to derive conditions for the Josephson junction to exhibit (horseshoe) chaos. To this end, the unperturbed system (i.e. when $\epsilon = 0$) is given by

$$\frac{dx_1}{d\tau} = x_2\,, \qquad \frac{dx_2}{d\tau} = \frac{\rho - \sin x_1 - x_2}{\beta}\,. \tag{6.47}$$

For the purpose of DC analysis (i.e. $\epsilon = 0$) we consider three cases (see [590]):

The case $\rho > 1$, $\beta > 0$:

The system has a unique periodic trajectory

$$x_2 = \psi(x_1) > 0, \qquad \text{for all} \quad x_1 \in [0, 2\pi),$$

with period 2π, that is, $\psi(x) = \psi(x + 2\pi)$. By implication x_2 is periodic with respect to time with period

$$T = \int_0^{2\pi} \frac{dx}{\psi(x)}.$$

This trajectory is globally asymptotically stable. No fixed points exist since

$$\rho > 1 \geq \sin x_1,$$

for each $x_1 \in \mathbf{R}$.

The case $0 < \rho \leq 1$, $\beta > \beta_0$:

For each $\rho \in (0, 1]$ there is a critical value $\beta_0 = \beta_0(\rho)$ such that for $\beta > \beta_0$ the unperturbed system (6.47) has a unique 2π-periodic locally asymptotically stable trajectory

$$x_2 = \psi(x_1) > 0, \quad \text{for all } x_1 \in [0, 2\pi),$$

which attracts all trajectories outside the domain of attraction of the fixed points. The fixed points are described by

$$\left\{ (\alpha, 0) \in \mathbf{R}^2 \middle| \sin \alpha = \rho \right\}. \tag{6.48}$$

For each $0 < \rho < 1$, the fixed points form an alternating sequence of stable nodes (or foci) and saddle points.

The case $0 < \rho \leq 1$, $0 < \beta \leq \beta_0$:

For this case the system has no periodic solutions other than fixed points described by (6.48). Considering the case $0 < \beta < \beta_0$ for $\alpha = 1$ all trajectories tend toward the unstable fixed points located at

$$\mathbf{x}_k^* := (\pi/2 + 2\pi k, 0)^T, \quad k \in \mathbf{Z},$$

while for $0 < \alpha < 1$ the trajectories converge toward the stable equilibria, except for pairs of trajectories which approach each saddle point. For $\beta = \beta_0$ the trajectories that connect saddle points form a separatrix. Trajectories originating above the separatrix tend toward it, while trajectories originating below it behave as in the case $\beta < \beta_0$. The above discussion is summarized in the DC bifurcation diagram presented by [686].

Recall that in this section we are discussing the case when only the amplitude of the periodic excitation is of ϵ-order. In order to use Melnikov's method, we must ensure

that the unperturbed system (6.47) has a homoclinic (or heteroclinic) trajectory. As shown in [686] there exists a heteroclinic trajectory for an appropriate choice of ρ which we denote by

$$\mathbf{x}_0(\tau) := (x_{0,1}(\tau), x_{0,2}(\tau))^T .$$

The Melnikov integral is given by [686]

$$M(\tau_0) := \int_{-\infty}^{\infty} \left(x_{0,2}(\tau) \frac{A'}{\beta} \sin\omega(\tau + \tau_0) \right) e^{\tau/\beta} \, d\tau . \tag{6.49}$$

The term $e^{\tau/\beta}$ necessitates checking the exponential convergence condition [683]. The existence of the Melnikov integral (6.49) is proved in [686]. The Melnikov integral may be simplified to (see [686])

$$M(\tau_0) = \frac{A'}{\beta} \left(I_1(\omega) \cos\omega\tau_0 + I_2(\omega) \sin\omega\tau_0 \right) ,$$

where I_1 and I_2 are defined by

$$I_1(\omega) := -\Im\left(\mathcal{F}(x_{0,2}(\tau) e^{\tau/\beta}) \right) , \quad I_2(\omega) := \Re\left(\mathcal{F}(x_{0,2}(\tau) e^{\tau/\beta}) \right) ,$$

with

$$\mathcal{F}(x(\tau)) := \int_{-\infty}^{\infty} x(\tau) e^{-j\omega\tau} \, d\tau ,$$

the Fourier transform of some time function $x(\tau)$. The function $x_{0,2}(\tau)$ is a bounded smooth function and $x_{0,2}(\tau) \to 0$ as $\tau \to \pm\infty$ (see [686]). We must show that the $x_{0,2} e^{\tau/\beta} \to 0$ fast enough as $\tau \to \pm\infty$ for the above integrals to exist. For τ close to $\pm\infty$ the rate at which $\mathbf{x}_0(\tau)$ approaches the saddle point

$$\mathbf{x}_s := (x_{1,s}, 0)^T , \qquad \rho = \sin x_{1,s} ,$$

is determined by the eigenvalues of

$$\mathbf{A} = \begin{pmatrix} 0 & 1 \\ -\frac{1}{\beta} \cos x_{1,s} & -\frac{1}{\beta} \end{pmatrix} ,$$

which is obtained from the linearization of the unperturbed system (6.47) about the saddle fixed point $\mathbf{x}_s$. These eigenvalues are given by

$$\begin{aligned} \lambda_1 &:= -\frac{1}{2\beta} - \frac{1}{2\beta}\sqrt{1 + 4\beta\sqrt{1-\rho^2}} < -\frac{1}{\beta} < 0 , \\ \lambda_2 &:= -\frac{1}{2\beta} + \frac{1}{2\beta}\sqrt{1 + 4\beta\sqrt{1-\rho^2}} > 0 , \end{aligned}$$

and therefore we have that $e^{(\lambda_1 + 1/\beta)\tau} \xrightarrow[-\infty]{\tau} 0$ and $e^{(\lambda_2 + 1/\beta)\tau} \xrightarrow[-\infty]{\tau} 0$.

Therefore, $x_{0,2}(\tau)e^{\tau/\beta}$ goes to zero exponentially as $\tau \to \pm\infty$ which finally proves that the Fourier transform $\mathcal{F}(x_{0,2}(\tau)e^{\tau/\beta})$ exists. Since $x_{0,2}(\tau)e^{\tau/\beta}$ is not identically zero, Parseval's theorem [775] guarantees that the support of $\mathcal{F}(x_{0,2}(\tau)e^{\tau/\beta})$ has nonzero Lebesgue measure. Moreover, due to the fact that $x_{0,2}(\tau)e^{\tau/\beta}$ is nonperiodic and smooth (actually analytic) the Fourier transform $\mathcal{F}(x_{0,2}(\tau)e^{\tau/\beta})$ is nonzero almost everywhere. Consequently $M(\tau_0)$ has transversal zeros (two in every interval $2\pi/\omega$) at almost every $\omega \in \mathbf{R}^+$, which guarantees the existence of P-homoclinic trajectory for the perturbed system.

The system in Figure 6.22 was also studied numerically by Salam and Sastry [686]. They observed chaos for $\rho = 0.7155$, $\beta = 8.5$. The case when $G \ll 1$, we find that the dimensionless differential equation (6.45) becomes singular. For this case an alternative normalization of the original system is given in [686] where it is studied in detail. For this resulting dimensionless system and its analysis based on Melnikov's method, refer to Example 2.40.

The Josephson junction was studied extensively in the literature. Ben-Jacob and coworkers studied the occurrence of intermittent chaos in Josephson junctions in [69]. The Josephson junction was analyzed by Odyniec and Chua (see [590], [591]) by means of integral manifolds. Different routes leading to chaos in the Josephson junction where studied by Huang and collaborators in [371]. The dynamical behaviour of coupled Josephson junctions was investigated in [225] and [806].

6.7 Cellular Neural Networks

The recent activity of studies on neurocomputing is forming a new trend towards parallel distributed processing based upon artificial neural networks. Artificial neural networks are composed of simple elements of artificial neurons that model biological neurons. A neuron model usually consists of a simple threshold element transforming a weighted summation of the inputs into the output through a nonlinear output function. However, from the viewpoint of neurophysiology, there is firm criticism that real neurons are in fact far more complicated than such simple elements. Despite this, great successes in problem solving have been achieved with neural networks consisting of such simple elements. Today it is known that chaos occurs in biological neural networks [846] [315] [335]. Chaos is also exhibited by some neuron models such as the Hodgkin-Huxley and FitzHugh-Nagumo equations and generalizations thereof. In this section we discuss cellular neural networks. The neural network architecture known as a *Cellular Neural Network* (CNN) was introduced by Chua and Yang [164] [163]. It consists of identical processing elements aggregatively spaced and interconnected directly to nearest neighbours. The output activation functions of a cellular neural network are continuous and bounded, based on the sum of weighted inputs from other cells, its own weighted outputs and a bias term.

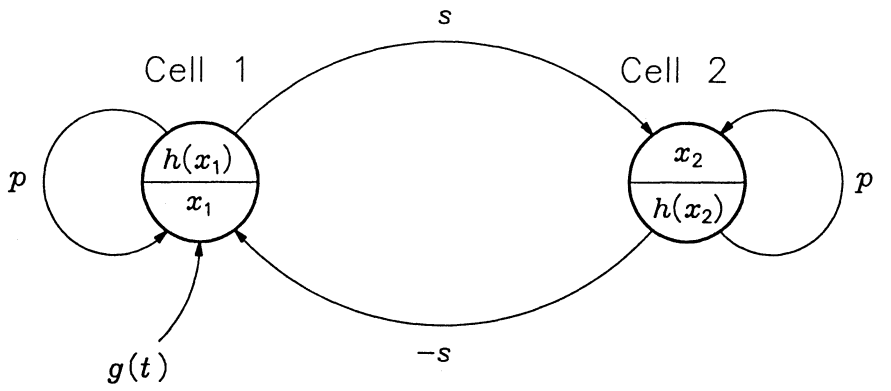

Figure 6.23: Two-cell cellular neural network studied by Zou and Nossek.

6.7.1 Theoretical and Numerical Results

For a detailed discussion of cellular neural networks the reader is referred to [164]. We restrict our discussion to the two-cell cellular neural network in Figure 6.23. This cellular neural network was first investigated for chaotic behaviour by Zou and Nossek in [879]. The dynamics of this two-cell cellular neural network are described by

$$\frac{dx_1}{dt} = ph(x_1) - x_1 - sh(x_2) + g(t), \tag{6.50}$$

$$\frac{dx_2}{dt} = sh(x_1) + ph(x_2) - x_2, \tag{6.51}$$

where $p > 1$, $s > 0$ and

$$h(x) := \text{sat}(x).$$

For the purpose of studying the dynamics of the system we first consider the autonomous case, i.e. when $g(t) = 0$ for each $t \in [0, \infty)$. For this purpose we define nine domains in state space namely:

$$R_1 := (-1,1) \times (-1,1), \qquad R_2 := (-1,1) \times [1,\infty),$$

$$R_3 := (-1,1) \times (-\infty,-1], \qquad R_4 := [1,\infty) \times (-1,1),$$

$$R_5 := (-\infty,-1] \times (-1,1), \qquad R_6 := (-\infty,-1] \times [1,\infty),$$

$$R_7 := [1,\infty) \times [1,\infty), \qquad R_8 := [1,\infty) \times (-\infty,-1],$$

$$R_9 := (-\infty,-1] \times (-\infty,-1].$$

Since the function h is piecewise-linear, we may rewrite the autonomous system as

$$\frac{d\mathbf{x}}{dt} = \mathbf{A}_i\mathbf{x} + \mathbf{b}_i, \quad \text{for each} \quad \mathbf{x} \in R_i,$$

where $i = 1, 2, \ldots, 9$. For clarity we list these matrices and vectors below:

$$\mathbf{A}_1 := \begin{pmatrix} p-1 & -s \\ s & p-1 \end{pmatrix}, \quad \mathbf{b}_1 := \begin{pmatrix} 0 \\ 0 \end{pmatrix},$$

$$\mathbf{A}_2 := \begin{pmatrix} p-1 & 0 \\ s & -1 \end{pmatrix}, \quad \mathbf{b}_2 := \begin{pmatrix} -2 \\ p \end{pmatrix},$$

$$\mathbf{A}_3 := \mathbf{A}_2, \qquad \mathbf{b}_3 := -\mathbf{b}_2$$

$$\mathbf{A}_4 := \begin{pmatrix} -1 & -s \\ 0 & p-1 \end{pmatrix}, \quad \mathbf{b}_4 := \begin{pmatrix} p \\ s \end{pmatrix},$$

$$\mathbf{A}_5 := \mathbf{A}_4, \qquad \mathbf{b}_5 := -\mathbf{b}_4,$$

$$\mathbf{A}_6 := -\mathbf{I}, \qquad \mathbf{b}_6 := \begin{pmatrix} -p-s \\ p-s \end{pmatrix},$$

$$\mathbf{A}_7 := -\mathbf{I}, \qquad \mathbf{b}_7 := \begin{pmatrix} p-s \\ p+s \end{pmatrix},$$

$$\mathbf{A}_8 := -\mathbf{I}, \qquad \mathbf{b}_8 := -\mathbf{b}_6,$$

$$\mathbf{A}_9 := -\mathbf{I}, \qquad \mathbf{b}_9 := -\mathbf{b}_7.$$

Now, for the case $0 < s < p-1$, the autonomous system has a unique fixed point in each of the nine domains, say $\mathbf{x}_i^* \in R_i$ for $i = 1, 2, \ldots, 9$ where

$$\mathbf{x}_1^* := (0,0)^T, \tag{6.52}$$

$$\mathbf{x}_2^* := \left(\frac{s}{p-1}, \frac{s^2}{p-1} + p\right)^T, \tag{6.53}$$

$$\mathbf{x}_3^* := -\mathbf{x}_2^*, \tag{6.54}$$

$$\mathbf{x}_4^* := \left(\frac{s^2}{p-1} + p, \frac{-s}{p-1}\right)^T, \tag{6.55}$$

$$\mathbf{x}_5^* := -\mathbf{x}_4^*, \tag{6.56}$$

$$\mathbf{x}_6^* := (-(p+s), p-s)^T, \tag{6.57}$$

$$\mathbf{x}_7^* := (p-s, p+s)^T, \tag{6.58}$$

$$\mathbf{x}_8^* := -\mathbf{x}_6^*, \tag{6.59}$$

$$\mathbf{x}_9^* := -\mathbf{x}_7^*. \tag{6.60}$$

To comment on the stability properties of these fixed points, we calculate their eigenvalues and associated eigenvectors. In the results below the subscripts s and u denote *stable* and *unstable* respectively. These are:

For fixed point $\mathbf{x}_1^*$:

$$\begin{aligned} \lambda_{u,1}, \lambda_{u,2} &:= (p-1) \pm js\,, \\ \mathbf{v}_{u,1}, \mathbf{v}_{u,2} &:= (\pm j, 1)^T\,, \end{aligned}$$

where $j := \sqrt{-1}$.

For fixed points $\mathbf{x}_2^*$ and $\mathbf{x}_3^*$:

$$\begin{aligned} \lambda_s &:= -1\,, \qquad \lambda_u := p-1\,, \\ \mathbf{v}_s &:= (0,1)^T\,, \quad \mathbf{v}_u := (p/s, 1)^T\,. \end{aligned}$$

For fixed points $\mathbf{x}_4^*$ and $\mathbf{x}_5^*$:

$$\begin{aligned} \lambda_s &:= -1\,, \qquad \lambda_u := p-1\,, \\ \mathbf{v}_s &:= (1,0)^T\,, \quad \mathbf{v}_u := (s/p, -1)^T\,. \end{aligned}$$

For fixed points $\mathbf{x}_6^*$, $\mathbf{x}_7^*$, $\mathbf{x}_8^*$ and $\mathbf{x}_9^*$:

$$\begin{aligned} \lambda_{s,1}, \lambda_{s,2} &:= -1\,, \\ \mathbf{v}_{s,1} &:= (1,0)^T\,, \quad \mathbf{v}_{s,2} := (0,1)^T\,. \end{aligned}$$

Reminding ourselves that $s > 0$, $p > 1$ we conclude that $\mathbf{x}_1^*$ is an unstable spiral, $\mathbf{x}_2^*, \ldots, \mathbf{x}_5^*$ are saddle points and $\mathbf{x}_6^*, \ldots, \mathbf{x}_9^*$ are stable nodes. What is interesting is the particular orientation of the unstable manifolds of saddles $\mathbf{x}_2^*, \ldots, \mathbf{x}_5^*$. As can be seen from Figure 6.24, each of the stable nodes lies at the point of intersection of two straight lines which are extensions of the unstable manifolds of a pair of saddle points. Together these straight lines form a parallelogram with a stable node at each vertex. As s approaches $p-1$ from below, each node and the saddle located counter clockwise from it move closer to each other until they coincide when $s = p-1$ as shown in Figure (6.25). Thus for this case

$$\mathbf{x}_7^* = \mathbf{x}_2^*\,, \quad \mathbf{x}_9^* = \mathbf{x}_3^*\,, \quad \mathbf{x}_8^* = \mathbf{x}_4^*\,, \quad \mathbf{x}_6^* = \mathbf{x}_5^*\,,$$

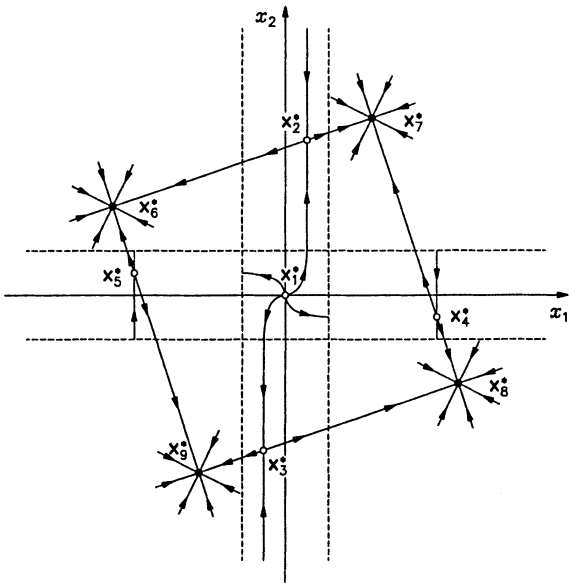

Figure 6.24: Location of the fixed points for $0 < s < p - 1$.

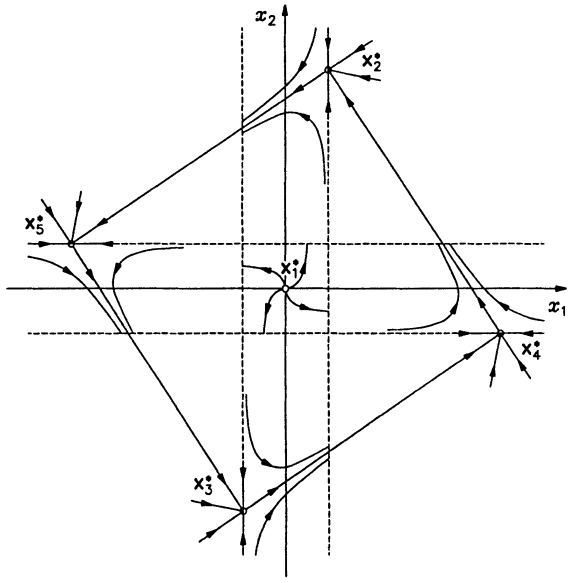

Figure 6.25: Location of the fixed points for $s = p - 1$.

and hence the autonomous system has only five fixed points, namely $\mathbf{x}_1^*, \ldots, \mathbf{x}_5^*$ described by (see (6.52) to (6.56)),

$$\mathbf{x}_1^* = (0,0)^T, \quad \mathbf{x}_2^* = (1, 2p-1)^T, \quad \mathbf{x}_3^* = -\mathbf{x}_2^*, \quad \mathbf{x}_4^* = (2p-1, -1)^T, \quad \mathbf{x}_5^* = -\mathbf{x}_4^*.$$

Notice that $\mathbf{x}_2^*, \ldots, \mathbf{x}_5^*$ lie on the boundaries of domains. The stability properties of $\mathbf{x}_1^*$ have remained unchanged. Concerning the other fixed points, with the amalgamation of a stable node with a saddle their stability properties have also combined. Take for instance $\mathbf{x}_2^*$ (a saddle for $s < p-1$) and $\mathbf{x}_7^*$ (a stable node for $s < p-1$). For $s = p-1$, $\mathbf{x}_2^*$ and $\mathbf{x}_7^*$ combine (i.e. $\mathbf{x}_2^* = \mathbf{x}_7^*$) to give what we now call $\mathbf{x}_2^*$. An arbitrary point $\mathbf{x} \in R_7$ will converge to $\mathbf{x}_2^*$ since it still looks like $\mathbf{x}_7^*$ from anywhere within R_7 while for an arbitrary point $\mathbf{x} \in R_2$, $\mathbf{x}_2^*$ looks like a saddle with its stable manifold along $\mathbf{x}_1 = 1$ and its unstable manifold extending into the domain R_2 along the direction $(-p/(p-1), -1)^T$. Put another way, R_7 is the domain of attraction of $\mathbf{x}_2^*$. It is clear that for $0 < s \leq p-1$ there exist no periodic solutions, since for any initial condition in state space its trajectory will eventually converge to a fixed point asymptotically.

For the case $s > p-1$ all fixed points except for the unstable spiral $\mathbf{x}_1^*$ disappear. We see that for this case each trajectory starting in domain R_1 spirals outward. What is the fate of these and in fact all trajectories of the autonomous system? To study the stability properties of an arbitrary trajectory we resort to Lyapunov's direct method. Consider the function $V : \mathbf{R}^2 \to [0, +\infty)$ defined by

$$V(\mathbf{x}) := \frac{1}{2}\left(x_1^2 + x_2^2\right).$$

Representing the autonomous system by $d\mathbf{x}/dt = \mathbf{f}(\mathbf{x})$, we may write the total time derivative of V along an arbitrary trajectory $\mathcal{T}$ of the autonomous system as

$$\left(\frac{dV}{dt}\right)_{\mathcal{T}} = \nabla V(\mathbf{y}(t)) \cdot \mathbf{f}(\mathbf{y}(t)),$$

where $\mathbf{y}(t)$ is the time parameterized representation of the trajectory $\mathcal{T}$. For $\mathbf{y} \in R_1$ we obtain

$$\begin{aligned}
\left(\frac{dV}{dt}\right)_{\mathcal{T}} &= \nabla V(\mathbf{y}) \cdot (\mathbf{A}_1\mathbf{y} + \mathbf{b}_1) \\
&= (y_1, \; y_2) \begin{pmatrix} p-1 & -s \\ s & p-1 \end{pmatrix} \begin{pmatrix} y_1 \\ y_2 \end{pmatrix} \\
&= (p-1)\left(y_1^2 + y_2^2\right) \\
&> 0, \qquad \text{for each} \quad \mathbf{y} \in R_1 \backslash \{\mathbf{0}\}.
\end{aligned} \tag{6.61}$$

For $\mathbf{y} \in R_2$,

$$\left(\frac{dV}{dt}\right)_{\mathcal{T}} = \nabla V(\mathbf{y}) \cdot (\mathbf{A}_2\mathbf{y} + \mathbf{b}_2)$$

$$
\begin{aligned}
&= (p-1)y_1^2 - sy_1 + sy_1y_2 + py_2 - y_2^2 \\
&= -sy_1 + py_2 + (p-1)y_1^2 + sy_1y_2 - y_2^2 \\
&\approx -y_2^2, \qquad \text{for} \quad y_2 \gg 1 \\
&< 0,
\end{aligned}
$$

for $\mathbf{y}$ sufficiently far from the origin. Similarly for each $\mathbf{y} \in R_3$ sufficiently far from the origin, we have that $y_2 \ll -1$ and hence

$$\left(\frac{dV}{dt}\right)_{\mathcal{T}} \approx -y_2^2 < 0\,.$$

For $\mathbf{y} \in R_i$ $(i = 4, 5)$ sufficiently far from the origin we obtain

$$\left(\frac{dV}{dt}\right)_{\mathcal{T}} \approx -y_1^2 < 0\,.$$

Finally, for $\mathbf{y} \in R_i$ $(i = 6, 7, 8, 9)$ sufficiently far from the origin $\sqrt{y_1^2 + y_2^2} \gg 1$ holds, giving

$$\left(\frac{dV}{dt}\right)_{\mathcal{T}} \approx \left(y_1^2 + y_2^2\right) < 0\,.$$

We have thus shown that sufficiently far from the origin all trajectories of the autonomous system intersect contours $V(\mathbf{x}) = C_1$ inward while for $V(\mathbf{x}) = C_2$ (with $0 < C_2 < 1 \gg C_1$) all trajectories intersect the contour outward. Since the autonomous system has no fixed point in the domain

$$P := \left\{\mathbf{x} \in \mathbf{R}^2 \middle| C_2 \leq V(\mathbf{x}) \leq C_1\right\},$$

for $s > p-1$, the Poincaré-Bendixson theorem (Appendix B) guarantees the existence of a periodic solution contained in P. Thus for each $s > p-1$ the autonomous system's response is either periodic or approaches a periodic trajectory asymptotically. A typical periodic solution of the autonomous system is shown in Figure 6.26. This completes our study of autonomous two-cell cellular neural network system.

Next consider the case when the system is sinusoidally excited with

$$g(t) = A\sin(2\pi t/T)\,.$$

For the case $A = 4.04$, $T = 4$ and $p = 2$, $s = 1.2$ the driven system exhibits chaos. A typical trajectory for this instance is shown in Figure 6.27. In Figure 6.28 Poincaré map of the chaotic attractor is shown. The horseshoe structure is clearly visible from Figure 6.28. The Poincaré map resembles a lady's shoe. For this reason this attractor is termed the *lady's shoe attractor* [880].

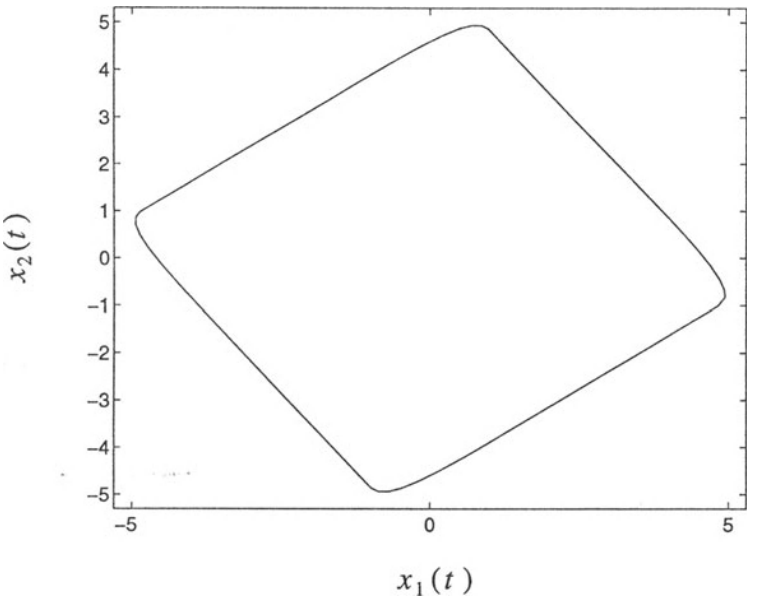

Figure 6.26: Periodic solution of the autonomous system for $s = 2.5$, $p = 3$.

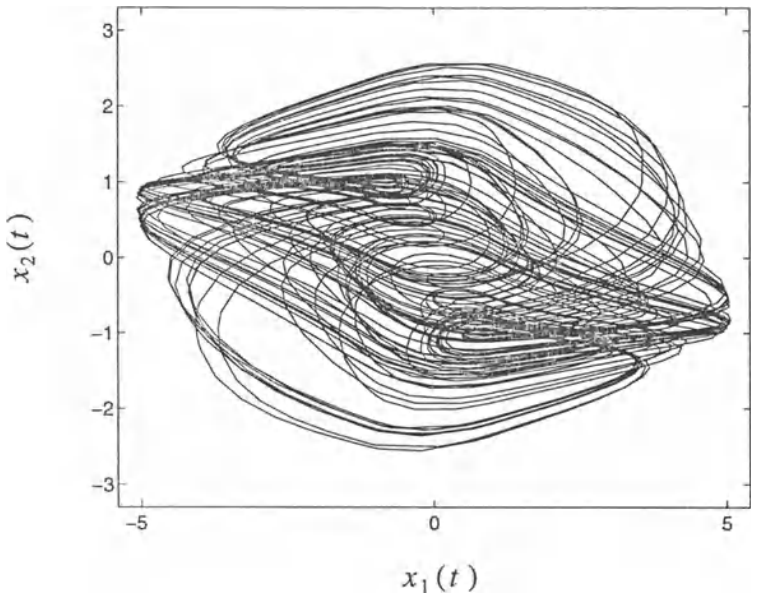

Figure 6.27: Chaotic trajectory of the driven two-cell cellular neural network.

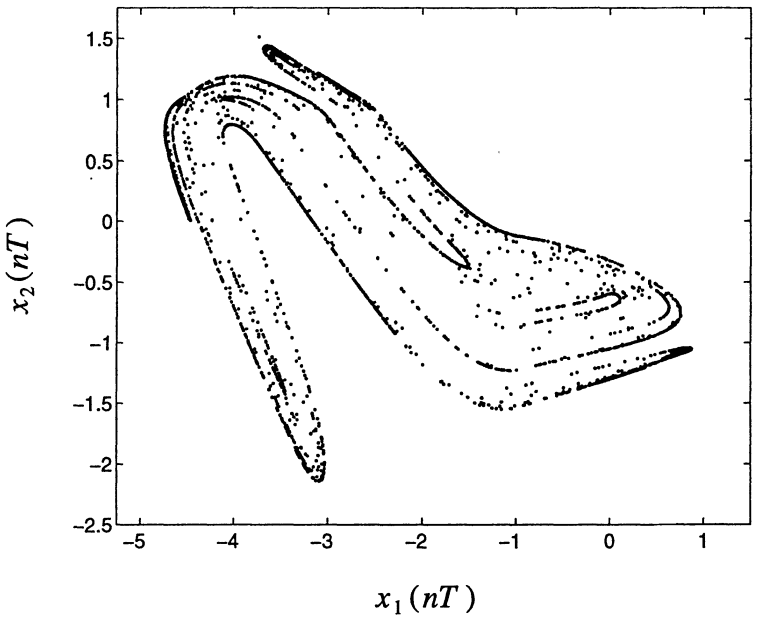

Figure 6.28: Lady's shoe attractor observed from the two-cell cellular neural network.

6.7.2 Experimental Cellular Neural Network Circuit

A circuit for realizing the two-cell nonreciprocal cellular neural network in Figure 6.23 was proposed by Zou and his coworkers in [880]. This circuit, shown in Figure 6.29, utilizes operational amplifiers, resistors and capacitors for the realization. In order to describe the operation of the circuit, consider the part of the circuit that constitutes Cell 1. Operational amplifier IC_1 together with C_1 and R_1 form the inner cell of Cell 1 which is a leaky integrator. Operational amplifier IC_2, R_5 and R_6 form an inverting amplifier which implements the nonlinear function $-\text{sat}(\cdot)$, which utilizes the inherent saturation property of the operational amplifer (Zou *et al.* used $R_5 = R$, $R_6 = 10R$). The second inverting amplifier consisting of IC_3, R_7 and R_8 inverts the polarity of the output of Cell 1 for use by Cell 2. The resistor R_2 and R_3 determine the weights with which the input $v_i(t)$ and the output of Cell 2 contribute to the input of Cell 1. The internal operation of Cell 2 is similar to that of Cell 1. For realization of the network in Figure 6.29 we put

$$R_2 = R_{10} = \frac{10R}{p}, \qquad R_3 = R_9 = \frac{10R}{s}.$$

Zou *et al.* [880] chose the following circuit parameters for their implementation:

$$R = 4.75\text{k}\Omega\,, \quad C_1 = 10\text{nF}\,, \quad R_1 = R_4 = R\,,$$

$$R_2 = R_{10} = 23.75\text{k}\Omega\ (p = 2.0)\,, \quad R_3 = R_9 = 30.583\text{k}\Omega\ (s = 1.2)\,, \quad V_{cc} = 10\text{V}\,.$$

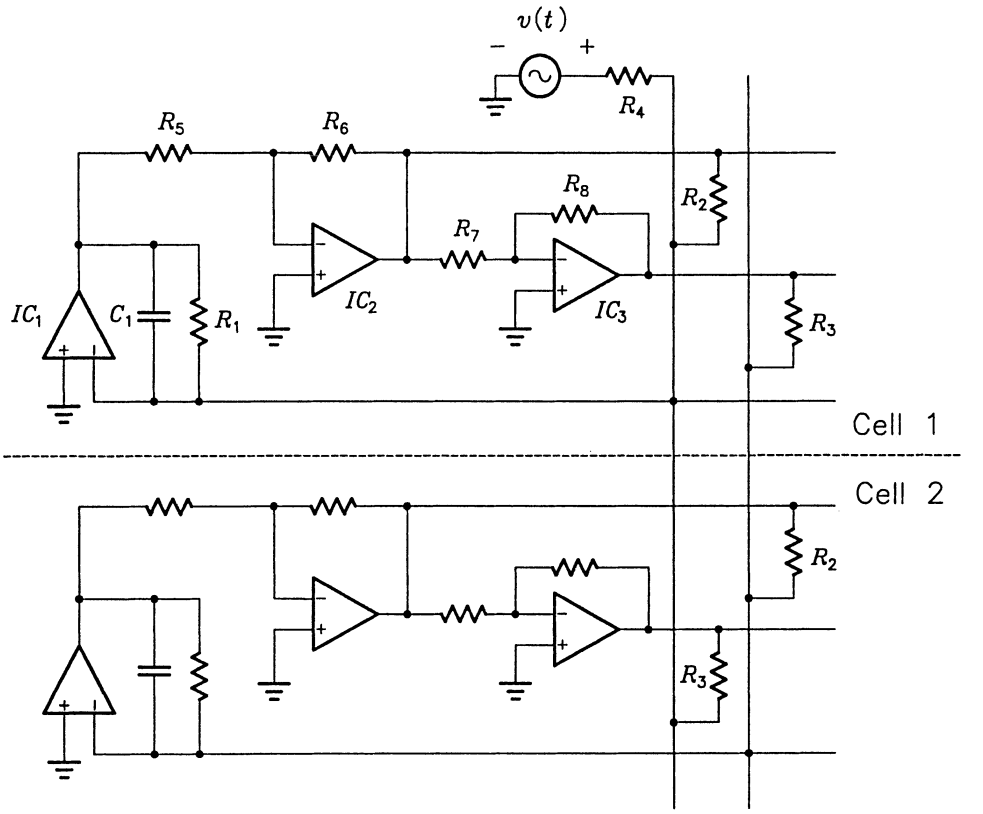

Figure 6.29: Electronic circuit realization of the two-cell cellular neural network.

For the sinusoidal forcing

$$v(t) = A \sin 2\pi f t\,,$$

with $A = 3.89$V, $f = 5.3$kHz Zou *et al.* observed the lady's shoe attractor from the their circuit. They also observed period-doubling bifurcations by fixing A to 3.96V and adjusting the frequency of the sinusoidal forcing. The experimental results observed by Zou *et al.* were found to be in excellent agreement with the numerical results.

Cellular neural networks have also been studied for nonlinear phenomena exhibited only by coupled nonlinear systems. In reseach contributions published in [140], cellular neural networks have been found to exhibit spatio-temporal chaos and autowaves. Concerning applications of cellular neural networks, their versatility has become apparent. These networks have been utilized in image processing applications [829] [163] [188], modelling of population dynamics [140] and nonlinear circuit modelling [36].

6.8 Phase Coupled Systems

In this section the stability of a class of coupled identical autonomous systems of first order nonlinear ordinary differential equations is investigated. These couplings play a central role in controlling chaotic systems and can be applied in electronic circuits. As applications we consider two coupled Van der Pol equations and two coupled logistic maps. When the uncoupled system admits a first integral we study whether a first integral exists for the coupled system. Gradient systems and the Painlevé property are also discussed. Finally the relation of the Lyapunov exponents of the uncoupled and coupled system are discussed.

Consider the autonomous system of first order ordinary differential equations

$$\frac{d\mathbf{u}}{dt} = \mathbf{F}(\mathbf{u}), \qquad \mathbf{u} = (u_1, u_2, \ldots, u_N)^T. \tag{6.62}$$

We assume that the functions $F_j : \mathbf{R}^N \to \mathbf{R}$ are analytic. Assume that $\mathbf{u}^*$ is a fixed point of (6.62). The variational equation of (6.62) is given by [754], [753]

$$\frac{d\mathbf{y}}{dt} = \frac{\partial \mathbf{F}}{\partial \mathbf{u}}(\mathbf{u}(t))\mathbf{y}, \tag{6.63}$$

where $\partial \mathbf{F}/\partial \mathbf{u}$ is the Jacobian matrix. Inserting the fixed point $\mathbf{u}^*$ into the Jacobian matrix results in an $N \times N$ matrix

$$\mathbf{A} := \frac{\partial \mathbf{F}}{\partial \mathbf{u}}(\mathbf{u}^*),$$

with constant coefficients. The eigenvalues $\lambda_1, \ldots, \lambda_N$ of this matrix determine the stability of the fixed point $\mathbf{u}^*$. Furthermore the eigenvalues provide information as to whether Hopf bifurcation can occur. In this case we assume that $\mathbf{F}$ depends on a (bifurcation) parameter. Moreover, the variational system (6.63) is used to find the one-dimensional Lyapunov exponents.

In controlling the chaos of the autonomous system (6.62) the coupling of two identical systems according to

$$\frac{d\mathbf{u}}{dt} = \mathbf{F}(\mathbf{u}) + c(\mathbf{v} - \mathbf{u}), \qquad \frac{d\mathbf{v}}{dt} = \mathbf{F}(\mathbf{v}), \tag{6.64}$$

and

$$\frac{d\mathbf{u}}{dt} = \mathbf{F}(\mathbf{u}) + c(\mathbf{v} - \mathbf{u}), \qquad \frac{d\mathbf{v}}{dt} = \mathbf{F}(\mathbf{v}) + c(\mathbf{u} - \mathbf{v}), \tag{6.65}$$

plays a central role [759]. Here $N \geq 3$ and $c \in \mathbf{R}$. First we realize that $(\mathbf{u}^*, \mathbf{v}^*)$ with $\mathbf{v}^* = \mathbf{u}^*$ is a fixed point of (6.64) and (6.65) if $\mathbf{u}^*$ is a fixed point of (6.62). Inserting the fixed point $(\mathbf{u}^*, \mathbf{u}^*)$ into the Jacobian matrix associated with (6.64) and (6.65) yields a $2N \times 2N$ matrix. We now show that the eigenvalues of this $2N \times 2N$ matrix can be found from the eigenvalues of the $N \times N$ matrix given by $\mathbf{A}$. Then

from the $2N$ eigenvalues of (6.63) we can determine the stability of the fixed point $(\mathbf{u}^*, \mathbf{u}^*)$ for the systems (6.64) and (6.65). First we consider system (6.64). To find the eigenvalues we present the following theorem.

Theorem 6.3 Let $\mathbf{A}$ be an $N \times N$ matrix over the real numbers. Let $\lambda_1, \ldots, \lambda_N$ be the eigenvalues of $\mathbf{A}$. Define the $2N \times 2N$ matrix $\mathbf{M}$ as

$$\mathbf{M} := \begin{pmatrix} \mathbf{A} - c\mathbf{I} & c\mathbf{I} \\ \mathbf{0} & \mathbf{A} \end{pmatrix},$$

where $\mathbf{I}$ is the $N \times N$ unit matrix. Then the eigenvalues of $\mathbf{M}$ are given by

$$\lambda_1, \lambda_2, \ldots, \lambda_N, \quad \lambda_1 - c, \lambda_2 - c, \ldots, \lambda_N - c.$$

Proof: There exists an $N \times N$ orthogonal matrix $\mathbf{Q}$ such that

$$\mathbf{Q}^T \mathbf{A} \mathbf{Q} = \mathbf{D} + \mathbf{U},$$

where $\mathbf{D} := \operatorname{diag}(\lambda_1, \lambda_2, \ldots, \lambda_N)$ and $\mathbf{U}$ is a strictly upper-triangular $N \times N$ matrix. Let

$$\mathbf{P} := \begin{pmatrix} \mathbf{Q} & \mathbf{0} \\ \mathbf{0} & \mathbf{Q} \end{pmatrix},$$

where $\mathbf{0}$ is the $N \times N$ zero matrix. Thus

$$\mathbf{P}^{-1} = \begin{pmatrix} \mathbf{Q}^T & \mathbf{0} \\ \mathbf{0} & \mathbf{Q}^T \end{pmatrix}.$$

It follows that

$$\mathbf{P}^{-1}\mathbf{M}\mathbf{P} = \begin{pmatrix} (\mathbf{D} - c\mathbf{I}) + \mathbf{U} & c\mathbf{I} \\ \mathbf{0} & \mathbf{D} + \mathbf{U} \end{pmatrix},$$

which then is an upper-triangular matrix. The entries on the diagonal are $\lambda_1, \ldots, \lambda_N$, $\lambda_1 - c, \ldots, \lambda_N - c$ which are the eigenvalues of $\mathbf{M}$. This proves the theorem. ■

For our purpose, the matrix $\mathbf{M}$ is the Jacobian matrix of system (6.64) evaluated at the fixed point $(\mathbf{u}^*, \mathbf{u}^*)$.

Next we consider the coupled system (6.65). To find these eigenvalues we prove the following theorem

Theorem 6.4 Let $\mathbf{A}$ be an $N \times N$ matrix over the real numbers. Let $\lambda_1, \ldots, \lambda_N$ be the eigenvalues of $\mathbf{A}$. Define the $2N \times 2N$ matrix $\mathbf{M}$ as

$$\mathbf{M} := \begin{pmatrix} \mathbf{A} - c\mathbf{I} & c\mathbf{I} \\ c\mathbf{I} & \mathbf{A} - c\mathbf{I} \end{pmatrix}.$$

Then the eigenvalues of $\mathbf{M}$ are given by

$$\lambda_1,\ \lambda_2,\ \ldots,\ \lambda_N,\quad \lambda_1 - 2c,\ \lambda_2 - 2c,\ \ldots\ , \lambda_N - 2c.$$

Proof: There exists an $N \times N$ orthogonal matrix $\mathbf{Q}$ such that $\mathbf{Q}^T\mathbf{A}\mathbf{Q} = \mathbf{D} + \mathbf{U}$, where $\mathbf{D} := \mathrm{diag}(\lambda_1, \lambda_2, \ldots, \lambda_N)$ and $\mathbf{U}$ is a strictly upper-triangular $N \times N$ matrix. Let

$$\mathbf{P} := \begin{pmatrix} \mathbf{Q} & \mathbf{0} \\ \mathbf{Q} & \mathbf{Q} \end{pmatrix}$$

where once again $\mathbf{0}$ is the $N \times N$ zero matrix. It follows that

$$\mathbf{P}^{-1} = \begin{pmatrix} \mathbf{Q}^T & \mathbf{0} \\ -\mathbf{Q}^T & \mathbf{Q}^T \end{pmatrix},$$

giving

$$\mathbf{P}^{-1}\mathbf{M}\mathbf{P} = \begin{pmatrix} \mathbf{D} + \mathbf{U} & c\mathbf{I} \\ \mathbf{0} & (\mathbf{D} - 2c\mathbf{I}) + \mathbf{U} \end{pmatrix}.$$

Now, $\mathbf{P}^{-1}\mathbf{M}\mathbf{P}$ is an upper-triangular matrix of which the entries on the diagonal are $\lambda_1, \ldots, \lambda_N, \lambda_1 - 2c, \ldots, \lambda_N - 2c$, the eigenvalues of $\mathbf{M}$. This proves the theorem. ■

As before, let $\mathbf{M}$ be the Jacobian matrix of system (6.64) after inserting the fixed point $(\mathbf{u}^*, \mathbf{u}^*)$.

Example 6.5 As an application let us consider the Van der Pol equation

$$\frac{du_1}{dt} = u_2, \qquad \frac{du_2}{dt} = r(1 - u_1^2)u_2 - u_1. \tag{6.66}$$

Then $\mathbf{u}^* = (0, 0)$ is a fixed point of (6.66). The eigenvalues of the functional matrix for this fixed point are given by $\lambda_{1,2} = r/2 \pm \sqrt{r^2/4 - 1}$. The uncoupled system shows Hopf bifurcation [766]. We find a Hopf bifurcation when the characteristic exponents cross the imaginary axis. For the Van der Pol equation a stable limit cycle is born. If we consider the coupling due to systems (6.65) we find that the eigenvalues of the coupled system are given by $\mu_1 = \lambda_1$, $\mu_2 = \lambda_2$, $\mu_3 = \lambda_1 - 2c$, $\mu_4 = \lambda_2 - 2c$. ■

Theorems 6.3 and 6.4 stated above also apply to coupled maps. For example Theorem 6.4 can be applied to

$$\mathbf{x}_{n+1} = \mathbf{f}(\mathbf{x}_n) + c(\mathbf{y}_n - \mathbf{x}_n), \qquad \mathbf{y}_{n+1} = \mathbf{f}(\mathbf{y}_n) + c(\mathbf{x}_n - \mathbf{y}_n).$$

Example 6.6 Consider the logistic map with $f(x) = rx(1-x)$. The map f admits the fixed points $x_1^* = 0$ and $x_2^* = (r-1)/r$. In the following we consider the fixed point x_2^*. Then we find that the Jacobian matrix (which is a 1×1 matrix) at this fixed point is given by $\mathbf{A} = \lambda = 2 - r$. Consequently the eigenvalues for the coupled system

$$x_{n+1} = 1 - ax_n^2 - b(x_n - y_n), \qquad y_{n+1} = 1 - ax_n^2 - b(y_n - x_n),$$

are $2 - r$ and $2 - r - 2c$. ■

Let us now study first integrals of system (6.62). Assume that (6.62) admits a first integral of the form $g(\mathbf{u})\mathrm{e}^{\epsilon t}$. Such first integrals appear in dissipative systems [760], [761], [762]. When $\epsilon = 0$ the non-dissipative case is obtained.

Theorem 6.7 Assume that (6.62) admits the first integral $g(\mathbf{u})\mathrm{e}^{\epsilon t}$. Then

$$(g(\mathbf{u}) + g(\mathbf{v}))\mathrm{e}^{\epsilon t}$$

is a first integral of the coupled system if

$$\frac{\partial g(\mathbf{u})}{\partial u_j} - \frac{\partial g(\mathbf{v})}{\partial v_j} = 0, \qquad j = 1, 2, \ldots, N.$$

Proof: From the condition that $g(\mathbf{u})\mathrm{e}^{\epsilon t}$ is a first integral of (6.62) we find

$$\sum_{j=1}^{N} \frac{\partial g(\mathbf{u})}{\partial u_j} F_j(\mathbf{u}) + \epsilon g(\mathbf{u}) = 0\,. \tag{6.67}$$

Inserting (6.67) and (6.65) into

$$\frac{d}{dt}\left((g(\mathbf{u}) + g(\mathbf{v}))\mathrm{e}^{\epsilon t}\right) = 0\,,$$

we obtain

$$c\sum_{j=1}^{N}\left(\frac{\partial g(\mathbf{u})}{\partial u_j} - \frac{\partial g(\mathbf{v})}{\partial v_j}\right)(v_j - u_j) = 0\,.$$

This completes the proof.

Example 6.8 An example where we can apply Theorem 6.7 is the Lotka-Volterra model

$$\begin{aligned}\frac{du_1}{dt} &= cu_1 + u_1(u_2 + u_3),\\ \frac{du_2}{dt} &= cu_2 + u_2(u_3 - u_1),\\ \frac{du_3}{dt} &= cu_3 + u_3(-u_1 - u_2).\end{aligned}$$

Here, an explicitly time-dependent first integral is given by

$$I(\mathbf{u}, t) = (u_1 + u_2 + u_3)\mathrm{e}^{-ct}\,.$$

■

Assume now that system (6.62) is a gradient system, i.e.

$$\mathbf{F}(\mathbf{u}) = -\mathrm{grad}W(\mathbf{u}),$$

where W is the potential. What can be said about the coupled system (6.65)? It is obvious that the coupled system (6.65) is also a gradient system, since it can be derived from the potential

$$W(\mathbf{u}) + W(\mathbf{v}) + \frac{1}{2}c(\mathbf{u} - \mathbf{v})^T(\mathbf{u} - \mathbf{v})\,.$$

Let us now discuss the Painlevé test. Let $\mathbf{u}(t) = \Phi(t; \mathbf{u}_0)$ be a solution of the initial value problem of (6.62). Let $\mathbf{v}(t) = \Phi(t; \mathbf{v}_0)$. Then $(\mathbf{u}(t), \mathbf{v}(t))$ is a particular solution of the coupled system (6.65) if $\mathbf{u}_0 = \mathbf{v}_0$. If $\mathbf{u}_0 \neq \mathbf{v}_0$, then $(\mathbf{u}(t), \mathbf{v}(t))$ is no longer a solution for (6.65). A similar argument can be applied to the Painlevé test [762]. If the uncoupled system (6.62) passes the Painlevé test, i.e. has an expansion (considered in the complex time domain) of

$$u_j(t) = (t - t_1)^{n_j} \sum_{j=0}^{\infty} a_j(t - t_1)^j, \qquad j = 1, 2, \ldots, N\,,$$

with the right number of Kowalevski exponents (see [762] for more details), then the coupled system (6.65) admits an expansion of the form $(\mathbf{u}(t), \mathbf{v}(t))$ around the singularity t_1, but the number of free parameters is one less than required. Thus the coupled system does not pass the Painlevé test in general if the uncoupled system (6.62) passes the test.

Let us now consider the Lyapunov exponents of the coupled system. To find a relation between the Lyapunov exponents of the coupled system (6.65) and uncoupled system

(6.62) we consider the time-evolution of $\Theta(t) := \mathbf{u}(t) - \mathbf{v}(t)$. We call Θ the *phase difference* [263]. It follows that

$$\frac{d\Theta}{dt} = \frac{d\mathbf{u}}{dt} - \frac{d\mathbf{v}}{dt} = \mathbf{F}(\mathbf{u}) - \mathbf{F}(\mathbf{v}) - 2c\Theta\,,$$

where we used (6.65). Using a Taylor expansion for $\mathbf{F}(\mathbf{u})$ and $\mathbf{F}(\mathbf{v})$ and the fact that

$$\frac{\partial \mathbf{F}}{\partial \mathbf{u}}(\mathbf{u}(t)) = \frac{\partial \mathbf{F}}{\partial \mathbf{v}}(\mathbf{u}(t)),$$

we obtain

$$\frac{d\Theta}{dt} = (\mathbf{A}(t) - 2cI)\Theta + O(\Theta^2), \qquad \mathbf{A}(t) := \frac{\partial \mathbf{F}}{\partial \mathbf{u}}(\mathbf{u}(t)), \tag{6.68}$$

and $O(\Theta^2)$ indicate higher order terms in Θ. Integrating (6.68) while neglecting the higher order terms yields

$$\Theta(t) = \left(e^{-2ct} T \exp\left(\int_0^t \mathbf{A}(s)\, ds \right) \right) \Theta(0),$$

where T is the time ordering operator. The eigenvalues μ_j $(j = 1, 2, \ldots, N)$ of

$$\lim_{t\to\infty} \left(T \exp\left(\int_0^t \mathbf{A}(s)\, ds \right) \right),$$

are related to the Lyapunov exponents λ_j $(j = 1, 2, \ldots, N)$ of system (6.62) via $\lambda_j = \ln |\mu_j|$. We find

$$\langle |\Theta(t)| \rangle \propto \mathrm{e}^{(\lambda_1 - 2c)t} \tag{6.69}$$

where the average is taken over all initial conditions $\mathbf{u}(0)$ and all directions of $\Theta(0)$ and λ_1 is the largest one-dimensional Lyapunov exponent. Equation (6.69) tells us that for $2c > \lambda_1$ both systems stay in phase. Consequently, they have the λ_1 of the uncoupled system (6.62). The two systems get out of phase at the value $c^* = \lambda_1$. Thus c^* provides the largest one-dimensional Lyapunov exponent.

From the trends in the field of chaos it is apparent that the study of coupled systems is of current interest. One of the fundamental reasons for this is that an array of coupled systems often describes natural processes more accurately. Another reason is that an array of coupled systems is by far more versatile than any such single system. Compare for instance the task performing capacity of a multi-layer perceptron to that of a single-layer perceptron which does not even have the capacity to represent a simple exclusive-or function [545]. With regard to coupled systems the reader is referred to [140], [865] and the references therein as well as the numerous references listed in the bibliography of this book.

Chapter 7

Controlling Chaos

7.1 Introduction

It is a well known fact that a chaotic attractor has embedded in it an infinite number of unstable periodic trajectories of different periods. This fact was exploited by Ott, Grebogi and Yorke [605] in an attempt to convert a chaotic trajectory of a chaotic system to (a selected) one of its unstable periodic trajectories. Until then all attempts at controlling chaos were focused on eliminating or suppressing the chaotic response of a chaotic system, often totally destroying the structure of the chaotic attractor which existed before the attempt to control the system. As pointed out by Ott and his collaborators, it is of fundamental importance to preserve the structure of the chaotic attractor, since, in essence this preserves the dynamical characteristics of the system, meaning amongst other things that the result of the control effort is known: a periodic trajectory on the chaotic attractor.

For example suppose a fighter aircraft is designed to move chaotically in the air. If desired, a fixed point of the associated attractor may be stabilized, resulting in smooth stable flight of the aircraft. However, if it becomes necessary to perform evasive manoeuvres, the controller that controls the aircraft may be adjusted to stabilize a periodic trajectory on the chaotic attractor. In this case, although the aircraft seems to be moving in a strange way, the motion exhibited by the aircraft still satisfies the equations of motion of the air frame. This will necessarily simplify other controller structures containing the aircraft dynamics in the loop. Stabilizing different periodic trajectories allows the aircraft to perform sometimes very different manoeuvres, adding to the flexibility and agility of the system.

Figure 7.1 classifies the methods for controlling chaos into categories. *Continuous control* represents all methods in which the control is applied to the system for all time, for instance conventional feedback (linear and nonlinear) whereas *discrete con-*

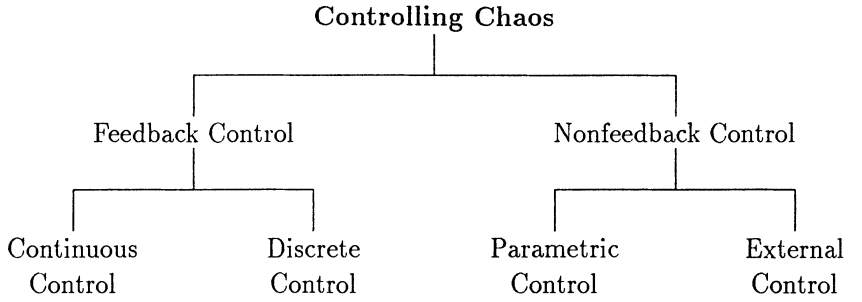

Figure 7.1: Classification of methods for controlling chaos.

trol represents all methods which apply control only on selected time instances, for example the OGY method [605], [606]. *Parametric control* refers to all attempts to control a chaotic system by introducing (usually) periodic perturbation to an accessible system parameter [485], [496]. *External control* represents all methods which apply control to the system input where the control signal is not derived from some form of state feedback [96].

Some methods attempt to stabilize existing unstable periodic trajectories. The *Ott-Grebogi-Yorke method* (OGY method for short) attempts to achieve this by controlling trajectories to approach the stable manifold of the periodic trajectory to be stabilized from where the trajectory is then approached with time. Conventional linear feedback however usually attempts to reduce positive characteristic exponents of the unstable periodic trajectory to be stabilized. Not all methods of controlling chaos attempts to stabilize existing unstable periodic orbits. Specifically the objective of nonfeedback control schemes is to extinguish chaos thereby usually modifying or totally destroying the attractor. In this chapter the OGY method which is a discrete method, is discussed in great detail. Other methods discussed are direct control and targeting, which are both discrete methods, and self-controlling feedback which is a continuous method. This is followed by a brief literature survey on the subject of controlling chaos.

7.2 Ott-Grebogi-Yorke Method

In practice, it is often desired that chaos be avoided and/or that the system performance be improved or changed in some way. Given a chaotic attractor, one approach might be to make some large and possibly costly alteration in the system which completely changes its dynamics in such a way as to achieve the desired behaviour.

Here we assume that this avenue is not available. Therefore, we address the following question: Given a chaotic system, how can improved performance and a desired attracting time-periodic motion be obtained by making only *small* time-dependent perturbations in an *accessible* system parameter?

The key observation (already mentioned earlier) is that a chaotic attractor typically has embedded within it an infinite number of unstable periodic trajectories. The OGY method takes advantage of this observation and may be outlined as follows. First some of the unstable low-period periodic trajectories that are embedded in the chaotic attractor are determined. Then these trajectories are examined to find one which yields improved system performance. Finally, the small time-dependent parameter perturbations must be made so as to *stabilize* this already existing trajectory. The parameter perturbations must be small enough to prevent the creation of new trajectories. It is interesting to note that if the situation is such that the suggested method is practically realizable, then the presence of chaos could be of great advantage because any one of a number of different trajectories can be stabilized, and the choice among those trajectories can be made to achieve the best system performance. If, on the other hand, the attractor is not chaotic but is, say, periodic, then small parameter perturbations will only change the trajectory slightly.

In addition one may want a system to be used for different purposes or under different conditions at different times. Thus, depending on the use, different requirements are expected of the system. If the system is chaotic, a multi-usability requirement might be accommodated without alteration of the gross system configuration. In particular, depending on the use desired, the system behaviour could be changed by switching the temporal programming of the small parameter perturbations to stabilize different orbits. In contrast, in the absence of chaos, completely separate systems might be required for each use. Therefore, when designing a system that is intended for multiple uses, purposely building chaotic dynamics into the system may allow for the desired flexibility.

7.2.1 Theory

The derivation is given for three-dimensional continuous-time autonomous dynamical systems which depend on one system parameter, which we denote by p (see [605], [606] and [663]). Such a system is described by a nonlinear differential equation of the form

$$\frac{d\mathbf{x}}{dt} = \mathbf{F}(\mathbf{x}, p)\,, \tag{7.1}$$

where $\mathbf{F} : \mathbf{R}^3 \times \mathbf{R} \to \mathbf{R}^3$ and $\mathbf{x} \in \mathbf{R}^3$. We assume that the parameter p is available for external adjustment, and we wish to temporally program our adjustment of p so as to achieve improved performance. It should be emphasized that the restriction here to three-dimensional systems is mainly for ease of presentation. For the case of

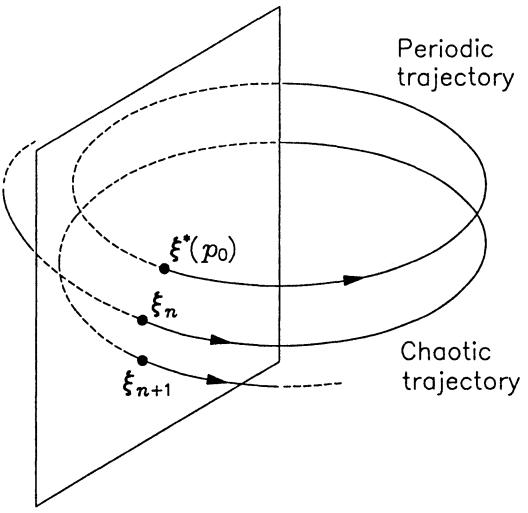

Figure 7.2: Periodic and chaotic trajectories and their orbits on the surface of section.

higher-dimensional (including infinite-dimensional) systems the reader is referred to [606]. In addition, we discuss only the stabilization of unstable periodic orbits. The stabilization of a fixed point is straightforward.

In order to simplify the presentation we first assume that i) the system equation is available, ii) all state variables are accessible and iii) the location of the unstable period-1 trajectory to be stabilized is known. (Here the term period-m trajectory refers to a periodic trajectory of period mT for T some positive real number.) Assume that for the parameter value $p = p_0$, the system is chaotic. By selecting an appropriate Poincaré section (i.e. a surface of section) for the dynamical system (7.1) we obtain the discrete-time system (the Poincaré map)

$$\boldsymbol{\xi}_{n+1} = \mathbf{G}(\boldsymbol{\xi}_n, p)\,, \tag{7.2}$$

where $\mathbf{G} : \mathbf{R}^2 \times \mathbf{R} \to \mathbf{R}^2$ and $\boldsymbol{\xi}_n \in \mathbf{R}^2$ specifies the position on the surface of section of the n-th piercing of the surface by the continuous trajectory. The unstable fixed point $\boldsymbol{\xi}^*(p_0)$ on the surface of section identifies with the unstable period-1 trajectory of the continuous-time system that is to be stabilized, i.e., this period-1 trajectory pierces the surface of section at the point with coordinate vector $\boldsymbol{\xi}^*(p_0)$. For a graphical illustration see Figure 7.2. Now, on the surface of section, in a small neighbourhood of the point $\boldsymbol{\xi} = \boldsymbol{\xi}^*(p_0)$ we can approximate the Poincaré map by

$$\Delta\boldsymbol{\xi}_{n+1} \approx \mathbf{A}\Delta\boldsymbol{\xi}_n + \mathbf{B}\Delta p_n\,, \tag{7.3}$$

where

$$\Delta p_n := p_n - p_0$$

and

$$\mathbf{A} := D_{\boldsymbol{\xi}}\mathbf{G}(\boldsymbol{\xi}^*(p_0), p_0)\,, \qquad \mathbf{B} := \frac{\partial \mathbf{G}}{\partial p}(\boldsymbol{\xi}^*(p_0), p_0)\,. \tag{7.4}$$

In order to prevent new trajectories from being created, the perturbations Δp_n should be kept very small. Also, in (7.3)

$$\Delta\boldsymbol{\xi}_k := \boldsymbol{\xi}_k - \boldsymbol{\xi}^*(p_0)\,, \quad k \in \mathbf{N}\,. \tag{7.5}$$

At this point we recall the following decomposition for the matrix $\mathbf{A}$:

$$\mathbf{A} = \lambda_u \mathbf{e}_u \mathbf{f}_u^T + \lambda_s \mathbf{e}_s \mathbf{f}_s^T\,. \tag{7.6}$$

Here $|\lambda_u| > 1$, $|\lambda_s| < 1$ where λ_u and λ_s represent the stable and unstable eigenvalues of $\mathbf{A}$, while $\{\mathbf{e}_u, \mathbf{e}_s\}$ and $\{\mathbf{f}_u, \mathbf{f}_s\}$ are the sets of left and right eigenvectors of $\mathbf{A}$, respectively. Recall that $\{\mathbf{e}_u, \mathbf{e}_s\}$ and $\{\mathbf{f}_u, \mathbf{f}_s\}$ form reciprocal bases, in other words

$$\mathbf{f}_s^T \mathbf{e}_s = \mathbf{f}_u^T \mathbf{e}_u = 1, \qquad \mathbf{f}_s^T \mathbf{e}_u = \mathbf{f}_u^T \mathbf{e}_s = 0\,.$$

Now, assume that $\boldsymbol{\xi}_n$ falls near the desired fixed point $\boldsymbol{\xi}^*(p_0)$ so that (7.3) applies. The control strategy is to choose p_n such that $\boldsymbol{\xi}_{n+1}$ falls on the stable manifold of $\boldsymbol{\xi}^*(p_0)$, that is, such that

$$\mathbf{f}_u^T \Delta\boldsymbol{\xi}_{n+1} = 0\,.$$

Using (7.3) and (7.6) in this expression, we obtain, after performing the necessary manipulation, that

$$\Delta p_n = -\mathbf{K}^T \Delta\boldsymbol{\xi}_n\,,$$

with $\mathbf{K}$ defined by (see [228])

$$\mathbf{K} := \frac{\lambda_u}{\mathbf{f}_u^T \mathbf{B}} \mathbf{f}_u\,. \tag{7.7}$$

Here, we assume that the condition $\mathbf{f}_u^T \mathbf{B} \neq 0$ is satisfied. The above considerations apply only in a small neighbourhood of $\boldsymbol{\xi}^*(p_0)$. To prevent $|p_n|$ from becoming too large and hence perhaps not meaningful any longer, we set

$$\Delta p_n = \begin{cases} -\mathbf{K}^T \Delta\boldsymbol{\xi}_n, & \text{if } |\mathbf{K}^T \Delta\boldsymbol{\xi}_n| < \Delta p_{\max} \\ 0, & \text{otherwise} \end{cases}\,, \tag{7.8}$$

where $\Delta p_{\max}$ is the maximum allowable parameter deviation. Finally, using (7.8) in (7.3) we obtain

$$\Delta\boldsymbol{\xi}_{n+1} \approx \mathbf{A}_c \Delta\boldsymbol{\xi}_n\,, \tag{7.9}$$

where $\mathbf{A}_c$ is the matrix

$$\mathbf{A}_c := \begin{cases} \mathbf{A} - \mathbf{B}\mathbf{K}^T, & \text{if } |\mathbf{K}^T \Delta\boldsymbol{\xi}_n| < \Delta p_{\max} \\ \mathbf{A}, & \text{otherwise} \end{cases} \tag{7.10}$$

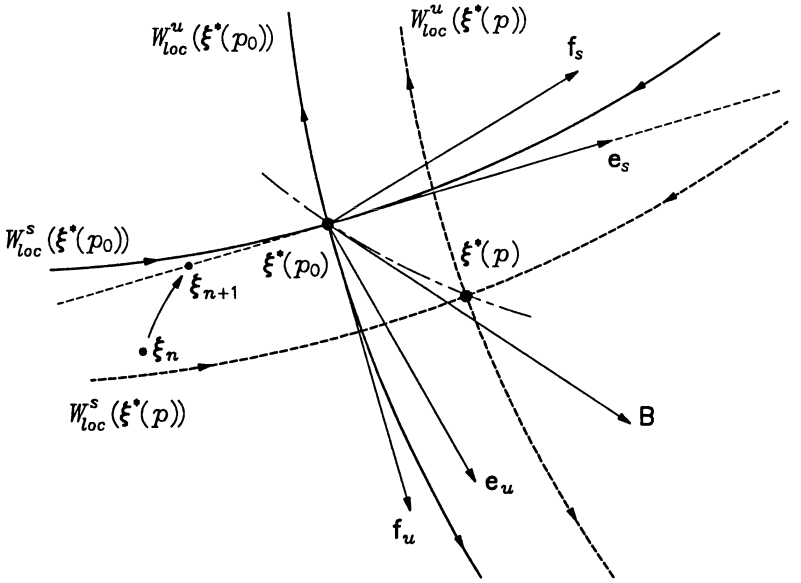

Figure 7.3: Geometric depiction of the OGY control method.

This completes the derivation of the OGY method for controlling chaos. A geometric view of the OGY control scheme is depicted in Figure 7.3. The expression (7.7) looks different from the expression given in [606]. The reason for this is that we have used linearization about $\xi^*(p_0)$ and p_0 and do not estimate the new position of the fixed point $\xi^*(p)$ with changing p as was done in [606]. However, it can be shown that these two approaches are equivalent (see [228]).

Using this method we can thus stabilize a periodic trajectory. However, for a typical initial condition, this is preceded in time by a chaotic transient in which the trajectory is similar to those on the uncontrolled chaotic attractor. The length τ of such a chaotic transient depends sensitively on the initial conditions and for randomly chosen initial conditions has an exponential probability distribution

$$P(\tau) \propto \mathrm{e}^{-\tau/\langle\tau\rangle},$$

for large τ. The estimated average time $\langle\tau\rangle$ to achieve control can be shown ([605], [606] and [663]) to be

$$\langle\tau\rangle \propto \Delta p_{\max}^{-\gamma}, \qquad \text{with} \quad \gamma = 1 - \frac{1}{2}\frac{\ln|\lambda_u|}{\ln|\lambda_s|}. \tag{7.11}$$

The OGY control algorithm is summarized below:

1. **Initialization**
   a. Identify the periodic trajectory to be stabilized.
   b. Calculate $\boldsymbol{\xi}^*(p_0)$.
   c. Calculate the matrices $\mathbf{A}$ and $\mathbf{B}$ (Equation (7.4)).
   d. Calculate $\{\lambda_u, \lambda_s\}$, $\{\mathbf{e}_u, \mathbf{e}_s\}$ and $\{\mathbf{f}_u, \mathbf{f}_s\}$ for $\mathbf{A}$.
   e. Calculate the vector $\mathbf{K}$ (Equation (7.7)).
   f. Select $\Delta p_{\max}$.
2. **Iteration**
   a. Calculate Δp_n (Equation (7.8)).

Example 7.1 Consider the Hénon map

$$\begin{pmatrix} x_{1,n+1} \\ x_{2,n+1} \end{pmatrix} = \begin{pmatrix} a - x_{1,n}^2 + bx_{2,n} \\ x_{1,n} \end{pmatrix}$$

with $b = 0.3$. We assume that the parameter a may be varied about $a_0 = 1.4$ for which the Hénon map is chaotic.

Accordingly we write

$$a_n = a_0 + \Delta a_n ,$$

and $\boldsymbol{\xi}_n := (x_{1,n}, x_{2,n})^T$. The fixed point $\boldsymbol{\xi}^*(a_0) = (x_1^*, x_2^*)^T$ and all the associated parameters and vectors required are [606]

$$\boldsymbol{\xi}^*(a_0) = \frac{1}{2}\left((b-1) + \sqrt{(b-1)^2 + 4a_0}\right)\begin{pmatrix} 1 \\ 1 \end{pmatrix},$$

$$\mathbf{A} = \begin{pmatrix} -2x_1^* & b \\ 1 & 0 \end{pmatrix},$$

$$\lambda_u = -x_1^* - \sqrt{x_1^{*2} + b}, \qquad \lambda_s = -x_1^* + \sqrt{x_1^{*2} + b},$$

$$\mathbf{e}_u = \frac{1}{\sqrt{\lambda_u^2 + 1}}\begin{pmatrix} \lambda_u \\ 1 \end{pmatrix}, \qquad \mathbf{e}_s = \frac{1}{\sqrt{\lambda_s^2 + 1}}\begin{pmatrix} \lambda_s \\ 1 \end{pmatrix},$$

$$\mathbf{f}_u = \frac{\sqrt{\lambda_u^2 + 1}}{\lambda_u - \lambda_s}\begin{pmatrix} 1 \\ -\lambda_s \end{pmatrix}, \qquad \mathbf{f}_s = \frac{\sqrt{\lambda_s^2 + 1}}{\lambda_s - \lambda_u}\begin{pmatrix} 1 \\ -\lambda_u \end{pmatrix},$$

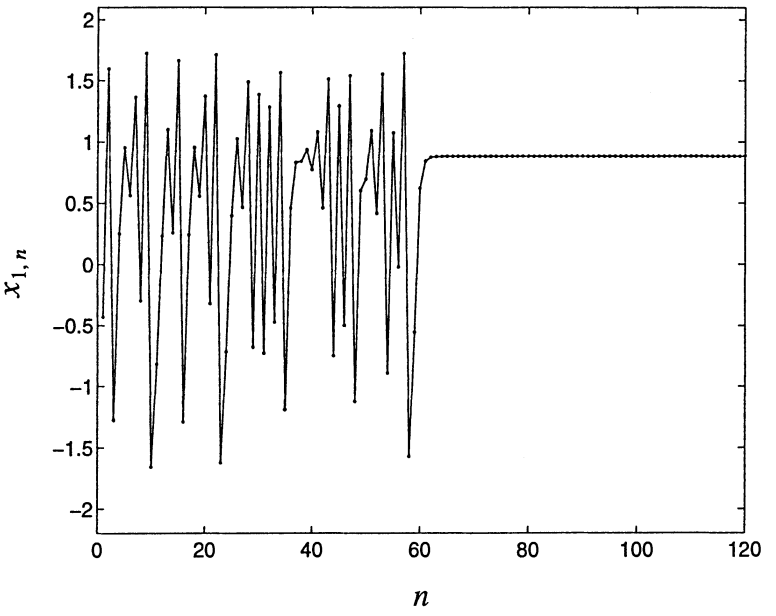

(a)

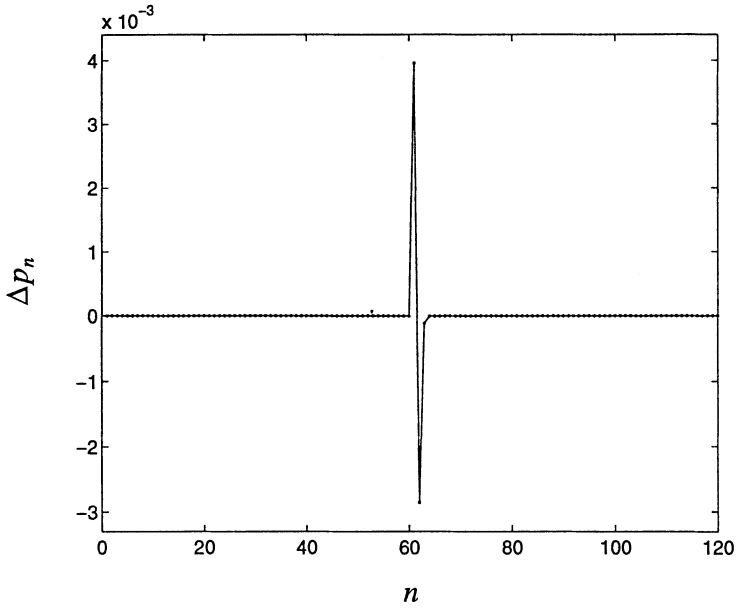

(b)

Figure 7.4: Stabilization of a period-1 state of the Hénon map by the OGY method.

$$\mathbf{B} = \begin{pmatrix} 1 \\ 0 \end{pmatrix}, \qquad \mathbf{K} = -\lambda_u \begin{pmatrix} 1 \\ -\lambda_s \end{pmatrix}.$$

As an illustration in Figure 7.4 we show the results of stabilizing the fixed point $\boldsymbol{\xi}^*(a_0)$ with $\Delta p_{\max} = 10^{-2}$. Starting at a randomly selected initial point

$$\boldsymbol{\xi}_0 = (-0.428060, 1.263923)^T$$

on the Hénon attractor, we see that for the first 60 iterations, the trajectory moves chaotically on the attractor, never falling within the desired strip about $\boldsymbol{\xi}^*(a_0)$, described by

$$\left|\mathbf{f}_u^T \Delta\boldsymbol{\xi}_n\right| < \Delta\xi_{\max}, \qquad \Delta\xi_{\max} := \left|\lambda_u^{-1}\mathbf{f}_u^T\mathbf{B}\right| \Delta p_{\max}.$$

Then on the 61-th iteration the state falls within the desired strip and the control is activated. After control is achieved the trajectory is held near $\boldsymbol{\xi}^*(a_0)$.

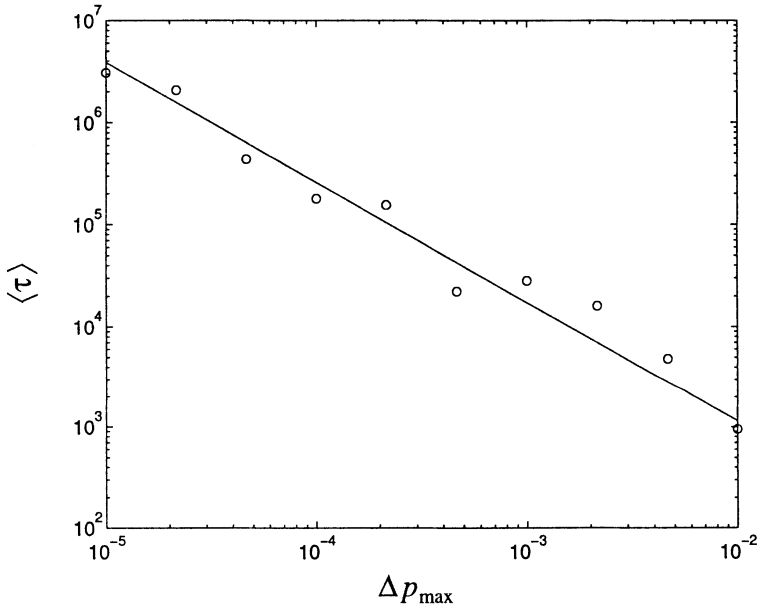

Figure 7.5: $\Delta p_{\max}$ vs. $\langle\tau\rangle$ for the Hénon map.

To evaluate the expression (7.11) for the estimated average time $\langle\tau\rangle$ to achieve control, we proceed as follows. We iterate the map with $a = a_0$ using a large number of randomly chosen initial conditions until all these initial conditions are distributed over the attractor (500 or more iterations should typically be used). We then turn on the control and for each of these orbits determine the additional iterations τ necessary before the orbit falls within a circle centred around $\boldsymbol{\xi}^*(a_0)$ with radius $\Delta\xi_{\max}/2$. We then calculate the average of these times. This is done for many different values of

$\Delta p_{\max}$. The graph of $\Delta p_{\max}$ vs. these average times is shown in Figure 7.5. The line in Figure 7.5 represents the theoretical estimate given by (7.11). The agreement between the experimental and theoretical estimates is satisfactory. ■

7.2.2 Unavailability of an Analytic Model

Often no analytical model (in this case (7.1)) is available. In such situations the suitable unstable periodic trajectory and local dynamical features of the system must be estimated from an experimentally measured trajectory of the system. In [300], [39], [317] and [469] it is shown how to locate periodic trajectories from experimental time series. Suppose $\{\boldsymbol{\xi}_k\}$ is a discrete orbit on the surface of section of a chaotic trajectory. If two successive piercings say $\boldsymbol{\xi}_n$ and $\boldsymbol{\xi}_{n+1}$ are close to each other then there will typically be a period-1 orbit nearby [300], [39], [724]. We denote this estimated fixed point by $\hat{\boldsymbol{\xi}}^*(p_0)$. To establish the dynamics local to the period-1 point $\hat{\boldsymbol{\xi}}^*(p_0)$, we collect a large number of pairs of successive piercings that lie close to $\boldsymbol{\xi}^*(p_0)$ say

$$\{(\boldsymbol{\xi}_n, \boldsymbol{\xi}_{n+1}),\ (\boldsymbol{\xi}_{n+k_1}, \boldsymbol{\xi}_{n+k_1+1}), \ldots, (\boldsymbol{\xi}_{n+k_N}, \boldsymbol{\xi}_{n+k_N+1})\}.$$

We then perform a least-squares fit of a local linear map to the collected data [231]. The least-squares estimate of the Jacobian matrix at $\boldsymbol{\xi}^*(p_0)$ is given by (Appendix C)

$$\hat{\mathbf{A}} = \left(\sum_{i=0}^{N} \Delta\boldsymbol{\xi}_{n+k_i+1} \Delta\boldsymbol{\xi}_{n+k_i}^T\right) \left(\sum_{j=0}^{N} \Delta\boldsymbol{\xi}_{n+k_j} \Delta\boldsymbol{\xi}_{n+k_j}^T\right)^{-1},$$

where $k_0 = 0$ and $\Delta\boldsymbol{\xi}_k = \boldsymbol{\xi}_k - \hat{\boldsymbol{\xi}}^*(p_0)$.

In order to determine $\hat{\mathbf{B}}$, the estimate of $\mathbf{B}$, we adjust the parameter p to $p = p_0 + \Delta p$, and determine $\hat{\boldsymbol{\xi}}(p)$ as mentioned earlier. Then we estimate $\hat{\mathbf{B}}$ from the approximation [724]

$$\hat{\mathbf{B}} = \left(\hat{\boldsymbol{\xi}}^*(p) - \hat{\boldsymbol{\xi}}^*(p_0)\right) / \Delta p.$$

Using the estimates $\hat{\boldsymbol{\xi}}^*(p_0)$, $\hat{\mathbf{A}}$ and $\hat{\mathbf{B}}$ we can calculate all other parameters and vectors required by the OGY control scheme.

7.2.3 Control of Period-m Orbits

The most direct way to analyze a period-m ($m > 1$) orbit corresponding with an mT-period continuous trajectory, is to take the m-th return map. The problem with this approach is that the update of the parametric corrections which occurs once in every interval mT, becomes rather infrequent and thus less effective. This approach is found to be very sensitive to noise. A better way is to use the first-return map

(with short intervals between piercings) and update the parameter correction at every piercing of the surface of section thereby adjusting the controlling parameter p more frequently.

Let the period-m orbit in the surface of section be

$$\boldsymbol{\xi}_1^*(p),\, \boldsymbol{\xi}_2^*(p), \ldots,\, \boldsymbol{\xi}_m^*(p)\,.$$

Let $\lambda_{u,n}, \lambda_{s,n}$, and $\mathbf{e}_{u,n}, \mathbf{e}_{s,n}$ be defined such that for small $|\boldsymbol{\xi}_n - \boldsymbol{\xi}_n^*(p_0)|$ and small p, the linearized dynamics in the neighbourhood of the period-m orbit is described by

$$\Delta\boldsymbol{\xi}_{n+1} \approx \left(\lambda_{u,n}\mathbf{e}_{u,n+1}\mathbf{f}_{u,n}^T + \lambda_{s,n}\mathbf{e}_{s,n+1}\mathbf{f}_{s,n}^T\right)\Delta\boldsymbol{\xi}_n + \mathbf{B}_n\Delta p_n\,, \tag{7.12}$$

where $\Delta\boldsymbol{\xi}_n := \boldsymbol{\xi}_n - \boldsymbol{\xi}_n^*(p_0)$, and $\{\mathbf{f}_{u,n}, \mathbf{f}_{s,n}\}$ is the contravariant basis of the basis $\{\mathbf{e}_{u,n}, \mathbf{e}_{s,n}\}$ and $\mathbf{B}_n = (\partial\boldsymbol{\xi}_n^*/\partial p)(p_0)$. Premultiplying (7.12) by $\mathbf{f}_{u,n+1}$ and requiring that

$$\mathbf{f}_{u,n+1}^T\Delta\boldsymbol{\xi}_{n+1} = 0\,,$$

we obtain

$$\Delta p_n = \left(\frac{\lambda_{u,n}}{\mathbf{f}_{u,n+1}^T\mathbf{B}}\mathbf{f}_{u,n}^T\right)\Delta\boldsymbol{\xi}_n\,.$$

The last two expressions obtained here are analogous to results obtained for period-1 trajectory stabilization. This is in essence *Occasional Proportional Feedback* (OPF) control.

7.2.4 Experimental Embedding

Suppose that the equations of motion of the system are not known, but that experimental time series of some scalar dependent variable $x(t)$ can be measured. Then, using delay coordinates with delay Δ one can form a delay coordinate vector

$$\tilde{\mathbf{x}}(t) := (x(t),\, x(t-\Delta),\, x(t-2\Delta), \ldots,\, x(t-N\Delta))^T\,.$$

The Whitney embedding theorem (Appendix B) states that, if $\mathcal{M}$ is a bounded manifold in a d-dimensional space with coordinates $\mathbf{y}$, then there exists a set of $2d+1$ functions, $h_i : \mathcal{M} \to \mathbf{R}$ for $i = 1, \ldots, 2d+1$, such that the map from $\mathcal{M}$ to $\mathbf{R}^{2d+1}$, namely

$$\mathbf{y} \mapsto \tilde{\mathbf{y}} = \mathbf{h}(\mathbf{y}) := (h_1(\mathbf{y}), \ldots, h_{2d+1}(\mathbf{y}))^T\,,$$

is an *embedding*. That is, if $\mathbf{h}(\mathbf{u}_1) = \mathbf{h}(\mathbf{u}_2)$ then $\mathbf{u}_1 = \mathbf{u}_2$, and the map on $\mathcal{M}$ is invertible. Therefore there are no self-intersections of the image of $\mathcal{M}$ in the embedding space. Using the Whitney embedding theorem, and viewing the map specified by the delay coordinate procedure as being a map into $\mathbf{R}^{N+1}$, it can be shown that $\tilde{\mathbf{x}}$ is an embedding for $\mathbf{x}$ if

$$N + 1 = 2D + 1\,,$$

with D the dimension of the dynamical system under investigation (which is $D = 3$ for our discussion). However, the OGY control procedure does not require reconstruction of the complete continuous-time dynamics in $\tilde{\mathbf{x}}$-space, since we are only interested in periodic orbits on the surface of section. This enables us to use a value of N substantially less than the value required above. To embed a small neighbourhood of a point from $\mathbf{x}$ to $\tilde{\mathbf{x}}$, we find that $N = D - 1$ is generally sufficient [606]. Thus, for the case $D = 3$, our surface of section need only be two-dimensional.

Using an experimental surface of section for the trajectory in the embedding space, we obtain many experimental points in the surface of section for $p = p_0$, say $\{\boldsymbol{\xi}_i\}$ where $\boldsymbol{\xi}_i$ denotes the coordinates on the surface of section at the i-th piercing of the surface of section by the trajectory $\tilde{\mathbf{x}}(t)$. For example, a possible choice of the surface of section would be $x(t - N\Delta) = C$ where C is some constant, and consequently

$$\boldsymbol{\xi}_i = (x(t_i), \ldots, x(t_i - (N-1)\Delta))^T ,$$

where $t = t_i$ denotes the time at the i-th piercing of the surface of section. From such experimentally determined sequences it has been demonstrated that a large number of distinct unstable periodic orbits on a chaotic attractor can be determined ([317] [469]). These unstable periodic orbits are then examined and the one which gives the best performance is selected. Using experimentally determined orbits in the surface of section, the stability properties of the selected periodic orbit is next determined (see previous section). Using the approximation methods of the previous section we can then calculate all parameters and vectors required by the OGY method. As pointed out in [228], in the presence of variation of the parameter p, delay coordinate embedding leads to a Poincaré map of a form different from (7.2). For example, say that the time instant on which the continuous-time trajectory pierces the surface of section at $\boldsymbol{\xi}_k$ is t_k and suppose

$$t_n - t_{n-r+1} \leq (N-1)\Delta < t_n - t_{n-r} ,$$

where r is a positive integer. Then the relevant map is of the form

$$\boldsymbol{\xi}_{n+1} = \mathbf{G}(\boldsymbol{\xi}_n, p_n, p_{n-1}, \ldots, p_{n-r}) .$$

For the case $r = 1$, this expression becomes

$$\boldsymbol{\xi}_{n+1} = \mathbf{G}(\boldsymbol{\xi}_n, p_n, p_{n-1}) . \tag{7.13}$$

Linearization of (7.13) gives

$$\Delta\boldsymbol{\xi}_{n+1} \approx \mathbf{A}\Delta\boldsymbol{\xi}_n + \mathbf{B}_0\Delta p_n + \mathbf{B}_1\Delta p_{n-1} , \tag{7.14}$$

where

$$\mathbf{A} = D_{\boldsymbol{\xi}}\mathbf{G}(\boldsymbol{\xi}^*(p_0), p_0, p_0) , \quad \mathbf{B}_k = \frac{\partial \mathbf{G}}{\partial p_{n-k}}(\boldsymbol{\xi}^*(p_0), p_0, p_0) , \quad k = 0, 1 .$$

Using the decomposition (7.6) and demanding that $\mathbf{f}_u^T \Delta\boldsymbol{\xi}_{n+1} = 0$, we obtain the control law [228]

$$\Delta p_n = -\frac{\lambda_u}{\mathbf{f}_u^T \mathbf{B}_0} \mathbf{f}_u^T \Delta\boldsymbol{\xi}_n - \frac{\mathbf{f}_u^T \mathbf{B}_1}{\mathbf{f}_u^T \mathbf{B}_0} \Delta p_{n-1} . \tag{7.15}$$

Clearly (7.15) has an *Infinite Impulse Response* (IIR) structure and will be unstable if $|\mathbf{f}_u^T \mathbf{B}_1 / \mathbf{f}_u^T \mathbf{B}_0| > 1$, but stable otherwise. Indeed, Dressler and Nitsche [228] have reported instances when the controller (7.15) was unstable. To overcome the possible instability of IIR structures, we require a control law for Δp_n such that Δp_{n+1} will automatically be zero. This is done by demanding that the system stabilizes on step $n+2$ and that Δp_{n+1} equals zero, i.e. by the requirements

$$\mathbf{f}_u^T \Delta\boldsymbol{\xi}_{n+2} = 0 , \quad \text{and} \quad \Delta p_{n+1} = 0 .$$

Using these two expressions, we obtain

$$\Delta p_{n+1} = \frac{-\lambda_u}{\mathbf{f}_u^T \mathbf{B}_0} \mathbf{f}_u^T \Delta\boldsymbol{\xi}_{n+1} - \frac{\mathbf{f}_u^T \mathbf{B}_1}{\mathbf{f}_u^T \mathbf{B}_0} \Delta p_n = 0 .$$

Finally, substituting (7.14) for $\Delta\boldsymbol{\xi}_{n+1}$ and performing the necessary manipulation, yields

$$\Delta p_n = \frac{-\lambda_u^2}{\lambda_u \mathbf{f}_u^T \mathbf{B}_0 + \mathbf{f}_u^T \mathbf{B}_1} \mathbf{f}_u^T \Delta\boldsymbol{\xi}_n - \frac{\lambda_u \mathbf{f}_u^T \mathbf{B}_1}{\lambda_u \mathbf{f}_u^T \mathbf{B}_0 + \mathbf{f}_u^T \mathbf{B}_1} \Delta p_{n-1} . \tag{7.16}$$

From numerical studies performed in [228] it is evident that the control law described by (7.16) out-performs both those described by (7.8) and (7.15).

Example 7.2 [228] The objective here is to control the Duffing oscillator

$$\frac{d^2x}{dt^2} + q\frac{dx}{dt} + x + x^3 = p\cos\omega t ,$$

where p is assumed to be the accessible parameter and $p_0 = 36$, $q = 0.2$ and $\omega = 0.661$. We take the maximum allowed perturbation to be $\Delta p_{\max} = 0.5$. We assume that only $x(t)$ is accessible. Using a three-dimensional embedding with delay time $T_d = T/4$ where $T = 2\pi/\omega$, we obtain a reconstructed state vector

$$\tilde{\mathbf{x}}(t) := (x(t),\, x(t - T_d),\, x(t - 2T_d))^T .$$

We select as the experimental surface of section

$$\tilde{x}_1(t) = 1 , \quad \tilde{x}_2(t) < 0 , \quad \frac{d\tilde{x}_1}{dt}(t) > 0 ,$$

where $\tilde{x}_i$ is the i-th component of the vector $\tilde{\mathbf{x}}$. Using the methods mentioned previously, an unstable fixed point,

$$\boldsymbol{\xi}_1^*(p_0) \approx (-2.846, -2.103)^T ,$$

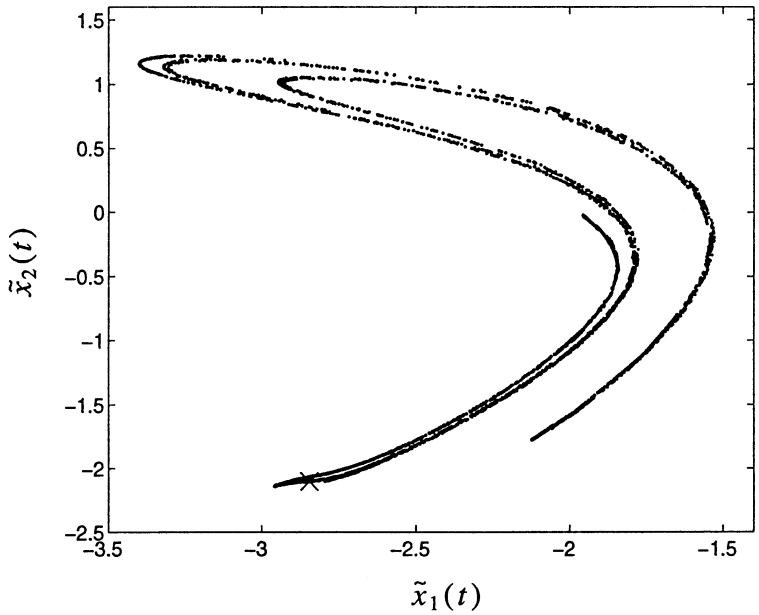

Figure 7.6: Location of the unstable fixed point in the surface of section $\tilde{x}_1(t) = 1$, $\tilde{x}_2(t) < 0$, $(d\tilde{x}_1/dt)(t) > 0$ ($\xi^*(p_0)$ is indicated by '$\times$').

was located. This fixed point is shown on the chaotic attractor in Figure 7.6. To obtain the vectors $\mathbf{B}_0$ and $\mathbf{B}_1$ we use the following procedure [228]. The perturbations Δp_i are alternately switched on and off at every piercing of the surface of section such that $\Delta p_i = 0$ for i odd and $\Delta p_i = \epsilon$ for i even, respectively. Here ϵ is a small real number. We regard all pairs $\left(\boldsymbol{\xi}_i, \boldsymbol{\xi}_{i+1}\right)$ for even i as one group and all pairs with odd i as another. Then, in the neighbourhood of $\boldsymbol{\xi}^*(p_0)$ affine mappings are fitted to $\mathbf{G}(\cdot, p_0, p_0 + \epsilon)$ using only pairs $\left(\boldsymbol{\xi}_i, \boldsymbol{\xi}_{i+1}\right)$ with i odd, and to $\mathbf{G}(\cdot, p_0 + \epsilon, p_0)$ using only pairs $\left(\boldsymbol{\xi}_i, \boldsymbol{\xi}_{i+1}\right)$ with i even. These maps then determine $\mathbf{B}_0$ and $\mathbf{B}_1$ by means of the relations

$$\mathbf{G}(\boldsymbol{\xi}^*, p_0, p_0 + \epsilon) \approx \boldsymbol{\xi}^* + \mathbf{B}_1\epsilon\,, \quad \text{and} \quad \mathbf{G}(\boldsymbol{\xi}^*, p_0 + \epsilon, p_0) \approx \boldsymbol{\xi}^* + \mathbf{B}_0\epsilon\,,$$

respectively. For ease of reference we restate the three respective control laws (7.9), (7.15) and (7.16), namely

$$\begin{aligned} \Delta p_n &= a\mathbf{f}_u^T \Delta\boldsymbol{\xi}_n\,, \\ \Delta p_n &= b_1\mathbf{f}_u^T \Delta\boldsymbol{\xi}_n + b_2\Delta p_{n-1}\,, \\ \Delta p_n &= c_1\mathbf{f}_u^T \Delta\boldsymbol{\xi}_n + c_2\Delta p_{n-1}\,. \end{aligned}$$

We now wish to stabilize $\boldsymbol{\xi}^*$ using each of the above control laws. Specializing the control laws to stabilize $\boldsymbol{\xi}^*$ yields

$$a = -16.43\,, \quad b_1 = -228.4\,, \quad b_2 = -12.9\,, \quad c_1 = 38.9\,, \quad c_2 = 2.2\,.$$

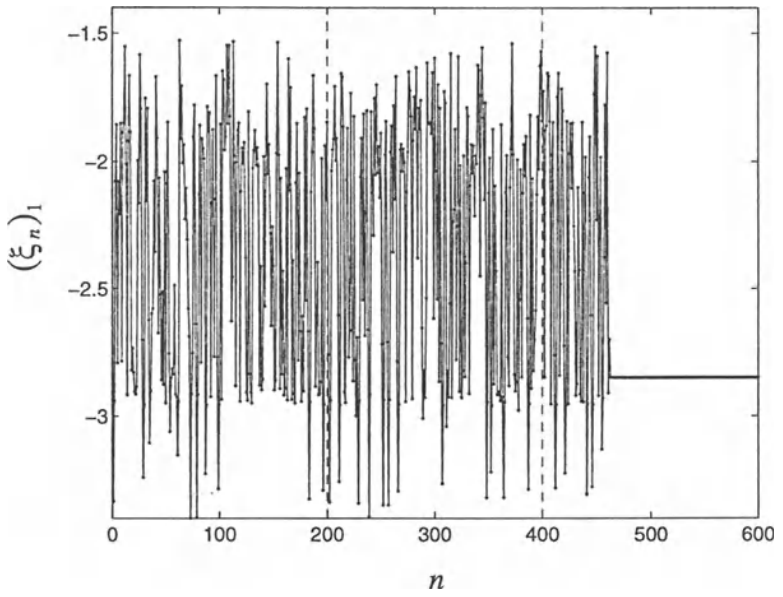

(a)

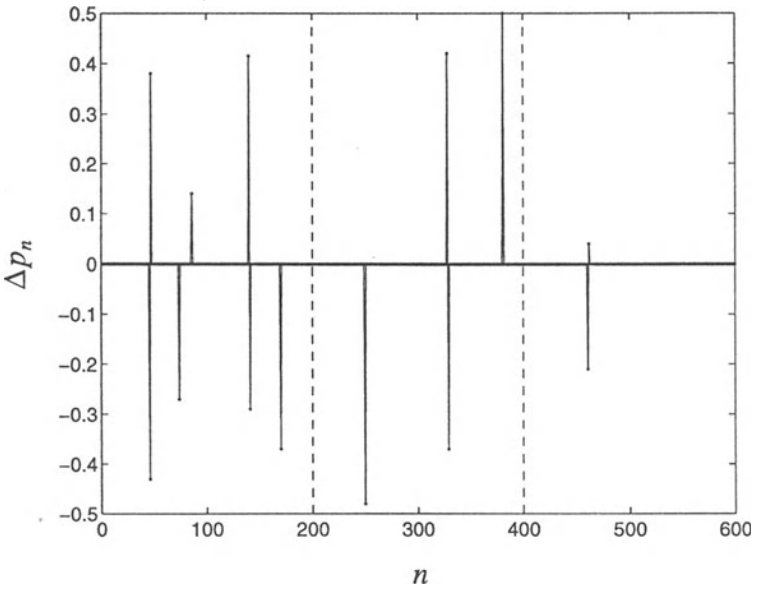

(b)

Figure 7.7: Successive application of the above control laws (in the order listed, each for 200 iterations) to the Duffing equation: (a) n vs. $(\boldsymbol{\xi}_n)_1$, the first component of the point $\boldsymbol{\xi}_n$. (b) Corresponding control parameter perturbations.

Applying the above control laws successively (each for 200 iterations) to the Duffing equation produced the results shown in Figure 7.7. As can be seen from the results, only the third control law listed above was successful in stabilizing the fixed point ξ^*. Moreover, this was achieved with perturbations drastically smaller than that used by the other control laws. Since $|b_2| > 1$ this explains why the second control law fails to stabilize ξ^*. The large absolute value of b_2 indicates further that the influence of the change of the preceding parameter p_{i-1} is relatively larger than that of the actual one, p_i which is exactly what is neglected if one applies the original OGY method without considering the implications of the time delay coordinate embedding. Results on the stabilization of other fixed points on the Poincaré section (Figure 7.7) can be found in [228]. ■

7.2.5 Survey on Applications of the OGY Method

The OGY control scheme have been utilized in both numerical and experimental studies of nonlinear dynamical systems. In numerical studies of the Hénon map and the kicked double rotor the OGY method was applied to stabilize existing unstable periodic trajectories (see [605], [606], [663], [724]). Ditto, Raueso and Spano [221] successfully used the OGY method in a physical system comprised of a gravitationally buckled, amorphous magnetoelastic ribbon. The ribbon material belongs to a new class of amorphous magnetostrictive materials that have been found to exhibit very large reversible changes of Young's modulus $E(H)$ with the application of small magnetic fields. The ribbon was clamped at the base to yield a free vertical length greater than the Euler buckling length, thus giving an initially buckled configuration. The ribbon was placed within three mutually orthogonal pairs of Helmholtz coils, which allowed for compensation of the Earth's magnetic field and application of an approximately uniform vertical magnetic field along the ribbon. The Young's modulus of the ribbon was then varied by applying a vertical magnetic field of the form

$$H(t) = H_{DC} + H_{AC}\cos(2\pi f t)\,.$$

To lowest order, the ribbon was not driven by magnetic forces, but was forced by gravity as $E(H)$ was varied. The magnetic-field amplitudes were typically set in the range 0.1 to 2.5 Oe. A sensor measured the curvature of the ribbon near its base. They were able to achieve stable period-1 and period-2 orbits in the chaotic regime by making perturbations, limited to less than 9% in one of the system's available parameters. They found an approximate linear mapping function in some neighbourhood of the desired fixed point, and used this to calculate the amount of feedback to apply in order to move the fixed point into the neighbourhood of the stable manifold. Because of experimental inaccuracies they could not get the system exactly on the stable manifold, and a new correction was applied each cycle. For period-2 the parameter was adjusted every other cycle.

In a microwave-pumped spin-wave-instability experiment performed by Azevedo and Rezende [45] the OGY method was used to suppress chaos due to spin-wave instabilities. The experiments were carried out with a polished sphere (diameter 1.0 mm) of the ferromagnet yttrium iron garnet (YIG) at room temperature, in the perpendicular-pumping, subsidiary-resonance configuration. The sample is located at the centre of a critically couple rectangular TE_{102} microwave cavity ($f_p = \omega_p/2\pi =$ 8.87GHz, $Q = 2000$) placed between the poles of an electromagnet, so that the microwave magnetic field $\mathbf{h}$ is perpendicular to the biasing field $\mathbf{H}$. However, a loop of diameter 1.5cm made with a 0.5mm copper wire was added inside the cavity to enable modulation of the sample biasing field

$$H(t) = H_0 + \delta H \cos(2\pi f_1 t), \quad \text{with} \quad \delta H/H_0 \approx 10^{-4},$$

over a broad frequency range 0 to 10MHz. The microwave radiation was provided by an X-band backward-wave oscillator with frequency stabilized by an external crystal oscillator and manually adjusted to the centre of the cavity resonance. The radiation was first amplified by a 1.8W traveling-wave tube, then attenuated with a variable precision attenuator, and then directed by a circulator to the resonant cavity where it drove spin waves in the sample. The nonlinear interaction between spin waves resulted in a low-frequency auto-oscillation of the microwave absorption which is detected with a sensitive Schottky-barrier diode at the output port of the circulator and recorded in a digital storage oscilloscope. To avoid sample heating pulsed microwave radiation with duration 100μs at 100 pulses/s was used. The usual experiment to study spin-wave phenomena is done with fixed values of H_0 and varying microwave power. At low power levels the steady-state reflection from the critically coupled cavity is negligible. As the driving field h was increased chaos emerged after a series of bifurcations. The fractal dimension of the attractor was found to be in the range 1.6 to 2.0 near the onset of chaos. The interaction of spin-wave modes is described by the autonomous nonlinear differential equations [199] containing the detuning parameter.

By applying a small modulation to the biasing magnetic field H with appropriate waveform, frequency and amplitude they were able to control the chaotic states. Waveforms used were sinusoidal, square wave and pulse modulation. The field modulation results in a corresponding modulation in the spin-wave frequency ω_k and so in the detuning parameter $\Delta\omega_k$, providing a handle to control the orbits.

The chaotic dynamics found in the diode resonator were converted into stable orbits with periods up to 23 drive cycles long. In this experimental study, Hunt [378] applied the OPF method to stabilize existing unstable periodic trajectories. By permitting fairly large parameter perturbations small alterations in the attractor were made, thereby permitting previously nonexistent periodic orbits to be stabilized. The system used in this work is the diode resonator, which consisted of a pn-junction rectifier in series with an inductor. When driven with an increasing sinusoidal voltage, the system exhibited the classic period-doubling route to chaos. It is know that this system is well characterized by a two-dimensional map [777]. The peak forward current through the diode was taken to be the accessible (chaotic) signal which had to be controlled.

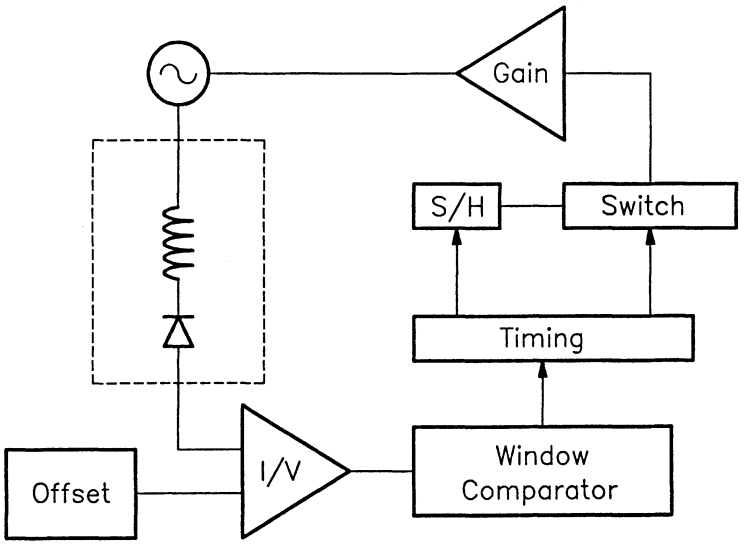

Figure 7.8: Block diagram depicting the experimental setup studied by Hunt.

In his experiment Hunt used a 1N2858 diode as resonator and a 100mH indicator with 25Ω DC resistance, and was driven at 53kHz. A block diagram of the complete system (i.e. diode resonator and the feedback control system) is shown in Figure 7.8. The current through the resonator is converted to a voltage by the I/V device after adding some offset. The purpose of this offset is that the current peaks may be offset, so that control may be attempted for any amplitude. If a peak current signal falls within the adjustable range of the window comparator, which is centred about zero, a trigger signal is generated for use by the timing circuit. The timing circuit in turn generates pulses for the sample/hold circuit (S/H) and the switch. The deviation of the peak from zero is switched through an amplifier to become the control (feedback) signal, which amplitude modulates the signal generator.

Occasional proportional feedback is used for the control. The peak current I_n is sampled, and if it is within a given window, the drive voltage is amplitude modulated by a signal proportional to the difference between I_n and the centre of the window. If it is not within the window, no modulation is applied. The maximum correction is proportional to the size of the window and the system gain, both of which are adjustable. For low-period trajectories this method is essentially the OGY method. However, for trajectories with longer periods the perturbations are allowed to become large enough to alter the attractor slightly, thereby creating new periodic trajectories. The control loop was implemented using using analogue devices, thereby enabling the control to be very fast. In the report [378] it is claimed that the whole correction process took less than 20μs to perform.

Roy and coworkers [668] have applied the OPF method to a multimode, autonomously chaotic solid state laser system. The laser used in their experiments was a diode-laser-pumped solid-state Nd-doped yttrium aluminum garnet (Nd:YAlG) system that contains a KTP (potassium titanyl phosphate) doubling crystal within a cavity of length approximately 3.5cm. The equations that describe the laser operation in several longitudinal modes are well known [851], [94]. However in the experiments reported in [668] it was not necessary to utilize a detailed model of the system. The laser was pumped at 60mW, about 3 times above threshold, and the chaotic operation was observed for a given rotational orientation between the YAlG and KTP crystal. At this level of excitation, the laser operates in anywhere from five to ten longitudinal modes, depending on the rotational orientation of the crystals and the length of the laser cavity.

In a periodically driven system it is convenient to sample a system variable at the driving frequency or its submultiples. However, in the autonomously chaotic laser, there is no driving signal applied, and hence some natural periodicity which is characteristic of the system has to be looked for. Such a periodicity is present in the form of relaxation oscillations in the laser with an intracavity nonlinear crystal and is representative of the fundamental periodicity in the exchange of energy between active atoms and light in the laser cavity. The frequency of the relaxation oscillations increases as the square root of the excitation level above threshold, and depends also on other parameters that characterize the laser. Such parameters are the cavity loss, fluorescence decay time of the active atoms, and the nonlinearity coefficient of the KTP crystal. The frequency of the relaxation oscillations is in the range 20 to 150kHz, for levels of excitation of the laser up to 5 times above threshold. The source of chaotic behaviour here is the coupling of the longitudinal modes through the nonlinear process of sum-frequency generation. This process causes destabilization of the relaxation oscillations which are normally heavily damped for such a system without the intracavity crystal. A block diagram of the laser system and controller studied in [668] is shown in Figure 7.9.

The operation of the laser system in Figure 7.9 is as follows. The fundamental 1.06 μm radiation is monitored by a photodiode, the output from which acts as the input to the control circuit. A stable oscillator is used to generate the synchronizing frequency with which is used to sample the output of the laser system. A variable offset is added to the laser signal to bring it within a window of adjustable width. The window comparator is activated when the signal passes through the window. When the synchronizing input is coincident with this event, the sample and hold acquires the voltage at this instant. The sampled signal is then passed through the gate for relatively short time intervals only. According to [668] a typical time period of application of the correction signal is less than 10μs. An inverting amplifier with variable offset and gain delivers the control signal to the diode-laser driver.

The basic technique for achieving dynamical control is essentially as follows. An accessible variable (in this case the total laser output intensity) is sampled within a

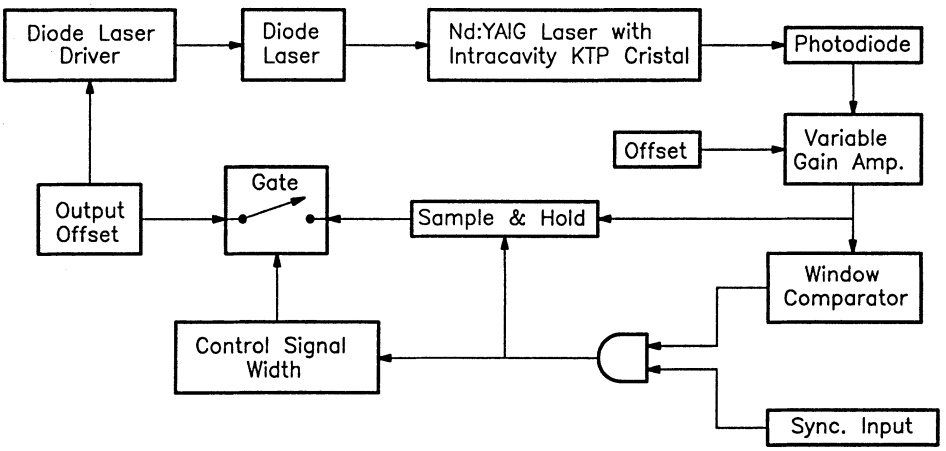

Figure 7.9: Schematic of the laser system and OPF control system.

window of selected offset and width. The sampling frequency is then related to the relaxation oscillation frequency of the system. A signal which is proportional to the difference between the sampled intensity signal and the centre of the window is generated and applied to perturb an accessible system parameter (the pump excitation) from its nominal value. This control signal repeatedly attempts to bring the system closer to an unstable periodic trajectory that is embedded in the chaotic attractor. The accuracy with which the unstable periodic trajectory is reproduced is limited by both the frequency and extent of the feedback as well as by the degree of instability of the trajectory.

The multimode laser system studied by Roy and coworkers is an example of a globally coupled system of nonlinear oscillators. The proportional control signal applied to the pump excitation results in an ordered, periodic state of the original chaotic ensemble of coupled oscillators. From the results reported in [668] it would seem that the technique of occasional proportional feedback should be widely applicable to a variety of systems including arrays of coupled oscillators. Such coupled arrays of nonlinear oscillators are of interest in Josephson-junction networks [851], Van der Pol oscillators, Chua circuits and many other models systems.

7.2.6 Further Aspects

In the derivation of the OGY method presented in Section 7.2 the vector $\mathbf{K}$ featuring in the control equation is given by (7.7). In [663], [724] the OGY method was considered for an arbitrary vector $\mathbf{K}$. For this more general case it was shown that the problem of selecting an appropriate $\mathbf{K}$ is exactly the *pole placement problem*, where $\mathbf{K}$ must be selected such that the eigenvalues of $(\mathbf{A} - \mathbf{B}\mathbf{K}^T)$ (in (7.10)) all lie in the

unit circle in the complex plane [455]. It is shown in [663], [724] that the optimal choice of $\mathbf{K}$ (i.e. the vector $\mathbf{K}$ that minimizes the average time to achieve control) is that $\mathbf{K}$ for which one eigenvalue of $(\mathbf{A} - \mathbf{B}\mathbf{K}^T)$ is zero and the other is the original stable eigenvalue of $\mathbf{A}$.

In the presentation of the OGY method, as it stands, the aspect of noise in the system has been neglected. By adding a noise term say $\rho \mathbf{w}_n$ on the righthand side of (7.3), the model is extended in this respect. Here ρ is the *signal-to-noise ratio* and $\mathbf{w}_n$ a noise vector with components being random variables having zero mean and unity variance [606]. For the case of small ρ the effect of noise is to "kick" the state out of the region where the control is on. Ott *et al.* [606] studied the effect of noise on the mean time, say $\langle T \rangle$, between kick-outs. They found that for $\langle T \rangle \ll \langle \tau \rangle$ control was still effective.

Ott and collaborators [606] also studied the effect of imperfect system identification. Imperfections of this nature are the result of measurement errors, due to measurement accuracy and measurement noise. Therefore $\hat{\boldsymbol{\xi}}^*(p_0)$ differs from $\boldsymbol{\xi}^*(p_0)$. Due to this and the estimation process $\hat{\mathbf{A}}$ will differ from $\mathbf{A}$, thereby causing deviations in the eigenvalues and eigenvectors of $\hat{\mathbf{A}}$ from that of $\mathbf{A}$. If the imperfection (in system identification) is small and the stable eigenvalue of $\mathbf{A}$ is not close to one in magnitude, control will still be achieved. If the imperfection is large, the magnitude of the previously stable eigenvalue might just become greater than one making the system uncontrollable. Furthermore, with large imperfections the deviation of the fixed point may be so severe that once again control may not be achieved. For a treatment of the higher dimensional case the reader is referred to [606].

We conclude this section by summarizing the advantages and disadvantages of the OGY method. All entities needed to achieve control can be obtained from an experimental signal. The controller can be implemented on computer in the system with a large time constant while it has been implemented using analogue components in the case of systems with small time constants. A major impairment of this method is its inability to cope with high dimensional transients resulting from parameter perturbations used in the control effort.

The method is based on the idea of the stabilization of unstable periodic trajectories embedded within a strange attractor. This is achieved by making a small time-dependent perturbation in the form of feedback to an accessible system parameter. This method turns the presence of chaos into an advantage. Due to the infinite number of different unstable periodic trajectories embedded in a strange attractor, a chaotic system can be tuned to a large number of distinct periodic regimes by switching the temporal programming of *small* parameter perturbation to stabilize different periodic orbits. The changes of the parameter, however are discrete in time since the method deals with the Poincaré map. This leads to some limitations. This method can stabilize only those periodic orbits whose maximal Lyapunov exponent is small compared to the reciprocal of the time interval between parameter changes. Since

the corrections of the parameter are infrequent and small, noise leads to occasional bursts of the system into regions far from the desired periodic orbit, and these bursts are more frequent for large noise [605].

7.3 Direct Control from Scalar Time Series

The OGY control method as well as those methods proposed by Dressler and Nitsche that were discussed in the previous section suffer from a fundamental limitation when applied to high dimensional physical systems evolving chaotically on a low dimensional attractor. For a chaotic system whose parameter values are held fixed, one often observes high dimensional transients that vanish with time as the dynamics settle down to a lower dimensional chaotic attractor. The application of even a minute short-term fluctuation in the parameters can reintroduce the higher dimensional transients, rendering it inappropriate to view the dynamics as low dimensional if parameters are frequently adjusted. Consequently, the most obvious approach for modelling a system in which an accessible parameter is to be varied is to follow the evolution in the entire set of phase space variables.

Consider a discrete-time N-dimensional autonomous system, which evolves chaotically at the nominal parameter value $p = p_0$, possessing an unstable equilibrium state $\boldsymbol{\xi}^*(p_0)$ that we wish to stabilize. Suppose that $\boldsymbol{\xi}^*(p_0)$ possesses a one-dimensional unstable manifold with associated eigenvalue λ_1. Thus, by assumption all remaining eigenvalues of the linearized system at $\boldsymbol{\xi}^*(p_0)$ are less than one in magnitude. (For the generalization of this control scheme to higher dimensional unstable manifolds, the reader is referred to [40].) During application of the control, the trajectory is forced to remain in the neighbourhood of $\boldsymbol{\xi}^*(p_0)$ and therefore the local dynamics can be modelled approximately by the linear relationship

$$\Delta\boldsymbol{\xi}_{n+1} \approx \mathbf{A}\Delta\boldsymbol{\xi}_n + \mathbf{B}\Delta p_n\,, \qquad n \in \mathbf{N}\,, \tag{7.17}$$

where

$$\Delta\boldsymbol{\xi}_n := \boldsymbol{\xi}_n - \boldsymbol{\xi}^*(p_0)\,, \qquad \text{and} \qquad \Delta p_n := p_n - p_0\,.$$

Take note that here, $\boldsymbol{\xi}_n$ is the state of the system in its full state space at time n. As before, the matrices $\mathbf{A}$ and $\mathbf{B}$ are given by (7.4).

Suppose that some scalar variable Δx_n is obtained as a linear projection of the relative state vector $\Delta\boldsymbol{\xi}_n$

$$\Delta x_n = P_x(\Delta\boldsymbol{\xi}_n) = \mathbf{p}_x^T\Delta\boldsymbol{\xi}_n\,, \qquad n \in \mathbf{N}\,, \tag{7.18}$$

where P_x is the linear *projection operator* onto the measurement direction x. Using (7.17) together with (7.18) we have

$$\Delta x_{n+1} = \mathbf{p}_x^T\mathbf{A}\Delta\boldsymbol{\xi}_n + \mathbf{p}_x^T\mathbf{B}\Delta p_n\,. \tag{7.19}$$

Now, we may write

$$\mathbf{A} = \lambda_1 \mathbf{e}_1 \mathbf{f}_1^T + \mathbf{\Lambda}\,, \tag{7.20}$$

where $\mathbf{e}_1$ and $\mathbf{f}_1$ are the right and left eigenvectors of $\mathbf{A}$ associated with the eigenvalue λ_1 , and are normalized such that $\mathbf{f}_1^T \mathbf{e}_1 = 1$. The $N \times N$ matrix $\mathbf{\Lambda}$ satisfies

$$\mathbf{\Lambda}^T \mathbf{f}_1 = \mathbf{\Lambda} \mathbf{e}_1 = \mathbf{0}\,. \tag{7.21}$$

For further reference we state the following vector decompositions,

$$\mathbf{y} = \mathbf{y}^u + \mathbf{y}^s = {}^u\mathbf{y} + {}^s\mathbf{y}\,, \tag{7.22}$$

where

$$\mathbf{y}^u || \mathbf{e}_1\,, \quad \mathbf{y}^s \perp \mathbf{f}_1\,, \quad {}^u\mathbf{y} || \mathbf{f}_1\,, \quad {}^s\mathbf{y} \perp \mathbf{e}_1\,, \tag{7.23}$$

for arbitrary $\mathbf{y} \in \mathbf{R}^N$. Using (7.20) to (7.23), we may rewrite (7.19) as

$$\begin{aligned}
\Delta x_{n+1} &= \mathbf{p}_x^T \mathbf{A} \left(\Delta \boldsymbol{\xi}_n^u + \Delta \boldsymbol{\xi}_n^s \right) + \mathbf{p}_x^T \mathbf{B} \Delta p_n \\
&= \mathbf{p}_x^T (\lambda_1 \mathbf{e}_1 \mathbf{f}_1^T + \mathbf{\Lambda}) \Delta \boldsymbol{\xi}_n^u + \mathbf{p}_x^T \mathbf{A} \Delta \boldsymbol{\xi}_n^s + \mathbf{p}_x^T \mathbf{B} \Delta p_n \\
&= \lambda_1 \mathbf{p}_x^T \Delta \boldsymbol{\xi}_n^u + \mathbf{p}_x^T \mathbf{A} \Delta \boldsymbol{\xi}_n^s + \mathbf{p}_x^T \mathbf{B} \Delta p_n \qquad (7.24) \\
&= \lambda_1 \mathbf{p}_x^T \Delta \boldsymbol{\xi}_n + \mathbf{p}_x^T \left(\mathbf{A} - \lambda_1 \mathbf{I} \right) \Delta \boldsymbol{\xi}_n^s + \mathbf{p}_x^T \mathbf{B} \Delta p_n \\
&= \lambda_1 \Delta x_n + a_x^1 \Delta p_n + \mathbf{p}_x^T \left(\mathbf{A} - \lambda_1 \mathbf{I} \right) \Delta \boldsymbol{\xi}_n^s \\
&= \lambda_1 \Delta x_n + a_x^1 \Delta p_n + \mathbf{p}_x^T \left(\mathbf{A} - \lambda_1 \mathbf{I} \right) \Delta \boldsymbol{\xi}_n\,, \qquad (7.25)
\end{aligned}$$

where $\mathbf{I}$ is the $N \times N$ identity matrix and

$$a_x^1 := \mathbf{p}_x^T \mathbf{B}\,.$$

To obtain the last term of (7.25) we have used the fact that for an arbitrary $\mathbf{y} \in \mathbf{R}^N$

$$\left(\mathbf{A} - \lambda_1 \mathbf{I} \right) \mathbf{A}^m \mathbf{y}^u = \lambda_1^m y^u \left(\mathbf{A} - \lambda_1 \mathbf{I} \right) \mathbf{e}_1 = \mathbf{0}\,, \qquad \mathbf{y}^u := y^u \mathbf{e}_1\,, \tag{7.26}$$

for each $m = 0, 1, \ldots$. Repeated iteration of the expression for $\Delta \boldsymbol{\xi}_n$ using (7.17) yields

$$\Delta \boldsymbol{\xi}_n = \sum_{j=0}^{k-2} \mathbf{A}^j \mathbf{B} \Delta p_{n-j-1} + \mathbf{A}^{k-1} \Delta \boldsymbol{\xi}_{n-k+1}\,,$$

and substitution thereof into (7.25) produces

$$\Delta x_{n+1} = \lambda_1 \Delta x_n + \sum_{j=1}^{k} a_x^j \Delta p_{n-j+1} + \mathbf{R}_x^k \Delta \boldsymbol{\xi}_{n-k+1}\,, \tag{7.27}$$

for $k \in \mathbf{N}$,

$$\mathbf{R}_x^k := \mathbf{p}_x^T \left(\mathbf{A} - \lambda_1 \mathbf{I} \right) \mathbf{A}^{k-1}\,,$$

and

$$a_x^j := \mathbf{p}_x^T \left(\mathbf{A} - \lambda_1 \mathbf{I} \right) \mathbf{A}^{j-2} \mathbf{B} = \mathbf{p}_x^T \left(\mathbf{A} - \lambda_1 \mathbf{I} \right) \mathbf{A}^{j-2} \mathbf{B}^s\,, \qquad \text{for } 2 \le j \le k\,. \tag{7.28}$$

The last step of (7.28) follows from (7.26). It is important to note that (7.27) is an exact description up to first order of the local dynamics in the neighbourhood of $\boldsymbol{\xi}^*(p_0)$ along the measurement direction x, in the presence of parameter perturbations. In contrast with the full state space model (7.17), a dependence on the entire history of the parameter perturbations is obtained in the above expansion. An important observation is that the sequence $\{a_x^j\}$ converges exponentially to zero. This can be observed by expanding $\mathbf{B}^s$ in terms of the right eigenvectors of $\mathbf{A}$, and using (7.20) in (7.28). The reason for this exponential convergence is that $\mathbf{B}^s$ has no component in the direction of the unstable left eigenvector of $\mathbf{A}$ and hence $\mathbf{A}^j\mathbf{B}^s$, $j \geq 1$ is a contraction. As will become evident later this may be exploited in the experimental application of the control scheme being derived here.

An alternative form of the expression for Δx_{n+1} can be obtained from (7.24), using (7.20) to (7.23), namely

$$\Delta x_{n+1} = \lambda_1 \Delta x_n^u + {}^u\mathbf{p}_x^T \mathbf{B}^u \Delta p_n + {}^s\mathbf{p}_x^T \mathbf{B}^s \Delta p_n + {}^s\mathbf{p}_x^T \mathbf{A} \Delta \boldsymbol{\xi}_n^s , \tag{7.29}$$

with Δx_n^u and Δx_n^s, respectively defined by

$$\begin{aligned} \Delta x_n^u &:= \mathbf{p}_x^T \Delta \boldsymbol{\xi}_n^u = {}^u\mathbf{p}_x^T \Delta \boldsymbol{\xi}_n = {}^u\mathbf{p}_x^T \Delta \boldsymbol{\xi}_n^u , \\ \Delta x_n^s &:= \mathbf{p}_x^T \Delta \boldsymbol{\xi}_n^s = {}^s\mathbf{p}_x^T \Delta \boldsymbol{\xi}_n = {}^s\mathbf{p}_x^T \Delta \boldsymbol{\xi}_n^s , \end{aligned} \tag{7.30}$$

such that

$$\Delta x_n = \Delta x_n^u + \Delta x_n^s .$$

From (7.29) we obtain

$$\Delta x_{n+1}^u = \Delta x_{n+1}|_{{}^s\mathbf{p}_x = 0} = \lambda_1 \Delta x_n^u + \mathbf{p}_x^T \mathbf{B}^u \Delta p_n . \tag{7.31}$$

If we evaluate (7.17) in the stable manifold, we get

$$\Delta \boldsymbol{\xi}_n^s = \mathbf{A} \Delta \boldsymbol{\xi}_{n-1}^s + \mathbf{B}^s \Delta p_{n-1} .$$

Repeated iteration of this expression produces

$$\Delta \boldsymbol{\xi}_n^s = \sum_{j=0}^{k-2} \mathbf{A}^j \mathbf{B}^s \Delta p_{n-j-1} + \mathbf{A}^{k-1} \Delta \boldsymbol{\xi}_{n-k+1}^s .$$

Substituting this expression into the expression for Δx_n^s obtained in (7.30) gives

$$\Delta x_n^s = \mathbf{p}_x^T \Delta \boldsymbol{\xi}_n^s = \sum_{j=0}^{k-2} \mathbf{p}_x^T \mathbf{A}^j \mathbf{B}^s \Delta p_{n-j-1} + \mathbf{p}_x^T \mathbf{A}^{k-1} \Delta \boldsymbol{\xi}_{n-k+1}^s . \tag{7.32}$$

The unstable fixed point $\boldsymbol{\xi}^*(p_0)$ can therefore be approached from its stable manifold by choosing the parameter perturbation in (7.31) such that $\Delta x_{n+1}^u = 0$. This yields the control law

$$\Delta p_n = \frac{-\lambda_1}{\mathbf{p}_x^T \mathbf{B}^u} \Delta x_n^u = \frac{-\lambda_1}{\mathbf{p}_x^T \mathbf{B}^u} (\Delta x_n - \Delta x_n^s) , \tag{7.33}$$

provided that $\mathbf{p}_x^T \mathbf{B}^u \neq 0$. Applying the parameter perturbation according to (7.33) displaces the trajectory onto the stable manifold. Once on the stable manifold, the trajectory will approach the fixed point $\boldsymbol{\xi}^*(p_0)$ at an exponential rate, determined solely by the local dynamics of the uncontrolled system itself. As in the previous section the parameter perturbation is applied only if $|\Delta p_n| < \Delta p_{\max}$, otherwise $p_n = p_0$ is used.

Now, suppose that no model is available for the system being studied. Then it may be impossible to determine the exact values of $\{\Delta x_n\}$ and $\mathbf{p}_x^T \mathbf{B}^u$ from measured data and hence we have to find a suitable approximation to (7.32) which is based on knowledge of λ_1 and finite many (say the first k) coefficients a_x^j. From the definition of a_x^j the constant coefficients appearing in the control law (7.32) can be expressed as [40]

$$\mathbf{p}_x^T \mathbf{B}^u \approx \sum_{j=1}^{k} \lambda_1^{-(j-1)} a_x^j + \lambda_1^{-(k-1)} \mathbf{p}_x^T \mathbf{A}^{k-1} \mathbf{B}^s , \tag{7.34}$$

$$\mathbf{p}_x^T \mathbf{A}^l \mathbf{B}^s \approx \sum_{j=1}^{l+1} \lambda_1^{l-j+1} a_x^j - \lambda_1^l \mathbf{p}_x^T \mathbf{B}^u , \tag{7.35}$$

for $l < k$. The k-th approximation to the control law (7.32) is obtained as follows. By definition $\mathbf{B}^s \perp \mathbf{f}_1$ and thus we conclude that

$$\mathbf{A}^k \mathbf{B}^s \xrightarrow[\infty]{k} \mathbf{0} ,$$

since all other eigendirections are contracting. In addition, $|\lambda_1| > 1$, so that

$$\lambda_1^{-(k-1)} \mathbf{p}_x^T \mathbf{A}^k \mathbf{B}^s \xrightarrow[\infty]{k} \mathbf{0} .$$

Using this we assume that k is large enough such that

$$\mathbf{p}_x^T \mathbf{B}^u \approx \sum_{j=1}^{k} \lambda_1^{-(j-1)} a_x^j .$$

The minimum value of k that is sufficient for control depends on the strength of the contraction along the contracting eigendirections of $\mathbf{A}$. For the case where the stable directions of the matrix $\mathbf{A}$ are very strongly contracting, $k = 1$ may perhaps suffice to achieve the desired control.

The problem now is to calculate the eigenvalue λ_1 and the set $\{a_x^j\}_{j=1}^k$. First an orbit is generated for no parameter perturbations (i.e. $p = p_0$). One method to calculate λ_1 is to use all successive pairs of iterates that fall within a small neighbourhood of the desired fixed point $\boldsymbol{\xi}^*(p_0)$ in order to calculate a least squares estimate $\hat{\mathbf{A}}$ of $\mathbf{A}$ as described in the previous section. From the estimate $\hat{\mathbf{A}}$ one can then calculate the estimate $\hat{\lambda_1}$ of eigenvalue λ_1 numerically (also refer to [39]). To calculate a_x^m for $m \geq 1$ (yet not too large) we generate an arbitrary orbit with $p = p_0$ until it falls within the (small) expected neighbourhood of $\boldsymbol{\xi}^*(p_0)$ at say time n. Then a parameter

perturbation Δp_n (with $|\Delta p_n| < p_{\max}$) which is small enough for the hypothesis of linearity to hold is applied for one iteration and removed thereafter. Acquiring the signal samples x_{n+m-1} and x_{n+m} we then have the equation

$$\Delta x_{n+m} \approx \hat{\lambda}_1 \Delta x_{n+m-1} + a_x^m \Delta p_n \,,$$

with a_x^m as the unknown. Repeating this process a number of times produces a set of these equations which may then be solved by least squares methods for $\hat{a}_x^m$, the estimate of a_x^m. For m large the estimate calculated using the technique above deteriorates due to nonlinear terms, since in m iteration steps the orbit may escape the neighbourhood of the fixed point $\boldsymbol{\xi}^*(p_0)$ in which linear approximation is valid. Therefore, to determine the a_x^m when m is large, all the coefficient estimates $\hat{a}_x^j$ for $j < m$ should be utilized in order to hold the orbit in the linear neighbourhood of $\boldsymbol{\xi}^*(p_0)$. This entails choosing the parameter perturbations

$$\Delta p_n, \ldots, \Delta p_{n+k-2} \,,$$

according to the $(m-1)$-order approximation of (7.32) which produces the expression (see (7.27))

$$\Delta x_{n+m} \approx \hat{\lambda}_1 \Delta x_{n+m-1} + \sum_{j=1}^{m-1} \hat{a}_x^j \Delta p_{n+m-j} + a_x^m \Delta p_n \,,$$

where the remainder term is disregarded on the assumption that $|\Delta \boldsymbol{\xi}_n| \ll 1$. Repeating this procedure a number of times, produces a set of equations of this form, which may then be used to obtain a least squares estimate $\hat{a}_x^m$ of the coefficient a_x^m. This completes the discussion on the practical aspects of the implementation of the control law (7.32).

A period-m orbit may be controlled using the current method either by controlling the fixed point of the m-th iterate of the system or by applying a control of the form of (7.32) at each orbit point. In the latter alternative however, it is necessary to determine a set of coefficients $\{a_x^j\}$ for each of the m orbit points. For large m, this iterative fit procedure leads to improved control compared with carrying out a single fit for the m-th iterate of the cycle. This is especially so in the presence of noise [40].

For a discussion on the usage of delay coordinate embedding with the control law (7.32), the use of error propagation in this method as well as applications of this method, the reader is referred to [40].

7.4 Targeting

Stabilizing a system by small perturbations as discussed in the preceding sections is extremely effective once the system's state comes close to the desired state. However, if it starts far from the desired state, it might take an unacceptably long time before a

typical trajectory comes close enough to the desired state to be captured by the controller. Shinbrot *et al.* [726] proposed a technique, which they have termed *targeting*, for directing the system to a desired neighbourhood of states in a short time.

For simplicity, we consider a three-dimensional continuous-time autonomous dynamical system. The extension to higher dimensions is given elsewhere [726]. The form of the system considered here is

$$\frac{d\mathbf{x}}{dt} = \mathbf{F}(\mathbf{x}, p)\,,$$

with $\mathbf{F} : \mathbf{R}^3 \times \mathbf{R} \to \mathbf{R}^3$ and $\mathbf{x} \in \mathbf{R}^3$. As in the previous section p is an accessible system parameter which is available for external adjustment. We assume that model equations describing the system are known, although they need not be exact. Next we select a surface of section and denote the coordinates in the surface of section by $\boldsymbol{\xi}$, and the Poincaré map by

$$\boldsymbol{\xi}_{n+1} = \mathbf{G}(\boldsymbol{\xi}_n, p)\,,$$

where the map $\mathbf{G} : \mathbf{R}^2 \to \mathbf{R}^2$ is necessarily invertible. Suppose that in state space we wish to go from a source point $\mathbf{x}_s$ to a small region about a target point, $\mathbf{x}_t$. Tracing the trajectory from $\mathbf{x}_s$ forward in time, we find its first intersection with the surface of section and denote this point $\boldsymbol{\xi}_s$. Tracing the trajectory through $\mathbf{x}_t$ backward in time, we similarly determine its first intersection with the surface of section and denote this point $\boldsymbol{\xi}_t$. By doing so we have reduced the problem to that of a two-dimensional map in which we wish to go from $\boldsymbol{\xi}_s$ to the vicinity of $\boldsymbol{\xi}_t$. Assuming that the system parameter p is available for adjustment at each iterate and that its nominal value is p_0, then its time dependence is described by

$$p_n = p_0 + \Delta p_n\,.$$

Once again we assume that the perturbation Δp_n may only be small.

If the unperturbed system is ergodic, then in the absence of perturbations (that is $\Delta p_n = 0$) the time τ required to travel from a source point $\boldsymbol{\xi}_s$ to a small neighbourhood say B_t of radius ϵ_t centred about the target point $\boldsymbol{\xi}_t$ in the ergodic set is determined by the natural probability measure μ of the system. Typically, we have

$$\tau \propto 1/\mu(B_t)\,.$$

If d_I is the information dimension of the system then we have (see [726])

$$\tau \propto 1/\epsilon_t^{d_I}\,,$$

for small ϵ_t. Therefore we conclude that in the absence of perturbations, the amount of time required to reach a desired target neighbourhood increases according to a power law as the size of this neighbourhood decreases. By applying targeting this power law can be converted to a much weaker logarithmic increase as will become evident.

By applying a perturbation Δp the change of state $\Delta\boldsymbol{\xi}$ after one iteration of the return map, relative to the point $\mathbf{G}(\boldsymbol{\xi}_s, p_0)$, is given by the Taylor expansion

$$\Delta\boldsymbol{\xi} \approx \Delta p \left[\frac{\partial \mathbf{G}}{\partial p}(\boldsymbol{\xi}_s, p)\right]_{p=p_0+\Delta p}, \qquad |\Delta p| < \Delta p_{\max}. \tag{7.36}$$

Here $\Delta p_{\max}$ is the maximum allowable perturbation of p. By varying Δp through the interval $(-\Delta p_{\max}, \Delta p_{\max})$ we find that (7.36) defines a line segment which passes through the point $\mathbf{G}(\boldsymbol{\xi}_s, p_0)$. We denote this line segment L and its length δL. Assuming that the system is chaotic for $p = p_0$, the length of the evolved line segment will grow roughly geometrically with each successive iteration of the map $\mathbf{G}(\boldsymbol{\xi}, p_0)$. Let n_1 denote the number of iterates required for the small line segment L to stretch to a length of order 1, that is, when

$$\delta L\, \mathrm{e}^{n_1 \lambda_1} \approx 1$$

if $\delta\xi$ is small, where λ_1 is the positive one-dimensional Lyapunov exponent of the system. From this we obtain an expression for n_1 in terms of δL and λ_1, namely

$$n_1 \approx \lambda_1^{-1} \ln(1/\delta L)\,.$$

Assuming the size of the relevant ergodic region to be of the order of 1, we see that it takes approximately n_1 iterates for the evolved line segment to span the ergodic region. Next consider the target region B_t. If we map this region backward in time, we find that its pre-image spans the ergodic region after, say, n_2 pre-iterates, where

$$n_2 \approx \lambda_2^{-1} \ln(1/\epsilon_t)\,,$$

if ϵ_t is small. Here λ_2 denotes the negative one-dimensional Lyapunov exponent of the system.

With the above results at our disposal we now describe the process of targeting. First iterate the (source) line segment L forward using $p_n = p_0$ until the evolved segment's length spans the ergodic region. Denote the number of iterates to achieve this by n_1. Then iterate the target region B_t backward until the evolved region first intersects the evolved line segment. Denote the number of backward iterations performed by n_2. Iterating a point in the middle of the intersection backward n_1 times, we find a point on the line segment L which is mapped to the target region B_t in $n_1 + n_2$ iterates. Knowing this point we can then determine the required perturbation Δp_1 to be applied on the first iterate from $\boldsymbol{\xi}_s$ by using (7.36). Thereafter, assuming no noise and no modelling error, the perturbation is switched off (i.e. $\Delta p_n = 0$ for $n \geq 2$) and the orbit lands in the target region after an additional $n_1 + n_2$ iterations. For small δL and B_t and under ideal conditions the total time required to direct the orbit in the surface of section, from the source point to the neighbourhood B_t of the target point, is thus given by

$$\tau \approx \left(\lambda_1^{-1} \ln(1/\delta L) + |\lambda_2|^{-1} \ln(1/\epsilon_t)\right) T\,.$$

Here T denotes the average time between intersections of a state space trajectory with the surface of section. Now, for $\delta L \approx \epsilon_t$, we have $\tau \propto \ln(1/\epsilon_t)$ which gives a logarithmic law in contrast to the power law for the uncontrolled system derived above.

We next discuss practical considerations involved with the implementation of the method of targeting in practice. In practice, one cannot actually iterate either the line L or the region B_t. Instead, we iterate discrete approximations to them and make successive refinements until a sufficiently accurate intersection is obtained. We do this by starting with a fixed number $N_s \gg 1$ of equally spaced points on L, iterating these points forward. In similar fashion we iterate $N_t \gg 1$ points on the perimeter of B_t backward. In order to determine intersections between the discretized versions of the evolved line segment and target region, we join consecutive points on these two objects with straight-line segments. Once an intersection is detected, its accuracy is refined by repeatedly halving the intersecting forward and backward line segments and determining which of the halves actually contains the intersection. The refinement process is repeated until at least one point on the forward iterated line segment falls inside the backward iterated target region. Notice that each refinement involves an increase in resolution by a factor of two at the expense of including three additional points (one on L and two on the perimeter of B_t). For a more elaborated discussion on the required number of points on L and B_t and its asymptotical behaviour the reader is referred to [726].

Example 7.3 Consider the Henón map

$$\mathbf{G}(\boldsymbol{\xi}_n, p) = \begin{pmatrix} p - bx_{2,n} - x_{1,n}^2 \\ x_{1,n} \end{pmatrix}, \qquad \boldsymbol{\xi}_n := (x_{1,n}, x_{2,n})^T,$$

with p the control parameter and $b = -0.3$. The nominal value of the control parameter p is $p_0 = 1.4$. The inverse map is given by

$$\mathbf{G}^{-1}(\boldsymbol{\xi}_n, p) = \begin{pmatrix} x_{2,n} \\ (p - x_{1,n} - x_{2,n}^2)/b \end{pmatrix}, \qquad b \neq 0.$$

Suppose the source point is

$$\boldsymbol{\xi}_s = (0.4772, -1.1880)^T,$$

and the target region is a small square with edge length $\epsilon_t = 0.0038$ centred about the target point

$$\boldsymbol{\xi}_t = (0.1371, -1.3280)^T.$$

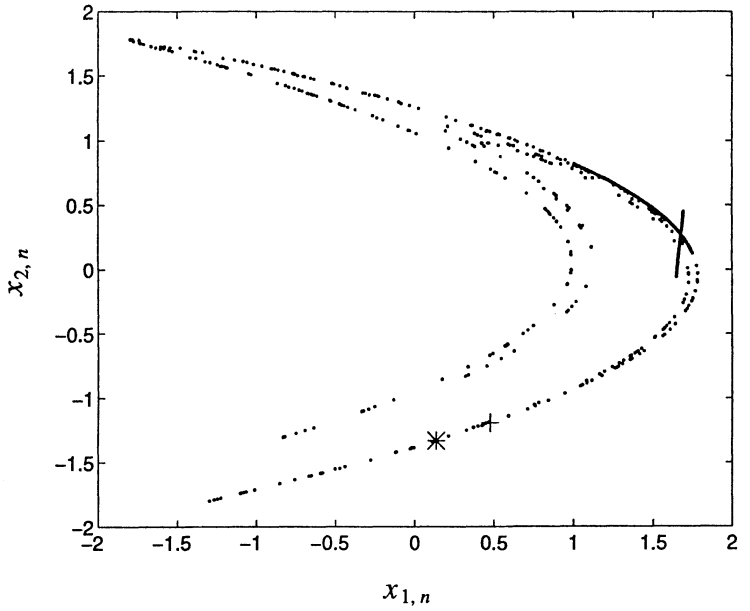

Figure 7.10: Intersection of the 10-th forward iterate of the source line segment and the second backward iterate of the target neighbourhood ($\boldsymbol{\xi}_s$ and $\boldsymbol{\xi}_t$ are indicated by '+' and '*' respectively).

Without utilizing targeting, 6062 iterations are required before the orbit originating at $\boldsymbol{\xi}_s$ visits the target neighbourhood. Suppose that the maximum allowable perturbation of the control parameter p is $\Delta p_{\max} = 2 \times 10^{-3}$ about its nominal value of $p_0 = 1.4$.

Figure 7.10 shows the intersection between the 10-th forward iterate of the source line segment and the second backward iterate of the target neighbourhood. A few points on the Hénon attractor are plotted in order to provide the necessary global perspective. Figure 7.11 provides a close-up view of this intersection. The portion of the forward iterated line segment lying in the backward iterated target region corresponds with control parameter values in the interval

$$P := [1.3988193, 1.3988225].$$

For the parametric control,

$$p_n = \begin{cases} 1.398821, & n = 1 \\ p_0, & n > 1 \end{cases},$$

the orbit of the controlled system is shown in Figure 7.12. A close-up view of the target region containing the target point and the 12-th iterate of the source point subject to the above parameter control, is shown in Figure 7.13. ■

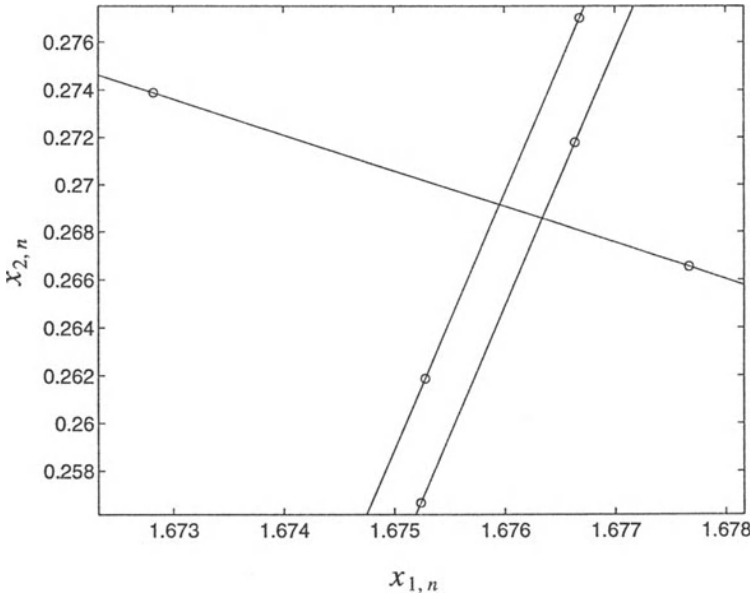

Figure 7.11: A close-up view of the intersection in Figure 7.10.

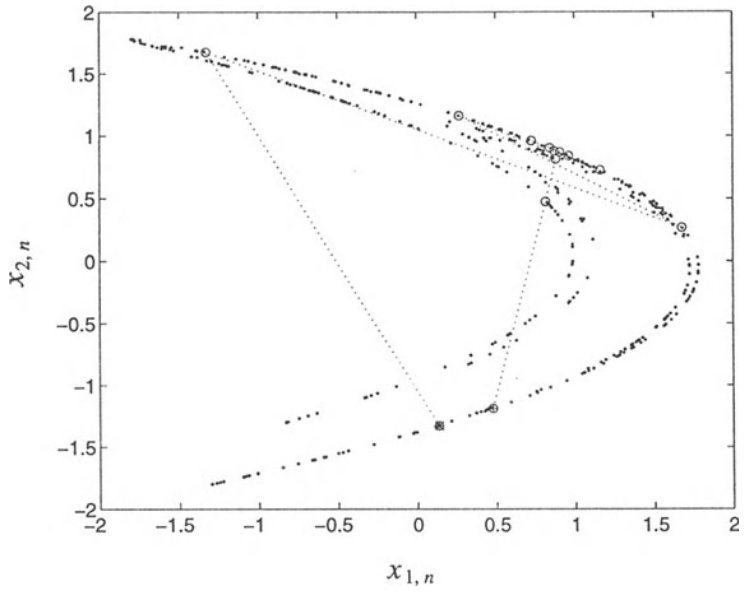

Figure 7.12: Orbit of the controlled system.

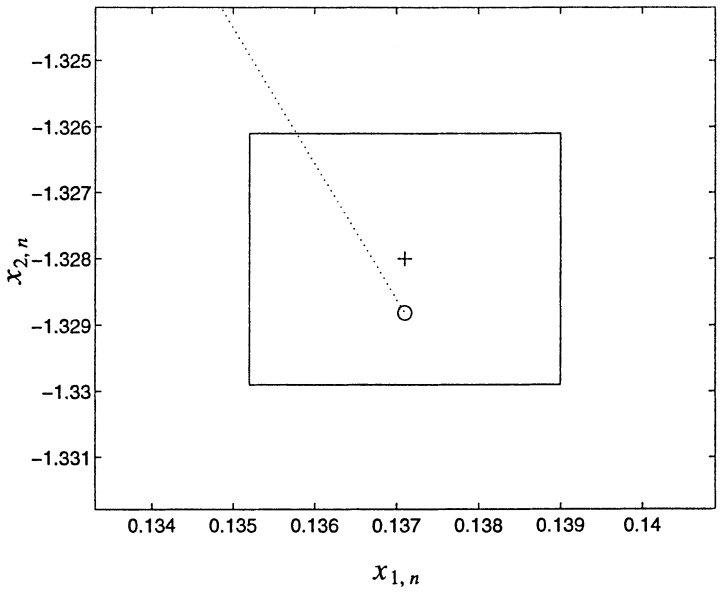

Figure 7.13: Close-up view of the target region containing the target point '+' and orbit point 'o'.

Shinbrot *et al.* [726] verified the above predicted logarithmic behaviour numerically. The results that they obtained were found to be in good agreement with the theoretically predicted results. They also found targeting to be effect in the presence of low power noise or when the system model is imperfect.

Kostelich *et al.* [446] applied the targeting method discussed here to the double rotor system which is a higher dimensional system. They found that it drastically reduced the time for the source point to visit the prescribed target neighbourhood.

Shinbrot and coworkers [723] were the first to apply the targeting method successfully to control of an experimental system. They used a vertically oriented, magnetoelastic ribbon, which is known to vibrate chaotically in response to an externally applied sinusoidal magnetic field with a DC component [220]. The ribbon was clamped at its base but was otherwise free to move. The modulus of elasticity of the ribbon was nonlinearly dependent on the applied field, so that as the field oscillates, the ribbon alternately buckles and stiffens under the influence of gravity. The position of the ribbon was measured at a point near its base by means of an optical sensor. They first constructed a discrete model from the experimental system. The DC magnetic field component was taken to be the control parameter. For nominal values of the magnitudes for the DC and AC fields and the frequency of the AC field, a delay plot consisting of samples of the position of the ribbon was obtained. The model of the system for these parameters values was obtained by fitting a spline curve. This

process was then repeated for a slightly lower and slightly higher value of the DC field thereby obtaining maps describing the perturbed system. These three maps were then used to implement the targeting method for this system.

7.5 Self-controlling Feedback

The OGY method for controlling chaos is a discrete method since it deals with the Poincaré map. This leads to some limitations. The OGY method can stabilize only those periodic orbits whose maximal Lyapunov exponent is small compared to the reciprocal of the time interval between parameter changes. Since the corrections of the parameter are infrequent and small, noise leads to occasional bursts of the system into the region far from the desired periodic orbit, and these bursts become more frequent as the signal-to-noise ratio decreases [605]. Therefore, time-continuous control seems very attractive in this context. Alternative terms for this type of control are continuous feedback control, self-controlling feedback and conventional control.

The response of chaotic systems to continuous periodic and aperiodic perturbations have been considered in a number of investigations. In [485], [96] and [496] the suppression of chaos, using continuous parametric perturbation, was studied. However, although this method is able to suppress chaos, in the process it often destroys the structure of the chaotic attractor. Therefore, this method cannot be used for stabilizing unstable periodic trajectories. Another disadvantage of this method is that the controlling perturbation must usually be comparatively large.

Pyragas [642] has proposed a method for controlling chaos based on continuous-time perturbation using feedback. His work mainly involves numerical simulations. Later Chen and Dong [130] provided a rigorous basis for this control scheme which they have verified by numerical simulations.

Consider an $(N+M)$-dimensional nonlinear dynamical system of the form

$$\frac{d\mathbf{x}}{dt} = \mathbf{f}(\mathbf{x},\mathbf{y},t)\,, \qquad \frac{d\mathbf{y}}{dt} = \mathbf{g}(\mathbf{x},\mathbf{y},t) + \mathbf{u}(\mathbf{x},\mathbf{y},t)\,, \tag{7.37}$$

where $\mathbf{x} \in \mathbf{R}^N$ $(N \geq 0)$ and $\mathbf{y} \in \mathbf{R}^M$ $(M > 0)$ with a control input $\mathbf{u} \in L_1(S \times \mathbf{R}^+)$ to the second subsystem with $S \subseteq \mathbf{R}^N \times \mathbf{R}^M$. $(L_1(S \times \mathbf{R}^+)$ denotes the set of all Lebesgue integrable functions on $S \times \mathbf{R}^+$.) We suppose that the two nonlinear vector-valued functions

$$\mathbf{f} : \mathbf{R}^N \times \mathbf{R}^M \times \mathbf{R}^+ \to \mathbf{R}^N \quad \text{and} \quad \mathbf{g} : \mathbf{R}^N \times \mathbf{R}^M \times \mathbf{R}^+ \to \mathbf{R}^M$$

are integrable and are such that the system has a unique solution trajectory $(\mathbf{x}(t), \mathbf{y}(t))$ in S and $t \geq t_0 \geq 0$, for any given initial point $(\mathbf{x}_0, \mathbf{y}_0, t_0) \in \mathcal{I} \subseteq S \times \mathbf{R}^+$. Self-controlling feedback then refers to a control input $\mathbf{u}$ (satisfying the above requirements) which achieves stabilization of an existing unstable periodic trajectory of the

system. Chen and Dong presented some general results for systems of the above form, in [130]. Here, we only restrict our attention to the following example, discussing a system of this form.

Example 7.4 [130] Consider the Duffing equation

$$\frac{dx}{dt} = y\,, \qquad \frac{dy}{dt} = -p_1 x - x^3 - py + q\cos\omega t\,. \tag{7.38}$$

Suppose that $(x^*(t), y^*(t))$ is a periodic solution of (7.38). By adding a linear correction term to (7.38), we obtain what we call the controlled Duffing equation given by

$$\begin{pmatrix} dx/dt \\ dy/dt \end{pmatrix} = \begin{pmatrix} y \\ -p_1 x - x^3 - py + q\cos\omega t \end{pmatrix} - \begin{pmatrix} K_{11} & K_{12} \\ K_{21} & K_{22} \end{pmatrix} \begin{pmatrix} x - x^* \\ y - y^* \end{pmatrix}. \tag{7.39}$$

Collecting similar terms then yields

$$\begin{aligned} \frac{dx}{dt} &= -K_{11}x + (1 - K_{12})y + (K_{12}x^* + K_{12}y^*)\,, \\ \frac{dy}{dt} &= -(K_{21} + p_1)x - x^3 - (K_{22} + p)y + (K_{21}x^* + K_{22}y^*) + q\cos\omega t\,. \end{aligned}$$

Clearly, if the solution $(x(t), y(t))$ coincides with $(x^*(t), y^*(t))$ then the controlled Duffing equation yields exactly the Duffing equation since then our control objective is being satisfied and no correction is required. However, if the solution $(x(t), y(t))$ differs from $(x^*(t), y^*(t))$ then there is a linear correcting term added to each equation in the Duffing system which attempts to stabilize $(x^*(t), y^*(t))$. The question now is whether there exists a feedback gain matrix

$$\mathbf{K} := \begin{pmatrix} K_{11} & K_{12} \\ K_{21} & K_{22} \end{pmatrix},$$

for the controller, which stabilizes the periodic solution $(x^*(t), y^*(t))$. In order to answer this question we must first determine constraints imposed on $\mathbf{K}$ for stability of the controlled Duffing equation. The Jacobian matrix associated with the controlled Duffing equation at the point $(x^*(t), y^*(t))$ is given by

$$\mathbf{J}_c(x^*(t), y^*(t)) := \begin{pmatrix} -K_{11} & 1 - K_{12} \\ -(K_{21} + p_1) - 3x^{*2} & -(K_{22} + p) \end{pmatrix}.$$

The characteristic equation of the controlled Duffing equation linearized about the point $(x^*(t), y^*(t))$ is

$$\begin{aligned}\det(s\mathbf{I} - \mathbf{J}_c) &= s^2 + (p + K_{11} + K_{22})s + \\ &\quad \Big(K_{11}(p + K_{22}) + (1 - K_{12})(K_{21} + p_1 + 3x^{*2})\Big) = 0\,,\end{aligned}$$

which is required to have all its roots located in the open left-half s-plane in order for the controlled system to be stable. A necessary and sufficient condition for this to be the case for a second order system is that all coefficients of the characteristic polynomial $\det(s\mathbf{I} - \mathbf{J}_c)$ have the same sign, that is,

$$\begin{aligned} p + K_{11} + K_{22} &> 0\,, \\ K_{11}(p + K_{22}) + (1 - K_{12})\left(K_{21} + p_1 + 3x^{*2}\right) &> 0\,. \end{aligned}$$

As in [130], we restrict our discussion to the case $K_{11} = K_{22} = 0$. Since $p > 0$, the first inequality is thus satisfied and the second inequality becomes

$$(1 - K_{12})\left(K_{21} + p_1 + 3x^{*2}\right) > 0\,.$$

If we assume in addition that $K_{12} = 0$ then we have

$$K_{21} > -p_1 - 3x^{*2}\,, \qquad t \geq 0\,,$$

and hence the controlled Duffing equation reduces to

$$\frac{dx}{dt} = y\,, \qquad \frac{dy}{dt} = -p_1 x - x^3 - py + q\cos\omega t - K_{21}(x - x^*)\,.$$

To be able to comment on the controllability of the controlled system we must first linearize the original system (7.38) about $(x^*(t), y^*(t))$ and then add the correction term as we have done previously for the nonlinear system. By doing so, we then obtain what we call the linearized controlled Duffing equation, namely

$$\begin{pmatrix} d\tilde{x}/dt \\ d\tilde{y}/dt \end{pmatrix} = \begin{pmatrix} 0 & 1 \\ -p_1 - 3x^{*2} & -p \end{pmatrix} \begin{pmatrix} \tilde{x} \\ \tilde{y} \end{pmatrix} + \begin{pmatrix} 0 \\ 1 \end{pmatrix} u\,,$$

which is completely controllable, and hence the controlled Duffing equation (7.39) is locally controllable by the feedback

$$u(t) = -K_{21}\left(x(t) - x^*(t)\right)\,.$$

In the linearized controlled Duffing equation $\tilde{x} := x - x^*$ and $\tilde{y} := y - y^*$.

For $p = 0.4$, $p_1 = -1.1$, $q = 2.1$ and $\omega = 1.8$ the projection of the state space onto the (x, y)-plane shows a chaotic attractor enclosed in a periodic trajectory with period $T = 2\pi/\omega \approx 3.490$. This period-1 trajectory is unstable on the inside but stable on

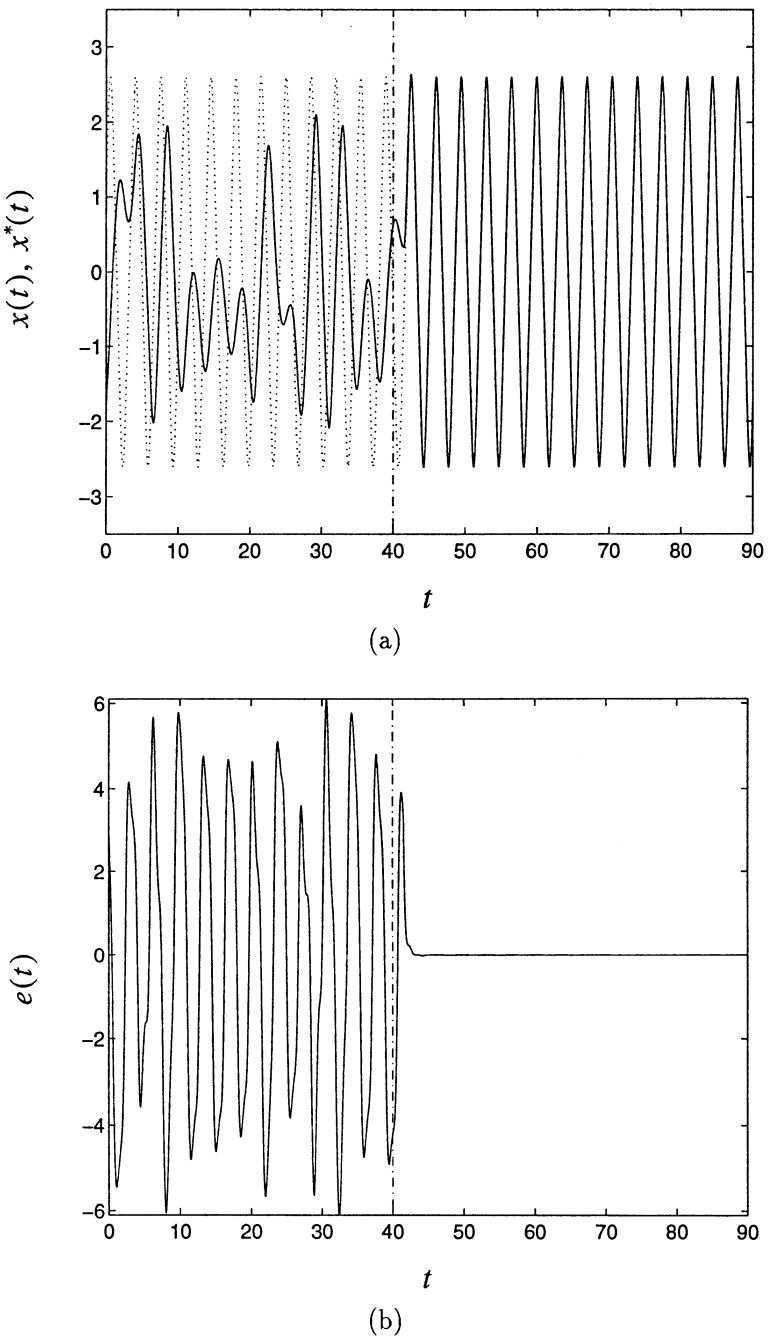

Figure 7.14: Controlling a chaotic trajectory of the Duffing equation to approach the periodic trajectory: (a) Signals $x(t)$ (solid line) and $x^*(t)$ (dotted line); (b) Feedback error signal $e(t) := x^*(t) - x(t)$.

the outside. Using this period-1 trajectory as the desired trajectory $(x^*(t), y^*(t))$ and setting $K_{21} = 5.0$ we have been able to achieve control of the chaotic trajectory in the sense that it asymptotically approaches the periodic trajectory $(x^*(t), y^*(t))$ once the control is switched on (see Figures 7.14 and 7.15). The vertical lines in Figures 7.14(a) and 7.14)(b) indicate the position in time when the control is switched on. By looking at the feedback error before the control was switched on (i.e. left of the vertical line in Figure 7.14(b)), we notice that the chaotic trajectory $x(t)$ and reference trajectory $x^*(t)$ differ significantly. However, after the control is switched on $x(t)$ converges to $x^*(t)$ very rapidly. Varying the position when the control is switched on results in a varying time to achieve control. Increasing K_{21} increases the convergence rate thereby reducing the time to achieve control. However, as with linear systems, there may exist a critical value of K_{21} beyond which the poles of the linearized system move across the $j\omega$-axis into the right half plane [455]. When this happens the linearized system becomes unstable. For the nonlinear system this means that it has become (at least locally) unstable, that is, the desired trajectory $x^*(t)$ is once again unstable. In severe cases the nonlinear system may become globally unstable, resulting in all trajectories in state space diverging towards infinity. What used to be an (chaotic) attractor will then have become a repeller. A general mathematical condition for the controllability of the Duffing equation is given by the following proposition.

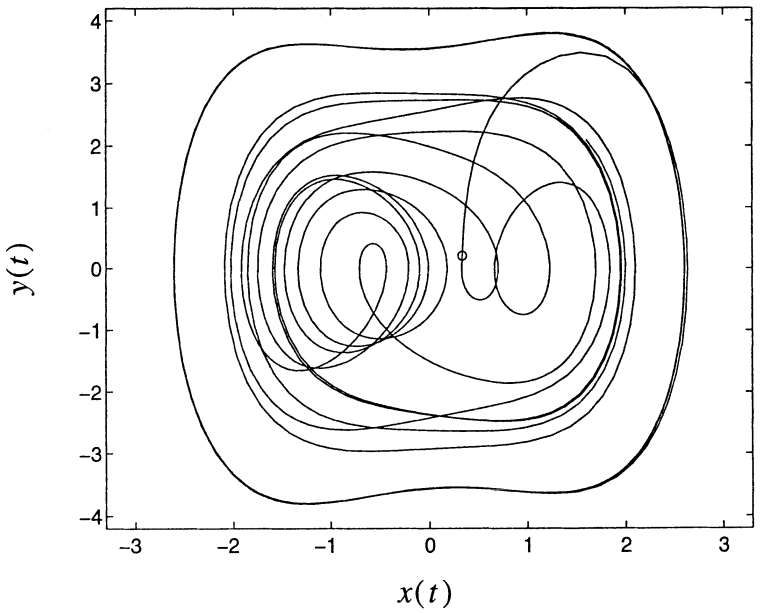

Figure 7.15: Time evolution in state space before and after control is switched on. The 'o' indicates the point where the control was switched on.

Proposition 7.5 [130] For any (stable or unstable) periodic solution $(x^*(t), y^*(t))$ of the Duffing equation (7.38) let the feedback control law be

$$u(t) = -K\left(x(t) - x^*(t)\right) + h(t, x, x^*)$$

with $K \geq -p_1$ and

i) $h(t, x, x^*) - 3xx^*(x - x^*) \in L_1([t', \infty) \times S)$ and

ii) $u \in L_1([t', \infty))$,

where $S \subseteq \mathbf{R}^2$ is the domain on which the system is defined. Then starting from any point of a system trajectory at $t = t' \geq t_0$, the trajectory of the controlled Duffing system converges to the desired periodic trajectory, in the sense that

$$\lim_{t\to\infty} |x(t) - x^*(t)| = 0 \qquad \text{and} \qquad \lim_{t\to\infty} |y(t) - y^*(t)| = 0\,.$$

Proof: Refer to [130].

□

Concerning this proposition, it is important to note that h, although nonlinear in general, may contain a linear term which cancels the linear term $K(x - x^*)$ of u. This results in a purely nonlinear controller controlling the system. This concludes our discussion of self-controlling feedback applied to the Duffing equation. ■

In their investigation of the Duffing equation, Chen and Dong [130] also studied the high gain case (i.e. $K_{21} \gg 1$) and found the control to be even more effective. They also studied the case when only an approximation of the desired periodic response (x^*, y^*) is available. They found that control could still be achieved fairly well.

So far it has been assumed that the desired periodic response $(\mathbf{x}^*(t), \mathbf{y}^*(t))$ or an approximation of it is available. However, this is rarely the case, especially for experimental systems for which poor models exists. In this regard, Pyragas [642] suggested that the delayed state, namely, $(\mathbf{x}(t-\tau), \mathbf{y}(t-\tau))$ could be used as the desired period-τ trajectory $(\mathbf{x}^*(t), \mathbf{y}^*(t))$. More precisely, Pyragas studied systems of the type for which $\mathbf{x}$ is inaccessible and $\mathbf{y}$ is a scalar. He considered a feedback controller of the form

$$u(t) = K(y^*(t) - y(t))\,,$$

where K is a real gain factor. To achieve stabilization of the desired unstable periodic trajectory $y^*(t)$, two parameters, the delay time τ and the weight K of the feedback must be adjusted.

Example 7.6 [642] Consider the Rössler system

$$\frac{dx_1}{dt} = -x_2 - y\,, \quad \frac{dx_2}{dt} = b + x_2(x_1 - c)\,, \quad \frac{dy}{dt} = x_1 + ay + u(t)\,, \tag{7.40}$$

for $a = b = 1/5$ and $c = 5.7$, with the control input given by

$$u(t) = K(y(t-\tau) - y(t))\,,$$

with K the feedback gain.

Experimentally it was discovered that the Rössler system possesses a periodic solution with period $T \approx 5.892$. By setting $\tau = 5.892$ and $K = 0.2$ this periodic solution could be stabilized. The results of the stabilization of this periodic trajectory can be seen in Figures 7.16 and 7.17. The time when the control was switched on is shown by the vertical line in Figure 7.16. Although the feedback error becomes very small it does not converge to zero. The fact that the feedback error doesn't decrease asymptotically to zero indicates that the value $\tau = 5.892$ assumed above differs slightly from the true period of the trajectory that we attempt to stabilize. Notice however that the convergence is still good when compared to the feedback error before the control is switched on. ■

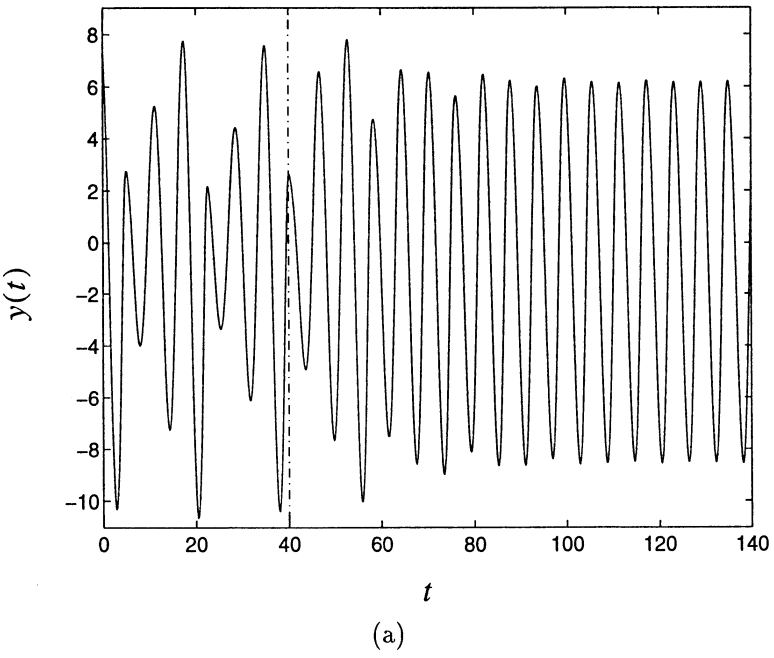

(a)

Figure 7.16: Results of stabilization of the periodic trajectory of the Rössler system for $\tau = 5.892$, $K = 0.2$: (a) State variable $y(t)$; (b) Feedback error signal $e(t) := y(t-\tau) - y(t)$.

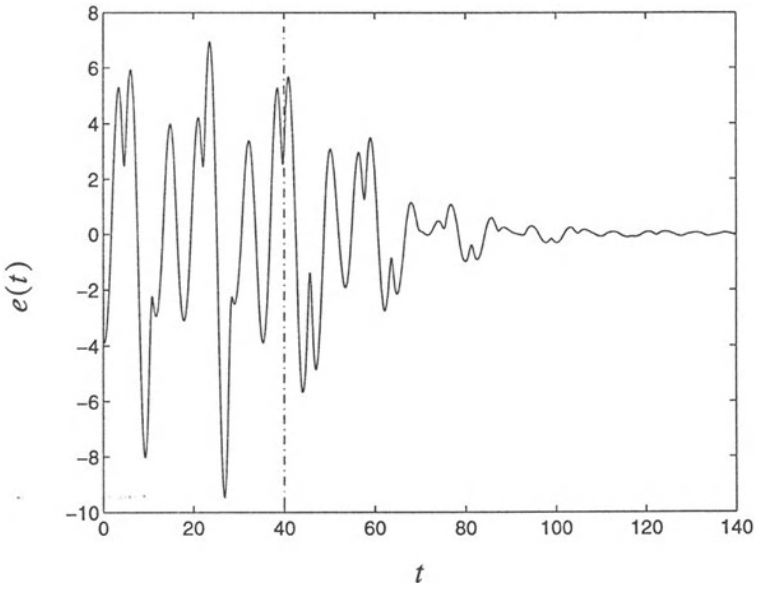

(b)

Figure 7.16: (Continued)

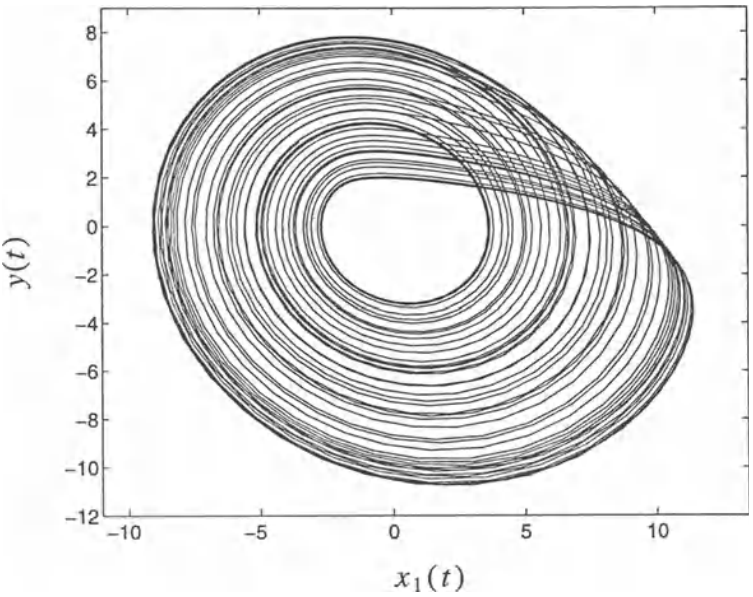

(a)

Figure 7.17: State space trajectories for the Rössler system: (a) Chaotic attractor; (b) Stabilized periodic trajectory for $\tau = 5.892$, $K = 0.2$.

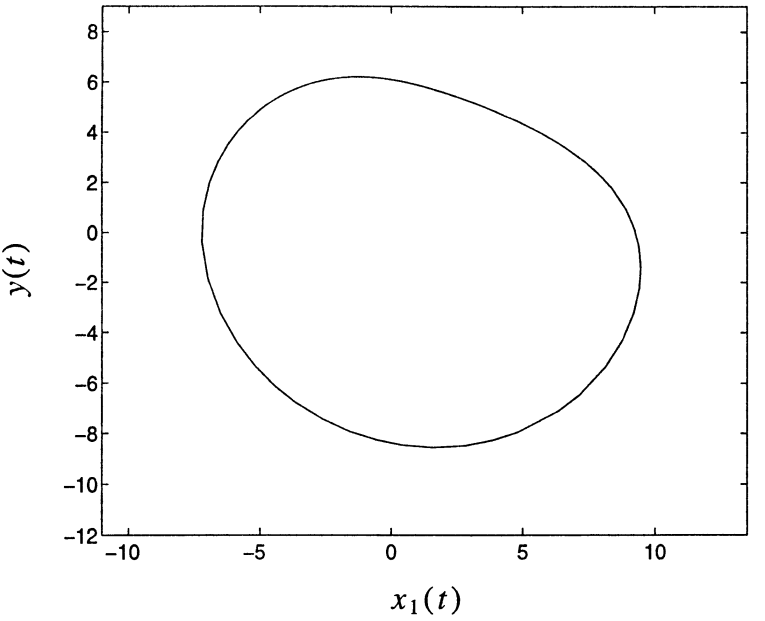

(b)

Figure 7.17: (Continued)

In an attempt to study the dependency of this control method on the setting of the delay time τ, Pyragas [642] analyzed the dispersion of the perturbation given by $\langle (y(t-\tau) - y(t))^2 \rangle$ for the Rössler system as a function of τ. (Here $\langle \cdot \rangle$ denotes time averaging.) He also studied the dependence of the perturbation on the weight K. Concerning the stabilization of existing unstable periodic solutions, Pyragas observed that this control method exhibits multistability. This means that if there exist more than one unstable periodic solution of period τ for the system, of which anyone can be stabilized, depending on the selected initial conditions of the system. Finally, he reached the following conclusion: In the case of an external control force the perturbation increases the dimension by one, as any external periodic signal $y_e(t)$ can be presented by one additional ordinary differential equation. The delayed feedback perturbation therefore increases the dimension to infinity and hence one can conclude that the stabilization in this method is achieved through additional degrees of freedom introduced in the system with the perturbation. The perturbation however does not change the projections of the unstable periodic trajectory on an original low-dimensional phase space but merely changes the Lyapunov exponent of the unstable periodic trajectory so that it becomes stable.

In [643] Pyragas and Tamaševičius demonstrated this control method by an experimental system consisting of the externally driven nonlinear oscillator which uses a tunnel-diode as a negative resistance device [643] with the feedback applied to it. This circuit is shown in Figure 7.18. The parameters of the circuit are as follows:

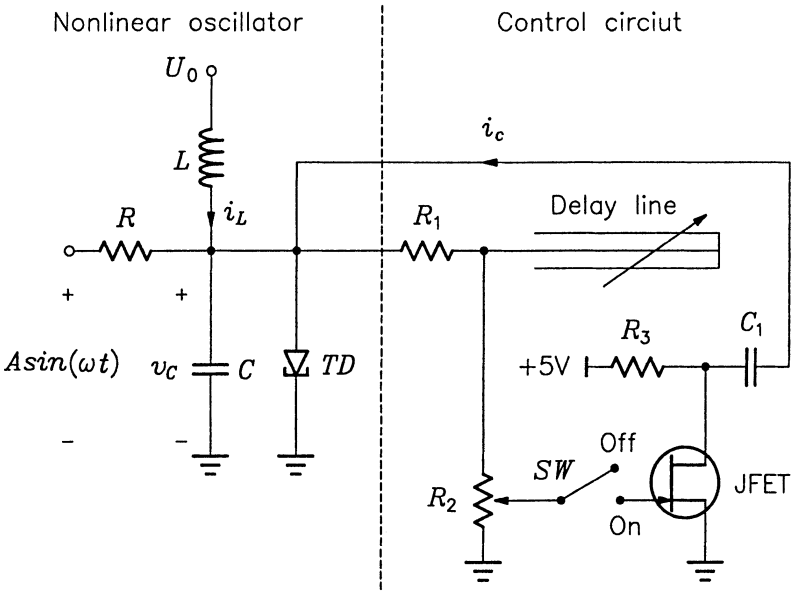

Figure 7.18: Experimental circuit studied by Pyragas and Tamaševičius.

$L = 17.4\mu$H, $C = 510$pF, $R = 5.1$kΩ. The external drive frequency f_e is 3.8MHz, the drive amplitude A is variable up to 3V, the DC bias U is always kept less than the critical value (approximately 70mV) for the appearance of self-sustained oscillations. The employed germanium tunnel-diode is characterized by the peak current $I_p = 1.5$mA and the peak voltage $U_p = 67$mV.

The dynamics of the oscillator are determined by the normalized equations

$$\frac{dx}{dt} = -y + c, \tag{7.41}$$

$$\frac{dy}{dt} = x - bN(y) - dy + a\sin\omega t + F(y,\tau), \tag{7.42}$$

with $F(y,\tau) \equiv 0$ when the feedback is switched off. The dimensionless quantities are

$$x := Zi_L/U_p, \quad y := v_C/U_p, \quad t \leftarrow t/T_0,$$

$$Z := \sqrt{L/C}, \quad T_0 := \sqrt{LC}, \quad a := ZA/RU_p,$$

$$b := ZI_p/U_p, \quad c := U_0/U_p, \quad d := Z/R_p,$$

$$\omega := 2\pi f_e T_0, \quad T := 2\pi/\omega, \quad F := Zi_c/U_p.$$

Here f_e is the external driving frequency, $v_C(t)$ is the voltage across the capacitor C, $i_L(t)$ is the current through the inductor L, $i_c(t)$ is the control current, R_c is the load

resistance due to the control circuit and

$$R_p := RR_c/(R + R_c)\,,$$

is the parallel combination of R and R_c. The normalized current-voltage characteristic of the tunnel-diode is of the form

$$N(y) = \frac{y^\alpha \mathrm{e}^{\alpha(1-y)} + \beta\,(\mathrm{e}^y - 1)}{1 + \beta\,(\mathrm{e} - 1)} \tag{7.43}$$

with $\alpha = 1.7$ and $\beta = 0.001$. The voltage v_C across the tunnel-diode is fed to a delay network with adjustable gain. The output of the delay network (i.e. the control current) is given in normalized form by

$$F(y,\tau) := K\,(y(t-\tau) - y(t))\,, \quad K := hpSZ, \quad \tau := T_d/T_0\,, \tag{7.44}$$

which is then fed into the node joining the tunnel-diode and the inductor L. Here

$$p := R_2 Z_d/(R_1 R_2 + R_1 Z_d + R_2 Z_d)\,,$$

and h denotes the attenuation as a result of R_2 and T_d is the adjustable double way delay time of the variable spiral line used by Pyragas and and Tamaševičius in [643]. The parameters of the control circuit used are as follows: $R_1 = 1.7\mathrm{k}\Omega$, $R_2 = 260\Omega$, the wave resistance of the delay line $Z_d = R_2 = 260\Omega$. The transconductance of the transistor $S = 11\mathrm{mA/V}$.

To control an unstable periodic trajectory the delay time T_d is adjusted close to the period of the desired trajectory by means of the adjustable delay line. (For the driven oscillator in Figure 7.18 T_d must be close to m/f_e, where $m \in \mathbf{N}$ is the periodicity number of the locked trajectory.) Then the switch SW is closed and the feedback coefficient K is increased by adjusting the potentiometer R_2 until stabilization occurs. If necessary the delay time T_d can be corrected and the whole adjustment procedure can be repeated to minimize the control signal. The stabilization of unstable periodic trajectories has been achieved in experiment only in definite intervals of the weight K of the feedback. Theoretically these intervals can be determined from variational equations, defining the Lyapunov exponents of corresponding trajectories (see [643], [646]). In [643] it is reported that the feedback signal remains nonzero even after locking has been achieved. This is due to the ohmic losses of about 10% in the long spiral delay line which has to be compensated for. Numerical results obtained from simulating this system are discussed in the next example.

Example 7.7 [643] Consider the system of equations (7.41) to (7.44) which models the circuit in Figure 7.18 for the parameter values

$$a = 1.40\,, \quad b = 4.10\,, \quad c = 0.92\,, \quad d = 0.15\,, \quad \omega = 2.25\,.$$

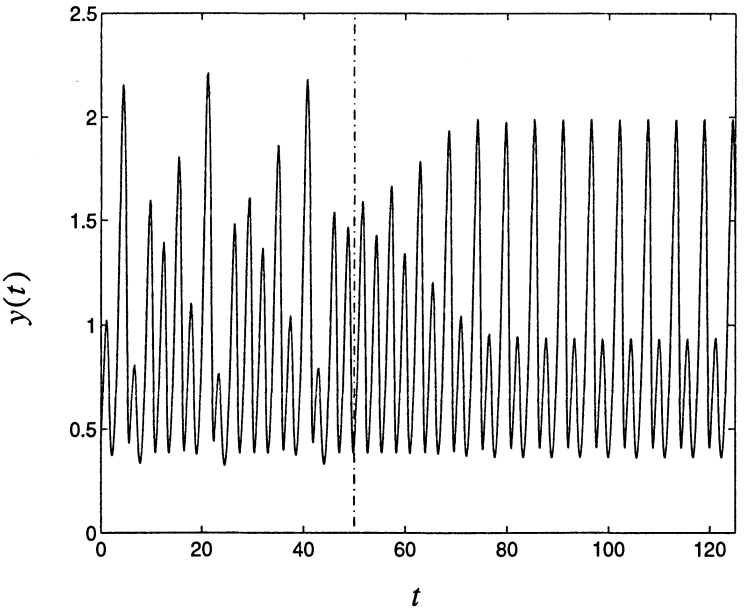

(a)

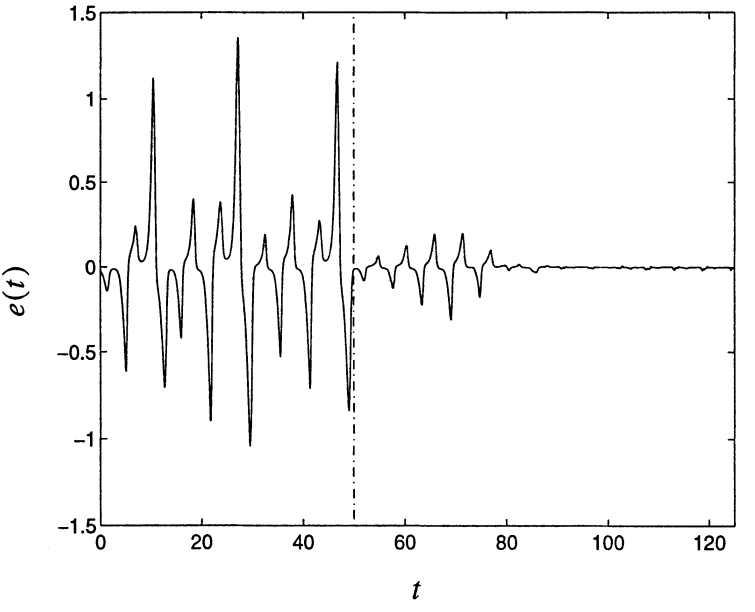

(b)

Figure 7.19: Time response of the RL-tunnel-diode oscillator before and after switching on the feedback control: (a) Output signal $y(t)$; (b) Feedback signal $e(t) := y(t-\tau) - y(t)$ with $\tau = 2T$ and $K = 0.5$.

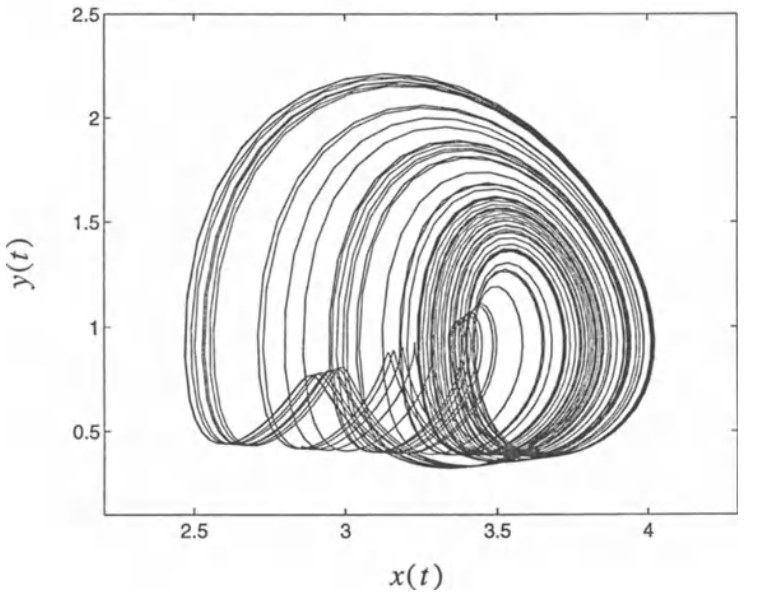

(a)

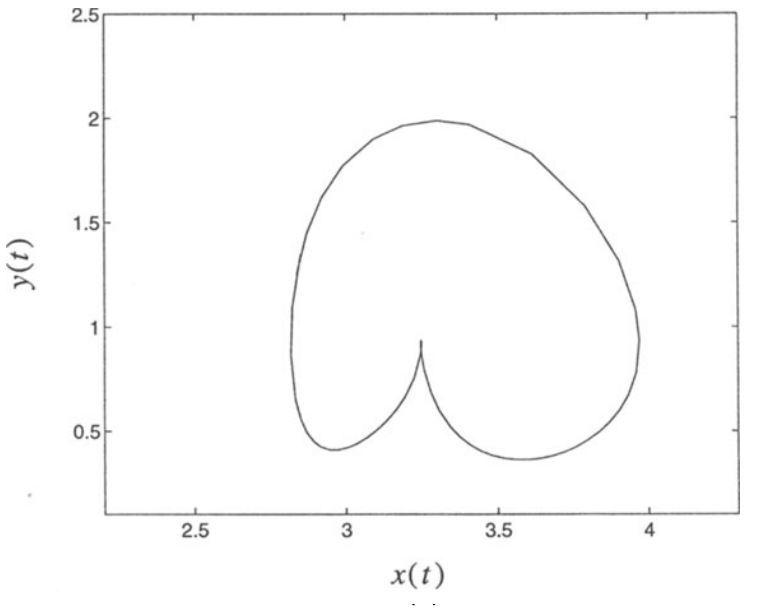

(b)

Figure 7.20: Calculated phase portraits for the RL-tunnel-diode oscillator: (a) Chaotic trajectory; (b) Controlled period-2 trajectory for $\tau = 5.585$, $K = 0.5$.

The delay time $\tau = 5.585$ approximates the period of an embedded unstable period-2 trajectory. Figure 7.19 illustrates the dynamics of the system before and after switching on the control. The control is switched on at the point in time indicated by the vertical line. The system without control is characterized by chaotic behaviour with asynchronous signals $y(t)$ and $y(t-\tau)$. This can be seen by viewing the feedback error signal $y(t-\tau)-y(t)$ in Figure 7.19(b) before the control is switched on. Switching on the control results in a periodic oscillation corresponding to an initially unstable periodic trajectory with period $2T \approx 5.585$. The signal $y(t)$ thus tends to an embedded unstable periodic trajectory with period $2T$ thereby causing the feedback correction $F(y,\tau)$ to reduce asymptotically towards zero as can be seen in Figure 7.19(b). The phase portraits of the chaotic and controlled trajectories in Figure 7.19 are shown in Figure 7.20. ■

Great care should be used when applying delayed feedback since increasing the delay beyond some critical value (which is system dependent) will cause the system to become unstable [783], [455]. By linearizing the system and using, for instance, the Nyquist stability criterion this critical value of the delay time may be determined. It will therefore not be possible in general to stabilize unstable periodic trajectories with arbitrarily long periods due to the stability problem.

For an enlightening discussion on continuous feedback control, the reader is referred to the article [646] by Qu, Hu and Ma. Herein it is shown by an example that positive feedback is required in some instances to reduce the largest Lyapunov exponent of a system in order to stabilize an existing periodic trajectory. In a paper by Chen and Dong self-controlling feedback was applied to discrete-time systems such as the Lozi map and the Hénon map. It was found that this type of controller is also able to control unstable periodic trajectories of these chaotic systems (see [131]). Chen later also applied this method to Chua's circuit (see [129]). In [129] a sufficient condition for controllability of Chua's circuit is derived.

7.6 Other Methods for Controlling Chaos

A method for controlling Hamiltonian chaos was proposed by Lai in cooperation with Ding and Grebogi (see [461]). The OGY method is not directly applicable to chaotic Hamiltonian systems. The reason is that a Hamiltonian system often exhibits complex conjugate eigenvalues at one or more points on an unstable periodic trajectory. Lai *et al.* extended the OGY method to control Hamiltonian chaos by incorporating the notion of stable and unstable directions at each of the desired periodic trajectory's points.

Kapitaniak and coworkers [418] proposed an effective method for controlling chaos by coupling one chaotic system (the main system) to another simple system (the

controller system) with easily adjustable parameters. In many methods for controlling chaos, the fact that there are infinitely many unstable periodic trajectories embedded in the chaotic attractor is exploited. However, Kapitaniak's method exploits the fact that in a small parameter neighbourhood of a quasi-attractor there exist many stable periodic trajectories. Moreover, this is achieved without feedback, by changing one of the parameters of the controller without changing any parameters of the main system. The goal is to change the dynamics of the system in such a way as to obtain stable periodic trajectories close to the original attractor. Depending on the application, a fixed point or a periodic trajectory having the desired properties may be stabilized. This method offers a way of controlling chaos without the necessity of following a response trajectory and targeting it to some desired domain of the phase space.

Kapitaniak's method can be especially useful in mechanical systems, where its simplicity offers important practical advantages compared to other controlling methods. The reason for this is that in mechanical systems the feedback controllers are usually very large (sometimes even larger than the controlled system) and have complicated dynamics. In contrast with such controllers the simplicity of the controller employing Kapitaniak's method offers a straightforward yet effective approach. For example the controller may be realizable by the simplest mechanical system, namely a mass and a spring with controllable stiffness. Another important use of this method is in VLSI circuits, where it is difficult, if not impossible to access the internal circuit parameters as required by other methods. This method is expected to be exploited in the design of fault-tolerant electrical systems where a previously built-in linear controller can be switched on by a remote signal to stabilize the system which had become chaotic due to, for example, aging of critical parts of the system.

A number of authors have investigated the use of adaptive control for the controlling of chaos. One of the first investigations linking chaos to adaptive control was done by Mareels and Bitmead [510]. Although they didn't consider controlling a chaotic system, they showed that, despite the complicated dynamics which the feedback gain exhibit, robust stabilization of the plant (the system to be stabilized) still occurs. To turn this in the direction of controlling a chaotic system by means of an adaptive controller, one might view their results as a system (in this case the plant) controlling a chaotic system (the gain scheduling subsystem of the controller).

Another investigation concerning adaptive control of chaos was done by Qammar and coworkers in [644]. They studied an indirect adaptive controller designed to drive the chaotic logistic system to a steady state. They found that although such a controller could achieve control, it could also add undesirable complexities to the system.

Fowler [255] applied stochastic control techniques to control chaotic systems. The algorithm studied by him used a Kalman filter as a state estimator. It yielded improved performance in at least some regions of the state space compared to that obtainable by use of a controller utilizing only the conditional mean of the state vector.

Open loop (i.e. nonfeedback) control schemes of chaos were studied by Lima and Pettini [485], Braiman and Goldhirsch [96] and Liu and Leite [496]. Lima and Pettini motivated their scheme of resonant parametric perturbations by an heuristic differential geometric based argument. This argument suggested that a stabilization of unstable geodesics could be attained by parametrically perturbing a chaotic system. As an example they studied the Duffing-Holmes equation with parametric perturbation. Liu and Leite used a similar scheme to control chaos generated by the Lorenz equations.

In an attempt to eliminate chaos in a dynamical system, Braiman and Goldhirsch applied a weak external forcing to the periodically driven pendulum. The application of the external forcing also results in other striking changes in the dynamics such as a stabilization of narrow subharmonic steps and the achievement of very low winding numbers.

In the paper [649], Rajasekar and Lakshmanan studied the problem of controlling chaos in the Bonhoeffer-Van der Pol oscillator using an adaptive control algorithm, (nonfeedback or open-loop) parametric perturbation, weak external forcing, (feedback or closed-loop) parametric control and additive noise control. The adaptive controller was used to reset the chaotic attractor to a prescribed limit cycle attractor. The feedback parametric controller used to stabilize an existing unstable periodic trajectory was a continuous-time bang-bang type controller. The feedback signal in this case was the difference between the actual chaotic response of the system and the desired periodic response expected of the system. In all cases they succeeded in extinguishing the chaotic response of the Bonhoeffer-Van der Pol oscillator by establishing a desired time-periodic motion.

The control of chaos finds applications in other fields as well. An example thereof is the synchronization of chaotic trajectories using control for application in, for instance, communication. The approach followed by Lai and Grebogi in [459] is to synchronize chaotic systems based on the OGY control scheme. In [459] they extend the OGY method to stabilize a chaotic trajectory of one system along a chaotic trajectory of another such system. The idea of stabilizing chaotic trajectories by using the OGY method was also proposed by Mehta and Henderson (see [541]). Their approach was to construct an artificial dynamical system evolving errors between the system's output and the target chaotic orbit. If the artificial system has a fixed point at the origin, parameter perturbations based on the OGY algorithm are then applied to stabilize the artificial system about the origin, which means that the original system's output is brought to the desired chaotic orbit [541]. They illustrated their method by using one-dimensional maps. Construction of the artificial map for more general dynamical systems may not be trivial. In the method proposed by Lai and Grebogi, on the other hand, parameter perturbations are applied directly to the original dynamical system and the method makes use of the geometrical structure of a chaotic trajectory.

In [408] derivative control is applied to Chua's circuit. It was found that a trajectory can be directed towards any of the two unstable fixed points of the system. Another use of the control of chaos was proposed by Hayes and coworkers (see [347]). In particular, they showed that the recent realization that chaos can be controlled with small perturbations can be employed to cause the symbolic dynamics of a chaotic system to track a prescribed symbol sequence, thus allowing any desired message to be encoded in the signal generated by a chaotic system. The natural complexity of chaos thus provides a vehicle for information transmission in the usual sense. This method of communication will often have technological advantages over existing techniques such as spread spectrum techniques.

Application of modern control techniques (such as fuzzy logic control [842] and artificial neural network control [711]) to the control of chaotic systems have also recieved attention recently.

In the past few years a whole new field has opened for research in chaos, namely synchronization of chaotic systems. For a brief discussion of the current trends of research in this field, the reader is referred to [219], [572] and to relevant references in the bibliography.

Chapter 8

Chaos in Electronics: The Future

8.1 Phases of Chaos Research: Past and Present

Looking back to the past chapters of this book and to the literature on chaos research in engineering, we observe that chaos research has gone through a number of phases. The first phase was the first encounters with chaos during which researchers became aware of the fact that they had come across results which could not be explained using the then existing theory (for example Lorenz who studied a simple model for convection [500]). This was followed by the formal recognition of the phenomenon and formal (mathematical) definition thereof (e.g. Li and Yorke's paper [482] in 1975). Then came what we call the craze, when everybody went searching for chaos in their fields of research. On discovery of chaos in their respective fields of interest, they published their observations. Only recently has chaos research begun to enter its fourth phase, in which researchers attempt to apply chaos in order to solve practical problems.

Regarding chaos research in electronic engineering, we see that research in this field is maturing. Only recently have attempts been made to apply chaos to solve engineering problems for the first time. Chaos has been applied to broaden the capture range of phase-locked loops [95]. A study has been conducted to apply chaos in $\Sigma\Delta$ modulators in an attempt to remove unwanted periodic interference occurring in such modulators [703]. In Chapter 5 we saw that ring self-excited oscillatory systems can be designed to be chaotic and can in addition satisfy constraints imposed on the spectral response. This enables one to apply such systems in spread spectrum applications where one would usually have used pseudorandom number generators. A number of studies concerning the use of chaos in secure communication [830] have also been performed [324], [347], [501], [621]. It was demonstrated in [113] that it is possible to separate multiple chaotic carriers with similar frequency characteristics which have been additively combined. The use of chaos in switched-mode power supplies to suppress

the injection of harmonics back into the power distribution network (thereby removing the need for filters which can be expensive) is also being investigated. Although chaotic signals may occupy a large frequency band, the energy is distributed more uniformly throughout the spectral band. Filter properties of the power network then reduce the energy of the chaotic signal even further. A chaotic integrated circuit for analyzing nonlinear discrete dynamical systems has been designed and manufactured by Yamakawa *et al.* [870]. This chip has three basic elements, namely a nonlinear delay element, a linear delay element and a summing element. Chaotic networks can be constructed by using one of more of these chips. The prototype chip was implemented using a 3 μm double polysilicon CMOS process. Synchronization of chaotic systems is emerging as a prominent research field. It already finds applications in secure communications [324].

8.2 Chaos Research: The Future

It is important to observe that, although researchers are starting to apply chaos to solve engineering problems, chaos research is still far from reaching its finally stage, namely the phase where refinement of existing engineering design procedures will occur. We are of the opinion that chaos research in engineering will eventually reach the point where it will lead to improved and refined design procedures, enabling a designer to design a system to deliberately be chaotic or not chaotic. We foresee that the control of chaos will play an important role not only in engineering and physics by in our general understanding of the nonlinear world that we live in. Ultimately, we may perhaps even one-day, understand the inner workings of the human brain [258], which is one of the most complex nonlinear systems that exists.

Researchers now only start to believe that in order for a system to be versatile it must be chaotic. Perhaps one-day the apparently long-term unpredictability of chaos which is still very much perceived as a negative property, will have positive results:

'... *Even the process of intellectual progress relies on the injection of new ideas. Innate creativity may have some underlying chaotic process that selectively amplifies small fluctuations and molds them into macroscopic coherent mental states that are experienced as thoughts. ... In this light chaos provides a mechanism that allows for free will within a world governed by deterministic laws.*'

Crutchfield *et al.* 1986 [189]

Appendix A

One-Dimensional Maps

A.1 Introduction

The objective of this Appendix is to provide an introduction to the theory of chaos. One-dimensional maps are used as a vehicle to convey the concepts required for studying chaos, firstly because fewer concepts are involved compared to higher dimensional maps and differential equations and secondly because of the fact that one-dimensional maps and their evolutions may easily be visualized, which helps to grasp ideas involved more rapidly. For generalization of these results to, and additional results on higher dimensional mappings and differential equations, the reader is referred to the bibliography. Some important theorems are stated in Appendix B without proof.

Consider an arbitrary one dimensional, N-th order discrete dynamical system whose time evolution is described by the homogeneous recurrence relation

$$x_{n+1} = f(x_n, x_{n-1}, \ldots, x_{n-N+1}),$$

where f is some function

$$f : \mathbf{R}^N \to \mathbf{R},$$

and x_n is the dynamical system's evolution on the n-th discrete time instant, i.e. $n = 0, 1, 2, \ldots$. In general f may be nonlinear and is usually at least piecewise differentiable. The function f which describes some dynamical system is termed a *mapping* or simply a *map*.

Example A.1 Consider the *logistic map* described by

$$x_{n+1} = f(x_n), \tag{A.1}$$

where

$$f : I \to \mathbf{R}, \qquad f(x) := rx(1 - x), \tag{A.2}$$

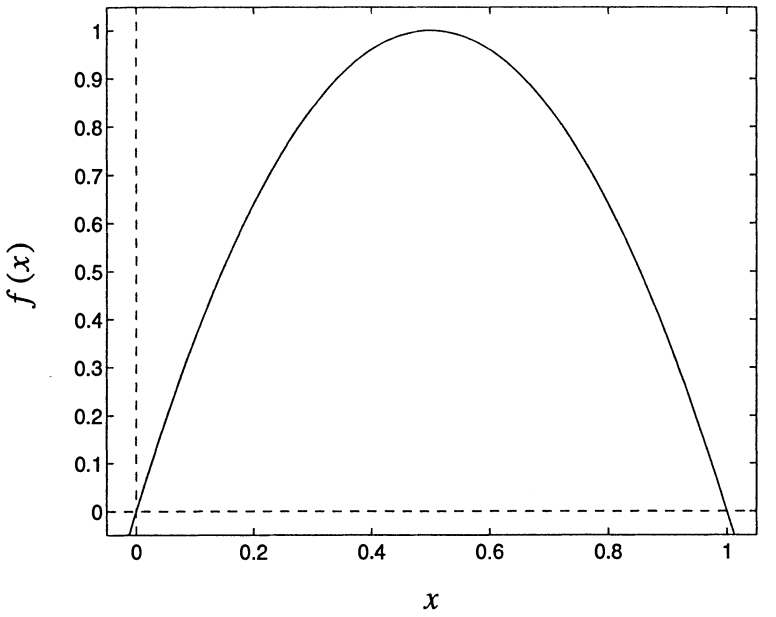

Figure A.1: The logistic map for $r = 4$.

with

$$I := \{x \mid 0 \leq x \leq 1\},$$

and $r \in \mathbf{R}^+$ a so-called *bifurcation parameter* of the system. From (A.2) we observe that f is of degree 2 in x and hence nonlinear in x. The map given by (A.2) is illustrated in Figure A.1. It is obvious that the logistic map is one-dimensional and of order one. ■

In this chapter we consider only one-dimensional, first order maps, that is, maps of the form

$$x_{n+1} = f(x_n), \tag{A.3}$$

where generally $f : \mathbf{R} \to \mathbf{R}$.

A.2 Orbits and Their Properties

Definition A.2 Consider the map $f : X \to X$, $X \subset \mathbf{R}$ defined by

$$x_{n+1} = f(x_n), \qquad n \in \mathbf{N}_0 \tag{A.4}$$

The set of points

$$\mathcal{O}^+(x_0) := \{x_0, x_1, x_2, \ldots\},$$

obtained from (A.4) is defined as the *forward orbit* of the point x_0. If f is a homeomorphism, we may also define the *backward orbit* of x_0 as the set of points

$$\mathcal{O}^-(x_0) := \{x_0, x_{-1}, x_{-2}, \ldots\},$$

and the *full orbit* of x_0 as the set

$$\mathcal{O}(x_0) := \mathcal{O}^-(x_0) \cup \mathcal{O}^+(x_0) = \{x_n \mid n \in \mathbf{Z}\},$$

obtained from (A.4). ■

At this point it is worthwhile to mention that another popular notation for representing the n-th iterate of the point x_0 under the map f is

$$x_n = f^{(n)}(x_0)$$

by application of the inductive definition

$$f^{(n)}(x_0) := f(f^{(n-1)}(x_0)), \quad n \in \mathbf{N},$$

where $f^{(1)}(x_0) = f(x_0)$. In the case of a causal dynamical system described by (A.4), the forward orbit of the system is its response to the initial condition x_0. In general an orbit of a dynamical system is the time evolution of the system coinciding with some predetermined value x_0 on iteration instance $n = 0$.

Since we classify a dynamical system based on its response to initial conditions (and inputs) it is therefore important to understand all orbits of a map. A particular type of orbit called a periodic orbit plays an important role in the study of dynamical systems.

Definition A.3 The point x^* is *periodic of prime period-n* if

$$f^{(n)}(x^*) = x^*,$$

but $f^{(m)}(x^*) \neq x^*$ for $1 \leq m < n$. The set of all iterates of a periodic point form a *periodic orbit* [50]. We denote the set of all points of prime period-n of the map f by $\mathrm{Per}_n(f)$. ■

Definition A.4 A *fixed point* (or *equilibrium point*) x^* of the map f is a point of period-1, that is,

$$f(x^*) = x^*.$$

The set of all fixed points of the map f will be denoted by $\mathrm{Fix}(f)$, i.e.

$$\mathrm{Fix}(f) := \mathrm{Per}_1(f).$$

■

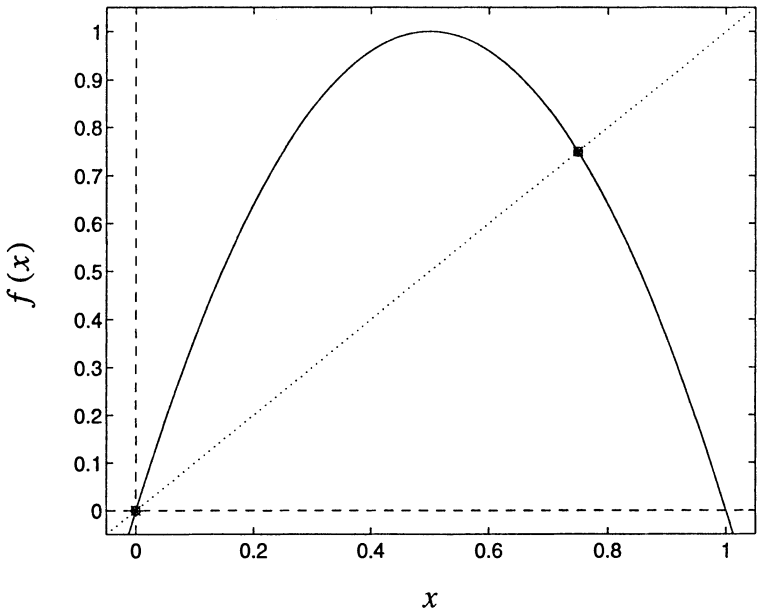

Figure A.2: Fixed points of the logistic map for $r = 4$.

To find the set of fixed points of a map f graphically we may overlay the curve $x_{n+1} = x_n$ onto $x_{n+1} = f(x_n)$ and look for all points of intersection.

Example A.5 Calculate the fixed points of the logistic map, $f : I \to I$,

$$f(x) = rx(1-x), \qquad 1 \leq r \leq 4\,.$$

From Figure A.2 we see that the logistic map has two fixed points as indicated by the dots. The set of fixed points of f can be shown to be $\mathrm{Fix}(f) = \{0, (r-1)/r\}$. ■

Example A.6 Find the fixed points of the map $f : I \to I$ defined by (refer to Section 6.3)

$$f(x) = 1 - (\alpha x + \beta)(\mathrm{mod}\ 1), \quad \alpha, \beta \in \mathbf{R}^+. \tag{A.5}$$

The graph of f is shown in Figure A.3. The fixed points are indicated by the dots in Figure A.3. To find the fixed points, consider

$$\begin{aligned}
& x^* = f(x^*) \\
\Longleftrightarrow \quad & x^* = 1 - (\alpha x^* + \beta)(\mathrm{mod}\ 1) \\
\Longleftrightarrow \quad & x^* = 1 - (\alpha x^* + \beta) + n, \quad \text{for some } n \in \mathbf{Z} \qquad \text{(see (A.6))} \\
\Longleftrightarrow \quad & x^* = \frac{n + 1 - \beta}{1 + \alpha}, \quad \text{for some } n \in \mathbf{Z}
\end{aligned}$$

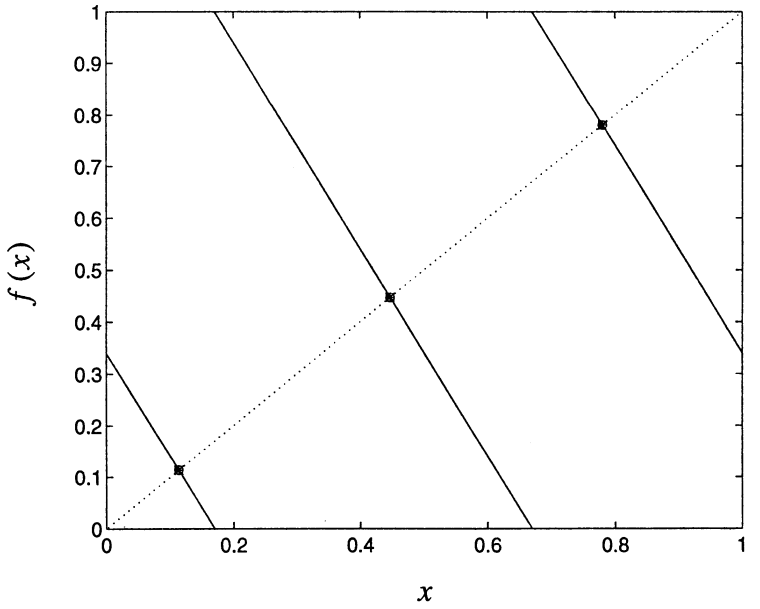

Figure A.3: The graph of f with the fixed points indicated by dots.

where we have used

$$x = y(\mathrm{mod}\ z) \iff x - y = kz, \quad \text{for some } k \in \mathbf{Z}. \tag{A.6}$$

Thus the set of fixed points of f is

$$\begin{aligned} \mathrm{Fix}(f) &= \left\{ x \in I \;\middle|\; x = \frac{n+1-\beta}{1+\alpha},\ n \in \mathbf{Z} \right\} \\ &= \left\{ \frac{n+1-\beta}{1+\alpha} \;\middle|\; n \in \mathbf{Z},\ \lceil \beta - 1 \rceil \le n \le \lfloor \beta + \alpha \rfloor \right\}, \end{aligned} \tag{A.7}$$

where $\lceil y \rceil$ (respectively $\lfloor y \rfloor$) denotes the least (respectively greatest) integer greater (respectively less) than or equal to the real number y. ■

Example A.7 Consider the logistic map. Then

$$\left\{ \frac{5-\sqrt{5}}{8},\ \frac{5+\sqrt{5}}{8} \right\}$$

is a period-2 orbit of the logistic map. ■

Example A.8 The map $f : I \to I$ given by

$$f(x) = \begin{cases} 2x, & \text{if } x \in [0, 1/2) \\ 2(1-x), & \text{if } x \in [1/2, 1] \end{cases} \tag{A.8}$$

is called the *tent map*. It can easily be verified that

$$\mathcal{O}^+(x_0) = \left\{\frac{1}{7}, \frac{2}{7}, \frac{4}{7}\right\},$$

is a period-3 orbit of the tent map. ■

In principle the set of points of period-n, $\mathrm{Per}_n(f)$ of the map $f : X \to X$, $X \subset \mathbf{R}$ can be determined analytically by solving the expression

$$x^* = f^{(n)}(x^*)$$

for x^*. However, because f is usually nonlinear this is sometimes only possible for small values of n (say $n = 1, 2$), while for greater values of n this is generally not possible. In the latter case the periodic points can only be determined either numerically or graphically.

To determine the set $\mathrm{Per}_n(f)$ graphically, we proceed as follows. First the set of all positive integer divisors for n, say $\mathcal{D} = \{1, n_1, n_2, \ldots, n_p\}$ is found. Then the graphs of the corresponding iterates of f are plotted, that is, the graphs of the set of functions

$$\{f, f^{(n_1)}, f^{(n_2)}, \ldots, f^{(n_p)}\},$$

overlayed onto one another. Next we overlay the graph of $y = x$ onto the aforementioned graphs. All points of intersection of the above set of iterates of f and the the diagonal (i.e. the graph of $y = x$) are then removed and then the graph of $f^{(n)}$ is overlaid onto the resulting graph. The intersections between $f^{(n)}$ and the disconnected segments of the diagonal are all periodic points of period-n. Mathematically this can be written as

$$\mathrm{Per}_n(f) = \left\{x \in X \;\middle|\; x = f^{(n)}(x)\right\} - \bigcup_{k \in \mathcal{D}} \left\{x \in X \;\middle|\; x = f^{(k)}(x)\right\}.$$

Example A.9 Find the points of period-3 for the logistic map with $r = 3.839$.

The graphs of f and $f^{(3)}$ are shown in Figure A.4. It can be verified that [217]

$$\mathrm{Per}_3(f) = \{a_1, a_2, a_3, b_1, b_2, b_3\}$$

where

$$\begin{aligned} a_1 &= 0.149888, \quad b_1 = 0.169040, \\ a_2 &= 0.489172, \quad b_2 = 0.539247, \\ a_3 &= 0.959299, \quad b_3 = 0.953837, \end{aligned}$$

up to six decimals.

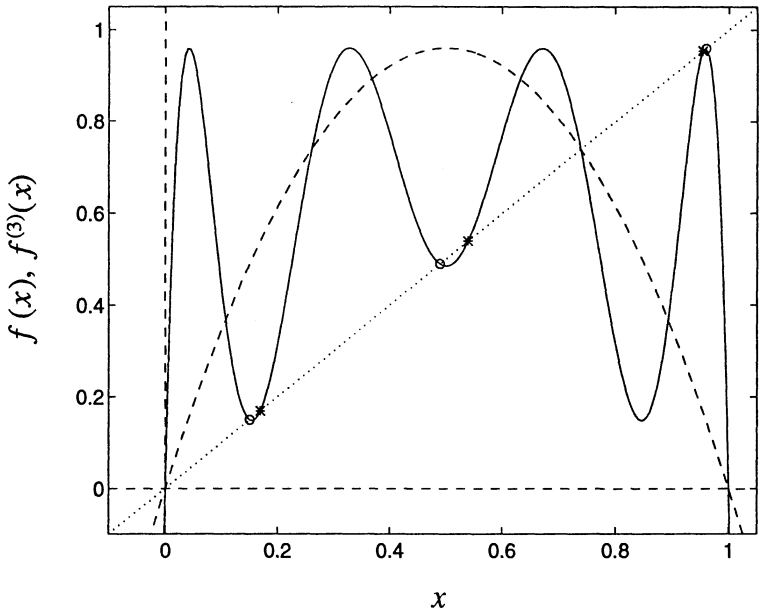

Figure A.4: The graphs of f (dashed line) and $f^{(3)}$ (solid line).

Note that the cardinality of $\mathrm{Per}_3(f)$ is 6. Since by definition a period-3 orbit contains exactly 3 points, this implies that f possesses two independent period-3 orbits. It may easily be verified numerically that the two period-3 orbits are $\{a_1, a_2, a_3, a_1, \ldots\}$ and $\{b_1, b_2, b_3, b_1, \ldots\}$. ■

Example A.10 For the map given by (A.5), determine $\mathrm{Per}_2(f)$.

The two cases $\alpha \neq 1$ and $\alpha = 1$ will be considered separately.

The case $\alpha \neq 1$:

We have

$$\begin{aligned} f^{(2)}(x^*) &= 1 - \{\alpha f(x^*) + \beta\} \,(\mathrm{mod}\ 1) \\ &= 1 - \{\alpha[1 - (\alpha x^* + \beta)(\mathrm{mod}\ 1)] + \beta\} \,(\mathrm{mod}\ 1) \\ &= 1 - \Big\{\alpha + \beta - (\alpha^2 x^* + \alpha\beta)(\mathrm{mod}\ \alpha)\Big\} \,(\mathrm{mod}\ 1) \qquad \text{(A.9)} \\ &= 1 - \Big\{\alpha + \beta - \alpha^2 x^* - \alpha\beta - n\alpha\Big\} + m, \quad \text{for some } n, m \in \mathbf{Z} \\ &= \alpha^2 x^* + (\alpha - 1)(\beta - 1) + \alpha n + m, \quad \text{for some } n, m \in \mathbf{Z}, \qquad \text{(A.10)} \end{aligned}$$

where (A.6) was used together with the identity

$$k(y(\mathrm{mod}\ z)) \equiv ky(\mathrm{mod}\ kz).$$

Solving (A.10) for x^*, we get

$$x^* = \frac{(\alpha-1)(\beta-1)+\alpha n+m}{(1-\alpha)(1+\alpha)} \quad \text{for some } n,m \in \mathbf{Z}.$$

Thus, the set of period-2 points of f is given by

$$\mathrm{Per}_2(f) = \left\{ x \in I \;\middle|\; x = \frac{(1-\alpha)(1-\beta)+\alpha n+m}{(1-\alpha)(1+\alpha)}, \quad n,m \in \mathbf{Z} \right\} - \mathrm{Fix}(f),$$

where $\mathrm{Fix}(f)$ is given by (A.7).

The case $\alpha = 1$:

Inserting $\alpha = 1$ into (A.9), we obtain

$$\begin{aligned} f^{(2)}(x) &= 1 - \{1+\beta-(x+\beta)(\mathrm{mod}\ 1)\}\,(\mathrm{mod}\ 1) \\ &= 1 - \{1+\beta-(x+\beta)\}\,(\mathrm{mod}\ 1) \\ &= x \quad \text{for each } x \in I, \end{aligned}$$

where we have made use of the identities

$$(y(\mathrm{mod}\ z))(\mathrm{mod}\ z) \equiv y(\mathrm{mod}\ z),$$

and

$$(x+y)(\mathrm{mod}\ z) \equiv (x(\mathrm{mod}\ z) + y(\mathrm{mod}\ z))(\mathrm{mod}\ z).$$

Finally we have

$$\mathrm{Per}_2(f) = I - \mathrm{Fix}(f),$$

where

$$\mathrm{Fix}(f) = \left\{ \frac{n+1-\beta}{2} \;\middle|\; n \in \mathbf{Z},\ \lceil \beta - 1 \rceil \le n \le \lfloor \beta + 1 \rfloor \right\}.$$

Hence for the case $\alpha = 1$ almost every point in I is of prime period-2. This implies that in this case infinitely many period-2 points (and hence period-2 orbits) exist.

The graphs of f and $f^{(2)}$ for an arbitrary case $\alpha \neq 1$ are shown (overlaid) in Figure A.5. ■

As will become evident later, our basic objective is to understand all orbits of a map. At this stage an orbit may be perceived as abstract. To give it a somewhat more concrete meaning we introduce the concept of the *phase portrait*. The phase portrait is a pictorial representation of the orbit of a map $f : X \to X$, $X \subset \mathbf{R}$ associated with an initial condition $x_0 \in X$.

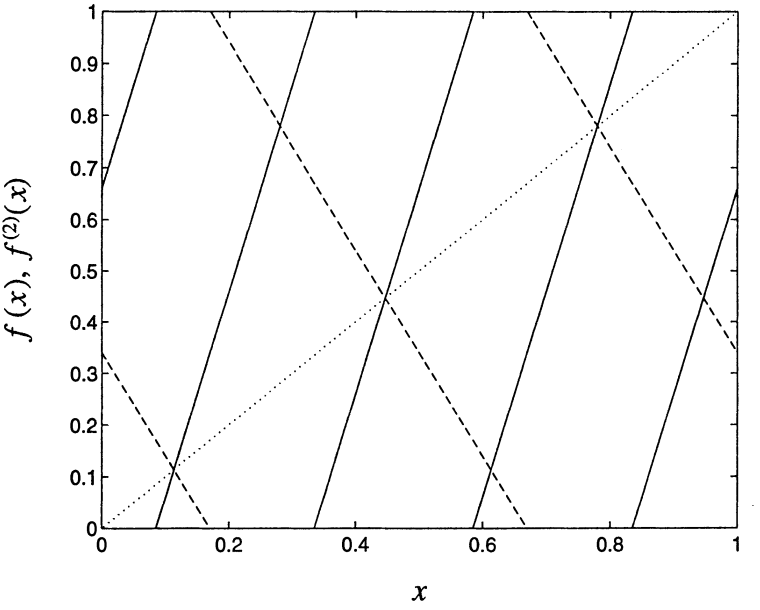

Figure A.5: The graphs of f (dashed line) and $f^{(2)}$ (solid line).

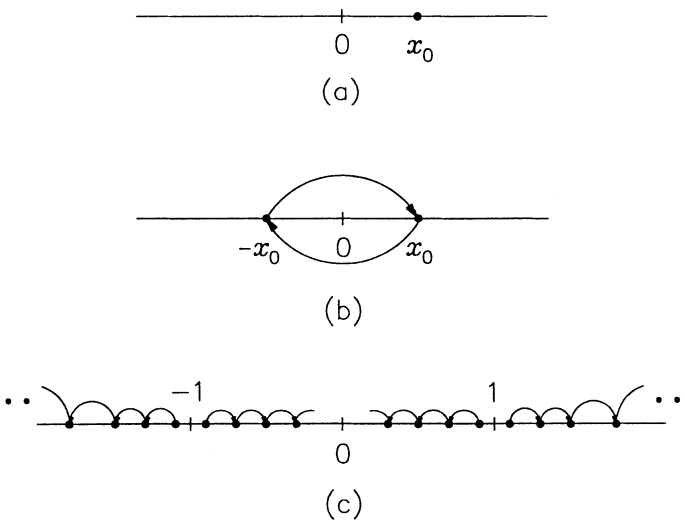

Figure A.6: The phase portraits of (a) $f(x) = x$, (b) $f(x) = -x$, (c) $f(x) = x^3$.

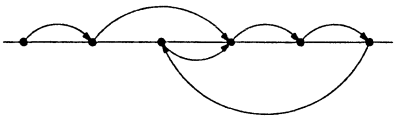

Figure A.7: Illustration of an eventually periodic point of period-4.

Example A.11 The phase portraits of the maps

$$f(x) = x\,, \quad f(x) = -x\,, \quad f(x) = x^3\,,$$

for $x \in \mathbf{R}$ are depicted in Figure A.6. ■

Definition A.12 Let $f : X \to X$, $X \subset \mathbf{R}$. The point $x \in X$ is *eventually periodic* of period-n if x is not periodic, yet there exists an integer $m > 0$ such that

$$f^{(n+k)}(x) = f^{(k)}(x)$$

for all $k \geq m$. ■

From the above definition it is clear that the point $f^{(k)}(x)$ is n-periodic if $k \geq m$. The concept of an eventually periodic point originating at the point x_0 is illustrated by the phase portrait in Figure A.7.

Example A.13 Let $f : S^1 \to S^1$ be the map defined by

$$f(\theta) := 2\theta\,,$$

where

$$S^1 := \left\{(x, y) \mid x^2 + y^2 = 1\right\}.$$

Note that $\theta = 0$ is a fixed point of f. For $\theta = k\pi/2^{n-1}$, $n \in \mathbf{N}$ it follows that $f^{(n)}(\theta) = 2k\pi$ and thus all such θ tend to the fixed point and are hence *eventually fixed*. ■

Example A.14 For the map $f : \mathbf{R} \to \mathbf{R}$

$$f(x) := x^2$$

the point $x = -1$ is eventually fixed. ■

Definition A.15 Suppose x^* is a n-periodic point of $f : X \to X$, $X \subset \mathbf{R}$. We say that $x \in X$ is *forward asymptotic* to x^* if

$$\lim_{k \to \infty} f^{(kn)}(x) = x^*.$$

The set of all points which are forward asymptotic to x^* is called the *stable set* of x^* and is denoted by $W^s(x^*)$.

If the inverse of f exists, then the *unstable set* $W^u(x^*)$ of the period-n point x^*, consisting of all points that are *backward asymptotic* to x^* may be defined by letting $k \to -\infty$ in the above. ■

For the case where x^* is a non-periodic point we may still define forward asymptotic points by requiring that

$$\lim_{k\to\infty} |f^{(k)}(x) - f^{(k)}(x^*)| = 0\,.$$

Example A.16 Let $f : \mathbf{R} \to \mathbf{R}$ be given by $f(x) = x^3$. Then we have

$$W^s(0) = (-1,1)\,, \quad W^u(-1) = \mathbf{R}^-\,, \quad W^u(1) = \mathbf{R}^+.$$

■

Example A.17 Consider the map $f : \mathbf{R}^+ \to \mathbf{R}^+$ defined by

$$f(x) = x + b\,\mathrm{sat}[a(1-x)] - c, \quad a, b, c \in \mathbf{R}^+, \tag{A.11}$$

where $\mathrm{sat}(\cdot)$ is the nonlinear saturation function defined by

$$\mathrm{sat}(x) := \begin{cases} 0, & \text{if } x \le 0 \\ x, & \text{if } 0 < x < 1 \\ 1, & \text{if } x \ge 1 \end{cases}.$$

This map is known as the *zigzag map*, and is illustrated in Figure A.8.

If $b > 0$ and $c > 0$, then f has exactly one fixed point, namely

$$x^* = 1 - \frac{c}{ab}.$$

From (A.11) we may derive expressions for each interval, that is

$$f(x) = \begin{cases} x + b - c, & \text{if } x \le (a-1)/a \\ x(1-ab) + ab - c, & \text{if } (a-1)/a < x < 1 \\ x - c, & \text{if } 1 \le x \end{cases}. \tag{A.12}$$

If $|1 - ab| < 1$ then $W^s(p) = \mathbf{R}^+$, else if $|1 - ab| > 1$ then $W^u(p) = [(a-1)/a, 1]$. ■

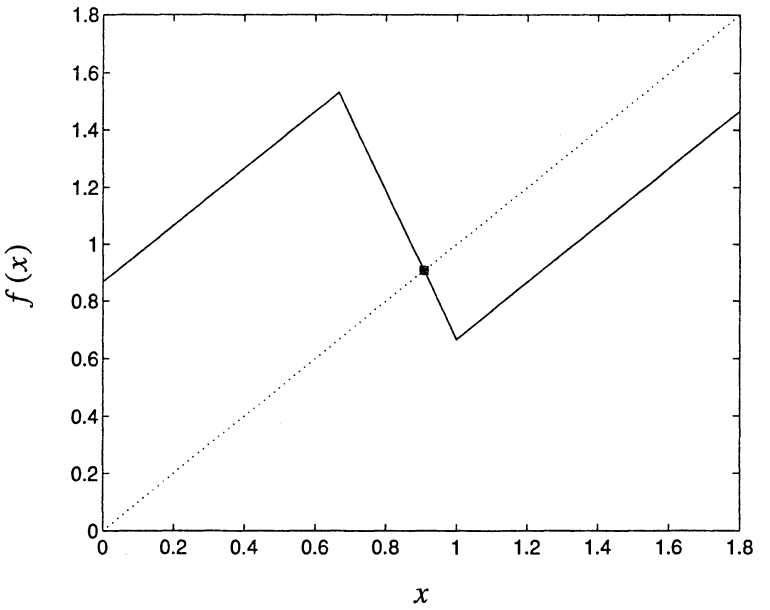

Figure A.8: Graph of the zigzag map.

Definition A.18 [482] Let $x^* \in X$ be any periodic point of the map $f : X \to X$. We say $x \in X$ is *asymptotically periodic* if

$$\lim_{n\to\infty} |f^{(n)}(x) - f^{(n)}(x^*)| = 0.$$

■

Definition A.19 Let $f : X \to X$ be a one-dimensional mapping. The *ω-limit set* of the point x is defined to be the set $L_\omega(x)$ of all $y \in X$ for which there exists a monotonic increasing sequence of positive integers $\{n_i\}_{i=1}^{\infty}$ such that

$$\lim_{i\to\infty} f^{(n_i)}(x) = y.$$

■

The next definition applies only to homeomorphisms.

Definition A.20 Let $f : X \to X$ be a one-dimensional mapping. The *α-limit set* of the point x is defined to be the set $L_\alpha(x)$ of all $y \in X$ for which there exists a monotonic decreasing sequence of negative integers $\{n_i\}_{i=1}^{\infty}$ such that

$$\lim_{i\to\infty} f^{(n_i)}(x) = y.$$

■

Example A.21 For the map $f : I \to I$ defined by (see Chapter 3)

$$f(x) := \begin{cases} \gamma x, & \text{if } 0 \le x \le 1/\gamma \\ \dfrac{\gamma}{\gamma - 1}\left(x - \dfrac{1}{\gamma}\right), & \text{if } 1/\gamma < x \le 1 \end{cases}$$

where $\gamma \in (1, \infty)$, calculate the ω-limit set.

Since the sequence $\{x_n\}_{n=0}^{\infty}$ is uniformly distributed (see Example A.62), any subinterval of I will include at least one point of $\{x_n\}_{n=0}^{\infty}$. Therefore we can construct the sequence $\{n_i\}_{i=1}^{\infty}$ for each $y \in (0,1)$ as follows. Let $\epsilon > 0$ be any real number such that $(y - \epsilon,\ y + \epsilon) \subset I$. Then n_1 can be chosen to satisfy

$$f^{(n_1)}(x) \in (y - \epsilon,\ y + \epsilon).$$

By considering $f^{(n_1)}(x_0)$ to be a new initial point, then a positive integer m_1 can be chosen such that

$$f^{(m_1)}(f^{(n_1)}(x)) \in (y - \epsilon/2,\ y + \epsilon/2).$$

Now define $n_2 := n_1 + m_1$. We thus have $f^{(n_2)}(x_0) \in (y - \epsilon/2,\ y + \epsilon/2)$. Continuing this procedure we eventually get

$$f^{(n_k)}(x) \in (y - \epsilon/k,\ y + \epsilon/k),$$

where $n_k > n_{k-1}$ for $k \in \mathbf{N}$. Consequently

$$\lim_{k \to \infty} f^{(n_k)}(x_0) = y.$$

By choosing the subintervals slightly differently, the cases where $y = 0$ and $y = 1$ can be proved. Thus $L_\omega(x_0) = [0,1]$. Since $x_0 \in (0,1) - \{1/\gamma\}$ was chosen arbitrarily we have that $L_\omega(x) = I$ for almost every (a.e.) $x \in I$. The phrase "almost every" will be clarified in Section A.9. ■

Earlier we introduced the concept of the phase portrait as a means of graphically representing how a point evolves under iteration of a given map. The same information can be obtained from the graph of the map by following a procedure called *graphical analysis* [217] as follows. Overlay graph of $y = x$ onto graph of $y = f(x)$. A vertical line from the point (x_0, x_0) intersects the graph of $y = f(x)$ at the point $(x_0, f(x_0))$. Next, a horizontal line through $(x_0, f(x_0))$ intersects the graph of $y = x$ at the point $(f(x_0), f(x_0))$. Continuing in this manner after n repetitions of the above process we end up at the point $(f^{(n)}(x_0), f^{(n)}(x_0))$ on the graph of $y = x$. The set of points $\left\{(f^{(k)}(x_0), f^{(k)}(x_0)) \mid k \in \mathbf{N}\right\}$ describes the evolution of the point x_0 under iteration of the map f. Thus the evolution described by this set of points on the graph of $y = x$ can be viewed as an enlarged (by factor $\sqrt{2}$) replica of the phase portrait.

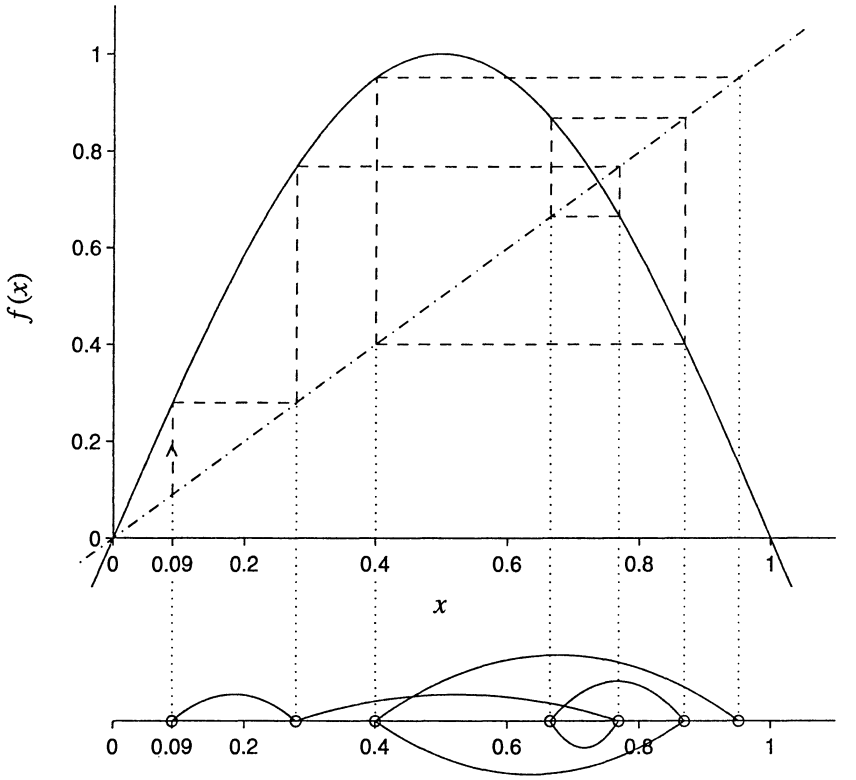

Figure A.9: Illustration of the relationship between graphical analysis and the phase portrait with $f(x) = \sin(\pi x)$.

Example A.22 Consider the *sine map* given by

$$f(x) = \sin(\pi x)\,.$$

Figure A.9 depicts the relationship between graphical analysis and the phase portrait for the map f with initial condition $x_0 = 0.09$. ■

A.3 Hyperbolicity

Definition A.23 Let x^* be a periodic point of prime period-n. If

$$\left|\frac{df^{(n)}}{dx}(x^*)\right| \neq 1$$

then x^* is said to be *hyperbolic*. ■

Example A.24 Determine those values of r for which both fixed points of the logistic map are hyperbolic.

The derivative of the logistic map (A.2) is given by

$$\frac{df}{dx}(x) = r(1-2x). \tag{A.13}$$

Evaluating df/dx at the fixed points of f gives

$$\left.\frac{df}{dx}(x)\right|_{x=0} = r, \qquad \text{and} \qquad \left.\frac{df}{dx}(x)\right|_{x=(r-1)/r} = 2-r,$$

where $r \in [1,4]$. Hence we see that both fixed points are hyperbolic for $r \in (1,2) \cup (2,4]$. ■

Example A.25 Consider the *Gauss map* $f : I \to I$ given by

$$f(x) = \begin{cases} 0, & \text{if } x = 0 \\ x^{-1} (\text{mod } 1), & \text{if } x \in (0,1] \end{cases}. \tag{A.14}$$

Comment on the hyperbolicity of its fixed points.

It can easily be shown that

$$\begin{aligned} \text{Fix}(f) &= \left\{ x \in I \;\middle|\; x^2 + kx - 1 = 0, \text{ for some } k \in \mathbf{N} \right\} \\ &= \left\{ x \in I \;\middle|\; x = \frac{\sqrt{k^2+4} - k}{2}, \text{ for some } k \in \mathbf{N} \right\}. \end{aligned}$$

The Gauss map has an infinite number of fixed points (this can easily be seen graphically). Using the fact that

$$\frac{d}{dx}[g(x)(\text{mod } z)] = \frac{dg}{dx}(x), \quad \text{if } g(x) \neq kz,$$

for $z \in \mathbf{R}$ and $k \in \mathbf{Z}$, we have

$$\frac{df}{dx}(x) = -\frac{1}{x^2}, \quad \text{if } x \neq \frac{1}{k}, \quad k \in \mathbf{N}.$$

Since the domain of f is $[0,1]$, we see that

$$\left| \frac{df}{dx}(x)|_{x=1} \right| = 1,$$

and

$$\left| \frac{df}{dx}(x^*) \right| > 1, \quad \text{for each } x^* \in \text{Fix}\,(f) - \{1\}.$$

Hence, except for the fixed point at $x = 1$, all other fixed points of the Gauss map are hyperbolic. ■

Example A.26 Comment on the hyperbolicity of the periodic orbits of the map $f : I \to I$ given by

$$f(x) = 2x(\text{mod } 1). \tag{A.15}$$

This map is called the *Bernoulli map*. Its second iterate is given by

$$\begin{aligned} f^{(2)}(x) &= [2f(x)](\text{mod } 1) \\ &= [2\{(2x)(\text{mod } 1)\}](\text{mod } 1) \\ &= [(4x)(\text{mod } 2)](\text{mod } 1) \\ &= (4x)(\text{mod } 1). \end{aligned}$$

In general the n-th iterate of the Bernoulli map is

$$f^{(n)}(x) = 2^n x(\text{mod } 1).$$

It can be shown that

$$\text{Fix}(f) = \{0\}$$

and for $n = 2, 3, 4, \ldots$ that

$$\text{Per}_n(f) = \left\{ x = \frac{k}{2^n - 1} \;\middle|\; k = 1, 2, 3, \ldots, 2^n - 2 \right\}.$$

The gradient of $f^{(n)}$ at x is obtained by differentiating $f^{(n)}$ once with respect to x, i.e.

$$\frac{df^{(n)}}{dx}(x) = 2^n, \quad \text{for } x \in I - \left\{ \frac{k}{2^n} \;\middle|\; k = 0, 1, 2, \ldots, 2^n \right\}, \quad n \in \mathbf{N}.$$

It follows that all periodic points of period-n, for each $n \in \mathbf{N}$, are hyperbolic. ■

A.4 Stability

In this section we discuss the stability properties of fixed points of one-dimensional mappings.

Proposition A.27 [217] Suppose that x^* is a hyperbolic fixed point of the C^1 map $f : X \to X$, $X \subset \mathbf{R}$ and that $|(df/dx)(x^*)| < 1$. Then there is an interval U about x^* such that if $x \in U$ then

$$\lim_{n \to \infty} f^{(n)}(x) = x^*.$$

Proof: Since f is of class C^1, there exists an $\epsilon > 0$ such that

$$\left| \frac{df}{dx}(x) \right| < A < 1 \quad \text{for } x \in [x^* - \epsilon, x^* + \epsilon].$$

Application of the mean value theorem yields

$$\begin{aligned} |f(x) - x^*| &= |f(x) - f(x^*)| \\ &= \left|\frac{df}{dx}(y)\right| |x - x^*|, \quad (y \in [x, x^*]) \\ &< A|x - x^*|, \quad (y \in [x^* - \epsilon, x^* + \epsilon]) \\ &< |x - x^*| \\ &\leq \epsilon . \end{aligned}$$

Hence $f(x) \in [x^* - \epsilon, x^* + \epsilon]$ for $x \in [x^* - \epsilon, x^* + \epsilon]$. In other words x is mapped into $[x^* - \epsilon, x^* + \epsilon]$. In general since $|(df/dx)(x)| < A$ for $x \in [x^* - \epsilon, x^* + \epsilon]$ it follows inductively that $f^{(n)}(x) \in [x^* - \epsilon, x^* - \epsilon]$, $n \in \mathbf{N}$. Applying the mean value theorem to $f^{(n)}$ we have

$$|f^{(n)}(x) - x^*| = |f^{(n)}(x) - f^{(n)}(x^*)| = \left|\frac{df^{(n)}}{dx}(r)\right| |x - x^*|, \quad r \in [x, x^*]. \tag{A.16}$$

The chain rule gives

$$\frac{df^{(n)}}{dx}(x) = \prod_{i=0}^{n-1} \frac{df}{dy}(y)\bigg|_{y=f^{(i)}(x)}, \quad n \in \mathbf{N} \tag{A.17}$$

for $x \in [x^* - \epsilon, x^* + \epsilon]$, (A.17) yields

$$\left|\frac{df^{(n)}}{dx}(x)\right| < A^n < 1, \tag{A.18}$$

since $f^{(i)}(x) \in [x^* - \epsilon, x^* + \epsilon]$, for $i = 0, 1, 2, \ldots, n$.

Using (A.18) and taking the limit as n approaches infinity, (A.16) becomes

$$|f^{(n)}(x) - x^*| < A^n |x - x^*| \xrightarrow[\infty]{n} 0 \quad \Longrightarrow \quad f^{(n)}(x) \xrightarrow[\infty]{n} x^*.$$

■

Next we will extend the above result to periodic points.

Proposition A.28 Suppose x^* is a hyperbolic period-n point, $n \in \mathbf{N}$ of the C^1 map $f : X \to X$, $X \subset \mathbf{R}$, and that $|(df^{(n)}/dx)(x^*)| < 1$. Then there is an open interval U about x^* such that if $x \in U$, then

$$\lim_{k \to \infty} f^{(nk)}(x) = x^*.$$

Proof: Since f is of class C^1, there exists an $\epsilon > 0$ such that

$$\left|\frac{df^{(n)}}{dx}(x)\right| < A < 1 \qquad \text{for } x \in [x^* - \epsilon, x^* + \epsilon].$$

Consequently (as was shown previously)

$$\frac{df^{(nk)}}{dx}(x) < A^k < 1, \quad x \in [x^* - \epsilon, x^* + \epsilon]$$

for arbitrary $k \in \mathbf{N}$. By the mean value theorem, we have

$$\begin{aligned} |f^{(nk)}(x) - x^*| &= |f^{(nk)}(x) - f^{(nk)}(x^*)| \\ &= \left|\frac{df^{(nk)}}{dx}(y)\right| |x - x^*|, \qquad (y \in [x, x^*]) \\ &< A^{nk}|x - x^*|. \end{aligned}$$

Hence

$$|f^{(nk)}(x) - x^*| \xrightarrow[\infty]{k} 0 \implies f^{(nk)}(x) \xrightarrow[\infty]{k} x^*.$$

■

Definition A.29 Let x^* be a hyperbolic period-n point of the map $f : X \to X$, $X \subset \mathbf{R}$ and $|(df/dx)(x^*)| < 1$. The point x^* is called an *attracting* period-n point (also called a *sink*). The maximal neighbourhood of the point x^* which converges to x^* under forward iteration of f is defined to be the *local stable set* of x^* denoted by $W^s_{loc}(x^*)$. ■

Next we consider the case where the derivative of a map is greater than one in absolute value.

Proposition A.30 Suppose x^* is a hyperbolic period-n point, $n \in \mathbf{N}$ of the C^1 map $f : X \to X$, $X \subset \mathbf{R}$, and that $|(df/dx)(x^*)| < 1$. Then there is an open interval U about x^* such that if $x \in U$ then

$$\lim_{k \to \infty} f^{(-nk)}(x) = x^*.$$

Proof: Since f is C^1 there is an $\epsilon > 0$ such that $|(df/dx)(y)| > A > 1$ for $y \in [x^* - \epsilon, x^* + \epsilon]$. By the mean value theorem

$$|f(y) - x^*| > A|y - x^*| > \epsilon. \tag{A.19}$$

It follows that

$$|y - x^*| < A^{-1}|f(y) - x^*|. \tag{A.20}$$

Substituting $y = f^{-1}(x)$ (since f is injective on the interval $[x^* - \epsilon, x^* + \epsilon]$) into (A.20) yields

$$|f^{-1}(x) - x^*| < A^{-1}|x - x^*|, \quad x \in [x^* - \delta, x^* + \delta]$$

where $\delta = f(\epsilon)$. From here onwards the proof is exactly the same as the proof of the previous two propositions. ■

Definition A.31 Let x^* be a hyperbolic period-n point of the map $f : X \to X$, $X \subset \mathbf{R}$ and $|(df/dx)(x^*)| > 1$. The point x^* is called a *repelling* period-n point (or a *source*). The maximal neighbourhood of the point x^* which converges to x^* under backward iteration of f is defined as the *local unstable set* of x^* denoted by $W^u_{loc}(x^*)$. ■

Example A.32 For the map given by (A.5) we have

$$\left|\frac{df}{dx}(x)\right| = \alpha, \quad \alpha \in \mathbf{R}^+$$

for $x \in I - \{y \in I | f(y) = 0\}$. Hence if $\alpha < 1$, then all fixed points and periodic orbits are attracting. If $\alpha > 1$ however, then all fixed points and periodic orbits are repelling. This follows easily from the fact that

$$\left|\frac{df^{(n)}}{dx}(x)\right| = \alpha^n, \quad x \in I - \left\{y \in I | f^{(n)}(y) = 0\right\}.$$

■

Example A.33 Consider the Gauss map, given by (A.14). Here

$$\left|\frac{df}{dx}(x)\right| = \frac{1}{x^2} > 1, \quad x \in I - \{y \in I | f(y) = 0\}. \tag{A.21}$$

By the chain rule and (A.21) we have

$$\left|\frac{df^{(n)}}{dx}(x)\right| = \prod_{k=0}^{n-1} \left|\frac{df}{dx}(f^{(k)}(x))\right| > 1, \ x \in I - \left\{y \in I | f^{(k)}(y) = 0, \ k = 0, 1, 2, \ldots, n-1\right\}. \tag{A.22}$$

Hence by (A.21) and (A.22) all fixed and periodic points are repelling. ■

A question which arises naturally is whether all points belonging to the same hyperbolic period-n orbit are equally attracting (or repelling) or are some of the points more attracting (or repelling) than others. The next proposition answers this question.

Proposition A.34 Consider the map $f : X \subset \mathbf{R} \to X$. The derivative of $f^{(n)}$ affords the same value at all points on a given period-n orbit.

Proof: Recall that

$$f^{(n)}(f^{(j)}(x)) \equiv f^{(j)}(f^{(n)}(x)), \quad j \in \mathbf{N}_0. \tag{A.23}$$

Differentiating (A.23) with respect to x gives

$$\frac{df^{(n)}}{dx}(f^{(j)}(x))\frac{df^{(j)}}{dx}(x) = \frac{df^{(j)}}{dx}(f^{(n)}(x))\frac{df^{(n)}}{dx}(x). \tag{A.24}$$

Suppose that x^* is a period-n point of f. Then, setting $x = x^*$ into (A.24) and using the fact that $f^{(n)}(x^*) = x^*$, we obtain

$$\frac{df^{(n)}}{dx}(f^{(j)}(x^*)) = \frac{df^{(n)}}{dx}(x^*),$$

for arbitrary $j \in \mathbf{N}_0$.

From this it is clear that all points on a periodic orbit have identical hyperbolicity characteristics. ■

Definition A.35 Consider the map $f : X \subset \mathbf{R} \to X$. If f has a period-n orbit and x^* is a point on this orbit, then this orbit is called

i) an *attracting hyperbolic period-n orbit* (or simply attracting period-n orbit) if $|(df^{(n)}/dx)(x^*)| < 1$,

ii) a *nonhyperbolic period-n orbit* if $|(df^{(n)}/dx)(x^*)| = 1$,

iii) a *repelling hyperbolic period-n orbit* (or simply repelling period-n orbit) if $|(df^{(n)}/dx)(x^*)| > 1$.

■

Example A.36 Classify the periodic orbits of the zigzag map for $ab > 2$ according to their hyperbolicity.

Differentiating the zigzag map (see (A.12)), we obtain

$$\frac{df}{dx}(x) = \begin{cases} 1, & \text{if } x \leq (a-1)/a \\ 1-ab, & \text{if } (a-1)/a < x < 1 \\ 1, & \text{if } 1 \leq x \end{cases}, \tag{A.25}$$

Hence $|(df/dx)(x)| \geq 1$, for $x \in \mathbf{R}^+$. Consider any period-n point (say x^*) of f, where $n \in \mathbf{N}$. Then from (A.25) we have

$$\left|\frac{df^{(n)}}{dx}(x^*)\right| = \prod_{k=0}^{n-1}\left|\frac{df}{dx}(f^{(k)}(x^*))\right| \geq 1\,. \tag{A.26}$$

To comment on the hyperbolicity of periodic orbits we must analyze these orbits more thoroughly.

Lemma A.37 The zigzag map possesses nonhyperbolic period-n orbits if

$$b = \left(\frac{n}{k}\right)c \tag{A.27}$$

and

$$a \geq \begin{cases} \dfrac{1}{c}, & \text{if } k = 1 \text{ and } l \in \mathbf{N} \\ \dfrac{k}{c}, & \text{if } k \in \mathbf{N} \text{ and } l = 1 \end{cases}$$

where in addition k and l satisfy $n = k + l$.

Proof: Let

$$f_L(x) := x + b - x\,, \qquad f_C(x) := (1 - ab)x + ab - c\,, \qquad f_R(x) := x - c.$$

From (A.26) we see that for the zigzag map to possess a nonhyperbolic period-n orbit we require that $|(df/dx)(f^{(k)}(x^*))| = 1$ for each $k = 0, 1, 2, \ldots, n-1$, implying that

$$f^{(k)}(x^*) \in \left[0, \frac{a-1}{a}\right) \cup (1, \infty), \quad k = 0, 1, 2, \ldots, n-1.$$

This means that a period-n orbit can only be nonhyperbolic if none of its points are contained in the interval $((a-1)/a\,,\, 1)$. Suppose that this orbit has k points in the interval $[0, (a-1)/a)$ and l points in the interval $(1, \infty)$ with $x^* \in [0, (a-1)/a)$. Thus

$$\begin{aligned} x^* &= f^{(n)}(x^*) \\ &= (f_R^{(l)} \circ f_C^{(0)} \circ f_L^{(k)})(x^*), \qquad n = k + l, \quad k, l \in \mathbf{N} \\ &= x^* + k(b - c) - lc\,, \end{aligned}$$

where $f \circ h$ denotes the composition of the functions f and h. Consequently

$$b = \left(\frac{k+l}{k}\right)c. \tag{A.28}$$

Furthermore we require that

$$\begin{aligned} & f_R^{(l)}\left(f_L\left(\frac{a-1}{a}\right)\right) > f_R(1) \\ \iff \quad & \frac{a-1}{a} + (b-c) - lc > 1 - c \\ \iff \quad & \phi(k,l)a < -\frac{k}{c}, \qquad \text{with } \phi(k,l) := kl - k - l, \end{aligned} \tag{A.29}$$

where we have used (A.28).

The case $k = 1,\ l \in \mathbf{N}$:

$$\phi(k,l) = -1 \quad \Longrightarrow \quad ac > 1\,.$$

The case $k \in \mathbf{N},\ l = 1$:

$$\phi(k,l) = -1 \quad \Longrightarrow \quad ac > k\,.$$

The case $k = l = 2$:

In this case $\phi(2,2) = 0$ and hence no value for a exists which satisfies (A.29).

The case: $k \geq 2,\ l > 2$ or $k > 2,\ l \geq 2$

$$\phi(k,l) > 0 \quad \Longrightarrow \quad a < \frac{-k}{c\phi(k,l)} < 0\,.$$

Since we required earlier that $a > 0$, only the first two cases apply. This completes the proof. □

Thus, if b is not of the form described by (A.27)), then every period-n orbit (if it exists) is hyperbolic according to (A.26), since it contains at least one point in the interval $((a-1)/a, 1)$. On the other hand, if b does satisfy (A.27), there will exist one or more period-n orbits of which at least one is nonhyperbolic. The conditions under which nonhyperbolic and hyperbolic period-n orbits will coexist is left for the reader to determine. ■

A.5 Topological Conjugacy

Definition A.38 Let $f : X \subset \mathbf{R} \to X$ and $g : Y \subset \mathbf{R} \to Y$ be two maps. The maps f and g are said to be *topologically conjugate* if there exists a homeomorphism $h : X \to Y$ such that $h \circ f = g \circ h$ or equivalently

$$g = h \circ f \circ h^{-1}.$$

■

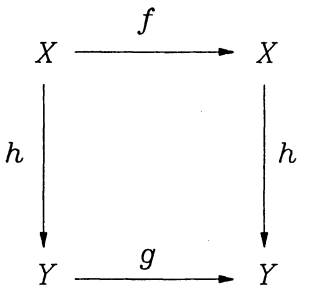

Figure A.10: Commutative diagram illustrating topological conjugacy.

The above definition is summarized in the commutative diagram in Figure A.10.

Example A.39 The Bernoulli map f given by (A.15) and the map $g : S^1 \to S^1$,

$$g(\theta) = 2\theta$$

are topologically conjugate through the map $h : I \to S^1$ given by

$$h(x) = 2\pi x.$$

■

Example A.40 Show that the map $f : I \to I$ defined by

$$f(x) = 4x(1-x) \tag{A.30}$$

(i.e. the logistic map with $r = 4$) and the tent map $g : I \to I$ defined by

$$g(x) = \begin{cases} 2x, & \text{if } x \in [0, 1/2) \\ 2(1-x), & \text{if } x \in [1/2, 1] \end{cases}$$

are topologically conjugate, i.e. $g = h \circ f \circ h^{-1}$ where $h : I \to I$ is defined by

$$h(x) := \frac{2}{\pi} \arcsin \sqrt{x}\,. \tag{A.31}$$

The inverse of h is defined on I with

$$h^{-1}(x) = \sin^2\left(\frac{\pi x}{2}\right) = \frac{1 - \cos(\pi x)}{2}. \tag{A.32}$$

Forming the composition $f \circ h^{-1}$ using (A.30) and (A.32) yields

$$\begin{aligned}(f \circ h^{-1})(x) &= 4\left(\frac{1-\cos \pi x}{2}\right)\left(1-\left(\frac{1-\cos \pi x}{2}\right)\right) \\ &= 1-\cos^2 \pi x \\ &= 1-\left(\frac{1+\cos 2\pi x}{2}\right) \\ &= \frac{1-\cos 2\pi x}{2} \\ &= \sin^2 \pi x. \end{aligned} \tag{A.33}$$

Substituting (A.33) into (A.31) gives

$$g(x) = (h \circ f \circ h^{-1})(x) = \frac{2}{\pi} \arcsin(\sin \pi x), \quad x \in I. \tag{A.34}$$

However, since $\sin \pi x$ is not injective on I we have to consider (A.34) separately on each subinterval where $\sin \pi x$ is injective.

For $x \in [0, 1/2]$ we have

$$\frac{2}{\pi} \arcsin(\sin \pi x) = 2x\,, \tag{A.35}$$

while for $x \in [1/2, 1]$ we have

$$\frac{2}{\pi} \arcsin(\sin \pi x) = 2(1-x)\,. \tag{A.36}$$

Using (A.35) and (A.36), (A.34) now becomes

$$g(x) = \begin{cases} 2x\,, & \text{if } x \in [0, 1/2) \\ 2(1-x)\,, & \text{if } x \in [1/2, 1] \end{cases}.$$

Thus f and g are topologically conjugate. ■

Proposition A.41 Let $f : X \subset \mathbf{R} \to X$ and $g : Y \subset \mathbf{R} \to Y$ be topologically conjugate, via the homeomorphism $h : X \to Y$. Then there is a one-to-one correspondence between periodic orbits of f and g. Moreover the hyperbolicity of a periodic orbit remains invariant under the transformation $g = h \circ f \circ h^{-1}$.

Proof: First we prove the one-to-one correspondence between period-n points of f and g. It follows that

$$g^{(n)} = (h \circ f \circ h^{-1})^{(n)} = h \circ f^{(n)} \circ h^{-1}, \quad n \in \mathbf{N}. \tag{A.37}$$

Now, suppose that x^* is a period-n point of f. Then from (A.37) it follows that

$$g^{(n)}(h(x^*)) = h(f^{(n)}(x^*)) = h(x^*)$$

and hence $h(x^*)$ is a period-n point of g. Since h is a homeomorphism there is a one-to-one correspondence between x^* and $h(x^*)$. Since x^* is an arbitrary period-n point of f, it follows that there is a one-to-one correspondence between period-n points of f and g.

Next we are going to prove the one-to-one correspondence between periodic orbits of f and g. By (A.37)

$$g^{(j)}(h(x^*)) = h(f^{(j)}(x^*)), \quad \text{for } j = 0, 1, 2, \ldots, n-1,$$

there is a one-to-one correspondence between these period-n orbits of f and g. Since this is true for all period-n orbits and since n was chosen arbitrarily we conclude that there is a one-to-one correspondence between periodic orbits of f and g.

Finally we have to prove the invariance of the hyperbolicity of periodic orbits under the transformation $g = h \circ f \circ h^{-1}$. From (A.37) we have

$$g^{(n)}(h(x)) = h(f^{(n)}(x)). \tag{A.38}$$

Differentiation of (A.38) yields

$$\frac{dg^{(n)}}{dx}(h(x))\frac{dh}{dx}(x) = \frac{dh}{dx}(f^{(n)}(x))\frac{df^{(n)}}{dx}(x), \qquad x \in X. \tag{A.39}$$

Inserting $x^* = f^{(n)}(x^*)$ into (A.39) we obtain

$$\frac{dg^{(n)}}{dx}(h(x^*))\frac{dh}{dx}(x^*) = \frac{dh}{dx}(f^{(n)}(x^*))\frac{df^{(n)}}{dx}(x^*) = \frac{dh}{dx}(x^*)\frac{df^{(n)}}{dx}(x^*).$$

If $(dh/dx)(x^*) \neq 0$, then

$$\frac{dg^{(n)}}{dx}(h(x^*)) = \frac{df^{(n)}}{dx}(x^*). \tag{A.40}$$

From (A.40) we see that the hyperbolicity of the corresponding period-n orbits of f and g are the same. Since n was chosen arbitrarily we conclude that the hyperbolicity of periodic orbits remains invariant under the transformation $g = h \circ f \circ h^{-1}$. ■

Example A.42 Calculate the hyperbolicity of the maps $f : I \to I$, and $g : I \to I$ defined by

$$f(x) = 4x(1-x)$$

and

$$g(x) = \begin{cases} 2x, & \text{if } x \in [0, 1/2) \\ 2(1-x), & \text{if } x \in [1/2, 1] \end{cases},$$

at their respective fixed points 3/4 and 2/3.

We have

$$\left.\frac{df}{dx}(x)\right|_{x=3/4} = -2, \quad \text{and} \quad \left.\frac{dg}{dx}(x)\right|_{x=2/3} = -2,$$

with

$$(h \circ f)(x)|_{x=3/4} = (g \circ h)(x)|_{x=2/3},$$

where h given by (A.31) was used. ■

A.6 Chaos

Chaos refers to the apparent random behaviour exhibited by a deterministic system under deterministic conditions. In the study of chaos one soon finds that there is not one single definition of chaos. There are two categories of definitions of chaos: topological and measure theoretical. In this section we shall restrict our attention to the topological definitions of chaos. Measure theoretical definitions of chaos will be considered in a subsequent section.

Definition A.43 The map $f : X \subset \mathbf{R} \to X$ is said to be *topologically transitive* if for open sets U, $V \subset X$ there exists $k > 0$ such that $f^{(k)}(U) \cap V \neq \emptyset$. ■

Intuitively topologically transitivity implies the displacement of points under iteration of the map f from one arbitrarily small neighbourhood to any other.

Example A.44 [217] The map $f : S^1 \to S^1$,

$$f(\theta) = \theta + 2\pi\gamma,$$

is topologically transitive if and only if γ is an irrational number. ■

Example A.45 The topological transitivity of the map $f : S^1 \to S^1$,

$$f(\theta) = \alpha\theta,$$

for $\alpha > 1$ follows easily from the fact that small arcs in S^1 are expanded to eventually cover S^1. Notice that f is topologically transitive if and only if $\alpha > 1$, since for $\alpha = 1$ and $0 < \alpha < 1$, the map f is the identity map and a contraction, respectively. The reader is referred to [217] for a detailed discussion of the case $\alpha = 2$.

Since we have established topological conjugacy between the Bernoulli map and the case $\alpha = 2$ earlier, we conclude that the Bernoulli map is also topologically transitive. ■

Definition A.46 The map $f : X \subset \mathbf{R} \to X$ exhibits *sensitive dependence on initial conditions* if there exists an $\epsilon > 0$ such that for any $x \in X$ and any neighbourhood B of x there exists a $y \in B$ and $n \in \mathbf{N}$ such that

$$|f^{(n)}(x) - f^{(n)}(y)| > \epsilon.$$

■

Example A.47 [217] The map $f : S^1 \to S^1$,

$$f(\theta) = \theta + 2\pi\gamma, \quad \gamma \in \mathbf{R}$$

does not exhibit sensitivity to initial conditions. ■

Example A.48 The map on the interval described by

$$x_{n+1} = (\alpha x_n)(\text{mod } 1),$$

exhibits sensitive dependence on initial conditions if and only if $\alpha > 1$. We observe that the special case $\alpha = 2$ produces the Bernoulli map. ■

Definition A.49 The map $f : X \subset \mathbf{R} \to X$ is said to be *chaotic* on $C \subseteq X$ if

i) C is closed under iteration of f,

ii) f exhibits sensitive dependence on initial conditions,

iii) f is topologically transitive on C,

iv) the set of all periodic points of f is dense in C.

■

The condition of sensitive dependence on initial conditions ensures unpredictability in the dynamical system, whereas the condition of topological transitivity ensures that the system is indecomposable (i.e., there does not exist a partition of the domain of the map describing the system such that the map is surjective on the disjoint sets in the partition). The density of periodic orbits ensures an element of regularity in the system's response. For example, the rational numbers in the interval are the (unstable) periodic points of the tent map. It is a well known fact that the set $\mathbf{Q}$ of rational numbers is dense in the set $\mathbf{R}$ of real numbers. The tent map is chaotic as will become evident shortly.

Example A.50 Show that the Bernoulli map is chaotic.

Since the Bernoulli map exhibits sensitive dependence on initial conditions (Example A.45), is topologically transitive on I (Example A.48), and the set of all its periodic points is $\mathbf{Q} \cap I$ which is dense in I, we conclude that the Bernoulli map is chaotic. ■

Example A.51 [217] The logistic map f, (A.1) is chaotic on I for $r = 4$. For all $r > 4$, the logistic map is chaotic on the Cantor set

$$\Lambda := I - \left(\bigcup_{k=0}^{\infty} A_k \right)$$

where

$$A_0 := \{x \in I \mid f(x) > 1\},$$

$$A_n := \left\{x \in I \mid f^{(n)}(x) \in A_0\right\} \quad \text{for } n \in \mathbf{N}.$$

■

Example A.52 Since the tent map, (A.8) is topologically conjugate to the logistic map with $r = 4$, we conclude that the tent map is therefore also chaotic. ■

A somewhat different definition of chaos is given by Li and Yorke [482].

Definition A.53 [482] The map $f : X \subset \mathbf{R} \to X$ is said to be *chaotic* in the *Li-Yorke sense* if

i) for each $k \in \mathbf{N}$ there is a periodic point in X having period k,

ii) there is an uncountable set $Y \subset X$ (containing no periodic points) which satisfies the conditions:

1) For each $x, y \in Y$ with $x \neq y$

$$\liminf_{n\to\infty} |f^{(n)}(x) - f^{(n)}(y)| = 0$$

but

$$\limsup_{n\to\infty} |f^{(n)}(x) - f^{(n)}(y)| > 0.$$

2) For every $y \in Y$ and periodic point $x^* \in X$,

$$\limsup_{n\to\infty} |f^{(n)}(y) - f^{(n)}(x^*)| > 0.$$

■

Thus, a one-dimensional map exhibits chaos in the Li-Yorke sense if the map possesses unstable (ii(b)) periodic orbits—i.e. no points in Y converge to any periodic point—of each period (i) and the forward orbits of any two nonperiodic points occasionally come arbitrarily close (ii(a)) to one another but always diverge thereafter (ii(a)).

Proposition A.54 [482] Let X be an interval of $\mathbf{R}$ and let $f : X \to X$ be a continuous map. Suppose that there is a point $x_1 \in X$ for which the points $x_2 = f(x_1), x_3 = f^{(2)}(x_1)$ and $x_4 = f^{(3)}(x_1)$ satisfy

$$x_4 \leq x_1 < x_2 < x_3\,, \qquad \text{or} \qquad x_4 \geq x_1 > x_2 > x_3\,.$$

Then f is chaotic in the Li-Yorke sense.

Proof: See [482]. ■

Example A.55 The zigzag map is chaotic in the Li-Yorke sense for the parameters $ab \geq 3$ and $a \leq 1/c$. This is proved in Chapter 3 Section 3.3 (refer to Proposition 3.2). ■

Remark If the map $f : X \subset \mathbf{R} \to X$ is chaotic then all the maps $f^{(n)}$, $n \in \mathbf{N}$ are also chaotic.

A.7 Invariant Density

Definition A.56 Consider the map $f : X \subset \mathbf{R} \to X$ which is chaotic on $C \subseteq X$. We define the *invariant (probability) density* of the iterates of f starting from an initial point $x_0 \in C$, by

$$\rho(x) := \lim_{N\to\infty} \frac{1}{N} \sum_{k=0}^{N-1} \delta(x - f^{(k)}(x_0)), \tag{A.41}$$

where δ is the *Dirac delta function*. ■

Proposition A.57 Suppose $f : X \subset \mathbf{R} \to X$ is chaotic on $C \subseteq X$. Then the invariant density ρ of f on C satisfies

$$\rho(y) = \int_C \delta(y - f^{(k)}(x))\rho(x)\,dx, \quad k \in \mathbf{N}_0. \tag{A.42}$$

Proof: The reader is referred to [438]. ■

Since the function $f^{(k)}$, $k = 2, 3, 4, \ldots$ is usually more complex than the function f, we obtain the simplest form of (A.42) by setting $k = 1$.

Definition A.58 Let $f : X \subset \mathbf{R} \to X$. Then the integral equation

$$\rho(y) = \int_C \delta(y - f(x))\rho(x)\, dx \tag{A.43}$$

is termed the *Frobenius-Perron integral equation.* ■

Proposition A.59 Suppose the map $f : X \subset \mathbf{R} \to X$ is chaotic on $C \subseteq X$. If the series

$$\rho_{k+1}(y) = \int_C \delta(y - f(x))\rho_k(x)dx, \quad k = 0, 1, 2, \ldots \tag{A.44}$$

is convergent and if ρ_0 is a normalized (Lebesgue integrable) function, i.e.

$$\int_C \rho_0(x)dx = 1, \tag{A.45}$$

then

$$\rho(x) := \lim_{k\to\infty} \rho_k(x) \tag{A.46}$$

is a normalized solution of the Frobenius-Perron equation and an invariant density for the map f.

Proof: Suppose the series

$$\rho_{k+1}(x) = \int_C \delta(y - f(x))\rho_k(x)\, dx, \quad k = 0, 1, 2, \ldots \tag{A.47}$$

is convergent and ρ_0 is a normalized integrable function. We must now prove that ρ given by (A.46) is a solution of the Frobenius-Perron equation and that ρ is normalized.

From (A.47) it follows that

$$\begin{aligned}
\rho(y) &= \lim_{k\to\infty} \rho_{k+1}(y) \\
&= \lim_{k\to\infty} \int_C \delta(y - f(x))\rho_k(x)\, dx \\
&= \int_C \delta(y - f(x)) \lim_{k\to\infty} \rho_k(x)\, dx \\
&= \int_C \delta(y - f(x))\rho(x)\, dx\,,
\end{aligned}$$

and hence ρ is a solution of the Frobenius-Perron equation.

Now, suppose that

$$\int_C \rho_0(x)\,dx = 1.$$

Then, for $k = 1$, using (A.47) we have

$$\begin{aligned}\int_C \rho_1(y)dy &= \int_C\int_C \delta(y - f(x))\rho_0(x)\,dx\,dy \\ &= \int_C \left(\int_C \delta(y - f(x))\,dy\right)\rho_0(x)\,dx \\ &= \int_C \rho_0(x)\,dx \\ &= 1.\end{aligned}$$

Assuming that for $k = n$ we have

$$\int_C \rho_n(x)dx = 1,$$

it follows that

$$\begin{aligned}\int_C \rho_{n+1}(y)dy &= \int_C\int_C \delta(y - f(x))\rho_n(x)\,dx\,dy \\ &= \int_C \left(\int_C \delta(y - f(x))\,dy\right)\rho_n(x)\,dx \\ &= \int_C \rho_n(x)\,dx \\ &= 1, \quad n = 0, 1, 2, \ldots\end{aligned}$$

and consequently we have finally proved inductively that ρ is normalized. This completes the proof. ■

Remark The following identity is useful in calculations involving the Dirac delta function δ:

$$\int \delta(f(x))g(x)\,dx \equiv \sum_n \frac{g(x_n)}{\left|\frac{df}{dx}(x_n)\right|},$$

where $\{x_n\}$ is the set of all solutions of $f(x) = 0$.

To illustrate the calculation of the invariant density of a map we consider some examples.

Example A.60 Obtain an expression for the invariant density of the tent map.

The tent map (A.8) may be written as

$$f(x) = \begin{cases} f_1(x), & \text{if } x \in [0, 1/2) \\ f_2(x), & \text{if } x \in [1/2, 1] \end{cases}$$

where $f_1(x) := 2x$ and $f_2(x) := 2(1-x)$. Using the Frobenius-Perron equation, we obtain

$$\begin{aligned}
\rho(y) &= \int_I \delta(y - f(x))\rho(x)\,dx \\
&= \int_0^{1/2} \delta(y - f_1(x))\rho(x)\,dx + \int_{1/2}^{1} \delta(y - f_2(x))\rho(x)\,dx \\
&= \int_{f_1(0)}^{f_1(1/2)} \delta(y-u)\rho(f_1^{-1}(u))\frac{df_1^{-1}}{du}(u)\,du + \int_{f_2(1/2)}^{f_2(1)} \delta(y-v)\rho(f_2^{-1}(v))\frac{df_2^{-1}}{dv}(v)\,dv \\
&= \int_0^1 \delta(y-u)\rho(f_1^{-1}(u))\frac{df_1^{-1}}{du}(u)\,du + \int_1^0 \delta(y-v)\rho(f_2^{-1}(v))\frac{df_2^{-1}}{dv}(v)\,dv \\
&= \rho(f_1^{-1}(y))\frac{df_1^{-1}}{dy}(y) - \rho(f_2^{-1}(y))\frac{df_2^{-1}}{dy}(y). \qquad \text{(A.48)}
\end{aligned}$$

Using the definitions for f_1 and f_2 in (A.48), we obtain

$$\rho(x) = \frac{1}{2}\rho\left(\frac{x}{2}\right) + \frac{1}{2}\rho\left(1 - \frac{x}{2}\right). \qquad \text{(A.49)}$$

To solve (A.49) we will make use of (A.44). First, we choose

$$\rho_0(x) = \chi_I(x), \qquad \text{(A.50)}$$

where, in general χ_A denotes the *characteristic function* of the set $A \subset \mathbf{R}^M$ and is defined as

$$\chi_A(x) := \begin{cases} 1, & \text{if } x \in A \\ 0, & \text{otherwise} \end{cases}.$$

It is obvious that (A.50) satisfies (A.45). Substituting (A.50) into (A.49) yields

$$\rho_1(x) = \frac{1}{2}\rho_0\left(\frac{x}{2}\right) + \frac{1}{2}\rho_0\left(1 - \frac{x}{2}\right) = \chi_I(x).$$

Continuing in this manner we observe that

$$\rho_k(x) = \chi_I(x), \quad k = 1, 2, \ldots$$

and hence the invariant density for the tent map is

$$\rho(x) = \chi_I(x).$$

■

Example A.61 The invariant density for the Bernoulli map (A.15) is given by

$$\rho(x) = \chi_I(x).$$

■

Example A.62 For the map $f : I \to I$,

$$f(x) = \begin{cases} \gamma x, & \text{if } 0 \le x \le 1/\gamma \\ \dfrac{\gamma}{\gamma - 1}\left(x - \dfrac{1}{\gamma}\right), & \text{if } 1/\gamma < x \le 1 \end{cases}$$

with $\gamma \in (1, \infty)$ we can easily show that the associated invariant density is

$$\rho(x) = \chi_I(x).$$

■

Example A.63 Derive the invariant density of the logistic map, (A.1) for $r = 4$.

The inverse of the logistic map is given by

$$f^{-1}(x) = \begin{cases} f_1^{-1}(x), & \text{if } 0 \le x < 1/2 \\ f_2^{-1}(x), & \text{if } 1/2 \le x < 1 \end{cases}$$

with

$$f_1^{-1}(x) = \frac{1}{2} - \frac{1}{2}\sqrt{1 - x}, \tag{A.51}$$

$$f_2^{-1}(x) = \frac{1}{2} + \frac{1}{2}\sqrt{1 - x}. \tag{A.52}$$

Substituting (A.51) and (A.52) into (A.48) gives

$$\rho(x) = \frac{1}{4\sqrt{1 - x}}\left[\rho\left(\frac{1 - \sqrt{1 - x}}{2}\right) + \rho\left(\frac{1 + \sqrt{1 - x}}{2}\right)\right] \tag{A.53}$$

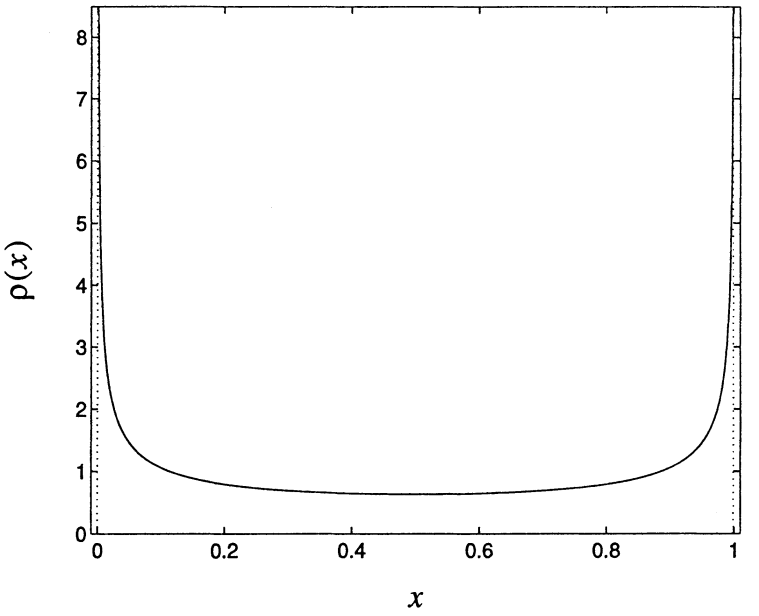

Figure A.11: The invariant density ρ for the logistic map for $r = 4$.

Now, choosing

$$\rho_0(x) = \chi_I(x),$$

and substituting ρ_0 into the right hand side of (A.53) yields

$$\rho_1(x) = \frac{1}{2\sqrt{1-x}}.$$

continuing in this way and then by taking the limit $n \to \infty$, we obtain

$$\rho(x) = \frac{1}{\pi\sqrt{x(1-x)}}. \tag{A.54}$$

The graph of (A.54) is shown in Figure A.11. ■

Example A.64 The circle map $f : [0, 2\pi) \to [0, 2\pi)$ (see [75]) describing the dynamics of a first-order nonuniformly sampling digital phase-locked loop circuit, is given by

$$f(x) = \left(x + \frac{k}{1 - A\sin x}\right) (\text{mod } 2\pi), \tag{A.55}$$

with $A, k \in \mathbf{R}$. The invariant density was calculated by iterating the Frobenius-Perron equation numerically. The invariant density obtained for $A = -0.25$ and $k = 8.5$ after 20 iterations, is shown in Figure A.12. The iteration was performed at 4096 uniformly spaced points in the interval $[0, 2\pi)$ for this particular experiment. ■

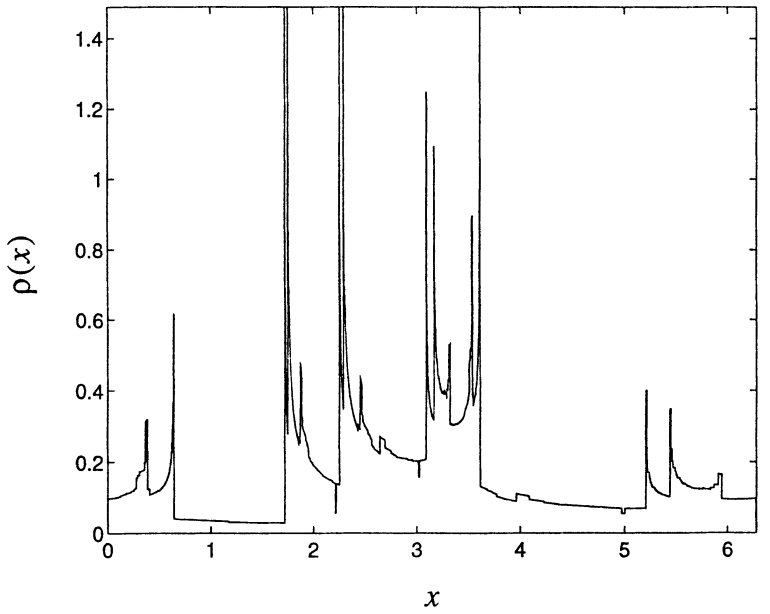

Figure A.12: Invariant density for the circle map (A.55): $A = -0.25$, $k = 8.5$.

Remarks

i) From Example A.64 we see that calculating estimates of the invariant density by means of histogram (i.e. box counting) methods provides unsatisfactory results in the sense that estimates obtained this way are very noisy, converge much slower and are of lower resolution than for estimates obtained by numerical iteration of the Frobenius-Perron operator. Histogram methods depend heavily on finding the post-transient part of the time series.

ii) The method of maximum entropy has also been utilized for estimating invariant densities in general [748]and more specifically for chaotic systems [758]. Moments are calculated from the time series. An entropy function is then maximized subject to these moments as constraints, thereby producing an estimate of the invariant density of the system. The estimate converges as the number of moments used as constraints increases.

Example A.65 Derive an expression for the invariant density of an arbitrary map

$$f : [x_0, x_n] \to [x_0, x_n], \qquad x_0, x_n \in \mathbf{R}, \quad n \in \mathbf{N}$$

which consists of n monotonic segments with the k-th segment defined on the interval $[x_{k-1}, x_k]$ for each $k = 1, 2, \ldots, n$.

From the Frobenius-Perron equation (A.43) we obtain

$$\begin{aligned}
\rho(y) &= \int_{x_0}^{x_n} \delta(y - f(x))\rho(x)\,dx \\
&= \int_{x_0}^{x_1} \delta(y - f_1(x))\rho(x)\,dx + \int_{x_1}^{x_2} \delta(y - f_2(x))\rho(x)\,dx + \\
&\qquad \cdots + \int_{x_{n-1}}^{x_n} \delta(y - f_n(x))\rho(x)\,dx \\
&= \sum_{k=1}^{n} \int_{x_{k-1}}^{x_k} \delta(y - f_k(x))\rho(x)\,dx \\
&= \sum_{k=1}^{n} \int_{f_k(x_{k-1})}^{f_k(x_k)} \delta(y - u)\rho\left(f_k^{-1}(u)\right) \frac{df_k^{-1}}{du}(u)\,du \\
&= \sum_{k=1}^{n} \rho(f_k^{-1}(y)) \left|\frac{df_k^{-1}}{dy}(y)\right| \chi_{[l_k,u_k)}(y)\,,
\end{aligned}$$

where

$$\begin{aligned}
l_k &:= \min\left(f_k(x_{k-1}), f_k(x_k)\right), \\
u_k &:= \max\left(f_k(x_{k-1})), f_k(x_k)\right),
\end{aligned}$$

for each $k = 1, 2, \ldots, n$. ■

Remark Thus far we have only considered the case where the map f is given and we attempt to find ρ. However, we could also consider the inverse problem where ρ is given and we have to find f which satisfies (A.41) (or equivalently (A.42)). In this case there is not necessarily a unique solution (refer to Examples A.60 to A.62), or for that matter, any solution at all. Moreover, it is even possible to generate random noise (i.e. a nonchaotic system) with the same invariant density as a given chaotic map. For example, the random noise generated by $\sin^2\theta$, where θ is noise that is uniformly distributed on the interval $[0, 2\pi]$ has the invariant density $\rho(x) = 1/\left(\pi\sqrt{x(1-x)}\right)$ [68] which is precisely the invariant density associated with the logistic map (see Example A.63).

A.8 Variational Equation and Lyapunov Exponent

Definition A.66 Consider the autonomous one-dimensional, first order dynamical system

$$x_{n+1} = f(x_n), \tag{A.56}$$

where $f : X \subset \mathbf{R} \to X$ is at least piecewise differentiable. We define the associated *variational equation* (or *linearized equation*) by

$$y_{n+1} = \frac{df}{dx}(x_n)y_n = \frac{df}{dx}(f^{(n)}(x_0))y_n. \tag{A.57}$$

■

We notice that variational equation (A.57) of a given map (A.56) is the linearized equation of that map. Therefore it describes the evolution of the tangent of f in the tangent space at x_n [231].

Definition A.67 Consider the map $f : X \subset \mathbf{R} \to X$. We define the *Lyapunov exponent* of the system described by the map f by

$$\lambda(x_0) := \lim_{N\to\infty} \frac{1}{N} \sum_{n=0}^{N-1} \ln \left| \frac{df}{dx}(f^{(n)}(x_0)) \right| \tag{A.58}$$

for a.e. $x_0 \in X$. ■

Using (A.57), we can write (A.58) as

$$\lambda(x_0) = \lim_{N\to\infty} \frac{1}{N} \sum_{n=0}^{N-1} \ln \left| \frac{y_{n+1}}{y_n} \right|. \tag{A.59}$$

From (A.59) it is evident that the Lyapunov exponent measures the average expansion of nearby trajectories. Equation (A.59) can also be written in the form

$$\lambda(x_0) = \lim_{N\to\infty} \frac{1}{N} \ln \left| \frac{y_N}{y_0} \right|.$$

With the definition of the Lyapunov exponent at our disposal we now give an alternative definition of a chaotic map.

Definition A.68 The map $f : X \subset \mathbf{R} \to X$ is said to be *chaotic* on $C \subseteq X$ if it has a nonperiodic orbit contained in C which has a positive Lyapunov exponent [18]. ■

Intuitively a positive Lyapunov exponent shows that the evolution of closely located points on nearby trajectories in the state space diverge in the mean. In other words, nearby trajectories repel one another in the mean.

Example A.69 Determine the Lyapunov exponent of the period-m orbits of the map $f : X \subset \mathbf{R} \to X$.

Suppose that $x_0 \in X$ is of period-m. Setting $N = km$ into (A.58) we have

$$\begin{aligned}
\lambda(x_0) &= \lim_{k\to\infty} \frac{1}{km} \sum_{n=0}^{km-1} \ln \left| \frac{df}{dx}(f^{(n)}(x_0)) \right| \\
&= \lim_{k\to\infty} \frac{1}{km} \left[k \sum_{n=0}^{m-1} \ln \left| \frac{df}{dx}(f^{(n)}(x_0)) \right| \right] \\
&= \frac{1}{m} \sum_{n=0}^{m-1} \ln \left| \frac{df}{dx}(x_n) \right|,
\end{aligned}$$

where we have used the facts $x_0 = f^{(m)}(x_0)$ and $x_n = f^{(n)}(x_0)$. Now, since

$$\begin{aligned}
\min_n \ln \left| \frac{df}{dx}(x_n) \right| &= \ln \left[\min_n \left| \frac{df}{dx}(x_n) \right| \right] \leq \ln \left| \frac{df}{dx}(x_k) \right|, \\
\max_n \ln \left| \frac{df}{dx}(x_n) \right| &= \ln \left[\max_n \left| \frac{df}{dx}(x_n) \right| \right] \geq \ln \left| \frac{df}{dx}(x_k) \right|,
\end{aligned}$$

for each $k = 0, 1, 2, \ldots, m-1$, we have

$$\ln \left[\min_n \left| \frac{df}{dx}(x_n) \right| \right] \leq \lambda(x_0) \leq \ln \left[\max_n \left| \frac{df}{dx}(x_n) \right| \right].$$

If the period-m orbit containing x_0 is attracting then

$$\max_n \left| \frac{df}{dx}(x_n) \right| < 1$$

and hence by the previous inequality we have

$$\lambda(x_0) \leq \ln \left[\max_n \left| \frac{df}{dx}(x_n) \right| \right] < 0.$$

If the period-m orbit containing x_0 is repelling then

$$\min_n \left| \frac{df}{dx}(x_n) \right| > 1$$

and hence

$$\lambda(x_0) \geq \ln \left[\min_n \left| \frac{df}{dx}(x_n) \right| \right] > 0.$$

■

Example A.70 Calculate the Lyapunov exponent of tent map ((A.8))

$$x_{n+1} = \begin{cases} 2x_n, & \text{if } x_n \in [0, 1/2) \\ 2(1 - x_n), & \text{if } x_n \in [1/2, 1] \end{cases}$$

to determine whether it is chaotic.

Since we are only interested in the chaotic orbits, we may therefore exclude all "uninteresting" orbits (i.e. periodic orbits and eventually periodic orbits) from consideration. Let $C' \subset I$ be the set of all points on nonperiodic orbits, i.e.

$$C' = I - \bigcup_{n=0}^{\infty} \mathrm{Per}_n(f).$$

The set C' contains among others all eventually periodic points. The maximal set $C \subset C'$ satisfying

$$C = f(C),$$

contains neither periodic points nor eventually periodic points and is the set that we are interested in. It can be shown that for the tent map f, the set C is precisely the set of irrational numbers. Since $1/2 \notin C$ the tent map is differentiable everywhere in C and hence the variational equation associated with the tent map is

$$y_{n+1} = \begin{cases} 2y_n, & \text{if } x_n \in [0, 1/2) \\ -2y_n, & \text{if } x_n \in (1/2, 1] \end{cases}.$$

Utilizing (A.59) we obtain the Lyapunov exponent as

$$\lambda(x_0) = \ln 2, \quad \text{for each } x_0 \in C.$$

Thus, since $\lambda > 0$ and the set C contains nonperiodicic orbits, we conclude that the tent map is chaotic. ■

A.9 Ergodic Theorem

Ergodic theory serves as the basis for the statistical theory of dynamical systems. The reason for this is that the computation of Lyapunov exponents involves averaging of derivatives along orbits, which leads to the study of ergodic theory. To this end, ergodic theory enables us to calculate statistical properties of the dynamical system such as entropy, characteristic exponents, dimensions and so on. For a detailed exposition of ergodic theory, the reader is referred to the introductory text by Friedman [260], and a more advanced treatment by Walters in [841]. An excellent discussion of the ergodic theory of chaos and strange attractors is given by Eckmann and Ruelle (1985) in [231].

Definition A.71 The map $f : X \subset \mathbf{R} \to X$ is said to be *decomposable* if X can be decomposed into two disjoint sets A and B satisfying

$$f(A) = A, \quad \text{and} \quad f(B) = B.$$

■

Remark It is important to realize the difference between $f^{-1}(A) = A$ and $f(A) = A$. Recall that for $A \subset X$,

$$f(A) := \{y \in X \,|\, y = f(x), \quad \text{for some } x \in A\}.$$

From this definition it follows easily that the former condition is stronger than the latter condition, namely

$$f^{-1}(A) = A \quad \Longleftrightarrow \quad f(A) \subseteq A, \quad A \cap f(X - A) = \emptyset.$$

Definition A.72 The map $f : X \subset \mathbf{R} \to X$ is *ergodic* if f is not decomposable. ■

Thus f is ergodic if $f(A) = A$ implies $m(A) = 0$ or $m(X - A) = 0$ where m denotes *Lebesgue measure* (see [179]). If $m(X) < 0$ then $m(X - A) = 0$ if and only if $m(A) = m(X)$. In this case f is ergodic if and only if $f^{-1}(A) = A$ implies $m(A) = 0$ or $m(X - A) = 0$.

Remarks

i) Any measure which is *absolutely continuous* with respect to Lebesgue measure would suffice in the above definition of ergodicity. For example, the measure $\mu : \mathcal{L}(X) \to \mathbf{R}^+$ defined by

$$\mu(A) := \int_A \rho(x)\, dx, \qquad A \in \mathcal{L}(X),$$

where $\mathcal{L}(X)$ denotes the set of all Lebesgue measurable subsets of X and $\rho : X \to \mathbf{R}^+$ is the invariant density associated with f. Here integration is in the Lebesgue sense.

ii) If some property is said to hold *almost everywhere* (a.e. for short) this means that this property holds everywhere except perhaps in a subset of Lebesgue measure zero.

It is clear that an ergodic system cannot be decomposed into two non-trivial subsystems that do not interact (i.e. are disjoint) with each other. All trajectories which are not in the m-negligible set of periodic orbits therefore approach every point x satisfying $\rho(x) > 0$, arbitrarily close over the course of time.

Example A.73 The map $f: I \to I$ defined by

$$f(x) := (x + a)(\text{mod } 1), \qquad a \in (0,1)$$

is ergodic if a is irrational [260]. ■

Example A.74 Show that the map $f: I \to I$ be given by

$$f(x) = \begin{cases} \gamma x, & \text{if } 0 \le x \le 1/\gamma \\ \dfrac{\gamma}{1-\gamma}\left(x - \dfrac{1}{\gamma}\right), & \text{if } 1/\gamma < x \le 1 \end{cases}$$

where $\gamma \in (1, \infty)$, is ergodic.

Notice that $f^{-1}(A) = A$ for some $A \subset I$ (if and only if $A = [0,1] - P$ or $A = P$, where $P := \bigcup_n \text{Per}_n(f)$). But by Proposition 3.5, Chapter 3, the number of periodic solutions of f is countable. Thus $\mu(A) = 1$ or $\mu(A) = 0$ and hence f is ergodic. ■

Theorem A.75 (Birkhoff Ergodic Theorem) Let $f: X \to X$ be a map that is measure preserving on $C \subseteq X$. For any integrable function $\phi: X \to \mathbf{R}$ the sequence of integrable functions $\{\phi_n : \mathbf{R} \to \mathbf{R}\}$ defined by

$$\phi_n(x) := \frac{1}{n} \sum_{k=0}^{n-1} \phi(f^{(k)}(x)), \qquad n \in \mathbf{N}$$

converges for a.e. $x \in C$ to the integrable function $\tilde{\phi}: \mathbf{R} \to \mathbf{R}$, i.e.

$$\tilde{\phi}(x) = \lim_{n \to \infty} \phi_n(x), \qquad \text{for a.e. } x \in C.$$

If f is ergodic with invariant density $\rho: X \to \mathbf{R}^+$ then

$$\tilde{\phi}(x) = \int_C \phi(y)\rho(y)\, dy,$$

for a.e. $x \in C$.

Proof: The proof of the ergodic theorem is given in [401], [260] and [841]. This theorem was originally proved by Birkhoff [81]. ■

Remark In the ergodic theorem as stated above, supp $\rho = C$.

Now, consider a map $f: X \to X$, which is measure preserving on $C \subseteq X$. Then, by setting

$$\phi(x) = \ln \left| \frac{df}{dx}(x) \right|,$$

we get

$$\frac{1}{n}\sum_{i=0}^{n-1}\phi(f^{(i)}(x)) = \frac{1}{n}\sum_{i=0}^{n-1}\ln\left|\frac{df}{dx}(f^{(i)}(x))\right| = \frac{1}{n}\ln\prod_{i=0}^{n-1}\left|\frac{df}{dx}(f^{(i)}(x))\right| = \frac{1}{n}\ln\left|\frac{df^{(n)}}{dx}(x)\right|. \tag{A.60}$$

From (A.60), the definition of the Lyapunov exponent (A.58) and the ergodic theorem we have

$$\lambda(x_0) = \lim_{n\to\infty}\frac{1}{n}\ln\left|\frac{df^{(n)}}{dx}(x_0)\right| = \int_C \ln\left|\frac{df}{dx}(x)\right|\rho(x)\,dx\,. \tag{A.61}$$

Equation (A.61) states that the Lyapunov exponent of a measure preserving, ergodic map f is equal to the ensemble average of the natural logarithm of the absolute valued slope of f on C.

Example A.76 Apply the ergodic theorem to calculate the Lyapunov exponent of the map $f : I \to I$ defined by

$$f(x) = \begin{cases} \gamma x, & \text{if } 0 \le x \le 1/\gamma \\ \dfrac{\gamma}{1-\gamma}\left(x - \dfrac{1}{\gamma}\right), & \text{if } 1/\gamma < x \le 1 \end{cases}$$

where $\gamma \in (1, \infty)$ is a parameter of the map.

Define $P := \bigcup_n \mathrm{Per}_n(f)$ and $C := I - P$. Since $m(P) = 0$, we get $m(C) = m(I) = 1$. By the ergodic theorem we have

$$\begin{aligned} \lambda &= \int_C \rho(x)\ln\left|\frac{df}{dx}(x)\right| dx \\ &= \int_I \rho(x)\ln\left|\frac{df}{dx}(x)\right| dx \\ &= \int_0^{1/\gamma} \ln\gamma\,dx + \int_{1/\gamma}^{1} \ln\left(\frac{\gamma}{\gamma-1}\right) dx \qquad \text{(see Example (A.62))} \\ &= \ln\gamma - \left(\frac{\gamma-1}{\gamma}\right)\ln(\gamma-1). \end{aligned} \tag{A.62}$$

From the expression for the derivative of λ,

$$\frac{d\lambda}{d\gamma} = -\frac{1}{\gamma^2}\ln(\gamma-1)\,,$$

we see that $d\lambda/d\gamma = 0$ for $\gamma = 2$ only, and hence λ has a single extremum, namely $\lambda = \ln 2$ at $\gamma = 2$. By using the transformation

$$\gamma = \frac{(e^\beta + 1)}{e^\beta}$$

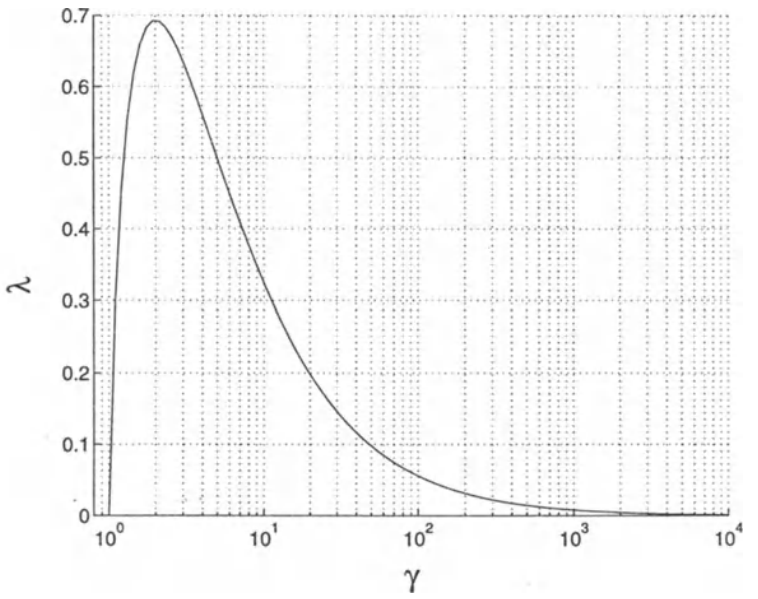

Figure A.13: Graph of λ vs. γ for the map f.

where $\beta \in \mathbf{R}$, it follows easily that $\lambda \downarrow 0$ as $\gamma \downarrow 1$ $(\beta \uparrow \infty)$ and $\gamma \uparrow \infty$ $(\beta \downarrow -\infty)$. Using the above two facts and the continuity of λ with respect to γ, we conclude that this extremum is a global maximum of λ and that $\lambda > 0$ for each $\gamma \in (1, \infty)$. Figure A.13 shows the graph of λ vs. γ.

■

Example A.77 Calculate the Lyapunov exponent for the logistic map with $r = 4$ by using the ergodic theorem.

The Lyapunov exponent for the logistic map with $r = 4$ is given by

$$\lambda(x_0) = \int_0^1 \ln|4 - 8x| \frac{1}{\pi\sqrt{x(1-x)}}\, dx = \ln 2\,,$$

where we have used (A.1) and (A.54) in (A.61). ■

Example A.78 Calculate the Lyapunov exponent of the tent map by using the ergodic theorem.

Differentiating the tent map

$$f(x) = \begin{cases} 2x, & \text{if } x \in [0, 1/2) \\ 2(1-x), & \text{if } x \in [1/2, 1] \end{cases},$$

we obtain

$$\frac{df}{dx}(x) = \begin{cases} 2, & \text{if } x \in [0, 1/2) \\ -2, & \text{if } x \in [1/2, 1] \end{cases}.$$

By application of the ergodic theorem we have

$$\lambda = \ln 2 \int_0^1 dx = \ln 2,$$

and hence the tent map is chaotic. Notice that its Lyapunov exponent is precisely equal to the Lyapunov exponent of the logistic map. That this must be true also follows from the fact that these two maps are topologically conjugate. ■

Example A.79 Calculate the Lyapunov exponent for the zigzag map for $ab = 3$ and $a \leq 1/c$.

For the parameter values $ab = 3$ and $a \leq 1/c$ it can be shown (see Chapter 3) that the domain of attraction of the zigzag map is the interval $\mathcal{A} = [1-c,\ 1+c]$ and that the zigzag map has the invariant density

$$\rho(x) = \frac{2}{3c}\left(\chi_{[1-c,1)}(x) + \frac{1}{2}\chi_{[1,1+c]}(x)\right). \tag{A.63}$$

From (A.25) we obtain

$$\frac{df}{dx}(x) = \begin{cases} 1, & \text{if } x \leq (a-1)/a \\ -2, & \text{if } (a-1)/a < x < 1 \\ 1, & \text{if } 1 \leq x \end{cases}.$$

Hence by the ergodic theorem the Lyapunov exponent is given by

$$\begin{aligned} \lambda &= \int_{\mathcal{A}} \ln\left|\frac{df}{dx}(x)\right| \rho(x)\, dx \\ &= \frac{2}{3c}\ln 2 \int_{1-c}^{1} dx + \frac{1}{3c}\ln 1 \int_{1}^{1+c} dx \\ &= \frac{2}{3}\ln 2. \end{aligned} \tag{A.64}$$

■

A.10 Information Exchange

Another important concept for describing the dynamics of a one-dimensional map is its information flow. As will be seen, the information flow [850] of a one-dimensional map is directly related to the stretching and folding of intervals under iteration of the map. We briefly discuss only the measure-theoretic entropy.

Definition A.80 Consider the map $f : X \subset \mathbf{R} \to X$ with an associated ergodic probability measure p. Let $\mathcal{A} = (A_1, A_2, \ldots, A_m)$ be a finite (p-measurable) partition of the support of p. The *average information content* or *entropy* of the partition $\mathcal{A}$ is defined as

$$H(\mathcal{A}) := -\sum_{i=1}^{m} p(A_i) \ln p(A_i).$$

■

Example A.81 Suppose the outcome of a measurement lies in an interval of the real line and we divide this interval uniformly into m subintervals. Suppose that the probability of the outcome is uniform, giving the probability of the outcome falling in the i-th subinterval as $p_i = 1/m$. Then the average information associated with the measurement is

$$H = -\sum_{i=1}^{m} \frac{1}{m} \ln m = \ln m.$$

Therefore, the finer our measurement resolution the more information we obtain about our system. ■

In general (as for the special case in the above example) we have that the finer the partition $\mathcal{A}$, the greater is the derived information $H(\mathcal{A})$ of the system.

Proposition A.82 The net change in information per iteration of the map $f : X \subset \mathbf{R} \to X$ is given by

$$\Delta H = S - F,$$

where S is the amount of information created by stretching and F is the amount of information lost by folding and these are given by

$$S := \int_X \rho(x) \ln \left| \frac{df}{dx}(x) \right| dx \tag{A.65}$$

and

$$F := \int_X \rho(x) R(x)\, dx \tag{A.66}$$

with

$$R(x) := -\sum_i \frac{\rho(x_i) \Big/ \left|\frac{df}{dx}(x_i)\right|}{\sum_j \rho(x_j) \Big/ \left|\frac{df}{dx}(x_j)\right|} \ln \left[\frac{\rho(x_i) \Big/ \left|\frac{df}{dx}(x_i)\right|}{\sum_k \rho(x_k) \Big/ \left|\frac{df}{dx}(x_k)\right|} \right], \tag{A.67}$$

and ρ is the invariant density associated with f. In (A.67) the summations for i, j and k are over all those points x_i, x_j and x_k respectively for which respectively $f(x_i) = f(x)$, $f(x_j) = f(x)$ and $f(x_k) = f(x)$, with x the argument of R.

Proof: See [850]. ■

Notice that S is precisely the Lyapunov exponent of the map f.

Example A.83 Calculate the average change of information per iteration for the Bernoulli map

$$f(x) = 2x (\text{mod } 1), \quad x \in I .$$

The invariant density for the Bernoulli map is (refer to Example A.61)

$$\rho(x) = \chi_I(x) .$$

The increase in information per iteration due to the stretching is

$$S = \int_I \chi_I(x) \ln 2 \, dx = \ln 2 .$$

In order to calculate the decrease in information per iteration due to the folding we first have to calculate the function R. For each $x \in (0, 1/2) \cup (1/2, 1)$

$$R(x) = \ln 2 .$$

Then, the decrease in information due to folding is

$$F = \int_I \ln 2 \, dx = \ln 2 .$$

Using values for the quantities S and F as calculated above, average change of information per iteration is

$$\Delta H = S - F = 0 .$$

■

Example A.84 Determine the average change in information per iteration for the zigzag map for $ab = 3$ and $a \leq 1/c$. Using (A.63) and (A.79) we find

$$R(x) = \begin{cases} 0, & \text{if } 1-c \leq x < 1-c/2 \\ \ln 2, & \text{if } 1-c/2 \leq x \leq 1+c \end{cases}.$$

Then

$$F = \frac{2}{3c}\int_{1-c}^{1-c/2} 0\,dx + \frac{2}{3c}\ln 2 \int_{1-c/2}^{1} dx + \frac{1}{3c}\ln 2 \int_{1}^{1+c} dx = \frac{2}{3}\ln 2.$$

By (A.64) we have

$$S = (2/3)\ln 2$$

giving the average change of information of

$$\Delta H = S - F = 0.$$

■

Example A.85 The derivative and invariant density of the logistic map for $r = 4$ are given by (A.13) and (A.54), respectively. According to Example A.77 we have

$$S = \lambda = \ln 2.$$

For the logistic map we find that

$$\sum_{i=1}^{2} \frac{\rho(x_i)}{\left|\frac{df}{dx}(x_i)\right|} = 2\frac{\rho(x_1)}{\left|\frac{df}{dx}(x_1)\right|}$$

since both f and ρ are symmetrical about $x = 1/2$ where the symmetry of f implies $x_1 + x_2 = 1/2$. Therefore R is easily shown to be given by

$$R(x) = \ln 2\,\chi_I(x),$$

giving

$$F = \ln 2 \int_I \rho(x)\,dx = \ln 2$$

and hence $\Delta H = S - F = 0$. ■

A.11 Connection with Higher Dimensional Maps

Let $f : X \subset \mathbf{R} \to X$ be a one-dimensional map and suppose that $g : Y \subset \mathbf{R}^N \to Y$ for $N \geq 2$ a fixed integer is a higher dimensional map.

Definition A.86 Let f be a one-dimensional map. Then f is called an *invariant* of the N-dimensional map g if

$$g\left(x, f(x), f^{(2)}(x), \ldots, f^{(N-1)}(x)\right) = f^{(N)}(x),$$

for each $x \in X$. ■

In this section we study the logistic map as an invariant of a class of two-dimensional maps. First we construct a class of two-dimensional maps, the members of which each admits the logistic map as an invariant. We then calculate their Lyapunov exponents. We show that the two-dimensional map can show hyperchaotic behaviour.

The logistic equation

$$x_{n+1} = 2x_n^2 - 1, \quad n = 0, 1, 2, \ldots \qquad x_0 \in [-1, 1], \tag{A.68}$$

is the most studied equation with chaotic behaviour. All quantities of interest in chaotic dynamics can be calculated exactly. Examples are the fixed points and their stability, the periodic orbits and their stability, the moments, the invariant density, topological entropy, the metric entropy, Lyapunov exponent, autocorrelation function. The exact solution of (A.68) takes the form

$$x_n = \cos\left(2^n \arccos(x_0)\right), \tag{A.69}$$

since $\cos(2\alpha) \equiv 2\cos^2(\alpha) - 1$. The Lyapunov exponent for almost all initial conditions is given by $\ln 2$. Let the logistic equation be an invariant of a class of second-order difference equations

$$x_{n+2} = g(x_n, x_{n+1}), \qquad n = 0, 1, 2, \ldots . \tag{A.70}$$

This means that if (A.68) is satisfied for a pair (x_n, x_{n+1}), then (A.70) implies that (x_{n+1}, x_{n+2}) also satisfies (A.68). In other words, let

$$x_{n+1} = f(x_n), \qquad n = 0, 1, 2, \ldots , \tag{A.71}$$

be a first-order difference equation. Then (A.71) is called an invariant of (A.70) if

$$g(x, f(x)) = f(f(x)). \tag{A.72}$$

The second-order difference equation (A.70) can be written as a system of first-order difference equations ($x_{1,n} \equiv x_n$)

$$x_{1,n+1} = x_{2,n}, \qquad x_{2,n+1} = g(x_{1,n}, x_{2,n}). \tag{A.73}$$

If x_0 and x_1 are the initial conditions of (A.70) ($x_0, x_1 \in [-1, 1]$) and assuming that (A.68) is an invariant of (A.70) as well as that x_0 and x_1 satisfy the logistic equation, then a one-dimensional Lyapunov exponent of (A.73) is given by $\ln 2$. Since system (A.73) is two-dimensional, we have a second one-dimensional Lyapunov exponent and a two-dimensional Lyapunov exponent. Let λ_1^1 and λ_2^1 be the two one-dimensional Lyapunov exponents. Let λ^2 be the two-dimensional Lyapunov exponent. Then we have

$$\lambda^2 = \lambda_1^1 + \lambda_2^1 .$$

Let us find the two-dimensional Lyapunov exponent. Consider the system of first-order difference equations

$$x_{1,n+1} = f_1(x_{1,n}, x_{2,n}), \qquad x_{2,n+1} = f_2(x_{1,n}, x_{2,n}). \tag{A.74}$$

The variational equation is given by ($\mathbf{x}_n = (x_{1,n}, x_{2,n})$)

$$y_{1,n+1} = \frac{\partial f_1}{\partial x_1}(\mathbf{x}_n) y_{1,n} + \frac{\partial f_1}{\partial x_2}(\mathbf{x}_n) y_{2,n}, \quad y_{2,n+1} = \frac{\partial f_2}{\partial x_1}(\mathbf{x}_n) y_{1,n} + \frac{\partial f_2}{\partial x_2}(\mathbf{x}_n) y_{2,n} . \tag{A.75}$$

Let $\mathbf{y}_n$ and $\mathbf{v}_n$ be two quantities satisfying the variational equation (A.75). Let $\{\mathbf{e}_1, \mathbf{e}_2\}$ be the standard basis in $\mathbf{R}^2$ and $\wedge$ be the exterior product (Grassmann product [766]). Then we find that

$$\mathbf{y}_n \wedge \mathbf{v}_n = (y_{1,n} v_{2,n} - y_{2,n} v_{1,n}) \mathbf{e}_1 \wedge \mathbf{e}_2 .$$

Now we define

$$w_n := y_{1,n} v_{2,n} - y_{2,n} v_{1,n} .$$

Thus the time evolution of w_n is given by

$$w_{n+1} = \left(\frac{\partial f_1}{\partial x_1}(\mathbf{x}_n) \frac{\partial f_2}{\partial x_2}(\mathbf{x}_n) - \frac{\partial f_1}{\partial x_2}(\mathbf{x}_n) \frac{\partial f_2}{\partial x_1}(\mathbf{x}_n) \right) w_n . \tag{A.76}$$

The two-dimensional Lyapunov exponent is given by

$$\lambda^2 = \lim_{N \to \infty} \frac{1}{N} \ln |w_N| .$$

Obviously, λ_1^1, λ_2^1 and λ^2 depend on the initial conditions of (A.74). If $f_1(x_1, x_2) = x_2$ and $f_2(x_1, x_2) = g(x_1, x_2)$ as in (A.73) we obtain from (A.76) that

$$w_{n+1} = -\frac{\partial g}{\partial x_1}(\mathbf{x}_n) w_n . \tag{A.77}$$

Without loss of generality we can set $w_0 = 1$.

We now derive a class of second-order difference equations with the logistic map as an invariant. We assume an arbitrary member g of this class to be of the form

$$g(x_1, x_2) = a_{1,0} x_1 + a_{0,1} x_2 + a_{2,0} x_1^2 + a_{1,1} x_1 x_2 + a_{0,2} x_2^2 + d .$$

Satisfying the condition (A.72) yields

$$g(x_1, x_2) = x_2 - 2x_1^2 + 2x_2^2 + d(1 + x_2 - 2x_1^2).$$

Since

$$\frac{\partial g}{\partial x_1} = -4x_1(d+1),$$

we find that (A.77) takes the form

$$w_{n+1} = -4x_{1,n}(d+1)w_n\,. \tag{A.78}$$

Let us now calculate the two-dimensional Lyapunov exponent λ^2. The initial values $x_{1,0}$, $x_{2,0}$ of the two-dimensional map $x_{1,n+1} = x_{2,n}$, $x_{2,n+1} = g(x_{1,n}, x_{2,n})$ satisfy the logistic map in the calculations that follow. Using (A.69) in (A.78), we obtain

$$\lambda^2(\theta_0) = \lim_{N\to\infty} \frac{1}{N} \ln\left(\prod_{n=1}^{N} 4|d+1|\,|\cos(2^n\theta_0)|\right), \quad d \neq -1, \quad \theta_0 := \arccos(x_0),$$

or

$$\lambda^2(\theta_0) = 2\ln 2 + \ln|d+1| + \gamma(\theta_0),$$

where

$$\gamma(\theta_0) := \lim_{N\to\infty} \frac{1}{N} \sum_{n=1}^{N} \ln|\cos(2^n\theta_0)|.$$

Now, since

$$\cos(2^n\theta_0) \equiv \cos(2^n\theta_0 \pmod{2\pi}),$$

we only need to study the Bernoulli shift map

$$\theta_{n+1} = 2\theta_n \pmod{2\pi}. \tag{A.79}$$

This map has the solution

$$\theta_n = 2^n\theta_0 \pmod{2\pi}.$$

The map (A.79) is ergodic with the invariant density

$$\rho(\theta) = \frac{1}{2\pi}\chi_{[0,2\pi)}(\theta)\,,$$

where χ is the characteristic function. Thus we may apply Birkhoff's ergodic theorem. This then gives

$$\gamma(\theta_0) = \int_0^{2\pi} \rho(\theta)\ln|\cos\theta|d\theta = \frac{1}{2\pi}\int_0^{2\pi} \ln|\cos\theta|d\theta = \frac{2}{\pi}\int_0^{\pi/2} \ln(\cos\theta)d\theta\,.$$

It follows that

$$\gamma(\theta_0) = -\ln 2, \quad \text{for} \quad \text{a.e.} \quad \theta_0 \in [0, 2\pi).$$

Thus

$$\lambda^2 = \ln 2 + \ln|d+1|, \quad d \neq -1 .$$

Now, since one of the one-dimensional Lyapunov exponent is $\ln 2$, and

$$\lambda^2 = \lambda_1^1 + \lambda_2^1, \qquad \lambda_1^1 \geq \lambda_2^1 ,$$

we find the two one-dimensional Lyapunov exponent as

$$\lambda_1^1 = \max\{\ln 2,\ \ln|d+1|\}, \qquad \lambda_2^1 = \min\{\ln 2,\ \ln|d+1|\}.$$

Obviously λ^2 can be made arbitrarily large positively or negatively by appropriate choice of d. This implies that the spectrum of the one-dimensional Lyapunov exponents may be $(+,-)$, $(+,0)$ or $(+,+)$. Thus, for the case $(+,+)$, hyperchaos would result if g is ergodic.

Now, recall the observation made above, namely that the solution (A.69) of the logistic map (A.68) is related to the Bernoulli shift map via the nonlinear transformation $x = \cos\theta$, and let $\{x_n(x_0)\}$ denote the orbit originating from x_0 for the logistic map. Then

$$\{x_n(x_0)\} \text{ is chaotic} \quad \Longleftrightarrow \quad \arccos(x_0) \in \mathbf{R}\backslash\mathbf{Q} .$$

This follows from the fact that the orbit of the Bernoulli shift map is chaotic if and only if $\theta_0 \in \mathbf{R}\backslash\mathbf{Q}$.

Appendix B

Important Definitions and Theorems

This appendix contains a list of definitions and theorems which are important in chaos, either directly or indirectly. Here we state theorems without giving proofs. However, with each theorem we give bibliographical references which either contain the proofs or give references where proofs may be found.

Definition B.1 (Sarkovskii's ordering)[217],[279] *Sarkovskii's ordering* of the natural numbers is given by

$$3 \rhd 5 \rhd 7 \rhd 9 \rhd \cdots$$

$$\cdots \rhd 2 \times 3 \rhd 2 \times 5 \rhd 2 \times 7 \rhd 2 \times 9 \rhd \cdots$$

$$\cdots \rhd 2^2 \times 3 \rhd 2^2 \times 5 \rhd 2^2 \times 7 \rhd 2^2 \times 9 \rhd \cdots$$

$$\cdots \rhd 2^3 \times 3 \rhd 2^3 \times 5 \rhd 2^3 \times 7 \rhd 2^3 \times 9 \rhd \cdots$$

$$\vdots$$

$$\cdots \rhd 2^3 \rhd 2^2 \rhd 2 \rhd 1 .$$

■

Theorem B.2 (Sarkovskii's Theorem) [217],[279] Suppose that $f : \mathbf{R} \to \mathbf{R}$ is continuous and f has a periodic point of prime period k. Then f has a period-l point for each l satisfying $k \rhd l$. ■

Definition B.3 (Li-Yorke Chaos in $\mathbf{R}^N$) [512] The map $\mathbf{f} : X \subset \mathbf{R}^N \to X$, $N > 1$ is said to be *chaotic* if there exists

i) a positive M such that for each integer $p \geq M$, $\mathbf{f}$ has a point of period p;

ii) a scrambled set of $\mathbf{f}$, (i.e. an uncountable set S containing no periodic points of $\mathbf{f}$) such that

1) $\mathbf{f}(S) \subset S$,

2) for every $\mathbf{x}, \mathbf{y} \in S$ with $\mathbf{x} \neq \mathbf{y}$

$$\limsup_{k\to\infty} \left\| \mathbf{f}^{(k)}(\mathbf{x}) - \mathbf{f}^{(k)}(\mathbf{y}) \right\| > 0\,,$$

3) for every $\mathbf{x} \in S$ and any periodic point $\mathbf{x}^*$ of $\mathbf{f}$

$$\limsup_{k\to\infty} \left\| \mathbf{f}^{(k)}(\mathbf{x}) - \mathbf{f}^{(k)}(\mathbf{x}^*) \right\| > 0\,;$$

iii) an uncountable subset $S_0 \subset S$ such that for every $\mathbf{x}, \mathbf{y} \in S_0$

$$\liminf_{k\to\infty} \left\| \mathbf{f}^{(k)}(\mathbf{x}) - \mathbf{f}^{(k)}(\mathbf{y}) \right\| = 0\,.$$

Theorem B.4 (Hartman's Theorem for Maps) [34], [279], [217] Let $\mathbf{x}^*$ be a hyperbolic fixed point of the diffeomorphism $\mathbf{f} : X \subset \mathbf{R}^N \to X$. Then there is a neighbourhood $B \subset X$ of $\mathbf{x}^*$ and a neighbourhood $B' \subset T_{\mathbf{x}^*}\mathbf{R}^N$ of $\mathbf{0}$ such that the restriction $\mathbf{f}|B$ is topologically conjugate to the restriction $T_{\mathbf{x}^*}\mathbf{f}|B'$ of the tangent map $T_{\mathbf{x}^*}\mathbf{f}$ ■

Theorem B.5 (Hartman's Theorem for Flows) [34], [279], [217] Let $\mathbf{x}^*$ be a hyperbolic fixed point of the system

$$\frac{d\mathbf{x}}{dt} = \mathbf{f}(\mathbf{x}), \qquad \mathbf{f} : X \subset \mathbf{R}^N \to \mathbf{R}^N\,,$$

with flow $\Phi : \mathbf{R}^+ \times \mathbf{R}^N \to \mathbf{R}^N$. Then there is a neighbourhood $B \subset X$ of $\mathbf{x}^*$ and a neighbourhood $B' \subset T_{\mathbf{x}^*}\mathbf{R}^N$ of $\mathbf{0}$ such that the restriction $\Phi|B$ is topologically conjugate to the restriction $T_{\mathbf{x}^*}\Phi|B'$ of the linearized flow $T_{\mathbf{x}^*}\Phi$. ■

Theorem B.6 (Whitney's Embedding Theorem) [42], [847] If $\mathcal{M}$ is a differentiable manifold, of dimension N, then there is a diffeomorphism $\mathbf{h} : \mathcal{M} \to \mathbf{R}^{2N+1}$ such that $\mathbf{h}(\mathcal{M})$ is closed in $\mathbf{R}^{2N+1}$. ■

Theorem B.7 (Stable and Unstable Manifold Theorem for Maps) [34], [134] Let $\mathbf{f} : X \subset \mathbf{R}^N \to X$ be a diffeomorphism with a hyperbolic fixed point $\mathbf{x}^* \in X$. Then on a sufficiently small neighbourhood $B \subset X$ of $\mathbf{x}^*$ there exist *local stable* and *local unstable manifolds*

$$W^s_{loc}(\mathbf{x}^*) := \left\{ \mathbf{x} \in B \,\middle|\, \mathbf{f}^{(n)}(\mathbf{x}) \xrightarrow[\infty]{n} \mathbf{x}^* \right\}, \qquad W^u_{loc}(\mathbf{x}^*) := \left\{ \mathbf{x} \in B \,\middle|\, \mathbf{f}^{(n)}(\mathbf{x}) \xleftarrow[\infty]{n} \mathbf{x}^* \right\},$$

of the same dimensions as the respective *stable* and *unstable eigenspaces* E^s and E^u and which are tangent to them at $\mathbf{x}^*$. Moreover, we define the *global stable* and *global unstable manifolds* at $\mathbf{x}^*$ as

$$W^s(\mathbf{x}^*) := \bigcup_{n \in \mathbf{N}} \mathbf{f}^{(-n)}\left(W^s_{loc}(\mathbf{x}^*)\right), \qquad W^u(\mathbf{x}^*) := \bigcup_{n \in \mathbf{N}} \mathbf{f}^{(n)}\left(W^u_{loc}(\mathbf{x}^*)\right),$$

respectively. ■

Theorem B.8 (Stable and Unstable Manifold Theorem for Flows) [34], [134] Consider the following N-dimensional system

$$\frac{d\mathbf{x}}{dt} = \mathbf{f}(\mathbf{x}), \qquad \mathbf{f} : X \subset \mathbf{R}^N \to \mathbf{R}^N,$$

with flow $\Phi : \mathbf{R}^+ \times \mathbf{R}^N \to \mathbf{R}^N$ and suppose that $\mathbf{x}^*$ is a hyperbolic fixed point of this system. Then on a sufficiently small neighbourhood $B \subset \mathbf{R}^N$ of $\mathbf{x}^*$ there exist *local stable* and *local unstable manifolds*

$$W^s_{loc}(\mathbf{x}^*) := \left\{ \mathbf{x} \in B \,\middle|\, \Phi(t;\mathbf{x}) \xrightarrow[\infty]{t} \mathbf{x}^* \right\}, \qquad W^u_{loc}(\mathbf{x}^*) := \left\{ \mathbf{x} \in B \,\middle|\, \Phi(t;\mathbf{x}) \xleftarrow[\infty]{t} \mathbf{x}^* \right\},$$

of the same dimensions as the respective *stable* and *unstable eigenspaces* E^s and E^u and are tangent to them at $\mathbf{x}^*$. Moreover, we define the *global stable* and *global unstable manifolds* at $\mathbf{x}^*$ as

$$W^s(\mathbf{x}^*) := \bigcup_{t \in \mathbf{R}} \Phi\left(t; W^s_{loc}(\mathbf{x}^*)\right), \qquad W^u(\mathbf{x}^*) := \bigcup_{t \in \mathbf{R}} \Phi\left(t; W^u_{loc}(\mathbf{x}^*)\right),$$

respectively. ■

Remarks

i) It is easy to see that if $W^s(\mathbf{x}^*)$ and $W^u(\mathbf{x}^*)$ intersect at one point, they must do so at infinitely many points.

ii) When the fixed point $\mathbf{x}^*$ is nonhyperbolic, the concept of a *centre manifold* must be introduced additionally [112], [392].

iv) The definition of invariant manifolds of a fixed point can easily be generalized to obtain a definition for the invariant manifolds of a periodic solution [134].

Definition B.9 If $W^s(\mathbf{x}^*)$ and $W^u(\mathbf{x}^*)$ intersect transversally at a point then they do so infinitely many times, giving a *homoclinic tangle.* Any such point is called a *transverse homoclinic point.* If the intersection at a point is tangential then it is so at infinitely many points and we say that *homoclinic tangencies* exist. ■

Definition B.10 (Kupka-Smale Diffeomorphism) [34], [134] Let $\mathcal{M}$ be a compact 2-manifold and let $\mathrm{Diff}^1(\mathcal{M})$ denote the set of all C^1 diffeomorphisms on $\mathcal{M}$. The elements of a residual subset of $\mathrm{Diff}^1(\mathcal{M})$ have the property that all their fixed and periodic points are hyperbolic and all intersections of stable and unstable manifolds are transverse. This subset is referred to as *Kupka-Smale diffeomorphisms.* ■

Theorem B.11 (Smale-Birkhoff Theorem) [34], [134] Let $\mathbf{f} \in \mathrm{Diff}^1(\mathcal{M})$ be Kupka-Smale and $\mathbf{x}^\times \neq \mathbf{x}^*$ be a transverse homoclinic point of a periodic point $\mathbf{x}^*$ of $\mathbf{f}$. Then there is a closed subset Λ of the hyperbolic nonwandering set $\Omega(\mathbf{f})$ [34], containing $\mathbf{x}^\times$ such that

i) Λ is a Cantor set;

ii) $\mathbf{f}^{(n)}(\Lambda) = \Lambda$ for some $n \in \mathbf{N}$;

iii) $\mathbf{f}|\Lambda$ is topologically conjugate to a shift on two symbols.

■

Theorem B.12 (Poincaré-Bendixson Theorem) [410], [307], [279] Suppose that $\mathcal{R}$ be a closed and bounded region in $\mathbf{R}^2$, consisting of nonsingular points of the second-order system

$$\frac{d\mathbf{x}}{dt} = \mathbf{f}(\mathbf{x}),$$

such that the trajectory $\mathbf{x}(t)$, $(t \geq 0)$ originating from $\mathbf{x}(0) = \mathbf{x}_0 \in \mathcal{R}$ lies entirely within $\mathcal{R}$. Then either $\mathbf{x}(t)$ is a periodic trajectory, or approaches a periodic trajectory, or terminates at a fixed point. ■

Theorem B.13 (Routh-Hurwitz Criterion) Consider the following N-dimensional system

$$\frac{d\mathbf{x}}{dt} = \mathbf{f}(\mathbf{x}), \qquad \mathbf{f} : \mathbf{R}^N \to \mathbf{R}^N,$$

with flow $\Phi : \mathbf{R}^+ \times \mathbf{R}^N \to \mathbf{R}^N$ and suppose that $\mathbf{x}^*$ is a fixed point of this system. Let

$$P(\lambda) := a_0\lambda^N + a_1\lambda^{N-1} + a_2\lambda^{N-2} + \ldots + a_{N-1}\lambda + a_N, \quad a_n \in \mathbf{R} \text{ for each } n = 0, \ldots, N, \tag{B.1}$$

be the *characteristic equation* of the corresponding Jacobian matrix of $\mathbf{f}$ evaluated at $\mathbf{x}^*$. Necessary but not sufficient conditions for the roots of (B.1) to have nonpositive real parts are

i) All coefficients $\{a_n\}_{n=0}^N$ of the polynomial $P(\lambda)$ have the same sign;

ii) None of the coefficients vanishes.

Necessary and sufficient conditions that all roots of (B.1) lie in the left half of the complex plane is that all Hurwitz determinants $\{D_n\}_{n=1}^N$ must be positive, where

$$D_1 := a_1\,, \quad D_2 := \det \begin{pmatrix} a_1 & a_3 \\ a_0 & a_2 \end{pmatrix}\,, \quad D_3 := \det \begin{pmatrix} a_1 & a_3 & a_5 \\ a_0 & a_2 & a_4 \\ 0 & a_1 & a_3 \end{pmatrix}\,, \quad \ldots$$

$$D_N := \det \begin{pmatrix} a_1 & a_3 & a_5 & \ldots & a_{2N-1} \\ a_0 & a_2 & a_4 & \ldots & a_{2N-2} \\ 0 & a_1 & a_3 & \ldots & a_{2N-3} \\ 0 & a_0 & a_2 & \ldots & a_{2N-4} \\ \vdots & \vdots & \vdots & \ddots & \vdots \\ 0 & 0 & 0 & \ldots & a_N \end{pmatrix}\,,$$

and $a_n := 0$ for each $n > N$. ■

Remarks

i) The amount of computation required for the evaluation of the Hurwitz determinants is drastically reduced by transforming the problem to obtain *Routh's tabulation* and using *Routh's procedure* to perform the evaluations [455].

ii) For discrete-time systems perhaps the easiest method to find unstable eigenvalues of the Jacobian matrix is to first transform the characteristic polynomial $P(\lambda)$ by means of the *bilinear transformation* and then to apply the above procedure directly [455].

Appendix C

Mathematical Methods

C.1 Least-Squares Linearized Flow Estimation

Consider the optimization problem presented in Chapter 2 namely

$$\min_{\mathbf{A}} J(\mathbf{A}), \tag{C.1}$$

where the cost function J was defined by

$$\begin{aligned} J(\mathbf{A}) &:= \frac{1}{M}\sum_{i=1}^{M} \|\mathbf{z}_i - \mathbf{A}\mathbf{y}_i\|_2^2 \\ &= \frac{1}{M}\sum_{i=1}^{M} (\mathbf{z}_i - \mathbf{A}\mathbf{y}_i)^T(\mathbf{z}_i - \mathbf{A}\mathbf{y}_i) \\ &= \frac{1}{M}\sum_{i=1}^{M} (\mathbf{z}_i^T\mathbf{z}_i - \mathbf{z}_i^T\mathbf{A}\mathbf{y}_i - \mathbf{y}_i^T\mathbf{A}^T\mathbf{z}_i + \mathbf{y}_i^T\mathbf{A}^T\mathbf{A}\mathbf{y}_i). \end{aligned} \tag{C.2}$$

Here $\mathbf{y}_i, \mathbf{z}_i \in \mathbf{R}^N$ for each $i = 1, 2, \ldots, M$ for M some positive integer and $\mathbf{A} \in \mathbf{R}^{N\times N}$. Before continuing, we introduce the *tensor representation* of vectors and matrices, namely

$$\mathbf{x} = \sum_{i=1}^{N} x_i \mathbf{e}_i, \qquad \mathbf{x} := (x_1, \ldots, x_N)^T \in \mathbf{R}^N, \tag{C.3}$$

$$\mathbf{A} = \sum_{i,j=1}^{N} a_{i,j}\mathbf{e}_i \otimes \mathbf{e}_j, \quad \mathbf{A} := (a_{i,j}) \in \mathbf{R}^{N\times N}, \tag{C.4}$$

where $\{\mathbf{e}_i\}_{i=1}^N$ is the standard basis in $\mathbf{R}^N$ and $\otimes$ denotes the *Kronecker product* (see [83]). To solve (C.2) we must differentiate J with respect to the matrix $\mathbf{A}$. To this

end we now introduce the differentiation of an arbitrary function of $\mathbf{A} \in \mathbf{R}^{N\times N}$, with respect to $\mathbf{A}$ as

$$\frac{\partial f}{\partial \mathbf{A}}(\mathbf{A}) := \nabla_{\mathbf{A}} \otimes f(\mathbf{A}), \tag{C.5}$$

where

$$\nabla_{\mathbf{A}} := \sum_{i,j=1}^{N} \mathbf{e}_i \otimes \mathbf{e}_j \frac{\partial}{\partial a_{i,j}}. \tag{C.6}$$

Using (C.5) and (C.6) we now calculate the derivative of each of $\mathbf{y}^T\mathbf{Az}$ and $\mathbf{y}^T\mathbf{Az}$ with respect to $\mathbf{A}$. Now,

$$\begin{aligned}
\frac{\partial}{\partial \mathbf{A}}\left(\mathbf{y}^T\mathbf{Az}\right) &= \nabla_{\mathbf{A}} \otimes \left(\mathbf{y}^T\mathbf{Az}\right) \\
&= \left(\sum_{i,j=1}^{N} \mathbf{e}_i \otimes \mathbf{e}_j \frac{\partial}{\partial a_{i,j}}\right) \otimes \left(\sum_{k,l=1}^{N} y_k a_{k,l} z_l\right) \\
&= \sum_{i,j,k,l=1}^{N} y_k z_l \frac{\partial a_{k,l}}{\partial a_{i,j}} \mathbf{e}_i \otimes \mathbf{e}_j \\
&= \sum_{i,j,k,l=1}^{N} y_k z_l \delta_{i,k}\delta_{j,l} \mathbf{e}_i \otimes \mathbf{e}_j \\
&= \sum_{i,j=1}^{N} x_i y_j \mathbf{e}_i \otimes \mathbf{e}_j \\
&= \sum_{i,j=1}^{N} (x_i \mathbf{e}_i) \otimes (y_j \mathbf{e}_j) \\
&= \mathbf{yz}^T.
\end{aligned} \tag{C.7}$$

By the same process

$$\frac{\partial}{\partial \mathbf{A}}(\mathbf{y}^T\mathbf{A}^T\mathbf{z}) = \mathbf{zy}^T. \tag{C.8}$$

Using (C.7) and (C.8) we may calculate the derivative of $\mathbf{y}^T\mathbf{A}^T\mathbf{Az}$ with respect to $\mathbf{A}$ as follows:

$$\begin{aligned}
\frac{\partial}{\partial \mathbf{A}}(\mathbf{y}^T\mathbf{A}^T\mathbf{Az}) &= \frac{\partial}{\partial \mathbf{A}}(\mathbf{u}^T\mathbf{Az}) + \frac{\partial}{\partial \mathbf{A}}(\mathbf{y}^T\mathbf{A}^T\mathbf{v}) \\
&= \mathbf{uz}^T + \mathbf{vy}^T \\
&= \mathbf{Ayz}^T + \mathbf{Azy}^T \\
&= \mathbf{A}(\mathbf{yz}^T + \mathbf{zy}^T),
\end{aligned} \tag{C.9}$$

where $\mathbf{u} := \mathbf{Ay}$ and $\mathbf{v} = \mathbf{Az}$.

Now we return to the problem of minimizing $J(\mathbf{A})$ with respect to $\mathbf{A}$. Obviously J is quadratic in the elements $\{a_{i,j}\}$ of $\mathbf{A}$. To find the $\mathbf{A} = \hat{\mathbf{A}}$ which minimizes J we must differentiate J with respect to $\mathbf{A}$, equate the derivative to the zero vector and then solve of $\mathbf{A} = \hat{\mathbf{A}}$:

$$\begin{aligned} \frac{\partial J}{\partial \mathbf{A}}(\hat{\mathbf{A}}) &= \frac{2}{M}\sum_{i=1}^{M}(-\mathbf{z}_i\mathbf{y}_i^T + \hat{\mathbf{A}}\mathbf{y}_i\mathbf{y}_i^T) = 0 \\ \Longrightarrow \quad \hat{\mathbf{A}}\left(\sum_{i=1}^{M}\mathbf{y}_i\mathbf{y}_i^T\right) &= \sum_{i=1}^{M}\mathbf{z}_i\mathbf{y}_i^T. \end{aligned} \tag{C.10}$$

If $M \geq N$ and there is no degeneracy then the inverse of the $N \times N$ matrix $\sum_{i=1}^{M}\mathbf{y}_i\mathbf{y}_i^T$ exists yielding

$$\hat{\mathbf{A}} = \left(\sum_{i=1}^{M}\mathbf{z}_i\mathbf{y}_i^T\right)\left(\sum_{i=1}^{M}\mathbf{y}_i\mathbf{y}_i^T\right)^{-1}. \tag{C.11}$$

Thus, $\hat{\mathbf{A}}$ is the least-squares solution to the problem $\mathbf{z}_i \approx \mathbf{A}\mathbf{y}_i$ for $i = 1, 2, \ldots, N$.

C.2 Line Intersection Algorithm

In this section we derive a simple algorithm for detecting the intersection of two line segments in a plane. Let the two line segments be l_1 and l_2. Suppose the endpoints of l_1 are the position vectors $\mathbf{x}_1$, and $\mathbf{x}_2$ and the endpoints of l_2 are the position vectors $\mathbf{y}_1$ and $\mathbf{y}_2$. Denote the point of intersection (if it exists) by $\mathbf{z}$. By assumption

$$\mathbf{x}_1\,,\ \mathbf{x}_2\,,\ \mathbf{y}_1\,,\ \mathbf{y}_2\,,\ \mathbf{z} \in \mathbf{R}^2\,.$$

Assuming l_1 and l_2 to be straightline segments ensures that $\mathbf{z}$ does exist although it need not lie on the line segments l_1 and l_2. In addition it enables us to write $\mathbf{z}$ as

$$\mathbf{z} = s(\mathbf{x}_2 - \mathbf{x}_1) + \mathbf{x}_1\,, \qquad s \in \mathbf{R}\,, \tag{C.12}$$

and

$$\mathbf{z} = t(\mathbf{y}_2 - \mathbf{y}_1) + \mathbf{y}_1\,, \qquad t \in \mathbf{R}\,, \tag{C.13}$$

that is, the point of intersection is a specific solution of each of two parametric equations with parameters s and t respectively. These two expressions may be manipulated into

$$(\mathbf{z} - \mathbf{x}_1) = s(\mathbf{x}_2 - \mathbf{x}_1)\,, \tag{C.14}$$

and

$$(\mathbf{z} - \mathbf{y}_2) = t(\mathbf{y}_2 - \mathbf{y}_1)\,. \tag{C.15}$$

Using (C.14), we have

$$(\mathbf{z} - \mathbf{x}_1) \times (\mathbf{y}_2 - \mathbf{y}_1) = s(\mathbf{x}_2 - \mathbf{x}_1) \times (\mathbf{y}_2 - \mathbf{y}_1)\,, \tag{C.16}$$

where the product $\times$ denotes the vector cross product. Substituting (C.13) for $\mathbf{z}$ in (C.16) and recalling that

$$(\mathbf{y}_2 - \mathbf{y}_1) \times (\mathbf{y}_2 - \mathbf{y}_1) = (0,0)^T,$$

we obtain

$$(\mathbf{y}_1 - \mathbf{x}_1) \times (\mathbf{y}_2 - \mathbf{y}_1) = s(\mathbf{x}_2 - \mathbf{x}_1) \times (\mathbf{y}_2 - \mathbf{y}_1). \tag{C.17}$$

By defining

$$\phi(\mathbf{a}, \mathbf{b}, \mathbf{c}, \mathbf{d}) := (\mathbf{a} - \mathbf{b}) \times (\mathbf{c} - \mathbf{d}), \qquad \mathbf{a},\ \mathbf{b},\ \mathbf{c},\ \mathbf{d} \in \mathbf{R}^2,$$

and letting $\mathbf{e}$ be the unit normal vector to the plane under consideration, (C.17) becomes

$$\phi(\mathbf{y}_1, \mathbf{x}_1, \mathbf{y}_2, \mathbf{y}_1)\mathbf{e} = s\phi(\mathbf{x}_2, \mathbf{x}_1, \mathbf{y}_2, \mathbf{y}_1)\mathbf{e},$$

giving

$$s = \frac{\phi(\mathbf{y}_1, \mathbf{x}_1, \mathbf{y}_2, \mathbf{y}_1)}{\phi(\mathbf{x}_2, \mathbf{x}_1, \mathbf{y}_2, \mathbf{y}_1)}.$$

From the symmetry of the problem we have

$$t = \frac{\phi(\mathbf{x}_1, \mathbf{y}_1, \mathbf{x}_2, \mathbf{x}_1)}{\phi(\mathbf{y}_2, \mathbf{y}_1, \mathbf{x}_2, \mathbf{x}_1)}.$$

Because of the anti-symmetric properties of ϕ, various permutations of the arguments of ϕ give the same result.

Now, for the line segments l_1 and l_2 to intersect it is clear that the conditions

$$0 \leq s \leq 1, \quad \text{and} \quad 0 \leq t \leq 1,$$

must be satisfied. For other values of s and t the intersection is beyond the endpoints of one or both of l_1 and l_2. Given samples of smooth stable and unstable manifolds for example, the above expressions for s and t, together with the above conditions on s and t may be used to find approximately the points of intersection.

Appendix D

MATLAB Program Listings

D.1 Lyapunov Exponents for Maps

```
% LYAP_MAP.M   Solves a system of first order maps, its variational
%              equations and simultaneously calculates the spectrum
%              of 1-D Lyapunov exponents.

close all, clear all

MAP_file = input('MAP Filename (HENONMAP) ','s');
if isempty(MAP_file)
  MAP_file = 'HENONMAP';
end

t_init = input('Initial Time [Sample No.] (0) ');
if isempty(t_init)
  t_init = 0;
end

t_span = input('Time Evolution Interval [No. of Samples] (5) ');
if isempty(t_span)
  t_span = 5;
end

t_final = t_init + t_span;

y_init = input('Initial State (Column) Vector ');
if isempty(y_init)
  y_init = [.2 .1]'
```

```
end

N = input('Total Order of System (4) ');
if isempty(N)
  N = 4;
end
Nd2 = N/2;

N_trials = input('Number of Consequtive Time Intervals (1000) ');
if isempty(N_trials)
  N_trials = 1000;
end

u_init = eye(Nd2);
u_final = zeros(u_init);
x_init = zeros(N,Nd2);
L = zeros(Nd2,1);

for i=1:Nd2
  x_init(:,i) = [y_init; u_init(:,i)];
end

fprintf('\n');

for j=1:N_trials

  fprintf('Trial: %g\n',j);

  for i=1:Nd2
    x = feval(MAP_file,t_init,t_final,x_init(:,i));
    u_final(:,i) = x(Nd2+1:N);
  end

  t_init  = t_final;
  t_final = t_final + t_span;

  y_init = x(1:Nd2);

  fprintf('\n');

  u_init = gra_schm(u_final);

  for i=1:Nd2
    L(i) = L(i) + log(u_final(:,i).'*u_init(:,i));
```

```
    fprintf(' L(%g) = %g, ',i,L(i)/j/t_span)
  end

  for i=1:Nd2
    x_init(:,i) = [y_init; u_init(:,i)];
  end

end

for i=1:Nd2
  L(i) = L(i)/N_trials/t_span;
end
```

D.2 Lyapunov Exponents for Flows

```
% LYAP_DE1.M   Solves a system of first order ODEs, its variational
%              equations and simultaneously calculates the spectrum
%              of 1-D Lyapunov exponents.

close all, clear all

ID = 'AV'; % Signature for Non-uniformly sampled data,
           % and Variational State evolution included.

ODE_file = input('ODE Filename (LORENZV) ','s');
if isempty(ODE_file)
  ODE_file = 'LORENZV';
end

t_init = input('Initial Time [sec.] (0) ');
if isempty(t_init)
  t_init = 0;
end

t_span = input('Time Evolution Interval [sec.] (0.05) ');
if isempty(t_span)
  t_span = 0.05;
end

t_final = t_init + t_span;
```

```
tol = input('Integration Error Tolerance (1e-6) ');
if isempty(tol)
  tol = 1e-6;
end

y_init = input('Initial State (Column) Vector ');
if isempty(y_init)
  y_init = [5.4566  -2.1775  42.7071]'
end

N = input('Total Order of System (6) ');
if isempty(N)
  N = 6;
end
Nd2 = N/2;

N_trials = input('Number of Consequtive Time Intervals (1000) ');
if isempty(N_trials)
  N_trials = 1000;
end

u_init = eye(Nd2);
u_final = zeros(u_init);
x_init = zeros(N,Nd2);
L = zeros(Nd2,1);

for i=1:Nd2
  x_init(:,i) = [y_init; u_init(:,i)];
end

fprintf('\n');

for j=1:N_trials

  fprintf('Trial: %g\n',j);

  clear t x;

  for i=1:Nd2
    [t,x] = ode45(ODE_file,t_init,t_final,x_init(:,i),tol);

    M = length(t);
    u_final(:,i) = x(M,Nd2+1:N).';
```

```
  end

  t_init = t(M);
  t_final = t_final + t_span;

  y_init = x(M,1:Nd2).';

  fprintf('\n');

  u_init = gra_schm(u_final);

  for i=1:Nd2
    L(i) = L(i) + log(u_final(:,i).'*u_init(:,i));
    fprintf(' L(%g) = %g, ',i,L(i)/j/t_span)
  end

  for i=1:Nd2
    x_init(:,i) = [y_init; u_init(:,i)];
  end

end

for i=1:Nd2
  L(i) = L(i)/N_trials/t_span;
end
```

D.3 Lyapunov Exponents from Time Series

```
% LYAP_TSV.M  Lyapunov exponents from the time series.

clear;
echo off;
visual = 0; % visual = 0/1

% Load the Uniformly sampled time evolution
DAT_file = input('Data Filename (LORENZI) ','s');
if isempty(DAT_file)
  DAT_file = 'LORENZI'; %'ISTATEVO';
end
```

```
cmd_str = ['load ', DAT_file];
eval(cmd_str);

if (ID == 'I')|(ID == 'U')  % If Interpolated/Uniformly Sampled Data
  [Nt Ns] = size(x);
else
  fprintf ('Invalid ID Code Encountered!\n');
  return;
end

Ni = input('Evolution Interval (No. of Samples) (5) ');
if isempty(Ni)
  Ni = 5;
end

ep = input('1/2 Cube Diagonal Length (1.0) ');
if isempty(ep)
  ep = 1.0;
end

Ng = input('Guard Band (0) ');
if isempty(Ng)
  Ng = 0;
end
Ng = Ng + 1;

% Input Cube Center Position
Nc = -inf;
while (Nc <= Ng | Nc > Nt-Ni-Ng)
  Nc = input('Initial Cube Center (Sample No.) ');
  if isempty(Nc)
    Nc = -inf;
  end
end

Np = -inf;
while (Np < Ns)
  Np = input('Max. No. of Points Required in Cube (30) ');
  if isempty(Np)
    Np = 30;
  end
end

Nmax = input('Max. No. of Iterations (500) ');
```

```
if isempty(Nmax)
  Nmax = 500;
end

fprintf('\n');
L = zeros(1,Ns);
B = eye(Ns);  % Basis vectors {e(i)} in tangent space

Y = zeros(Ns,Np);
Z = zeros(Ns,Np);
k = 0;
while (k<Nmax)&(Nc+Ni+Ng<=Nt)

  k = k+1;
  fprintf('Trial: %g\n',k);

% Find Np nearest ep-neighbours
  xc = x(Nc,:);

  di = [x(1:Nc-Ng,:); x(Nc+Ng:Nt-Ni,:)];
  di = (di-ones(di(:,1))*xc).';
  di = sum(di.*di);
  di = di.^(.5);
  [ans, id] = sort(di);

  p = id(1:Np);
  Nn = sum(di(p)<=ep);
  p = p(1:Nn);

  fprintf(' No. of Neighbours found: %g,  ',Nn);
  fprintf('Max. norm = %g\n',max(di(p)));

  if Nn>=Ns

% Calculate y-tangent vectors
  for j=1:Nn
    Y(:,j) = (xc - x(p(j),:)).';
  end

% Calculate corresponding z-tangent vectors
  for j=1:Nn
    Z(:,j) = (x(Nc+Ni,:) - x(p(j)+Ni,:)).';
  end
```

```
% Calculate LMSE estimate of the linearized flow map A(i)
  A = (Z*Y.')*inv(Y*Y.');

  end

% Transform basis vectors {e(i)}
  C = A*B;
  det(C)


  B = mod_gs(C); %  B = gra_schm(C);

  for i=1:Ns
    L(i) = L(i) + log(C(:,i).'*B(:,i));
    fprintf(' L(%g) = %g,',i,L(i)/k/Ni/dt)
  end

  fprintf('\n\n')

  Nc = Nc+Ni; % Translate the cube.

end  % while

fprintf('Lyapunov exponents:\n')
L = L/Nmax/Ni/dt;  % Perform scaling assoc. with averaging
```

D.4 Standard Gram-Schmidt Procedure

```
function A = Gram_Schmidt(A)
% gra_schm   Performs Gram-Schmidt Orthonormalisation on the
%            column vectors of a square matrix.
%
%            Function Call:
%
%              B = gra_schm(A);
%
%             where
%
%                A = M x N  matrix
```

```
%                B = M x N  matrix containing orthonormal columns
%
%            See also: MOD_GS

s = size(A);

for k=1:s(2)
  if (k > 1)
    A(:,k) = A(:,k) - A(:,1:k-1) * (A(:,1:k-1)' * A(:,k));
  end
  A(:,k) = A(:,k)/norm(A(:,k));
end
```

D.5 Modified Gram-Schmidt Procedure

```
function A = Mod_Gram_Schmidt(A)
% mod_gs     Performs Gram-Schmidt Orthonormalisation on the
%            column vectors of a square matrix using the Modified
%            Gram-Schmidt procedure (Golub & Van Loan, p 152)
%
%            Function Call:
%
%              B = mod_gs(A);
%
%             where
%
%                A = M x N  matrix
%                B = M x N  matrix containing orthonormal columns
%
%           See also: GRA_SCHM

s = size(A);
R = zeros(s(2),s(2));

for k=1:s(2)
  R(k,k) = norm(A(:,k));

  for i=1:s(1)
    A(i,k) = A(i,k)/R(k,k);
  end
```

```
  for j=k+1:s(2)
    R(k,j) = A(1:s(1),k).'*A(1:s(1),j);

    for i=1:s(1)
      A(i,j) = A(i,j)-A(i,k)*R(k,j);
    end

  end

end
```

Bibliography

[1] Abarbanel H.D.I., Sushchik M.M., "Local or Dynamical Dimensions of Nonlinear Systems Inferred from Observations," *Int. J. Bifurcation and Chaos*, vol. 3, no. 3, pp. 543–550, 1993.

[2] Abed E.H., "Singularly Perturbed Hopf Bifurcation," *IEEE Trans. Circuits Syst.*, vol. CAS-32, no. 12, pp. 1270–1280, 1985.

[3] Abed E.H., Varaiya P.P., "Nonlinear Oscillations in Power Systems," *Elect. Power Energy Systems*, vol. 6, no. 1, pp. 37–43, 1984.

[4] Abed E.H., Wang H.O., Alexander J.C., Hamdan A.M.A., Lee H.-C., "Dynamic Bifurcations in a Power System Modeling Exhibiting Voltage Collapse," *Int. J. Bifurcation Chaos*, vol. 3, no. 5, pp. 1169–1176, 1993.

[5] Abelson H., Eisenberg M., Halfant M. et al., "Intelligence in Scientific Computing," *Communications of the ACM*, vol. 32, no. 5, pp. 546–562, 1989.

[6] Abidi A.A., Chua L.O., "On the Dynamics of Josephson-Junction Circuits," *Electronic Circuits Syst.*, vol. 3, pp. 186–200, 1979.

[7] Abraham N.B., "Complexities and Progress in Studies of Optical Chaos," *Optics News*, pp. 8–12, 1989.

[8] Abraham R., Robbin J., *Transversal Mappings and Flows.* W.A. Benjamin Inc., New York, 1967.

[9] Abraham R.H., Shaw C.D., *Dynamics—The Geometry of Behavior, Part 2: Chaotic Behavior.* Santa Cruz, CA: Aerial Press Inc., 1984.

[10] Abuelma'atti M.T., "Approximate Method for Hand Computation of Nonlinear Distortion Performance of Varactor Tuning Circuits," *IEE Proc.*, vol. 133, pt. G, no. 5, pp. 265–270, 1986.

[11] Afraimovich V.S., Shereshevsky M.A., "The Hausdorff Dimension of Attractors Appearing by Saddle-Node Bifurcations," *Int. J. Bifurcation and Chaos*, vol. 1, no. 2, pp. 309–325, 1991.

[12] Aihara K., Takabe T., Toyoda M., "Chaotic Neural Networks," *Phys. Lett. A*, vol. 144, no. 6,7, pp. 333–340, 1990.

[13] Akashi S., "A Relation Between Kolmogorov-Prokhorov's Condition and Ohya's Fractal Dimensions," *IEEE Trans. on Information Theory*, vol. 38, no. 5, pp. 1567–1570, 1992.

[14] Alder R.L., Konheim A.G., Mcandrew M.H., "Topological Entropy," *Trans. Amer. Math. Soc.*, vol. 114, pp. 309–319, 1965.

[15] Alekseev V.M., "Quasirandom Dynamical Systems, I." *Math. USSR Sb.*, vol. 5, pp. 73–128, 1968.

[16] Alekseev V.M., "Quasirandom Dynamical Systems, II." *Math. USSR Sb.*, vol. 6, pp. 505–560, 1968.

[17] Alekseev V.M., "Quasirandom Dynamical Systems, III." *Math. USSR Sb.*, vol. 7, pp. 1–43, 1969.

[18] Alligood K.T., Yorke J.A., "Fractal Basin Boundaries and Chaotic Attractors," *Chaos and Fractals the Mathematics Behind the Computer Graphics, Proc. of Symposia in Applied Math.*, vol. 39, pp. 41–55, 1989.

[19] Amari S.-I., "Field Theory of Self-Organizing Neural Nets," *IEEE Trans. Systems, Man, and Cybernetics*, vol. SMC-13, no. 5, pp. 741–748, 1983.

[20] Amos D.E., Burgmeier J.W., "Computation with Three-Term, Linear, Nonhomogeneous Recursion Relations," *SIAM Review*, vol. 15, no. 2, pp. 335–??, 1973.

[21] Anazia C.O., "The Inverted World of Gyrators," *Electronics World & Wireless World*, pp. 414–417, 1992.

[22] Andronov A.A., Leontovich E.A., Gordon I.I., Maier A.G., *Qualitative Theory of Second-Order Dynamic Systems*. New York, NY: John Wiley & Sons, 1973.

[23] Androulakakis S.P., Hartley T.T., Greenspan B., Qammar H., "Practical Considerations on the Calculation of the Uncertainty Exponent and the Fractal Dimension of Basin Boundaries," *Int. J. Bifurcation and Chaos*, vol. 1, no. 2, pp. 327–333, 1991.

[24] Anishchenko V.S., Safonova M.A., Chua L.O., "Stochastic Resonance in Chua's Circuit," *Int. J. Bifurcation and Chaos*, vol. 2, no. 2, pp. 397–401, 1992.

[25] Anishchenko V.S., Vadivasova T.E., Postnov D.E., Safonova M.A., "Synchronization of Chaos," *Int. J. Bifurcation and Chaos*, vol. 2, pp. 633–644, 1992.

[26] Antonian A., Naidu K.S., "Modeling of a Gyrator Circuit," *IEEE Trans. Circuit Theory*, vol. CT-20, no. 5, pp. 553–540, 1973.

[27] Aprille T.J., Trick T.N., "A Computer Algorithm to Determine the Steady-State Response of Nonlinear Oscillators," *IEEE Trans. Circuits Syst.*, vol. CAS-4, pp. 354–360, 1972.

[28] Arapostathis A., Sastry S.S., Varaiya P.P., "Global Analysis of the Swing Dynamics," *IEEE Trans. Circuits Syst.*, vol. 29, no. 10, pp. 673–679, 1982.

[29] Aref'yev A.A., Baskakov E.N., Stepanov L.M., *Radiotekhnichevskiy Ustroistva na Tranzistornykh ekvivalentakh p-n-p-n-Strucktur.* (*Radio Devices based on Transistor Equivalents of p-n-p-n-Structures*), Moscow: Radio i Svyaz Press, 1982.

[30] Arnol'd V.I., *Catastrophe Theory.* Berlin: Springer-Verlag, 1984.

[31] Arnol'd V.I., *Geometrical Methods in the Theory of Ordinary Differential Equations.* New York, NY: Springer-Verlag, 1983.

[32] Arnol'd V.I., *Ordinary Differential Equations.* Cambridge, MA: MIT Press, 1973.

[33] Arrowsmith D.K., Place C.M., *An Introduction to Dynamical Systems.* Cambridge: Cambridge University Press, 1990.

[34] Arrowsmith D.K., Place C.M., *Dynamical Systems, Differential Equations, Maps and Chaotic Behaviour.* London: Chapman & Hall, 1992.

[35] Arrowsmith D.K., Place C.M., *Ordinary Differential Equations.* London: Chapman & Hall, 1982.

[36] Arena P., Baglio S., Fortuna L., Manganaro G., "Analogic CNN Algorithms for some Image Compression and Restoration Tasks," *IEEE Trans. Circuits Syst.—I: Fund. Theory and Appl.*, vol. 42, no. 5, pp. 278–284, 1995.

[37] Ascheid G., Meyr H., "Cycle Slips in Phase-Locked Loops: a Tutorial Survey," *IEEE Trans. Commun.*, vol. COM-30, no. 10, pp. 2228–2241, 1982.

[38] Ash R.B., *Measure, Integration, and Functional Analysis.* New York, NY: Academic Press, 1972.

[39] Auerbach D., Cvitanovic P., Eckmann J.-P., Gunaratne G., Procaccia I., "Exploring Chaotic Motion through Periodic Orbits," *Phys. Rev. Lett.*, vol. 58, pp. 2387–2389, 1987.

[40] Auerbach D., Grebogi C., Ott E., Yorke J.A., "Controlling Chaos in High Dimensional Systems," *Phys. Rev. Lett.*, vol. 69, no. 24, pp. 3479–3482, 1992.

[41] Auslander L., *Differentiable Geometry.* New York, NY: Harper & Row, 1967.

[42] Auslander L., MacKenzie R.E., *Introduction to Differentiable Manifolds.* New York, NY: McGraw-Hill, 1963.

[43] Ayers D., "The Twisted World of Nonlinear Electronics," *Electronics World & Wireless World*, pp. 102–107, 1993.

[44] Ayrom F., Zhong G.-Q., "Chaos in Chua's Circuit," *IEE Proc.*, vol. 133, pt. D, no. 6, pp. 307–312, 1986.

[45] Azevedo A., Rezende S.M., "Controlling Chaos in Spin-Wave Instabilities," *Phys. Rev. Lett.*, vol. 66, no. 10, pp. 1342–1345, 1991.

[46] Azzouz A., Duhr R., Hasler M., "Transition to Chaos in a Simple Nonlinear Circuit Driven by a Sinusoidal Voltage Source," *IEEE Trans. Circuits Syst.*, vol. CAS-30, no. 12, pp. 913–914, 1983.

[47] Azzouz A., Hasler M., "Orbits of the *R-L*-Diode Circuit," *IEEE Trans. Circuits Syst.*, vol. 37, no. 11, pp. 1330–1338, 1990.

[48] Baghious E.H., Jarry P., ""Lorenz Attractor" from Differential Equations with Piecewise-Linear Terms," *Int. J. Bifurcation and Chaos*, vol. 3, no. 1, pp. 201–210, 1993.

[49] Baier G., Klein A., "Maximum Hyperchaos in Generalized Henon Maps," *Phys. Lett. A.* vol. 151, no. 6,7, pp. 281–284, 1990.

[50] Baillieul J., Brockett R.W., Washburn R.B., "Chaotic Motion in Nonlinear Feedback Systems," *IEEE Trans. Circuits Syst.*, vol. CAS-27, no. 11, pp. 990–997, 1980.

[51] Baker G.L., Gollub J.P., *Chaotic Dynamics: an Introduction.* Cambridge: Cambridge University Press, 1990.

[52] Baris Ya.S., Fodchuk V.I., "Bounded Solutions in Nonlinear Singularly Perturbed Systems via Integral Manifolds," *Ukr. Math. J.*, vol. 22, no.1, pp. 3–11, 1970.

[53] Barnsley M., *Fractals Everywhere.* New York, NY: Academic Press, 1988.

[54] Bartissol P., Chua L.O., "The Double Hook," *IEEE Trans. Circuits Syst.*, vol. 35, no. 12, pp. 1512–1522, 1988.

[55] Bartram J.E., "The Effect of Quantization of Sampled-Feedback Systems," *Aiee Trans. Appl. Ind.*, pt. 2, vol. 77, pp. 177–182, 1985.

[56] Baxter J.H., Bocko M.F., Douglass D.H., "Behaviour of a Nonlinear Resonator Driven At Subharmonic Frequencies," *Phys. Rev. A*, vol. 41, no. 2, pp. 619–625, 1990.

[57] Beard N., "The Science of Chaos," *Electronics World & Wireless World*, pp. 462–466, 1991.

[58] Beardon A.F., *Iteration of Rational Functions.* New York, NY: Springer-Verlag, 1991.

[59] Bedford T., Keane M., Series C. (eds.), *Ergodic Theory, Symbolic Dynamics, and Hyperbolic Spaces.* Oxford: Oxford University Press, 1991.

[60] Bedford T., Swift J. (eds.), *New Directions in Dynamical Systems.* Cambridge: Cambridge University Press, 1988.

[61] Beige H., Diestelhorst M., "Chaos near Structural Phase Transition," *Z. Naturforsch., vol. 45a*, pp. 958–964, 1990.

[62] Bel'skii YU.L., Dmitriyev A.S., Panas A.I., Starkov S.O., "The Synthesis of Broadband Chaotic Signals in Self-Excited Oscillatory Systems," *Scripta Technica, Inc.*, pp. 74–82, 1992.

[63] Belmonte A.L., Vinson M.J., Glazier J.A., Gunaratne G.M., Kenny B.G., "Trajectory Scaling Functions At the Onset of Chaos: Experimental Results," *Phys. Rev. Lett.*, vol. 61, no. 5, pp. 539–542, 1988.

[64] Belogortsev A.B., "Analytical Approach to the Torus Bifurcations in the Quasiperiodically Forced Van der Pol Oscillators," *Phys. Lett. A*, vol. 161, pp. 352–356, 1992.

[65] Belogortsev A.B., Poliashenko M.F., Tretjakov O.A., Vavriv D.M., "Stochastic Instability of Oscillator with Coupled Stabilising Resonator," *Electronic Letters*, vol. 26, no. 17, pp. 1354–1355, 1990.

[66] Belogortsev A.B., Vavriv D.M., Poliashenko M.F., Chernyshov I. YU., "Chaos During Resonant Interaction of Active and Passive Oscillators," *Soviet J. of Comm. Tech. and Elec. (USA)*, vol. 36, no. 6, pp. 142–148, 1991.

[67] Belykh V.N., Pedersen N.F., Soerensen O.H., "Shunted Josephson-Junction Model I, II," *Phys. Rev. B*, vol. 16, pp. 4853–4871, 1977.

[68] Bendat J.S., Piersol A.G., *Random Data: Analysis and Measurement Procedures.* New York, NY: Wiley, 1971.

[69] Ben-Jacob E., Goldhirsch I., Imry Y., Fishman S., "Intermittent Chaos in Josephson Junctions," *Phys. Rev. Lett.*, vol. 49, pp. 1599–1602, 1982.

[70] Benettin G., Galgani L., Giorgilli A., Strelcyn J.-M., "Lyapunov Characteristic Exponents for Smooth Dynamical Systems and for Hamiltonian Systems; a Method for Computing All of Them: Part 1," *Meccanica*, pp. 9–20, 1980.

[71] Benettin G., Galgani L., Giorgilli A., Strelcyn J.-M., "Lyapunov Characteristic Exponents for Smooth Dynamical Systems and for Hamiltonian Systems; a Method for Computing All of Them: Part 2," *Meccanica*, pp. 21–30, 1980.

[72] Benettin G., Galgani L., Strelcyn J.-M., "Kolmogorov Entropy and Numerical Experiments," *Phys. Rev. A*, vol. 14, no. 6, pp. 2338–2345, 1976.

[73] Benlynkh V.N., Pederen N.F., Soerensen O.H., "Shunted Josephson-Junction Model—I the Autonomous Case and II the Nonautonomous Case," *Phys. Rev. B*, vol. 16, pp. 4853–4871, 1977.

[74] Berge P., Pomeau Y., Vidal C., *Order within Chaos.* New York, NY: Wiley, 1984.

[75] Bernstein G.M., Lieberman M.A., "Secure Random Number Generation using Chaotic Circuits," *IEEE Trans. Circuits Syst.*, vol. 39, no. 9, pp. 1157–1164, 1990.

[76] Berzruchko B.P., "The Features of the Excitation of Subharmonic and Chaotic Oscillators," *Scripta Technica, Inc.*, pp. 58–61, 1992.

[77] Best R.E., *Phase-Locked Loops.* New York, NY: McGraw-Hill, 1984.

[78] Bhatia N.P., Szëgo G.P., *Dynamical Systems: Stability Theory and Applications.* Berlin: Springer-Verlag, 1967.

[79] Birkhoff G., Rota G.-C., *Ordinary Differential Equations.* New York, NY: Wiley, 1978.

[80] Birkhoff G.D., "Nouvelles Recherches sur les systèmes dynamiques," *Mem. Point. Acad. Sci. Novi. Lyncaei*, vol. 1, pp. 85–216, 1935.

[81] Birkhoff G.D., "Proof of the Ergodic Theorem," *Proc. Natl. Acad. Sci. USA*, vol. 17, pp. 656–660, 1931.

[82] Birkhoff G.D., "Dynamical Systems," *A.M.S. Coll. Publications*, vol. 9, reprinted 1966, Providence: American Mathematical Society 1927.

[83] Bishop R.L., Goldberg S.I., *Tensor Analysis on Manifolds.* Toronto, Ontario: Dover, 1980.

[84] Blázquez C.M., Tuma E., "Dynamics of the Double Scroll Circuit," *IEEE Trans. Circuits Syst.*, vol. 37, no. 5, pp. 589–593, 1990.

[85] Blázquez C.M., Tuma E., "Strange Attractors of the Shil'nikov type in Chua's Circuit," *Int. J. Bifurcation and Chaos*, vol. 3, no. 5, pp. 1293–1298, 1993.

[86] Block A., Von Bloh W., Schellnhuber H.J., "Efficient Box-Counting Determination of Generalized Fractal Dimensions," *Phys. Rev. A*, vol. 42, no. 4, pp. 1869–1874, 1990.

[87] Block L.S., Coppel W.A., *Dynamics in One Dimension.* Berlin: Springer-Verlag, 1992.

[88] Block L.S., Guckenheimer J., Misiurewicz M., Young L.S., *Periodic Points and Topological Entropy of One-Dimensional Maps.* Nitecki Z., Robinson C. (eds.), Global Theory of Dynamical Systems, New York, NY: Springer-Verlag, 1980.

[89] Bogoliubov N.N., Mitropolskii Y.A., *Asymptotic Methods in the Theory of Nonlinear Systems.* New York, NY: Gordon and Breach, 1961.

[90] Bowen R., "Bernoulli Maps of the Interval," *Israel J. Math.*, vol. 28, no. 1–2, pp. 161–168, 1977.

[91] Boyarsky A., Lou Y.S., "A Matrix Method for Approximating Fractal Measures," *Int. J. Bifurcation and Chaos*, vol. 2, no. 1, pp. 176–175, 1992.

[92] Boyd S., Chua L.O., "Dynamical System need not have Spectrum," *IEEE Trans. Circuits Syst.*, vol. CAS-32, no. 9, pp. 968–969, 1985.

[93] Boyes E., "Understanding the *P-N* Junction," *Phys. Educ.*, vol. 25, pp. 53–59, 1990.

[94] Bracikowski C., Roy R., *Chaos*, vol. 1, pp. 49–60, 1991.

[95] Bradley E., "Using Chaos to Broaden the Capture Range of a Phase-Locked Loop," *IEEE Trans. Circuits Syst.—I: Fund. Theory and Appl.*, vol. 40, no. 11, pp. 808–818, 1993.

[96] Braiman Y., Goldhirsch I., "Taming Chaotic Dynamics with weak Periodic Perturbations," *Phys. Rev. Lett.*, vol. 66, no. 20, pp. 2545–2548, 1991.

[97] Briggs K., "An Improved Method for Estimating Liapunov Exponents of Chaotic Time Series," *Phys. Lett. A*, vol. 151, no. 1,2, pp. 27–32, 1990.

[98] Briggs K., "Simple Experiments in Chaos Dynamics," *Am. J. Phys.*, vol. 55, no. 12, pp. 1083–1089, 1987.

[99] Brigham E.O., *The Fast Fourier Transform.* Englewood Cliffs, NJ: Prentice-Hall Inc., 1974.

[100] Brockett R.W., "Nonlinear Systems and Differential Geometry," *Proc. IEEE*, vol. 64, no. 1, pp. 61–72, 1976.

[101] Broomhead D.S., Lowe D., "Multivariate Functional Interpolation and Adaptive Networks," *Complex Systems*, vol. 2, pp. 321–355, 1988.

[102] Brophy J.J., *Basic Electronics for Scientists.* Third Edition, Tokyo: McGraw-Hill, 1977.

[103] Brorson S.D., Dewey D., Linsay P.S., "Self-Replicating Attractor of a Driven Semiconductor Oscillator," *Phys. Rev. A*, vol. 28, no. 2, pp. 1201–1203, 1983.

[104] Broucke M.E., "One Parameter Bifurcation Diagram for Chua's Circuit," *IEEE Trans. Circuits Syst.*, vol. CAS-34, no. 2, pp. 208–209, 1987.

[105] Brown D.P., "Matrix Tests for Period 1 and 2 Limit Cycles in Discrete Threshold Networks," *IEEE Trans. Systems, Man, and Cybernetics*, vol. 22, no. 3, pp. 552–554, / 1992.

[106] Brown R., Chua L.O., "Dynamical Integration," *Int. J. Bifurcation and Chaos*, vol. 3, no. 1, pp. 217–222, 1993.

[107] Bröcker T., *Differentiable Germs and Catastrophes.* Cambridge: Cambridge University Press, 1975.

[108] Budelli R., Torres J., Catsigeras E., Enrich H., "Two-Neuron Network I. Integrate and Fire Pacemaker Models," *Biol. Cybern.*, vol. 66, pp. 95–101, 1991.

[109] Bulsara A.R., Schieve W.C., Jacobs E.W., "Homoclinic Chaos in Systems Perturbed by Weak Langevin Noise," *Phys. Rev. A*, vol. 41, no. 2, pp. 668–681, 1990.

[110] Cambell D., Crutchfield J., Farmer D., Jen E., "Experimental Mathematics: the Role of Computation in Nonlinear Science," *Communications of the ACM*, vol. 28, no. 4, pp. 374–384, 1985.

[111] Candy J.C., "A use of Limit Cycle Oscillations to obtain Robust Analog-to-Digital Converters," *IEEE Trans. Commun.*, vol. COM-22, , pp. 298–305, 1974.

[112] Carr J., *Applications of Centre Manifold Theory.* New York, Springer-Verlag, 1981.

[113] Carroll T.L., "Communicating with use of Filtered, Synchronized, Chaotic Signals," *IEEE Trans. Circuits Syst.—I: Fund. Theory and Appl.*, vol. 42, no. 3, pp. 105–110, 1995.

[114] Carroll T.L., Pecora L.M., "A Circuit for Studying the Synchronization of Chaotic Systems," *Int. J. Bifurcation and Chaos*, vol. 2, no. 2, pp. 659–667, 1992.

[115] Cartwright M.L., Littlewood J.E., "On Non-Linear Differential Equations of the Second Order: I. The Equation $\ddot{y} - k(1 - y^2)\dot{y} + y = b\lambda k \cos(\lambda t + a)$, k Large," *J. London Math. Soc.*, vol. 20, pp. 180–189, 1945.

[116] Cascais J., Dilão R., Da Costa A.N., "Chaos and Reverse Bifurcation in a RCL Circuit," *Phys. Lett. A*, vol. 93, no. 5, pp. 213–216, 1983.

[117] Casdagli M., "Nonlinear Prediction of Chaotic Time Series," *Physica D*, vol. 35, pp. 335–356, 1989.

[118] Casdagli M., Eubank S., Farmer J.D., Gibson J., "State Space Reconstruction in the Presence of Noise," *Physica D*, vol. 51, pp. 52–98, 1991.

[119] Celletti A., Falcolini C., Tedeschini-Lalli L., "The Basin of Attraction of a Spin-Orbit Resonance," *Int. J. Bifurcation and Chaos*, vol. 3, no. 5, pp. 1305–1309, 1993.

[120] Ceschia M., Zecchin G., "Asymptotic Amplitude from a Three-Parameter Oscillator," *IEEE Trans. Circuits Syst.*, vol. CAS-28, no. 5, pp. 456–459, 1981.

[121] Ceschia M., Zecchin G., "Asymptotic Amplitude from a Two-Parameter Strongly Nonlinear Oscillator," *IEEE Trans. Circuits Syst.*, vol. CAS-28, no. 5, pp. 448–455, 1981.

[122] Chacón R., Batres Y., Cuadros F., "Teaching Deterministic Chaos through Music," *Phys. Educ.*, vol. 27, pp. 151–154, 1992.

[123] Chakraborty T., Rand R.H., "The Transition from Phase-Locking to Drift in a System of Two Weakly Coupled Van der Pol Oscillators," *Int. J. Non-Linear Mechanics*, vol. 23, no. 5/6, pp. 369–376, 1988.

[124] Challis R.E., Kitney R.I., "Biomedical Signal Processing (in Four Parts) Part 1 Time-Domain Methods," *Med. & Biol. Eng. & Comput.*, vol. 28, no. 6, pp. 509–524, 1990.

[125] Chang F-J., Twu S.-H., Chang S., "Global Bifurcation and Chaos from Automatic Gain Control Loops," *IEEE Trans. Circuits Syst.—I: Fund. Theory and Appl.*, vol. 40, no. 6, pp. 403–411, 1993.

[126] Chapeau-Blondeau F., Chauvet G., "Stable, Oscillatory, and Chaotic Regimes in the Dynamics of Small Neural Networks with Delay," *Neural Networks*, vol. 5, no. 5, pp. 735–743, - 1992.

[127] Chase C., Serrano J., Ramadge P.J., "Periodicity and Chaos from Switched Flow Systems: Contrasting Examples of Discrete Continuous Systems," *IEEE Trans. Automat. Contr.*, vol. 38, no. 1, pp. 70–83, 1993.

[128] Chaundy T.W., Phillips E., "The Convergence of Sequences Defined by Quadratic Recurrence-Formulae," *Quart. J. of Math. (Oxford)*, pp. 74–80, 1936.

[129] Chen G., "Controlling Chua's Global Unfolding Circuit Family," *IEEE Trans. Circuits Syst.—I: Fund. Theory and Appl.*, vol. 40, no. 11, pp. 829–832, 1993.

[130] Chen G., Dong X., "On Feedback Control of Chaotic Continuous-Time Systems," *IEEE Trans. Circuits Syst.*, vol. 40, no. 8, pp. 591–601, 1993.

[131] Chen G., Dong X., "On Feedback Control of Chaotic Nonlinear Dynamic Systems," *Int. J. Bifurcation and Chaos*, vol. 2, no. 2, pp. 407–411, 1992.

[132] Chialina S., Hasler M., Premoli A., "Fast and Accurate Calculation of Lyapunov Exponents for Piecewise-Linear Systems," *Int. J. Bifurcation and Chaos*, vol. 4, no. 1, pp. 127–136, 1994.

[133] Chiang H.-D., Hirsch M.W., Wu F.F., "Stability Regions on Nonlinear Autonomous Dynamical Systems," *IEEE Trans. Automat. Contr.*, vol. 33, no. 1, pp. 16–26, 1988.

[134] Chillingworth D.R.J., *Differential Topology with a View to Applications.* London: Pitman, 1976.

[135] Chorin A.J., "Numerical Estimates of Hausdorff Dimension," *J. Comp. Phys.*, vol. 46, pp. 390–396, 1982.

[136] Chow S.W., Hale J.K., *Methods of Bifurcation Theory.* New York, NY: Springer-Verlag, 1982.

[137] Chu Y-H., Chou J.-H., Chang S., "Chaos from Third-Order Phase-Locked Loops with Slowly Varying Parameter," *IEEE Trans. Circuits Syst.*, vol. 37, no. 9, pp. 1104–1115, 1990.

[138] Chu Y.H., Chou J.-H., Chang S., "Chaos in Phase-Locked Loops," *Electron. Lett.*, vol. 27, no. 9, pp. 750–751, 1991.

[139] Chu Y.H., Chou J.-H., Chang S., "Reply to the "Comments of Chaos from Third-Order Phase-Locked Loops with a Slowly Varying Parameter"," *IEEE Trans. Circuits Syst.*, vol. 38, no. 6, pp. 677–678, 1991.

[140] Chua L.O., (ed.), *Special Issue on Nonlinear Waves, Patterns and Spatio-Temporal Chaos in Dynamic Arrays.* IEEE Trans. Circuits Syst.—I Fund. Theory and Appl., vol. 42, no. 10, 1995.

[141] Chua L.O., "Dynamic Nonlinear Networks: State-Of-The-Art," *IEEE Trans. Circuits Syst.*, vol. CAS-27, no. 11, pp. 1059–1087, 1980.

[142] Chua L.O., "Global Unfolding of Chua's Circuits," *IEICE Trans. on Fundamentals of Electronics, Communication and Computer Sciences*, vol. E 76-A, no. 5, pp. 704–734, 1993.

[143] Chua L.O., "Nonlinear Circuits," *IEEE Trans. Circuits Syst.*, vol. CAS-31, no. 1, pp. 69–87, 1984.

[144] Chua L.O., "The Genesis of Chua's Circuit," *AEÜ*, vol. 46, no. 4, pp. 250–257, 1992.

[145] Chua L.O., Ayrom F., "Designing Non-Linear Single Op-Amp Circuits: a Cook-Book Approach," *Int. J. Circuit Theory Appl.*, vol. 13, pp. 235–268, 1985.

[146] Chua L.O., Brayton R.K., Guckenheimer J., Mees A.I. (eds.), *Special Issue on Nonlinear Phenomena, Modeling, and Mathematics: Part I: Contributed Papers.* IEEE Trans. Circuits Syst., vol. CAS-30, no. 9, 1983.

[147] Chua L.O., Brayton R.K., Guckenheimer J., Mees A.I. (eds.), *Special Issue on Nonlinear Phenomena, Modeling, and Mathematics: Part I: Tutorial Papers.* IEEE Trans. Circuits Syst., vol. CAS-30, no. 8, 1983.

[148] Chua L.O., Deng A-C., "Negative Resistance Devices: Part II," *Int. J. Circuit Theory Appl.*, vol. 12, pp. 337–373, 1984.

[149] Chua L.O., Desoer C.A., Kuh E.S., *Linear and Nonlinear Circuits.* Electrical Engineering Series, Singapore: McGraw-Hill, 1987.

[150] Chua L.O., Green D.N., "A Qualitative Analysis of the Behavior of Dynamic Nonlinear Networks: Steady-State Solutions of Nonautonomous Networks," *IEEE Trans. Circuits Syst.*, vol. CAS-23, pp. 530–550, 1976.

[151] Chua L.O., Hasler M. (eds.), *Special Issue on Chaos in Nonlinear Electronic Circuits: Part A. Tutorials and Reviews.* IEEE Trans. Circuits Syst.—I: Fund. Theory and Appl., vol. 40, no. 10, 1993.

[152] Chua L.O., Hasler M. (eds.), *Special Issue on Chaos in Nonlinear Electronic Circuits: Part B. Bifurcation and Chaos.* IEEE Trans. Circuits Syst.—I: Fund. Theory and Appl., vol. 40, no. 11, 1993.

[153] Chua L.O., Hasler M., Neirynck J., Verburgh P., "Dynamics of a Piecewise-Linear Resonant Circuit," *IEEE Trans. Circuits Syst.*, vol. CAS-29, no. 8, pp. 535–547, 1982.

[154] Chua L.O., Komuro M., Matsumoto T., "The Double Scroll Family," *IEEE Trans. Circuits Syst.*, vol. CAS-33, no. 11, pp. 1072–1118, 1986.

[155] Chua L.O., Lin G.-N., "Canonical Realization of Chua's Circuit Family," *IEEE Trans. Circuits Syst.*, vol. 37, no. 7, pp. 885–902, 1990.

[156] Chua L.O., Lin G.-N., "Intermittency in a Piecewise-Linear Circuit," *IEEE Trans. Circuits Syst.*, vol. 38, no. 5, pp. 510–520, 1991.

[157] Chua L.O., Lin T., "Chaos and Fractals Form Third-Order Digital Filters," *Int. J. Circuit Theory Appl.*, vol. 18, pp. 241–255, 1990.

[158] Chua L.O., Lin T., "Chaos in Digital Filters," *IEEE Trans. Circuits Syst.*, vol. 35, no. 6, pp. 648–658, 1988.

[159] Chua L.O., Madan R.N., "Sights and Sounds of Chaos," *IEEE Circuits & Devices Magazine*, pp. 3–13, 1988.

[160] Chua L.O., Matsumoto T., Ichiraku S., Correction to "Geometric Properties of Resistive Nonlinear n-Ports: Transversality, Structural Stability, Reciprocity, and Anti-Reciprocity," *IEEE Trans. Circuits Syst.*, vol. CAS-28, no. 2, p. 168, 1981.

[161] Chua L.O., Matsumoto T., Ichiraku S., "Geometric Properties of Resistive Nonlinear n-Ports: Transversality, Structural Stability, Reciprocity, and Anti-Reciprocity," *IEEE Trans. Circuits Syst.*, vol. CAS-27, pp. 577–603, 1980.

[162] Chua L.O., Tang Y.S., "Nonlinear Oscillation via Volterra Series," *IEEE Trans. Circuits Syst.*, vol. CAS-29, no. 3, pp. 150–168, 1982.

[163] Chua L.O., Yang L., "Cellular Neural Networks: Applications," *IEEE Trans. Circuits Syst.*, vol. 35, no. 10, pp. 1273–1290, 1988.

[164] Chua L.O., Yang L., "Cellular Neural Networks: Theory," *IEEE Trans. Circuits Syst.*, vol. 35, no. 10, pp. 1257–1272, 1988.

[165] Chua L.O., Yao Y., Yang Q., "Devil's Staircase Route to Chaos in a Nonlinear Circuit," *Int. J. Circuit Theory Appl.*, vol. 14, pp. 315–329, 1986.

[166] Chua L.O., Yao Y., Yang Q., "Generating Randomness from Chaos and Constructing Chaos with Desired Randomness," *Int. J. Circuit Theory Appl.*, vol. 18, pp. 215–240, 1990.

[167] Chua L.O., Ying L.P., "Canonical Piecewise-Linear Analysis," *IEEE Trans. Circuits Syst.*, vol. CAS-30, no. 3, pp. 125–140, 1983.

[168] Chua L.O., Yu J.B., Yu Y.Y., "Bipolar-JFET-MOSFET Negative Resistance Devices," *IEEE Trans. Circuits Syst.*, vol. CAS-32, no. 1, pp. 46–61, 1985.

[169] Chua L.O., Yu J.B., Yu Y.Y., "Negative Resistance Devices," *Int. J. Circuit Theory Appl.*, vol. 11, pp. 161–186, 1983.

[170] Chua L.O. (ed.), *Special Issue on Chaotic Systems.* Proc. IEEE, vol. 75, no. 8, 1987.

[171] Chui C.K., *An Introduction to Wavelets.* New York, NY: Academic Press, 1992.

[172] Chui C.K. (ed.), *Wavelets Analysis and Its Applications vol. 2, Wavelets: A Tutorial in Theory and Applications.* San Diego, CA: Academic Press, 1992.

[173] Cicogna G., Fronzoni L., "Effects of Parametric Perturbations on the Onset of Chaos in the Josephson-Junction Model: Theory and Analog Experiments," *Phys. Rev. A*, vol. 24, no. 4, pp. 1901–1906, 1990.

[174] Claasen T.A.C.M., Mecklenbräuker W.F.G., Peek J.B.H., "Effect of Quantization and Overflow in Recursive Digital Filters," *IEEE Trans. Acoust. Speech, Signal Process.*, vol. ASSP-24, pp. 517–529, 1976.

[175] Clarke K.K., Hess D.T., *Communication Circuits: Analysis and Design.* Reading, MA: Addison-Wesley, 1978.

[176] Clay R., *Nonlinear Networks and Systems.* A Wiley-Interscience Publication, New York, NY: Wiley, 1971.

[177] Coddington E.A., Levinson N., *Theory of Ordinary Differential Equations.* New York, NY: McGraw-Hill, 1955.

[178] Cody M.A., "The Fast Wavelet Transform," *Dr. Dobb's J.*, pp. 16–28, 100–101, 1992.

[179] Cohn D.L., *Measure Theory.* Boston, MA: Birkhäuser, 1980.

[180] Cole J.D., *Perturbation Methods in Applied Mathematics.* Waltham, MA: Ginn-Glaisdell, 1968.

[181] Collet P., Eckmann J.-P., *Iterated Maps of the Interval As Dynamical Systems.* Boston, MA: Birkhäuser, 1980.

[182] Collet P., Eckmann J.-P., Lanford O.E., "Universal Properties of Maps on an Interval," *Comm. Math. Phys.*, vol. 76, pp. 211–254, 1980.

[183] Cook A.E., Roberts P.H., "The Rikitake Two-Disc Dynamo System," *Proc. Camb. Phil. Soc.*, vol. 68, pp. 547–569, 1970.

[184] Coste J., Peyraud J., Coullet P., "Asymptotic Behaviours in the Dynamics of Competing Species," *SIAM J. Appl. Math.*, vol. 36, pp. 516–543, 1978.

[185] Coullet P., Tresser C., "Iterations D'endomorphismes et Groupe de Renormalisation," *J. De Physique*, vol. C5, pp. 25–28, 1978.

[186] Cowan C.F.N., Grant P.M. (eds.), *Adaptive Filters.* Englewood Cliffs, NJ: Prentice-Hall Inc., 1985.

[187] Cronin J., *Mathematical Aspects of Hodgkin-Huxley Neural Theory.* Cambridge: Cambridge University Press, 1987.

[188] Crounse K.R., Roska T., Chua L.O., "Image Halftoning with Cellular Neural Networks," *IEEE Trans. Circuits Syst.—II: Analog and Digital Signal Processing*, vol. 40, no. 4, pp. 267–283, 1993.

[189] Crutchfield J.P., Farmer J.D., Packard N.H., Shaw R.S., "Chaos," *Scientific American*, pp. 38–49, 1986.

[190] Crutchfield J.P., Huberman B.A., "Fluctuations and the Onset of Chaos," *Phys. Lett. A*, vol. 77, no. 6, pp. 407–410, 1980.

[191] Crutchfield J.P., Packard N.H., "Symbolic Dynamics of One-Dimensional Maps: Entropies, Finite Precision, and Noise," *Int. J. Theor. Phys.*, vol. 21, no. 6-7, pp. 433–466, 1982.

[192] Cruz J.M., Chua L.O., "A CNN Chip for Connected Component Detection," *IEEE Trans. Circuits Syst.*, vol. 38, no. 7, pp. 812–817, 1991.

[193] Curry J.H., Yorke J.A., "A Transition from Hopf Bifurcation to Chaos: Computer Experiment with Maps on $\mathbf{R}^2$," *Lecture Notes in Maths.*, vol. 668, pp. 48–66, 1978.

[194] D'humieres D., Beasley M.R., Huberman B.A., Libchaber A., "Chaotic States and Routes to Chaos in the Forced Pendulum," *Phys. Rev. A.*, vol. 26, no. 6, pp. 3483–3496, 1982.

[195] Damljanovic D.D., "Remodeling the P-N Junction," *Circuits & Devices Magazine*, pp. 35–37, 1993.

[196] Dämmig M., Mitschke F., "Estimation of Lyapunov Exponents from Time Series: the Stochastic Case," *Phys. Lett. A*, vol. 178, pp. 385–394, 1993.

[197] Danielson D.A., *Vectors and Tensors in Engineering and Physics.* Reading, MA: Addison-Wesley, 1992.

[198] Davies M., "Noise Reduction by Gradient Descent," *Int. J. Bifurcation and Chaos*, vol. 3, no. 1, pp. 113–118, 1992.

[199] De Aguiar F.M., Rezende S.M., "Observation of Subharmonic Routes to Chaos in Parallel-Pumped Spin Waves in Yttrium Iron Garnet," *Phys. Rev. Lett.*, vol. 56, no. 10, pp. 1070–1073, 1986.

[200] De Barra G., *Measure Theory and Integration.* Ellis Norwood Series, New York, NY: John Wiley & Sons, 1981.

[201] De Bellescize H., "La Recéption Synchrone," *Onde Electrique*, vol. 11, pp. 230–240, 1932.

[202] De Melo W., Van Strien S., *One-Dimensional Dynamics.* Berlin: Springer-Verlag, 1993.

[203] de Silva C.P., "Shil'nikov's Theorem—A Tutorial," *IEEE Trans. Circuits Syst.—I: Fund. Theory and Appl.*, vol. 40, no. 10, pp. 675–682, 1993.

[204] De Sousa Vieira M., Khoury P., Lichtenberg A.J., Lieberman M.A., Wonchoba W., "Numerical and Experimental Studies of Self-Synchronization and Synchronized Chaos," *Int. J. Bifurcation and Chaos*, vol. 2, no. 3, pp. 645–657, 1992.

[205] De Sousa Vieira M., Lichtenberg A.J., Lieberman M.A., "Nonlinear Dynamics of Self-Synchronizing Systems," *Int. J. Bifurcation and Chaos*, vol. 1, no. 3, pp. 691–699, 1991.

[206] De-Souza-Machado S., Rollins R.W., Jacobs D.T., Hartman J.L., "Studying Chaotic Systems using Microcomputer Simulations and Lyapunov Exponents," *Am. J. Phys.*, vol. 35, no. 4, pp. 321–329, 1990.

[207] Deane J.H., Hamill D.C., "Instability, Subharmonics, and Chaos in Power Electronic Systems," *IEEE Trans. Power Electronics*, vol. 5, no. 3, pp. 260–268, 1990.

[208] Deane J.H.B., "Chaos in a Current-Mode Controlled Boost DC-DC Converter," *IEEE Trans. Circuits Syst.—I: Fund. Theory and Appl.*, vol. 39, no. 8, pp. 680–679, 1992.

[209] Delaney P.A., Walsh D.O., "A Bibliography of Higher-Order Spectra and Cumulants," *IEEE Signal Processing Magazine*, pp. 61–70, 1994.

[210] Delgado-Restituto M., Rodriguez-Vasquez A., "A CMOS Monolithic Chua's Circuit," *J. Circuits, Systems and Computers*, vol. 3, no. 2, pp. 259–268, 1993.

[211] Delgado-Restituto M., Rodriquez-Vasquez A., Huertas J.L., "A Chaotic Switched-Capacitor Circuit for $1/f$ Noise Generation," *IEEE Trans. Circuits Syst.—I: Fund. Theory and Appl.*, vol. 39, no. 4, pp. 325–328, 1992.

[212] Dempsey G.L., Mcvey E.S., "Circuit Implementation of a Peak Detector Neural Network," *IEEE Trans. Circuits Syst.*, vol. 40, no. 9, pp. 585–591, 1993.

[213] Dennis J.E., Woods J.A., "New Computing Environments: Microcomputers in Large-Scale Computing, Ed. A. Wouk," *SIAM*, pp. 116–122, 1987.

[214] Desoer C.A., Haneda H., "The Measure of a Matrix As a Tool to Analyze Computer Algorithms for Circuit Analysis," *IEEE Trans. Circuit Theory*, vol. 19, no. 5, pp. 480–486, 1972.

[215] Dessouky K., Lindsey W.C., "Phase and Frequency Transfer Between Mutually Synchronized Oscillators," *IEEE Trans. Commun.*, vol. COM-32, pp. 110–117, 1984.

[216] Deutsch S., Deutsch A., *Understanding the Nervous System: an Engineering Perspective*. New York, NY: IEEE Press, 1993.

[217] Devaney R.L., *An Introduction to Chaotic Dynamical Systems*. Second Edition, Redwood City, CA: Addison-Wesley, 1989.

[218] Dick S., "Exploring Negative Resistance: the Lambda Diode," *Elektor Electronics*, pp. 54–55, 1992.

[219] Ditto W.L., Pecora L.M., "Mastering Chaos," *Scientific American*, pp. 62–68, 1993.

[220] Ditto W.L., Rauseo S., Cawley R., Grebogi C., Hsu G.-H., Kostelich E., Ott E., Savage H.T., Segnan R., Spano M.L., Yorke J.A., *Phys. Rev. Lett.*, vol. 63, pp. 923–930, 1989.

[221] Ditto W.L., Rauseo S.N., Spano M.L., "Experimental Control of Chaos," *Phys. Rev. Lett.*, vol. 65, no. 26, pp. 3211–3214, 1990.

[222] Dmitriyev, A.S., Kislov V.Ya., *Stockhasticheskiyec Kolebaniya v Radiofizike i Elektronike. (Stochastic Oscillations in Radio Physics and Electronics)*, Moscow: Nauka Press, 1989.

[223] Dobson I., "Observations on the Geometry of Saddle-Node Bifurcation and Voltage Collapse in Electrical Power Systems," *IEEE Trans. Circuits Syst.—I: Fund. Theory and Appl.*, vol. 39, no. 3, pp. 240–243, 1992.

[224] Dobson I., Lu L., "Voltage Collapse Precipitated by the Immediate Change in Stability when Generator Reactive Power Limits are Encountered," *IEEE Trans. Circuits Syst.—I: Fund. Theory and Appl.*, vol. 39, no. 9, pp. 762–766, 1992.

[225] Doedel E.J., Aronson D.G., Othmer H.G., "The Dynamics of Coupled Current-Biased Josephson Junctions: Part I," *IEEE Trans. Circuits Syst.*, vol. 35, no. 7, pp. 810–819, 1988.

[226] Dolezal V., Newcomb R.W., "A Nonlinear Impedance Converter," *IEEE Trans. Circuits Syst.*, vol. CAS-28, no. 2, pp. 149–152, 1981.

[227] Dracopoulos D.C., Jones A.J., "Modeling Dynamic Systems," *World Conference on Neural Networks*, 1993.

[228] Dressler U., Nitsche G., "Controlling Chaos using Time Delay Coordinates," *Phys. Rev. Lett.*, vol. 68, no. 1, pp. 1–4, 1992.

[229] Duong-Van M., "The Physics of the Logistic Map in the Continuous-Time Limit," *Phys. Lett. A*, vol. 151, no. 9, pp. 493–499, 1990.

[230] Eckmann J.-P., Oliffson Kamphorst S., Ruelle D., Ciliberto S., "Liapunov Exponents from Time Series," *Phys. Rev. A*, vol. 34, no. 6, pp. 4971–4979, 1986.

[231] Eckmann J.-P., Ruelle D., "Ergodic Theory of Chaos and Strange Attractors," *Rev. Mod. Phys.*, vol. 57, no. 3, Part 1, pp. 617–656, 1985.

[232] Elgar S., Chandran V., "Higher-Order Spectral Analysis to Detect Nonlinear Interactions in Measured Time Series and an Application to Chua's Circuit," *Int. J. Bifurcation and Chaos*, vol. 3, no. 1, pp. 19–34, 1993.

[233] Ellison J.A., Saenz A.W., Dumas H.S., "Improved N-th Order Averaging Theory for Periodic Systems," *J. of Differential Equations*, vol. 84, no. 2, pp. 383–403, 1990.

[234] El-Sayed M.L., "Partitioned Matrix Derivative using Kronecker Products," *IEEE Trans. Circuits Syst.*, vol. CAS-27, no. 12, pp. 1268–1269, 1980.

[235] Elton J.H., "An Ergodic Theorem for Iterated Maps," *Ergodic Theory Dynamical System*, vol. 7, pp. 481–488, 1987.

[236] Endo T., Chua L.O., "Piecewise-Linear Analysis of High-Damping Chaotic Phase-Locked Loops using Melnikov's Method," *IEEE Trans. Circuits Syst.—I Fund. Theory and Appl.*, vol. 40, no. 11, pp. 801–807, 1993.

[237] Endo T., Chua L.O., "Bifurcation Diagrams and Fractal Basin Boundaries of Phase-Locked Loop Circuits," *IEEE Trans. Circuits Syst.*, vol. 37, no. 4, pp. 534–540, 1990.

[238] Endo T., Chua L.O., "Chaos from Phase-Locked Loops," *IEEE Trans. Circuits Syst.*, vol. 35, no.8, pp. 987–1003, 1988.

[239] Endo T., Chua L.O., "Chaos from Two Coupled Phase-Locked Loops," *IEEE Trans. Circuits Syst.*, vol. 37, no. 9, pp. 1183–1187, 1990.

[240] Endo T., Chua L.O., "Synchronization of Chaos in Phase-Locked Loops," *IEEE Trans. Circuits Syst.*, vol. 38, no. 12, pp. 1580–1588, 1991.

[241] Endo T., Chua L.O., Narita T., "Chaos from Phase-Locked Loops-Part II: High-Dissipation Case," *IEEE Trans. Circuits Syst.*, vol. 36, no. 2, pp. 255–263, 1989.

[242] Endo T., Mori S., "Mode Analysis of a Ring of a Large Number of Mutually Coupled Van der Pol Oscillators," *IEEE Trans. Circuits Syst.*, vol. CAS-25, no. 1, pp. 7–18, 1978.

[243] Endo T., Tada K., "Analysis of the Pull-In Range of Phase-Locked Loops by the Galerkin's Method," *IECE Trans.*, vol. J68-B, pp. 236–243, 1985.

[244] Essex C., Nerenberg M.A.H., "Fractal Dimension: Limit Capacity or Hausdorff Dimension?," *Am. J. Phys.*, vol. 58, no. 10, pp. 986–987, 1990.

[245] Estabrook F.B., Wahlquist H.D., "The Geometric Approach to Sets of Ordinary Differential Equations and Hamiltonian Dynamics," *SIAM Review*, vol. 17, no. 2, pp. 201–220, 1975.

[246] Falzarano J.M., Shaw S.W., Troesch A.W., "Application of Global Methods for Analyzing Dynamical Systems to Ship Rolling Motion and Capsizing," *Int. J. Bifurcation and Chaos*, vol. 2, no. 1, pp. 101–115, 1992.

[247] Farmer J.D., Ott E., Yorke J.A., "The Dimension of Chaotic Attractors," *Physica D*, vol. 7, pp. 153–180, 1983.

[248] Farmer J.D., Sidorowich J.J., "Optimal Shadowing and Noise Reduction," *Physica D*, vol. 47, pp. 373–392, 1991.

[249] Farmer J.D., Sidorowich J.J., "Predicting Chaotic Time Series," *Phys. Rev. Lett.*, vol. 59, pp. 845–848, 1987.

[250] Feely O., Chua L.O., "Nonlinear Dynamics of a Class of Analog-To-Digital Converters," *Int. J. Bifurcation and Chaos*, vol. 2, no. 2, pp. 325–340, 1992.

[251] Feigenbaum M.J., "Quantitative Universality for a Class of Nonlinear Transformations," *J. Stat. Phys.*, vol. 19, no. 1, pp. 1–25, 1978.

[252] Feit S.D., "Characteristic Exponents and Strange Attractors," *Comm. Math. Phys.*, vol. 61, pp. 249–260, 1978.

[253] Fenichel N., "Geometric Singular Perturbation Theory for Ordinary Differential Equations," *J. of Differential Equations, 31*, pp. 53–98, 1979.

[254] Fike C.T., *Computer Evaluation of Mathematical Functions.* Englewood Cliffs, NJ: Prentice-Hall Inc., 1968.

[255] Fowler T.B., "Application of Stochastic Control Techniques to Chaotic Nonlinear Systems," *IEEE Trans. Automat. Contr.*, vol. 34, no. 2, pp. 201–205, 1989.

[256] Franceshetti D.R., Jones D.W., Campbell B.W., "Hamming Sets, Ising Sets, Cellular Automata, Neural Nets, and the Random Walk," *Am. J. Phys.*, vol. 61, no. 1, pp. 50–53, 1993.

[257] Frederickson P., Kaplan J.L., Yorke E.D., Yorke J.A., "The Lyapunov Dimension of Strange Attractors," *J. Diff. Equ.*, vol. 49, pp. 185–207, 1983.

[258] Freeman W.J., "Strange Attractors that Govern Mammalian Brain Dynamics shown by Trajectories of Electroencephalographic (EEG) Potential," *IEEE Trans. Circuits Syst.*, vol. 35, no. 7, pp. 781–783, 1988.

[259] Freire M., Franquelo L.G., Aracil J., "Periodicity and Chaos in an Autonomous Electronic System," *IEEE Trans. Circuits Syst.*, vol. CAS-31, no. 3, pp. 237–247, 1984.

[260] Friedman N.A., *Introduction to Ergodic Theory.* New York, NY: Van Nostrand Reinhold Co., 1970.

[261] Froyland J., "Some Symmetric, Two-Dimensional, Dissipative Maps," *Physica D*, vol. 8, pp. 423–434, 1983.

[262] Fujisaka H., Sato C., "An Algebraic Analysis for Bifurcation Problems," *Electronics and Communications in Japan, Part 3*, vol. 74, no. 9, pp. 22–32, 1991.

[263] Fujisaka H., Yamada T., *Prog. Theor. Phys.*, vol. 69, pp. 32–36, 1983.

[264] Fukushima K., Yamada T., Yazaki T., "Fluctuation Spectrum for a New type of Intermittency in a Coupled Electronic Circuit," *J. Phys. Soc. Japan*, vol. 59, no. 8, pp. 2659–2666, 1990.

[265] Gambart-Ducros D., Maral G., "An Efficient Algorithm Reduces Computing Time in Solving Stiff Ordinary Differential Equations," *IEEE Trans. Circuits Syst.*, vol. CAS-27, no. 9, pp. 747–755, 1980.

[266] Gambaudo J.-M., Procaccia I., Thomae S., Tresser C., "New Universal Scenarios for the Onset of Chaos in Lorenz-Type Flows," *Phys. Rev. Lett.*, vol. 57, no. 8, pp. 925–928, 1986.

[267] Gardini L., Abraham R., Record R.J., Fournier-Prunaret D., "A Double Logistic Map," *Int. J. Bifurcation and Chaos*, vol. 4, no. 1, pp. 145–176, 1994.

[268] Gardner F.M., *Phaselock Techniques*. New York, NY: Wiley, 1966.

[269] Geist K., Parlitz U., Lauterborn W., "Comparison of Different Methods for Computing Lyapunov Exponents," *Progr. Theor. Phys.*, vol. 83, no. 5, pp. 875–893, 1990.

[270] Genchev Z.D., Ivanov Z.G., Todorov B.N., "Effect of a Periodic Perturbation on Radio Frequency Model of Josephson Junction," *IEEE Trans. Circuits Syst.*, vol. CAS-30, no. 9, pp. 633–636, 1983.

[271] Genesio R., Tesi A., "A Harmonic Balance Approach for Chaos Prediction: Chua's Circuit," *Int. J. Bifurcation and Chaos*, vol. 2, no. 1, pp. 61–79, 1992.

[272] Genesio R., Tesi A., "Chaos Prediction in Nonlinear Feedback Systems," *IEE Proc. D*, vol. 138, no. 4, pp. 313–320, 1991.

[273] Genesio R., Tesi A., "Harmonic Balance Methods for the Analysis of Chaotic Dynamics in Nonlinear Systems," *Automatica*, vol. 28, no. 1, pp. 521–548, 1992.

[274] Genesio R., Tesi A., "On Limit Cycles in Feedback Polynomial Systems," *IEEE Trans. Circuits Syst.*, vol. 35, no. 12, pp. 1523–1526, 1988.

[275] Genesio R., Tesi A., Villoresi F., "A Frequency Approach for Analyzing and Controlling Chaos in Nonlinear Circuits," *IEEE Trans. Circuits Syst.—I: Fund. Theory and Appl.*, vol. 40, no. 11, pp. 819–828, 1993.

[276] Germond A., "Computation of Ferroresonant Overvoltages in Actual Power Systems by Galerkin's Method," *IEEE PICA Conf.* New Orleans, LA, 1975.

[277] Gil S., Gupta S.C., "First-Order Discrete Phase-Locked Loop with Applications to Demodulation of Angle-Modulated Carrier," *IEEE Trans. Commun.*, vol. 20, pp. 454–462, 1972.

[278] Gil S., Gupta S.C., "On Higher Order Discrete Phase-Locked Loops," *IEEE Trans. Aerosp. Electron. Syst.*, vol. 8, pp. 615–623, 1972.

[279] Glendinning P., *Stability, Instability and Chaos: An Introduction to the Theory of Nonlinear Differential Equations.* Cambridge Texts in Applied Mathematics, Cambridge: Cambridge University Press, 1994.

[280] Glendinning P., Sparrow C., "Local and Global Behaviour near Homoclinic Orbits," *J. Stat. Phys.*, vol. 35, pp. 645–697, 1984.

[281] Gluskin E., "The Internal Resonance Relations in the Pause States of a Nonlinear *LCR* Circuit," *Phys. Lett. A*, vol. 175, pp. 121–132, 1993.

[282] Goedhart D., Van de Plassche R., Stikvoort E., "Digital-to-Analog Conversion in playing a Compact Disc," *Phillips Tech. Rev.*, vol. 40, , pp. 174–179, 1982.

[283] Goetz A., *Introduction to Differential Geometry.* Reading, MA: Addison-Wesley, 1970.

[284] Goffmann C., *Calculus of Several Variables.* New York, NY: Harper & Row, 1965.

[285] Goffmann C., *Introduction to Real Analysis.* New York, NY: Harper & Row, 1967.

[286] Goldberger A.L., Rigney D.R., West B.J., "Chaos and Fractals in Human Physiology," *Scientific American*, pp. 34–41, 1990.

[287] Goldstein H., *Classical Mechanics.* Reading, MA: Addison-Wesley, 1980.

[288] Goldstein L.J., *Abstract Algebra: A First Course.* Englewood Cliffs, NJ: Prentice-Hall, 1973.

[289] Gollub J.P., Brunner T.O., Danly B.G., "Periodicity and Chaos in Coupled Nonlinear Oscillators," *Science*, vol. 200, no. 7, pp. 48–50, 1978.

[290] Golub G.H., Van Loan C.F., *Matrix Computations.* Second Edition, Baltimore: Johns Hopkins University Press, 1989.

[291] Gonchenko S.V., Shil'nikov L.P., Turaev D.V., "Models with nonrough Poincaré Homoclinic Curves," *Phys. D*, vol. 62, pp. 1–14, 1993.

[292] Graeme J.G., *Applications of Operational Amplifiers: Third-Generation Techniques.* The Burr-Brown Electronics Series, Tokyo: McGraw-Hill, 1973.

[293] Graeme J.G., Tobey G.E., Huelsman L.P., *Operational Amplifiers: Design and Applications.* The Burr-Brown Electronics Series, Tokyo: McGraw-Hill, 1971.

[294] Graf R.F., *The Modern Oscillator Circuit Encyclopedia.* Blue Ridge Summit, PA: Tab Books, 1976.

[295] Grafton R.G.T., "Algorithm As 157: the Run-Up and Run-Down Tests," *Applied Statistics*, vol. 30, pp. 81–85, 1982.

[296] Grassberger P., Procaccia I., "Characterization of Strange Attractors," *Phys. Rev. Lett.*, vol. 50, no. 5, pp. 346–349, 1983.

[297] Grassberger P., Schreiber T., Schaffrath C., "Nonlinear Time Sequence Analysis," *Int. J. Bifurcation and Chaos*, vol. 1, pp. 521–547, 1992.

[298] Gray R.M., Chou W., Wong P.-W., "Quantization Noise in Single-Loop Sigma-Delta Modulation with Sinusoidal Inputs," *IEEE Trans. Commun.*, vol. COM-37, pp. 956–968, 1989.

[299] Grebogi C., Ott E., "Fractal Basin Boundaries, Long-Lived Chaotic Transients, and Unstable-Unstable Pair Bifurcation," *Phys. Rev. Lett.*, vol. 50, no. 13, pp. 935–938, 1983.

[300] Grebogi C., Ott E., Yorke J.A., "Unstable Periodic Orbits and the Dimension of Multifractal Chaotic Attractors," *Phys. Rev. A*, vol. 37, no. 5, pp. 1711–1724, 1988.

[301] Grebogi C., Ott E., Yorke J.A., "Chaotic Attractors in Crisis," *Phys. Rev. Lett.*, vol. 48, no. 22, pp. 1507–1510, 1982.

[302] Grebogi C., Ott E., Yorke J.A., "Crises, Sudden Changes in Chaotic Attractors, and Transient Chaos," *Physica D*, vol. 7, pp. 181–200, 1983.

[303] Green D.N., "Global Stability Analysis of Automatic Gain Control Circuits," *IEEE Trans. Circuits Syst.*, vol. CAS-30, no. 2, pp. 78–83, 1983.

[304] Green M.M., Willson A.N., "How to Identify Unstable DC Operating Points," *IEEE Trans. Circuits Syst.—I: Fund. Theory and Appl.*, vol. 39, no. 10, pp. 820–823, 1993.

[305] Greenside H.S., Wolf A., Swift J., Pignataro T., "Impracticality of a Box-Counting Algorithm for Calculating the Dimensionality of Strange Attractors," *Phys. Rev. A*, vol. 25, no. 6, pp. 3453–3456, 1982.

[306] Greenspan B.D., Holmes P.J., *Homoclinic Orbits, Subharmonics and Global Bifurcations in Forced Oscillations.* Nonlinear Dynamics and Turbulence, Barenblatt G.I., Iooss G., Joseph D.D., Eds., Marshfield, MA: Pitman, 1983.

[307] Grimshaw R., *Nonlinear Ordinary Differential Equations.* Applied Mathematics and Engineering Science Texts, Oxford: Blackwell Scientific Publ., 1990.

[308] Grobman D., "Homeomorphisms of Systems of Differential Equations," *Dokl. Akad. Nauk.*, vol. 128, pp. 880-881, 1959.

[309] Grossmann S., Schnedler E. Thomae S., *Ergodicity and Entrainment in a System of Electrical Relaxation Oscillators.* Annalen der Physik, 7 Folge, Band 42, Heft 3, pp. 307–318, 1985.

[310] Gruendler J., Thesis, Department of Mathematics, Univeristy of North Carolina, 1981.

[311] Guckenheimer J., "Computational Environments for Exploring Dynamical Systems," *Int. J. Bifurcation and Chaos.*, vol. 1, no. 2, pp. 269–276, 1991.

[312] Guckenheimer J., "Dynamics of the Van der Pol Equation," *IEEE Trans. Circuits Syst.*, vol. CAS-27, no. 11, pp. 983–989, 1980.

[313] Guckenheimer J., "Symbolic Dynamics and Relaxation Oscillations," *Physica D*, vol. 1, pp. 227–235, 1980.

[314] Guckenheimer J., Holmes P., *Nonlinear Oscillations, Dynamical Systems, and Bifurcations of Vector Fields.* New York, NY: Springer-Verlag, 1983.

[315] Guevara M.R., Glass L., Mackey M.C., Shrier A., "Chaos in Neorobiology," *IEEE Trans. Systems, Man and Cybernetics*, vol. SMC-13, no. 5, pp. 790–798, 1983.

[316] Gumowski I., Mira C., *Dynamique Chaotique.* Cepadues Editions, 1980.

[317] Gunaratne G.H., Linsay P.S., Vinson M.J., "Chaos Beyond Onset: a Comparison of Theory and Experiment," *Phys. Rev. Lett.*, vol. 63, no. 1, pp. 1–4, 1989.

[318] Gusev Ye.A., Karpel'son A.Ye., "The Concept of Deterministic Chaos and Problems of Nondestructive Testing," *Originally Published in Tekhnicheskaya Kibernetika*, no. 6, pp. 157–164, 1989.

[319] Gutzwiller M.C., "Quantum Chaos," *Scientific American*, pp. 26–32, 1992.

[320] Hadamard J., "Les surfaces à courbures opposés et leur lignes géodésiques," *J. Math. Pures Appl.*, vol. 4/5, pp. 27–73, 1981.

[321] Hajj I., Skelboe S., "Steady-State Analysis of Piecewise-Linear Dynamical Systems," *IEEE Trans. Circuits Syst.*, vol. CAS-28, no. 3, pp. 234–242, 1981.

[322] Haken H., "At least one Lyapunov Exponent vanishes if the Trajectory of an Attractor does not contain a Fixed Point," *Phys. Lett. A*, vol. 94, no. 2, pp. 71–72, 1983.

[323] Hale J.K., *Ordinary Differential Equations.* New York: Krieger, 1980.

[324] Halle K.S., Wu C.W., Itoh M., Chua L.O., "Spread Spectrum Communication through Modulation of Chaos," *Int. J. Bifurcation and Chaos*, vol. 3, no. 2, pp. 469–477, 1993.

[325] Halmos P.R., *Measure Theory.* Princeton, NJ: D. Van Nostrand Co., 1950.

[326] Hamill D.C., "Learning about Chaotic Circuits with Spice," *IEEE Trans. Education*, vol. 36, no. 1, pp. 28–35, 1993.

[327] Hamill D.C., Deane J.H.B., Jefferies D.J., "Modeling of Chaotic DC-DC Converters by Iterated Nonlinear Mappings," *IEEE Trans. Power Electronics*, vol. 7, no. 1, pp. 25–35, 1992.

[328] Hamill D.C., Jeffries D.J., "Subharmonics and Chaos in a Controlled Switched-Mode Power Converter," *IEEE Trans. Circuits Syst.*, vol. 35, no. 8, pp. 1059–1061, 1988.

[329] Hammel S.M., "A Noise Reduction Method for Chaotic Systems," *Phys. Lett. A*, vol. 148, no. 8,9, pp. 421–428, 1990.

[330] Handley J.W., Jaenisch H.M., Bjork C.A., Richardson L.T., Carruth R.T., "Chaos and Fractal Algorithms Applied to Signal Processing and Analysis," *Simulation*,vol. 60, no. 4, pp. 261–278, 1993.

[331] Hanselman D., Littlefield B., *The Student Edition of Matlab: Version 4 User's Guide.* Englewood Cliffs, NJ: Prentice-Hall Inc., 1995.

[332] Hao B.-L. (ed.), *Chaos.* Singapore: World Scientific, 1984.

[333] Hao B.-L. (ed.), *Chaos II.* Singapore: World Scientific, 1990.

[334] Hardy G.H., Littlewood J.E., Pólya G., *Inequalities.* Cambridge: Cambridge University Press, 1959.

[335] Harth E., "Order and Chaos in Neural Systems: an Approach to the Dynamics of Higher Brain Functions," *IEEE Trans. Systems, Man, and Cybernetics*, vol. SMC-13, no. 5, pp. 782–789, / 1983.

[336] Hartman P., "A Lemma on the Theory of Structural Stability of Differential Equations," *Proc. Amer. Math. Soc.*, vol. 11, pp. 610–620, 1960.

[337] Hartman P., "On the Local Linearization of Differential Equations," *Proc. AMS*, vol. 14, pp. 568–573, 1963.

[338] Hartman P., *Ordinary Differential Equations.* New York, NY: John Wiley & Sons, 1964.

[339] Hasler M.J., "Electrical Circuits with Chaotic Behavior," *Proc. IEEE*, vol. 75, no. 8, pp. 1009–1021, 1987.

[340] Hasler M.J., Verburgh P., "On the Uniqueness of the Steady State for Nonlinear Circuits with Time Dependent Sources," *IEEE Trans. Circuits Syst.*, vol. CAS-31, no. 8, pp. 702–713, 1984.

[341] Hassard B.D., Kazarinoff N.D., *Theory and Applications of the Hopf Bifurcation*. Cambridge: Cambridge University Press, 1981.

[342] Hassard B.D., Wan Y.-H., "Bifurcation Formulae Derived from Center Manifold Theory," *J. Math. Anal. Appl.*, vol. 63, pp. 297–312, 1978.

[343] Hata M., "Euler's Finite Difference Scheme and Chaos in $\mathbf{R}^n$," *Proc. Japan Acad.*, vol. 58(a), pp. 178–181, 1982.

[344] Hawksford M.O.J., "Chaos, Oversampling, and Noise Shaping in Digital-To-Analog Conversion," *J. Audio Eng. Socl.* vol. 37, no. 12, pp. 980–1001, 1989.

[345] Hayashi C., *Nonlinear Oscillations in Physical Systems*. New York, NY: McGraw-Hill, 1964.

[346] Hausdorff F., "Dimension und Auβeres Maβ," *Math. Anallen*, vol. 79, pp. 157–179, 1918.

[347] Hayes S., Grebogi C., Ott E., "Communicating with Chaos," *Phys. Rev. Lett.*, vol. 70, no. 20, pp. 3031–3034, 1993.

[348] Haykin S., *Adaptive Filter Theory*. Second Edition, Englewood Cliffs, NJ: Prentice-Hall Inc., 1991.

[349] Haykin S., *Communication Systems*. Second Edition, Toronto, Canada: Wiley, 1983.

[350] Heidemann G., Bode M., Purwins H.-G., "Fronts Between Hopf- and Turing-Type Domains in a Two-Component Reaction-Diffusion System," *Phys. Lett. A*, vol. 177, pp. 225–230, 1993.

[351] Helleman R.H.G., "Self-Generated Chaotic Behaviour in Non-Linear Mechanics," *In Fundamental Problems in Statistical Mechanics*, vol. 5, pp. 165–233, 1980.

[352] Helton J.W., "Systems with Infinite-Dimensional State Space: the Hilbert Space Approach," *Proc. IEEE*, vol. 64, no. 1, pp. 145–160, 1976.

[353] Hermes H., "A Survey of Recent Results in Differential Equations," *SIAM Review*, vol. 15, no. 2, pp. 453–468, 1973.

[354] Higuchi T., "Approach to an Irregular Time Series on the Basis of the Fractal Theory," *Physica D*, vol. 31, pp. 277–283, 1988.

[355] Hilborn R.C., "Quantitative Measurement of the Parameter Dependence of the Onset of a Crisis in a Driven Nonlinear Oscillator," *Phys. Rev. A*, vol. 31, no. 1, pp. 378–382, 1985.

[356] Hinch E.J., *Perturbation Methods.* Cambridge: Cambridge University Press, 1991.

[357] Hirai K., Chinen H., "A Synthesis of a Nonlinear Discrete-Time System Having a Periodic Solution," *IEEE Trans. Circuits Syst., Vol CAS-29*, no. 8, pp. 574–577, 1982.

[358] Hirsch M.W., *Differential Topology.* New York, NY: Springer-Verlag, 1976.

[359] Hirsch M.W., Pugh C.C., Shub M., *Invariant Manifolds.* New York, NY: Springer-Verlag, 1977.

[360] Hirsch M.W., Smale S., *Differential Equations, Dynamical Systems, and Linear Algebra.* New York, NY: Academic Press, 1974.

[361] Hockett K., Holmes P., "Nonlinear Oscillators, Iterated Maps, Symbolic Dynamics, and Knotted Orbits," *Proc. IEEE*, vol. 75, no. 8, pp. 1071–1080, 1987.

[362] Holmes P., "Averaging and Chaotic Motions in Forced Oscillations," *SIAM. J. Appl. Math.*, vol. 38, pp. 68–80 and vol. 40, pp. 167–168, 1980.

[363] Holmes P., Marsden J., "A Partial Differential Equation with Infinitely Many Periodic Orbits: Chaotic Oscillations of a Forced Beam," *Arch. Rat. Mech. Anal.*, vol. 76, no. 2, pp. 135–166, 1981.

[364] Holmes P.J., Moon F.C., "Strange Attractors and Chaos in Nonlinear Mechanics," *J. Applied Mechanics*, vol. 50, pp. 1021–1032, 1983.

[365] Holmgren R.A., *A First Course in Discrete Dynamical Systems.* New York, NY: Springer-Verlag, 1994.

[366] Hoover W.G., Posch H.A., "Direct Measurement of Lyapunov Exponents," *Phys. Lett. A*, vol. 113, no. 2, pp. 82–84, 1985.

[367] Hsu C.S., "A Theory of Cell-To-Cell Mapping Dynamical Systems," *J. Appl. Mech.*, vol. 47, pp. 931–939, 1980.

[368] Hsu C.S., Cheng W.H., "Steady-State Response of a Non-Linear System Under Impulsive Periodic Parametric Excitation," *J. of Sound and Vibration*, vol. 50, no. 1, pp. 95–116, 1977.

[369] Hsu I.-D., "Existence of Periodic Solutions for the Belousov-Zaikin- Zhabotinskii Reaction by a Theorem of Hopf," *J. of Differential Equations*, vol. 20, pp. 339–403, 1976.

[370] Hua X.-J., Gilmore R., Mindlin G.B., Solari H.G., "An Efficient Algorithm for Fast O(N*ln(N)) Box Counting," *Phys. Lett. A.*, vol. 151, no. 1,2, pp. 43–46, 1990.

[371] Huang J.C., Chin C.H., Lee P.S., Yao Y.H., Gou Y.S., "The Computer-Assisted Study of Routes to Chaos in the Current- Driven Josephson Junction," *Chinese J. Phys.*, vol. 22, no. 3, pp. 53–93, 1984.

[372] Huang Y., Huang J.C., Gou Y.S., "Physical Properties of Transition to Chaos in RF-Driven Josephson Junction Analog," *J. Low Temp. Phys.*, vol. 63, Nos. 3/4, pp. 287–295, 1986.

[373] Hudgins J.L., "A Review of Modern Power Semiconductor Devices," *Microelectronics J.*, vol. 24, pp. 41–54, 1993.

[374] Hudson J.L., Rossler O.E., Killory H.C., "Chaos in a Four-Variable Piecewise-Linear System of Differential Equations," *IEEE Trans. Circuits Syst.*, vol. 35, pp. 902–908, 1989.

[375] Huertas J.L., Chua L.O., Rodriguez-Vazquez A.B., Rueda A., "Nonlinear Switched-Capacitor Networks: Basic Principles and Piecewise-Linear Design," *IEEE Trans. Circuits Syst.*, vol. CAS-32, no. 4, pp. 305–319, 1985.

[376] Hunt E.R., *Comment on a Driven Nonlinear Oscillator.* Phys. Rev. Lett., vol. 49, no. 14, p. 1054, 1982.

[377] Hunt E.R., *High-Period Orbits Stabilized in the Diode Resonator.* Proc. 1st Experimental Chaos Conference, Arlington, Virginia, eds. Vohra S., Spano M., Shlesinger M., Pecora L., Ditto W., 1991.

[378] Hunt E.R., "Stabilizing High-Period Orbits in a Chaotic System: the Diode Resonator," *Phys. Rev. Lett.*, vol. 67, no. 15, pp. 1953–1955, 1991.

[379] Hunt E.R., Johnson G., "Keeping Chaos at Bay," *IEEE Spectrum*, pp. 32–36, 1993.

[380] Hunt E.R., Rollins R.W., "Exactly Solvable Model of a Physical System Exhibiting Multidimensional Chaotic Behavior," *Phys. Rev. A*, vol. 29, no. 2, pp. 1000–1002, 1984.

[381] Hutchison J., Lee F.F., "Some Notes on Practical FDNR Filters," *IEEE Trans. Circuits Syst.*, vol. CAS-28, no. 3, pp. 242–???, 1981.

[382] Hénon M., "A two-dimensional Mapping with a Strange Attractor," *Commun. Math. Phys.*, vol. 50, pp. 69–77, 1976.

[383] Ikeda K., Daido H., "Optical Turbulence: Chaotic Behaviour of Transmitted Light from a Ring Cavity," *Phys. Lett. Rev.*, vol. 45, no. 9, pp. 709–712, 1980.

[384] Ikezi H., deGrassie J.S., Jensen T.H., "Observation of Multiple-Valued Attractors and Crises in a Driven Nonlinear Circuit," *Phys. Rev. A*, vol. 28, pp. 1207–1209, 1983.

[385] Inaba N., Mori S., "Chaos via Torus Breakdown in a Piecewise-Linear Forced Van der Pol Oscillator with a Diode," *IEEE Trans. Circuits Syst.*, vol. 38, no. 5, pp. 398–409, 1991.

[386] Inaba N., Mori S., "Folded Torus in the Forced Rayleigh Oscillator with a Diode Pair," *IEEE Trans. Circuits Syst.—I: Fund. Theory and Appl.*, vol. 39, no. 5, pp. 402–411, 1992.

[387] Inose H., Yasuda Y., "A Unity Bit Coding Method by Negative Feedback," *Proc. IEEE*, vol. 51, pp. 1524–1535, 1963.

[388] Iooss G., *Bifurcation of Maps and Applications.* North-Holland, Amsterdam, 1979.

[389] Iooss G., Adelmeyer M., *Topics in Bifurcation Theory and Applications.* Advanced Series in Nonlinear Dynamics, Singapore: World Scientific, 1992.

[390] Iooss G., Joseph D.D., *Elementary Stability and Bifurcation Theory.* New York, NY: Springer-Verlag, 1980.

[391] Irwin M.C., *Smooth Dynamical Systems.* New York, NY: Academic Press, 1980.

[392] Isidori A., *Nonlinear Control Systems.* Second Edition, Berlin: Springer-Verlag, 1989.

[393] Ito K., "Periodicity and Chaos in Great Earthquake Occurrence," *J. Geophys. Research*, vol. 85, no. B3, pp. 1399–1408, 1980.

[394] Ito K., Oono Y., Yamazaki H., Hirakawa K., "Chaotic Behavior in Great Earthquakes-Coupled Relaxation Oscillator Model, Billiard Model and Electronic Circuit Model," *J. Phys. Soc. Japan*, vol. 49, no. 1, pp. 43–52, 1980.

[395] Ito S., Tanaka S., Nakada H., "On Unimodal Linear Transformations and Chaos II," *Tokyo J. Math.*, vol. 2, no. 2, pp. 241–259, 1979.

[396] Jackson E.A., "The Entrainment and Migration Controls of Multiple-Attractor Systems," *Phys. Lett. A.* vol. 151, no. 9, pp. 478–484, 1990.

[397] Janssen H.J., Beerden L., Flerackers E.L.M., "An Experimental Look at the Resonant Behaviour of a Nonlinear *LC* Circuit," *Eur. J. Phys.*, vol. 5, pp. 94–100, 1984.

[398] Janssens H., *Hysteresis Magnetique et Ferroresonance Modeles Mathematiques et Application aux Reseaux de Puissance.* PhD Thesis, University of Louvain, Louvain, Belgium, 1981.

[399] Jefferies D.J., "Bifurcation to Chaos in Clocked Digital Systems Containing Autonomous Timing Circuits," *Phys. Lett.*, vol. 115, no. 3, pp. 89–92, 1986.

[400] Jefferies D.J., Deane J.H.B., Johnstone G.G., "An Introduction to Chaos," *Elect. & Comm. Eng. J.*, pp. 115–123, / 1989.

[401] Jeffery R.L., *The Theory of Functions of a Real Variable.* Toronto, Ontario: Dover, 1985.

[402] Jeffries C., Perez J., "Direct Observation of Crises of the Chaotic Attractor in a Nonlinear Oscillator," *Phys. Rev. A*, vol. 27, no. 1, pp. 601–603, 1983.

[403] Jeffries C., Perez J., "Observation of a Pomeau-Manneville Intermittent Route to Chaos in Nonlinear Oscillator," *Phys. Rev. A*, vol. 26, no. 4, pp. 2117–2122, 1982.

[404] Jeffries C., Wiesenfeld K., "Observation of Noisy Precursors of Dynamic Instabilities," *Phys. Rev. A*, vol. 31, no. 2, pp. 1077–1084, 1985.

[405] Jeffries C.D., "Chaotic Dynamics of Instabilities in Solids," *Physica Scripta*, vol. T9, pp. 11–26, 1985.

[406] Jimenez A.J., Director S.W., "New Families of Algorithms for Solving Nonlinear Circuit Equations," *IEEE Trans. Circuits Syst.*, vol. CAS-25, no. 1, pp. 1–6, 1978.

[407] Johnson C.R., "Adaptive IIR Filtering: Current Results and Open Issues," *IEEE Trans. Inform. Theory*, vol. It-30, pp. 237–250, 1984.

[408] Johnston G.A., Hunt E.R., "Derivative Control of the Steady State in Chua's Circuit Driven in the Chaotic Region," *IEEE Trans. Circuits Syst.—I: Fund. Theory and Appl.*, vol. 40, no. 11, pp. 833–835, 1993.

[409] Jones M.C., Lotwick H.L., "A Remark on Algorithm As 176. Kernel Density Estimation using the Fast Fourier Transform," *Royal Statistical Soc. (Series C), Applied Statistics*, vol. 33, pp. 120–122, 1984.

[410] Jordan D.W., Smith P., *Nonlinear Ordinary Differential Equations.* Second Edition, Oxford Applied Mathematics and Computing Science Series, Oxford: Clarendon Press, 1987.

[411] Judd K., Mees A.I., "Estimating Dimensions with Confidence," *Int. J. Bifurcation and Chaos*, vol. 1, no. 2, pp. 467–470, 1991.

[412] Kahlert C., "Globale Aspekte Homokliner Bahnen," *AEÜ*, vol. 46, no. 4, pp. 266–273, 1992.

[413] Kahlert C., "The Chaos Producing Mechanism in Chua's Circuit and Related Piecewise-Linear Dynamical Systems," *Proc. 1987 European Conference on Circuit Theory and Design, Paris*, pp. ??–??, 1987.

[414] Kalman R.E., "Nonlinear Aspects of Sampled-Data Control Systems," *Proc. Symp. on Nonlinear Circuit Analysis*, vol. 6, pp. 273–312, 1956.

[415] Kaneko K., "On the Period-Adding Phenomena At the Frequency Locking in a One Dimensional Mapping," *Prog. Theor. Phys.*, vol. 68, no. 2, pp. 669–672, 1982.

[416] Kaneko K., "Transition of Torus to Chaos Accompanied by Frequency Locking with Symmetry Breaking," *Prog. Theor. Phys.*, vol. 69, no. 5, 1983, pp. 1427–1442, 1983.

[417] Kanwal R.P., *Generalized Functions: Theory and Technique.* Mathematics in Science and Engineering, vol. 171, New York, NY: Academic Press, 1983.

[418] Kapitaniak T., Kocarev LJ., Chua L.O., "Controlling Chaos without Feedback and Control Signals," *Int. J. Bifurcation and Chaos*, vol. 3, no. 2, pp. 459–468, 1993.

[419] Katok A. (ed.), *Ergodic Theory and Dynamical Systems II.* Boston, MA: Birkhäuser, 1982.

[420] Kawakami H., "Bifurcation of Periodic Responses in Forced Dynamic Nonlinear Cir- Cuits: Computation of Bifurcation Values of the System Parameters," *IEEE Trans. Circuits Syst.*, vol. CAS-31, pp. 248–260, 1984.

[421] Kearney M.J., Stark J., "An Introduction to Chaotic Signal Processing," *GEC J. of Research*, vol. 10, no. 1, pp. 52–58, 1992.

[422] Keener J.P., "Analog Circuitry for the Van der Pol and Fitzhugh-Nagumo Equations," *IEEE Trans. on Systems, Man, and Cybernetics*, vol. SMC-13, no. 5, pp. 1010–1014, 1983.

[423] Keener J.P., "Chaotic Behavior in Piecewise-Linear Difference Equations," *Trans. Am. Math. Soc.*, vol. 261, pp. 589–604, 1980.

[424] Keener J.P., *Principles of Applied Mathematics: Transformation and Approximation.* Reading, MA: Addison-Wesley, 1988.

[425] Kelley A., "The Stable, Center Stable, Center, Center Unstable, Unstable Manifolds," *J. Diff. Equ.*, vol. 3, pp. 546–570, 1967.

[426] Kelley A., "The Stable, Center-Stable, Center, Center-Unstable and Unstable Manifolds," Abraham R., Robbin J., eds., *Transversal Mappings and Flows*, New York, NY: Benjamin, Appendix C, pp. 134–154, 1967.

[427] Kennedy M.P., "Three Steps to Chaos," *Trans. Circuits Syst.*, vol. 40, no. 10, pp. 657–674, 1993.

[428] Kennedy M.P., "Experimental Chaos via Chua's Circuit," *Proc. 1st Experimental Chaos Conference*, Arlington, Virginia, eds. Vohra S., Spano M., Shlesinger M., Pecora L., Ditto W., 1991.

[429] Kennedy M.P., "Robust Op-Amp Realization of Chua's Circuit," *Frequenz*, vol. 46, pp. 66–80, 1992.

[430] Kennedy M.P., Chua L.O., "Van der Pol and Chaos," *IEEE Trans. Circuits Syst.*, vol. CAS-33, no. 10, pp. 974–980, 1986.

[431] Kennedy M.P., Dedieu H., *Experimental Demonstration of Binary Chaos—Shift Keying using Self-Synchronising Chua's Circuits.* Preprint, 1992.

[432] Kennedy M.P., Krieg K.R., Chua L.O., "The Devil's Staircase: The Electrical Engineer's Fractal," *Trans. Circuits Syst.*, vol. 36, no. 8, pp. 1133–1139, 1989.

[433] Ketema Y., "A Physical Interpretation of Melnikov's Method," *Int. J. Bifurcation and Chaos*, vol. 2, no. 1, pp. 1–9, 1992.

[434] Ketema Y., "An Oscillator with Cubic and Piecewise-Linear Springs," *Int J. Bifurcation and Chaos*, vol. 1, no. 2, pp. 349–356, 1991.

[435] Kim S.-Y., Kook H., "Renormalization Analysis of Two Coupled Maps," *Phys. Lett. A*, vol. 178, no. 3,4, pp. 258–264, 1993.

[436] Kirillov A.A., Gvishiani A.D., *Theorems and Problems in Functional Analysis.* New York, NY: Springer-Verlag, 1982.

[437] Klinker T., Meyer-Ilse W., Lauterborn W., "Period Doubling and Chaotic Behavior in a Driven Toda Oscillator," *Phys. Lett. A*, vol. 101, no. 8, pp. 371–375, 1984.

[438] Kluiving R., Capel H.W., "Phase-Transition-Like Phenomenon in a Piecewise Linear Map," *Physica A*, vol. 164, pp. 593–624, 1990.

[439] Kocarev L., Shang A., Chua L.O., "Transitions in Dynamical Regime by Drving: a Method of Control and Synchronisation of Chaos," *Int. J. Bifurcation and Chaos*, vol. 3, no. 2, pp. 479–483, 1993.

[440] Kocarev Lj., Chua L.O., "On Chaos in Digital Filters: Case $b = -1$," *IEEE Trans. Circuits Syst.*, vol. 40, no. 6, pp. 404–407, 1993.

[441] Kocarev Lj., Halle K.S., Eckert K., Chua L.O., "Experimental Demonstration of Secure Communication via Chaos Synchronization," *Int. J. Bifurcation and Chaos*, vol. 2, no. 3, pp. 709–713, 1992.

[442] Kohda T., Murao K., "Piecewise Polynomial Galerkin Approximation to Invariant Densities of One Dimensional Difference Equations," *Electronics and Communications in Japan*, vol. 65-A, no. 6, pp. 1–11, 1982.

[443] Kohda T., Shitanda K., "Time-Correlation Functions of Chaotic Solutions Observed in a Certain Class of Piecewise-Linear Difference Equations," *Electronics and Communications in Japan*, vol. 66-A, no. 8, pp. 16–25, 1983.

[444] Kolmogorov A.N., "A New Invariant for Transitive Dynamical Systems," *Dokl. Akad. Nauk SSSR*, vol. 119, pp. 861–864, 1958.

[445] Kopell N., Washburn R.B., "Chaotic Motions in the Two-Degree-Of-Freedom Swing Equations," *IEEE Trans. Circuits Syst.*, vol. CAS-29, no. 11, pp. 738–746, 1982.

[446] Kostelich E.J., Grebogi C., Ott E., Yorke J.A., "Higher-Dimensional Targeting," *Phys. Rev. E.*, vol. 47, no. 1, pp. 305–310, 1993.

[447] Kouda A., Mori S., "Analysis of a Ring of Mutually Coupled Van der Pol Oscillators with Coupling Delay," *IEEE Trans. Circuits Syst.*, vol. CAS-28, no. 3, pp. 247–253, 1981.

[448] Kovacs Z., Tel T., "Scaling in Multifractals: Discretization of an Eigenvalue Problem," *Phys. Rev. A*, vol. 40, no. 8., pp. 4641–4646, 1989.

[449] Kowalski J.M., Albert G.L., Rhoades B.K., Gross G.W., "Neural Networks with Spontaneous, Correlated Bursting Activity: Theory and Simulations," *Neural Networks*, vol. 5, no. 5, pp. 805–822, 1992.

[450] Kreyszig E., *Introduction to Functional Analysis with Applications*. New York, NY: John Wiley & Sons, 1978.

[451] Kriegsmann G.A., "The Rapid Bifurcation of the Wien Bridge Oscillator," *IEEE Trans. Circuits Syst.*, vol. CAS-34, no. 9, pp. 1093–1096, 1987.

[452] Krylov N., Bogoliubov N., *Introduction to Nonlinear Mechanics*. Princeton: Princeton University Press, 1949.

[453] Kullstam P.A., "Heaviside's Operational Calculus: Oliver's Revenge," *IEEE Trans. Education*, vol.34, no. 2, pp. 155–166, 1991.

[454] Kunick A., Steeb W.-H., "Coupled Chaotic Oscillators," *J. Phys. Soc. Japan*, vol. 54, no. 4, pp. 1220–1223, 1985.

[455] Kuo B.C., *Automatic Control Systems*. Sixth Edition, Englewood Cliffs, NJ: Prentice-Hall Inc., 1991.

[456] Kuszta B., Bailey J.E., "Nonlinear Model Identification by Analysis of Feedback-Stimulated Bifurcation," *IEEE Trans. Automat. Contr.*, vol. AC-27, no. 1, pp. 227–228, 1982.

[457] Kwatny H.G., Pasrija A.K., Bahar L.Y., "Static Bifurcation in Electric Power Networks: Loss of Steady-State Stability and Voltage Collapse," *IEEE Trans. Circuits Syst.*, vol. CAS-33, no. 10, pp. 981–986, 1986.

[458] Kwatny H.G., Piper G.E., "Frequency Domain Analysis of Hopf Bifurcations in Electrical Power Networks," *IEEE Trans. Circuits Syst.*, vol. 37, no. 10, pp. 1317–1321, 1990.

[459] Lai Y-C., Grebogi C., "Synchronization of Chaotic Trajectories using Control," *Phys. Rev. E*, vol. 47, no. 4, pp. 2357–2360, 1993.

[460] Lai Y-C., Grebogi C., Tél T., *Controlling Transient Chaos in Dynamical Systems.* Towards the Harnessing of Chaos - Proc. of the 7-th Toyota Conference, Lake Hamana, Japan, ed. M. Yamaguchi, Elsevier, 1993.

[461] Lai Y-C., Ding M., Grebogi C., "Controlling Hamiltonian Chaos," *Phys. Rev. E*, vol. 47, no. 1, pp. 86–92, 1993.

[462] Lai Y-C., Tél T., Grebogi C., "Stabilizing Chaotic-Scattering Trajectories using Control," *Phys. Rev. E*, vol. 48, no. 2, pp. 709–717, 1993.

[463] Landau I.D., "A Survey of Model Reference Adaptive Techniques—Theory and Applications," *Automatica*, vol. 10, pp. 353–379, 1974.

[464] Landau I.D., "Unbiased Recursive Identification using Model Reference Adaptive Techniques," *IEEE Trans. Automat. Contr.*, vol. AC-21, no. 2, pp. 194–202, 1976.

[465] Lang S., *Analysis I.* Reading, MA: Addison-Wesley, 1969.

[466] Lang S., *Linear Algebra.* Reading, MA: Addison-Wesley, 1967.

[467] Lasota A., Mackey M.C., *Chaos, Fractals, and Noise: Stochastic Aspects of Dynamics.* New York, NY: Springer-Verlag, 1994.

[468] Lasota A., Yorke J.A., "On the Existence of Invariant Measure for Piecewise Monotonic Transformations (1)," *Trans. Amer. Math. Soc.*, vol. 186, pp. 481–488, 1973.

[469] Lathrop D.P, Kostelich E.J., "Characterization of an Experimental Strange Attractor by Periodic Orbits," *Phys. Rev. A*, vol. 40, pp. 4028–4031, 1989.

[470] Lauterborn W., Meyer-Ilse W., "Chaos," *Physik in Unserer Zeit, 17. Jabrg., Nr. 6*, pp. 177–187, 1986.

[471] Le Roux G.J., *Numerical Homoclinic Instabilities.* M.Sc Thesis, University of the Orange Free State, Bloemfontein, South Africa, 1993.

[472] Leakey D.M., "Chaos in Communications," *Telkom93 Proceedings*, Cape Town, Chapter 2, pp. 1–6, 1993.

[473] Leonov N.N., "Map of the Line into Itself," *Radiofisica*, vol. 2, pp. 942–956, 1959.

[474] Leonov N.N., "Piecewise Linear Map," *Radiofisica*, vol. 3, pp. 496–510, 1960.

[475] Lesurf J., "Chaos in Electronics," *Electronics World & Wireless World*, pp. 467–472, 1991.

[476] Levi M., Hoppensteadt F.C., Miranker W.L., "Dynamics of the Josephson Junction," *Quart. Appl. Math.*, pp. 167–198, 1978.

[477] Levin U.L., Narendra K.S., "Control of Nonlinear Dynamical Systems using Neural Networks: Controllability and Stabilization," *IEEE Trans. on Neural Networks*, vol. 4, no. 2, pp. 192–206, 1993.

[478] Levinsen M.T., "The Chaotic Oscilloscope," *Am. J. Phys.*, vol. 61, no. 2, pp. 155–158, 1993.

[479] Levinson N., "A Second Order Differential Equation with Singular Solutions," *Annals of Mathematics*, vol. 50, no. 1, pp. 127–153, 1949.

[480] Lewis J.E., Glass L., "Nonlinear Dynamics and Symbolic Dynamics of Neural Networks," *Neural Computation*, vol. 4, pp. 621–642, 1992.

[481] Li T.-Y., "Finite Approximation for Frobenius-Perron Operator. A Solution to Ulam's Conjecture," *J. Approx. Theory*, vol. 17, pp. 173–186, 1976.

[482] Li T.-Y., Yorke J.A., "Period Three Implies Chaos," *Amer. Math. Monthly*, vol. 82, pp. 985–992, 1975.

[483] Li T.Y., Yorke J.A., "Ergodic Transformation from an Interval into Itself," *Trans. Amer. Math. Soc.*, vol. 235, pp. 183–192, 1978.

[484] Lichtenberg A.J., Lieberman M.A., *Regular and Stochastic Motion*. New York, NY: Springer-Verlag, 1983.

[485] Lima R., Pettini M., "Suppression of Chaos by Resonant Parametric Perturbations," *Phys. Rev. A.*, vol 41, no. 2, pp. 726–733, 1990.

[486] Lin P.M., Chua L.O., "Topological Generation and Analysis of Voltage Multiplier Circuits," *IEEE Trans. Circuits Syst.*, vol. CAS-24, no. 10, pp. 517–530, 1977.

[487] Lin T., Chua L.O., "On Chaos of Digital Filters in the Real World," *IEEE Trans. Circuits Syst.*, vol. 38, no. 5, pp. 557–558, 1991.

[488] Lindsey W.C., Chie C.M., "A Survey of Digital Phase-Locked Loops," *Proc. IEEE*, vol. 69, pp. 410–431, 1981.

[489] Lindsey W.C., Chie C.M., "Performance Measures for Phase-Locked Loops–A Tutorial," *IEEE Trans. Commun.*, vol. COM-30, no. 10, pp. 2224–2227, 1982.

[490] Lindsey W.C., Dobrogowski A., Kantak A., "Mutual Synchronization Properties of a System of Two Oscillators with Sinusoidal Phase-Detectors," *IEEE Trans. Commun.*, vol. COM-24, pp. 1321–1326, 1976.

[491] Ling F.H., Schmidt G., Kook H., "Universal Behaviour of Coupled Nonlinear Oscillators," *Int. J. Bifurcation and Chaos*, vol. 1, no. 2, pp. 363–368, 1991.

[492] Linkens D.A., "The Stability of Entrainment Conditions for *RLC* Coupled Van der Pol Oscillators used as a Model for Intestinal Electrical Rhythms," *Bulletin of Math. Biol.*, vol. 39, pp. 359–372, 1977.

[493] Linsay P.S., "Period Doubling and Chaotic Behavior in a Driven Anharmonic Oscillator," *Phys. Rev. Lett.*, vol. 47, no. 19, pp. 1349–1352, 1981.

[494] Linsay P.S., Brailove A., "Experiments with Coupled Nonlinear Oscillators," *Proc. 1st Experimental Chaos Conference*, Arlington, Virginia, eds. Vohra S., Spano M., Shlesinger M., Pecora L., Ditto W., 1991.

[495] Liu R.W., *Special Issue on Nonlinear Circuits and Systems.* IEEE Trans. Circuits Syst., vol. CAS-27, no. 11, 1980.

[496] Liu Y., Leite J.R.R., "Control of Lorenz Chaos," *Phys. Lett. A*, vol. 185, pp. 35–37, 1994.

[497] Lonngren K.E., "Notes to Accompany a Student Laboratory Experiment on Chaos," *IEEE Trans. Education*, vol. 34, no. 1, pp. 123–128, 1991.

[498] Loparo K.A., Feng X., "Probabilistic Characterization of Chaotic Behaviour in a Family of Feedback Control Systems," *Proc. 29th Confererence on Decision and Control*, Honolulu, Hawaii, pp. 1306–1311, 1990.

[499] López-Ruiz R., Pérez-García C., "Dynamics of Two Logistic Maps with a Multiplicative Coupling," *Int. J. Bifurcation and Chaos*, vol. 2, no. 2, pp. 421–425, 1992.

[500] Lorenz E.N., "Deterministic Non-Periodic Flow," *J. Atmos. Sci.*, vol. 20, pp. 130–141, 1963.

[501] Lozi R., Chua L.O., "Secure Communications via Chaotic Synchronization II: Noise Reduction by Cascading Two Identical Receivers," *Int. J. Bifurcation and Chaos*, vol. 3, no. 5, pp. 1319–1325, 1993.

[502] Luprano J., Hasler M., "More Details on the Devil's Staircase Route to Chaos," *IEEE Trans. Circuits Syst.*, vol. 36, no. 1, pp. 146–148, 1989.

[503] Lyubimov D.V., Pikovsky A.S., Zaks M.A., *Universal Scenarios of Transitions to Chaos via Homoclinic Bifurcations.* Churchill: Harwood Academic, 1989.

[504] Macchi O., Jaidane-Saidane M., "Adaptive IIR Filtering and Chaotic Dynamics: Application to Audio Frequency Coding," *IEEE Trans. Circuits Syst.*, vol. 36, no. 4, pp. 591–599, 1989.

[505] Maginu K., "Spatially Homogeneous and Inhomogeneous Oscillations and Chaotic Motion in the Active Josephson Junction Line," *SIAM J. Appl. Math.*, vol. 43, pp. 225–243, 1983.

[506] Maldonado O., Markus M., Hess B., "Coexistence of Three Attractors and Hysteresis Jumps in a Chaotic Spinning Top," *Phys. Lett. A*, vol. 144, no. 3, pp. 153–158, 1990.

[507] Maloberti F., "An Efficient Method for the Numerical Analysis of Transients in Linear-Dynamic Circuits," *IEEE Trans. Circuits Syst.*, vol. CAS-32, no. 8, pp. 848–851, 1985.

[508] Mandelbrot B.B., *The Fractal Geometry of Nature.* W.H. Freeman, San Fransisco, 1982.

[509] Mareels I.M.Y., Bitmead R.R., "Bifurcation Effects in Robust Adaptive Control," *IEEE Trans. Circuits Syst.*, vol. 35, no. 7, pp. 835–841, 1988.

[510] Mareels I.M.Y., Bitmead R.R., "Non-Linear Dynamics in Adaptive Control: Chaotic and Periodic Stabilization," *Automatica*, vol. 22, no. 6, pp. 641–655, 1986.

[511] Marino R., Kokotovic P.V., "A Geometric Approach to Nonlinear Singularly Perturbed Control Systems," *Automatica* vol. 24, no. 1, pp. 31–41, 1988.

[512] Marotto F.R., "Perturbations of Stable and Chaotic Difference Equations," *J. Math. Anal. Appl.*, vol. 72, pp. 716–729, 1979.

[513] Marotto F.R., "Snap-Back Repellers Imply Chaos in $\mathbf{R}^n$," *J. of Mathematical Analysis and Applications.* vol. 63, pp. 199–223, 1978.

[514] Marsden J., Scheurle J., "The Construction and Smoothness of Invariant Manifolds by the Deformation Method," *SIAM, J. Math. Anal.*, vol. 18, pp. 1261–1274, 1987.

[515] Marsden J.E., McCracken M., *The Hopf Bifurcation and Its Applications.* Applied Mathematical Sciences, vol. 19, New York, NY: Springer-Verlag, 1976.

[516] Maschke B.M., Van Der Schaft A.J., Breedveld P.C., "An Intrinsic Hamiltonian Formulation of the Dynamics of *LC*-Circuits," *IEEE Trans. Circuits Syst.—I: Fund. Theory and Appl.*, vol. 42, no. 2, pp. 73–82, 1995.

[517] Massara R.E., Al-Najjar A.R., "FDNR Realisation of All-Pole Low Pass Filter," *IEE Proc.*, vol. 128, no. 4, pp. 195–197, 1981.

[518] Matsumoto T., "A Chaotic Attractor from Chua's Circuit," *IEEE Trans. Circuits Syst.*, vol. CAS-31, no. 12, pp. 1055–1058, 1984.

[519] Matsumoto T., Chua L.O., Ayaki K., "Reality of Chaos in the Double Scroll Circuit: a Computer-Assisted Proof," *IEEE Trans. Circuits Syst.*, vol. 35, no. 7, pp. 909–925, 1988.

[520] Matsumoto T., Chua L.O., Kawakami H., Ichiraku S., "Geometric Properties of Dynamic Nonlinear Networks: Transversality, Local Solvability and Eventual Passivity," *IEEE Trans. Circuits Syst.*, vol. CAS-28, no. 5, pp. 406–428, 1981.

[521] Matsumoto T., Chua L.O., Kobayashi K., "Hyperchaos: Laboratory Experiment and Numerical Confirmation," *IEEE Trans. Circuits Syst.*, vol. CAS-33, no. 11, pp. 1143–1147, 1986.

[522] Matsumoto T., Chua L.O., Komuro M., "The Double Scroll," *IEEE Trans. Circuits Syst.*, vol. CAS-32, no. 8, pp. 797–818, 1985.

[523] Matsumoto T., Chua L.O., Komuro M., "The Double Scroll Bifurcations," *Int. J. Circuit Theory Appl.*, vol. 14, no. 1, pp. 117–146, 1986.

[524] Matsumoto T., Chua L.O., Tanaka S., "Simplest Chaotic Nonautonomous Circuit," *Phys. Rev. A*, vol. 30, N0. 2, pp. 1155–1157, 1984.

[525] Matsumoto T., Chua L.O., Tokumasu K., "Double Scroll via a Two-Transistor Circuit," *IEEE Trans. Circuits Syst.*, vol. CAS-33, no. 8, pp. 828–835, 1986.

[526] Matsumoto T., Chua L.O., Tokunaga R., "Chaos via Torus Breakdown," *IEEE Trans. Circuits Syst.*, vol. CAS-34, no. 3, pp. 240–253, 1987.

[527] Matsumoto T., Ikegami G., Chua L.O., "Strong Structural Stability of Resistive Nonlinear n-Ports," *IEEE Trans. Circuits Syst.*, vol. CAS-30, no. 4, pp. 197–222, 1983.

[528] Matsumoto T., Salam F.M.A., "Editorial," *IEEE Trans. Circuits Syst.*, vol. 35, no. 7, pp. 766–767, 1988.

[529] McCulloch W.S., Pitts W., "A Logical Calculus of the Ideas Imminent in Nervous Activity," *Bull. Math. Biophys.*, vol. 5, pp. 115–133, 1943.

[530] McGonigal G.C., Elmasry M.I., "Generation of Noise by Electronic Iteration of the Logistic Map," *IEEE Trans. Circuits Syst.*, vol. CAS-34, no. 8, pp. 981–983, 1987.

[531] Mees A.I., Jackson M.F., Chua L.O., "Device Modeling by Radial Basis Functions," *IEEE Trans. Circuits Syst.—I: Fund. Theory and Appl.*, vol. 39, no. 1, pp. 19–27, 1992.

[532] Mees A.I., "A Plain Man's Guide to Bifurcations," *IEEE Trans. Circuits Syst.*, vol. CAS-30, no. 8, pp. 512–517, 1983.

[533] Mees A.I., "Describing Function, Circle Criteria and Multiple-Loop Feedback Systems," *Proc. IEE*, vol. 120, no. 1, pp. 126–130, 1973.

[534] Mees A.I., "Describing Functions: Ten Years On," *IMA J. of Applied Mathematics*, vol. 32, pp. 221–233, 1984.

[535] Mees A.I., *Dynamics of Feedback Systems.* New York, NY: Wiley, 1981.

[536] Mees A.I., Chapman P.B., "Homoclinic and Heteroclinic Orbits in the Double Scroll Attractor," *IEEE Trans. Circuits Syst.*, vol. CAS-34, no. 9, pp. 1115–1120, 1987.

[537] Mees A.I., Chua L.O., "The Hopf Bifurcation Theorem and Its Applications to Nonlinear Circuits and Systems," *IEEE Trans. Circuits Syst.*, vol. CAS-26, no. 4, pp. 235–254, 1979.

[538] Mees A.I., Rapp P.E., Jennings L.S., "Singular-Value Decomposition and Embedding Dimension," *Phys. Rev. A*, vol. 36, no. 1, pp. 340–346, 1987.

[539] Mees A.I., Sparrow C., "Some Tools for Analyzing Chaos," *Proc. IEEE*, vol. 75, no. 8, pp. 1058–1070, 1987.

[540] Mees A.I., Sparrow C.T., "Chaos," *IEE Proc.*, vol. 128, pt. D, no. 5, pp. 201–205, 1981.

[541] Mehta N.J., Henderson R.M., *Phys. Rev. A*, vol. 44, pp. 4861–4863, 1991.

[542] Melnikov V.K., "On the Stability of the Center for Time Periodic Perturbations," *Trans. Moscow Math. Soc.*, vol. 12, pp. 1–57, 1963.

[543] Mielczarek E.V., Turner J.S., Leiter D., Davis L., "Chemical Clocks: Experimental and Theoretical Models of Nonlinear Behavior," *Am. J. Phys.*, vol. 51, no. 1, pp. 32–42, 1983.

[544] Minorsky N., *Nonlinear Oscillations.* New York, NY: Krieger, 1974.

[545] Minsky M., Papert S., *Perceptrons: An Introduction to Computational Geometry.* Cambridge, MA: The MIT Press, 1969.

[546] Mira C., *Chaotic Dynamics. from a One-Dimensional Endomorphism to a Two-Dimensional Diffeomorphism.* Singapore: World Scientific, 1987.

[547] Misawa T., Iwerson J., Loporcaro L., Ruch J., "Single-Chip per Channel Codec with Filters utilizing $\Sigma\Delta$ Modulation," *IEEE J. Solid State Circuits*, vol. SC-16, pp. 333–341, 1981.

[548] Mishina T., Kohmoto T., Hashi T., "Simple Electronic Circuit for the Demonstration of Chaotic Phenomena," *Am. J. Phys.*, vol. 53, no. 4, pp. 332–334, 1985.

[549] Mitobe K., Adachi N., "Hopf Bifurcation in an Adaptive D.C. Servo System," *Int. J. Control*, vol. 54, no. 4, pp. 831–847, 1991.

[550] Mitropolskii Y.A., Lykova O.B., *Integral Manifolds in Nonlinear Mechanics.* Nauka, Moscow, 1973.

[551] Mitschke F., "Acausal Filters for Chaotic Signals," *Phys. Rev. A*, vol. 41, no. 2, pp. 1169–1171, 1990.

[552] Mohamed A.M., Emad F.P., "Nonlinear Oscillations in Magnetic Bearing Systems," *IEEE Trans. Automat. Contr.*, vol. 38, no. 8, pp. 1242–1245, 1993.

[553] Mohler R.R., *Nonlinear Systems, Volume 1, Dynamics and Control.* Englewood Cliffs, NJ: Prentice-Hall Inc., 1991.

[554] Mohler R.R., *Nonlinear Systems, Volume 2, Applications to Bilinear Control.* Englewood Cliffs, NJ: Prentice-Hall Inc., 1991.

[555] Montandon B., "Almost Periodic Solutions and Integral Manifolds for Weakly Nonlinear Conservative Systems," *J. Diff. Equ.*, vol. 12, pp. 417–425, 1972.

[556] Moon F.C., *Chaotic and Fractal Dynamics: An Introduction for Applied Scientists and Engineers.* A Wiley-Interscience Publication, New York, NY: Wiley & Sons, 1992.

[557] Moon F.C., Li G.-X., "Fractal Basin Boundaries and Homoclinic Orbits for Periodic Motion in a Two-Well Potential," *Phys. Rev. Lett.*, vol. 55, no. 14, pp. 1439–1442, 1985.

[558] Moore K.L., *Iterative Learning Control for Deterministic Systems.* Berlin: Springer-Verlag, 1993.

[559] Moroney P., Willsky A.S., Houpt P.K., "The Digital Implementation of Control Compensators: The Coefficient Wordlength Issue," *IEEE Trans. Automat. Contr.*, vol. CAS-25, no. 4, pp. 621–630, 1980.

[560] Morse M., Hedlund G.A., "Symbolic Dynamics," *IEEE Amer. J. Math.*, vol. 60, pp. 815–866, 1938.

[561] Moser J., *Stable and Random Motions in Dynamical Systems.* Princeton: Princeton University Press, 1973.

[562] Mossayebi F., Qammar H.K., Hartley T.T., "Adaptive Estimation and Synchronisation of Chaotic Systems," *Phys. Lett. A*, vol. 161, pp. 255–262, 1991.

[563] Munkres J.R., *Topology a First Course.* Englewood Cliffs, NJ: Prentice-Hall, 1975.

[564] Murali K., Lakshmanan M., "Bifurcation and Chaos of the Sinusoidally-Driven Chua's Circuit," *Int. J. Bifurcation and Chaos*, vol. 1, no. 2, pp. 369–384, 1991.

[565] Murali K., Lakshmanan M., "Effect of Sinusoidal Excitation on the Chua's Circuit," *IEEE Trans. Circuits Syst.—I: Fund. Theory and Appl.*, vol. 39, no. 4, pp. 264–270, 1992.

[566] Murali K., Lakshmanan M., "Observation of Many Bifurcation Sequences in a Driven Piecewise-Linear Circuit," *Phys. Lett. A*, vol. 151, no. 8, pp. 412–419, 1990.

[567] Murao K., Kohda T., Noda K., Yanase M., "$1/f$ Noise Generator using Logarithmic and Antilogarithmic Amplifiers," *IEEE Trans. Circuits Syst.—I: Fund. Theory and Appl.*, vol. 39, no. 10, pp. 851–853, 1992.

[568] Murch A.R., Bates R.H.T., "Colored Noise Generation through Deterministic Chaos," *IEEE Trans. Circuits Syst.*, vol. 37, no. 5, pp. 608–613, 1990.

[569] Nagumo J., Sato S., "A Response Characteristic of a Mathematical Neuron Model," *Electronics and Communications in Japan*, vol. 55-D, no. 4, pp. 123–130, 1972.

[570] Nakamura A., Hamada N., "Identification of Nonlinear Dynamical System by Piecewise-Linear System," *Electronics and Communications in Japan, Part 3*, vol. 74, no. 9 pp. 102–115, 1991.

[571] Nayfeh A.H., Mook D.T., *Nonlinear Oscillations.* New York, NY: John Wiley & Sons, 1979.

[572] Neff J., Carroll T.L., "Circuits that get Chaos in Sync," *Scientific American*, pp. 101–103, 1993.

[573] Nekorkin V.I., Chua L.O., "Spatial Disorder and Wave Fronts in a Chain of Coupled Chua's Circuits," *Int. J. Bifurcation and Chaos*, vol. 3, no. 5, pp. 1281–1291, 1993.

[574] Nelder J.A., Mead R., "A Simplex Method for Function Minimization," *Computer J.*, vol. 7, pp. 308–313, 1986.

[575] Neubert R., "Predictor-Corrector Techniques for Detecting Hopf Bifurcation Points," *Int. J. Bifurcation and Chaos*, vol. 3, no. 5, pp. 1311–1318, 1993.

[576] Newcomb R.W., "The Semistate Description of Nonlinear Time-Variable Circuits," *IEEE Trans. Circuits Syst.*, vol. CAS-28, no. 1, pp. 62–71, 1981.

[577] Newcomb R.W., Sathyan S., "An *RC* Op Amp Chaos Generator," *IEEE Trans. Circuits Syst.*, vol. CAS-30, no. 1, pp. 54–56, 1983.

[578] Nicolis C., Nicolis G., "Finite Time Behaviour of Small Errors in Deterministic Chaos and Lyapunov Exponents," *Int. J. Bifurcation and Chaos*, vol. 3, no. 5, pp. 1339–1342, 1993.

[579] Niedernostheide F.-J., Ardes M., Or-Guil M., Purwins H.-G., "Spatiotemporal Behavior of Localized Current Filaments in *P-N-P-N* Diodes: Numerical Calculations and Comparison with Exper. Results," *Phys. Rev. B*, vol. 49, no. 11, pp. 7370–7382, 1994.

[580] Nikias C.L., Mendel J.M., "Signal Processing with Higher-Order Spectra," *IEEE Signal Processing Magazine*, pp. 10–37, 1993.

[581] Nishio Y., Inaba N., Mori S., Saito T., "Rigorous Analysis of Windows in a Symmetric Circuit," *IEEE Trans. Circuits Syst.*, vol. 37, no. 4, pp. 473–487, 1990.

[582] Nitecki Z., Robinson C. (eds.), *Global Theory of Dynamical Systems*. New York, NY: Springer-Verlag, 1980.

[583] Noakes L, "Densities and Dynamics," *Int. J. Bifurcation and Chaos*, vol. 2, no. 2, pp. 371–381, 1992.

[584] Noakes L., "The Takens Embedding Theorem," *Int. J. Bifurcation and Chaos*, vol. 1, no. 4, pp. 867–872, 1991.

[585] Noble B., Daniel J.W., *Applied Linear Algebra*. Third Edition, Englewood Cliffs, NJ: Prentice-Hall Inc., 1988.

[586] Noldus E., "Perturbation Theory for the Analysis of Nonlinear Oscillations," *Benelux Quarterly J. of Automatic Control, Journal A*, vol. 33, no. 2, pp. 18–23, 1992.

[587] O'droma M.S., "Dynamic Range and Other Fundamentals of the Complex Bessel Function Series Approximation Model for Memoryless Nonlinear Devices," *IEEE Trans. Commun.*, vol. 37, no. 4, pp. 397–398, 1989.

[588] Octavio M., Dacosta A., Aponte J., "Nonuniversality and Metric Properties of a Forced Nonlinear Oscillator," *Phys. Rev. A*, vol. 34, no. 2, pp. 1512–1515, 1986.

[589] Odessey P.H., Weber E., "Critical Conditions in Ferroresonance," *AIEE Trans.*, vol. 57, no. 8, pp. 444–452, 1938.

[590] Odyniec M., Chua L.O., "Josephson-Junction Circuit Analysis via Integral Manifolds," *IEEE Trans. Circuits Syst.*, vol. CAS-30, no. 5, pp. 308–320, 1983.

[591] Odyniec M., Chua L.O., "Josephson-Junction Circuit Analysis via Integral Manifolds: Part II," *IEEE Trans. Circuits Syst.*, vol. CAS-32, no. 1, pp. 34–45, 1985.

[592] Ogorzalek M.J., "Chaotic Regions from Double Scroll," *IEEE Trans. Circuits Syst.*, vol. CAS-34, no. 2, pp. 201–203, 1987.

[593] Ogorzalek M.J., "Complex Behavior in Digital Filters," *Int. J. Bifurcation and Chaos*, vol. 2, no. 1, pp. 11–29, 1992.

[594] Ogorzalek M.J., "Taming Chaos—Part I: Synchronization," *IEEE Trans. Circuits Syst.—I: Fund. Theory and Appl.*, vol. 40, no. 10, pp. 693–699, 1993.

[595] Ogorzalek M.J., "Taming Chaos—Part II: Control," *IEEE Trans. Circuits Syst.—I: Fund. Theory and Appl.*, vol. 40, no. 10, pp. 700–706, 1993.

[596] Ohlson J.E., "Exact Dynamics of Automatic Gain Control," *IEEE Trans. Commun.*, vol. COM-22, no. 1, pp. 72–75, 1974.

[597] Ohta Y., "Qualitative Analysis of Nonlinear Quasi-Monotone Dynamical Systems Described by Functional-Differential Equations," *IEEE Trans. Circuits Syst.*, vol. CAS-28, no. 2, pp. 138–??, 1981.

[598] Ono Y., Fukushima K., "A Scaling Property of the Fluctuation Spectrum for an Intermittency Observed in the Chua Circuit," *Phys. Lett. A*, vol. 163, pp. 173–175, 1992.

[599] Oono Y., Osikawa M., "Chaos in Nonlinear Difference Equations I. Qualitative Study of (formal) Chaos," *Prog. Theor. Phys.*, vol. 64, no. 1, pp. 54–67, 1980.

[600] Oono Y., Takahashi Y., "Chaos, External Noise and Fredholm Theory," *Prog. Theor. Phys.*, vol. 63. no. 5, pp. 1804–1807, 1980.

[601] Oppenheim A.L., Wornell G.W., Isabelle S.H., Cuomo K.M., "Signal Processing in the Context of Chaotic Signals," *Proc. IEEE ICASSP IV*, San Francisco, CA, vol. 4, pp. 117–120, 1992.

[602] Orchard H.J., Sheahan D.F., "Inductorless Bandpass Filters," *IEEE J. Sold-State Circuits*, vol. Sc-5, pp. 108–118, 1970.

[603] Oseledec V.I., "A Multiplicative Ergodic Theorem. Lyapunov Characteristic Numbers for Dynamical Systems," *Trans. Moscow Math. Soc.* vol. 19, pp. 197–231, 1968.

[604] Ott E., *Chaos in Dynamical Systems.* New York, NY: Cambridge University Press, 1993.

[605] Ott E., Grebogi C., Yorke J.A., "Controlling Chaos," *Phys. Rev. Lett.*, vol. 64, no. 11, pp. 1196–1199, 1990.

[606] Ott E., Grebogi C., Yorke J.A., "Controlling Chaotic Dynamical Systems," *Chaos: Soviet-American Perspectives on Nonlinear Science*, ed. D.K. Campbell Amer. Inst. Phys., New York, pp. 153–172, 1990.

[607] Ottino J.M., "The Mixing of Fluids," *Scientific American*, pp. 40–49, 1989.

[608] Ovsyannikov I.M., Shil'nikov L.P., "Systems with Homoclinic Curve of the Multi-dimensional Saddle-Focus and Spiral Chaos," *Math. Sbornik*, vol. 182, pp. 1043–1073, 1991.

[609] Packard N.H., Crutchfield J.P., Farmer J.D., Shaw R.S., "Geometry from a Time Series," *Phys. Rev. Lett.*, vol. 45, no. 9, pp. 712–716, 1980.

[610] Palis J., deMelo W., *Geometric Theory of Dynamical Systems: An Introduction.* New York, NY: Springer-Verlag, 1982.

[611] Papoulis A., *The Fourier Integral and Its Applications.* New York, NY: McGraw-Hill, 1962.

[612] Papoulis A., *Probability, Random Variables, and Stochastic Processes.* Electrical Engineering Series, Singapore: McGraw-Hill, 1984.

[613] Park S.J., Gray R.M., "Sigma-Delta Modulation with Leaky Integration and Constant Input," *IEEE Trans. on Information Theory*, vol. 38, no. 4, pp. 1512–1533, 1992.

[614] Parker S.P., Hess S.F., "Limit Cycle Oscillations in Digital Filters," *IEEE Trans. Circuits Syst.*, vol. CAS-18, pp. 687–697, 1971.

[615] Parker T.S., Chua L.O., "A Computer-Assisted Study of Forced Relaxation Oscillations," *IEEE Trans. Circuits Syst.*, vol. CAS-30, no. 8, pp. 518–533, 1983.

[616] Parker T.S., Chua L.O., "Chaos: a Tutorial for Engineers," *Proc. IEEE*, vol. 75, no. 8, pp. 982–1008, 1987.

[617] Parker T.S., Chua L.O., *Practical Numerical Algorithms for Chaotic Systems.* Berlin: Springer-Verlag, 1989.

[618] Parker T.S., Chua L.O., "The Dual Double Scroll Equation," *IEEE Trans. Circuits Syst.*, vol. CAS-34, no. 9, pp. 1059–1073, 1987.

[619] Parker T.S., Kennedy M.P., Liao Y., Chua L.O., "Qualitative Nonlinear Circuit Analysis using Computers," *IEEE Trans. Circuits Syst.*, vol. CAS-33, no. 8, pp. 794–804, 1986.

[620] Parlitz U., "Identification of True and Spurious Lyapunov Exponents from Time Series," *Int. J. Bifurcation and Chaos*, vol. 2, pp. 155–165, 1992.

[621] Parlitz U., Chua L.O., Kocarev Lj., Halle K.S., Shang A., "Transmission of Digital Signals by Chaotic Synchronization," *Int. J. Bifurcation and Chaos*, vol. 2, pp. 973–977, 1992.

[622] Parlitz U., Lauterborn W., "Period-Doubling Cascades and Devil's Staircase of the Driven Van der Pol Oscillator," *Phys. Rev. A*, vol. 36, no. 3, pp. 1428–1433, 1987.

[623] Pawelzik K., Schuster H.G., "Errata: Generalized Dimensions and Entropies from a Measured Time Series," *Phys. Rev. A*, vol. 36, no. 9, p. 4529–4529, 1987.

[624] Pawelzik K., Schuster H.G., "Generalized Dimensions and Entropies from a Measured Time Series," *Phys. Rev. A*, vol. 35, no. 1, pp. 481–484, 1987.

[625] Pecora L.M., Carroll T.L., "Driving Systems with Chaotic Signals," *Phys. Rev. A*, vol. 44, pp. 2374–2383, 1991.

[626] Pecora L.M., Carroll T.L., "Synchronizing Chaotic Circuits," *IEEE Trans. Circuits Syst.*, vol. 38, no.4, pp. 453–456, 1991.

[627] Pecora L.M., Carroll T.L., "Synchronization in Chaotic Systems," *Phys. Rev. Lett.*, vol. 64, no. 8, pp. 821–824, 1990.

[628] Pei L-Q., Guo F., Wu S-X., Chua L.O., "Experimental Confirmation of a Period Adding Route to Chaos in a Nonlinear Circuit," *IEEE Trans. Circuits Syst.*, vol. CAS-33, no. 4, pp. 438–442, 1986.

[629] Peitgen H.-O. (ed.), *Newton's Method and Dynamical Systems*. Dordrecht: Kluwer, 1989.

[630] Percival I., Richards D., *Introduction to Dynamics*. Cambridge: Cambridge University Press, 1982.

[631] Percora L.M., Carroll T.L., "Synchronized Chaotic Signals and Systems," *Proc. IEEE ICASSP IV*, San Francisco, CA, vol. 4, pp. 137–140, 1992.

[632] Perez J., Jeffries C., "Effects of Additive Noise on a Nonlinear Oscilltor Exhibiting Period Doubling and Chaotic Behavior," *Phys. Rev. B*, vol. 26, no. 6, pp. 3460–3462, 1982.

[633] Perez J.M., Yu Z., Kowalski J.M., Albert G., Littler C.L., Song X.N., "Synchronization of Chaos in Coupled Tunnel Diode Relaxation Oscillators," *Proc. 1st Experimental Chaos Conference*, Arlington, Virginia, eds. Vohra S., Spano M., Shlesinger M., Pecora L., Ditto W., 1991.

[634] Perez-Munuzuri V., Perez-Villar V., Chua L.O., "Propagation Failure in Linear Arrays of Chua's Circuits," *Int. J. Bifurcation and Chaos*, vol. 2, no. 2, pp. 403–406, 1992.

[635] Pettini M., Vulpiani A., "Possible Failure of Arnold Diffusion in Nonlinear Hamiltonian Systems with More That Two Degrees of Freedom," *Phys. Lett. A*, vol. 106, no. 5,6, pp. 207–211, 1984.

[636] Phillips C.L., Nagle H.T. Jr., *Digital Control System Analysis and Design.* Englewood Cliffs, NJ: Prentice-Hall Inc., 1984.

[637] Pickover C.A., *Computers, Pattern, Chaos, and Beauty.* New York, NY: St. Martin's Press, 1990.

[638] Pippard A.B., *Response and Stability: an Introduction to the Physical Theory.* Cambridge: Cambridge University Press, 1985.

[639] Poincaré H., *Les Methodes Nouvelles De La Mécanique Celeste.* Gauthier-Villars, Paris, 1899.

[640] Poliashenko M., McKay S.R., Smith C.W., "Chaos and Nonisochronism in Weakly Coupled Nonlinear Oscillators," *Phys. Rev. A*, vol. 44, no. 6, pp. 3452–3456, 1991.

[641] Pool R., *Is it Healthy to be Chaotic?* Science, vol. 243, p. 604, 1989.

[642] Pyragas K., "Continuous Control by Self-Controlling Feedback," *Phys. Lett. A*, vol. 170, pp. 421–428, 1992.

[643] Pyragas K., Tamaševičius A., "Experimental Control of Chaos by Delayed Self-Controlling Feedback," *Phys. Lett. A*, vol. 180, pp. 99–102, 1993.

[644] Qammar H.K., Mossayebi F., Murphy L., "Dynamical Complexity Arising in the Adaptive Control of a Chaotic System," *Phys. Lett. A*, vol. 178, pp. 279–283, 1993.

[645] Qin G., Gong D., Li R., Wen X., "Rich Bifurcation Behaviors of the Driven Van der Pol Oscillator," *Phys. Lett. A*, vol. 141, no. 8,9, pp. 412–416, 1989.

[646] Qu Z., Hu G., Ma B., "Controlling Chaos via Continuous Feedback," *Phys. Lett. A*, vol. 178, pp. 265–270, 1993.

[647] Rainville E.D., *Intermediate Differential Equations.* Second Edition, New York, NY: Macmillan, 1964.

[648] Rainville E.D., Bedient P.E., *Elementary Differential Equations.* Fourth Edition, New York, NY: Macmillan, 1974.

[649] Rajasekar S., Lakshmanan M., "Controlling Chaos in Bonhoeffer-Van der Pol Oscillator," *Int. J. Bifurcation and Chaos*, vol. 2, no. 1, pp. 201–204, 1992.

[650] Rand R.H., Holmes P.J., "Bifurcation of Periodic Motion in Two Weakly Coupled Van der Pol Oscillators," *Int. J. Non-Linear Mechanics*, vol. 15, pp. 387–399, 1980.

[651] Raven F.H., *Automatic Control Engineering.* Third Edition, Singapore: McGraw-Hill, 1978.

[652] Reich S., "Differential-Algebraic Equations and Applications in Circuit Theory," *AEÜ*, vol. 46, no. 4, pp. 298–304, 1992.

[653] Rey G.J., Bitmead R.R., Johnson C.R., "The Dynamics of Bursting in Simple Adaptive Feedback Systems with Leakage," *IEEE Trans. Circuits Syst.*, vol. 38, no. 5, pp. 476–488, 1991.

[654] Ridders C.J.F., "Accurate Determination of Threshold Voltage Levels of a Schmitt Trigger," *IEEE Trans. Circuits Syst.*, vol. CAS-32, no. 9, pp. 969–970, 1985.

[655] Rikitake T., "Oscillations of a Systems of Discs Dynamos," *Proc. Camb. Phil. Soc.*, vol. 54, pp. 89–105, 1958.

[656] Rioul O., Vetterli M., "Wavelets and Signal Processing," *IEEE Signal Processing Magazine*, pp. 14–38, 1991.

[657] Robbins K.A., "A New Approach to Subcritical Instability and Turbulent Transitions in a Simple Dynamo," *Math. Proc. Camb. Phil. Soc.* vol. 82, pp. 309–325, 1977.

[658] Robinson F.N.H., "The Modified Van der Pol Oscillator," *IMA J. of Applied Mathematics*, vol. 38, pp. 135–150, 1987.

[659] Rodriguez-Vazquez A.B., Huertas J.L., Chua L.O., "Chaos in a Switched-Capacitor Circuit," *IEEE Trans. Circuits Syst.*, vol. CAS-32, no. 10, pp. 1083–1084, 1985.

[660] Rodriquez-Vazquez A., Huertas J.L., Rueda A., Perez-Verdu B., Chua L.O., "Chaos from Switched-Capacitor Circuits: Discrete Maps," *Proc. IEEE*, vol. 75, no. 8, pp. 1090–1106, 1987.

[661] Rollins R.W., Hunt E.R., "Exactly Solvable Model of a Physical System Exhibiting Universal Chaotic Behavior," *Phys. Rev. Lett.*, vol. 49, no. 18, pp. 1295–1298, 1982.

[662] Romeiras F.J., "Controlling Chaotic Dynamical Systems," *American Control Conference (IEEE)*, 1991.

[663] Romeiras F.J., Grebogi C., Ott E., Dayawansa W.P., "Controlling Chaotic Dynamical Systems," *Physica D*, vol. 58, pp. 165–192, 1992.

[664] Roska T., "The Limits of Modeling of Nonlinear Circuits," *IEEE Trans. Circuits Syst.*, vol. CAS-28, no. 3, pp. 212–216, 1981.

[665] Rössler O.E., "An Equation for Hyperchaos," *Phys. Lett. A*, vol. 71, pp. 155–157, 1979.

[666] Rössler O.E., "Chaotic Oscillations—An Example of Hyperchaos," *Nonlinear Oscillations in Biology, Lectures on Applied Mathematics*, vol. 17, Amer. Math. Soc. pp. 141–156, 1979.

[667] Rössler O.E., "Chemical Turbulence: Chaos in a Small Reaction-Diffusion System," *Z. Naturforsch.*, vol. 31a, pp. 1168–1172, 1976.

[668] Roy R., Murphy T.W., Maier T.D., Gills Z., Hunt E.R., "Dynamical Control of a Chaotic Laser: Experimental Stabilization of a Globally Coupled System," *Phys. Rev. Lett.*, vol. 68, no. 9, pp. 1259–1262, 1992.

[669] Rubio F.R., Aracil J., Camacho E.F., "Chaotic Motion in an Adaptive Control System," *Int. J. Control*, vol. 42, no. 2, pp. 353–360, 1985.

[670] Rudin W., *Principles of Mathematical Analysis.* Second Edition, Mexico: McGraw-Hill, 1964.

[671] Ruelle D., *Chaotic Evolution and Strange Attractors.* Cambridge: Cambridge University Press, 1990.

[672] Ruelle D., *Elements of Differentiable Dynamics and Bifurcation Theory.* Boston, MA: Academic Press, 1989.

[673] Ruelle D., "Strange Attractors," *The Mathematical Intelligencer*, vol. 2, pp. 126–137, 1980.

[674] Rul'kov N.F., Volkovskii A.R., Rodriquez-Lozano A., del Rio E., Velarde M.G., "Mutual Synchronization of Chaotic Self-Oscillators with Dissipative Coupling," *Int. J. Bifurcation and Chaos*, vol. 2, pp. 669–676, 1992.

[675] Saeks R., "State in Hilbert Space," *SIAM Review*, vol. 15, no. 2, pp. 283–??, 1973.

[676] Sain M.K., "The Growing Algebraic Presence in Systems Engineering: An Introduction," *Proc. IEEE*, vol. 64, no. 1, pp. 96–111, 1976.

[677] Saito T., "A Chaos Generator Based on a Quasi-Harmonic Oscillator," *IEEE Trans. Circuits Syst.*, vol. CAS-32, no.4, pp. 320–331, 1985.

[678] Saito T., "On a Coupled Relaxation Oscillator," *IEEE Trans. Circuits Syst.*, vol. 35, no. 9, pp. 1147–1155, 1988.

[679] Saito T., "A Chaotic Circuit Family Including One Diode," *Elec. & Comm. in Japan, Part 3*, vol. 72, no. 8, pp. 52–59, 1989.

[680] Saito T., "An Approach toward Higher Dimensional Hysteresis Chaos Generators," *IEEE Trans. Circuits Syst.*, vol. 37, no. 3, pp. 399–409, 1990.

[681] Saito T., "Reality of Chaos in Four-Dimensional Hysteretic Circuits," *IEEE Trans. Circuits Syst.*, vol. 38, no. 12, pp. 1517–1524, 1991.

[682] Saito T., Fujita H., "Chaotic Phenomenon in a Tuning Circuit Including Variable Capacitor or Variable Resistor," *Trans. IECE Japan*, vol. 65-A, no. 4, pp. 305–309, 1982.

[683] Salam F.M., Marsden J.E., Varaiya P.P., "Chaos and Arnold Diffusion in Dynamical Systems," *IEEE Trans. Circuits Syst.*, vol. CAS-30, no. 9, pp. 697–708, 1983.

[684] Salam F.M.A., Bai S., "Complicated Dynamics of a Prototype Continuous-Time Adaptive Control System," *IEEE Trans. Circuits Syst.*, vol. 35, no. 7, pp. 842–851, 1988.

[685] Salam F.M.A., Marsden J.E., Varaiya P.P., "Arnold Diffusion in the Swing Equations of a Power System," *IEEE Trans. Circuits Syst.*, vol. CAS-31, no. 8, pp. 673–688, 1984.

[686] Salam F.M.A., Sastry S.S., "Dynamics of the Forced Josephson Junction Circuit: the Regions of Chaos," *IEEE Trans. Circuits Syst.*, vol. CAS-32, no. 8, pp. 784–796, 1985.

[687] Salerno M., "Phase-Locking Chaos in Long Josephson Junctions," *Phys. Lett. A*, vol. 144, no. 8,9, pp. 453–458, 1990.

[688] Sandberg I.W., "On Volterra Expansions for Time-Varying Nonlinear Systems," *IEEE Trans. Circuits Syst.*, vol. CAS-30, no. 2, pp. 61–67, 1983.

[689] Sandberg I.W., "Volterra-Like Expansions for the Solutions of Nonlinear Integral Equations and Nonlinear Differential Equations," *IEEE Trans. Circuits Syst.*, vol. CAS-30, no. 2, pp. 68–77, 1983.

[690] Sandler Y.M., "Model of Neural Networks with Selective Memorization and Chaotic Behavior," *Phys. Lett. A*, vol. 144, no. 8,9, pp. 462–466, 1990.

[691] Sano M., Sawada Y., "Measurement of the Lyapunov Spectrum from a Chaotic Time Series," *Phys. Rev. Lett.*, vol. 55, no. 10, pp. 1082–1085, 1985.

[692] Saphir W.C., Hasegawa H.H., "Spectral Representations of the Bernoulli Map," *Phys. Lett. A*, vol. 171, pp. 317–322, 1992.

[693] Sastry S., Bodson M., *Adaptive Control: Stability, Convergence, and Robustness.* Prentice Hall Information and System Sciences Series, Englewood Cliffs, NJ: Prentice-Hall Inc., 1989.

[694] Sastry S.S., Desoer C.A., "Jump Behavior of Circuits and Systems," *IEEE Trans. Circuits Syst.*, vol. CAS-28, no. 12, pp. 1109–1115, 1981.

[695] Sauer T., Yorke J.A., Casdagli M., "Embedology," *J. Stat. Phys.*, vol. 65, no. 3/4, pp. 579–616, 1991.

[696] Sayed A.H., Kailath T., "A State-Space Approach to Adaptive RLS Filtering," *IEEE Signal Processing Magazine*, pp. 18–60, 1994.

[697] Schieve W.C., Bulsara A.R., "Multiplicative Noise and Homoclinic Crossing: Chaos," *Phys. Rev. A*, vol. 41, no. 2, pp. 1172–1174, 1990.

[698] Schiff S.J., Chang T., "Differentiation of Linearly Correlated Noise from Chaos in a Biological System using Surrogate Data," *Biol. Cybern.*, vol. 67, pp. 387–393, 1992.

[699] Scholl E., "Impact Ionization Mechanism for Self-Generated Chaos in Semiconductors," *Phys. Rev. B*, vol. 34, no. 2, pp. 1395–1398, 1986.

[700] Scholten W.B., Gaggioli R.A., "Differentiation of Tensor Fields," *SIAM Review*, vol. 14, no. 2, pp. 271–277, 1972.

[701] Scholten W.B., Gaggioli R.A., "Normals to Coordinate Hypersurfaces as Weight Minus-One Covariant Base Vectors," *SIAM Review*, vol. 15, no. 2, pp. 275–282, 1973.

[702] Schreier R., "An Empirical Study of High-Order Single-Bit Delta-Sigma Modulators," *IEEE Trans. Circuits Syst.—II: Analog and Digital Signal Processing*, vol. 40, no. 8, pp. 461–466, 1993.

[703] Schreier R., "Destabilizing Limit Cycles in Delta-Sigma Modulators with Chaos," *SIAM Conference on Applic. Dynamical Systems*, Snowbird, Utha, 1992.

[704] Schuss Z., "Singular Perturbation Methods in Stochastic Differential Equations of Mathematical Physics," *SIAM Review*, vol. 22, no. 2, pp. 119–155, 1980.

[705] Schuster H., *Deterministic Chaos: An Introduction*. VCH Publishers, Weinheim, 1989.

[706] Schuster H.G., Martin S., Martienssen W., "New Method for Determining the Largest Liapunov Exponent of Simple Nonlinear Systems," *Phys. Rev. A*, vol. 33, no. 5, pp. 3547–3549, 1986.

[707] Schwarz F., "Symmetries of Differential Equations: from Sophus Lie to Computer Algebra," *SIAM Review*, vol. 30, no. 3, pp. 450–481, 1988.

[708] Schwegler H., Mackey M.C., "A Simple Model for the Approach of Entropy to Thermodynamic Equilibrium," *J. Phys. A: Math. Gen.*, vol. 27, pp. 1939–1951, 1994.

[709] Sedra A.S., Smith K.C., *Microelectronic Circuits*. Holt-Saunders, Japan, 1982.

[710] Servizi G., Turchetti G., "Normal Form Singularities in Area-Preserving Maps and Analytic Continuation by Padé Approximants," *Phys. Lett. A*, vol. 151, no. 9, pp. 485–492, 1990.

[711] Shahar Dror L., Collins D.J., "Identification and Control of Non-Linear Time-Varying Dynamical Systems using Neural Networks," *World Conference on Neural Networks*, 1993.

[712] Shannon C.E., "The Mathematical Theory of Communication," *Bell Syst. Tech. J.*, vol. 27, pp. 379–423, 1948.

[713] Sharkovsky A.N., "Chaos from a Time-Delayed Chua's Circuit," *IEEE Trans. Circuits Syst.—I: Fund. Theory and Appl.*, vol. 40, no. 10, pp. 781–783, 1993.

[714] Shaw R., "Strange Attractors, Chaotic Behavior and Information Flow," *Z. Naturforsch.*, vol. 36a, no. 1, pp. 80–112, 1982.

[715] Shaw S.W., "The Dynamics of a Harmonically Excited System Having Rigid Amplitude Constraints," *J. Appl. Mech.*, vol. 52, pp. 453–465, 1985.

[716] Shil'nikov L.P., "A Case of the Existence of a Denumerable Set of Periodic Motions," *Soviet Math. Dokl.*, vol. 6, pp. 163–166, 1965.

[717] Shil'nikov L.P., "A Contribution to the Problem of a Structurally Stable Equilibrium State of Saddle-Focus type," *Math. Ussr. Sb.*, vol. 10, pp. 91–102, 1970.

[718] Shil'nikov L.P., "Chua's Circuit: Rigorous Results and Future Problems," *IEEE Trans. Circuits Syst.—I: Fund. Theory and Appl.*, vol. 40, no. 10, pp. 784–786, 1993.

[719] Shil'nikov L.P., "Existence of a Countable Set of Periodic Motions in a Four-Dimensional Space in an Extended Neighbourhood of a Saddle-Focus," *Soviet Math. Dokl.*, vol. 8, pp. 54–58, 1967.

[720] Shil'nikov L.P., "On a New type of Bifurcation of Multidimensional Dynamical Systems," *Sov. Math.*, vol. 10, pp. 1368–1371, 1969.

[721] Shil'nikov L.P., "On the Generation of a Periodic Motion from Trajectories Doubly Asymptotic to an Equilibrium State of Saddle-Type," *Math. Ussr. Sb.*, vol. 6, pp. 427–438, 1968.

[722] Shimada I., Nagashima T., "A Numerical Approach to Ergodic Problem of Dissipative Dynamical Systems," *Prog. of Theor. Phys.*, vol. 61, no. 6, pp. 1605–1614, 1979.

[723] Shinbrot T., Ditto W., Grebogi C., Ott E., Spano M., Yorke J.A., "Using the Sensitive Dependence of Chaos (the "Butterfly Effect") to Direct Trajectories in an Experimental Chaotic System," *Phys. Rev. Lett.*, vol. 68, no. 19, pp. 2863–2866, 1992.

[724] Shinbrot T., Grebogi C., Ott E., Yorke J.A., "Using Small Perturbations to Control Chaos," *Nature*, vol. 363, pp. 411–417, 1993.

[725] Shinbrot T., Ott E., Grebogi C., Yorke J.A., "Using Chaos to Direct Orbits to Targets in Systems Describable by a One-Dimensional Map," *Phys. Rev. A*, vol. 45, no. 6, pp. 4165–4168, 1992.

[726] Shinbrot T., Ott E., Grebogi C., Yorke J.A., "Using Chaos to Direct Trajectories to Targets," *Phys. Rev. Lett.*, vol. 65, no. 26, pp. 3215–3218, 1990.

[727] Shinbrot T., Ott E., Grebogi C., Yorke J.A., "Using Chaos to Target Stationary States of Flows," *Phys. Lett. A*, vol. 169, pp. 349–354, 1992.

[728] Shinriki M., Yamamoto M., Mori S., "Multimode Oscillations in a Modified Van der Pol Oscillator Containing a Positive Nonlinear Conductance," *Proc. IEEE*, vol. 69, no. 3, pp. 394–395, 1981.

[729] Shiraiwa K., Kurata M., "A Generalization of a Theorem of Marotto," *Nagoya Math. J.*, vol. 82, pp. 83–97, 1981.

[730] Sieradski A.J., *An Introduction to Topology and Homotopy*. Boston, MA: PWS-Kent Publishing Co., 1992.

[731] Silverman B.W., "Kernel Density Estimation using the Fast Fourier Transform," *Royal Statistical Soc. (Series C), Applied Statistics*, vol. 31, pp. 93–97, 1982.

[732] Silvermann B.W., *Density Estimation for Statistics and Data Analysis*. London: Chapman & Hall, 1986.

[733] Simon M.K., "A Note on the Generation of Phase Plane Plots on a Digital Computer," *IEEE Trans. Commun.*, vol. COM-28, no. 1, pp. 144–149, 1980.

[734] Sinai Ya.G., *Introduction to Ergodic Theory*. Princeton: Princeton University Press, 1977.

[735] Singer J., Wang Y.-Z., Bau H.H., "Controlling a Chaotic System," *Phys. Rev. Lett.*, vol. 66, pp. 1123–1125, 1991.

[736] Singer S., "Loss-Free Gyrator Realization," *IEEE Trans. Circuits Syst.*, vol. 35, no. 1, pp. 26–34, 1988.

[737] Singh R., Prasad P.S.R., Bhattacharjee J.K., Thareja R.K., "Effect of Internal Noise and Hopf Bifurcations in a Hollow Cathode Discharge," *Phys. Lett. A*, vol. 178, pp. 284–288, 1993.

[738] Sira-Ramirez H., "Nonlinear P-I Controller Design for Switchmode DC-to-DC Power Converters," *IEEE Trans. Circuits Syst.*, vol. 38, no. 4, pp. 410–417, 1991.

[739] Skelboe S., "Computation of the Periodic Steady-State Response of Nonlinear Networks by Extrapolation Methods," *IEEE Trans. Circuits Syst.*, vol. CAS-27, no. 3, pp. 161–??, 1980.

[740] Skoog R.A., Blankenship G.I., "Generalized Pulse-Modulated Feedback Systems: Norms, Gains, Lipschitz Constants, and Stability," *IEEE Trans. Automat. Contr.*, vol. AC-15, no. 3, pp. 300–315, 1970.

[741] Slaughter J.B., "Quantization Errors in Digital Control Systems," *IEEE Trans. Automat. Contr.*, vol. AC-9, pp. 70–74, 1964.

[742] Slotine J.-J.E., Li W., *Applied Nonlinear Control.* Englewood Cliffs, NJ: Prentice-Hall Inc., 1991.

[743] Smale S., *The Mathematics of Time (Essays on Dynamical Systems, Economic Processes, and Related Topics).* New York, NY: Springer-Verlag, 1980.

[744] Smale S. (ed.), *The Mathematics of Time.* New York, NY: Springer-Verlag, 1980.

[745] Smale S., "On the Mathematical Foundations of Electrical Circuit Theory," *J. Diff. Geom.*, vol. 7, pp. 193–210, 1972.

[746] Smale S., "Differentiable Dynamical Systems," *Bull. Amer. Math. Soc.*, vol. 73, pp. 747–817, 1967.

[747] Smale S., "Diffeomorphisms with many Periodic Points," *Differential and Combinatorial Topology*, Cairns S.S. (ed.), Princeton: Princeton University Press, pp. 63–80, 1967.

[748] Solms F., "Inferring with Incomplete Information: The Maximum Entropy Principle," Internal Report, Department of Applied Mathematics, Rand Afrikaans University, 1993.

[749] Sparrow C.T., "An Introduction to the Lorenz Equations," *IEEE Trans. Circuits Syst.*, vol. CAS-30, no. 8, pp. 533–542, 1983.

[750] Sparrow C.T., "Chaos in a Three Dimensional Single Loop Feedback System with a Piecewise Linear Feedback Function," *J. Math. Anal. and Appl.*, vol. 83, pp. 275–291, 1981.

[751] Sparrow C.T., *The Lorenz Equations: Bifurcations, Chaos, and Strange Attractors.* New York, NY: Springer-Verlag, 1982.

[752] Spivak M., *Calculus on Manifolds.* W.A. Benjamin Inc., New York, 1965.

[753] Steeb W.-H., *A Handbook of Terms used in Chaos and Quantum Chaos.* Mannheim: BI Wissenschaftsverlag, 1992.

[754] Steeb W.-H., *Chaos und Quantenchaos in Dynamischen Systemen.* Mannheim: BI Wissenschaftsverlag, 1994.

[755] Steeb W.-H., *Continuou Symmetries, Lie Algebras, Differential Equations and Computer Algebra.* World Scientific, Singapore, 1996.

[756] Steeb W.-H., "On a Driven Nonlinear Circuit and Chaotic Behaviour," *J. Chinese Inst. of Engineers*, vol. 10, no.6, pp. 717–720, 1987.

[757] Steeb W.-H., Erig W., Kunick A., "Chaotic Behaviour and Limit Cycle Behaviour of Anharmonic Systems with Periodic External Pertubations," *Phys. Lett. A*, vol. 93, no. 6, pp. 267–270, 1983.

[758] Steeb W.-H., Solms F., Stoop R., "Chaotic Systems and Maximum Entropy," *J. Phys. A: Math. Gen.*, vol. 27, pp. L399–L402, 1994.

[759] Steeb W.-H., Stoop R., Lai Choy Heng, Villet C.M., "Coupled Chaotic Oscillators and Control of Chaos," *South African Journal of Science*, vol. 91, pp. 273–274, 1995.

[760] Steeb W.-H., "Continuous Symmetries of the Lorenz Model and the Rikitake Two-Disc Dynamo System," *J. Phys. A: Math. Gen.*, vol. 15, pp. L389–L390, 1982.

[761] Steeb W.-H., "On Constants of Motion of the Generalized Lotka-Volterra Model," *Lettre al Nuovo Cimento*, vol. 36, pp. 188–192, 1983.

[762] Steeb W.-H., Euler N., *Nonlinear Evolution Equations and Painlevé Test.* Singapore: World Scientific, 1988.

[763] Steeb W.-H., Van Wyk M.A., "Invariants and Chaotic Maps," *Int. J. Theor. Phys.*, vol. 35, no. 5, pp. 1253–1257, 1996.

[764] Steeb W.-H., Van Wyk M.A., *Stability, First Integral and Ljapunov Exponents of Phase-Coupled Nonlinear Dynamical Systems.* Submitted for Publication, 1996.

[765] Steeb W.-H., in collab. Van Wyk M.A., *Algorithms and Computations with Turbo C.* Mannheim: BI Wissenschaftsverlag, 1992.

[766] Steeb W.-H., in collab. Van Wyk M.A., *Chaos and Fractals: Algorithms and Computations.* Mannheim: BI Wissenschaftsverlag, 1992.

[767] Steenekamp A.P., Nel A.L., "Die Chaotiese Vibrasie van 'n Magneto-Elastiese Balk," Internal Report, no. Kd-72, Rand Afrikaans University, South Africa, us 1990.

[768] Stephens S.A., Thomas J.B., "Controlled-Root Formulation for Digital Phase-Locked Loops," *IEEE Trans. Aerosp. Electron. Syst.*, vol. 31, no. 1, pp. 78–96, 1995.

[769] Stevens S.N., Lin P.-M., "Analysis of Piecewise-Linear Resistive Networks using Complementary Pivot Theory," *IEEE Trans. Circuits Syst.*, vol. CAS-28, no. 5, pp. 429–441, 1981.

[770] Stewart I., *Does God Play Dice?: The Mathematical Theory of Chaos.* England: Penguin Books, 1990.

[771] Stoop R., Meier P.F., "Evaluation of Lyapunov Exponents and Scaling Functions from Time Series," *J. Opt. Soc. Am. B*, vol. 5, no. 5, pp. 1037–1045, 1988.

[772] Stoop R., Parisi J., "Calculation of Lyapunov Exponents avoiding Spurious Elements," *Physica D*, vol. 50, pp. 89–94, 1991.

[773] Strang G., "Wavelet Transforms versus Fourier Transforms," *Bull. Amer. Math. Soc.*, vol. 28, no. 2, pp. 288–305, 1993.

[774] Strang G., "Wavelets," *American Scientist*, vol. 82, pp. 250–255, 1994.

[775] Stremler F.G., *Introduction to Communication Systems.* Second Edition, Reading, MA: Addison-Wesley, 1982.

[776] Su Z., Rollins R.W., Hunt E.R., "Universal Properties at the Onset of Chaos in Driven Diode Resonator Systems," *Phys. Rev. A*, vol. 40, no. 5, pp. 2689–2697, 1989.

[777] Su Z., Rollins R.W., Hunt E.R., "Simulation and Characterization of Strange Attractors in Driven Diode Resonator Systems," *Phys. Rev. A*, vol. 40, no. 5, pp. 2698–2705, 1989.

[778] Su Z., Rollins R.W., Hunt E.R., "Measurements of $f(\alpha)$ Spectra of Attractors at Transitions to Chaos in Driven Diode Resonator Systems," *Phys. Rev. A*, vol. 36, no. 7, pp. 3515–3517, 1987.

[779] Swift J.W., "Hopf Bifurcation with the Symmetry of the Square," *Nonlinearity*, vol. 1, pp. 333–377, 1988.

[780] Szemplińska-Stupnicka W., Iooss G., Moon F.C., *Chaotic Motions in Nonlinear Dynamical Systems.* CISM Courses and Lectures no. 298, Wien, NY: Springer-Verlag, 1988.

[781] Szemplińska-Stupnicka W., Troger H., *Engineering Applications of Dynamics of Chaos.* CISM Courses and Lectures no. 319, Wien, NY: Springer-Verlag, 1991.

[782] Tadeusiewicz M., "A Method for Finding Bounds on all the DC Solutions of Transistor Circuits," *IEEE Trans. Circuits Syst.—I: Fund. Theory and Appl.*, vol. 39, no. 7, pp. 557–564, 1992.

[783] Takahashi Y., Rabins M.J., Auslander D.M., *Control and Dynamic Systems.* Reading, MA: Addison-Wesley, 1991.

[784] Takens F., "Detecting Strange Attractors in Turbulence," *Lecture Notes in Mathematics*, no. 898, NewYork, NY: Springer-Verlag, 1981.

[785] Takizawa T., Liu Y., Ohtsubo J., "Chaos in a Feedback Fabry-Perot Interferometer," *IEEE J. of Quantum Electronics*, vol. 30, no. 2, pp. 334–338, 1994.

[786] Tan N., Eriksson S., "Delta-Sigma Modulators using Unity-Gain Buffers," *Electronic Letters*, vol. 29, no. 5, pp. 478–480, 1993.

[787] Tanaka S., Matsumoto T., Chua L.O., "Bifurcation Scenario in a Driven R-L-Diode Circuit," *Physica D*, vol. 28, pp. 317–344, 1987.

[788] Tang Y.S., Mees A.I., Chua L.O., "Synchronization and Chaos," *IEEE Trans. Circuits Syst.*, vol. CAS-30, no. 9, pp. 620–626, 1983.

[789] Tanzke S., "Ein Beitrag zur Berechnung der Periodischen Lösung in Stark Nicht-Linearen Selbsterregten Netzwerken," *Wiss. Z. Th. Ilmenau*, vol. 36, Heft 4, Sektion Informationstechnik und Theoretische Electrotechnik, pp. 107–116, 1990.

[790] Tavares G., Piedade M.S., "High Performance Algorithms for Digital Signal Processing AGC," *IEEE Int. Symp. on Circuits Syst.*, New Orleans, LA, USA, vol. 2, pp. 1529–1532, 1990.

[791] Taylor A.E., Lay D.C., *Introduction to Functional Analysis.* Second Edition, New York, NY: John Wiley & Sons, 1980.

[792] Temam R., *Infinite-Dimensional Dynamical Systems in Mechanics and Physics.* Applied Mathematcal Sciences, vol. 68, New York, NY: Springer-Verlag, 1988.

[793] Testa J., Pérez J., Jeffries C., "Evidence for Universal Chaotic Behavior of a Driven Nonlinear Oscillator," *Phys. Rev. Lett.*, vol. 48, no. 11, pp. 714–717, 1982.

[794] Testa J., Pérez J., Jeffries C., "Testa, Perez, and Jeffries Respond," *Phys. Rev. Lett.*, vol. 49, no. 14, p. 1055, 1982.

[795] Thomas B., "The Runge-Kutta Methods: Approximating Solutions to ODEs," *Byte Mag.*, pp. 191–210, 1986.

[796] Thompson J., Stewart H., *Nonlinear Dynamics and Chaos: Geometrical Methods for Engineers and Scientists.* John Wiley, New York, 1986.

[797] Tokunaga R., Chua L.O., Matsumoto T., "Bifurcation Analysis of a Cusp-Constrained Piecewise-Linear Circuit," *Int. J. Circuit Theory Appl.*, vol. 17, pp. 283–346, 1989.

[798] Tokunaga R., Komuro M., Matsumoto T., Chua L.O., "'Lorenz Attractor' from an Electrical Circuit with Uncoupled Continuous Piecewise-Linear Resistor," *Int. J. Circuit Theory Appl.*, vol. 17, pp. 71–85, 1989.

[799] Tokunaga R., Matsumoto T., Chua L.O., Miyama S., "The Piecewise-Linear Lorenz Circuit Is Chaotic in the Sense of Shilnikov," *IEEE Trans. Circuits Syst.*, vol. 37, no. 6, pp. 766–786, 1990.

[800] Toumazou C., Lidgey F.J., "Wide-Band Precision Rectification," *IEE Proceedings*, vol. 134, pt. G. no. 1, pp. 7–15, 1987.

[801] Trajkovic L., Correction to "Negative Differential Resistance in Transistor Circuits," *IEEE Trans. Circuits Syst.*, vol. CAS-34, no. 1, p. 109, 1987.

[802] Trajkovic L., "Negative Differential Resistance in Transistor Circuits," *IEEE Trans. Circuits Syst.*, vol. CAS-33, no. 7, p. 736, 1986.

[803] Travis I., Weygandt C.N., "Subharmonics in Circuits Containing Iron-Cored Reactors," *AIEE Trans.*, vol. 57, no. 8, pp. 423–430, 1938.

[804] Tresser C., "About Some Theorems of L.P. Shilnikov," *Annales l'inst. Henri Poincaré*, vol. 40, pp. 441–461, 1984.

[805] Tresser C., *On Some Theorems of L.P. Shil'nikov and Some Applications.* Preprint, Univ. of Nice, France, 1982.

[806] Tsang K.Y., Strogatz S.H., Wiesenfeld K., "Reversibility and Noise Sensitivity of Josephson Arrays," *Phys. Rev. Lett.*, vol. 66, no. 8, pp. 1094–1097, 1991.

[807] Ueda Y., "Explosion of Strange Attractors Exhibited by Duffing's Equation," *Ann. N. Y. Acad. Sci.*, vol. 357, pp. 422–434, 1980.

[808] Ueda Y., Akamatsu N., "Chaotically Transitional Phenomena in a Forced Negative-Resistance Oscillator," *IEEE Trans. Circuits Syst.*, vol. CAS-28, no. 3, pp. 217–224, 1981.

[809] Uhlmann H., Finger L., "Identifikation Irregularen Verhaltens Zur Globalen Analyse Nichtlinearer Dynamischer Netwerke und Systeme Durch Optimierte ..," *AEÜ*, vol. 46, no. 4, pp. 258–265, 1992.

[810] Urabe M., "Galerkin's Procedure for Nonlinear Periodic Systems," *Arch. Rat. Mech. Anal.*, vol. 72, pp. 121–152, 1965.

[811] Ushio T., Hirai K., "Bifurcation and Chaos in Non-Linear Sampled-Data Control System," *IFAC 9-th World Congress*, Budapest, Hungary, 1984.

[812] Ushio T., Hirai K., "Chaos in Non-Linear Samples-Data Control Systems," *Int. J. Control*, vol. 38, no. 5, pp. 1023–1033, 1983.

[813] Ushio T., Hirai K., "Chaotic Behavior in Piecewise-Linear Sampled-Date Control Systems," *Int. J. Non-Linear Mechanics*, vol. 20, no. 5/6, pp. 493–506, 1985.

[814] Ushio T., Hsu C.S., "Chaotic Rounding Error in Digital Control Systems," *IEEE Trans. Circuits Syst.*, vol. CAS-34, no. 2, pp. 133–139, 1987.

[815] Van Buskirk B., Jeffries C., "Observation of Chaotic Dynamics of Coupled Nonlinear Oscillators," *Phys. Rev. A*, vol. 31, no. 5, pp. 3332–3357, 1985.

[816] Van der Pol B., Van der Mark J., "Frequency Demultiplication," *Nature*, vol. 120, no. 3019, pp. 363–364, 1927.

[817] Van der Pol B., Van der Mark J., "The Heartbeat Considered as a Relaxation Oscillation, and an Electrical Model of the Heart," *Phil. Mag.*, vol. 6, pp. 763–775, 1928.

[818] Van Exter M., Lagendijk A., "Observation of Fine Structure in the Phase Locking of a Non-Linear Oscillator," *Phys. Lett. A*, vol. 99, no. 1, pp. 1–4, 1983.

[819] Van Rooij A.C.M., *Non-Archimedean Functional Analysis.* Marcel Dekker Inc., New York, 1978.

[820] Van Wyk M.A., *Statistical Properties of the Zigzag map.* In Preparation, 1996.

[821] Van Wyk M.A., *Periodic Orbits of the Frobenius-Perron Operator of a Piecewise-Linear Map.* In Preparation, 1996.

[822] Van Wyk M.A., "Chaos in Engineering Systems," *SAIEE Talk*, Rand Afrikaans University, Johannesburg, South Africa, 1993.

[823] Van Wyk M.A., "Chaos and Computer Algebra," *Fractales y Caos*, Universidad Internacional Menendez Pelayo, Valencia, Spain, 1992.

[824] Van Wyk M.A., *Toepassing van Komplekse Interpolasie by Rignetantennes.* (Application of Complex Interpolation to Antenna Arrays), M.Eng Thesis: Rand Afrikaans University, Johannesburg, South Africa, 1989.

[825] Varghese M., Fuchs A., Mukundan R., "Chaotic Zero Dynamics in Kinematically Redundant Robots," *IEEE Trans. Aerosp. Electron. Syst.*, vol. 27, no. 5, pp. 784–795, 1991.

[826] Varghese M., Thorp J.S., "An Analysis of Truncated Fractal Growths in the Stability Boundaries of Three-Node Swing Equations," *IEEE Trans. Circuits Syst.*, vol. 35, no. 7, pp. 825–834, 1988.

[827] Varrientos J.E., Sachez-Sinencio E., Ramirez-Angulo J., "A Current-Mode Cellular Neural Network Implementation," *IEEE Trans. Circuits Syst.—II: Analog and Digital Signal Processing*, vol. 40, no. 3, pp. 147–155, 1993.

[828] Veitch D., Glendinning P., "Explicit Renormalisation in Piecewise-Linear Bimodal Maps," *Physica D*, vol. 44, pp. 149–167, 1990.

[829] Venetianer P.L., Werblin F., Roska T., Chua L.O., "Analogic CNN Algorithms for some Image Compression and Restoration Tasks," *IEEE Trans. Circuits Syst.—I: Fund. Theory and Appl.*, vol. 42, no. 5, pp. 278–284, 1995.

[830] Vernam G.S., "Cipher Printing Telegraph Systems for Secret Wire and Telegraphic Communications," *J. Amer. Inst. Elec. Eng.*, vol. 55, pp. 109–115, 1926.

[831] Vetter W.J., Correction to "Derivative Operations on Matrices," *IEEE Trans. Automat. Contr.*, vol. AC-16, p. 113, 1971.

[832] Vetter W.J., "Derivative Operations on Matrices," *IEEE Trans. Automat. Contr.*, vol. AC-15, pp. 241–244, 1970.

[833] Vetter W.J., "Matrix Calculus Operations and Taylor Expansions," *SIAM Review*, pp. 352–369, 1973.

[834] Vidyasagar M., *Nonlinear Systems Analysis.* Second Edition, Englewood Cliffs, NJ: Prentice-Hall Inc., 1993.

[835] Vidyasagar M., Bertschmann R.K., "Some Simplifications of the Graphical Nyquist Criterion," *IEEE Trans. Automat. Contr.*, vol. 33, no. 3, pp. 301–305, 1988.

[836] Villet C.M., Steeb W.-H., "The Coupled Logistic Equations and Domain of Attraction," Internal Report, Rand Afrikaans University, South Africa, 1993.

[837] Vilms J., "Differentiation of Tensor Fields. II," *SIAM Review*, vol. 16, no. 3, pp. 303–308, 1974.

[838] Vohra S., Spano M., Shlesinger M., Pecora L., Ditto W., (eds.) *Proceedings of the 1st Experimental Chaos Conference, 1–3, 1991, Arlington, Virginia.* Singapore: World Scientific, 1992.

[839] Voges W., Atmanspancher H., Scheingraber H., "Deterministic Chaos in Acreting Systems: Analysis of the X-Ray Variability of Hercules X-1," *The Astrophys. J.*, vol. 320, pp. 794–802, 1987.

[840] Vu K. T., Liu C.-C., "Shrinking Stability Regions and Voltage Collapse in Power Systems," *IEEE Trans. Circuits Syst.—I: Fund. Theory and Appl.*, vol. 39, no. 4, pp. 271–289, 1992.

[841] Walters P., *An Introduction to Ergodic Theory.* New York, NY: Springer-Verlag, 1982.

[842] Wang L.-X., *Adaptive Fuzzy Systems and Control: Design and Stability Analysis.* Englewood Cliffs, NJ: Prentice-Hall Inc., 1994.

[843] Weatherburn C.E., *Differential Geometry in Three Dimensions.* Cambridge: Cambridge University Press, 1927.

[844] Weinberg A., Liu B., "Noise and Transmission Delays in Mutual Synchronized Systems," *IEEE Trans. Aerosp. Electron. Syst.*, vol. AES-11, pp. 756–767, 1975.

[845] Weiss L.G., "Wavelets and Wideband Correlation Processing," *IEEE Signal Processing Magazine*, pp. 13–32, 1994.

[846] West B.J., *Fractal Physiology and Chaos in Medicine.* Studies of Nonlinear Phenomena in Life Science – vol. 1, Singapore: World Scientific, 1992.

[847] Whitney H., "Differentiable Manifolds," *Ann. Math.*, vol. 37, pp. 645–680, 1936.

[848] Wichmann B., Hill D., "Building a Random Number Generator," *Byte Mag.*, pp. 123–128, 1987.

[849] Widom H., *Lectures on Measure and Integration.* New York, NY: Van Nostrand Reinhold, 1969.

[850] Wiegerinck W., Tennekes H., "On the Information Flow for One-Dimensional Maps," *Phys. Lett. A*, vol. 144, no. 3, pp. 145–152, 1990.

[851] Wiesenfeld K., Bracikowski C., James G.E., Roy R., "Observation of Antiphase States in a Multimode Laser," *Phys. Rev. Lett.*, vol. 65, pp. 1749–1752, 1990.

[852] Wiggins S., *Global Bifurcations and Chaos.* Applied Mathematical Sciences, vol. 73, New York, NY: Springer-Verlag, 1988.

[853] Wiggins S., *Introduction to Applied Nonlinear Dynamical Systems and Chaos.* Text in Applied Mathematics, vol. 2, New York, NY: Springer-Verlag, 1990.

[854] Wiggins S., Holmes P.J., "Erata: Homoclinic Orbits in Slowly Varying Oscillators," *SIAM J. Math. Anal.*, vol. 19, no. 5, pp. 1254–1255, 1988.

[855] Wiggins S., Holmes P.J., "Homoclinic Orbits in Slowly Varying Oscillators," *SIAM J. Math. Anal.*, vol. 18, no. 3, pp. 612–629, 1987.

[856] Wilke C., Leven R.W., Deutsch H., "Experimental and Numerical Study of Prechaotic and Chaotic Regimes in a Helium Glow Discharge," *Phys. Lett. A*, vol. 136, no. 3, pp. 114–120, 1989.

[857] Williams G.E., *Practical Transistor Circuit Design and Analysis.* New York, NY: McGraw-Hill, 1973.

[858] Williamson D., *Digital Control and Implementation: Finite Wordlength Considerations.* Englewood Cliffs, NJ: Prentice-Hall, 1991.

[859] Wittenburg J., *Dynamics of Systems of Rigid Bodies.* Germany: B.G. Teubner Stuttgart, 1977.

[860] Wolf A., Swift J.B., Swinney H.L., Vastano J.A., "Determining Lyapunov Exponents from the Time Series," *Physica D*, vol. 16, pp. 285–317, 1985.

[861] Wolff S., *How to be a Phd Student.* New Scientist, p. 49, 1992.

[862] Wood K., "Chaos, Fractals and Computers," *Electronics World & Wireless World*, pp. 957–966, 1989.

[863] Wornell G.W., Oppenheim A.V., "Estimation of Fractal Signals from Noisy Measurements using Wavelets," *IEEE Trans. Signal Processing.* vol. 40, no. 3, pp. 611–623, 1992.

[864] Wu C.W., Chua L.O., "On a Conjecture regarding the Synchronization in an Array of Linearly Coupled Dynamical Systems," *IEEE Trans. Circuits Syst.—I: Fund. Theory and Appl.*, vol. 43, no. 2, pp. 161–165, 1996.

[865] Wu C.W., Chua L.O., "Synchronization in an Array of Linearly Coupled Dynamical Systems," *IEEE Trans. Circuits Syst.—I: Fund. Theory and Appl.*, vol. 42, no. 8, pp. 430–447, 1995.

[866] Wu S., "Chua's Circuit Family," *IEEE Proc., Special Issue on Chaotic Systems*, pp. 1022–1032, 1987.

[867] Wyatt J.L., Chua L.O., Gannett J.W., Gocknar I.C., Green D.N., "Energy Concepts in the State-Space Theory of Nonlinear n-Ports: Part II—Losslessness," *IEEE Trans. Circuits Syst.*, vol. CAS-29, no. 7, pp. 417–431, 1982.

[868] Wyatt J.L., Chua L.O., Gannett J.W., Gocknar I.C., Green D.N., "Energy Concepts in the State-Space Theory of Nonlinear n-Ports: Part I-Passivity," *IEEE Trans. Circuits Syst.*, vol. CAS-28, no. 1, pp. 48–63, 1981.

[869] Yamaguti M., Ushiki S., "Chaos in Numerical Analysis of Ordinary Differential Equations," *Physica D*, vol. 3, pp. 618–626, 1981.

[870] Yamakawa T., Miki T., Uchino E., "A Chaotic Chip for Analyzing Nonlinear Discrete Dynamical Network Systems," *Proceedings of the 2nd International Conference on Fuzzy Logic and Neural Networks*, Iizuka, Japan, pp. 563–566, 1992.

[871] Young L.-S., "Entropy, Lyapunov Exponents and Hausdorff Dimension in Differential Dynamical Systems," *IEEE Trans. Circuits Syst.*, vol. CAS-30, no. 8, pp. 599–607, 1983.

[872] Zeeman E.C., *Catastrophe Theory.* Reading, MA: Addison-Wesley, 1977.

[873] Zein D.A., "On the Periodic Steady-State Problem by the Newton Method," *IEEE Trans. Circuits Syst.*, vol. CAS-27, no. 12, pp. 1263–1268, 1980.

[874] Zhong G.-Q., Ayrom F., "Experimental Confirmation of Chaos in Chua's Circuit," *Int. J. Circuit Theory Appl.*, vol. 13, pp. 93–98, 1985.

[875] Zhong G.-Q., Ayrom F., "Periodicity and Chaos in Chua's Circuit," *IEEE Trans. Circuits Syst.*, vol. CAS-32, no. 5, pp. 501–503, 1985.

[876] Zhou T., Moss F., Bulsara A., *Simulations of a Strange Non Chaotic Attractor in a Squid.* Proc. 1st Experimental Chaos Conference, Arlington, Virginia, eds. Vohra S., Spano M., Shlesinger M., Pecora L., Ditto W., 1991.

[877] Zlatev M.P., Nenov G.A., "Synthesis of Active *RC* Systems with Multiport Gyrators and defined Structure," *IEEE Trans. Circuits Syst.*, vol. CAS-27, no. 3, pp. 191–199, 1980.

[878] Zou F., Nossek J.A., "Stability of Cellular Neural Networks with Opposite-Sign Templates," *IEEE Trans. Circuits Syst.*, vol. 38, no. 6, pp. 675–677, 1991.

[879] Zou F., Nossek J.A., "A Chaotic Attractor with Cellular Neural Networks," *IEEE Trans. Circuits Syst.*, vol. 38, no. 7, pp. 811–812, 1991.

[880] Zou F., Seiler G., Schuler A.J., Eppinger B., Nossek J.A., "Experimental Confirmation of the Lady's Shoe Attractor," *IEEE Trans. Circuits Syst.—I: Fund. Theory and Appl.*, vol. 39, no. 10, pp. 844–846, 1992.

[881] Zurada J.M., "Analog Implementation of Neural Networks," *Circuits & Devices Magazine*, pp. 36–41, 1992.

Index

MATHEMATICAL MODELLING:
Theory and Applications

---

1. M. Křížek and P. Neittaanmäki: *Mathematical and Numerical Modelling in Electrical Engineering.* Theory and Applications. 1996 ISBN 0-7923-4249-6
2. M.A. van Wyk and W.-H. Steeb: *Chaos in Electronics.* 1997 ISBN 0-7923-4576-2

KLUWER ACADEMIC PUBLISHERS – DORDRECHT / BOSTON / LONDON